

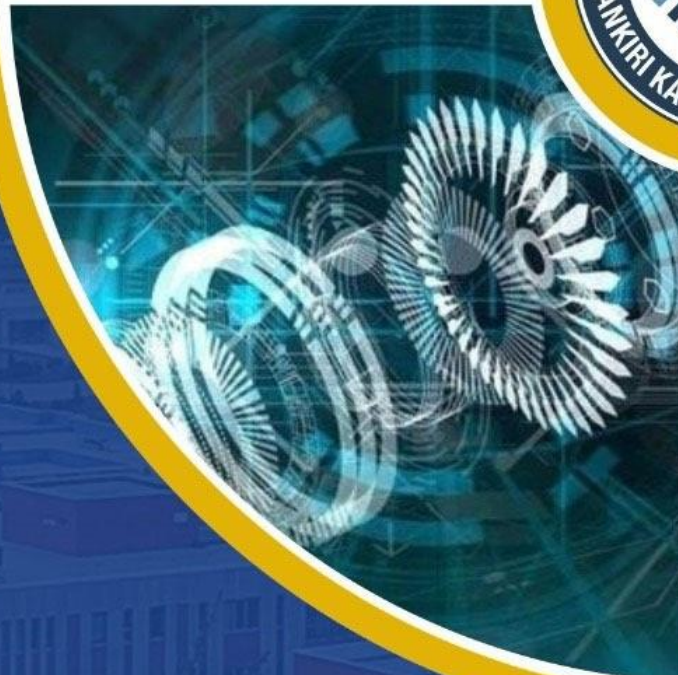


/karatekinuni

<https://ikstc.karatekin.edu.tr>

3rd INTERNATIONAL KARATEKIN SCIENCE AND TECHNOLOGY CONFERENCE

21-22 November 2024
ÇANKIRI, TÜRKİYE



Fulltext

Proceeding Book



Science from Çankırı to the World

www.karatekin.edu.tr



IKSTC3rd

**3rd International Karatekin Science and Technology Conference
(IKSTC3rd)**

FULLTEXT PROCEEDING BOOK

November 21-22, 2024 – Çankırı, Türkiye

Editors

Dr. Muhammed Bora AKIN

Dr. Zehra Gülten YALÇIN

ISBN: 978-625-98655-7-7



IKSTC3rd 2024

3rd International Karatekin Science and Technology Conference (IKSTC3rd)

Fulltext Proceeding Book

ISBN: 978-625-98655-7-7

ÇANKIRI KARATEKİN UNIVERSITY PUBLICATION®

TÜRKİYE

TR: +90 376 218 95 00

<https://ikstc.karatekin.edu.tr/>

All rights reserved to Çankırı Karatekin University.

It cannot be copied or reproduced without permission.

Whole legal and ethical responsibilities belong to the authors.

ÇAKU Publications - 2024©

Draft Publish Date: November 29th, 2024

Final Publish Date: December 6th, 2024

ISBN: 978-625-98655-7-7

ABOUT THE CONFERENCE

CONFERENCE NAME

3rd International Karatekin Science and Technology Conference (IKSTC3rd)

DATE AND PLACE

November 21-22, 2024 Çankırı – Türkiye

ORGANIZING AGENCY

ÇAKU – Çankırı Karatekin University

CHAIRMAN OF THE CONFERENCE

Prof. Dr. Harun ÇİFTÇİ

GENERAL COORDINATOR

Assoc. Prof. Dr. Hüseyin GÖKÇE

OFFICIAL LANGUAGE OF THE CONFERENCE

English

PARTICIPANT COUNTRIES

Azerbaijan, Bangladesh, Bosnia and Herzegovina, Djibouti, Iraq, Libyan Arab Jamahiriya, Nigeria,
Pakistan, Türkiye, United Arab Emirates, Uzbekistan



IKSTC3rd 2024

Conference Chairman

Prof. Dr. Harun ÇİFTÇİ, Rector, Çankırı Karatekin University, Türkiye

Conference Vice Chairman

Prof. Dr. Hüseyin ODABAŞ, Vice Rector, Çankırı Karatekin University, Türkiye

Prof. Dr. İbrahim ÇİFTÇİ, Vice Rector, Çankırı Karatekin University, Türkiye

Prof. Dr. Yavuz DEMİREL, Vice Rector, Çankırı Karatekin University, Türkiye

Organization Chairman

Assoc. Prof. Dr. Hüseyin GÖKÇE, Çankırı Karatekin University, Türkiye

University Independent Representative

Prof. Dr. Şevki ADEM, Çankırı Karatekin University, Türkiye



IKSTC3rd 2024

Organization Committee

Prof. Dr. Faruk KARAASLAN, Çankırı Karatekin University, Türkiye
Prof. Dr. Gonca DURMAZ GÜNGÖR, Çankırı Karatekin University, Türkiye
Prof. Dr. Volkan EYÜPOĞLU, Çankırı Karatekin University, Türkiye
Assoc. Prof. Dr., Ayşenur KAYABAŞ AVŞAR Çankırı Karatekin University, Türkiye
Assoc. Prof. Dr. Ceyhun TURKMEN, Çankırı Karatekin University, Türkiye
Assoc. Prof. Dr. Ender BUGDAY, Çankırı Karatekin University, Türkiye
Assoc. Prof. Dr. Ercan AYDOGMUS, Fırat University, Türkiye
Assoc. Prof. Dr. Hüdayi ERÇOŞKUN, Çankırı Karatekin University, Türkiye
Assoc. Prof. Dr. Irmak POLAT, Çankırı Karatekin University, Türkiye
Assoc. Prof. Dr. Melike BİLGİ, Çankırı Karatekin University, Türkiye
Assoc. Prof. Dr. Mustafa KARHAN, Çankırı Karatekin University, Türkiye
Assoc. Prof. Dr. Selim BUYRUKOĞLU, Çankırı Karatekin University, Türkiye
Assoc. Prof. Dr. Selma AKÇAY, Çankırı Karatekin University, Türkiye
Assoc. Prof. Dr. Tuğba GÜRKOK TAN, Çankırı Karatekin University, Türkiye
Asst. Prof. Dr. Enis SERT, Çankırı Karatekin University, Türkiye
Asst. Prof. Dr. Fatih ISSI, Çankırı Karatekin University, Türkiye
Asst. Prof. Dr. Filiz SARIKAYA PEKACAR, Çankırı Karatekin University, Türkiye
Asst. Prof. Dr. Mehmet Ali BIBERCI, Çankırı Karatekin University, Türkiye
Asst. Prof. Dr. Muhammed Bora AKIN, Çankırı Karatekin University, Türkiye
Asst. Prof. Dr. Murat KONCA, Çankırı Karatekin University, Türkiye
Asst. Prof. Dr. Mücahit UĞUR, Çankırı Karatekin University, Türkiye
Asst. Prof. Dr. Pembe Merve KARABULUT, Çankırı Karatekin University, Türkiye
Asst. Prof. Dr. Ruhan ALTUN ANAYURT, Çankırı Karatekin University, Türkiye
Asst. Prof. Dr. Sakine KIRATLI, Çankırı Karatekin University, Türkiye
Asst. Prof. Dr. Salih YILMAZ, Çankırı Karatekin University, Türkiye
Asst. Prof. Dr. Serap KOCABIYIK ÇAŞKURLU, İstanbul University - Cerrahpaşa, Türkiye
Asst. Prof. Dr. Taha ETEM, Çankırı Karatekin University, Türkiye
Asst. Prof. Dr. Zehra Gülten YALÇIN, Çankırı Karatekin University, Türkiye
Dr. Adem ÇİÇEK, Çankırı Karatekin University, Türkiye
Dr. Çağatay ERSİN, Çankırı Karatekin University, Türkiye
Dr. Dilek AKIN, Çankırı Karatekin University, Türkiye
Dr. Enes BEKTAŞ, Çankırı Karatekin University, Türkiye
Dr. Mahmud Esad YİĞİT, Çankırı Karatekin University, Türkiye
Dr. Mehmet GÜNEŞ, Çankırı Karatekin University, Türkiye
Dr. Sezgin YAŞA, Çankırı Karatekin University, Türkiye
Dr. Vedat Arda KÜÇÜK, Çankırı Karatekin University, Türkiye
Eren YURDAKUL, Çankırı Karatekin University, Türkiye
Hüsamettin ŞERBETÇİ, Çankırı Karatekin University, Türkiye
İrem Nur ECEMİŞ, Çankırı Karatekin University, Türkiye
Mehmet Ali BOZ, Çankırı Karatekin University, Türkiye
Mehmet Emin ÖZDEMİR, Çankırı Karatekin University, Türkiye
Selim SÜRÜCÜ, Çankırı Karatekin University, Türkiye



IKSTC3rd 2024

Scientific Committee

- Prof. Dr. Abdullah Emin AKAY, Bursa Teknik University, Türkiye
Prof. Dr. Alberto BORGHETTI, University of Bologna, Italy
Prof. Dr. Alpaslan KUŞVURAN, Çankırı Karatekin University, Türkiye
Prof. Dr. Avni BERISHA, Pristina University, Kosovo
Prof. Dr. Ayşe ŞAHİN YAĞLIOĞLU, Amasya University, Türkiye
Prof. Dr. Cemil ALKAN, Tokat Gaziosmanpaşa University, Türkiye
Prof. Dr. Faruk POLAT, Çankırı Karatekin University, Türkiye
Prof. Dr. Hayati MAMUR, Manisa Celal Bayar University, Türkiye
Prof. Dr. Ilhan BUŞATLIĆ, University of Zenica, Bosnia &Herzegovina
Prof. Dr. İlyas İNCİ, Çankırı Karatekin University, Türkiye
Prof. Dr. Malic ĆABARAVIDIĆ, University of Zenica, Bosnia &Herzegovina
Prof. Dr. Muhammed RIAZ, University of The Punjab, Pakistan
Prof. Dr. Murat YAYLACI, Recep Tayyip Erdoğan University, Türkiye
Prof. Dr. Naim ÇAĞMAN, Tokat Gaziosmanpaşa University, Türkiye
Prof. Dr. Sinan AKSÖZ, Pamukkale University, Türkiye
Assoc. Prof. Dr. Bogdan STRIMBU, Oregon State University, USA
Assoc. Prof. Dr. Canan CİMŞİT, Kocaeli University, Türkiye
Assoc. Prof. Dr. Damla AMUTKAN MUTLU, Gazi University, Türkiye
Assoc. Prof. Dr. Harun GÖKÇE, Gazi University, Türkiye
Assoc. Prof. Dr. Hasan ARSLANOĞLU, Çanakkale Onsekiz Mart University, Türkiye
Assoc. Prof. Dr. Hülya SİPAHİ, Eskişehir Osmangazi University, Türkiye
Assoc. Prof. Dr. Mirela MARIANA NICULESCU, University of Craiova, Romania
Assoc. Prof. Dr. Nadira BUŞATLIĆ, University of Zenica, Bosnia &Herzegovina
Assoc. Prof. Dr. Nursel ALTAN ÖZBEK, Düzce University, Türkiye
Assoc. Prof. Dr. Onur ÖZBEK, Düzce University, Türkiye
Assoc. Prof. Dr. Ömer Cem KARAKOÇ, Çankırı Karatekin University, Türkiye
Assoc. Prof. Dr. Özlem DOĞAN AYDENİZ, Yıldız Teknik University, Türkiye
Assoc. Prof. Dr. Tamer ÇANKAYA, Bolu Abant İzzet Baysal University, Türkiye
Assoc. Prof. Dr. Ümit Nazlı TEMEL, Cumhuriyet University, Türkiye
Asst. Prof. Dr. Burçak DEMİRBAKAN, Çanakkale Onsekiz Mart University, Türkiye
Asst. Prof. Dr. Didar ÜÇÜNCÜOĞLU, Çankırı Karatekin University, Türkiye
Asst. Prof. Dr. Esmâ ÖZHÜNER, Çankırı Karatekin University, Türkiye
Asst. Prof. Dr. Haluk KORUCU, Çankırı Karatekin University, Türkiye
Asst. Prof. Dr. Mehmet Burak KAYNAR, Hacettepe University, Türkiye
Asst. Prof. Dr. Mehmet Fikret GELİBOLU, Hatay Mustafa Kemal University, Türkiye
Asst. Prof. Dr. Musa Faruk ÇAKIR, Çankırı Karatekin University, Türkiye
Asst. Prof. Dr. Mustafa TEKE, Çankırı Karatekin University, Türkiye
Asst. Prof. Dr. Mustafa YAZ, Yozgat Bozok University, Türkiye
Asst. Prof. Dr. Nuray ÇİÇEK, Çankırı Karatekin University, Türkiye
-



IKSTC3rd 2024

Scientific Committee (Continued)

Asst. Prof. Dr. Seda ERKAN BUĞDAY, Çankırı Karatekin University, Türkiye

Asst. Prof. Dr. Sercan BASİT, Kırşehir University, Türkiye

Asst. Prof. Dr. Tuğba ARSLAN, Çankırı Karatekin University, Türkiye

Asst. Prof. Dr. Zeliha ERBAŞ, Çankırı Karatekin University, Türkiye

Dr. Dursun Kemal BAYRAKTAR, Kastamonu University, Türkiye

Dr. Emel EKİNCİ, Çankırı Karatekin University, Türkiye

Dr. Yusuf Alperen ŞİŞMAN, Ondokuz Mayıs University, Türkiye

Baran ARAS, Çankırı Karatekin University, Türkiye

Müslüm GÜR, Çankırı Karatekin University, Türkiye

Tevfik ATAMAN, Çankırı Karatekin University, Türkiye



IKSTC3rd 2024

Conference Moderators

Prof. Dr. Gonca DURMAZ GÜNGÖR, Çankırı Karatekin University, Türkiye
Assoc. Prof. Dr. Ayşenur KAYABAŞ AVŞAR, Çankırı Karatekin University, Türkiye
Assoc. Prof. Dr. Ceyhun TÜRKMEN, Çankırı Karatekin University, Türkiye
Assoc. Prof. Dr. Tuğba GÜRKOK TAN, Çankırı Karatekin University, Türkiye
Asst. Prof. Dr. Filiz SARIKAYA PEKCAR, Çankırı Karatekin University, Türkiye
Asst. Prof. Dr. Murat KONCA, Çankırı Karatekin University, Türkiye
Asst. Prof. Dr. Mücahit UĞUR, Çankırı Karatekin University, Türkiye
Asst. Prof. Dr. Pembe Merve KARABULUT, Çankırı Karatekin University, Türkiye
Asst. Prof. Dr. Ruhan ALTUN ANAYURT, Çankırı Karatekin University, Türkiye
Asst. Prof. Dr. Salih YILMAZ, Çankırı Karatekin University, Türkiye
Asst. Prof. Dr. Taha ETEM, Çankırı Karatekin University, Türkiye
Dr. Adem ÇİÇEK, Çankırı Karatekin University, Türkiye
Dr. Enes BEKTAŞ, Çankırı Karatekin University, Türkiye
Dr. Mahmud Esat YİĞİT, Çankırı Karatekin University, Türkiye
Dr. Sezgin YAŞA, Çankırı Karatekin University, Türkiye
Dr. Vedat Arda KÜÇÜK, Çankırı Karatekin University, Türkiye
Eren YURDAKUL, Çankırı Karatekin University, Türkiye
Hüsamettin ŞERBETÇİ, Çankırı Karatekin University, Türkiye
İkbal AY KEÇELİ, Çankırı Karatekin University, Türkiye
Mehmet Ali BOZ, Çankırı Karatekin University, Türkiye
Mehmet Emin ÖZDEMİR, Çankırı Karatekin University, Türkiye



IKSTC3rd 2024

Invited Speakers

Prof. Dr. Bilge Hilal ÇADIRCI, Tokat Gaziosmanpaşa University, Türkiye

Prof. Dr. Emel AKYOL, Yıldız Teknik University, Türkiye

Prof. Dr. Malik ČABARAVIDIĆ, University of Zenica, Bosnia & Herzegovina

Prof. Dr. Mustafa Kemal SEZGİNTÜRK, Çanakkale Onsekiz Mart University, Türkiye

Assoc. Prof. Dr. Harun GÖKÇE, Gazi University, Türkiye

Asst. Prof. Dr. Ravi RAVAT, UPES University, India

Dr. Yashar S. HAJIMOLANA, University of Twente, Netherland

Adem TEMEL, Private Sector Executive, Pir-Inci A.S Türkiye

Feyzullah ÇINAR, - Deputy Director General of Civil Aviation, Türkiye



IKSTC3rd 2024

Conference Topics

Agricultural Science and Engineering
Biology
Chemical Engineering
Chemistry
Civil Engineering
Combustion and Fuels
Computer Engineering
Electric and Electronics Engineering
Environmental Engineering
Food Engineering
Forest Engineering
Health Sciences
Landscape Architecture
Mathematics
Material Science
Metallurgy and Materials Engineering
Mechanical Engineering
Medicinal Science
Occupational Health and Safety
Physics
Statistics



IKSTC3rd 2024

Dear Participant,

The total number of speakers at “3rd International Karatekin Science and Technology Conference” was 84 together with the invited speakers.

A total of 9 invited speakers, 3 of whom are foreign and 6 of whom are Turkish nationals, made presentations at the conference.

In addition to the invited speakers, 45 foreign speakers from various countries made presentations at the conference. 54% of the 84 speakers in total were foreigners.

Thank you to all the participants who gave generously of their time, especially the speakers who shared their studies and experiences and the institutions who assisted in.

3rd International Karatekin Science and
Technology Conference Organizing
Committee



T.C.
ÇANKIRI KARATEKİN ÜNİVERSİTESİ
Genel Sekreterlik

Sayı : E-52133317-051-222788
Konu : Görevlendirme (Akademisyen Temsilcisi)

DAĞITIM YERLERİNE

İlgi : 14.11.2024 tarihli ve E-37619811-209-222372 sayılı yazı.

Üniversitemiz ev sahipliğinde 21–22 Kasım 2024 tarihleri arasında yüz yüze ve çevrimiçi (hibrit) olarak düzenlenecek olan 3. Uluslararası Karatekin Bilim ve Teknoloji Konferansına (3. International Karatekin Science and Technology ConferanceIKSTC3rd), Fen Fakültesi Kimya Bölümü öğretim üyesi Prof. Dr. Şevki ADEM’in “Konferans Akademisyen Temsilcisi” olarak katılım sağlaması Rektörlüğümüzce uygun görülmüştür.

Bilgilerini ve gereğini rica ederim.

Prof. Dr. Harun ÇİFTÇİ
Rektör

Dağıtım:
Mühendislik Fakültesi Dekanlığına
Fen Fakültesi Dekanlığına

Bu belge, güvenli elektronik imza ile imzalanmıştır.

Belge Doğrulama Kodu : 0L17-YPP3-0GEB Belge Doğrulama Adresi : <https://ebyssorgu.karatekin.edu.tr>

Adres: Çankırı Karatekin Üniversitesi Uluyazı Kampüsü Rektörlük Binası Merkez/

Çankırı

Telefon No : 0 376 218 95 05

e-Posta : genelsekreterlik@karatekin.edu.tr

Fax No : 0 376 218 95 09

İnternet Adresi :

<https://www.karatekin.edu.tr/>

Bilgi İçin :Nurullah CANSIZ

Şef V.

Telefon No:7212





Index

NDWI ANALYSIS FOR DETECTION OF WATER BODY EXTRACTION OF BEYSEHİR LAKE BETWEEN 1984-2024	1
STATISTICAL STUDIES IN THE PHARMACEUTICAL INDUSTRY	6
SOLAR CHIMNEY POWER SYSTEMS AS A RENEWABLE ENERGY SOLUTION IN LIBYA	12
GREEN CHEMICALS TO OBTAIN REDUCED GRAPHENE OXIDE	18
SUSTAINABLE ENERGY SOLUTIONS WITH FOREST BIOMASS IN TURKEY	23
R,S,T-SPHERICAL FUZZY SOFT SETS.....	29
AN EXPERIMENTAL STUDY OF DC MOTOR APPLICATION BASED ON MPPT DC-DC BUCK-BOOST CONVERTER POWERED BY PHOTOVOLTAIC GENERATORS USING AKBABA MODEL	34
HEARING HEALTH AND OCCUPATIONAL SAFETY RISKS FOR CONSTRUCTION WORKERS.....	40
THE ROLE OF BIOMASS ENERGY IN SUSTAINABLE DEVELOPMENT AND ITS CONTRIBUTION TO ENVIRONMENTAL SUSTAINABILITY GOALS.....	45
HEAT TRANSFER ANALYSIS IN A TRAPEZOIDAL CORRUGATED CHANNEL WITH CIRCULAR OBSTACLES AT DIFFERENT LOCATIONS.....	51
LITHIUM ION BATTERIES: BATTERY FAILURE & FIRE AND INTERVENTION METHODS FOR BATTERY FIRE IN ELECTRICAL VEHICLES	58
HEALTH PROFESSIONAL DOULAS INTERVENTIONS AND BIRTH STYLE: A PILOT STUDY.....	63
SALT RADIOACTIVITY	67
PHOTOCATALYTIC APPLICATIONS OF METAL OXIDES FOR ENVIRONMENTAL AND ENERGY SOLUTIONS	70
DESIGNING FIBER-REINFORCED CONCRETE OVERLAYS ADAPTED TO COLD CLIMATE REGIONS IN TÜRKİYE	75
APPLICATION AND ESSENTIAL COMPONENTS OF SERIAL AND PARALLEL CHOPPER CONVERTERS	81
COMPARISON OF THE PERFORMANCE OF DIFFERENT PV SYSTEM CONFIGURATIONS UNDER PARTIAL SHADING	87
INVESTIGATION OF MIDWIVES' SATISFACTION WITH SUPPORTIVE PERSONNEL ASSIGNED TO VAGINAL BIRTH AND THEIR PRACTICE: MIXED METHOD RESEARCH.....	93
FLOW AND HEAT TRANSFER IN AN ASYMMETRIC TRAPEZOIDAL DUCT WITH TURBULATORS.....	97
INVESTIGATION OF PROPERTIES OF WASTE CONCRETE POWDER SUBSTITUTED CEMENT-BASED MORTARS	103
THE REACTIVE POWER COMPENSATION TO IMPROVE WIND TURBINE STABILITY	108
OPTIMIZATION BASED ENERGY MANAGEMENT APPROACH FOR PROSUMERS LOCATED IN	



SMALL-SCALE MICROGRIDS.....	114
LUNG CANCER DETECTION WITH MACHINE LEARNING SUPPORTED IMAGE PROCESSING TECHNIQUES.....	120
AN EVALUATION OF DYNAMIC COMPACTION: LIMITS AND EFFECTS ON GEOTECHNICAL PERFORMANCE.....	126
COMPARATIVE ANALYSIS OF FLOATING AND GROUND-MOUNTED PHOTOVOLTAIC SYSTEMS: PERFORMANCE, ENVIRONMENTAL AND ECONOMIC PERSPECTIVES IN ISTANBUL.....	132
BLOCKCHAIN AND THE NUCLEAR SUPPLY CHAIN: THE TRACKING TECHNOLOGY OF THE FUTURE....	138
BIOCOMPOSITES AS ALTERNATIVES TO SYNTHETIC FIBER COMPOSITES: TYPES, PRODUCTION METHODS, AND MECHANICAL PROPERTIES	143
HYDROGEN PRODUCTION FROM NATURAL GAS	147
THE DUAL ROLE OF LIVER ENZYMES IN THE DIAGNOSIS AND MONITORING OF NAFL	152
TRANSFORMATION OF FOOD WASTE INTO ADSORBENTS AND METHYLENE BLUE DYE REMOVAL...	158
CAN ARTIFICIAL INTELLIGENCE BE TRAINED TO ACCOUNT FOR THE GROWTH LAWS AND BIOLOGICAL PATTERNS INHERENT IN TREE GROWTH?	164
THE EFFECT OF DOMINANT SIDE ON LOWER EXTREMITY FLEXIBILITY IN ADOLESCENT SHOOTING ATHLETES.....	170
USE OF PROBABILITY DENSITY FUNCTIONS TO PREDICT DIAMETER DISTRIBUTIONS IN FORESTRY...	176
MEETING COMMON AREA ENERGY NEEDS IN MULTI-DWELLING BUILDINGS WITH PHOTOVOLTAIC (PV) PANELS: DESIGN AND CALCULATIONS.....	182
INFLUENCE OF ADDITIVES ON CALCIUM SULFATE CRYSTAL SIZE AND MORPHOLOGY	187
INTEGRATION OF GAS CHROMATOGRAPHY MASS SPECTROMETRY ANALYSIS OF PHYTOCHEMICALS IN ZIZIPHUS JUJUBA TARGETING MULTIDRUG RESISTANT SHIGELLA SPECIES COMPLEMENTED BY MOLECULAR DOCKING STUDY	192
DETERMINATION OF THE POTENTIAL INHIBITORY POTENTIALS OF SOME THIOSEMICARBAZONE COMPOUNDS ON GLYCERALDEHYDE-3-PHOSPHATE DEHYDROGENASE ENZYME	197
TARGETING REPROGRAMMED GLUCOSE METABOLISM IN CANCER THERAPY	202
DETERMINATION OF THE POTENTIAL INHIBITORY POTENTIALS OF SOME THIOSEMICARBAZONE COMPOUNDS ON GLYCOGEN SYNTHASE KINASE 3 ENZYME AS IN SILICO	208
AN INVESTIGATION OF THE EFFECT OF CUPPING (AL-HIJIMA) ON HEMATOLOGICAL, AND LIPID PROFILE PARAMETERS IN MISSAN PROVINCE/ SOUTH IRAQ.....	213
DEEP LEARNING BASED FAULT DETECTION FOR PCB QUALITY CONTROL USING YOLO	219
GUT MICROBIOME AND SALT CONSUMPTION	225
TURKISH FOOD CODEX SALT COMMUNIQUÉ.....	231
THE NEW TRENDS IN OPTODE APPLICATIONS AND TECHNOLOGY.....	236



MOLECULAR DOCKING STUDIES AND ITS APPLICATIONS	241
MODELING AND SIMULATION OF ELECTRIC VEHICLES: AN APPROACH USING MATLAB	246
MANSYS-BASED INTAKE MANIFOLD FLOW ANALYSIS: A COMPUTATIONAL FLUID DYNAMICS APPROACH.....	251
SWOT ANALYSIS OF THE THERAPY USE OF ÇANKIRI ROCK SALT MINE IN HEALTH TOURISM	256
DYNAMIC RESYNCHRONIZATION UNITS IN MICROGRIDS TRANSITIONS	261



NDWI Analysis for Detection of Water Body Extraction of Beyşehir Lake Between 1984-2024

Erkan KARAKOYUN^{1,*} 

¹ Faculty of Engineering and Architecture, Mus Alparslan University, Mus, Türkiye

Abstract

This study investigates the long-term changes in the water surface area of Beyşehir Lake, the largest freshwater lake in Türkiye, between 1984 and 2024. Using Landsat satellite images and the Normalized Difference Water Index (NDWI), we analyze decade-interval data to monitor changes in the lake's surface area in response to climate-driven water resource pressures. Our findings show a significant decline in the lake's surface area from 658 km² in 1984 to 581 km² in 2024, marking an 11.7% reduction. This shrinkage is attributed to increased drought conditions linked to climate change, impacting local agriculture and biodiversity. Remote sensing and GIS tools prove effective for such environmental monitoring, highlighting critical trends and offering insights for local water management strategies to mitigate further decline. The outcomes emphasize the importance of sustainable water resource management in the context of global climate change and provide a basis for planning and preservation efforts in regional hydrology and agriculture.

Keywords: Beyşehir Lake, NDWI, GIS, Remote Sensing, Landsat

1. Introduction

Every species needs water to sustain their life in our world. Water is the most important component in the hydrological cycle, which includes the basic cycle of life. Therefore, if water resources are negatively affected, vital consequences may occur for living things. For this reason, it is important to protect water resources, plan them and observe their changes over time.

The increasing human population and developing industrialization increase the need for water resources over time. As a natural result of this, water resources such as rivers and lakes tend to decrease over time [1]. Due to the increasing greenhouse gas effect in the world's atmosphere, there have been changes in climate parameters such as precipitation and temperature. Türkiye is also in danger under these changing climate conditions. Due to decreasing precipitation and increasing temperatures, droughts are experienced on a regional scale. As a result of this situation, sectors such as agriculture, food, and industry are negatively affected, lakes and dams are drying up and water quality is decreasing [2].

In recent years, increasing computer technology has provided benefits to studies in many different areas. Remote sensing and geographic information systems have also increased in use in many different areas with the developing computer technology and capacity. Especially with the use of satellite images and GIS, high-resolution maps of the desired location can be created and with the help of these images, land use maps of the region can be created. There are many studies in the literature with the help of satellite images and GIS.

Normalized Difference Water Index (NDWI) [3] is a method widely used in the literature to determine the water boundaries of the region with the help of data obtained from satellite images. [4] successfully performed water body extraction using NDWI in their study. [5] investigated using NDWI for the extraction of surface water from Landsat data. [6] indicated the spatiotemporal changes of Burdur Lake between the years 1987-2000 by using NDWI, modified NDWI (MNDWI) and Automated Water Extraction Index (AWEI) from Landsat data.

In Türkiye, studies have been carried out by researchers on determining water-covered areas and monitoring their changes over the years using remote sensing and GIS [6-8]. [7] investigated the water surface and land use changes in Mogan Lake between 1998 and 2010 using Landsat TM5 and Landsat 8 OLI_TIRS satellite images. [6] conducted a study on Burdur Lake using time series analysis and performed water body extraction and change detection between 1987 and 2011.

* Corresponding author. e-mail address: e.karakoyun@alparslan.edu.tr

In this study, the water surface changes on Lake Beyşehir, located in the lake district region of Türkiye, between 1984 and 2024 were examined using Landsat satellite images. Considering that many lakes in the region experience drought problems, it is important to know in which direction Lake Beyşehir has changed over a 40-year period with this study.

2. Materials and Methods

2.1. Study Area

Beyşehir Lake is located in the lake region of Türkiye between Isparta and Konya provinces. It is the largest freshwater lake in Türkiye. 80% of the lake is located within the borders of Konya and 20% within the borders of Isparta province. It is a very important place for bird watching and many fish species live in the lake. The location of Beyşehir Lake is shown in Figure 1.

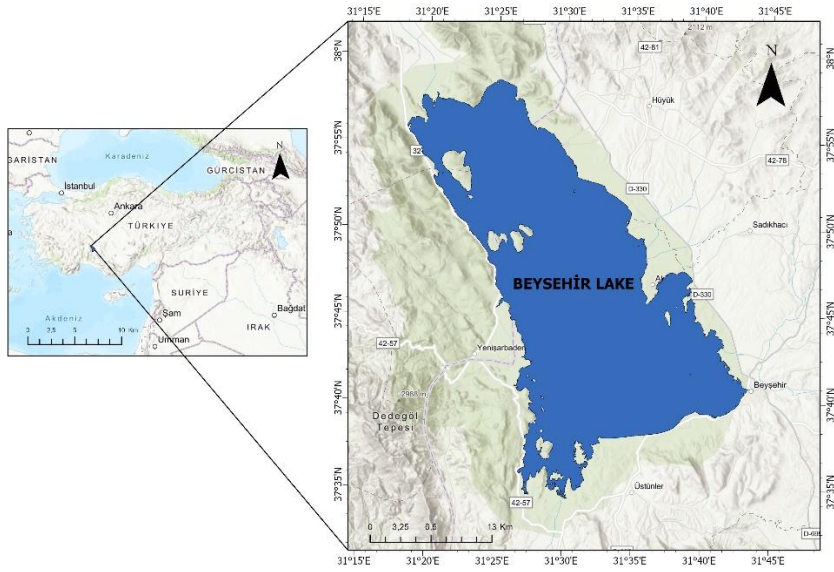


Figure 1. The location of Study Area

2.2. Data and Methods

The details of Landsat images obtained for this study is given in Table 1. The Landsat 9 satellite data were used for the year 2024, Landsat 8 satellite data were used for the year 2014, and Landsat 5 satellite data were used for the years 1984, 1994, and 2004. For each year that satellite images were used, the same months of that year were tried to be selected. ArcGIS Pro software was used for processing and classifying satellite images. Satellite images with low cloudiness were selected. Satellite images were selected for the study area at 10-year intervals starting from 1984 and downloaded from the United States Geological Survey (USGS) Earth Explorer site [9].

Table 1. Satellite description used in this study.

Satellite	Date	Path/Row	Cloud Cover (%)	Satellite Launch Date
Landsat 5	10-20-1984	178/34	0	
Landsat 5	10-16-1994	178/34	3	Marc 1,1984
Landsat 5	10-11-2004	178/34	0	
Landsat 8	10-07-2014	178/34	0.14	Feb 11, 2013
Landsat 9	08-07-2024	178/34	0.71	Oct 27, 2021

Normalized Difference Water Index

The Normalized Difference Water Index (NDWI) was initially proposed by [3] to identify surface water in wetland areas and to assess the extent of surface water bodies. The NDWI is calculated for Landsat 5, Landsat 8, and Landsat 9 as Equation 1.

$$NDWI = \frac{B3 - B5}{B3 + B5} \quad (1)$$

First of all, in the analyses, Landsat satellite images were downloaded from NASA USGS [3] website in a way that would include Beyşehir Lake. Since the satellite images cover a very wide area, they were cropped using ArcGIS Pro software to include Beyşehir Lake and its immediate surroundings in order to increase time and program performance. The subsequent analyses were made on this cropped frame. Then, NDWI analysis was performed using the Raster Calculator function on ArcGIS Pro software. Wetlands and remaining parts were defined from the obtained images using the Reclassify function. The defined areas were calculated separately for the years 1984, 1994, 2004, 2014, and 2024 using various operations on the program, and the surface areas of Beyşehir Lake were calculated.

3. Results and Discussion

Beyşehir Lake surface area was examined using Landsat satellite images for changes in water surface area at 10-year intervals from 1984 to 2024. Figure 2 (a, b, c, d, e) shows the Beyşehir Lake water surface area obtained by NDWI analysis for the years 1984, 1994, 2004, 2014, and 2024. In order to observe the changes between the analysis start year 1984 and 2024, the water surface maps for the years 1984 and 2024 are superimposed in Figure 2e. As can be seen from the figure, there are visible water losses especially in the northwest and southwest of Beyşehir Lake.

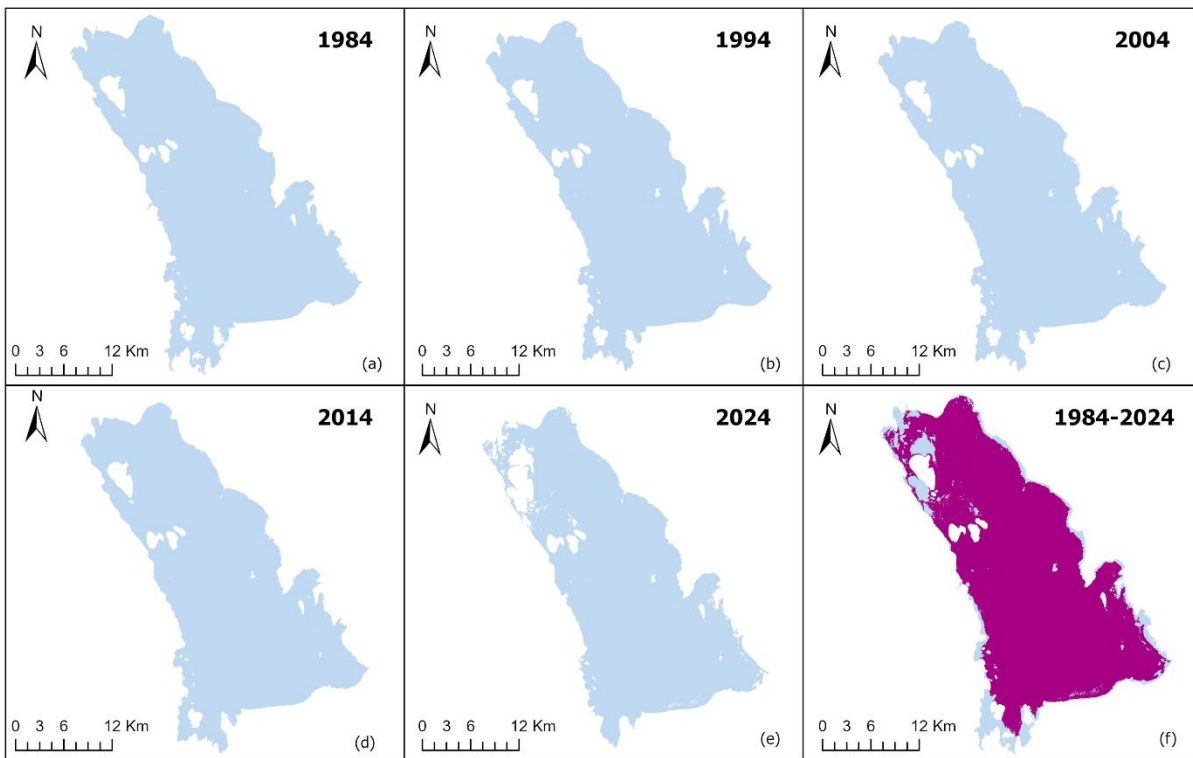


Figure 2. The water surface of Beyşehir Lake by years.

When we consider the Figure 2 (a,b,c,d,e) it is clearly seen that the water area of Lake Beyşehir has been decreasing over the years and will reach its lowest level in 2024. Global drought and water resource losses are seen in our country, and the lake region is also affected by this situation. Table 2 shows the water surface areas of Lake Beyşehir obtained by NDWI analysis for the years 1984, 1994, 2004, 2014, and 2024, respectively. It can be seen from the table that the surface area, which was 658 km² in 1984, decreased to 619 km² in 1994. An increase in the water surface area was observed only in 2004 within the 10-year period analyzed. The water surface area, which was 619 km² in 1994, was calculated as 631 km² in 2004. Although a small change was observed between 2004 and 2014, the water surface area, which was 630 km² in 2014, decreased to 581 km². In the last 40-year period analyzed, the decline accelerated, especially due to the effects of climate change and drought.

Table 2. Changes in Beyşehir Lake Water Surface Areas over the Years

Year	Area (km ²)
1984	658
1994	619
2004	631
2014	630
2024	581

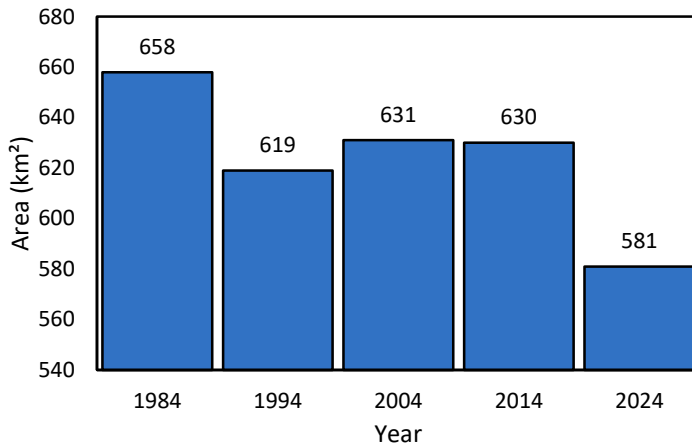


Figure 3. Water surface area change of Beyşehir Lake between 1984-2024.

In order to observe the changes in the water surface areas of Lake Beyşehir between the analyzed years 1984-2024, the changes in the water surface area by year are given in Figure 3. It is clearly seen that a serious decrease in the water surface areas was observed especially after 2014.

4. Conclusion

In this study, water body surface of Beyşehir Lake is determined between the years 1984-2024. In order to the Landsat satellite data were used and the Normalized Difference Water Index (NDWI) analysis applied for these data. The maps were created for every 10-year interval from 1984 to 2024. From NDWI analysis, the water body surface area was found as 658 km² which is the highest area of last 40 years while the lowest body surface area was detected in the year 2024 with 581 km². From the year 1984 to 2024 the water surface area of Beyşehir Lake decreased 11.7 %.

As a result, it is clear that the global climate change resulting in drought is adversely affecting Beyşehir Lake. The observation of the changing water surface area of Beyşehir Lake with remote sensing technology is an effective method in the field of water resources and agriculture. The results obtained from this study show that

the water surface of Lake Beysehir has decreased over time, and it is thought that it will guide local administrators to prevent this situation.

References

- [1] Bayrak, M., Yulu, A., & Öztürk, Y. (2022). Balıkgöl (Ağrı) Kıyılarında Arazi Örtüsü/Kullanımının Zamansal Değişimi (1989-2021). *Coğrafi Bilimler Dergisi*, 20(1), 282–309. <https://doi.org/10.33688/aucbd.1063557>
- [2] Kaya, Ö. A., & Kaplan, G. (2021). Uzaktan Algılama Yöntemleri İle Burdur Gölü’ndeki Alansal Değişiminin Belirlenmesi. *Doğal Afetler ve Çevre Dergisi*, 7(1), 1–12. <https://doi.org/10.21324/dacd.760805>
- [3] McFeeters, S. K. (1996). The use of the Normalized Difference Water Index (NDWI) in the delineation of open water features. *International Journal of Remote Sensing*, 17(7), 1425–1432. <https://doi.org/10.1080/01431169608948714>
- [4] Ji, L., Zhang, L., & Wylie, B. (2009). Analysis of dynamic thresholds for the normalized difference water index. *Photogrammetric Engineering and Remote Sensing*, 75(11), 1307–1317. <https://doi.org/10.14358/PERS.75.11.1307>
- [5] Rokni, K., Ahmad, A., Selamat, A., & Hazini, S. (2014). Water feature extraction and change detection using multitemporal landsat imagery. *Remote Sensing*, 6(5), 4173–4189. <https://doi.org/10.3390/rs6054173>
- [6] Sarp, G., & Ozcelik, M. (2017). Water body extraction and change detection using time series: A case study of Lake Burdur, Turkey. *Journal of Taibah University for Science*, 11(3), 381–391. <https://doi.org/10.1016/j.jtusci.2016.04.005>
- [7] Özçalık, H., Torun, A. T., & Bilgilioglu, S. S. (2020). Landsat uydu görüntüleri kullanılarak Mogan Gölü ’ nün su yüzeyi ve arazi örtü değişiminin belirlenmesi. *Turkish Journal of Remote Sensing*, 2(2), 77–84.
- [8] Özelkan, E. (2020). Water body detection analysis using NDWI indices derived from landsat-8 OLI. *Polish Journal of Environmental Studies*, 29(2), 1759–1769. <https://doi.org/10.15244/pjoes/110447>
- [9] <https://earthexplorer.usgs.gov/> (Accessed on November 2, 2024)



Statistical Studies in the Pharmaceutical Industry

Şebnem ŞENOL^{1,*} , Aynur DEMİR¹ , Emel AKYOL³

¹ Institute of Natural Sciences, Faculty of Chemistry-Metallurgy, Chemical Engineering, Yildiz Technical University, Istanbul, Turkey

Abstract

In this study, the data from the article "Synthesis and characterization of hydrogels based on poly(2-hydroxyethyl methacrylate) for drug delivery under UV irradiation" were used within the scope of statistical study in the pharmaceutical industry. Two statistical methods called "Artificial Neural Networks (ANN)" in the Matlab programme and "Response Surface Method (RSM)" in the Minitab package programme were used. It was determined how close the results obtained in the programme are to the results found in the laboratory experiment. Today, with the developing technology, both time and cost are becoming increasingly valuable. For this reason, it is aimed to find results close to reality by saving time and cost with statistical methods.

Keywords: Artificial Neural Networks, Response Surface Method, Matlab, Minitab, Drug release

1. Introduction

With the development of technology, prediction modeling is performed to solve complex structures in some areas for the future. "Artificial Neural Networks (ANN)" is one of the methods that make predictions by using artificial intelligence [1]. "Artificial Neural Networks (ANN)", which was discovered by being inspired by the human brain, is a computer system and prediction method that serves this purpose in addition to the fact that it performs many abilities such as producing, designing and predicting information just like our brain without any help [2]. Artificial Neural Networks perform non-linear modelling between input and output parameters without the need for prior knowledge and without making a prediction. Inputs are introduced to the network and then output variables are given in response to the inputs. The network is trained by learning the relationship between input and output. The reason why this method is preferred is learning by teaching [3].

The artificial nerve cell consists of five parts;

- Input variables
- Weights
- Collection function
- Activation function
- Output variables [4].

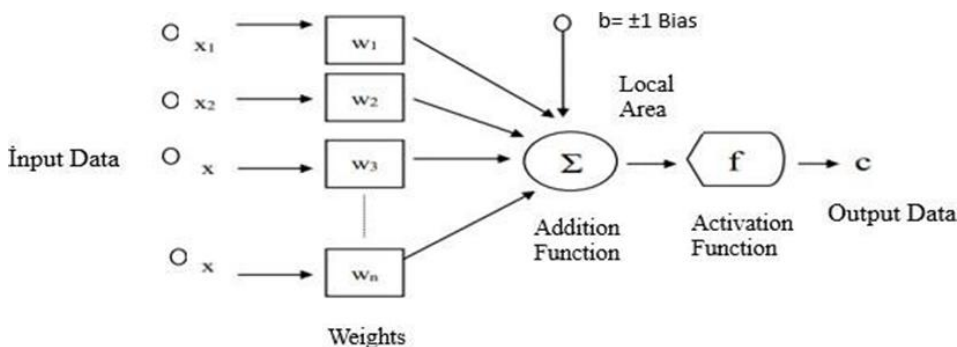


Figure 1. Working Principle of Artificial Neural Network [4]

The sum function is a type of function that calculates the effect of all inputs and weights on this processing element. The sum function calculates the net input to the cell. If all of the net input collected in the cell is,

* Corresponding author. e-mail address: sebnemsenol_@hotmail.com

$$net = \sum_{i=1}^n w_{ij}x_i + b$$

is obtained as. In this equation

x_i : input value of neuron i ,

w_{ij} : weight coefficients,

n : the total number of inputs to a cell,

b is the threshold value and Σ is the sum function [5].

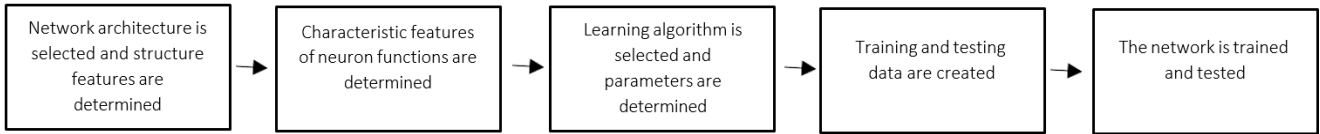


Figure 2. Artificial Neural Networks Workflow

The Response Surface Method is a technique that combines mathematics and statistics, which is used in analysis and modeling in some applications where the answers sought are affected by different variables and these answers are aimed to reach optimized conditions. The response surface method, which is used in industry and many other fields, is frequently used in scientific research as it enables us to reach the most appropriate answer with fewer experiments [6]. The response surface method consists of 3 stages: model validation, mathematical modeling and design of experiments. With the design of the experiment, it is possible to establish a relationship between the dependent and independent parameters and to determine which parameter is the most important. Polynomial equations created in the response surface method are widely used because they provide ease in estimating the response surface function. To see to what extent the estimated model represents the real values and how accurate it is, the model should be validated [7].

2. Materials and Methods

In the present study, the article "Synthesis of HEMA (Poly 2-hydroxyethylmethacrylate) based hydrogels for controlled drug release under the influence of photoinitiators"[8] was used. In this article, HEMA-based hydrogels were prepared with photoinitiators (Irg 184, Irg 651, Irg 2959) and crosslinker (ethylene glycol dimethacrylate). Donepezil HCL, HAp or TiO₂, the active ingredient of the drug used in the treatment of Alzheimer's disease, was added to HEMA-based hydrogels by photopolymerization method and the swelling and release effects of hydrogels were investigated. Release analyses were performed in different pH environments and the most suitable release environment was determined. It was determined that the synthesized hydrogels can be used in the release of Donepezil HCl drug active substance. The results [8] were predicted by Artificial Neural Network (ANN) and Response Surface Method (RSM). For Artificial Neural Networks (ANN), Matlab programme R2018b version Neural Network Toolbox was used. For the Response Surface Method (RSM), the Minitab package programme Design Of Experiment (DOE) was used. The prediction results were statistically compared with the experimental results.

3. Results and Discussion

Firstly, predictions were made with Artificial Neural Network and compared with the results in the paper.

HEMA-based hydrogels were synthesized using ethylene glycol dimethacrylate crosslinker and Irgacure 184, Irgacure 651, Irgacure 2959 photoinitiators and HAp as additive. The following table shows the hydrogels synthesized at different times according to pH 1.2 taken from the article "Synthesis of HEMA (Poly 2-hydroxyethyl methacrylate) based hydrogels for controlled drug release under the influence of photoinitiators"[8]. The detected results were predicted by Artificial Neural Network and the results were statistically compared.

Table 1. Formulation of HEMA-based hydrogels

Hydrogels	HEMA (%)	EGDMA (%)	Irg 651 (%)	Irg 184 (%)	Irg 2959 (%)	HAp (%)
Hydrogel 1 (H1)	50	3	0.1	–	–	–
Hydrogel 2 (H2)	50	3	0.5	–	–	–
Hydrogel 3 (H3)	50	3	1	–	–	–
Hydrogel 4 (H4)	50	3	–	0.1	–	–
Hydrogel 5 (H5)	50	3	–	0.5	–	–
Hydrogel 6 (H6)	50	3	–	1	–	–
Hydrogel 7 (H7)	50	3	–	–	2	–
Hydrogel 8 (H8)	50	3	–	–	3	–
Hydrogel 9 (H9)	50	3	0.1	–	–	0.5
Hydrogel 10 (H10)	50	3	0.5	–	–	0.5
Hydrogel 11 (H11)	50	3	1	–	–	0.5
Hydrogel 12 (H12)	50	3	–	0.1	–	0.5
Hydrogel 13 (H13)	50	3	–	0.5	–	0.5
Hydrogel 14 (H14)	50	3	–	1	–	0.5
Hydrogel 15 (H15)	50	3	–	–	2	0.5
Hydrogel 16 (H16)	50	3	–	–	3	0.5

Table 2. Drug Release Value at pH 1.2

PH 1.2																
Time(min)	H1	H2	H3	H4	H5	H6	H7	H8	H9	H10	H11	H12	H13	H14	H15	H16
10	14	18	30	12	13	14	27	53	6	19	34	3	12	14	26	36
20	15	27	41	14	16	20	32	69	21	34	49	11	14	15	30	45
30	22	28	44	15	22	25	36	73	32	37	61	23	30	31	35	50
60	39	44	70	20	24	26	46	83	33	54	87	29	39	40	40	56
120	41	65	80	32	34	37	58	94	41	80	87	42	44	45	55	75
180	70	84	93	43	43	52	67	94	49	80	87	45	46	47	71	89
240	74	91	93	48	49	53	68	94	49	80	87	46	48	50	71	89
300	74	91	93	50	51	53	72	94	52	80	87	47	50	51	71	89
360	74	91	93	50	51	53	72	94	70	80	87	49	50	51	71	89

MATLAB programme was used in the development of the ANN model. With the help of the codes written in the MATLAB programme, the data set was introduced to the network and training was performed. The most appropriate network architecture was determined and the model was created. In the study, a feed-forward network structure was used to predict the drug release rate of the hydrogel. The first step of the prediction process in artificial neural networks starts with the selection of input, output and test data. Input data consists of 3 columns as Irg 651, Irg 184, Irg 2959. The output data are synthesized hydrogels. The number of neurons in the input layer of the network is 3, the number of neurons in the intermediate layer is 10 and the number of neurons in the output layer is 1. The Sigmoid transfer function was used in the hidden (intermediate) and output layers. The number of hidden layers and the number of neurons in the layers were determined by trial and error. Levenberg-Marquardt optimization method was chosen for training the network and adjusting the weights. A total of 16 data were obtained as a result of the experimental studies. In the table given above, separate predictions were made in Artificial Neural Networks for pH 1.2 in the time period from 10 minutes to 360 minutes, and the most efficient result was obtained for 360 minutes. The prediction study at pH 1.2 at 360 minutes is shown in the image below. The data were normalized before being introduced to the network. The normalization process is applied to increase model success. Firstly, the data were transferred to the Matlab programme. Input variables are assigned to the input section, output variables are assigned to the output section and variables to be tested are assigned to the test section. The 16 variables from H1 to H16 in Table 2 were transferred as both input and test data. The resulting artificial neural network model according to the selections on the screen above is shown in Figure 4.

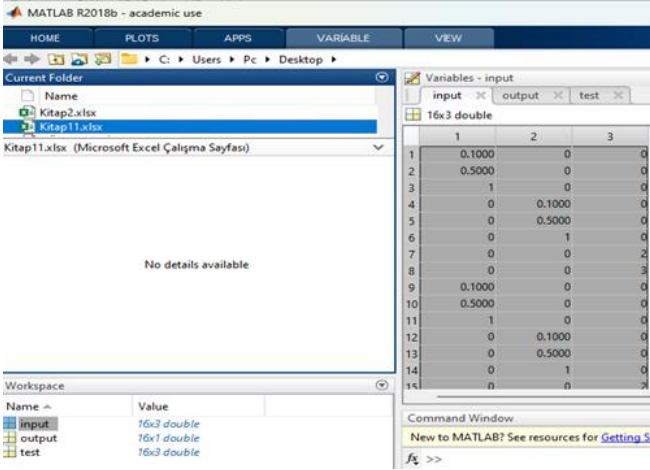


Figure 3. Data transfer screen in ANN

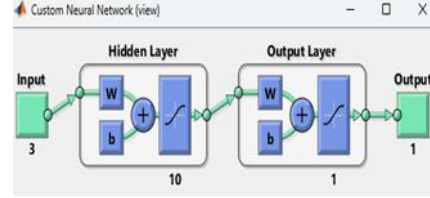


Figure 4. Structure of ANN

The training for the test data in ANN was completed and the prediction processes were performed and the results are as follows. The training performance of the selected model is given in the graph in Figure 6.

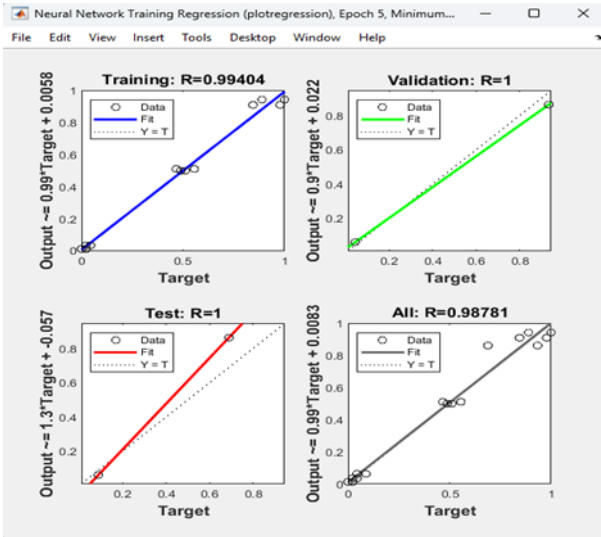


Figure 5. Regression graph in ANN

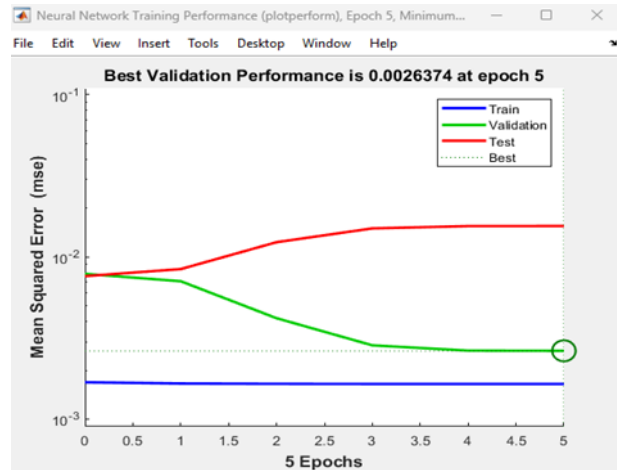


Figure 6. ANN training performance

The regression equation resulting from the experimental result values and the results generated by the Artificial Neural Network is as follows

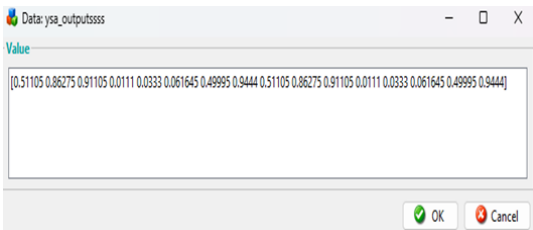


Figure 7. ANN result screen

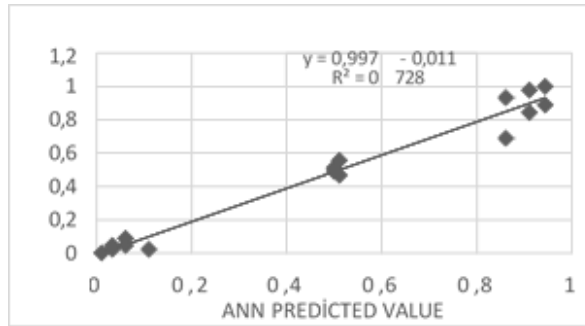


Figure 8. Release graph of predicted values and actual values

Table 3. ANN training result screen

	A	B	C	D	E	F
1	IRG 651	IRG 184	IRG 2959	HYDROGELS	YSA SONUÇ	FARK
2	0,1	0	0	0,5555	0,51105	0,04445
3	0,5	0	0	0,9333	0,86275	0,07055
4	1	0	0	0,9777	0,91105	0,06665
5	0	0,1	0	0,0222	0,0111	0,0111
6	0	0,5	0	0,0444	0,0333	0,0111
7	0	1	0	0,0888	0,061645	0,027155
8	0	0	2	0,5111	0,49995	0,01115
9	0	0	3	1	0,9444	0,0556
10	0,1	0	0	0,4666	0,51105	0,04445
11	0,5	0	0	0,6888	0,86275	0,17395
12	1	0	0	0,8444	0,91105	0,06665
13	0	0,1	0	0	0,0111	0,0111
14	0	0,5	0	0,0222	0,03333	0,01113
15	0	1	0	0,0444	0,061645	0,017245
16	0	0	2	0,4888	0,49995	0,01115
17	0	0	3	0,8888	0,9444	0,0556
18						

After the artificial neural network study, the study with the Minitab response surface method (RSM) is as follows. As a first step, the Minitab programme is opened, central composite is selected as the design type from the create response surface design option, the number of factors is selected as 3 for our 3 variables [8] and a design is created. After selecting the central composite design type, input and output variables are assigned.

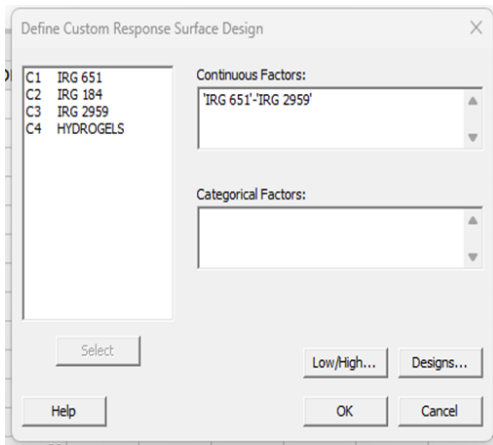


Figure 9. Data transfer screen in Minitab

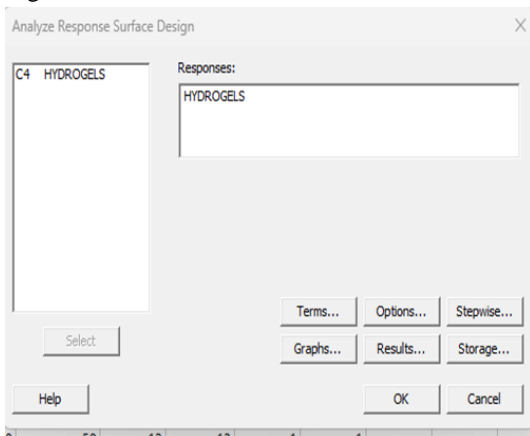


Figure 10. Entering input variables

	A	B	C	D	E	F
1	IRG 651	IRG 184	IRG 2959	HYDROGELS	MINITAB SONUÇ	FARK
2	0,1	0	0	74	66,304	7,696
3	0,5	0	0	91	87,56	3,44
4	1	0	0	93	89,56	3,44
5	0	0,1	0	50	55,196	5,196
6	0	0,5	0	51	48,46	2,54
7	0	1	0	53	52,46	0,54
8	0	0	2	72	71,5	0,5
9	0	0	3	94	91,5	2,5
10	0,1	0	0	70	66,304	3,696
11	0,5	0	0	80	87,56	7,56
12	1	0	0	87	89,56	2,56
13	0	0,1	0	49	55,196	6,196
14	0	0,5	0	50	48,46	1,54
15	0	1	0	51	52,46	1,46
16	0	0	2	71	71,5	0,5
17	0	0	3	89	91,5	2,5

Table 4. Analysis results

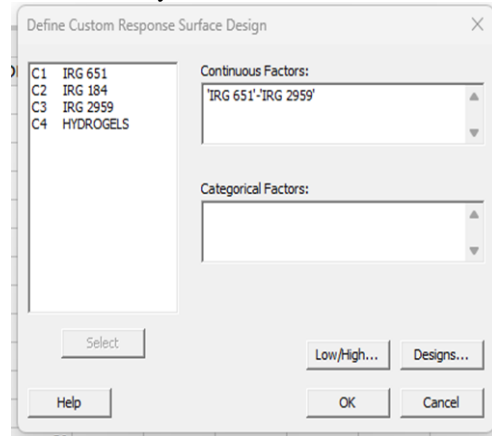


Figure 11. Entering output variable

The regression equation resulting from the experimental result values and the results generated by the Response Surface Method (RSM) is as follows

Model Summary

S	R-sq	R-sq(adj)	R-sq(pred)
5,26938	94,53%	90,88%	85,11%

Figure 12. R-value results

Regression Equation in Uncoded Units

$$\text{HYDROGELS} = 58,26 + 85,9 \text{ IRG } 651 - 33,4 \text{ IRG } 184 - 2,30 \text{ IRG } 2959 - 54,6 \text{ IRG } 651 * \text{IRG } 651 \\ + 27,6 \text{ IRG } 184 * \text{IRG } 184 + 4,46 \text{ IRG } 2959 * \text{IRG } 2959$$

Figure 13. Equation found as a result of the analysis

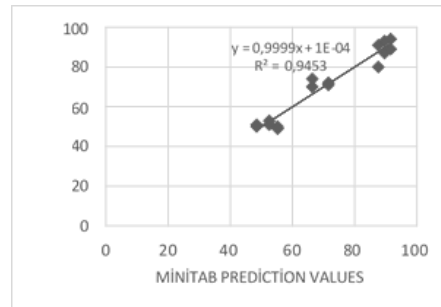


Figure 14. Release graph of predicted values and actual values

4. Conclusion

When the data obtained by using Artificial Neural Networks and Response Surface Method in this study are analyzed, the following results emerge:

In the article "Synthesis and characterization of hydrogels based on poly(2-hydroxyethyl methacrylate) for drug delivery under UV irradiation"[8], ANN gave the closest result to the data obtained as a result of the experimental study. In Figure 5, the correlation coefficient shows the relationship between outputs and targets. The values between outputs and targets are very close to 1. The correlation values of the model are 0.99404 for training, 1 for validation and 1 for testing. The overall correlation coefficient of the data set is 0.98781. The fact that the values are close to 1 for all data shows that the data obtained with ANN training and the real data are compatible with each other. Correlation coefficient values close to 1 means that the model is successful. As the mean squared error approaches zero, it means that better results are produced, that is, it can be said that the error is lower and more successful results are obtained. The lowest MSE value for the validation set was 0.0026374. This result again shows that the model is successful. When the Minitab analysis reports are examined, it is seen that the regression equation is significant at a 5% significance level ($P = 0.000 < \alpha = 0.05$) $R^2 = 94.53\%$. When the results of Artificial Neural Networks training and Minitab analysis are graphed separately with experimental values, R^2 value is 0.9728 for ANN and 0.9453 for RSM. In this way, the results found in the programme were verified. Based on all these, the R^2 value obtained in the Artificial Neural Network prediction was higher than the Response Surface Method. According to the performance values obtained in the study, it is seen that the Artificial Neural Network model performs more effectively than the Response Surface Method. Thus, it is seen that Artificial Neural Networks have higher prediction ability and less error than the Response Surface Method. In this case, it is possible to prefer Artificial Neural Networks in cases where regression analysis assumptions are not met and the analysis cannot be performed.

References

- [1] Ataseven, B. (2013). Forecasting Modelling with Artificial Neural Networks. *Öneri Journal*, 10(39), 101-115.
- [2] Erdoğan, E., & Özyürek, H. (2012). Price Forecasting with Artificial Neural Networks. *Journal of Social and Human Sciences*, 4(1), 85-92.
- [3] Yavuz, S., & Deveci, M. (2012). The effect of statistical normalization techniques on artificial neural network performance. *Erciyes University Journal of Faculty of Economics and Administrative Sciences*, (40), 167-187.
- [4] Damla, Y., Temiz, T., & Keskin, E. (2020). Estimation of Water Level Using Artificial Neural Network: Yalova Gökçe Dam Example. *Kırklareli University Journal of Engineering and Science*, 6(1), 32-49
- [5] Terzi, Ö. (2009). Prediction of Lake Egirdir Water Temperature with Artificial Neural Networks Method. *Journal of Süleyman Demirel University Institute of Science and Technology*, 10(2), 297-302.
- [6] Ateş, Ç., Bayraktar, B. and Bilen, M. (2018). Determination of the Optimum Conditions of a Boron Factory Wastewater Chemical Treatment Process by Response Surface Method. *Gazi University Journal of Faculty of Engineering and Architecture*, 33(1).
- [7] Albayrak, S. Optimisation of Noise Levels in Machine Tools by Response Surface Method).
- [8] Senol, S., & Akyol, E. (2018). Synthesis and characterization of hydrogels based on poly (2- hydroxyethyl methacrylate) for drug delivery under UV irradiation. *Journal of Materials Science*, 53, 14953-14963



Solar chimney power systems as a renewable energy solution in Libya

Abrayik Abdulslam Abrayik ALFAKHAKHIRI^{1,*} , Abdullah AKBULUT² , Ethar Sulaiman Yaseen YASEEN³ 

¹ Institute of Graduate Studies, Department of Mechanical Engineering, Çankırı Karatkin University, Çankırı, Türkiye

² Institute of Graduate Studies, Department of Mechanical Engineering, Çankırı Karatkin University, Çankırı, Türkiye

³ Institute of Graduate Studies, Department of Electrical and Electronics Engineering, Çankırı Karatkin University, Çankırı, Türkiye

Abstract

This study investigates the potential of Solar Chimney Power Systems (SCPS) as a sustainable energy solution for Libya. SCPS technology leverages solar energy to drive air through a tall chimney, generating electricity via turbines, making it an attractive option for regions with high solar irradiance. This research proposes a system design optimized for Libyan conditions, particularly in Derna-Al-Fataih, where climatic and solar characteristics are conducive to efficient operation. An economic analysis, reveals promising financial metrics, including an annual revenue of \$290,138, a net profit of \$240,138, and a payback period of 6.25 years, resulting in a 16.01% return on investment (ROI). These results suggest that SCPS technology could provide a reliable and profitable renewable energy source for Libya, contributing to energy diversification and sustainability. This study addresses existing gaps in SCPS research and offers recommendations for future work on hybrid systems and region-specific adaptations.

Keywords: Solar chimney, Renewable energy, Hybrid energy systems, Libya.

1. Introduction

Solar Chimney Power Systems (SCPS), also known as Solar Aero-Electric Power Plants (SAEP), are innovative structures that convert solar energy into electrical power through the natural process of buoyancy-driven airflow. The system consists of three main components: a solar collector, a chimney, and a turbine. Sunlight heats the air trapped under a transparent collector, creating a greenhouse effect that increases the temperature of the air. The warmer air rises through the chimney, where it drives a turbine to generate electricity. This process uses a simple yet effective method to capture solar energy and convert it into a sustainable power source. The concept of the solar chimney was first introduced by Cabanyes [1], who envisioned using it to heat air within a building, with an attached wind blade for electricity generation. Since the 1970s, various countries, including Australia, the USA, and Canada, have registered patents to explore the potential of this technology [2]. The first operational prototype was constructed in Manzanares, Spain, between 1981 and 1982 by Schlaich and his team [3][4]. This pioneering project inspired additional proposals globally, including some notable large-scale initiatives. For instance, a 200 MW solar chimney was proposed for Mildura, Australia, featuring a 1000-meter chimney and a 7000-meter-diameter collector, with the capacity to power around 200,000 households [5][6]. In Rajasthan, India, a 100 MW plant was scheduled but later canceled due to political tensions between India and Pakistan [7]. Meanwhile, Spain saw a proposal for a 40 MW Ciudad Real Torre Solar project, which would include a 750-meter-high chimney and a 3.5 km² collector [8]. In Namibia, the "Green Tower" project planned a 1500-meter chimney integrated with agricultural greenhouses, generating 400 MW [9]. In China, a 1000-meter-high solar chimney was proposed in Shanghai, combining power generation with tourism potential [10]. Over time, researchers have examined various design enhancements and applications for solar chimney systems. Zhou et al. [10] provided an overview of the early experimental and theoretical research on solar chimneys up to 2010, discussing design variations like floating chimneys and sloped collectors. Chikere et al. [11] reviewed methods for enhancing SCPS performance, including the use of waste heat from flue gases to boost energy input. Zhai et al. [12] summarized applications of solar chimneys integrated into buildings, particularly on rooftops and walls, while Dhahri and Omeri [13] categorized research into project developments, numerical studies, and unconventional designs. Olorunfemi and Bamisile [14] focused on desert applications, with specific attention to northern Nigeria. Although these reviews

* Corresponding author. e-mail address: 228117200@ogrenci.karatekin.edu.tr

provided valuable insights, they were often limited in scope, region-specific, or outdated. Figure 1 shows the visualization of solar chimney.



Figure 1. Solar chimney [15]

This study aims to address existing gaps by offering a design of solar chimney, focusing particularly on its potential applications in Libya. The design also includes an analysis of hybrid systems that integrate solar chimneys with other renewable energy sources, providing insights into optimizing these systems for improved efficiency tailored to Libyan conditions. Furthermore, we identify key research gaps and propose a roadmap for future studies, encouraging advancements in hybrid configurations, more precise simulation models, and exploration of solar chimney potential specifically adapted to Libya's environment and energy needs.

2. Materials and Methods

2.1 System overview

For this mission focused on designing an efficient and durable solar chimney that optimizes both cost and performance, the selection of materials and corresponding parameters for the collector area, chimney structure, and insulation needs to carefully balance these factors. Figure 2 shows the general scheme of solar chimney.

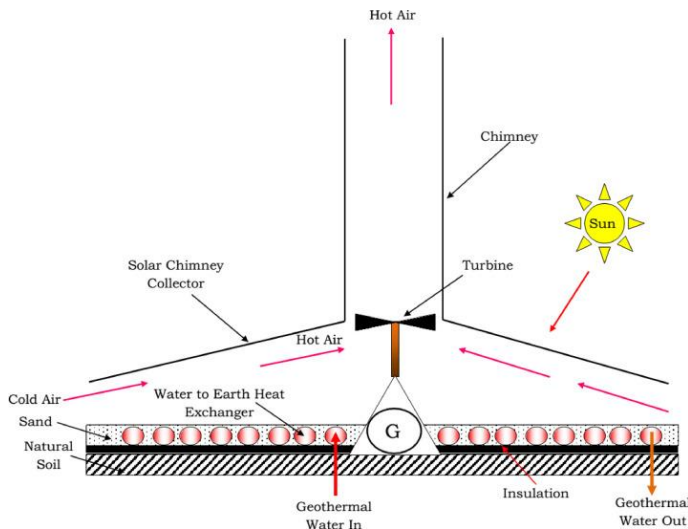


Figure 2. Scheme of solar chimney [16]

Solar chimney collector consists of a sloped, transparent structure designed to capture sunlight. This collector creates a greenhouse effect, trapping solar radiation and heating the air beneath it. As the air warms, it becomes less dense and rises toward the chimney. This heated airflow is crucial to driving the system, as it moves naturally toward the chimney due to the temperature-induced pressure difference.

At the center of the system, the chimney provides the primary pathway for the hot air, channeling it upward through the tall, vertical structure. The chimney height enhances the stack effect, which intensifies the upward flow of air by creating a stronger pressure gradient. Positioned at the base of the chimney is a turbine, which harnesses the kinetic energy of the rising hot air. As the air flows through, it drives the turbine, generating mechanical energy that is converted to electrical power via a generator.

2.2 Proposed Location

This study suggests Derna-Al-Fataih in Libya as a location for this study (Figure 3). Darna Al-Fataih, a district in the historic city of Darna, Libya, is distinguished by its favorable Mediterranean climate, characterized by hot, dry summers and mild, wet winters. With a population of approximately 100,000 [17] and over 3,200 hours of sunshine annually, the area is highly suitable for solar energy initiatives like Solar Chimney technology. This technology generates electricity by harnessing solar energy to create an updraft within a tall chimney, a process well-suited to the region's sunny conditions.

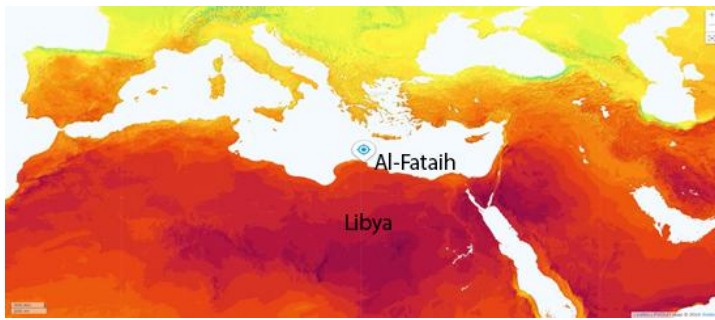


Figure 3. Map of the proposed location

As shown in Figure 4 seasonal variations in the solar path are marked by distinct lines for the equinoxes, June solstice, and December solstice. During the summer solstice, the sun follows the highest path in the sky, giving the longest day and the most intense solar radiation. Conversely, during the winter solstice, the sun's lower path results in shorter days and reduced solar intensity.

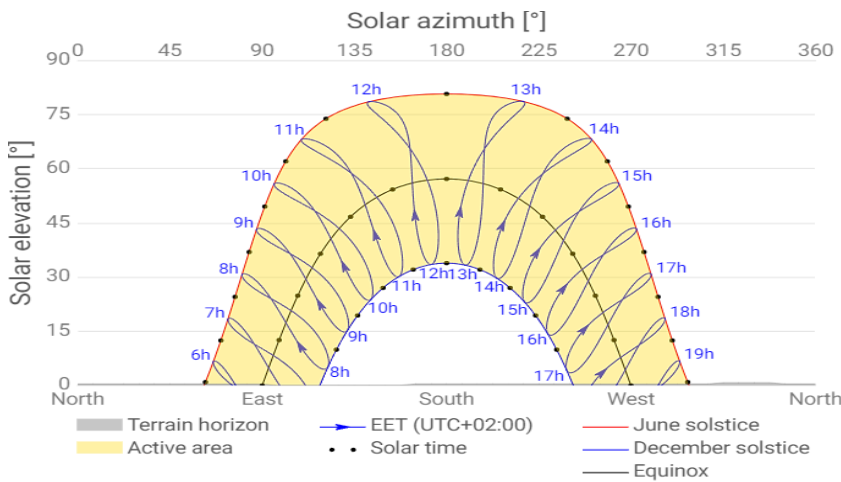


Figure 4. Elevation [°] and azimuth [°] solar

The monthly average values of direct normal irradiation (DNI) in Libya offer critical insights for designing and evaluating the efficiency of hybrid solar and wind chimney power systems. Measured in kilowatt-hours per square meter (kWh/m²), DNI displays seasonal trends, with peak levels occurring in the summer and lower values in the

winter. These seasonal fluctuations have a substantial effect on the design and operational efficiency of hybrid systems, making careful planning and optimization essential for achieving optimal performance.

2.3 Economic analysis

In this economic analysis, the profitability of the project is evaluated with an electricity price set at \$60 per megawatt-hour (MWh). Key financial metrics such as annual revenue, net profit, payback period, and return on investment (ROI) are calculated to assess the viability of the project. To determine the annual revenue, the total amount of electricity generated annually, 4,835.64 MWh, is multiplied by the fixed electricity price of \$60 USD per MWh. This results in an annual revenue of \$290,138 USD. This revenue forms the basis for further profitability calculations by providing a clear picture of the project's income potential. The net profit calculation involves subtracting the total operating costs from the annual revenue. With annual revenue at \$290,138 USD and operating costs at \$100,000 USD per year, the resulting net profit amounts to \$240,138 USD per year. This value represents the actual income that the project is expected to generate annually after accounting for operating expenses. Next, the payback period is calculated to determine the time required to recover the initial investment of \$1,500,000 USD through the annual net profit. By dividing the initial investment by the annual net profit, we find that the payback period is approximately 6.24 years. This metric is crucial as it indicates the timeframe within which the project will start to yield returns beyond the original capital expenditure. Finally, the ROI is computed to evaluate the project's profitability in percentage terms. By dividing the annual net profit by the initial investment and multiplying by 100, we arrive at an ROI of 16.1%. This ROI provides a straightforward indication of the financial efficiency of the investment, with a higher percentage reflecting a more attractive return relative to the initial expenditure. In summary, the economic analysis indicates that with an electricity price of \$60/MWh, the project yields an annual revenue of \$290,138 USD and a net profit of \$240,138 USD. The payback period is approximately 6.24 years, and the ROI stands at 16.1%, suggesting a profitable and viable investment opportunity. These metrics collectively provide a comprehensive view of the project's economic potential and its capacity to generate sustained returns.

3. Results and Discussion

3.1. Analysis of daily temperature and solar radiation variations

Over a 365-day cycle, Earth's orbit around the sun creates four distinct seasons, each marked by significant changes in temperature and solar radiation. Additionally, Earth's rotation on its axis every 24 hours results in day and night, which affects ambient temperature and solar energy availability. In January, ambient temperatures and solar radiation levels are moderate, averaging 16.7°C and 362 W/m², respectively. These conditions support efficient solar panel operation, as temperatures are within the optimal range to avoid losses from excessive heat. Although January's solar radiation is lower than in warmer months, its consistency and mild temperatures provide a stable energy generation base. February exhibits similar moderate conditions, with an average daytime temperature of 15.35°C and solar radiation of 301 W/m². While solar radiation is slightly lower than in January, it remains adequate for effective solar generation, with moderate temperatures sustaining system efficiency. In March, temperatures peak at midday, reaching 25°C, with solar radiation hitting a high of 510 W/m², also around midday. These midday peaks indicate the most productive time for solar energy generation, where both temperature and solar radiation align optimally. April sees a temperature increase, peaking at 28°C at midday, while solar radiation rises to 560 W/m². The alignment between peak solar radiation and temperature in April further optimizes energy generation around midday. May experiences significant increases in both temperature and solar radiation, enhancing solar productivity. Daytime temperatures average 29.4°C, ranging from 22°C in the morning to a midday peak of 34°C. Solar radiation averages 488.33 W/m², reaching 710 W/m² at midday, marking 10:00–14:00 as the prime period for energy collection due to sustained high radiation levels. June, marked by high temperatures and solar radiation, represents the onset of summer. Average temperatures are 33.88°C, beginning at 26°C and peaking at 39°C at midday. Solar radiation averages 600.83 W/m², reaching a peak of 860 W/m² at midday and staying high between 11:00 and 14:00. This combination of prolonged daylight and intense solar radiation makes June an exceptionally productive month for solar generation, even with minor efficiency losses from heat. Overall, the high temperatures and strong solar radiation in spring and early summer provide optimal conditions for hybrid solar chimney systems, with midday hours offering the most efficient energy collection due to the alignment of temperature and solar intensity. Figure 5 show the summarized of finding.

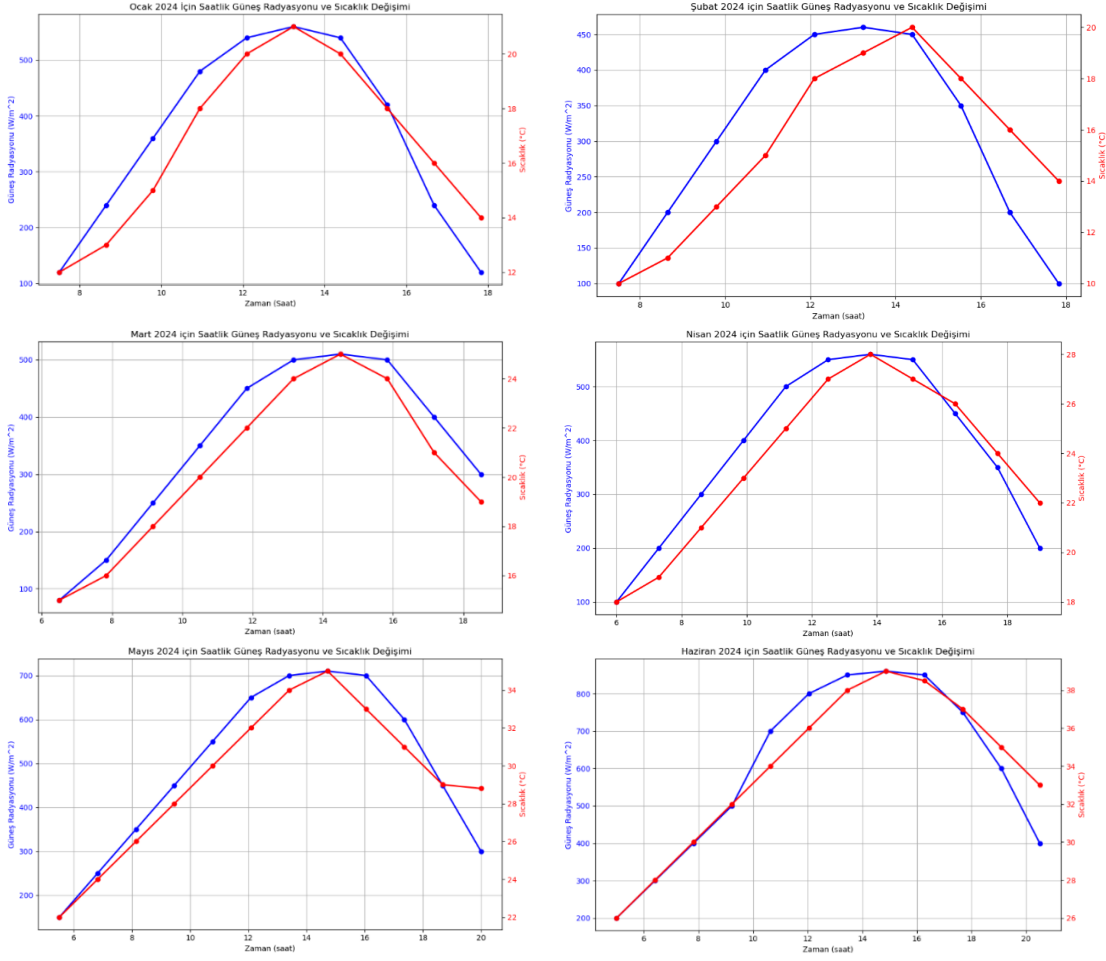


Figure 5. Analysis of daily temperature and solar radiation variations from January to July 2024

3.2 Economic feasibility analysis of solar chimney power generation system

In this study, an economic analysis for a Solar Chimney Power Generation System was conducted. The analysis focuses on essential financial metrics such as Annual Revenue, Net Profit, Payback Period, and Return on Investment (ROI), providing a comprehensive view of the project's financial viability. These parameters offer insights into the project's potential to generate income, cover operational costs, repay its initial investment, and deliver returns to investors. The annual revenue of the system is derived by multiplying the total energy produced by the system with the electricity price, resulting in an annual revenue of \$290,138. This value represents the total income generated each year through the sale of electricity produced by the solar chimney. The net profit, calculated by subtracting the annual operating expenses (OPEX) from the annual revenue, is \$240,138. This net profit figure highlights the earnings available after operational costs are covered, serving as a primary indicator of the system's profitability. The payback period is calculated by dividing the initial investment by the net profit, yielding a result of 6.25 years (Table 1).

Table 1. Economic analysis conducted for a base electricity price of \$60/MWh

PARAMETER	VALUE
Annual Energy Production (E_{annual})	4,835.64 MWh/year
Annual Revenue	\$290,138
Initial Investment	\$1,500,000
Annual Net Profit	\$240,138
Payback Period	6.25 years
Return on Investment (ROI)	16.01%

4. Conclusion

This study demonstrates the feasibility and potential benefits of implementing Solar Chimney Power Systems (SCPS) as a renewable energy source in Libya, particularly in regions like Derna-Al-Fataih with favorable solar and climatic conditions. These financial metrics underscore the system's ability to provide a steady income stream while recouping the initial investment within a reasonable timeframe, marking it as a viable alternative to conventional energy sources. This research not only fills a gap in region-specific renewable energy studies but also suggests that SCPS technology can contribute to Libya's energy diversification and reduce dependency on fossil fuels. Additionally, the integration of SCPS with hybrid renewable systems, as proposed in this study, presents further avenues for enhancing efficiency and reliability, particularly in meeting Libya's energy demands sustainably. Future studies are encouraged to explore advanced design optimizations, hybrid configurations, and precise simulation models to adapt solar chimney systems more effectively to Libya's unique environmental and economic landscape.

References

- [1] Cabanyes, I. (1903). *Las chimeneas solares (Solar chimneys)*. *La Energía Eléctr.*
- [2] Lucier, R. E. (1981). System for converting solar heat to electrical energy. *Google Patents*.
- [3] Richards, R. (1982). Hot air starts to rise through Spain's solar chimney. *Electrical Review*, 210, 26–27.
- [4] Haaf, W., Friedrich, K., Mayr, G., & Schlaich, J. (1983). Solar chimneys (part I): principle and construction of the pilot plant in Manzanares. *International Journal of Solar Energy*, 2, 3–20.
- [5] Nizetic, S., Ninic, N., & Klarin, B. (2008). Analysis and feasibility of implementing solar chimney power plants in the Mediterranean region. *Energy*, 33, 1680–1690.
- [6] EnviroMission Limited. (2006). Technology: Technology overview. Retrieved from <http://www.enviromission.com.au>
- [7] Jiakuan, Y., Jin, L., & Po, X. (2003). A novel technology of solar chimney for power generation. *ACTA Energiae Solaris Sinica*, 24, 570–573.
- [8] Sagasta, F. M. (2003). Torre solar de 750 metros de altura en Ciudad Real (España).
- [9] Cloete, R. (2008). Solar Tower sheds light on little-used technology. *Engineering News Online*. Retrieved from <http://www.engineeringnews.co.za/article.php>
- [10] Zhou, X., Wang, F., & Ochieng, R. M. (2010). A review of solar chimney power technology. *Renewable and Sustainable Energy Reviews*, 14, 2315–2338.
- [11] Chikere, A. O., Al-Kayiem, H. H., & Karim, Z. A. A. (2011). Review on the enhancement techniques and introduction of an alternate enhancement technique of solar chimney power plant. *Journal of Applied Sciences*, 11, 1877–1884.
- [12] Zhai, X. Q., Song, Z. P., & Wang, R. Z. (2011). A review for the applications of solar chimneys in buildings. *Renewable and Sustainable Energy Reviews*, 15(8), 3757–3767.
- [13] Dhahri, A., & Omri, A. (2013). A review of solar chimney power generation technology. *International Journal of Engineering and Advanced Technology*, 2.
- [14] Olusola Olorunfemi, & Bamisile. (2014). A review of solar chimney technology: Its application to desert-prone villages/regions in Northern Nigeria. *International Journal of Scientific and Engineering Research*, 5, 1210–1216.
- [15] Saleh, M. J., Atallah, F. S., Sameer Algburi, & Ahmed, O. K. (2023). Enhancement methods of the performance of a solar chimney power plant: Review. *Results in Engineering*, 19, 101375–101375. <https://doi.org/10.1016/j.rineng.2023.101375>
- [16] Sharon, H. (2023). A detailed review on sole and hybrid solar chimney based sustainable ventilation, power generation, and potable water production systems. *Energy Nexus*, 10, 100184.
- [17] Motamedi, M. (2023, September 13). Why did Derna's dams break when Storm Daniel hit Libya? *Www.aljazeera.com*. <https://www.aljazeera.com/news/2023/9/13/why-did-dernas-dams-break-when-storm-daniel-hit-libya>



Green Chemicals to Obtain Reduced Graphene Oxide

Mahdi Mohamed DAHER¹, Mahad Ousleyeh ALI¹, Mücahit UĞUR¹ , Didar ÜÇÜNCÜOĞLU² ,
Haluk KORUCU^{1,*} 

¹ Department of Chemical Engineering, Faculty of Engineering, Çankırı Karatekin University, Ulyazı, Çankırı 18100, Türkiye

² Department of Food Engineering, Faculty of Engineering, Çankırı Karatekin University, Ulyazı, Çankırı 18100, Türkiye

Abstract

To develop sustainable and environmentally friendly processes, researchers have focused on unhazardous compounds, such as reduced graphene oxide (rGO) instead of graphene oxide (GO). One of the synthesis methods is chemical reduction in which hydrazine and sodium boron hydride are intensively used. In this study, urea, glucose and sodium boron hydride were used during the chemical reduction method of GO as natural and green reducing compounds. The structural characterization, reduction performance, surface area measurements of rGO samples were determined with FTIR, SEM+EDS, and BET respectively to characterize the synthesis performance of rGO. According to the results obtained, SEM+EDS and BET surface area recovery results gave the best results with urea at 161.2% and 138.69%. FTIR analysis approved the preferred compounds were significantly effective to get rGO successfully. Overall outcomes of this research suggest urea performs better for the synthesis of rGO than sodium boron hydride and glucose.

Keywords: Graphene Oxide, Reduced Graphene Oxide, Hummers TOUR Method, Chemical reduction method

1. Introduction

Graphene oxide (GO), a specific type of graphene, is defined by the presence of oxygen-containing functional groups such as carboxyl, epoxy, and hydroxyl. These groups keep GO hydrophilic, which increases its dispersibility in water and other organic solvents. Improved dispersibility is critical in applications such as drug delivery, where GO's high surface area and biocompatibility allow for successful drug loading and release. [1]. Furthermore, GO's functional groups provide active sites for additional chemical modifications, broadening its use in composite materials and sensor technologies [2]. One of GO's most powerful reducing agents is L Hydrazine, which is well-known for its ability to restore graphene's conjugated structure. Hydrazine reduction often produces high-quality reduced graphene oxide (rGO) with improved electrical conductivity. The main drawbacks of hydrazine are its severe toxicity and environmental concerns, which discourage large-scale and ecologically sensitive uses [3]. Other frequent reducing agents for GO include sodium borohydride (NaBH₄). At low temperatures, it successfully decreases GO while being less harmful than hydrazine. Although the reduction is occasionally insufficient, leaving some oxygen-containing groups on the graphene lattice, NaBH₄-reduced GO has good electrical properties [4]. The reduction of GO using urea and glucose presents a novel and sustainable method, notable for its ease of use and efficiency, which is attracting considerable interest. Because of its low cost and high organic component concentration, it makes it easier to heat out groups that contain oxygen. The technique yields rGO, exhibiting electrical and thermal properties remarkably like those of graphene. In contrast to conventional reducing agents such as hydrazine, the reduction process that employs urea and sugar presents advantages due to its reduced environmental impact and lower toxicity. In addition to being a promising green reductant for the manufacture of rGO, urea and sugar reduced graphene oxide demonstrate enhanced electrical conductivity and mechanical strength, making it a desirable material for a variety of technological applications [5]. This study utilized urea, glucose, and sodium boron hydride to create reduced graphene oxide using chemical reduction from graphene oxide, which was previously generated via the modified Hummers method. The objective of this study was to characterize the synthesis of reduced graphene oxide. For the characterisation investigation,

* Corresponding author. e-mail address: halukkorucu@karatekin.edu.tr

structural analysis was conducted using FTIR, surface area was measured by BET, and the degree of reduction was assessed using SEM coupled with EDS. The evaluation of GO was conducted in relation to the quality criteria and metrics associated with urea, glucose, and sodium boron-reduced graphene oxide, focusing on the performance assessment of recovery rates and chemical properties.

2. Materials and Methods

This study focused on the production of graphene oxide by the Hummers technique from graphite and the characterisation of reduced graphene oxide produced through an environmentally friendly chemical reduction strategy. This study utilized glucose, urea, and sodium boron hydride, commonly referenced in the literature for comparative analysis, as reducing agents. All synthesized samples will be subjected to surface area analysis using the BET technique, the degree of reduction by SEM+EDS, and structure characterization by FTIR spectrum scanning. For graphene oxide synthesis by modified Hummers method from graphite, 10 g of graphite sample, and 30 g of KMnO_4 were mixed with 100 mL of H_2SO_4 and 10 mL of H_3PO_4 at 5 °C for 24 h. The mixture was then mixed for another 6 h at the reaction temperature of 95 °C by adding 100 milliliters of distilled water. The mixture was allowed to cool down at the end of the reaction and 10 mL of H_2O_2 and 1 mL of HCl were added. Washing was performed using the decantation method until the pH was 3. GO synthesis was performed by subjecting the samples to centrifugation, washing, and drying steps at 60 °C. After 5 g of sodium borohydride, urea and glucose were added to the 2 g of GO samples obtained for three different experiments. 300 mL of distilled water was added at 80 °C. The experiments were carried out for a period of 24 h. At the end of the trials, each sample was washed with pure water by decantation method until it reached pH 7. Then, they were washed with ethyl alcohol and acetone for the last time and dried in a vacuum oven set to 70 °C. The quality standards established for the characterization of GO and rGO samples are listed in **Table 1**.

Table 1. Quality standards of the graphene oxide and reduced graphene oxide

Quality Criteria	Symbol	Purpose	Provided Information
1	FTIR	Characatarizaton of the structure	Functional groups
2	SEM+EDS	Carbon/Oxygen ratio	Reduction degree
3	BET	Surface Area	Degree of porosity

3. Results and Discussion

The improvement rates of reduced graphene oxide synthesis are given in Table 2. The best result in terms of reduction performance (C/O) and surface area was obtained in the reduced graphene oxide sample synthesized using urea with 161.2% and 138.69%, respectively. The reduction performance of glucose is almost the same as that of sodium boron hydride. The results obtained have shown that it has been found possible to use urea and glucose, which are environmentally friendly and low-cost compounds, instead of sodium boron hydride, which is a costly and toxic compound commonly used in the literature.

Table 2 Recovery rates between graphene oxide and reduced graphene oxide samples

Answers	GO-Ref	rGO-Sodium Borhydre	rGO-Urea	rGO-Glucose	Recovery Rate rGO- Sodium Borhydre (%)	Recovery Rate rGO- Urea (%)	Recovery Rate rGO- Glucose (%)
BET (SA- m^2/g)	13,36	24,75	31,89	14,73	85,2*	138,69	10,25
SEM+EDS (C/O)	2,32	4,48	6,06	4,41	93,1	161,2	90

Calculation of the % recovery rate of the experiment performed reference graphene oxide

*Percentage change = $\frac{((\text{New value}/\text{Old value})-1)}{1} \times 100$. * was caltulated as $\frac{(24,75 / 13,36)-1}{1} \times 100 = 85,2$ (plus value means improvement)*

The produced graphene oxide samples FT-IR analysis model reveals that the vibration peak at 1721 cm^{-1} is C = O, whereas the vibration and deformation peaks of the O-H groups at 3391 cm^{-1} and 1410 cm^{-1} are C-O. The graphite structure does not have the C-O stress peak at 1221 cm^{-1} , C-O stress peak at 1046 cm^{-1} , and the C = C stress peak at $1680\text{-}1620\text{ cm}^{-1}$. On the other hand, it was discovered that sodium boron hydride had mostly vanished during the synthesis of reduced graphene oxide for urea and glucose, and the peaks created by graphene oxide synthesis began to resemble graphite when measured in cm^{-1} .

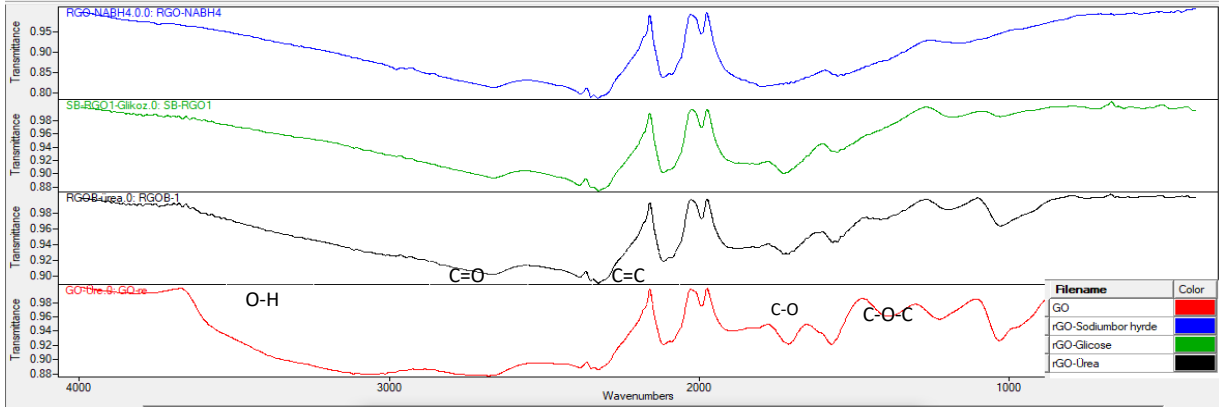


Figure 1. FTIR images of experimental samples

Figure 1 shows that the produced GO samples' FT-IR analysis model reveals that the vibration peak at 1721 cm^{-1} is C = O, whereas the vibration and deformation peaks of the O-H groups at 3391 cm^{-1} and 1410 cm^{-1} are C-O. The graphite structure does not have the C-O stress peak at 1221 cm^{-1} , C-O stress peak at 1046 cm^{-1} , and the C = C stress peak at $1680\text{-}1620\text{ cm}^{-1}$ [6]. On the other hand, it was discovered that sodium boron hydride, urea, and glucose had mostly vanished GO structure during the synthesis of rGO, and the peaks created by GO synthesis began to resemble graphite.

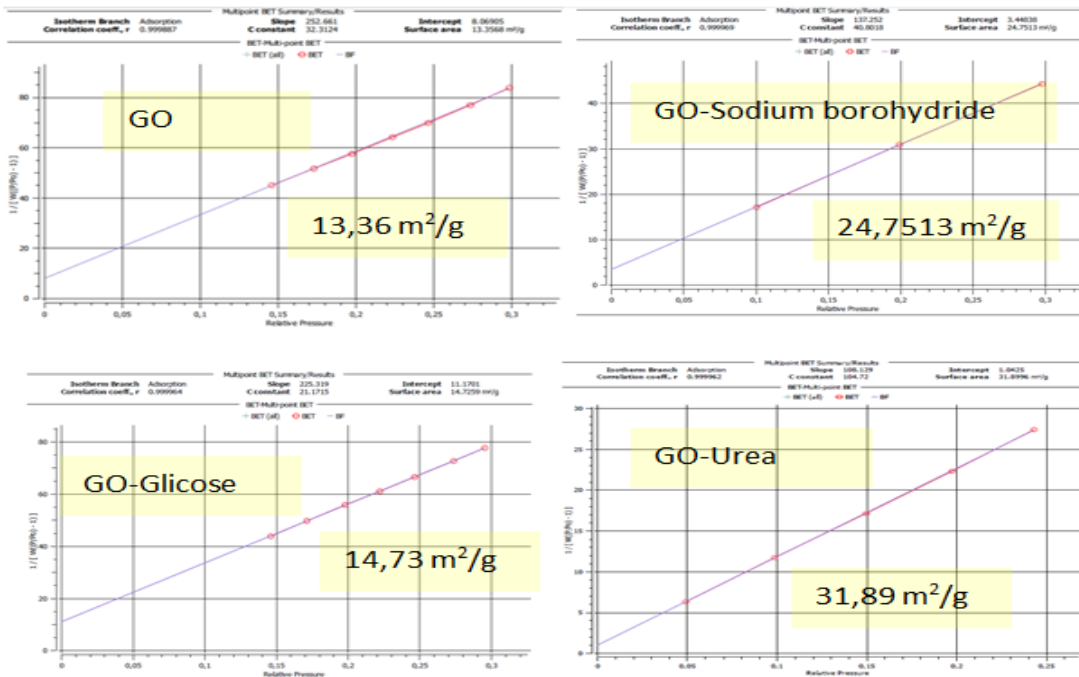


Figure 2. BET images of experimental samples

Multi-point BET surface area measurements of graphene oxide and reduced graphene oxide samples are given in Figure 2. Reduced graphene oxide samples are expected to have higher surface areas than graphene oxide. As expected, surface areas increased during the manufacture of reduced graphene oxide. Urea produced the best results, while glucose produced the lowest results. The huge surface area is due to the creation of a porous structure; however, contaminants in the structure may have prevented this increase by blocking the pores.

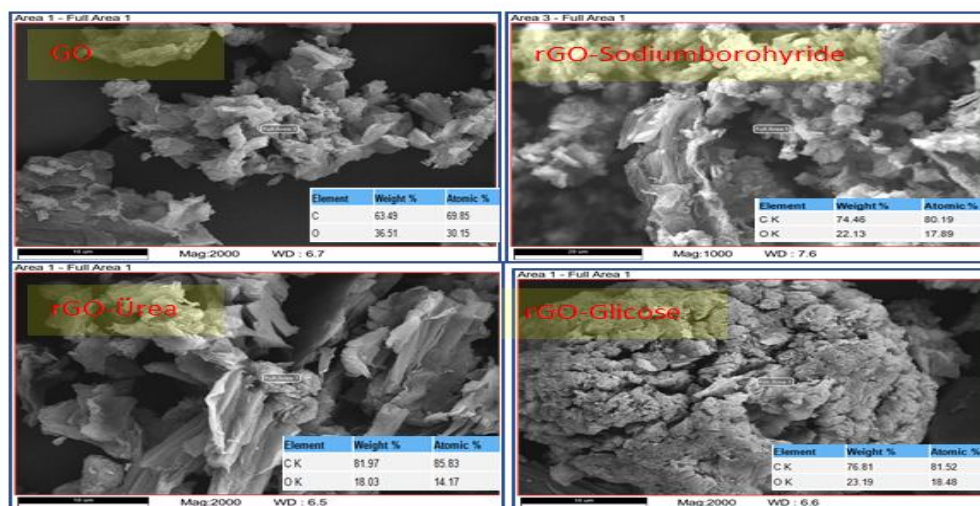


Figure 3 SEM+EDS results of experimental samples

Figure 3 shows the SEM images and EDS results. It has been discovered that urea has significantly better reduction performance than sodium boron hydride and glucose, while sodium boron hydride and glucose have similar reduction performance. This indicates that urea offers a more sustainable approach for the reduction of graphene oxide compared to the commonly utilized sodium boron hydride found in existing studies.

4. Conclusion

Reduction performance (C/O) was measured by SEM+EDS analysis and C/O atomic ratios were aimed to be large values because it was desired to reduce functional groups with oxygen content for reduction performance. According to the BET method, the surface area results have been analyzed and it is requested that the surface area values be high. As the surface area value increases, the porosity in the structure increases and provides an advantage in the adsorption ability of the material, mass transfer rate, and its use as a catalyst. In addition, the high surface area is an indicator of the formation of micro-pores and lamellar structures. The optimal outcomes for C/O and surface area recovery rates in reduced graphene oxide samples were achieved in the sample synthesized with urea, yielding 161.2% and 138.69%, respectively. The reducing efficacy of glucose is about equivalent to that of sodium borohydride. The findings indicate that environmentally benign and inexpensive molecules, urea and glucose, can substitute for sodium borohydride, a costly and poisonous substance commonly referenced in the literature.

Acknowledgment

The authors acknowledge that this research was supported financially by Çankırı Karatekin University, Scientific Research Project (MF081123B33). All experimental activities were carried out in the Research Laboratory of Çankırı Karatekin University. The author expresses gratitude to all sponsors for their valuable input.

References

- [1] Korucu, H. (2025). Multi response optimization of synthesis of boron compounds by Dopting to graphene oxide in the Modified Hummers method. *Materials Science and Engineering: B*, 311, 117839.

- [2] Toda, K., Furue, R., & Hayami, S. (2015). Recent progress in applications of graphene oxide for gas sensing: A review. *Analytica chimica acta*, 878, 43-53.
- [3] Park, S., An, J., Potts, J. R., Velamakanni, A., Murali, S., & Ruoff, R. S. (2011). Hydrazine-reduction of graphite-and graphene oxide. *Carbon*, 49(9), 3019-3023
- [4] Korucu, H. (2022). Evaluation of the performance on reduced graphene oxide synthesized using ascorbic acid and sodium borohydride: Experimental designs-based multi-response optimization application. *Journal of Molecular Structure*, 1268, 133715.
- [5] De Silva, K. K. H., Huang, H. H., Joshi, R. K., & Yoshimura, M. (2017). Chemical reduction of graphene oxide using green reductants. *Carbon*, 119, 190-199.
- [6] Alam, S. N., Sharma, N., & Kumar, L. (2017). Synthesis of graphene oxide (GO) by modified hummers method and its thermal reduction to obtain reduced graphene oxide (rGO). *Graphene*, 6(1), 1-18.



Sustainable Energy Solutions with Forest Biomass In Turkey

D. Kemal BAYRAKTAR^{1,*} , Mehmet GÜNEŞ² , Shakhzoda KHOLIKULOVA³ 

¹ Department of Forest Industrial Engineering, Karadeniz Technical University, Trabzon, Türkiye

² Çankırı Vocational School, Department of Design, Çankırı Karatekin University, Çankırı, Türkiye

³ Department of Mechanical Engineering, Çankırı Karatekin University, Çankırı, Türkiye

Abstract

Renewable energy sources are essential in addressing climate change, achieving energy independence, and meeting sustainable development goals. Turkey has a significant potential for forest biomass thanks to its rich natural resources and large forest areas. Forest biomass is a renewable energy source obtained by using organic materials such as trees and plants in energy production. According to 2024 data, Turkey's forested areas cover about %29 of the total land surface and 6 million tons of oil equivalent energy is produced annually from forest biomass. Utilization of this energy source has the potential to meet the energy needs of local communities, while supporting environmental sustainability and reducing carbon emissions. However, sustainable forest management practices are necessary, as there can be negative impacts such as overcutting. Sustainable forest management includes a range of strategies and practices for the conservation and efficient use of forest resources. In this context, forestry policies in Turkey aim to maintain the integrity of forest ecosystems to ensure environmental sustainability. Projects carried out by the General Directorate of Forestry focus on protecting the biodiversity of forests, promoting afforestation efforts and improving the health of existing forests.

Existing policies include laws and regulations to protect forest areas, incentives for biomass energy projects, environmental protection and rehabilitation programs. Turkey collaborates with the European Union and various international organizations to expand the adoption of renewable energy sources. This cooperation includes issues such as the transfer of innovative technologies and raising awareness of the local population.

In conclusion, sustainable management of forest biomass offers great opportunities for energy security and environmental sustainability. By taking the necessary steps to utilize the potential of forest biomass and achieve sustainable development goals, Turkey can increase its energy independence and support environmental protection efforts.

Keywords: Forest Biomass, Sustainable Energy, Energy Generation

1. Introduction

The importance of renewable energy sources is increasing today with efforts to combat climate change and achieve energy independence. The limited resources of fossil fuels and environmental pollution increase the need for alternative energy sources. Forest biomass plays an important role by utilizing organic materials such as trees and plants in energy production. Turkey is in an important position in terms of biomass energy potential with its large forest areas and rich natural resources. Turkey's forested areas cover about 29% of the total land surface, which strengthens its biomass potential.

The utilization of forest biomass in energy production not only fulfills the energy demands of local communities but also enhances the nation's energy autonomy. In addition, trees and other waste salvaged from forest fires are included in this energy capacity. By 2024, Turkey will produce 6 million tons of oil equivalent energy from forest biomass, which is an important step towards achieving sustainable energy solutions. Biomass energy plays an important role in achieving carbon emission reduction targets and effective biomass management and responsible forest policies contribute to the conservation of forest cover [1].

This study aims to examine the potential of forest biomass in Turkey and its contribution to sustainable energy solutions. Together with the sustainable management of Turkey's natural resources and forest structure, the role of forest biomass in modern energy production is of great importance for rural development and environmental sustainability. Starting from the definition of forest biomass, the study will comprehensively address its potential in Turkey, its utilization in energy production, its environmental impacts and its impacts on rural development.

* Corresponding author. e-mail address: profdukebay@gmail.com

In this context, effective management of Turkey's forest biomass resources is critical for both increasing energy independence and ensuring environmental sustainability. In this context, in order to better understand the potential of Turkey's forest biomass resources and the role of these resources in energy production, Fig. 1. is shown.



Figure 1. The potential of Turkey's forest biomass resources.

2. Definition and Importance of Forest Biomass

Forest biomass is the organic mass of trees, shrubs and other plant material. This mass can be used in many fields such as energy production, materials science and agriculture. The importance of forest biomass as a renewable energy source lies in the fact that it provides both environmental and economic benefits in line with sustainability principles. Forest biomass is renewable within natural cycles, thus playing an effective role in combating climate change by maintaining ecosystem balances [2].

The use of biomass in energy production balances the carbon cycle, reducing the amount of carbon dioxide released into the atmosphere. Plants take carbon dioxide from the atmosphere through the process of photosynthesis and gain mass through growth. Therefore, planting new trees to replace those used as biomass contributes to offsetting greenhouse gas emissions. Turkey's vast forest areas have great potential for biomass energy production. Communities, especially in rural areas, can meet their own energy needs by utilizing these energy sources.

Forest biomass in Turkey generally consists of various materials such as forest residues, pruning waste and industrial by-products. Efficient utilization of these resources has a positive impact on the local economy. The use of biomass energy in rural areas increases local employment and supports rural development. As a result, forest biomass is an important energy source for both environmental sustainability and economic development.

3. Forest Biomass Potential in Turkey

Turkey's forest biomass potential is quite high thanks to the country's rich natural resources and diverse climatic conditions. By 2024, the total area of Turkey's forests is around 23 million hectares, covering about 29% of the total land surface. These large forest areas indicate a huge potential in terms of biomass resources. Forests are an important source not only for wood production but also for energy production [3].

Forest biomass resources are derived from logging, forest management activities, trees salvaged after fires and natural wastes within the forest. In Turkey, the efficient utilization of these resources both meets the energy needs of local communities and contributes to national energy policy. Turkey produces about 6 million tons of oil equivalent energy per year from forest biomass. This is an important step to increase the country's energy independence.

In addition, sustainable management of forest biomass is also critical for maintaining environmental balance. Sustainable forest management practices ensure that nature is protected in the process of logging and biomass production. Reforestation and rehabilitation of forests help to increase biomass potential and strengthen ecosystem services. In conclusion, the potential of forest biomass in Turkey offers a great opportunity for sustainable energy solutions and environmental protection.

4. Energy Production through the Use of Forest Biomass

The utilization of forest biomass for energy production can be realized through various methods. These include techniques such as direct combustion, gasification, pyrolysis and anaerobic digestion. Direct combustion is the burning of biomass materials to produce heat. This method is often used in heating systems or power plants.

However, it is important to control the emissions released during the combustion process to reduce environmental impacts.

Gasification is the heating of biomass at high temperatures and low oxygen levels to produce gas, which is then converted into energy. This gas can then be converted into energy. Gasification offers a more efficient method of energy production compared to combustion. Furthermore, pyrolysis is the process by which biomass is broken down under heat to form liquid and gaseous products. This method provides more energy efficiency by changing the chemical structure of the biomass.

Anaerobic digestion is the process by which organic matter is broken down by microorganisms without oxygen. This method is used to produce biogas and combines waste management and energy production. These various methods of energy production from forest biomass offer significant opportunities to meet Turkey's energy needs and develop sustainable energy solutions. In this context, the following image is presented to illustrate the potential of anaerobic digestion and various energy production methods from forest biomass in meeting Turkey's energy needs [4].



Figure 2. The potential for meeting Turkey's energy needs.

In Turkey, the use of forest biomass for energy production plays an important role in rural areas. Local people meet their energy needs by utilizing biomass resources, thereby reducing energy costs. In addition, the use of forest biomass supports local economies and creates jobs. As a result, the utilization of forest biomass in energy production is a vital element for Turkey's energy strategy [5].

5. Environmental Impacts and Reducing Carbon Emissions

The use of biomass produces significantly less carbon emissions compared to fossil fuels. Turkey is utilizing biomass energy resources to achieve its greenhouse gas emission reduction targets by 2030. Forest biomass supports environmental sustainability with its carbon sequestration capacity [6].

Utilizing forest biomass for energy production can lead to both beneficial and adverse environmental effects. Positive impacts include being a renewable energy source, reducing dependence on fossil fuels and the potential to reduce greenhouse gas emissions. As forest biomass is a renewable resource within natural cycles, it helps to develop sustainable energy solutions. In this context, biomass utilization is becoming an important tool in combating climate change by increasing energy security [7].

However, there are also some negative impacts associated with the use of forest biomass. Over-cutting practices can lead to the destruction of forest ecosystems and reduced biodiversity. Furthermore, deforestation or insufficient reforestation can lead to increased carbon emissions. Therefore, managing forest biomass sustainably is critical to minimizing environmental impacts. Sustainable forest management practices contribute to maintaining ecosystem balance by ensuring the efficient and environmentally friendly use of biomass resources.

Figure 3 shows the trend values related to forest biomass and sustainable energy in Turkey from 2015 to 2024 [8].

The green line represents the increase in forest areas (in million hectares) over the years, while the blue dashed line illustrates annual biomass energy production (in million tons of oil equivalent). In line with sustainability principles, an integrated approach should be adopted for the utilization of forest biomass in energy production. This approach should ensure that environmental impacts are minimized and economic benefits are maximized in

energy production. Thus, the utilization of forest biomass will both enhance energy security and support environmental sustainability [9].

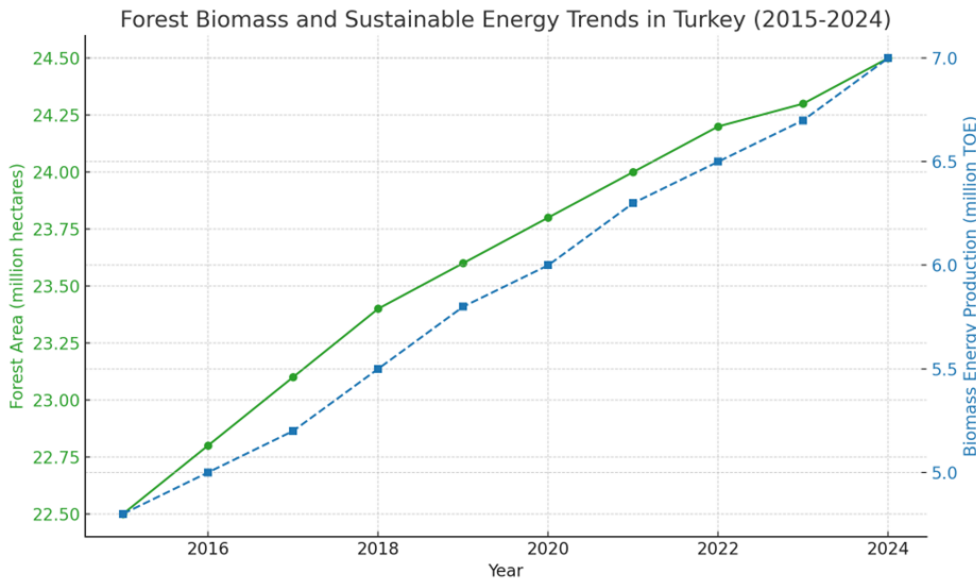


Figure 3. Trend values related to forest biomass and sustainable energy in Turkey from 2015 to 2024.

6. Impacts on Rural Development

The use of forest biomass offers significant opportunities in terms of rural development and energy access. Rural regions of Turkey experience difficulties in terms of energy access. Problems such as distance to electricity networks, high energy costs and inadequate energy infrastructure make it difficult for rural communities to meet their energy needs. At this point, forest biomass stands out as a sustainable solution that can be used to meet the energy needs of local people.

In rural areas, the use of forest biomass not only meets the energy needs of local people, but also has the potential to create employment. Employing local labor in forest management, biomass collection and energy production processes contributes to the strengthening of the rural economy. This process, together with the increase in local job opportunities, supports rural development and increases the economic well-being of the society [11].

The use of forest biomass also helps to increase energy security by utilizing local energy resources. Local people can meet their own energy needs using biomass resources, thus reducing external dependency. This strengthens the energy independence of rural communities while also contributing to environmental sustainability.

As a result, the use of forest biomass is an important tool for Turkey's rural development policies and energy access strategies. In this context, local governments and relevant institutions need to evaluate the potential of forest biomass in energy production and develop sustainable energy solutions.

7. Current Policy and Management Strategies

The use of forest biomass in energy production in Turkey is supported by various policy and management strategies. As of 2024, the Republic of Turkey provides a comprehensive framework for the development of renewable energy sources and implements various programs and incentives to evaluate this potential. The Ministry of Energy and Natural Resources develops strategies for increasing biomass energy and raises awareness in this area.

Existing laws for the use of forest biomass in energy production encourage sustainable forest management. The Forest Law and the Renewable Energy Resources Support Mechanism (YEKDEM) ensure the support of biomass projects and the effective implementation of these projects. These regulations increase the participation of local governments and the private sector in biomass projects and support energy production processes.

In addition, universities and research institutions in Turkey are investigating the potential of forest biomass in energy production and developing innovative solutions. These studies cover topics such as the efficient use of biomass resources, the application of energy production technologies and the reduction of environmental impacts.

Collaborations at the local level ensure that forest biomass is utilized more effectively and offer innovative approaches in energy production.

The active role of local governments and non-governmental organizations (NGOs) in this process contributes to the sustainable management of forest biomass. Raising awareness in society about the use of biomass in energy production helps local people understand how they can benefit from these resources. Education programs and information seminars are organized to increase knowledge and ensure participation in biomass energy.

In summary, Turkey's current policy and management strategies encourage the use of forest biomass in energy production and support renewable energy projects. Sustainable forest management and the effective use of biomass resources both increase energy security and offer great opportunities in terms of environmental sustainability.

8. Challenges Encountered in the Use of Forest Biomass and Policy Recommendations for Sustainable Biomass Use in Turkey

Although the use of forest biomass in energy production provides many benefits, it faces various challenges. These challenges may affect the sustainable management of biomass resources and the efficiency of energy production processes.

First of all, the difficulties experienced in the supply of biomass resources are noteworthy. Sustainable management of forests is of critical importance for the efficient use of biomass resources. However, excessive cutting practices can lead to the destruction of forest ecosystems and the reduction of biodiversity. This situation poses a significant threat to the sustainability of biomass production. Therefore, forest management practices need to be reviewed and improved.

Secondly, the cost of technologies used in energy production processes can be a significant obstacle, especially for small-scale enterprises. The implementation of innovative technologies and reducing the cost of these technologies are critical factors for the success of biomass energy projects. In addition, the installation and operating costs of biomass energy systems may make it difficult for local people and small enterprises to benefit from these resources.

Thirdly, the lack of sufficient knowledge and experience in the operation and management of biomass energy systems is also a significant challenge. Local people and small businesses may not have the knowledge and skills required to effectively use biomass resources. Therefore, it is important to increase training programs and technical support services.

Finally, legal and regulatory barriers encountered in biomass energy production should also be taken into account. Local and national regulations need to be updated to support biomass energy projects. This will contribute to increasing energy production by paving the way for biomass energy projects.

Appropriate policies and incentive mechanisms need to be established for the dissemination of biomass energy. The government's provision of supportive laws and incentives for biomass projects will accelerate developments in the sector. In addition, initiatives that increase cooperation with the private sector will help Turkey use its biomass potential more effectively.

The future potential of forest biomass plays an important role in meeting Turkey's energy needs. Developing technology and increasing energy demand enable more efficient and effective use of biomass resources. Global trends towards renewable energy provide opportunities for Turkey to evaluate its forest biomass potential. In particular, the use of forest biomass is of great importance in meeting the energy needs of local people and ensuring environmental sustainability.

However, there are also some challenges related to the use of forest biomass. Excessive cutting practices can lead to the destruction of forest ecosystems and the reduction of biodiversity. In addition, bureaucratic obstacles encountered during the financing and implementation of biomass energy projects can make it difficult to implement the projects. Raising awareness and educating local people about biomass energy is important in overcoming these challenges.

In order to realize the future potential of forest biomass, innovative technologies must be used and an integrated approach must be adopted. In this context, sustainable management of forest biomass will both increase energy security and support environmental sustainability. Turkey can increase its energy independence and achieve its sustainable development goals by taking the necessary steps to evaluate its forest biomass potential.

9. Future Potential and Opportunities

The future potential of forest biomass in energy production is directly related to Turkey's rich natural resources and increasing energy needs. The increasing demand for renewable energy means that forest biomass will gain more importance. Turkey can increase energy security and contribute to environmental sustainability by utilizing its forest biomass potential in a sustainable way.

In the future, diversification of biomass energy projects offers more opportunities in energy production. For example, small-scale biomass energy systems established to meet the energy needs of local people can support rural development and create employment. In addition, the local implementation of biomass energy systems will increase energy independence and contribute to the strengthening of local economies [10].

In addition to biomass energy, forest biomass has other potential areas of use in Turkey. The processing and transformation of forest products can provide efficient use of biomass resources. In this context, supporting research and development activities can help to emerge innovative solutions. In addition, organizing awareness-raising campaigns on the use of forest biomass will contribute to informing the society on this issue.

As a result, the use of forest biomass in energy production offers great opportunities for Turkey. Sustainable forest management and efficient use of biomass resources play an important role in terms of energy security, environmental sustainability and rural development. Turkey can achieve its renewable energy targets and take important steps for a sustainable future by efficiently evaluating forest biomass.

10. Conclusion

This study examines the potential of forest biomass in energy production, its environmental impacts, its role in rural development and current management strategies in Turkey. Turkey's rich natural resources and large forest areas offer a great potential for forest biomass in terms of energy production. The use of forest biomass both meets the energy needs of local people and contributes to the country's energy independence.

The use of forest biomass in energy production supports environmental sustainability and has the potential to reduce carbon emissions. However, sustainable forest management practices need to be adopted to prevent negative impacts such as excessive cutting practices. Current policy and management strategies in Turkey encourage the use of forest biomass in energy production and support renewable energy projects.

As a result, sustainable management of Turkey's forest biomass offers great opportunities in terms of energy security and environmental sustainability. The efficient use of forest biomass plays an important role in rural development, employment creation and strengthening of local economies. By efficiently utilizing forest biomass, Turkey can develop sustainable energy solutions and take important steps towards a greener future.

References

- [1] Kaygusuz, K., & Türker, M. F. (2002). Biomass energy potential in Turkey. *Renewable Energy*, 26(4), 661-678.
- [2] Parde, J. (1980). *Forestry Abstracts*, Forest biomass, 41(8), 343-362.
- [3] Ersoy, A. E., & Ugurlu, A. (2024). Bioenergy's role in achieving a low-carbon electricity future: A case of Türkiye. *Applied Energy*, 372, 123799.
- [4] Hobson, P. N., Bousfield, S., Summers, R., & Kirsch, E. J. (1974). Anaerobic digestion of organic matter. *Critical Reviews in Environmental Science and Technology*, 4(1-4), 131-191.
- [5] Karayılmazlar, S., Saraçoğlu, N., Çabuk, Y., & Kurt, R. (2011). Biyokütlenin Türkiye'de enerji üretiminde değerlendirilmesi. *Bartın Orman Fakültesi Dergisi*, 13(19), 63-75
- [6] Cairns, M. A. ve Meganck, R. A. (1994). Karbon tutma, biyolojik çeşitlilik ve sürdürülebilir kalkınma: entegre orman yönetimi. *Çevre yönetimi*, 18(1), 13-22.
- [7] Hall, J. P. (2002). Sustainable production of forest biomass for energy. *The Forestry Chronicle*, 78(3), 391-396.
- [8] Toklu, E. (2017). Biomass energy potential and utilization in Turkey. *Renewable Energy*, 107, 235-244.
- [9] Ayan, A., & Senturk, A. (2023). E. Exploring of Biomass Energy Specific to Turkey.
- [10] Janssen, R., Rutz, D., Janssen, R., & Rutz, D. (2012). *Bioenergy for sustainable development in Africa* 5393-5398, Berlin, Springer.
- [11] Mukherjee, M., & Shaw, R. (2021). Forward-looking lens to mainstream blue-green infrastructure. *Ecosystem-Based Disaster and Climate Resilience: Integration of Blue-Green Infrastructure in Sustainable Development*, 501-512.



r,s,t-Spherical Fuzzy Soft Sets

Fatih KARAMAZ^{1,*} , ***Faruk KARAASLAN¹*** 

¹ Department of Mathematics, Faculty of Sciences, Çankırı Karatekin University, 18100, Çankırı, Turkey

Abstract

This study introduces the concept of r,s,t-Spherical Fuzzy Soft Sets (rst-SFSS), building upon and extending the traditional T-Spherical Fuzzy Soft Sets (T-SFSS) framework. The proposed rst-SFSS model enhances the flexibility and applicability of fuzzy soft sets by incorporating distinct degrees for membership, neutral membership, and non-membership, allowing for a more comprehensive representation of uncertain and imprecise information. Within this extended framework, various fundamental operations such as complement, subethood, equality, union, and intersection are rigorously defined, providing a foundational structure for complex data analysis. Additionally, the properties of these operations are thoroughly examined to establish their logical coherence and practical applications, particularly in fields that rely on multi-criteria decision-making processes.

Keywords: *r,s,t-spherical fuzzy sets, soft set, fuzzy soft set, r,s,t-spherical fuzzy soft sets*

1. Introduction

Fuzzy set theory, established by Zadeh [1] in 1965, has proven to be an essential instrument for addressing uncertainty and ambiguity across diverse scientific and technical domains. Numerous generalizations of fuzzy sets have been proposed over the years to improve their applicability and tackle more intricate decision-making challenges. Prominent among these are Intuitionistic Fuzzy Sets (IFS) [2], Pythagorean Fuzzy Sets (PyFS) [3], Picture Fuzzy Sets (PFS) [4], and Spherical Fuzzy Sets (SFS) [5], each offering different ways to addressing degrees of membership, non-membership, and hesitation.

The notion of Spherical Fuzzy Sets (SFS) [5] was established to offer a more adaptable and thorough framework by integrating degrees of membership, neutral membership, and non-membership within a spherical context. This development facilitated the emergence of T-Spherical Fuzzy Sets (T-SFS) [6], which further expanded the model by employing a parameter n to regulate the total of the degrees.

Building on these developments, this paper introduces the r,s,t-Spherical Fuzzy Soft Set (rst-SFSS), a novel extension that incorporates three parameters r , s , and t to provide an even more flexible and powerful tool for decision-making. The rst-SFSS framework allows for a more nuanced representation of uncertainty and offers improved capabilities for handling multi-criteria decision-making (MCDM) problems.

This study introduces the concept of r,s,t-Spherical Fuzzy Soft Sets (rst-SFSS), expanding on the traditional T-Spherical Fuzzy Soft Sets (T-SFSS) framework. The proposed rst-SFSS model increases the flexibility and applicability of fuzzy soft sets by incorporating distinct levels for membership, neutral membership, and non-membership, enabling a more detailed representation of uncertain and imprecise information. In this extended framework, fundamental operations like complement, subethood, equality, union, and intersection are rigorously defined, establishing a solid foundation for complex data analysis. Furthermore, the properties of these operations are thoroughly examined to ensure logical consistency and practical application, especially in fields dependent on multi-criteria decision-making processes.

2. Preliminaries

This section presents some fundamental principles related to T-SFS and r,s,t-SFS, which are well-documented in the literature.

Definition 2.1. [1] Let U be a nonempty set called initial universe. A fuzzy set (FS) is denoted by Ω and is defined by its membership function κ_{Ω} as follows:

$$\kappa_{\Omega} : U \rightarrow [0,1]$$

* Corresponding author. e-mail address: karamaz@karamaz.com

the value of $\kappa_\Omega(\alpha)$ is called the membership degree of $\alpha \in U$. This numerical value $\kappa_\Omega(\alpha)$ expresses belonging the degree of α to the fuzzy set Ω . Also, fuzzy set Ω on U can be written as follows:

$$\Omega = \{(\alpha, \kappa_\Omega(\alpha)) : \alpha \in U, \kappa_\Omega(\alpha) \in [0,1]\}.$$

The following notions explain the generalization process from IFSs to r,s,t-SFSs.

Let U be the universe of discourse with $\mu_A : U \rightarrow [0,1]$ and $\nu_A : U \rightarrow [0,1]$ which are the degrees of membership and non-membership, respectively. The set of $A = \{(\alpha, \mu_A(\alpha), \nu_A(\alpha)) \mid \alpha \in U\}$ is called:

- **Intuitionistic Fuzzy Set (IFS) [2]:** A in U if it satisfies the condition $0 \leq \mu_A + \nu_A \leq 1$ with the degree of indeterminacy given by

$$\pi_A(\alpha) = 1 - \mu_A(\alpha) - \nu_A(\alpha)$$

- **Pythagorean Fuzzy Set (PyFS) [3]:** A in U if it satisfies the condition $0 \leq \mu_A^2(\alpha) + \nu_A^2(\alpha) \leq 1$ with the degree of indeterminacy given by

$$\pi_A(\alpha) = \sqrt{1 - \mu_A^2(\alpha) - \nu_A^2(\alpha)}$$

To have further generalization, we consider the universe of discourse U with $\mu_A : U \rightarrow [0,1]$, $\eta_A : U \rightarrow [0,1]$, and $\nu_A : U \rightarrow [0,1]$ being the degree of membership, degree of neutral membership, and degree of non-membership, respectively. The set $A = \{(\alpha, \mu_A(\alpha), \eta_A(\alpha), \nu_A(\alpha)) \mid \alpha \in U\}$ is called as follows:

- **Picture Fuzzy Set (PFS) [4]:** A in U if it satisfies the condition $0 \leq \mu_A(\alpha) + \eta_A(\alpha) + \nu_A(\alpha) \leq 1$ with the degree of refusal given by

$$r_A(\alpha) = 1 - (\mu_A(\alpha) + \eta_A(\alpha) + \nu_A(\alpha))$$

- **Spherical Fuzzy Set (SFS) [5]:** A in U if it satisfies the condition $0 \leq \mu_A^2(\alpha) + \eta_A^2(\alpha) + \nu_A^2(\alpha) \leq 1$ with the degree of refusal given by:

$$r_A(\alpha) = \sqrt{1 - (\mu_A^2(\alpha) + \eta_A^2(\alpha) + \nu_A^2(\alpha))}$$

- **T-Spherical fuzzy set (T-SFS) [6]:** Let n be any natural number. A set A in U if it satisfies the condition $0 \leq \mu_A^n(\alpha) + \eta_A^n(\alpha) + \nu_A^n(\alpha) \leq 1$ with the degree of refusal given by:

$$r_A(\alpha) = \sqrt[n]{1 - (\mu_A^n(\alpha) + \eta_A^n(\alpha) + \nu_A^n(\alpha))}$$

- **r,s,t-Spherical fuzzy set (r,s,t-SFS) [7,8]:** Let r, s, t be any natural numbers. A set A in U if it satisfies the condition $0 \leq \mu_A^r(\alpha) + \eta_A^s(\alpha) + \nu_A^t(\alpha) \leq 1$ with the degree of refusal given by:

$$r_A(\alpha) = \sqrt[lcm(r,s,t)]{1 - (\mu_A^r(\alpha) + \eta_A^s(\alpha) + \nu_A^t(\alpha))}$$

Similarly, the extension of Soft Sets to T-Spherical fuzzy soft sets, accompanied with illustrative examples, is documented in the literature, as detailed below.

Let $U = \{\alpha_1, \alpha_2, \dots, \alpha_m\}$ be the universe of discourse and $E = \{\sigma_1, \sigma_2, \dots, \sigma_n\}$ be the set of parameters. The pair (φ, E) is called:

- **Soft Set (SS) [9]** over U iff $\varphi : E \rightarrow P(U)$, where $P(U)$ is the power set of U ;
- **Fuzzy Soft Set (FSS) [10]** over $\varphi(U)$, where φ is a mapping given by $\varphi : E \rightarrow F(U)$ and $F(U)$ denotes the set of all fuzzy set of U ;
- **Intuitionistic Fuzzy Soft Set (IFSS) [11]** over U if $\varphi : E \rightarrow IFS(U)$ and can be represented as:

$$(\varphi, E) = \{(\sigma, \varphi(\sigma)) : \sigma \in E, \varphi(\sigma) \in IFS(U)\},$$

where $IFS(U)$ represents the set of all IFSs of U ;

- **Pythagorean Fuzzy Soft Set (PyFSS) [12]** over U if $\varphi : E \rightarrow PYFS(U)$ and can be represented as:

$$(\varphi, E) = \{(\sigma, \varphi(\sigma)) : \sigma \in E, \varphi(\sigma) \in PYFS(U)\},$$

where $PYFS(U)$ represents the set of all PyFSs of U ;

- **Picture Fuzzy Soft Set (PFSS) [4]** over U if $\varphi : E \rightarrow PFS(U)$ and can be represented as:

$$(\varphi, E) = \{(\sigma, \varphi(\sigma)) : \sigma \in E, \varphi(\sigma) \in PFS(U)\},$$

where $PFS(U)$ represents the set of all PFSs of U ;

- **Spherical Fuzzy Soft Set (SFSS) [13]** over U if $\varphi : E \rightarrow SFS(U)$ and can be represented as:

$$(\varphi, E) = \{(\sigma, \varphi(\sigma)) : \sigma \in E, \varphi(\sigma) \in SFS(U)\},$$

where $SFS(U)$ represents the set of all SFSs of U ;

- **T-Spherical Fuzzy Soft Set (T-SFSS)** [14] over U if $\varphi: E \rightarrow TSFS(U)$ and can be represented as:

$$(\varphi, E) = \{(\sigma, \varphi(\sigma)) : \sigma \in E, \varphi(\sigma) \in TSFS(U)\},$$

where $TSFS(U)$ represents the set of all T-SFSSs of U .

3. r,s,t-Spherical Fuzzy Soft Set

In this section, we introduce r,s,t-Spherical Fuzzy Soft Set (rst-SFSS) as an extension to T-SFSS. Further, the score and accuracy function for the defined rst-SFSS have been proposed along with various operations and different properties.

Definition 3.1. Let U be the universe of discourse and SFS^{rst} be the collection of all rst-SFS over U . Let E be the set of parameters. The pair (φ, E) is a r,s,t-Spherical Fuzzy Soft Set over U iff $\varphi: E \rightarrow SFSS^{rst}$. For any parameter $\sigma_k \in E$, φ_{σ_k} is a r,s,t-Spherical Fuzzy Soft Set given by:

$$\varphi_{\sigma_k} = \{(\alpha_i, \mu_k(\alpha_i), \eta_k(\alpha_i), \nu_k(\alpha_i)) \mid \alpha_i \in U\}$$

where $\mu_k(\alpha_i)$, $\eta_k(\alpha_i)$, and $\nu_k(\alpha_i)$ are the degrees of membership, neutral membership, and non-membership, respectively, with the condition:

$$0 \leq \mu_k^r(\alpha_i) + \eta_k^s(\alpha_i) + \nu_k^t(\alpha_i) \leq 1,$$

and the degree of refusal:

$$r_k(\alpha_i) = \sqrt[lcm(r,s,t)]{1 - (\mu_k^r(\alpha) + \eta_k^s(\alpha) + \nu_k^t(\alpha))}$$

where r,s, and t are natural numbers.

Example 3.1. Consider the set of four houses, say, $H = \{\alpha_1, \alpha_2, \alpha_3, \alpha_4\}$ and the set of parameters under consideration, say, $E = \{\sigma_1 = \text{expensive}, \sigma_2 = \text{wooden}, \sigma_3 = \text{cheap}, \sigma_4 = \text{beautiful}, \sigma_5 = \text{good location}\}$. Then, the perception for the attractiveness of the houses may be described as a rst-SFSS given by:

$$(\varphi, E) = \{\varphi_{\sigma_1}, \varphi_{\sigma_2}, \varphi_{\sigma_3}, \varphi_{\sigma_4}, \varphi_{\sigma_5}\}$$

where,

$$\varphi_{\sigma_1} = \{(\sigma_1, 0.01, 0.9, 0.2), (\sigma_2, 0.9, 0.01, 0.1)\}$$

$$\varphi_{\sigma_2} = \{(\sigma_3, 0.2, 0.3, 0.9), (\sigma_4, 0.1, 0.9, 0.3), (\sigma_5, 0.3, 0.2, 0.9)\}$$

$$\varphi_{\sigma_3} = \{(\sigma_1, 0.4, 0.01, 0.8), (\sigma_4, 0.8, 0.3, 0.1)\}$$

$$\varphi_{\sigma_4} = \{(\sigma_1, 0.05, 0.95, 0.2), (\sigma_4, 0.7, 0.1, 0.05), (\sigma_5, 0.02, 0.8, 0.6)\}$$

$$\varphi_{\sigma_5} = \{(\sigma_2, 0.9, 0.1, 0.01), (\sigma_4, 0.1, 0.85, 0.15)\}$$

3.1. Operations on r,s,t-Spherical Fuzzy Soft Sets

In this subsection, we propose some basic operations on rst-SFSSs.

Definition 3.2. Let (φ, Q) and (ψ, R) be two rst-SFSS on the same universe of discourse U . Let $Q, R \subseteq E$ be the set of parameters; then:

- **Complement:** $(\varphi, Q)^c = (\varphi^c, Q)$ where $\varphi^c: Q \rightarrow SFSS^{rst}(U)$ is a mapping given by

$$\varphi^c(\sigma) = (\varphi(\sigma))^c, \text{ for all } \sigma \in Q;$$

- **Subsethood:** $(\varphi, Q) \subseteq (\psi, R)$, iff $Q \subseteq R$ and for all $\sigma \in Q$, $\varphi(\sigma) \subseteq \psi(\sigma)$;
- **Equality:** $(\varphi, Q) = (\psi, R)$, if $(\varphi, Q) \subseteq (\psi, R)$ and $(\psi, R) \subseteq (\varphi, Q)$;
- **Union:** $(\varphi, Q) \cup (\psi, R) = (T, S)$, where $S = Q \cup R$ for all $p \in S$ and

$$T(\rho) = \begin{cases} \varphi(\rho) & \rho \in Q - R \\ \psi(\rho) & \rho \in R - Q \\ \varphi(\rho) \cup \psi(\rho) & \rho \in Q \cap R \end{cases}$$

In other words, for all $\rho \in Q \cap R$

$$T(\rho) = \{\alpha, \max(\mu_{\varphi(\rho)}(\alpha), \mu_{\psi(\rho)}(\alpha)), \min(\eta_{\varphi(\rho)}(\alpha), \eta_{\psi(\rho)}(\alpha)), \min(v_{\varphi(\rho)}(\alpha), v_{\psi(\rho)}(\alpha))\}$$

- **Intersection:** $(\varphi, Q) \cap (\psi, R) = (T, S)$, where $S = Q \cap R$ for all $\rho \in S$ and

$$T(\rho) = \begin{cases} \varphi(\rho) & \rho \in Q - R \\ \psi(\rho) & \rho \in R - Q \\ \varphi(\rho) \cap \psi(\rho) & \rho \in Q \cap R \end{cases}$$

In other words, for all $\rho \in Q \cap R$

$$T(\rho) = \{\alpha, \min(\mu_{\varphi(\rho)}(\alpha), \mu_{\psi(\rho)}(\alpha)), \min(\eta_{\varphi(\rho)}(\alpha), \eta_{\psi(\rho)}(\alpha)), \max(v_{\varphi(\rho)}(\alpha), v_{\psi(\rho)}(\alpha))\}$$

Proposition 3.1. Suppose that (φ, Q) and (ψ, R) are two rst-SFSSs on the universal set U . Let $Q, R \subseteq E$ be two subsets of the set of parameters; then, as per their definitions, the following properties clearly hold:

- i. $((\varphi, Q)^c)^c = (\varphi, Q)$
- ii. $((\varphi, Q) \cap (\psi, R))^c = (\varphi, Q)^c \cup (\psi, R)^c$
- iii. $((\varphi, Q) \cup (\psi, R))^c = (\varphi, Q)^c \cap (\psi, R)^c$

Further, for simplicity and necessary computations, rst-SFSS can also be regarded as $\tau_u = (\mu_u, \eta_u, \nu_u)$ and called as r,s,t-Spherical Fuzzy Soft Number (rst-SFSN), where u is referential subscript used for establishing a connection between alternatives and parameters in computational examples. For application purposes, to rank these numbers, we propose the score and accuracy functions for the r,s,t-spherical fuzzy soft numbers as follows:

4. Conclusion

In this paper, we introduced the r,s,t-Spherical Fuzzy Soft Set (rst-SFSS) as a generalization of the existing T-Spherical Fuzzy Soft Sets (T-SFSS). This new framework enhances the flexibility and applicability of fuzzy set theory in dealing with complex decision-making problems by incorporating the degrees of membership, neutral membership, and non-membership in a more comprehensive manner. We defined various operations on rst-SFSS, including complement, subethood, equality, union, and intersection, and explored their properties. Additionally, we proposed score and accuracy functions to facilitate the ranking of alternatives, which is crucial in decision-making processes. Furthermore, we developed aggregation operators for rst-SFSS, which play a significant role in the information fusion process. In future research, we aim to explore the potential of rst-SFSS in other domains and develop more sophisticated aggregation operators to further enhance its applicability and efficiency.

References

- [1] Zadeh, L. A. (1965). Fuzzy Sets. *Information and Control*, 8, 338–353.
- [2] Atanassov, K.T. (1986). Intuitionistic fuzzy sets. *Fuzzy Sets Syst.*, 20(1), 87–96.
- [3] Yager, R.R. (2013). Pythagorean fuzzy subsets. In: *Proceedings of Joint IFSA World Congress and NAFIPS Annual Meeting, Edmonton, Canada*, pp. 57–61.
- [4] Cuong, B.C. (2013). Picture Fuzzy Sets First Results. *Part 1, in Preprint of Seminar on Neuro-Fuzzy Systems with Applications. Institute of Mathematics, Hanoi.*
- [5] Gündogdu, F.K. and Kahraman, C. (2018). Spherical fuzzy sets and spherical fuzzy TOPSIS method. *J. Intell. Fuzzy Syst.*, 36, 1–16.

- [6] Mahmood, T., Ullah, K., Khan, Q. and Jan, N. (2019). An approach toward decision-making and medical diagnosis problems using the concept of spherical fuzzy sets. *Neural Computing and Applications*, vol. 31, no. 11, pp. 7041–7053.
- [7] Ali, J. and Naeem, M. (2023). r,s,t-spherical fuzzy VIKOR method and its application in multiple criteria group decision making. *IEEE Access*, 11, 46454-46475.
- [8] Karamaz, F. and Karaaslan, F. (2024) Distance Measures of r,s,t-Spherical Fuzzy Sets and Their Applications in MCGDM Based on TOPSIS. *Journal of Supercomputing*, (Accepted).
- [9] Molodtsov D. A. (1999) Soft set theory-first results, *Comput Math Appl*, 37, 19-31.
- [10] Çağman, N., Enginoğlu, S., Çıtak, F. (2011). Fuzzy soft set theory and its applications, *Iran. J. Fuzzy Syst.*, 8(3), 137–147.
- [11] Maji, P.K., Biswas, R., and Roy, A.R. (2001). Intuitionistic fuzzy soft sets, *Journal of Fuzzy Mathematics*, 9, 677–692.
- [12] Peng, X., Yang, Y., Song, J., and Jiang, Y. (2015). Pythagorean fuzzy soft set and its application, *Computer Engineering*, 41, 224–229.
- [13] Perveen P.A., Fathima et al. (2019). Spherical Fuzzy Soft Sets and Its Applications in Decision-making Problems. *1 Jan. 2019*, 8237 – 8250.
- [14] Guleria A., Bajaj R.K. (2021). T-spherical fuzzy soft sets and its aggregation operators with application in decision-making, 28(2), 1014–1029.



An Experimental Study of DC Motor Application Based on MPPT DC-DC Buck-Boost Converter Powered by Photovoltaic Generators using Akbaba model

Nurettin GÖKŞENLİ¹ , Enes BEKTAŞ^{2,*} , Taha A. TAHA³

¹ Vocational School, Electronics and Automation Department, Çankırı Karatekin University, Çankırı, Türkiye

² Engineering Faculty, Electrical and Electronics Engineering Department, Çankırı Karatekin University, Çankırı, Türkiye

³ Renewable Energies Researches Unit, Northern Technical University, Kirkuk, Iraq

Abstract

Photovoltaic generators (PVGs) are a kind of renewable energy technology that transforms solar radiation into electrical power. The Maximum Power Point Tracker (MPPT) optimizes power generation on a small scale for independent PVG systems. This study aims to develop, evaluate, and use an innovative MPPT circuit for small-scale PVGs. The control circuit utilizes a microcontroller, while the Akbaba Model represents the I-V characteristics of the PVG. The suggested system utilizes a DC/DC buck-boost converter. The microcontroller calculates the converter's duty cycle by using feedback from the output voltage and converts the intensity of solar radiation into a reference value for control. A prototype is created to empirically verify the suggested methodology.

Keywords: Akbaba model, DC motor, MPPT, Photovoltaic generators, Renewable energy

1. Introduction

In recent years, the global energy scene has changed significantly, with an increasing focus on renewable energy sources and technological developments allowing their integration into the power system. The desire to solve environmental issues, lower greenhouse gas emissions, and improve energy security drives this change. Solar photovoltaic (PV) systems have become crucial among the many renewable energy sources because they can use plenty of solar energy and transform it into electrical power. Particularly in industrialized nations, research on renewable energy use and how it affects economic development has been thorough. For example, Balcilar et al. [1] used a historical decomposition approach to investigate the link between renewable energy usage and growth in the G-7 nations. Their results stress the importance of ongoing investment in renewable technology as they show the positive contribution of renewable energy to economic development.

Utilizing maximum power point tracking (MPPT) techniques is essential for optimizing solar energy conversion efficiency, making it a crucial component of PV systems. Researchers have developed numerous MPPT techniques to adapt to load fluctuations and changing environmental conditions. For instance, Goksenli and Akbaba [2] presented a novel microcontroller-based MPPT technique based on the Akbaba model, proving its efficiency via simulation and application. Likewise, Xu et al. [3] suggested a quick and effective MPPT method for changing solar irradiance and load resistance conditions. Developed for fast-changing partial shade situations, Kermadi et al. [4] developed a high-performance global MPPT tracker for fast-changing partial shade situations, demonstrating its excellence in preserving optimum power output

Berrezek et al. [5] also explored the potential of neural networks for effective MPPT, observing significant improvements in speed and tracking accuracy. Priyanka and Dash [6] closely examined clever MPPT techniques, stressing developments in artificial intelligence (AI) uses. Emphasizing artificial intelligence's role in recent developments, Boubaker [7] methodically examined present trends in MPPT approaches. Offering a thorough overview of MPPT methods, Kathe et al. [8] underlined the need for sophisticated algorithms for improving PV system performance. Kumar et al. [9] presented a novel wide-input voltage DC-DC converter for solar PV systems using a hybrid MPPT controller, and demonstrated its performance through experimental data.

Researchers have carefully investigated the financial factors of PV systems, in addition to MPPT approaches. Bazilian et al. [10] reviewed the economics of solar electricity, addressing elements such as cost reductions, technical developments, and legislative frameworks that contribute to the general acceptance of PV systems. Reviewing photovoltaic solar cells holistically, Al-Ezzi and Ansari [11] discussed their technical development, efficiency gains, and economic feasibility.

Researchers also investigate the integration of solar PV systems with motor-driven applications, particularly in water pumping. While Appelbaum and Sarma [13] examined the behavior of permanent magnet DC motors run by solar cells, Akbaba [12] examined the matching of induction motors to PV generators for optimal power transmission. Saied and Monji [14] investigated ideal solar array layouts and DC motor field characteristics for the highest yearly mechanical energy output. For dynamic matching of a solar-electrical/photovoltaic system, Zinger and Braunstein [15] approximated the minimal Z requirements on the matching system. Akbaba and Akbaba [16] examined a DC motor pump system driven by a photovoltaic-boost converter. Akbaba [17] has investigated the ideal matching characteristics of an MPPT unit used for a PVG-powered water pumping system. Presenting an FPGA-based active disturbance rejection control method for a DC motor drive driven by solar photovoltaic energy, Guerrero-Ramirez et al. [18] for water-pumping uses, Shukla and Nikolovski [19] looked at a solar photovoltaic array with a brushless DC motor drive supplied from a grid. Using solar cells and an MPPT technique via the incremental conductance approach, Mahmoud et al. [20] created an induction motor speed control method.

Thus, with its financial advantages and pragmatic uses, the continuous developments in renewable energy technologies, especially solar PV systems, and MPPT methods, highlight the essential function renewable energy plays in determining a sustainable energy future.

This research concentrates on developing, testing, and implementing a unique Maximum Power Point Tracking (MPPT) circuit, primarily for small-scale solar generators (PVG). A microcontroller-based control circuit is employed, with the Akbaba Model utilized to simulate the I-V characteristics of the PVG. The system integrates a DC/DC buck-boost converter, where the microcontroller computes the duty cycle based on feedback from the output voltage and converts the solar radiation intensity into a reference value for optimal control. A prototype of the system is constructed to empirically validate the proposed methodology.

2. Materials and Methods

This paper presents the development and experimental implementation of an MPPT method using permanent magnet DC motors as the load. The photovoltaic generator (PVG) characteristics are modeled using the Akbaba model, which accurately captures the I-V relationship of the PVG. The Akbaba model is defined by Equation (1) [4].

$$I = \frac{V_{oc}-V}{A+BV^2-CV} \quad (1)$$

Where A is given by Equation (2),

$$A = \frac{V_{oc}}{I_{sc}} \quad (2)$$

In these equations, V_{oc} represents the open-circuit voltage, and I_{sc} is the short-circuit current of the PV panel.

The power output of the PVG can be expressed as in Equation (3):

$$P = I \cdot V = \frac{V(V_{oc}-V)}{A+BV^2-CV} \quad (3)$$

The parameters A , B , C , V_{oc} , and I_{sc} are derived for different values of solar irradiance (S). The detailed parameter extraction process is described in [2]. A sample of measured solar irradiance values is provided in Table 1.

Table 1. V_{oc} , I_{sc} , A , B , and C values at selected % solar radiation values

%S	V_{oc}	I_{sc}	A	B	C
50	18.3	0.35	51.8	0.0257	3.10
75	19.16	0.51	37.7	0.022	2.275
85	19.6	0.58	32.7	0.0167	1.915
100	19.8	0.68	28.94	0.008528	1.574

By performing further mathematical processes, the voltage at the maximum power point V_{max} can be stated as shown in Equation (4).

$$V_{max} = \left[\frac{V_{oc}}{I_{sc}} (C - BV_{oc}) \right] \left[\frac{1}{1 - \sqrt{1 - I_{sc}(C - BV_{oc})}} \right] \quad (4)$$

Equations (3) and (4) determine the current and power at the maximum power point I_{max} and P_{max} , respectively, as given in Equations (5) and (6).

$$I_{max} = \frac{V_{oc} - V_{max}}{A + BV_{max}^2 - CV_{max}} \quad (5)$$

$$P_{max} = V_{max} \cdot I_{max} \quad (6)$$

The accuracy of the I-V characteristics defined by parameters A, B, and C are validated through comparison with conventional I-V data, as referenced in [4]. The derived model parameters for the PVG, based on solar irradiance (S), are presented as given in Equation (7).

$$\begin{aligned} A &= 0.005347S^2 - 1.258S + 101.3 \\ B &= -6.832 \times 10^{-6}S^2 + 0.00068S + 0.0088 \\ C &= 0.0001788S^2 - 0.05736S + 5.523 \end{aligned} \quad (7)$$

In the proposed method, system performance is primarily influenced by the levels of solar radiation and the output load voltage. The control circuit measures solar radiation, converting it into a voltage signal for the microcontroller. The microcontroller then calculates the model parameters A, B, C, V_{out} , I_{sc} , V_{max} , and the duty cycle (dc).

The duty cycle is determined by Equation (8):

$$dc = 1 - \frac{V_{max}}{V_{out}} \quad (8)$$

where V_{max} is the maximum power voltage of the PVG, and V_{out} is the instantaneous measured output voltage.

The microcontroller, programmed with embedded software, generates the required duty cycle to maximize the output power. Solar radiation is detected by the voltage drop across a resistor (R), providing an input voltage (V_R) to the microcontroller for the duty cycle. Figure 1 illustrates the system's block diagram.

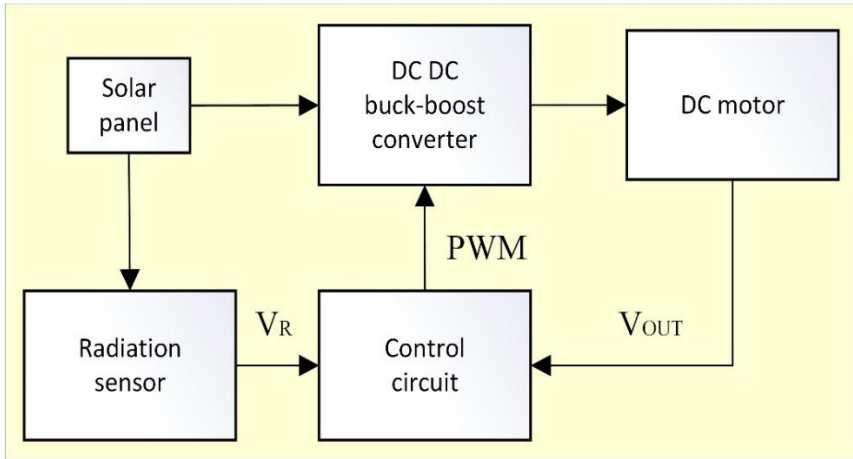


Figure 1. Block diagram of the system

The microcontroller is programmed to apply the $V_{max} = f(S)$ relationship to determine the required duty cycle based on Equation (8), enabling the PVG to operate at maximum power. The system requires only two inputs: solar radiation (S) and output load voltage (V_{out}) with other parameters depending on S and embedded within the microcontroller program. The MPPT circuit output aligns with the output of the DC-DC buck-boost converter.

3. Experimental Application and Results

The experimental study is conducted using the application circuit depicted in Figure 2, specifically under varying solar radiation conditions, represented as $S = 74\%$ and 93% . Many variables like voltage, current, and power output are carefully monitored and noted throughout the experiment. These tests gave important new perspectives on the operating qualities and efficiency of the system components, including the DC-DC buck-boost converter, microcontroller, and sensor.

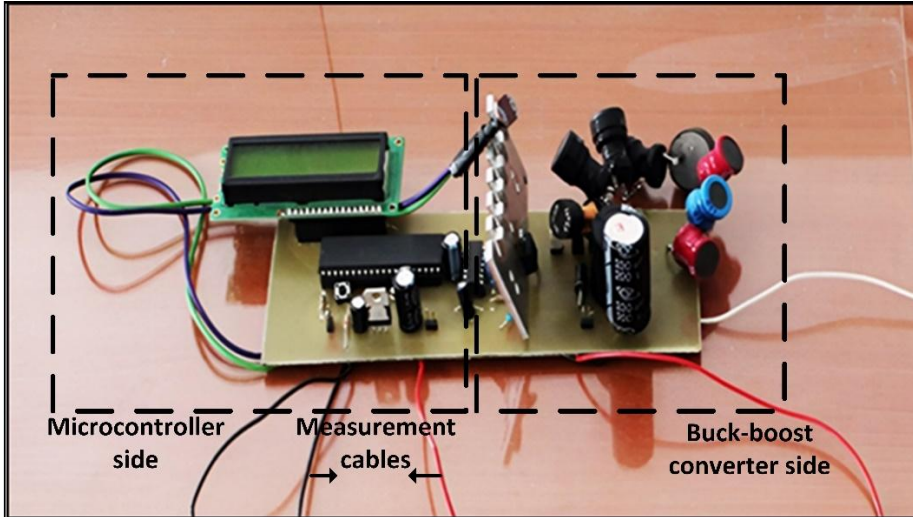


Figure 2. Application circuit of the system

For the boost converter, inductance and capacitor are determined as 6mH and 140uF. With these values, the converter operates with a 20% inductance current ripple and a 1% voltage ripple. Consequently, the oscilloscope graphics and DC-DC buck-boost converter design process are acquired and are given in Figure 3. Here, altering the L and C variables can provide various outcomes. Finding the best suitable value to achieve better outcomes is essential in practice.

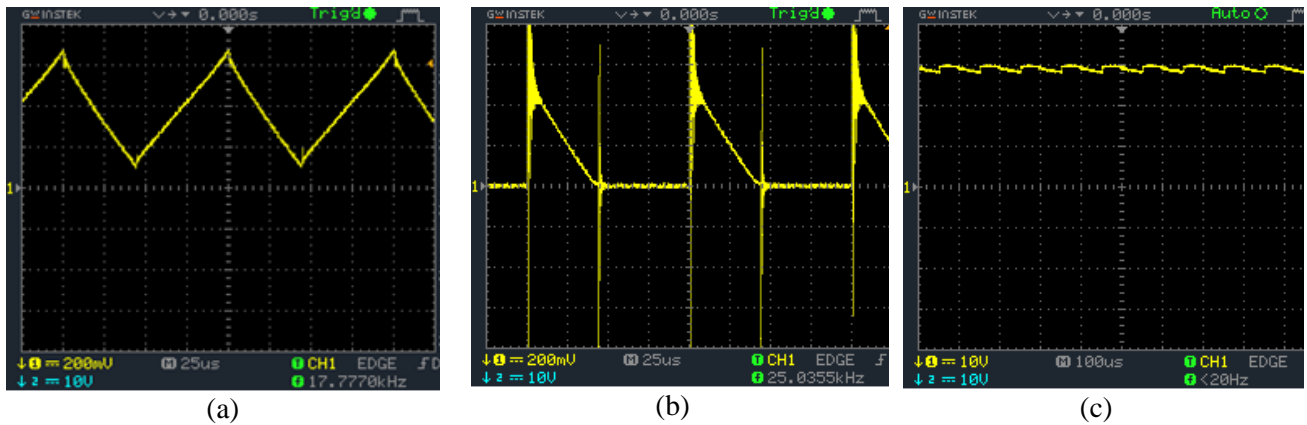


Figure 3. Experimental results a) Inductance current, b) Diode current, c) Output voltage of converter (capacitor voltage)

To determine the conditions for the DC load operating at maximum power, permanent magnet motor combinations that can operate at 24 V and 0.5 W-2W output are used. For different S values (74% and 93%) input/output voltages of the converter, currents of the panel, and load are measured as in Tables 2-3.

Table. 2 Measured system parameters for parallel connection at S=74%

Number of motors	V_{Load}	I_{Load}	P_{Load}	V_{Panel}	I_{Panel}	P_{Panel}
1	18.24	0.068	1.24	14.9	0.2	2.98
2	17.87	0.137	2.459	14.85	0.258	3.83
3	17.42	0.196	3.41	14.8	0.311	4.6
4	17.22	0.240	4.133	14.75	0.353	5.21

Table 3. Measured system parameters for parallel connection at S=93%

Number of motors	V_{Load}	I_{Load}	P_{Load}	V_{Panel}	I_{Panel}	P_{Panel}
1	18.8	0.105	1.974	16	0.24	3.84
2	18.5	0.17	3.145	15.9	0.3	4.77
6	15.4	0.54	8.316	15.6	0.612	9.54
7	15.3	0.567	8.675	15.5	0.623	9.66
8	15.1	0.584	8.818	15.3	0.635	9.72

By connecting DC motors in parallel, the resistance of the load decreases. It can be concluded that as the load resistance decreases, the Solar Panel approaches the appropriate load resistance and the losses decrease. It can be assumed that the solar panel is producing power that is nearly at its maximum when S is 93%. In this instance, the proposed algorithm follows the V-I curve produced by the Akbaba method to modify the converter voltage. As a result, the expected maximum power is obtained and minimum loss is realized.

4. Conclusion

In this study, the I-V characteristics of the PVG are simulated using the Akbaba Model in a microcontroller-based control circuit. A DC/DC buck-boost converter is part of the system. The microcontroller figures out the duty cycle by using feedback from the output voltage and turns the amount of solar radiation into a reference value for the best MPPT control. The system aims to draw more power from the PV panel as the number of parallel-connected DC motors increases. At 74% solar irradiance, the panel voltage fluctuates between 14.9 and 14.75 V, with the converter output set to 17-18 V. However, at 93% solar radiation, the proposed MPPT control technique effectively reduces the load voltage to 15 V. Consequently, the system achieves a loss of approximately 0.5 W and a power transfer of 9.5 W.

References

- [1] Balcilar, M., Ozdemir, Z. A., Ozdemir, H., & Shahbaz, M. (2018). The renewable energy consumption and growth in the G-7 countries: Evidence from historical decomposition method. *Renewable Energy*, 126, 594-604. <https://doi.org/10.1016/j.renene.2018.03.066>
- [2] Goksenli, N., & Akbaba, M. (2016). Development of a new microcontroller based MPPT method for photovoltaic generators using Akbaba model with implementation and simulation. *Solar Energy*, 136, 622-628. <https://doi.org/10.1016/j.solener.2016.07.037>
- [3] Xu, L., Cheng, R., & Yang, J. (2020). A New MPPT Technique for Fast and Efficient Tracking under Fast Varying Solar Irradiation and Load Resistance. *International Journal of Photoenergy*, 2020, 1-18. <https://doi.org/10.1155/2020/6535372>
- [4] Kermadi, M., Salam, Z., Ahmed, J., & Berkouk, E. M. (2021). A High-Performance Global Maximum Power Point Tracker of PV System for Rapidly Changing Partial Shading Conditions. *IEEE Transactions on Industrial Electronics*, 68(3), 2236-2245. <https://doi.org/10.1109/tie.2020.2972456>
- [5] Berrezzek, F., Khelil, K., & Bouadjila, T. (2020). Efficient MPPT scheme for a photovoltaic generator using neural network. In *International Conference on Control, Circuit and System Science and Processing (CCSSP)* (pp. 1-8). <https://doi.org/10.1109/ccssp49278.2020.9151551>
- [6] Priyanka, G., & Dash, S. K. (2020). A Detailed Review on Intelligent Maximum Power Point Tracking Algorithms. In *International Conference on Industrial Instrumentation and Control (ICIC)* (pp. 1-8). <https://doi.org/10.1109/icimia48430.2020.9074861>
- [7] Boubaker, O. (2023). MPPT techniques for photovoltaic systems: A systematic review in current trends and recent advances in artificial intelligence. *Discovery Energy*, 3, 9. <https://doi.org/10.1007/s43937-023-00024-2>
- [8] Kathe, M. L., Makokha, A. B., Zachary, S. O., & Adaramola, M. S. (2023). A Comprehensive Review of Maximum Power Point Tracking (MPPT) Techniques Used in Solar PV Systems. *Energies*, 16(5), 2206. <https://doi.org/10.3390/en16052206>
- [9] Kumar, S., Sunil, S., & Balakrishna, K. (2024). A new wide input voltage DC-DC converter for solar PV systems with hybrid MPPT controller. *Scientific Reports*, 14(1). <https://doi.org/10.1038/s41598-024-61367-x>
- [10] Bazilian, M., Onyeji, I., Liebreich, M., MacGill, I., Chase, J., Shah, J., Gielen, D., Arent, D., Landfear, D., & Zhengrong, S. (2013). Re-considering the economics of photovoltaic power. *Renewable Energy*, 53, 329-338. <https://doi.org/10.1016/j.renene.2012.11.029>
- [11] Al-Ezzi, A. S., & Ansari, M. N. M. (2022). Photovoltaic Solar Cells: A Review. *Applied System Innovation*, 5(4), 67. <https://doi.org/10.3390/asi5040067>
- [12] Akbaba, M. (2007). Matching Induction Motors to PVG for Maximum Power Transfer. *Desalination*, 209(1), 31-38. <https://doi.org/10.1016/j.desal.2007.04.005>
- [13] Appelbaum, J., & Sarma, M. S. (1989). The Operation of Permanent Magnet DC Motors Powered by a

- Common Source of Solar Cells. *IEEE Transactions on Energy Conversion*, 4(4), 635-642. <https://doi.org/10.1109/MPER.1989.4310423>
- [14] Saied, M. M., & Monji, G. J. (1989). Optimal Solar Array Configuration and DC Motor Field Parameters for Maximum Annual Output Mechanical Energy. *IEEE Transactions on Energy Conversion*, 4(3), 459-465. <https://doi.org/10.1109/MPER.1989.4310963>
- [15] Zinger, Z., & Braunstein, A. (1981). Dynamic Matching of a Solar-electrical/Photovoltaic/System - An Estimation of the Minimum Z Requirements on the Matching System. *IEEE Transactions on Power Apparatus Systems*, PAS-100(March), 1189-1192. <https://doi.org/10.1109/TPAS.1981.316588>
- [16] Akbaba, M., & Akbaba, M. C. (2001). Dynamic Performance of a Photovoltaic-Boost Converter Powered DC Motor-Pump System. In *Electric Machines and Drives Conference* (pp. 356-361). <https://doi.org/10.1109/IEMDC.2001.939325>
- [17] Akbaba, M. (2006). Optimum Matching Parameters of an MPPT Unit Used for a PVG- Powered Water Pumping System for Maximum Power Transfer. *International Journal of Energy Research*, 30, 395-409. <https://doi.org/10.1002/er.1157>
- [18] Guerrero-Ramirez, E., Martinez-Barbosa, A., Contreras-Ordaz, M. A., Guerrero-Ramirez, G., Guzman-Ramirez, E., Barahona-Avalos, J. L., & Adam-Medina, M. (2022). DC Motor Drive Powered by Solar Photovoltaic Energy: An FPGA-Based Active Disturbance Rejection Control Approach. *Energies*, 15(18), 6595. <https://doi.org/10.3390/en15186595>
- [19] Shukla, T., & Nikolovski, S. (2023). A Solar Photovoltaic Array and Grid Source-Fed Brushless DC Motor Drive for Water-Pumping Applications. *Energies*, 16(17), 6133. <https://doi.org/10.3390/en16176133>
- [20] Mahmmoud, O. N., Gaeid, K. S., Nashi, A. F., & Siddiqui, K. M. (2020). Induction Motor Speed Control with Solar Cell Using MPPT Algorithm by Incremental Conductance Method. *Tikrīt Journal of Engineering Sciences*, 27(3), 8-16. <https://doi.org/10.25130/tjes.27.3.02>



Hearing Health And Occupational Safety Risks For Construction Workers

Beyza DEMİRTAŞ YILMAZ¹, ^{ID}, Salih YILMAZ^{2*}, ^{ID}, Buket ÇAM³, ^{ID}

¹ Faculty of Health Science, Audiology Department, Erciyes University, Kayseri, Türkiye

² Faculty of Engineering, Civil Engineering Department, Çankırı Karatekin University, Çankırı, Türkiye

³ Faculty of Health Science, Nursing Department, Erciyes University, Kayseri, Türkiye

Abstract

Noise is a significant public health problem, especially in the auditory system, but also in general health. Workers with hearing loss face challenges in terms of personal safety. They are also at higher risk of work-related injuries and are more likely to be unemployed. Noise has become an increasingly important issue, and its effects are being discussed in many sectors. Noise, which can affect individuals in many cognitive, social, and physiological aspects, is important to address from many angles, especially since it is a large part of the working lives of construction sector workers. In noisy work environments, communication is critical for work performance and/or safety. It is known that noise negatively affects interpersonal communication and reduces work efficiency. It has been determined that the effects of noise are evaluated in many sectors, but there is no comprehensive research in the construction field in Turkey. Today, it is essential to determine the share of occupational health and safety practices applied in all business areas in the construction sector and the measures to be taken. Unlike businesses in the industry in general, activities in the construction sector are not always fixed and carried out in a single location. Therefore, noise levels are constantly changing. It is important to discuss the national regulations and assessments that address general occupational health and safety practices in relation to hearing health and noise, and the effects of these measures on hearing health. This review discusses the interactions of noise with hearing loss and tinnitus and the rules that workers must follow in this sector.

Keywords: hearing loss, noise, workplace health and safety, civil engineering

1. Introduction

Noise is a major public health problem, with particular effects on the auditory system but also with adverse effects on general health. Hearing loss and tinnitus are common risks associated with occupations with high levels and prolonged exposure to noise, such as construction, agriculture, and music industries [1]. Between 7% and 21% of hearing loss in adults is attributable. Noise-induced hearing loss is one of the most common occupational diseases [2]. In a study conducted in the United States, hearing loss and tinnitus symptoms of workers exposed and not exposed to noise were evaluated and hearing loss was detected in 7% of workers who were not exposed to noise and 23% of those who were exposed. In this study, the proportion of patients with tinnitus complaints was 15% in workers with noise exposure and 5% in those without noise exposure. [3]. In another study involving different sectors, hearing loss was reported in 25% of American construction workers and 37-58% of musicians exposed to noise [4], [5]. In different studies evaluating the noise exposure of construction workers, musicians, and agricultural workers, the average noise equivalent exposures were 72-112 dBA for construction workers, 75-98 dBA for musicians, and 62.6-92.1 for agricultural workers for 8 hours. [6], [7].

When international and national studies are evaluated, it is seen that different sectors have been investigated together. Still, especially in Turkey, there is no comprehensive research on noise exposure of construction workers and general occupational health and safety measures. This review investigated international studies in the field of construction, occupational health and safety regulations in Turkey, and the measures taken.

Some studies have reported that noise is not the only workplace risk factor for hearing loss. Some chemicals used in industrial processes have also been shown to have ototoxic effects in combination with noise or other chemicals. Ototoxic chemicals fall into four main categories: solvents (e.g., toluene, styrene, ethylbenzene, trichloroethylene), asphyxiants (e.g., carbon monoxide, hydrogen cyanide, acrylonitrile), heavy metals (e.g., mercury, lead, tin) and polychlorinated biphenyls. The effects of ototoxic chemicals can sometimes mimic the

* Corresponding author. E-mail address: salihyilmaz@karatekin.edu.tr

effects of noise through similar physiological processes, making it difficult to determine the specific impact of individual factors on workers [8].

Noise-induced hearing loss is caused by damage to the outer hair cells present in the cochlea. The damage can occur through multiple mechanisms, including mechanical, ischemic, or metabolic. Regardless of the pathway leading to hair cell destruction, hair cells in mammalian species do not regenerate, so noise-induced hearing loss is permanent [9].

An auditory exposure of sufficiently high intensity can separate the organ of Corti, located in the inner ear, from the basilar membrane and reach a force that can disrupt the integrity of the barrier between endolymph and perilymph [10].

Studies show that noise exposure of at least 130 dB sound pressure level (SPL) is required to cause direct mechanical damage to the ear [9].

Permanent sensorineural hearing loss is the most common and most serious effect of noise-related occupational exposure, characterized by a “notch” in the configuration of audiometry thresholds. The weakest thresholds occur in the 3000-6000 Hz range, with better thresholds above and below these frequencies. The primary notch frequency is related to the spectrum of the noise source, the size of the ear canal, and its associated resonant frequency. With continuous exposure, the noise notch deepens and spreads to adjacent frequencies, as shown in Figure 1. Noise has been found to be associated with and potentially affects the auditory system and cardiovascular health. Whether there is a causal relationship between noise and cardiovascular pathologies is still debated. Although the pathophysiology is unknown, it is theorized to work through the autonomic nervous and endocrine systems. The stress response to noise can trigger elevated heart rate and blood pressure. Over time, chronic stress leads to a chronic stress response and can contribute to risks of hypertension (chronically high blood pressure), high cholesterol, and coronary heart disease. The literature has consistently shown a moderate association between occupational noise exposure and hypertension [11], [12].

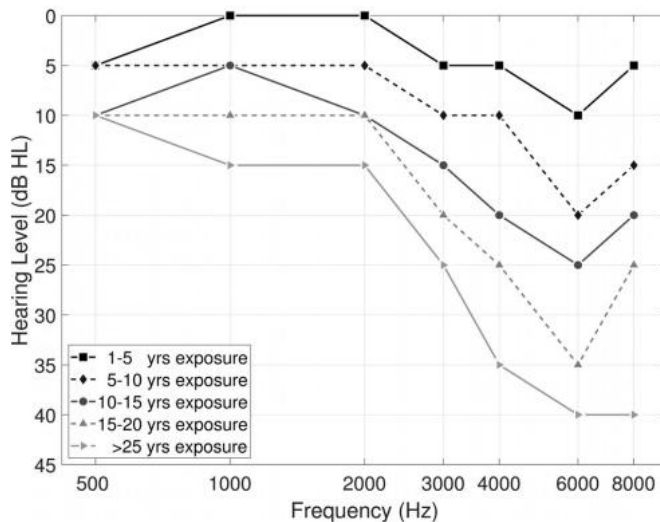


Figure 1. Progression of noise-induced hearing loss with repeated exposure [13].

Middendorff et al. (2004) reported that in their study between 1979 and 1999, the highest average exposure levels were recorded in Construction (94.9-96.7 dBA), followed by Mining (93.6-93.7 dBA), Manufacturing (89.9-91.9 dBA), Agriculture (89.9-91.6 dBA) and Wholesale Trade (89.7-91.2 dBA). [14].

Choi et al. (2012) analyzed occupational information network data to identify the occupations where noise exposure occurs most frequently. They reported that Transportation and Material Handling technicians, Extraction and Precision Manufacturing occupations, Vehicle and Mobile Equipment Mechanics and Repairers, and Machine Operators ranked highest in noise exposure assessments [15].

In many work environments, communication is critical to work performance and safety. High noise levels especially have a negative impact on speech communication. In general, a signal-to-noise ratio between 6-12 dB is required for clear speech understanding [16].

Studies have shown that noise exposure is the primary cause of preventable hearing loss. The most common protective equipment used to protect against the effects of noise and maintain healthy communication is ear protection plugs. Ear protectors used to protect against the effects of loud noise can change speech intelligibility in noise. Studies have shown that noise levels of 90 dB_A and above have a very positive effect on speech intelligibility, but if the noise level is below 85 dB_A, speech intelligibility is negatively affected. [9], [13], [17].

Although ear protectors can improve the ability of normal hearing individuals to accurately detect speech signals in the presence of loud background noise, workers with hearing loss are reported to have more difficulty hearing warning signals [18]. However, left untreated, hearing loss can lead to stress and fatigue, as well as communication difficulties and social isolation. [17].

Stress is reported to be associated with depression, cognitive decline, dementia, falls, increased hospitalizations and healthcare costs, and mortality associated with the effects of fatigue and social isolation. Workers with hearing loss face challenges not only psychosocially but also in terms of their personal safety. Individuals with sensory deficits are at higher risk of work-related injuries and are more likely to be unemployed [13], [17], [19], [20], [21].

Unlike other noisy environments, in construction work sites, the sound elements are not always constant and in one place. Therefore, noise levels and exposures are constantly changing. Construction work is often done outdoors, under the influence of weather conditions, wind tunnels, topography, atmosphere, and the environment. In addition, noise sources in construction, e.g., heavy excavation machinery, may move from one location to another; their intensity may vary considerably during working hours [22].

The equipment commonly used in the construction industry and the sound levels they generate are presented in Table 1. Looking at this frequently used equipment, it is seen that the sounds at construction sites are at serious heights.

Table 1. Noise Levels of Construction Equipment [22]

Construction Equipment	Audio Range dBA	Construction Equipment	Audio Range dBA
Wheel Loader	85-91	Battering-Ram	82-105
Digger Loader	79-89	Hydraulic Breaker	90-100
Road Roller	79-93	Generator	<85
Dozer	89-103	Asphalt Paver	100-102
Truck	88-103	Skreyper	84-102
Concrete Mixer	<85	Pneumatic Breaker	94-111
Crane	97-102	Greyder	<85

2. Results

The construction sector has always been the locomotive sector of countries with the added value and employment opportunities it provides to the economy. However, occupational accidents in the sector constitute major problems for our country as in many countries of the world. In order to prevent occupational accidents, minimize losses, and raise awareness of all parties in the sector, the occupational health and safety legislation in the European acquis within the framework of the European Union harmonization process was introduced into the working life of our country with the regulations published in 2003 and 2004 based on Article 78 of the Labor Law No. 4857. These legislations were updated within the scope of the Occupational Health and Safety Law No. 6331 dated 20/6/2012.

Among these regulations, the “Regulation on Occupational Health and Safety in Construction Work”, which is based on the Council Directive 92/57/EEC of the European Union, determines the minimum health and safety requirements for construction workplaces.

In order to reduce noise-related accidents and diseases in construction work sites, a detailed analysis of sound sources should be made as a priority. Workers working with sources that produce noise above the risky level must use their personal protective equipment fully and completely. In addition, efforts should be made to reduce

the sound production of these noise elements as much as possible. All employees and employers should be made aware of occupational health and safety. This study presents a preliminary investigation of noise and its effects at construction sites.

References

- [1] D. I. Nelson, R. Y. Nelson, M. Concha-Barrientos, and M. Fingerhut, "The global burden of occupational noise-induced hearing loss," *Am J Ind Med*, vol. 48, no. 6, pp. 446–458, Dec. 2005, doi: 10.1002/ajim.20223.
- [2] S. A. Fausti, D. J. Wilmington, P. V. Helt, W. J. Helt, and D. Konrad-Martin, "Hearing health and care: The need for improved hearing loss prevention and hearing conservation practices," *The Journal of Rehabilitation Research and Development*, vol. 42, no. 4s, p. 45, 2005, doi: 10.1682/JRRD.2005.02.0039.
- [3] E. A. Masterson, C. L. Themann, S. E. Luckhaupt, J. Li, and G. M. Calvert, "Hearing difficulty and tinnitus among U.S. workers and non-workers in 2007," *Am J Ind Med*, vol. 59, no. 4, pp. 290–300, Apr. 2016, doi: 10.1002/ajim.22565.
- [4] O. Hong, "Hearing loss among operating engineers in American construction industry," *Int Arch Occup Environ Health*, vol. 78, no. 7, pp. 565–574, Aug. 2005, doi: 10.1007/s00420-005-0623-9.
- [5] S. Couth, N. Mazlan, D. R. Moore, K. J. Munro, and P. Dawes, "Hearing Difficulties and Tinnitus in Construction, Agricultural, Music, and Finance Industries: Contributions of Demographic, Health, and Lifestyle Factors," *Trends Hear*, vol. 23, Jan. 2019, doi: 10.1177/2331216519885571.
- [6] M. D. Fernández, S. Quintana, N. Chavarría, and J. A. Ballesteros, "Noise exposure of workers of the construction sector," *Applied Acoustics*, vol. 70, no. 5, pp. 753–760, May 2009, doi: 10.1016/j.apacoust.2008.07.014.
- [7] R. Neitzel, N. S. Seixas, J. Camp, and M. Yost, "An Assessment of Occupational Noise Exposures in Four Construction Trades," *Am Ind Hyg Assoc J*, vol. 60, no. 6, pp. 807–817, Nov. 1999, doi: 10.1080/00028899908984506.
- [8] A. Lie *et al.*, "Occupational noise exposure and hearing: a systematic review," *Int Arch Occup Environ Health*, vol. 89, no. 3, pp. 351–372, Apr. 2016, doi: 10.1007/s00420-015-1083-5.
- [9] T. N. Le, L. V. Straatman, J. Lea, and B. Westerberg, "Current insights in noise-induced hearing loss: A literature review of the underlying mechanism, pathophysiology, asymmetry, and management options," *Journal of Otolaryngology- Head & Neck Surgery*, vol. 46, no. 1, Jan. 2017, doi: 10.1186/s40463-017-0219-x.
- [10] A. Kurabi, E. M. Keithley, G. D. Housley, A. F. Ryan, and A. C.-Y. Wong, "Cellular mechanisms of noise-induced hearing loss," *Hear Res*, vol. 349, pp. 129–137, Jun. 2017, doi: 10.1016/j.heares.2016.11.013.
- [11] E. Kerns, E. A. Masterson, C. L. Themann, and G. M. Calvert, "Cardiovascular conditions, hearing difficulty, and occupational noise exposure within US industries and occupations," *Am J Ind Med*, vol. 61, no. 6, pp. 477–491, Jun. 2018, doi: 10.1002/ajim.22833.
- [12] M. Skogstad, H. A. Johannessen, T. Tynes, I. S. Mehlum, K.-C. Nordby, and A. Lie, "Systematic review of the cardiovascular effects of occupational noise," *Occup Med (Chic Ill)*, vol. 66, no. 1, pp. 10–16, Jan. 2016, doi: 10.1093/occmed/kqv148.
- [13] C. L. Themann and E. A. Masterson, "Occupational noise exposure: A review of its effects, epidemiology, and impact with recommendations for reducing its burden," *J Acoust Soc Am*, vol. 146, no. 5, pp. 3879–3905, Nov. 2019, doi: 10.1121/1.5134465.
- [14] P. J. Middendorf, "Surveillance of occupational noise exposures using OSHA's Integrated Management Information System," *Am J Ind Med*, vol. 46, no. 5, pp. 492–504, Nov. 2004, doi: 10.1002/ajim.20092.
- [15] Y.-H. Choi, H. Hu, S. Tak, B. Mukherjee, and S. K. Park, "Occupational noise exposure assessment using O*NET and its application to a study of hearing loss in the US general population," *Occup Environ Med*, vol. 69, no. 3, pp. 176–183, Mar. 2012, doi: 10.1136/oem.2011.064758.

- [16] G. S. Robinson *et al.*, “Chapter 14: Speech Communications and Signal Detection in Noise,” in *The Noise Manual, Revised 5th edition*, 2700 Prosperity Ave., Suite 250 Fairfax, VA 22031: American Industrial Hygiene Association, pp. 567–600. doi: 10.3320/978-1-931504-02-7.567.
- [17] C. Themann, A. Suter, and M. Stephenson, “National Research Agenda for the Prevention of Occupational Hearing Loss—Part 1,” *Semin Hear*, vol. 34, no. 03, pp. 145–207, Aug. 2013, doi: 10.1055/s-0033-1349351.
- [18] C. Themann, A. Suter, and M. Stephenson, “National Research Agenda for the Prevention of Occupational Hearing Loss—Part 2,” *Semin Hear*, vol. 34, no. 03, pp. 208–252, Aug. 2013, doi: 10.1055/s-0033-1349352.
- [19] M. Basner *et al.*, “Auditory and non-auditory effects of noise on health,” *The Lancet*, vol. 383, no. 9925, pp. 1325–1332, Apr. 2014, doi: 10.1016/S0140-6736(13)61613-X.
- [20] A. Dzhambov and D. Dimitrova, “Occupational noise and ischemic heart disease: A systematic review,” *Noise Health*, vol. 18, no. 83, p. 167, 2016, doi: 10.4103/1463-1741.189241.
- [21] R. L. Neitzel, T. K. Swinburn, M. S. Hammer, and D. Eisenberg, “Economic Impact of Hearing Loss and Reduction of Noise-Induced Hearing Loss in the United States,” *Journal of Speech, Language, and Hearing Research*, vol. 60, no. 1, pp. 182–189, Jan. 2017, doi: 10.1044/2016_JSLHR-H-15-0365.
- [22] <https://guvenliinsaat.csgeb.gov.tr/>



The Role of Biomass Energy in Sustainable Development and Its Contribution To Environmental Sustainability Goals

D. Kemal BAYRAKTAR¹, ***Mehmet GÜNEŞ²***

¹ Department of Forest Industrial Engineering, Karadeniz Technical University, Trabzon, Türkiye

² Çankırı Vocational School, Department of Design, Çankırı Karatekin University, Çankırı, Türkiye

Abstract

Bioenergy, being a key element in sustainable development strategies, holds the promise of fostering inventive and eco-conscious solutions in energy generation to bolster economic advancement and contribute significantly to meeting ecological preservation objectives. Biomass energy is crucial in advancing sustainable development efforts and plays a key part in reaching environmental sustainability objectives. In developed nations, biomass stands out as a key energy source, originating from diverse biological resources like agricultural leftovers, wood chips, animal byproducts, and specialized energy crops. In a well-established country, about 342 million tons of biomass are used each year, meeting approximately 5% of the energy requirements. This involves utilizing corn grain for ethanol production, and wood or wood residues for generating heat and electricity. By tripling biomass production, the country has the potential to produce approximately 60 billion gallons of low greenhouse gas emission liquid fuel, meeting the future demands for food, animal feed, fiber, traditional forestry products, and exports. Untapped biomass resources possess the potential to greatly enhance the country's bioeconomy, potentially increasing the annual biomass supply by approximately 350 million tons on top of existing levels. In a mature market down the road, energy crops have the potential to provide over 400 million tons of biomass annually. The analysis highlights sustainability by taking into account potential effects on soil, air, and water quality, as well as ensuring the preservation of biodiversity. The range of methods encompassed in the technological processes for converting biomass into energy consists of incineration, pyrolysis, gasification, and anaerobic digestion. The study highlights the significant environmental advantages of biomass, including its carbon neutrality, ability to decrease dependency on fossil fuels, and capacity to provide energy access in rural regions while boosting local economies. Moreover, this study places a significant emphasis on the potential of biomass to fulfill the energy requirements of rural areas in developing nations and enhance its efficiency using contemporary biomass technologies. In summary, it is important to highlight that to unlock the full potential of biomass for achieving sustainable development objectives, it is crucial to address environmental and economic obstacles through cooperation among managers, scientists, and industry professionals.

Keywords: Biomass Energy, Sustainable Development, Environmental Impact

1. Introduction

Biomass is perceived as a key component of renewable energy solutions in driving towards environmental sustainability objectives. In natural ecosystems, there is a continuous cycle that offers sustainable energy and materials through the recycling of organic waste. Organic matter produced by living organisms (plants, animals, and microorganisms) is composed of a combination of fundamental elements such as carbon, hydrogen, and oxygen, and can be utilized for energy production, biochemical processes, and industrial applications.

These substances could potentially be utilized to provide energy through various methods. Biomass stands uniquely among other forms of renewable energy because it can easily be converted into liquid fuels, electricity, and heat. The extensive variety of biomass sources, such as agricultural residues, wood chips, animal waste, and purpose-grown energy crops, makes it a very versatile resource for generating energy.

Forest energy projects in developing countries that are sustainable have the ability to make a notable impact on fulfilling local energy requirements as well as global climate objectives. By blending forest management with energy production, such projects have the potential to improve rural livelihoods and lessen deforestation [1].

Finland's energy strategy underscores the importance of wood energy, particularly emphasizing the use of forest chips from small-sized trees and residual biomass from cuttings. It prioritizes the target of generating 5

million cubic meters of forest chips by 2010, amounting to 10 TWh. This highlights the significance of forest energy in achieving sustainable development objectives and decreasing carbon emissions[2].

"Biomass is organic material obtained from living organisms that can be harnessed as an energy source through different technological methods. " Biomass is composed of organic materials that come from plants, animals, and microorganisms, making it a versatile resource for energy production [3].

Biomass, particularly liquid fuels (biofuels), have a significant impact on the generation of electricity and heat. This occurs because biomass has the unique capability to be converted directly into different types of energy, a characteristic not shared by other renewable energy sources such as solar, wind, or hydropower [4].

The diversity of biomass sources is what makes biomass such a crucial resource in energy production. Agricultural residues such as. Materials such as straw, husks, corn cobs, wood chips, and animal wastes like manure), and energy crops grown in a specially tailored manner (e. g. Miscanthus and willow are among the various biomass sources mentioned [5].

The diversity of available sources greatly enhances the acknowledgment of biomass as a sustainable and renewable choice for generating energy. The versatility and adaptability of biomass energy enable it to undertake a crucial function in the worldwide energy shift. Moreover, biomass is being more widely used as a component of renewable energy sources to decrease reliance on fossil fuels and lower its carbon emissions [6].

Particularly in developing countries, biomass has a vital role in meeting the energy needs of rural areas and increasing access to energy sources [7].

- **Agricultural residues:** This involves crop residues like straw, husks, and bagasse. The figure displayed in Figure 1 illustrates how these leftover residues in the field post-harvest can be collected for energy production.



Fig. 1. Value-added agricultural residues.

- **Wood and Forestry Residues:** Wood chips, sawdust and other timber industry by-products are common sources of biomass. It is also shown in Figure 2 that forest thinning and logging residues provide an important biomass supply.

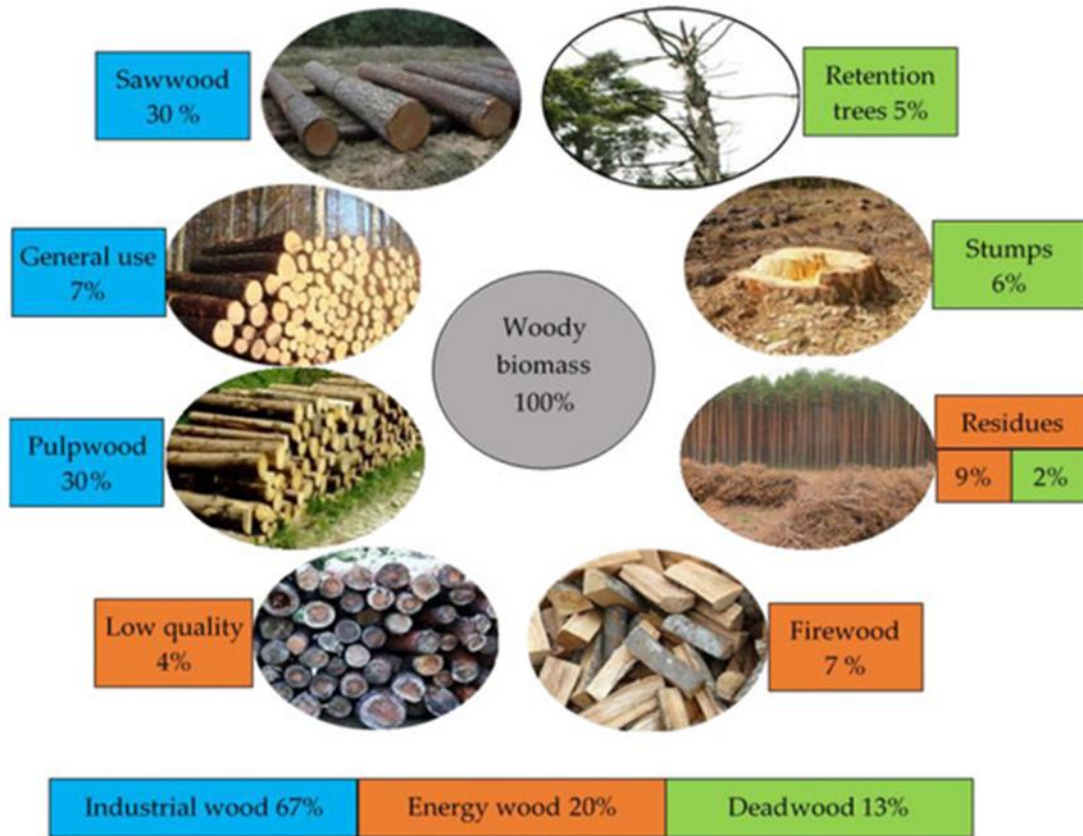


Fig. 2. Utilization of wood and wood residues as a renewable resource in sustainable forest management.

- **Animal Wastes:** Animal manure and other organic waste generated from animal husbandry operations serve as highly valuable resources for producing biogas, as illustrated in Figure 3.

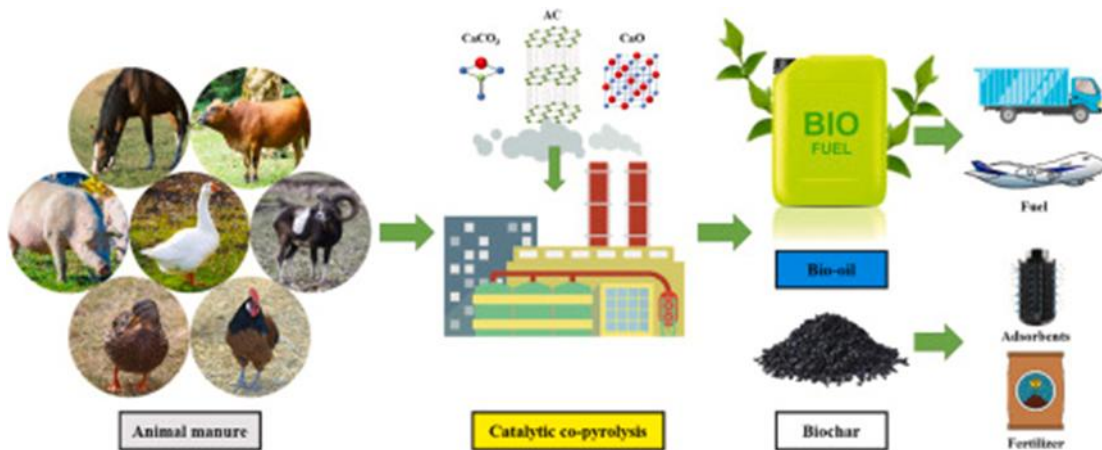


Figure 3. Utilization of animal manure through pyrolysis for bioenergy.

- **Municipal Solid Waste (MSW):** The organic fractions of MSW can be converted into energy through anaerobic digestion or incineration, including food waste and green waste.

Municipal and solid waste comprise a diverse range of materials that can be recycled, all gathered without prior sorting. Besides organic waste, there are various recyclable materials included in the input. Municipal and solid waste typically ranges in density from 0.1 to 0.3 Mg/cubic meter. To develop a captivating economic concept, it's crucial to gather and consider customer details on throughput capacity, waste composition, and objectives. A strong plant's bandwidth covers a spectrum from semi-automated to fully automated solutions. A considerable amount of flexibility and stability is needed. The illustration in Figure 4 displays the process of handling municipal and solid waste.



Fig. 4. Municipal and solid waste treatment.

- **Energy Plants:** These plants are grown with the specific purpose of producing energy, such as switchgrass, miscanthus, and rapidly growing trees like poplar and willow. The depiction in Figure 5 showcases the future of energy crops



Fig. 5. Next generation energy.

3. Transformation Technologies

Biomass can be converted into energy in various technological ways:

- **Incineration:** The simplest method, incineration is the burning of biomass to produce heat. This heat can be used directly or converted into electricity.
- **Gasification:** In this process, biomass is converted into a combustible gas mixture through partial oxidation. This synthesis gas can be used for electricity generation or as a chemical feedstock.

- **Anaerobic Digestion:** Organic matter is broken down by bacteria in the absence of oxygen, producing biogas (a mixture of methane and carbon dioxide) and digestion products that can be used as fertilizer.
- **Pyrolysis:** Biomass is heated in the absence of oxygen to produce bio-oil, syngas and biochar. Pyrolysis is a promising technology for converting biomass into liquid fuels.
- **Fermentation:** Biomass, especially plants rich in sugar and starch, is fermented by microorganisms to produce ethanol, a widely used biofuel.

4. Environmental Impacts

The environmental impacts of biomass energy are multifaceted:

- **Carbon Neutrality:** Biomass is generally considered carbon neutral because the CO₂ released during combustion is approximately equal to the CO₂ absorbed during the growth of the biomass. However, factors such as land use changes and transportation emissions can upset this balance.
- **Deforestation and Land Use:** Large-scale production of energy crops can lead to deforestation and competition with food production, raising concerns about food security and biodiversity loss.
- **Air Quality:** Burning biomass can result in the emission of particulates, NO_x and other pollutants, which can affect air quality.
- **Waste Management:** Biomass energy can help reduce waste disposal challenges by converting waste into useful energy.

5. Biomass in Sustainable Development

Biomass plays an important role in sustainable development, especially in rural and developing regions:

- **Access to Energy:** Biomass is often the primary source of energy in rural areas, providing cooking fuel and heat. Modern biomass technologies can increase energy access and reduce health risks associated with traditional biomass use.
- **Economic Development:** Biomass production and processing can create jobs and boost local economies, especially in agricultural regions.
- **Tackling Climate Change:** As a renewable energy source, biomass can contribute to reducing greenhouse gas emissions, provided that sustainable practices are employed in its production and utilization.

6. Biomass Energy in Developing Countries

In developing countries, biomass is a critical component of energy systems and often accounts for a significant share of total energy consumption. Traditional use of biomass for cooking and heating (such as wood, dung and crop residues) is common, but this use comes with health and environmental challenges. The transition to modern biomass technologies, such as improved cookstoves, biogas plants and biomass-based electricity generation can increase energy efficiency, reduce indoor air pollution and lower greenhouse gas emissions.

7. Policies and Programs

Governments and international organizations have recognized the importance of biomass in achieving the sustainable development goals (SDGs). Policies and programs that promote the sustainable production and use of biomass energy are vital. These include subsidies for renewable energy projects, incentives for growing energy crops, and research and development funds for advanced biomass technologies.

South-South cooperation for climate adaptation and sustainable development" was authored by the United Nations Conference on Trade and Development (UNCTAD). It discusses the severe impact of climate change on developing countries and proposes South-South cooperation as a viable solution for building climate resilience. The paper advocates for sharing green industrial policies and establishing a supportive trade and environment agenda at the World Trade Organization (WTO) to help these countries adapt to climate changes while achieving their sustainable development goals. It highlights successful examples of cooperation for climate mitigation and adaptation, offering valuable lessons for the Global South [8].

8. Challenges and Future Perspectives

Despite its potential, widespread adoption of biomass energy faces several challenges:

- **Technological Barriers:** Advanced biomass conversion technologies are often expensive and require significant research and development to become commercially viable.
- **Sustainability Concerns:** Ensuring that biomass production does not lead to deforestation, biodiversity loss or food insecurity is a critical challenge.
- **Infrastructure Needs:** Improving infrastructure for the collection, processing and distribution of biomass is essential to support the growth of the biomass energy sector.

However, the future of biomass energy is promising. Advances in technology and the growing need for sustainable energy solutions are likely to spur the expansion of biomass energy globally. Integrating biomass with other renewable energy sources, such as solar and wind, can also increase the resilience and sustainability of energy systems.

9. Conclusion

Biomass energy offers a versatile and renewable option to reduce dependence on fossil fuels and contribute to sustainable development. In developing countries, it plays a vital role by providing accessible, affordable and sustainable energy solutions. However, realizing the full potential of biomass energy requires addressing environmental, economic and technological challenges through comprehensive policies, sustainable practices and continuous innovation.

It highlights the importance of biomass in the global energy transition and calls for coordinated efforts to maximize the benefits of biomass while mitigating its potential downsides.

References

- [1] Smith, A., & Johnson, L. (2021). Integrating forest energy into sustainable development: Challenges and opportunities. *Renewable and Sustainable Energy Reviews*, 134, 110245. <https://doi.org/10.1016/j.rser.2020.110245>
- [2] Hakkila, P. (2003). Wood fuel from small-sized trees and cuttings in meeting Finland's energy strategy. *Journal of Sustainable Energy*, 5(2), 45-56.
- [3] Demirbas, A. (2009). Biomass feedstocks. *Biofuels: Securing the Planet's Future Energy Needs*, 45-85.
- [4] Panwar, N. L., Kaushik, S. C., & Kothari, S. (2011). Solar greenhouse an option for renewable and sustainable farming. *Renewable and Sustainable Energy Reviews*, 15(8), 3934-3945.
- [5] Arora, R., Behera, S., & Kumar, S. (2015). Bioprospecting thermophilic/thermotolerant microbes for production of lignocellulosic ethanol: a future perspective. *Renewable and sustainable energy reviews*, 51, 699-717.
- [6] McKendry, P. (2002). Energy production from biomass (part 1): overview of biomass. *Bioresource technology*, 83(1), 37-46.
- [7] Bauen, A., Berndes, G., Junginger, M., Londo, M., & Vuille, F. (2009). *Bioenergy-a Sustainable and Reliable Energy Source Main Report*.
- [8] UNCTAD, (2022). *South-South cooperation for climate adaptation and sustainable development*. United Nations Conference on Trade and Development.



Heat Transfer Analysis in a Trapezoidal Corrugated Channel with Circular Obstacles at Different Locations

Nasser Abdoul Halim ISMAEL¹ , Selma AKÇAY^{2*} , Maher Abdulhameed Sadeq SADEQ³

¹ Çankırı Karatekin University, Department of Mechanical Engineering, Çankırı, Türkiye

² Çankırı Karatekin University, Engineering Faculty, Department of Mechanical Engineering, Çankırı, Türkiye

³ Çankırı Karatekin University, Department of Mechanical Engineering, Çankırı, Türkiye

Abstract

Corrugated surfaces significantly improve heat transfer compared to straight channels [1, 2]. For this reason, these surfaces are widely used in many engineering applications, especially in heat exchangers [1-3]. It is reported that obstacles or turbulators placed inside corrugated channels increase heat transfer [4, 5]. The geometry of these obstacles and their location inside the channel significantly affect the flow and heat transfer. This study numerically analyzes the effect of circular obstacles placed at different positions in an asymmetric trapezoidal corrugated channel on the flow and heat transfer. Numerical solutions are carried out with the ANSYS Fluent program. The working fluid is air. There are adiabatic straight sections at the inlet and outlet of the channel. Trapezoidal corrugated surfaces are maintained at a constant temperature ($T_w=340K$). The study was applied for three different locations of circular obstacles (t : 7 mm, 9 mm and 11 mm) and four different Reynolds numbers (Re : 3000, 4000, 5000 and 6000). For these parameters, channel outlet temperature (T_{out}), heat transfer coefficient (h), Nusselt number (Nu) and heat transfer enhancement ratio (ER) in the channel were obtained and the results were presented in graphs. To observe the effects of channel geometry, circular obstacles and Reynolds number on flow and heat transfer, flow and temperature contours were obtained at different parameters. As a result of the numerical study, it was observed that heat transfer increased with the increase in channel inlet velocity. It was seen that the location of circular obstacles affected the flow and heat transfer. This study showed that if appropriate parameters were selected, obstacles placed in corrugated channels could significantly increase heat transfer.

Keywords: Circular obstacle, Heat transfer, Trapezoidal corrugated channel

1. Introduction

Corrugated surfaces significantly improve heat transfer compared to straight channels [1, 2]. For this reason, these surfaces are widely used in many engineering applications, especially in heat exchangers [1-3]. It is reported that obstacles, turbulators or winglets placed inside corrugated channels increase heat transfer [4, 5]. Geometries of these obstacles and their locations inside the channel significantly affect the flow and heat transfer. For this purpose, many experimental and numerical studies have been carried out. The results of these studies have shown that the geometric structure and location of the turbulators or winglets added to the channel change the heat transfer behavior. [6].

Uysal and Akçay [3] conducted a numerical study on flow and heat transfer behaviour in hybrid corrugated channels and reported that the hybrid corrugated channels improved the heat transfer compared to the uniform wave geometry. Zheng et al. [4] carried out a numerical work investigating the effects of the vortex generators with different geometries on flow and heat transfer and reported that the fluid flow and heat transfer significantly changed by the geometries of the vortex generations. Brodniansk'a, & Kot'smíd [5] examined the heat transfer improvement in a new type of wavy channel heat exchanger with circular cylinders. They found that the circular vortex cylinders significantly enhanced heat transfer. Also, they reported that the heat transfer in wavy channels was increased by 1.98 times compared to the straight channel. In a numerical study, Akçay [6] investigated the flow and heat transfer characteristics of winglets placed at the center of a zigzag wavy channel. It was reported that the channel geometry and winglets have a significant effect on improving the heat transfer.

The shape of the wave profile, the geometry of the turbulators added into the channel, their locations, flow and fluid conditions affect the flow and heat transfer [7, 8]. Due to the many parameters to be examined, new research is needed. Therefore, in this study, effects on the flow and heat transfer of the different locations of

* Corresponding author. e-mail address: selmaakcay@karatekin.edu.tr

circular obstacles in an asymmetric trapezoidal wavy channel were numerically examined for turbulent flow regime.

2. Materials and Methods

2.1. Numerical geometry

In Figure 1 is given the geometry of the asymmetric trapezoidal duct with circular obstacles used in the study. There are adiabatic straight parts with a length of $L_1 = 100$ mm at the inlet and outlet of the duct. The asymmetric trapezoidal duct part (L_2) is heated. This part is kept at a constant temperature of 340 K. Circular cylinders are placed inside the wavy duct. Analyses were performed for three different locations of circular obstacles (t : 7 mm, 9 mm and 11 mm). The dimensions of the geometric parameters of the numerical model are indicated in Figure 1.

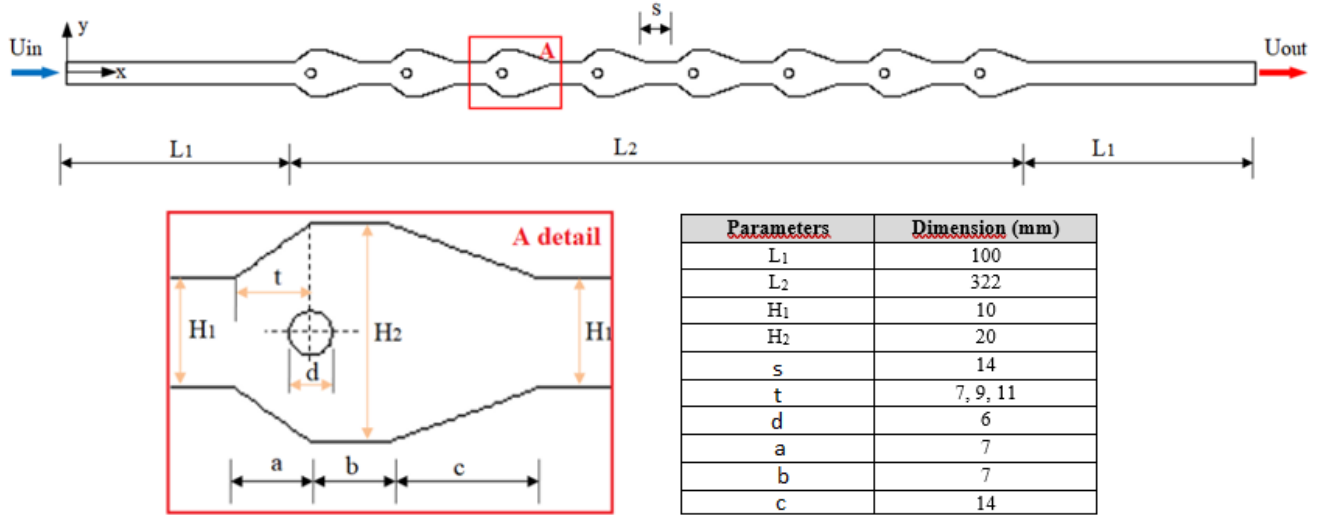


Figure 1. Geometry of the numerical model (with details)

2.2. Governing equations

In present study, the flow field is two dimensional (2d). Working fluid is air. Air is considered incompressible, single-phase and Newton type. The working fluid flows in turbulent regime and steady case. Viscous terms are ignored. It is assumed that the thermophysical properties of the fluid do not change with temperature and pressure. The effects of radiation and gravity are neglected. The governing equations are given below:

$$\frac{\partial}{\partial x_i}(\rho \bar{u}_i) = 0 \quad (1)$$

$$\frac{\partial}{\partial t}(\rho \bar{u}_i) + \frac{\partial}{\partial x_j}(\rho \bar{u}_i \bar{u}_j) = -\frac{\partial \bar{p}}{\partial x_i} + \frac{\partial}{\partial x_j} \left[\left(\mu + \mu_t \right) \left(\frac{\partial \bar{u}_i}{\partial x_j} + \frac{\partial \bar{u}_j}{\partial x_i} \right) \right] - \rho \overline{u'_i u'_j} \quad (2)$$

$$\frac{\partial}{\partial t}(\rho c \bar{T}) + \frac{\partial}{\partial x_j}(\rho \bar{u}_j \bar{T}) = \frac{\partial}{\partial x_j} \left[\left(\Gamma + \Gamma_t \right) \left(\frac{\partial \bar{T}}{\partial x_j} \right) \right] \quad (3)$$

$$-\rho \overline{u'_i u'_j} = (\mu_t) \left(\frac{\partial u_i}{\partial x_j} + \frac{\partial u_j}{\partial x_i} \right) \quad (4)$$

$$\frac{\partial}{\partial t}(\rho k) + \frac{\partial}{\partial x_i}(\rho k \bar{u}_i) = \frac{\partial}{\partial x_j} \left[\left(\mu + \frac{\mu_t}{\sigma_k} \right) \frac{\partial k}{\partial x_j} \right] + G_k - \rho \varepsilon \quad (5)$$

$$\frac{\partial}{\partial t}(\rho \varepsilon) + \frac{\partial}{\partial x_i}(\rho \varepsilon \bar{u}_i) = \frac{\partial}{\partial x_j} \left[\left(\mu + \frac{\mu_t}{\sigma_\varepsilon} \right) \frac{\partial \varepsilon}{\partial x_j} \right] + C_{1\varepsilon} \frac{\varepsilon}{k} G_k - C_{2\varepsilon} \rho \frac{\varepsilon^2}{k} \quad (6)$$

In this study, the heat transfer in the asymmetric trapezoidal wavy duct with different locations of circular obstacles was investigated at different Reynolds numbers (Re: 3000, 4000, 5000 and 6000).

2.3. Numerical procedure and boundary conditions

The numerical study was carried out with the ANSYS Fluent program, which solves with a finite volume approach. The standard k- ϵ turbulence model was used as the viscous flow model. Governing equations were discretized with the finite volume approach and the velocity-pressure relationship was solved with the SIMPLE algorithm. The convergence criterion was as 10^{-7} for the energy equations and 10^{-4} for the other equations. For the mesh independence testing, the Nusselt numbers were calculated for different element numbers. As a result of mesh independence testing, it was determined that 169134 element numbers (for the channel without obstacles) are sufficient for the solutions. The mesh structure of the numerical model is given in detail in Figure 2.

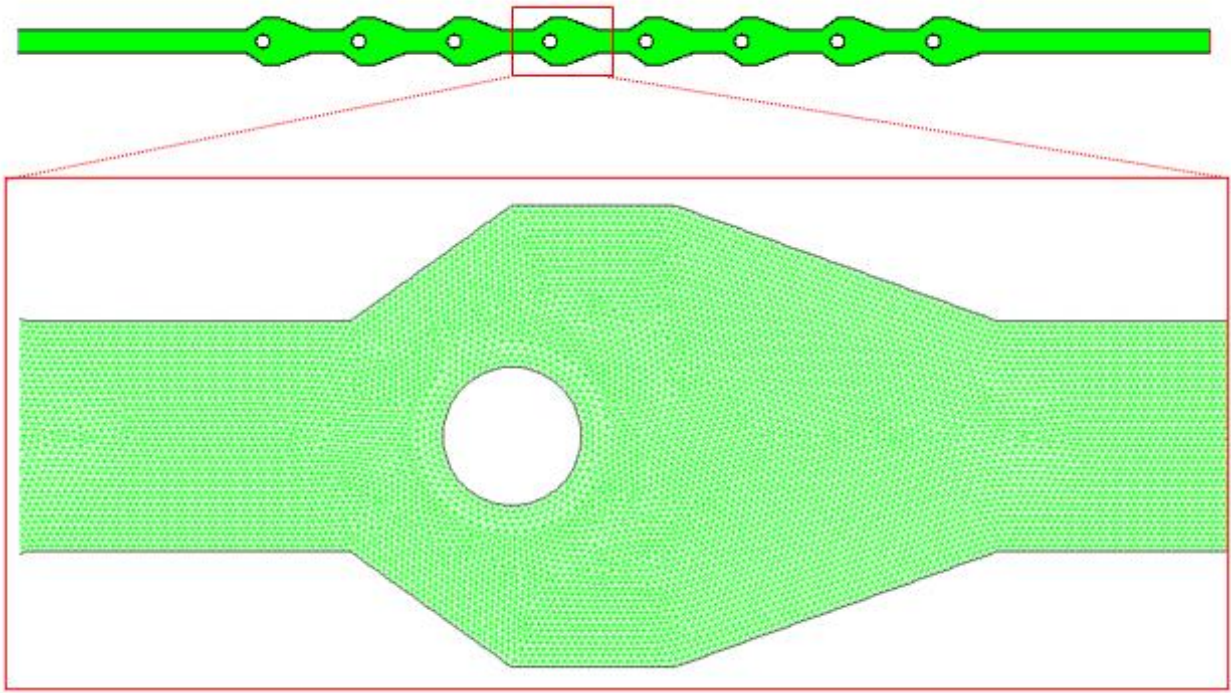


Figure 2. Element structures of the numerical model (with details)

The working fluid enters the channel at a constant velocity (U_{in}) and temperature ($T_{in}=293$ K). In the study, Reynolds number varied in the range of $3000 \leq Re \leq 6000$. The surfaces of the wavy duct (L_2) were kept constant at $T_w=340$ K. The non-slip wall condition is defined for the all walls. The circular obstacles are assumed to be adiabatic and non-slip conditions. The straight parts at the inlet and outlet of the channel are adiabatic.

2.4. Mathematical Model

The Reynolds number (Re) is given by Equation (7):

$$Re = \frac{\rho U_{in} D_h}{\mu} \quad (7)$$

where, D_h is the hydraulic diameter, ρ is the density, μ is the dynamic viscosity, and U_{in} is the inlet velocity.

The average Nusselt number (Nu) is calculated by Equation (8):

$$Nu = \frac{h D_h}{k_f} \quad (8)$$

where, h and k_f are convective heat transfer coefficient and thermal conductivity, respectively.

$$h = \frac{q''}{\Delta T_{log}}$$

where, q'' and ΔT_{\log} are heat flux and logarithmic temperature difference, respectively.

Logarithmic temperature difference is calculated by Equation (9):

$$\Delta T_{\log} = \frac{[(T_w - T_{out}) - (T_w - T_{in})]}{\ln \left[\frac{(T_w - T_{out})}{(T_w - T_{in})} \right]} \quad (9)$$

where, T_{in} , T_{out} , and T_w represent the inlet and outlet temperatures of the fluid and the temperature of the wavy surface, respectively.

The heat transfer enhancement ratio (ER) is described with Equation (10).

$$ER = \frac{Nu_w}{Nu_o} \quad (10)$$

where, Nu_w shows the Nusselt number obtained in the asymmetric trapezoidal wavy duct with circular obstacles, and Nu_o indicates the Nusselt number obtained in the asymmetric trapezoidal wavy duct without circular obstacles.

Results and Discussion

2.5. Validation of the numerical results

The numerical results obtained in this work were validated with the results of previous studies. Wang et al. [9] experimentally investigated heat transfer for the turbulent flow case of air in a straight duct. Figure 3 shows the comparison of the results of this study and Wang et al. [9].

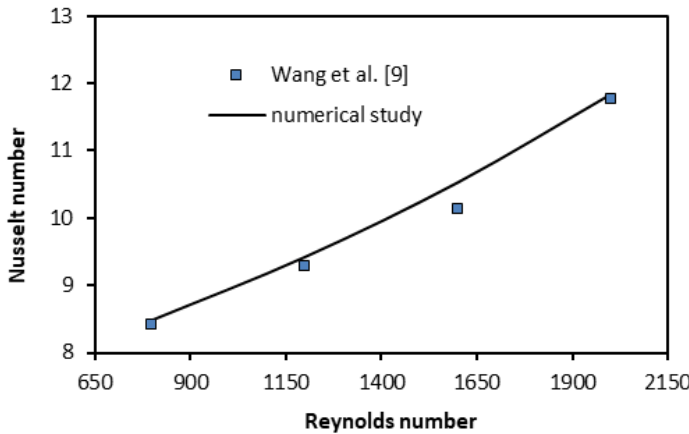


Figure 3. Validation of the numerical study

In this study, the velocity, temperature and turbulent kinetic energy contours were obtained to indicate the effects on flow and heat transfer of different locations of the circular obstacles in the asymmetric trapezoidal wavy duct. The contour images were also compared for the case without circular obstacles ($t=0$).

Figure 4 presents the velocity contours in different locations of the circular obstacles for $Re=6000$. The circular obstacles in the wavy channel affected the flow fields. The presence of stagnant fluid regions in the wavy cavities in the channel where there are no circular obstacles is noteworthy. It was observed that the fluid contacted the wavy surfaces better at $t = 7$ mm of the obstacle position. The shift of the obstacles in the flow direction increased the stagnant fluid area in the trapezoidal cavity. It was also observed that the flow passing around the circular obstacles converged at a longer distance at $t = 7$ mm and at a shorter distance at $t = 11$ mm.

In Figure 5 indicates the temperature contours in different locations of the circular obstacles for $Re=6000$. The locations of the circular obstacles significantly affected the temperature distributions. It was observed that the temperature gradient in the channel without obstacles ($t=0$) was higher than in the channel with obstacles. In channels with obstacles, the temperature gradient was increased by shifting the circular obstacles towards the flow direction. It seen that the temperature gradient of the obstacles at $t=7$ mm position was lower than that at $t=11$ mm position.

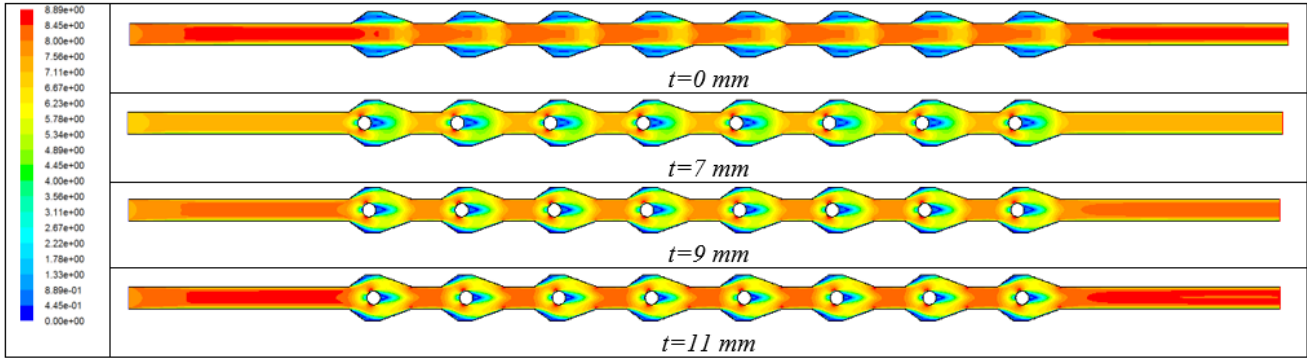


Figure 4. Velocity contours for different locations of the circular obstacles at $Re=6000$

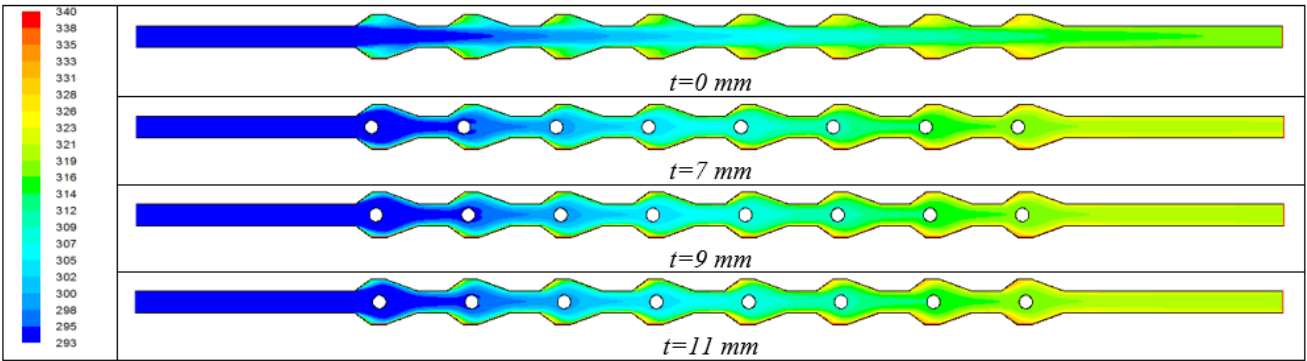


Figure 5. Temperature contours for different locations of the circular obstacles at $Re=6000$

Figure 6 indicates turbulent kinetic energy contours in the asymmetric trapezoidal wavy duct with different locations of circular obstacles for $Re=6000$. In the channel without circular obstacles, a significant increase in kinetic energy is observed in trapezoidal cavities. In channels with circular obstacles, an increase in kinetic energy is observed around circular obstacles. The shift of circular obstacles in the flow direction has increased the area where turbulent kinetic energy is effective.

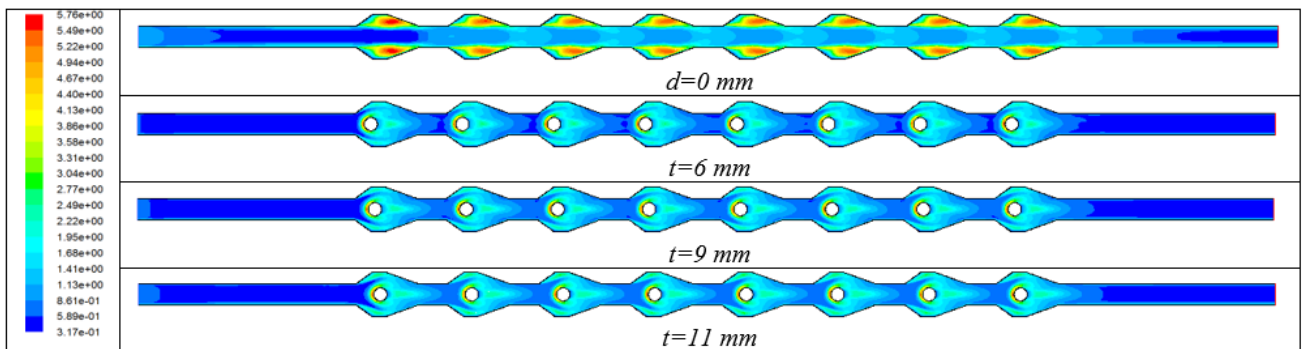


Figure 6. Turbulent kinetic energy contours for different locations of the circular obstacles at $Re=6000$

Figure 7 presents the outlet temperature of the fluid (a), heat transfer coefficient (W/m^2K) (b), Nusselt number (c), and heat transfer enhancement ratio (d) with Reynolds number for the asymmetric trapezoidal wavy duct with/without obstacles. It was seen that the outlet temperature decreased with increasing Reynolds number for all channel cases. The highest outlet temperature was found in the channel with $t=7$ mm obstacle location (Fig. 5a). Increasing Re increased the heat transfer coefficient in all channel flows. The highest heat transfer coefficient was obtained to be $h = 51.06 W/m^2K$ in the obstacle location of $t=7$ mm (Fig. 5b). Increasing Re also increased the Nusselt number in all ducts. It is seen that the higher Nusselt number is found to be $Nu = 34.47$ in the obstacle location of $t=7$ mm (Fig. 5c). In Figure 5d, the channel without obstacles is taken as reference and the effects of different obstacle locations on heat transfer enhancement ratio are calculated. Heat

transfer enhancement ratio decreased with increasing obstacle locations. At $Re=6000$, heat transfer in the obstacle location of $d=7$ mm increased by 1.27 times compared to the channel without obstacles (Fig. 5d).

As seen in Figure 7, the channel outlet temperature, heat transfer coefficient, Nusselt number and heat transfer enhancement ratio obtained at the $t=7$ mm obstacle location caused a more significant change compared to the other obstacle locations ($t=9$ mm and $t=11$ mm). The outlet temperature of the channel, heat transfer coefficient, Nusselt number and enhancement rate values obtained at the $t=9$ and $t=11$ mm obstacle locations were found to be very close to each other.

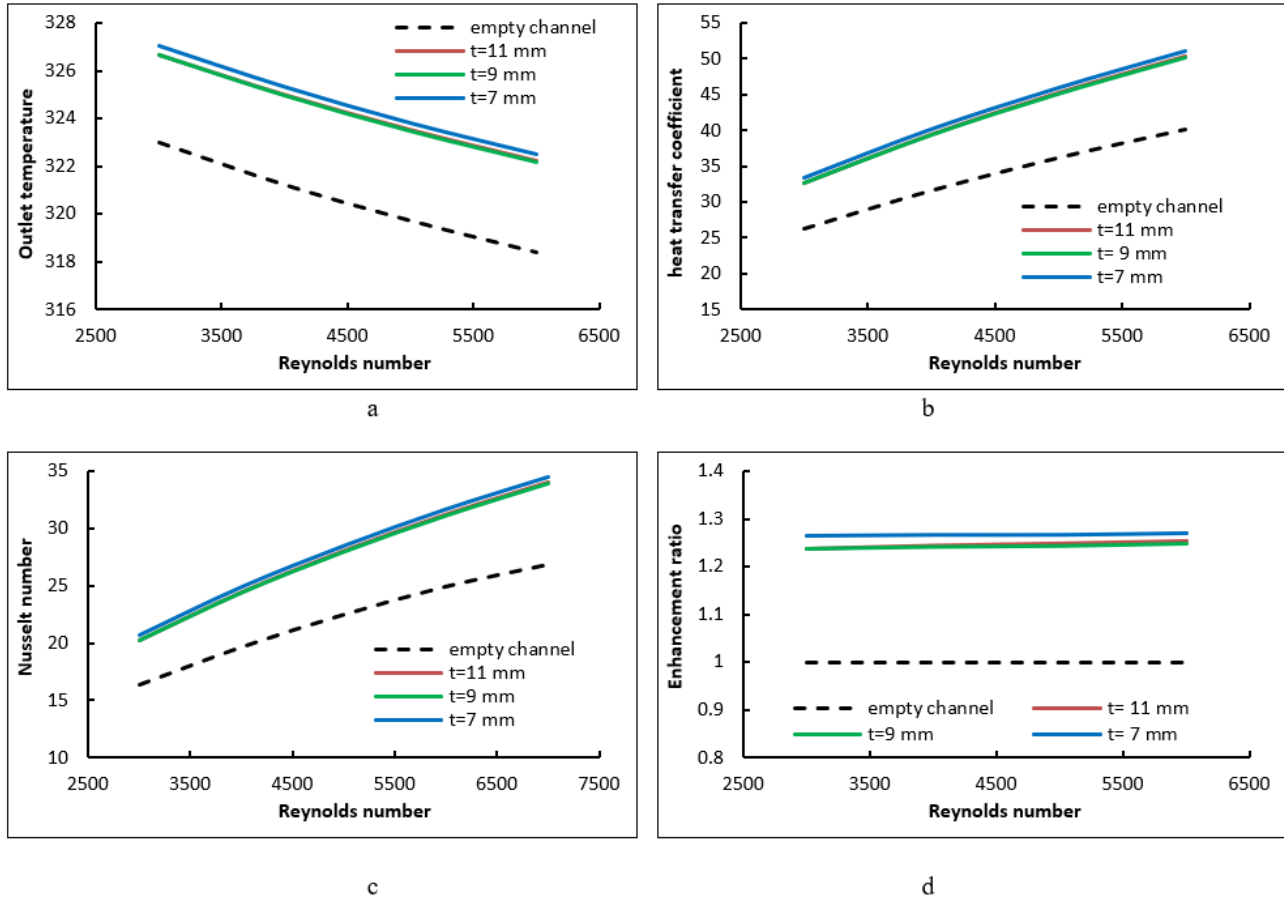


Figure 7. a- Outlet temperature, b- Heat transfer coefficient (W/m^2K), c- Nusselt number, d- Enhancement ratio with Reynolds number

3. Conclusion

In this study, the effects of locations of the circular obstacles on the flow and heat transfer in an asymmetric trapezoidal wavy channel were numerically investigated under turbulent flow regime. The analyses were conducted for different locations of circular obstacles and Reynolds numbers in the range of $3000 \leq Re \leq 6000$. In the study, the channel outlet temperature (T_{out}), heat transfer coefficient (h), Nusselt number (Nu) and heat transfer enhancement ratio (ER) obtained for different parameters were given as graphs. The velocity, temperature and turbulent kinetic energy contours were presented in the channel. The main results were given below:

- The locations of the circular obstacles added to the channel affected the flow and heat transfer.
- The outlet temperature of the channel decreased with increasing Reynolds number for all channel flows. The highest outlet temperature was obtained in the channel with $t=7$ mm obstacle location.
- Increasing Reynolds number increased the heat transfer coefficient in all channel flows. The highest heat transfer coefficient was found in the obstacle location of $t=7$ mm.

- Increasing Reynolds number increased the Nusselt number in all cases. It is seen that higher heat transfer was provided in $t=7$ mm obstacle location.
- The heat transfer enhancement ratio decreased with the shift of circular obstacles in the flow direction. At $Re=6000$, the heat transfer in the obstacle location of $t=7$ mm increased by 1.27 times compared to the channel without obstacles.
- The outlet temperature of the channel, heat transfer coefficient, Nusselt number and enhancement ratio obtained at the $t=9$ and $t=11$ mm obstacle locations were found to be very close to each other.

Acknowledgement

In this study, the financial support was provided by The Scientific and Technological Research Council of Turkey (TUBITAK), Project No: 1919B012319076 (2209A, University Students Research Projects Support Program, 2023-2). All numerical work was conducted in Çankırı Karatekin University Computer Laboratory. The authors would like to thanks to all supporters due to their precious contributions.

References

- [1] Alam, T., & Kim, M. H. (2018). A comprehensive review on single phase heat transfer enhancement techniques in heat exchanger applications. *Renewable and Sustainable Energy Reviews*, 81, 813-839.
- [2] Zhang, J., Zhu, X., Mondejar, M. E., & Haglind, F. (2019). A review of heat transfer enhancement techniques in plate heat exchangers. *Renewable and Sustainable Energy Reviews*, 101, 305-328.
- [3] Uysal, D., & Akçay, S. (2024). Numerical study of thermal and hydrodynamic characteristics of turbulent flow in hybrid corrugated channels with different wave profiles. *Journal of Mechanical Engineering and Sciences*, 18(2), 10026–10045.
- [4] Zheng, Y., Yang, H., Mazaheri, H., Aghaei, A., Mokhtari, N., & Afrand, M. (2021). An investigation on the influence of the shape of the vortex generator on fluid flow and turbulent heat transfer of hybrid nanofluid in a channel. *Journal Thermal Analysis and Calorimetry*, 143,1425–1438.
- [5] Brodniansk'a, Z., & Kot'smíd, S. (2023). Heat transfer enhancement in the novel wavy shaped heat exchanger channel with cylindrical vortex generators. *Applied Thermal Engineering*, 220, 119720.
- [6] Akcay, S. (2023). Numerical analysis of hydraulic and thermal performance of Al_2O_3 -water nanofluid in a zigzag channel with central winglets, *Gazi University Journal of Science*, 36 (1), 383-397.
- [7] Akcay, S. (2021). Investigation of thermo-hydraulic performance of nanofluids in a zigzag channel with baffles. *Adıyaman Üniversitesi Mühendislik Bilimleri Dergisi*, 8(15), 525-534.
- [8] Akcay, S. (2022). İçerisinde dik bölmeler bulunan trapez bir kanalda bölme yüksekliğinin akış ve ısı transferine etkisinin incelenmesi. *Bitlis Eren Üniversitesi Fen Bilimleri Dergisi*, 11 (2), 479-490.
- [9] Wang, G., Qia, C., Liu, M., Li, C., Yan, Y., & Liang, L. (2019). Effect of corrugation pitch on thermo-hydraulic performance of nanofluids in corrugated tubes of heat exchanger system based on exergy efficiency. *Energy Conversion and Management*, 186, 51–65.



Lithium Ion Batteries: Battery Failure & Fire and Intervention Methods for Battery Fire in Electrical Vehicles

Sezgin YAŞA^{1,*} , Sedat BARUTCU²

¹ Engineering Faculty, Mechanical Engineering Department, Çankırı Karatekin University, Çankırı, Türkiye

² Social Sciences Vocational School, Civil Defense and Firefighting Program, Çankırı Karatekin University, Çankırı-Türkiye

Abstract

Lithium-ion batteries (LiBs) are widely used and especially with the widespread use of electric vehicles, the use of LiBs are increasing. Lithium-ion batteries simply consist of anode, cathode, electrolyte, separator and current collectors such as copper and aluminum. LiBs are intricate industrial products that may cause mistakes in design, manufacture, and usage, which can result in safety incidents. To improve battery safety, it's critical to have a thorough understanding of the failure mechanisms that might arise in different scenarios. In particular, the types of damage that can occur can be classified as mechanical damage, thermal damage and electrical damage. Another important issue is the intervention method to be applied to lithium-ion batteries after the damage occurs. In the scope of this study, the structure of LiBs, LiB types, the types of damage that can occur in LiBs used in electric vehicles in particular and the methods of intervention in possible fires will be discussed.

Keywords: Li-ion Battery, Failure, Battery Fire, Intervention

1. Introduction

In contrast to other rechargeable systems, lithium ion batteries (LIBs) have dominated the energy sector because of their unparalleled qualities, which include a high energy density, a small size, and the capacity to fulfill a variety of performance requirements. Li-ion battery research is being conducted extensively by both government organizations and businesses in an effort to create an economy that is energy-sustainable [1].

The anode, cathode, and electrolyte are the three main functioning parts of a lithium ion battery. In a typical lithium ion cell, the electrolyte is a lithium salt in an organic solvent, the cathode is a metal oxide, and the anode is composed of carbon. Graphite is the most often used anode material in commerce. One of three substances is often used as the cathode: a spinel (like lithium manganese oxide), a polyanion (like lithium iron phosphate), or a layered oxide (like lithium cobalt oxide). Usually, complexes of lithium ions are present in the electrolyte, which is a combination of organic carbonates like ethylene carbonate (EC) or diethyl carbonate (DEC). Non-coordinating anion salts including lithium hexafluorophosphate (LiPF₆), lithium hexafluoroarsenate monohydrate (LiAsF₆), lithium perchlorate (LiClO₄), and lithium tetrafluoroborate (LiBF₄) are typically used in these non-aqueous electrolytes. The anode and cathode must be separated using a separator. A extremely thin sheet of plastic with tiny holes in it serves as the divider. It divides the positive and negative electrodes while permitting ions to flow through, and it is situated between the cathode and the anode [2]. The Schematic of LiB and main component of it are shown in Fig 1.

There are many types of different battery cathode materials such as; LiCoO₂ (LCO, Year introduced: 1991), LiFePO₄ (LFP, Year introduced: 1996) LiMn₂PO₄ (LMO, Year introduced: 1996) Li(Ni-Co-Al) (NCA, Year introduced: 1999) Li(Ni-Co-Mn) (NMC, Year introduced: 2008), (Fig 2) [3]. Efforts are ongoing to reduce cobalt usage in NMC due to cost and ethical concerns [4].

EV driving range is mostly determined by battery energy density, and existing Li-ion batteries, even with high densities (250 to 693 Wh L⁻¹), still can't match gasoline, underscoring the need for more development and study. With balanced energy density, power density, safety, and overall performance, NMC, LFP, and LMO are excellent options for EVs and energy storage systems [4].

* Corresponding author. e-mail address: sezginyasa@karatekin.edu.tr

Maintaining this temperature range is essential. It is highly advised to use liquid or air cooling management and monitoring systems to protect the battery, the car, and its occupants [6].

Battery casing damage, cell compression, crushing, puncturing, and bending are examples of mechanical damage. Internal short circuits, excessive power output (high C-rate), overcharging, and overdischarging can all result in electrical damage. Both self-heating and heating from an external heat source are examples of thermal damage. In the event of mechanical damage, the separator may rupture as a result of battery deformation. The separator may be punctured by dendritic development in the battery in the event of electrical damage. The separator may collapse in cases of thermal damage due to the high internal heat produced in the battery [6].

Thermal failure can also be brought on by external overheating and high ambient temperatures, in addition to overheating brought on by electrical or physical causes. Rapid increases in battery temperature due to thermal variables can result in a number of problems, including the melting of the membrane, the breakdown of electrodes and electrolytes, and a host of adverse effects [7].

Notably, the separator is compromised in each of the three damage situations. When the separator is damaged, the insulation between the anode and the cathode is removed, allowing electrons to flow and creating a short circuit that may ignite a fire [6].

Exothermic electrochemical reactions can cause a rapid rise in temperature, which influences aging, cell deterioration, and the kinetics of electrochemical processes. Strict temperature management hence prolongs battery life and gets rid of undesirable circumstances like thermal runaway and layer deterioration. Thermal runaway and overheating are two unavoidable and dangerous scenarios that threaten high-performance battery systems. To maintain the peak temperature level below the critical temperatures, the battery thermal management systems must meet the requirements for uniform temperature distribution and thermal control [8].

Fig. 3 shows how a battery failure in a LiB used in an electric vehicle develops and the stages that develop as a result of the fire. It is seen that even in the event of extinction, the battery can continue to burn again. The main reason for this is that the battery contains a large number of cells and the other cells are affected by the exposure and the combustion continues as they start to burn.

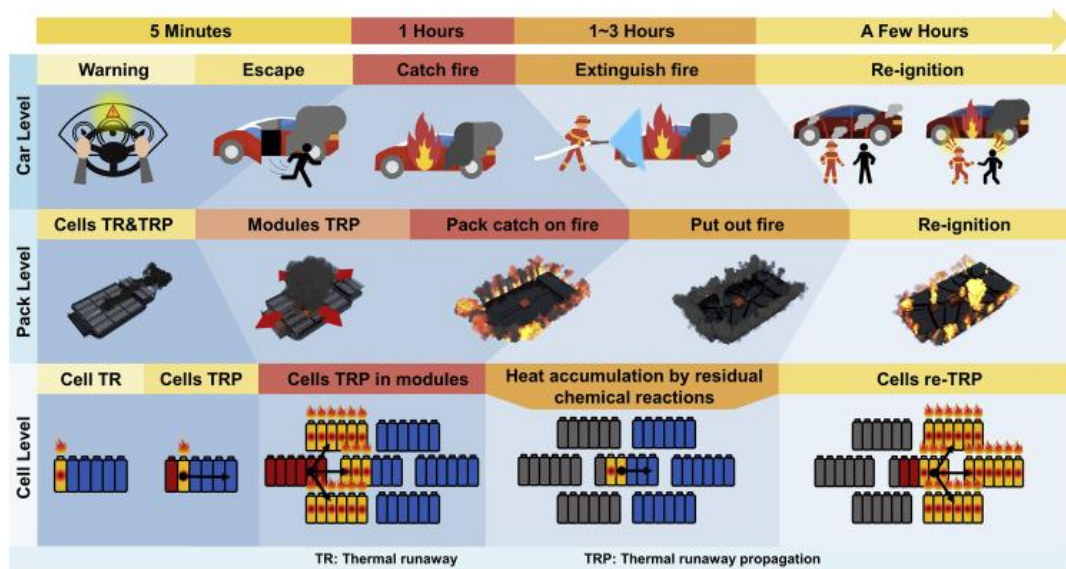


Figure 3. The Mechanism of Accidents in Electric Vehicles Associated with Battery Failure [9]

3. Intervention Methods for Battery Fire in Electrical Vehicles

When the oxidation level in the lithium-ion battery is examined, especially in battery fires, very different intervention methods are used.

Although there are few literature studies, some step inferences have been formed from the events experienced and the experiences gained. The findings made from these inferences; It is quite difficult and difficult to bring together the controls of these products when nitrogen-ion batteries burn and change as a result of this burning, it is revealed that a lot of extinguishers are needed to extinguish explosions and that a re-ignition is likely to occur no matter what. First of all, in order to cool down an electric vehicle fire that has occurred for any reason, the extinguishing equipment called a fire blanket is laid in such a way that the top of the vehicle is completely covered. Although electric vehicles are not as complex as internal combustion engines with atmospheric engines in terms of mechanics, they pose many risks when the risks they pose are taken into consideration. Fire departments are trying to eliminate many risks by developing intervention methods within the possibilities [10].

Some hazards and intervention status for safe operation;

- Risks posed by high voltage hazards
- Risks posed by fire situation and safe intervention
- Effects of fire extinguishing kits
- Application of protective fire blanket before battery extinguishing
- Continuous monitoring of temperature values with thermal camera

4. Conclusion

The number of electric vehicles in particular has been rapidly increasing in the world and in our country in recent years. Therefore, it is inevitable that we will see more electric vehicles around us as time goes by. Therefore, battery safety systems in electric vehicles and the method of intervention in case of any battery fire will gain more importance. In this study, the structure of battery systems, error and fire mechanisms and the method of intervention in case of any battery fire that may occur are emphasized. In particular, the production of effective solutions on the safety of battery systems and the methods of intervention in case of any error and fire that may occur is an important necessity.

References

- [1] G. Kaur, B.D. Gates, Review — Surface Coatings for Cathodes in Lithium Ion Batteries : From Crystal Structures to Electrochemical Performance Review — Surface Coatings for Cathodes in Lithium Ion Batteries : From Crystal Structures to Electrochemical Performance, *J. Electrochem. Soc.* 169 (2024) 043504. <https://doi.org/10.1149/1945-7111/ac60f3>.
- [2] Q. Wang, P. Ping, X. Zhao, G. Chu, J. Sun, C. Chen, Thermal runaway caused fire and explosion of lithium ion battery, *J. Power Sources* 208 (2012) 210–224. <https://doi.org/10.1016/j.jpowsour.2012.02.038>.
- [3] G. Harper, P. Slater, R. Stolkin, A. Walton, P. Christensen, O. Heidrich, Recycling lithium-ion batteries from electric vehicles, *Nature* 575 (2019) 75–86. <https://doi.org/10.1038/s41586-019-1682-5>.
- [4] A.K. Koech, G. Mwandila, F. Mulolani, P. Mwaanga, South African Journal of Chemical Engineering Lithium-ion battery fundamentals and exploration of cathode materials : A review, *South African J. Chem. Eng.* 50 (2024) 321–339. <https://doi.org/10.1016/j.sajce.2024.09.008>.
- [5] Y. Yang, R. Wang, Z. Shen, Q. Yu, R. Xiong, W. Shen, Towards a safer lithium-ion batteries: A critical review on cause, characteristics, warning and disposal strategy for thermal runaway, *Adv. Appl. Energy* 11 (2023) 100146. <https://doi.org/10.1016/J.ADAPEN.2023.100146>.
- [6] M.İ. Karamangil, A. Sürmen, M. Tekin, Elektrikli Araçlarda Batarya Yangınlarına Genel Bakış, *Uluslararası Yakıtlar Yanma Ve Yangın Derg.* 11 (2023) 29–40. <https://doi.org/10.52702/fce.1224612>.
- [7] M. Buldu, S. Altın, F. Bulut, Lityum İyon Bataryaları İçin Güvenlik Riskleri ve Çözüm Önerileri, *J. Sustain. Eng. Appl. Technol. Dev.* 7 (2024) 131–142.

- <https://doi.org/10.51764/smutgd.1511977>.
- [8] S. Gungor, S. Gocmen, E. Cetkin, A review on battery thermal management strategies in lithium-ion and post-lithium batteries for electric vehicles, J. Therm. Eng. 9 (2023) 1078–1099. <https://doi.org/10.18186/thermal.1334238>.
- [9] W. Huang, X. Feng, X. Han, W. Zhang, F. Jiang, Questions and Answers Relating to Lithium-Ion Battery Safety Issues, Cell Reports Phys. Sci. 2 (2021) 100285. <https://doi.org/10.1016/j.xcrp.2020.100285>.
- [10] Tengilimoğlu E. S., & Barutcu S. (2024), *Sosyal Bilimler, Elektrikli Araçlardaki Yangına Müdahale Stratejilerinin Belirlenmesi; İtfaiye Teşkilatlarının Hazırlık Seviyeleri*, Afyonkarahisar, Türkiye, YAZ yayınları



Health Professional Doulas Interventions And Birth Style: A Pilot Study

Engin DİNÇ¹ , Tuğba ARSLAN^{2,*} , Serdar ARSLAN³

¹Department of Public Health Services, Konya Provincial Health Directorate, Konya, Türkiye

²Faculty of Health Sciences, Department of Occupational Therapy, Çankırı Karatekin University, Çankırı, Türkiye

³Nezahat Keleşoğlu Faculty of Health Sciences, Department of Physiotherapy and Rehabilitation, Necmettin Erbakan University, Konya, Türkiye

Abstract

The aim of the study was to examine the selection rate of interventions performed by health professional doulas and the types of births accompanied by doulas. The universe of the study consisted of birth records where vaginal birth was planned by the physician and the pregnant woman and where births were accompanied by a doula (N=49). 47 records kept by professional doulas were retrospectively analysed. The variables of the study were the techniques applied by the doula and the mode of delivery. Of the births accompanied by a doula, 44 (93.6%) were vaginal, 2 (4.3) were cesarean, and 1 (2.1%) was vaginal after cesarean. Doulas used medical techniques more than communication techniques or complementary techniques. The most common practices used by mothers to facilitate labor were breathing exercises and massage. The least preferred practices were music and shower. It was determined that approximately half of the pregnant women were nulliparous and that the doula practices performed according to the type of birth were similar. The number of cesarean sections and vaginal births after cesarean sections, which are too low to be statistically calculated, are clinically significant outcomes. This research is also important because it presents the content and effects of free services provided in a public hospital.

Keywords: Doulas, Parturition, Vaginal Birth after Cesarean

1. Introduction

From antiquity to the present day, there have been individuals who have provided assistance to women during childbirth. In the present era, births occur in a hospital setting, with support provided by a multidisciplinary team of health professionals, family members offering spiritual support to the expectant mother, and trained doulas. To supplement the assistance provided by hospital personnel and family members, an increasing number of women in labor are opting to utilize the services of doulas [1]. Doulas receive training in order to provide emotional and physical support to women and their partners throughout the stages of pregnancy, labour and the postpartum period. While some doulas possess a background in nursing or midwifery, the majority of them are women with no previous healthcare training [2]. Doulas provide spiritual support to the expectant mother before, during and after birth, employing a range of techniques to facilitate the birthing process and enhance the quality of life for the expectant mother. These techniques encompass breathing exercises, massage, positional changes, aromatherapy, point pressure techniques, meditation, imagery, and the use of water. A substantial body of evidence attests to the advantages of intrapartum doula care, including a reduced likelihood of caesarean section and a shorter duration of labour. In one study, it was emphasised that bathing, massage, touching, changing position, moving and walking were found to reduce labour pain and increase satisfaction with labour [3]. In the Cochrane review, it was emphasised that walking and standing in the first stage of labour in pregnant women shortened the duration of labour by approximately one hour, reduced the need for caesarean section and epidural, and it was reported that walking and standing had no adverse effects on maternal and neonatal health [4]. A review highlighted the necessity for a more comprehensive integration of doula care into the existing maternity care system, accompanied by an increase in the reimbursement rates for doula services [5]. The aim of the study was to examine the selection rate of interventions performed by health professional doulas and the types of births accompanied by doulas.

* Corresponding author. e-mail address: tugbaarslan@karatekin.edu.tr

2. Materials and Methods

The study was conducted in a retrospective descriptive manner. In order to enhance the quality of care provided during vaginal births, midwives with undergraduate degrees were provided with in-service training by the Konya Public Health Presidency. These midwives were then assigned to provide supportive interventions and continuous care alongside the midwife responsible for medical intervention. The birth records examined included births that occurred at Dr. Ali Kemal Berivanlı Gynecology and Obstetrics Hospital between January 01 and January 31, 2019. The universe of the study consisted of birth records where vaginal birth was planned by the physician and the pregnant woman and where births were accompanied by a doula (N=49). Among these women, all of those who met the following criteria constituted the sample of the study. The inclusion criteria were labour delivery (36-42 weeks of gestation), fetus with head presentation. The exclusion criteria were high-risk pregnancy, multiple pregnancies, and a caesarean section decided by the physician in charge at the time of application. Two birth records were excluded from the study because the gestational age was less than 36 weeks. 46 birth records with doulas were examined.

Data Collection Methods

Records kept by professional doulas were retrospectively analysed. The variables of the study were the techniques applied by the doula and the mode of delivery.

Data Analysis

All data are presented in numerical and percentage form. In the planning of the study, the birth records of nulliparous pregnant women were grouped as vaginal and caesarean. The practices of doulas were to be compared with the chi-square test; however, this was not done due to the lack of sufficient data, with only one birth being recorded via caesarean.

Ethical Considerations

Ethical approval for the research was obtained from Çankırı Karatekin University Ethics Committee (unique decision code: fedf8ef36abb4e53).

3. Results

In this birth records the number of pregnant women with 0 births was 23 (48.9%). Of the births accompanied by a doula, 44 (93.6%) were vaginal, 2 (4.3%) were caesarean, and 1 (2.1%) was vaginal after caesarean. The neonatal mortality rate was determined as 1 (2.1%). The average time the doula accompanies the pregnant woman is 273.15 ± 158.27 minutes. When the practices of the doulas were analysed, a total of 37 women (78.7%) received massage treatments on the lower abdomen, sacral region, upper thighs, shoulders and legs. 42 doulas (89.4%) performed controlled breathing exercises with pregnant women. 28 (59.6%) doulas performed practices that enabled the pregnant women to be active such as squatting, kneeling, standing and pelvic tilt on a Swiss ball. A total of 10 (21.3%) pregnant women underwent acupressure, which is defined as the constant stimulation of acupuncture points using the fingertips, thumb, joints, or a suitable acupuncture instrument. A total of 13 (27.7%) pregnant women were provided with the opportunity to relax by listening to the music or sounds of their choice during the course of their labour. Eighteen percent 18(38.3%) of doulas conducted progressive relaxation training during the latent phase of labour. A total of 13(27.7%) of pregnant women were provided with a hot shower. As there was no data available on the previous mode of delivery for multiparous pregnant women, it was not possible to analyse the effect of the doula's practices on the mode of delivery. For this reason, the birth records of nulliparous pregnant women were grouped as vaginal (n=22) and caesarean (n=1). Doula practices were examined and it was determined that massage, breathing, active positions, muscle relaxation and music were applied to this pregnant woman who gave birth via caesarean section. Despite this, the birth was via caesarean section due to narrow pelvis.

4. Discussion

In this study, birth records were examined with a midwife responsible for medical care and a midwife working as a professional doula. It was found that the majority of the births were vaginal and only 4.3% were caesarean. The most common practices used by mothers to facilitate labor were breathing exercises and massage. The least

preferred practices were music and shower. It was determined that approximately half of the pregnant women were nulliparous and that the doula practices performed according to the type of birth were similar. In the birth records with professional doulas, it was found that the majority of births were vaginal and only 4.3% were via cesarean section. This is an expected situation since the records examined were the records of non-high-risk pregnancies where the physician deemed vaginal birth appropriate and the pregnant woman preferred vaginal birth. The literature also suggests that the presence and support of a trained doula reduces the likelihood of cesarean birth [2,6,7]. Since there is no control group data in this study, it is not possible to make a definitive judgment on this issue. Despite this, it is undeniable that the cesarean rate in this study is quite low. The most common practices used by doulas to facilitate labor are breathing and massage. It is reported that slow and deep breathing is used during contractions in the first stage of labor and breathing associated with pushing efforts in the second stage [8]. The least preferred practices are music and shower practices. It is reported that doulas use more communicative methods such as verbal communication, eye contact, and asking client's questions [9]. In this study, more medical techniques such as breathing were used, the reason for which is that they did not report communicative approaches as a technique. Since this study was conducted by examining retrospective data records, it is not possible to know their thoughts on reporting. In this study, when nulliparous pregnant women were grouped according to the type of birth, it was determined that the practices were similar. This contradicts the research conducted. The possible effect of doula support on reducing the cesarean rate has been shown [5] and there are various studies on the effectiveness of the practices [10,11]. Professional doulas preferred the application that the pregnant woman needed during labor. This finding is expected since they are the ones who know best which techniques to use at what time. The lack of a control group in the study made it difficult to determine the effectiveness of the applications. The number of cesarean sections and vaginal births after cesarean sections, which are too low to be statistically calculated, are clinically significant outcomes. Support from doulas not only contributes to positive maternal and neonatal outcomes, but has also been shown to help reduce health disparities among women of different socioeconomic status [9]. This research is also important because it presents the content and effects of free services provided in a public hospital.

Acknowledgement

There is no financial support for the research.

References

- [1] Ireland, S., Montgomery-Andersen, R., & Geraghty, S. (2019). Indigenous Doulas: A literature review exploring their role and practice in western maternity care. *Midwifery*, 75, 52–58. <https://doi.org/10.1016/j.midw.2019.04.005>
- [2] Fortier JH, Godwin M. Doula support compared with standard care: Meta-analysis of the effects on the rate of medical interventions during labour for low-risk women delivering at term. *Can Fam Physician*. 2015 Jun;61(6):e284–92. PMID: PMC4463913.
- [3] Simkin, P. P., & O'hara, M. (2002). Nonpharmacologic relief of pain during labor: systematic reviews of five methods. *American journal of obstetrics and gynecology*, 186(5 Suppl Nature), S131–S159. <https://doi.org/10.1067/mob.2002.122382>
- [4] Lawrence, A., Lewis, L., Hofmeyr, G. J., & Styles, C. (2013). Maternal positions and mobility during first stage labour. *The Cochrane database of systematic reviews*, (10), CD003934. <https://doi.org/10.1002/14651858.CD003934.pub4>
- [5] Font, G., & Testani, E. (2020). Doula Programs Improve Cesarean Section Rate, Breastfeeding Initiation, Maternal and Perinatal Outcomes [11P]. *Obstetrics & Gynecology*, 135, 170S.
- [6] Chen, I., Opiyo, N., Tavender, E., Mortazhejri, S., Rader, T., Petkovic, J., Yogasingam, S., Taljaard, M., Agarwal, S., Laopaiboon, M., Wasiak, J., Khunpradit, S., Lumbiganon, P., Gruen, R. L., & Betran, A. P. (2018). Non-clinical interventions for reducing unnecessary caesarean section. *The Cochrane database of systematic reviews*, 9(9), CD005528. <https://doi.org/10.1002/14651858.CD005528.pub3>
- [7] Sobczak, A., Taylor, L., Solomon, S., Ho, J., Kemper, S., Phillips, B., Jacobson, K., Castellano, C., Ring, A., Castellano, B., & Jacobs, R. J. (2023). The Effect of Doulas on Maternal and Birth Outcomes: A Scoping Review. *Cureus*, 15(5), e39451. <https://doi.org/10.7759/cureus.39451>
- [8] Heim, M. A., & Makuch, M. Y. (2023). Breathing Techniques During Labor: A Multinational Narrative

- Review of Efficacy. *The Journal of perinatal education*, 32(1), 23–34. <https://doi.org/10.1891/JPE-2021-0029>
- [9] Paterno, M. T., Van Zandt, S. E., Murphy, J., & Jordan, E. T. (2012). Evaluation of a student-nurse doula program: an analysis of doula interventions and their impact on labor analgesia and cesarean birth. *Journal of midwifery & women's health*, 57(1), 28-34.
- [10] Tracy, S. K., Sullivan, E., Wang, Y. A., Black, D., & Tracy, M. (2007). Birth outcomes associated with interventions in labour amongst low risk women: a population-based study. *Women and Birth*, 20(2), 41-48.
- [11] Issac, A., Nayak, S. G., Priyadarshini, T., Balakrishnan, D., Halemani, K., Mishra, P., ... & Stephen, S. (2023). Effectiveness of breathing exercise on the duration of labour: A systematic review and meta-analysis. *Journal of global health*, 13, 04023. <https://doi.org/10.7189/jogh.13.04023>



Salt Radioactivity

Alaa MOHAMMED GHANI HASSAN^{1,*} , Hüdayi ERÇOŞKUN² 

¹ Ministry of Agriculture - Tikrit Research Department, Tikrit, Iraq

² Faculty of Engineering, Department of Food Engineering, Çankırı Karatekin University Çankırı, Türkiye

Abstract

Salt is a widely used mineral, prized for its culinary and medicinal benefits, but certain types of salt may contain natural radioactivity due to the presence of radioactive isotopes such as potassium-40 (K-40) and radon-226 (Ra-226). These isotopes contribute to background radiation, which can have varying effects depending on the salt's source. This article reviews the natural radioactivity in salt, exploring the radioactive isotopes present, their potential environmental impact, and the health implications for human consumption. While the radiation levels in most salts are low and do not pose significant health risks, prolonged exposure to high levels may cause health concerns. The paper also investigates the radioactivity levels in various salts, including Himalayan and sea salts, and concludes that the radioactive content in most salts is too low to affect human health. A balanced approach to salt consumption, with attention to its source, is advised to minimize any potential risks.

Keywords: Salt, Radioactivity, Potassium-40, Radon-226, Natural Isotopes

1. Introduction

Salt, a naturally occurring mineral compound, has been an integral part of human culture for centuries, serving both culinary and medicinal purposes. The most common form of salt, sodium chloride (NaCl), is generally regarded as safe for everyday use [1]. However, certain salts contain isotopes that may introduce natural radioactivity, raising concerns regarding their potential health effects [2]. This article delves into the radioactive properties of salt, examining its origins, the levels of radioactivity it may contain, and the potential health risks associated with such exposure.

2. Radioactive Properties of Salt

Salts primarily consist of minerals that naturally occur in the Earth's crust, many of which contain radioactive isotopes. These isotopes are the source of radiation that emanates from naturally occurring elements. Natural radioactivity results from the decay of various elements within the Earth's crust, particularly those of uranium (U), thorium (Th), and potassium-40 (K-40) [3]. These elements contribute to the radioactive properties of salts in the following ways:

- K-40 (Potassium-40): Potassium is a ubiquitous element found in nature and is naturally radioactive. Potassium-40 may be present in the composition of salts and contributes to the environmental background radiation. Although the effect of potassium-40 in salt is minimal, its absorption by the human body contributes to a slight increase in biological radiation exposure [4].
- Ra-226 (Radon-226): Radon is a radioactive gas produced from the decay of uranium found in the Earth's crust. Its release in salt mines may influence the radiation levels in nearby environments. However, these effects are usually minimal, and radon exposure from salt is rarely a cause for concern [5].

3. Radioactivity in Salt and Environmental Impacts

The radioactivity levels in salt vary significantly based on its geographical source [6]. Salt mines located in regions with uranium- and thorium-rich rocks typically exhibit higher levels of natural radioactivity due to the geological composition of the area from which the salt is extracted [7]. These areas can produce salts with elevated radiation levels that may influence both human health and the surrounding environment.

While radiation levels in most salt mines are too low to cause significant environmental harm, there are cases where the release of radioactive materials during mining operations may affect local ecosystems [8]. In general, these occurrences remain localized and pose minimal long-term risks to surrounding areas.

* Corresponding author. e-mail address: alaa.93mohammd@gmail.com

4. Effects of Salt on Human Health

The radioactive content of most salts is typically so low that it does not present a health risk. The concentration of radioactive isotopes usually falls below thresholds that would cause significant harm under normal consumption patterns [9]. However, prolonged exposure to high levels of radiation can lead to health issues over time [10].

- **Radioactive Potassium (K-40) and Human Health:** Potassium-40, a naturally occurring isotope, is found in the human body and plays a crucial role in various physiological processes. The levels of potassium-40 found in salt are far too low to pose a health risk, and the body metabolizes it without any adverse effects. Therefore, potassium-40 intake from salt is not a health concern [11].
- **Radon and Health:** Prolonged radon exposure, especially in confined spaces like salt mines, can increase the risk of lung cancer [10]. However, the radon levels typically found in salt deposits are insufficient to pose significant health risks [5]. While extended exposure to elevated radon concentrations in certain mining environments may lead to health concerns, such instances are rare and localized.

4.1. Radioactive Salts: Types of Salt with Higher Radioactivity

Certain types of salt, particularly those extracted from specific geological regions, may contain higher natural radioactivity levels. Himalayan salt and some sea salts, for example, may contain radioactive elements due to the surrounding rocks and water sources [1]. Despite these elevated radioactivity levels, the health risks associated with consuming these salts regularly remain minimal [2].

- **Himalayan Salt:** Himalayan salt is renowned for its mineral-rich composition and may contain natural radioactive isotopes. However, these levels are typically so low that they do not present any health risks [4]. Although the geological characteristics of the Himalayan region influence its radioactivity, studies suggest that the salt remains safe for human consumption due to the low concentrations of radioactive elements [8].
- **Sea Salt:** Sea salt, which is harvested through the evaporation of seawater, can contain trace amounts of natural radioactive elements [7]. The radioactivity in sea salt depends on factors such as the quality of the seawater and the extent of local pollution [3]. Despite these factors, the radioactive content in most sea salts is too low to pose any significant biological effect [5].

5. Conclusion

Salt is a naturally abundant compound that may contain trace levels of natural radioactivity, primarily from potassium-40 and other isotopes. However, the levels of radioactivity in most salts are well within safe limits and do not pose significant health risks. In fact, radiation levels in salt are generally too low to cause harm, and in most cases, they do not have any adverse effects on human health. Salt mines located in regions rich in uranium or thorium may exhibit higher levels of radioactivity, but such cases generally pose minimal environmental or health risks. It is important to consider the source and quality of salt to ensure its safety and align with healthy lifestyle practices.

Although the potential health impacts of radioactive salts are generally minimal, it remains prudent to monitor the quality of salt consumed, particularly from sources with known higher radioactivity levels. Awareness of the origin and geological context of salt can help minimize any potential health risks, ensuring a safe and informed approach to salt consumption.

References

- [1] Ercoşkun, H. (2021). Tuz ve gıda. In H. Ercoşkun (Ed.), *Her yönüyle tuz* (pp. 77-106). Nobel Akademik Yayıncılık.
- [2] Abdul Sani, S. F., Muhamad Azim, M. K., Marzuki, A. A., Khandaker, M. U., Almugren, K. S., Daar, E., Alkallas, F. H., & Bradley, D. A. (2022). Radioactivity and elemental concentrations of natural and commercial salt. *Radiation Physics and Chemistry*, 190, 109790. <https://doi.org/10.1016/j.radphyschem.2021.109790>

- [3] Ali Baloch, M., et al. (2012). A study on natural radioactivity in Khewra Salt Mines, Pakistan. *Journal of Radiation Research*, 53(3), 411-421. <https://doi.org/10.1269/jrr.11162>
- [4] Caridi, F., Messina, M., Belvedere, A., D'Agostino, M., Marguccio, S., Settineri, L., & Belmusto, G. (2019). Food salt characterization in terms of radioactivity and metals contamination. *Applied Sciences*, 9(14), 2882. <https://doi.org/10.3390/app9142882>
- [5] El-Bahi, S. M. (2003). Radioactivity levels of salt for natural sediments in the northwestern desert and local markets in Egypt. *Applied Radiation and Isotopes*, 58(1), 143-148. [https://doi.org/10.1016/S0969-8043\(02\)00270-1](https://doi.org/10.1016/S0969-8043(02)00270-1)
- [6] Ferruccio, G. (1972). Review of salt tectonics in relation to the disposal of radioactive wastes in salt formations. *GSA Bulletin*, 83(12), 3551–3574. [https://doi.org/10.1130/0016-7606\(1972\)83\[3551:ROSTIR\]2.0.CO;2](https://doi.org/10.1130/0016-7606(1972)83[3551:ROSTIR]2.0.CO;2)
- [7] Gera, F. (1972). Review of salt tectonics in relation to the disposal of radioactive wastes in salt formations. *GSA Bulletin*, 83(12), 3551–3574. [https://doi.org/10.1130/0016-7606\(1972\)83\[3551](https://doi.org/10.1130/0016-7606(1972)83[3551)
- [8] Lewis, R. S. (1971). The radioactive salt mine. *Bulletin of the Atomic Scientists*, 27(6), 27–30. <https://doi.org/10.1080/00963402.1971.11455377>
- [9] Ravisankar, R., Rajalakshmi, A., Eswaran, P., Gajendiran, V., & Meenakshisundram, V. (2007). Radioactivity levels in soil of salt field area, Kelambakkam, Tamilnadu, India. *Nuclear Science and Techniques*, 18(6), 372-375. [https://doi.org/10.1016/S1001-8042\(08\)60011-1](https://doi.org/10.1016/S1001-8042(08)60011-1)
- [10] Tahir, S. N. A., & Alaamer, A. S. (2008). Determination of natural radioactivity in rock salt and radiation doses due to its ingestion. *Journal of Radiological Protection*, 28, 233. <https://doi.org/10.1088/0952-4746/28/2/N01>
- [11] Bolívar, J. P., García-Tenorio, R., & García-León, M. (1995). Enhancement of natural radioactivity in soils and salt-marshes surrounding a non-nuclear industrial complex. *Science of The Total Environment*, 173–174, 125-136. [https://doi.org/10.1016/0048-9697\(95\)04735-2](https://doi.org/10.1016/0048-9697(95)04735-2)



Photocatalytic Applications of Metal Oxides for Environmental and Energy Solutions

Housseina GOHAR MAHAMMAD¹ , ***Mehmet Ali BOZ***² , ***Muhammed Bora AKIN***^{2,*} 

¹ Institute of Graduate Studies, Department of Chemical Engineering, Çankırı Karatekin University, Çankırı, Türkiye

² Faculty of Engineering, Department of Chemical Engineering, Çankırı Karatekin University, Çankırı, Türkiye

Abstract

Metal oxides hold a significant place in the field of photocatalysis due to their wide range of applications in environmental remediation, energy conversion, and biomedical sciences. These materials exhibit unique electronic, optical, and structural properties, such as wide band gaps, chemical stability, and tunable surface characteristics, making them highly attractive for various catalytic applications. Their potential for addressing critical environmental challenges, including the degradation of organic pollutants, water splitting for hydrogen production, and carbon dioxide reduction, positions metal oxides as key materials for transitioning to sustainable technologies.

Recent advances in materials science have highlighted the importance of innovative strategies to enhance the photocatalytic performance of metal oxides. Methods such as structural modifications, defect engineering, and nano-composite formulations have proven effective in overcoming intrinsic limitations like electron-hole recombination and limited visible light absorption. These strategies enable bandgap tuning, improved charge carrier dynamics, and optimized surface reactivity, significantly boosting their performance.

This brief review presents an analysis of these innovations aimed at improving the photocatalytic efficiency of metal oxides and scientifically compares various approaches. It examines how these materials are modified and integrated into composite systems, elucidating the fundamental mechanisms behind performance enhancements and identifying promising research directions for environmental and energy applications.

Keywords: Metal oxides, Photocatalysis, Environmental sustainability

1. Introduction

Photocatalysis has become a significant field in modern science as a method for controlling light-induced chemical reactions. The first systematic studies date back to the early 20th century, focusing on the interaction of light with matter. Notably, Giacomo Ciamician's works in 1912 laid the groundwork by advocating for the use of solar energy in chemical transformations. However, the first major breakthrough in modern photocatalysis occurred in 1972 with Fujishima and Honda's study, which demonstrated the splitting of water into hydrogen and oxygen using TiO₂. This discovery highlighted the potential of photocatalysis in sustainable energy production [1].

Photocatalysis holds critical importance in combating environmental pollution and advancing renewable energy. Since the 1980s, environmental applications have focused on the degradation of organic pollutants and water purification. Modern research, enabled by advancements in nanotechnology and semiconductor materials, has led to the development of photocatalysts capable of utilizing visible light more efficiently [2].

Research in photocatalysis began with theoretical studies on light-induced chemical reactions from 1900 to 1970. The discovery of TiO₂ as a photocatalyst marked a significant scientific milestone [3]. From 1980 to 2000, environmental photocatalysis emerged as an effective method for addressing industrial pollutants, and materials like strontium titanate (SrTiO₃) broadened the range of applications [4]. Since the 2000s, advanced semiconductors and nanomaterials have significantly contributed to the integration of photocatalysis into applications ranging from energy production to environmental remediation. Photocatalysis using materials like TiO₂ has demonstrated remarkable efficiency in degrading organic pollutants and treating wastewater, making it a subject of extensive research [5,6]. Additionally, integrating photocatalytic processes into microbial fuel cells has shown dual benefits in wastewater treatment and energy generation, underscoring the potential of photocatalytic technologies in both environmental and energy sectors [5,7].

* Corresponding author. e-mail address: mbakin@karatekin.edu.tr

Moreover, advancements in nanomaterials have enhanced the efficiency and applicability of photocatalytic systems. For instance, TiO_2 nanoparticles have significantly improved the degradation of various organic pollutants, making them a preferred choice in many applications [8, 9]. The versatility of these nanomaterials extends to hybrid systems, combining technologies such as ozonation or advanced oxidation processes (AOPs), which further optimize pollutant removal [10, 11]. This synergy not only improves degradation efficiency but also enables the treatment of a wider range of contaminants, including pharmaceuticals and industrial effluents [12, 13].

In the biomedical field, photocatalysis has shown promise in applications such as disinfection and the degradation of antibiotic residues, which are critical for maintaining environmental and public health [14, 15]. The ability of photocatalytic systems to harness solar energy further enhances their appeal, offering a sustainable solution to water treatment challenges, particularly in regions with limited access to clean water [16, 17]. Overall, the integration of advanced semiconductors and nanomaterials in photocatalysis represents a significant advancement in environmental technologies and energy production, providing innovative solutions to global challenges.

Photocatalysis offers sustainable solutions for clean energy production and environmental remediation. For instance, water splitting for hydrogen production is seen as an alternative solution to both the energy crisis and environmental issues caused by fossil fuels. Additionally, the use of photocatalysts for the removal of organic pollutants is of great importance for environmental cleanliness and human health [18]. This rich history and scientific foundation demonstrate that photocatalysis is not merely a laboratory technology but also a powerful tool for addressing societal and environmental challenges.

2. Photocatalytic Applications of Metal Oxides

Pollution Remediation with ZnO and TiO_2

Zinc oxide (ZnO) and titanium dioxide (TiO_2) are widely recognized for their high photocatalytic activity in degrading organic pollutants under UV light. These metal oxides facilitate the breakdown of harmful contaminants into less toxic products, with surface modification shown to improve degradation efficiency [19]. The photocatalytic process involves the generation of electron-hole pairs upon light exposure, where the electrons and holes react with water and oxygen to form reactive species, such as hydroxyl radicals, which actively degrade pollutants.

Energy and Water Treatment with Defect-Rich Metal Oxides

Defect-rich metal oxides, containing purposeful lattice imperfections, have demonstrated enhanced photocatalytic properties. The engineered defects trap charge carriers, reducing electron-hole recombination rates and increasing the efficiency of the photocatalytic reaction [20]. This structural approach has shown significant potential in water purification and energy applications, such as hydrogen production via water splitting.

Degradation of Organic Pollutants with Metal Oxide Nanocomposites

Nanocomposite structures combining multiple metal oxides offer an effective solution for environmental cleanup, especially in decomposing organic pollutants. Such nanocomposites improve light absorption and facilitate electron transfer, optimizing photocatalytic performance [21]. By combining metal oxides with complementary properties, these composites show improved charge separation and reduced recombination, making them ideal for wastewater treatment.

Metal Oxides in Environmental Sustainability

Metal oxides play an essential role in sustainable practices, offering recyclable and non-toxic options for pollution control. Danish et al. (2020) review their applications in reducing environmental pollutants, emphasizing their stability and low environmental impact [22]. These oxides convert toxic contaminants into benign products, supporting sustainable environmental practices.

Antimicrobial Coatings Using TiO_2 and ZnO

TiO_2 and ZnO are utilized as antimicrobial agents in surface coatings, particularly in the food industry, due to their ability to produce reactive oxygen species (ROS) under light, which destroy microbial cell walls [23]. This photocatalytic disinfection approach provides a non-toxic solution for surfaces requiring strict hygiene, such as in food processing.

Solar Energy Conversion via Transition Metal Oxides

Transition metal oxides are increasingly explored for solar energy conversion due to their adjustable bandgaps, which enable effective light absorption and transformation [24]. These oxides, by optimizing bandgap structures, efficiently capture solar energy, which is then converted to chemical energy, a key process in applications like solar cells and hydrogen production.

Degradation of Pharmaceutical Pollutants with TiO₂

The photocatalytic degradation of pharmaceutical contaminants in water systems has become an important application for TiO₂, which breaks down persistent pharmaceutical residues that resist conventional treatments [25]. This application is crucial in minimizing the environmental impact of pharmaceutical waste.

Light-Driven Organic Reactions with Metal Oxide Semiconductors (MOS)

Metal oxide semiconductors (MOS) facilitate light-driven organic transformations, offering an environmentally friendly alternative for organic synthesis. The generation of electron-hole pairs in MOS drives these reactions efficiently, supporting green chemistry initiatives [26].

Environmental Remediation with Metal Oxide Heterostructures

Heterostructures, created by integrating different metal oxides, exhibit enhanced photocatalytic activity due to improved charge separation and light absorption. These heterostructures are effective for degrading a wide range of environmental pollutants, making them suitable for environmental remediation [27].

Biomedical and Environmental Applications of Nanostructured Metal Oxides

Nanostructured metal oxides provide high photocatalytic activity, benefiting both biomedical and environmental applications. Their large surface area and high reactivity allow targeted applications such as cancer treatment, antimicrobial surfaces, and environmental cleanup [28].

Table 1. Photocatalytic Applications of Metal Oxides

Study Focus	Metal Oxide(s)	Key Findings	Ref.
Pollution Remediation	ZnO, TiO ₂	Enhanced pollutant degradation efficiency in water due to modified surface structures	[1]
Energy and Water Treatment	Defect-rich Metal Oxides	Surface defects optimize photocatalytic properties for water and energy applications	[2]
Organic Pollutant Degradation	Various Metal Oxides	Metal oxides with nanocomposite structures show significant photocatalytic degradation of organic pollutants	[3]
Environmental Sustainability	Metal Oxides	Systematic review showing practical applications of metal oxides in pollution control	[4]
Antimicrobial Coatings	TiO ₂ , ZnO	Metal oxides as antimicrobial coatings with effective photocatalytic disinfection potential	[5]
Solar Energy Conversion	Transition Metal Oxides	Improved solar energy capture and photocatalysis using engineered metal oxide layers	[6]
Pharmaceutical Pollutants Degradation	TiO ₂ , Metal Oxides	Effective in breaking down pharmaceutical residues in water systems	[7]
Light-Driven Organic Reactions	MOS (Metal Oxide Semiconductors)	Metal oxide catalysts promote organic transformations under light, ideal for green chemistry	[8]
Environmental Remediation	Metal Oxide Heterostructures	Heterostructure-based metal oxides achieve high photocatalytic performance in degrading pollutants	[9]
Biomedical and Environmental Use	Nanostructured Metal Oxides	Multi-application potential in biomedical and environmental fields due to enhanced photocatalytic action	[10]

3. Conclusion

Metal oxides have emerged as pivotal materials in photocatalysis, offering a versatile platform for addressing critical challenges in environmental sustainability and energy production. The extensive body of literature highlights their exceptional potential in degrading organic pollutants, splitting water for hydrogen generation, and reducing carbon dioxide into value-added products. Semiconductors like TiO₂ and SrTiO₃ have demonstrated their efficacy as photocatalysts, with further advancements driven by nanotechnology and structural engineering, such as defect manipulation and the integration of hybrid systems.

The integration of nanomaterials has enhanced the functional efficiency of these systems, expanding their applicability to include biomedical disinfection, pharmaceutical residue removal, and wastewater treatment. Furthermore, hybrid technologies combining photocatalysis with advanced oxidation processes have exhibited significant improvements in degradation rates and the scope of treatable contaminants.

Despite these advancements, challenges remain in optimizing visible-light absorption, charge carrier dynamics, and large-scale application feasibility. Future research should focus on developing cost-effective and environmentally friendly photocatalysts with improved efficiency under solar irradiation. Additionally, integrating photocatalytic technologies into existing energy and environmental frameworks holds promise for addressing global challenges in clean energy and sustainable development. Thus, innovations in metal oxide-based photocatalysis demonstrate a transformative role in creating a more sustainable future by offering both environmental benefits and long-term energy solutions.

References

- [1] Fujishima, A., & Honda, K. (1972). Electrochemical photolysis of water at a semiconductor electrode. *Nature*, 238(5358), 37–38. <https://doi.org/10.1038/238037a0>
- [2] Kowalska, E.; Zheng, S. Theme Issue in Memory to Professor Jiro Tsuji (1927–2022). *Catalysts* 2024, 14, 396. <https://doi.org/10.3390/catal14070396>
- [3] Yaemsunthorn, K., Macyk, W., & Ortyl, J. (2024). Semiconductor photocatalysts in photopolymerization processes: Mechanistic insights, recent advances, and future prospects. *Progress in Polymer Science*, 158, 101891. <https://doi.org/10.1016/j.progpolymsci.2024.101891>
- [4] Hossain, A., Bhagya, T. C., Mukhanova, E. A., Soldatov, A. V., Henaish, A. M. A., Mao, Y., & Shibli, S. M. A. (2024). Engineering strontium titanate-based photocatalysts for green hydrogen generation: Recent advances and achievements. *Applied Catalysis B: Environmental*, 342, 123383. <https://doi.org/10.1016/j.apcatb.2023.123383>
- [5] Yao, T., Wei, J., Mo, R., Ma, H., & Ai, F. (2022). Photocatalytic microbial fuel cells and performance applications: a review. *Frontiers in Chemistry*, 10. <https://doi.org/10.3389/fchem.2022.953434>
- [6] Wu, D., Li, C., Zhang, D., Wang, L., Zhang, X., & Lin, Q. (2019). Photocatalytic improvement of γ -TiO₂ modified TiO₂ prepared by a ball milling method and application in shrimp wastewater treatment. *RSC Advances*, 9(26), 14609–14620. <https://doi.org/10.1039/c9ra02307k>
- [7] Dong, F., Zhen, P., Yang, S., Lin, Q., Li, L., Li, C., ... & Nie, S. (2022). Improving wastewater treatment by triboelectric-photo/electric coupling effect. *Acs Nano*, 16(3), 3449–3475. <https://doi.org/10.1021/acsnano.1c10755>
- [8] Singh, T., Srivastava, N., Mishra, P., Bhatiya, A., & Singh, N. (2016). Application of TiO₂ nanoparticle in photocatalytic degradation of organic pollutants. *Materials Science Forum*, 855, 20–32. <https://doi.org/10.4028/www.scientific.net/msf.855.20>
- [9] Mathew, R. and Kanmani, S. (2020). Photocatalytic degradation of carbamazepine using ozonation and photocatalytic ozonation with TiO₂ and WO₃. *Water Practice & Technology*, 15(3), 645–651. <https://doi.org/10.2166/wpt.2020.050>
- [10] Tijani, J., Fatoba, O., Madzivire, G., & Petrik, L. (2014). A review of combined advanced oxidation technologies for the removal of organic pollutants from water. *Water Air & Soil Pollution*, 225(9). <https://doi.org/10.1007/s11270-014-2102-y>
- [11] Lincho, J., Gomes, J., & Martins, R. (2021). Paraben compounds—part ii: an overview of advanced oxidation processes for their degradation. *Applied Sciences*, 11(8), 3556. <https://doi.org/10.3390/app11083556>
- [12] Datta, P. and Roy, S. (2023). Recent development of photocatalytic application towards wastewater treatment. *Catalysis Research*, 03(03), 1–23. <https://doi.org/10.21926/cr.2303020>
- [13] Lama, G., Meijide, J., & Sanromán, Á. (2022). Heterogeneous advanced oxidation processes: current approaches for wastewater treatment. *Catalysts*, 12(3), 344. <https://doi.org/10.3390/catal12030344>
- [14] Pretali, L., Maraschi, F., Cantalupi, A., Albin, A., & Sturini, M. (2020). Water depollution and photo-detoxification by means of TiO₂: fluoroquinolone antibiotics as a case study. *Catalysts*, 10(6), 628. <https://doi.org/10.3390/catal10060628>
- [15] Yu, H., Wang, S., Zhang, Z., Chen, S., Quan, X., & Liang, H. (2019). Fabrication of a double-helical photocatalytic module for disinfection and antibiotics degradation. *Water Environment Research*, 91(9),

- 918-925. <https://doi.org/10.1002/wer.1132>
- [16] Zhang, Y., Sivakumar, M., Yang, S., Enever, K., & Ramezaniapour, M. (2018). Application of solar energy in water treatment processes: a review. *Desalination*, 428, 116-145. <https://doi.org/10.1016/j.desal.2017.11.020>
- [17] Njoku, D., Oluwasola, H., Onyekuru, S., & Oguzie, E. (2022). Review of solar energy applications for water treatment; a global and african perspective. *Geoinformatica Polonica*, 21, 57-82. <https://doi.org/10.4467/21995923gp.22.005.17083>
- [18] Mukherjee, U., Shah, J. A., & Ngai, M.-Y. (2024). Visible light-driven excited-state copper-BINAP catalysis for accessing diverse chemical reactions. *Chem Catalysis*, 101, 101184. <https://doi.org/10.1016/j.checat.2024.101184>
- [19] Arora, A. K., Jaswal, V. S., Singh, K., & Singh, R. (2016). Applications of metal/mixed metal oxides as photocatalyst: A review. *Oriental Journal of Chemistry*, 32(4), 2035–2046. <https://doi.org/10.13005/ojc/320430>
- [20] Raizada, P., Soni, V., Kumar, A., Singh, P., Khan, A. A. P., Asiri, A. M., Thakur, V. K., & Nguyen, V.-H. (2021). Surface defect engineering of metal oxides photocatalyst for energy application and water treatment. *Journal of Materiomics*, 7(2), 388–418. <https://doi.org/10.1016/j.jmat.2020.10.009>
- [21] Khan, M. M., Adil, S. F., & Al-Mayouf, A. (2015). Metal oxides as photocatalysts. *Journal of Saudi Chemical Society*, 19(5), 462–464. <https://doi.org/10.1016/j.jscs.2015.01.003>
- [22] Danish, M. S. S., Bhattacharya, A., Stepanova, D., & Mishra, Y. K. (2020). A systematic review of metal oxide applications for energy and environmental sustainability. *Metals*, 10(12), 1604. <https://doi.org/10.3390/met10121604>
- [23] Yemmireddy, V. K., & Hung, Y.-C. (2017). Using photocatalyst metal oxides as antimicrobial surface coatings to ensure food safety—Opportunities and challenges. *Comprehensive Reviews in Food Science and Food Safety*, 16(4), 617–631. <https://doi.org/10.1111/1541-4337.12267>
- [24] Elumalai, N. K., Vijila, C., Jose, R., Uddin, A., & Ramakrishna, S. (2015). Metal oxide semiconducting interfacial layers for photovoltaic and photocatalytic applications. *Materials for Renewable and Sustainable Energy*, 4(3), 11. <https://doi.org/10.1007/s40243-015-0054-9>
- [25] Velempini, T., Prabakaran, E., & Pillay, K. (2021). Recent developments in the use of metal oxides for photocatalytic degradation of pharmaceutical pollutants in water—a review. *Materials Today Chemistry*, 19, 100380. <https://doi.org/10.1016/j.mtchem.2020.100380>
- [26] Riente, P., & Noël, T. (2019). Application of metal oxide semiconductors in light-driven organic transformations. *Catalysis Science & Technology*, 9(19), 5186–5232. <https://doi.org/10.1039/C9CY01170F>
- [27] Theerthagiri, J., Chandrasekaran, S., Salla, S., Madhavan, J., & Ashokkumar, M. (2018). Recent developments of metal oxide based heterostructures for photocatalytic applications towards environmental remediation. *Journal of Solid State Chemistry*, 267, 35–52. <https://doi.org/10.1016/j.jssc.2018.07.009>
- [28] Kannan, K., Radhika, D., Sadasivuni, K. K., Reddy, K. R., & Raghu, A. V. (2020). Nanostructured metal oxides and its hybrids for photocatalytic and biomedical applications. *Advances in Colloid and Interface Science*, 281, 102178. <https://doi.org/10.1016/j.cis.2020.102178>



Designing Fiber-Reinforced Concrete Overlays Adapted to Cold Climate Regions in Türkiye

Duygu KAPLANCA¹ , **Emin ŞENGÜN^{2,*}** 

¹Graduate School of Natural and Applied Sciences, Master's Program in Civil Engineering, Ankara Yildirim Beyazıt University, Ankara, Türkiye

²Faculty of Engineering and Natural Sciences, Department of Civil Engineering, Ankara Yildirim Beyazıt University, Ankara, Türkiye

Abstract

Data from Türkiye's Ministry of Transport and Infrastructure highlight that highways accounts for approximately 89% of freight and 91% of passenger transport. Over the past decade, records from the General Directorate of Highways reveal a 44% rise in freight and a 30% increase in passenger transport, suggesting a substantial future demand on road infrastructure due to heavy traffic loads. In contrast to practices in developed nations, awareness of rigid pavements (concrete roads) in Türkiye is relatively promising, with flexible pavements like asphalt and seal coats predominating. These types of pavements typically require frequent preventive maintenance, rehabilitation, and overlay applications under heavy traffic load. This study investigates bonded concrete overlay on asphalt (BCOA) as an alternative approach, which has garnered increasing interest in developed countries. The analysis focuses on three pilot cities (Erzurum, Kayseri, and Afyonkarahisar) that represent harsh climatic conditions. For each city, overlay design was developed considering two levels of existing pavement distress (moderate and severe), four traffic volume categories (low, low-moderate, moderate-high, high), and three subgrade conditions (poor, moderate, good). Additionally, with the growing interest in fiber reinforcement for thin concrete overlays, this study examines design variations for both non-reinforced and fiber-reinforced scenarios at dosages of 0, 2.5, and 3.5 kg/m³. These designs are evaluated under two different joint spacing configurations: 1x1 m and 2x2 m. The findings propose customized overlay designs for each city, considering subgrade quality, traffic volume, unique climate conditions, and other relevant factors. As expected, the required overlay thickness increases with higher traffic volumes, poorer subgrade quality, and deteriorated existing pavement conditions. Notably, in addition to the primary benefit of mitigating plastic shrinkage cracking through the fiber bridging effect, the incorporation of fibers enabled a reduction in the recommended overlay thickness by up to 30%.

Keywords: Concrete Overlay, Rigid Pavement Design, Mechanistic-Empirical Approach, Thickness Design Chart

1. Introduction

As of 2024, data from Türkiye's General Directorate of Highways (GDH) reveals that approximately 65% of the nation's highways and state roads are surfaced with asphalt concrete (flexible pavement), while 33% are covered with chip-seal pavements. Furthermore, statistics from the Ministry of Transport and Infrastructure indicate that highways dominate freight and passenger transportation in Türkiye, accounting for 89.3% and 91.2%, respectively, compared to maritime, air, and rail transport. Although highways and state roads comprise roughly half of Türkiye's total road network, they bear a disproportionately large share of transport demand. This heavy dependence on the road network for transport, coupled with significant increases in both freight (44%) and passenger (30%) traffic over the past decade, has led to a pushing need for regular maintenance, and major rehabilitation. In 2022, road freight transport in Türkiye reached 323.5 billion ton-km, while passenger transport totaled 348.5 billion passenger-km, with overall road usage amounting to 140.5 billion vehicle-km. Between 2005 and 2022, the vehicle-km metric increased by 143.3%, ton-km by 106.3%, and passenger-km by 99.9%, highlighting significant growth in road transportation demand over the past two decades [1]. As of 2023, approximately 13% of the nation's highways required major pavement rehabilitation, which entails significant structural reconstruction. Maintenance demands have been met by substantial efforts, including 839 km of HMA pavement construction and rehabilitation and 6,374 km of chip-seal pavement work completed in 2023 alone. Cumulatively, between 2003 and 2023, these figures amounted to 31,395 km of HMA pavement and 273,698 km of chip-seal pavement. The allocated budget for highway and state road repairs in 2024 underscores this effort, with 4.7 billion TL designated for highways and 37.1 billion TL for state roads [2]. Additionally, Türkiye's increasing vehicle ownership—currently standing at around 28.7 million registered vehicles, according to TÜİK December 2023 data—increases the demand for higher-standard roads. With vehicle

* Corresponding author. e-mail address:@.....

ownership rates of 167 cars per 1,000 people (compared to an EU average of 531), Türkiye is projected to see continued growth in traffic density, placing further strain on the existing infrastructure. As traffic volume and heavy-load transport requirements rise, maintenance costs increase, showing the need to explore new, more resilient pavement technologies [3].

In many developed countries, concrete pavements are preferred for roads subjected to heavy traffic due to their durability and load-bearing capacity. For instance, in the United States, concrete pavements support a substantial share of traffic on high-volume highways. Similarly, in Canada's Quebec province, although concrete roads comprise only 4% of the network, they accommodate approximately 75% of total traffic. In Europe, concrete pavements are extensively utilized, particularly in Germany, Austria, and Belgium. In Germany, concrete accounts for about one-fourth of high-traffic highways; in Austria, three-fourths; and in Belgium, nearly half. Furthermore, in Belgium, concrete overlays are used for 60% of village roads, highlighting their versatility and long-term performance [4]. In Türkiye, concrete pavements are anticipated to play a crucial role in extending the service life of high-traffic, deformation-prone roads while reducing life cycle costs. Although GDH released technical specifications for concrete pavements in 2016, rigid pavement usage remains limited, with only 8.1 km of concrete roads under the GDH's purview, including pilot projects in Afyon-İşçehisar, Hasdal Kavşağı-Kemerburgaz, Ordu-Ulubey National Road, and Karamürsel City Crossing. Efforts to expand concrete road networks continue through new bidding processes. At this time, the urgent need in Türkiye's infrastructure lies not in new road construction but in the rehabilitation of existing roads through overlay applications to extend service life, restore ride and increase capacity. In this regard, bonded concrete overlays on asphalt (BCOA) have emerged as a promising alternative, attracting increased interest in developed countries as a cost-effective and durable solution.

Bonded concrete overlays are applied to existing asphalt in fair to good condition in order to repair surface flaws and/or restore structural capacity (Figure 1). To form a monolithic pavement layer, these overlays typically have a thickness of 5 to 15 cm. and are predicated on the idea that the overlay and the existing surface will form a long-lasting physical link. For a pre-overlay surface to be clean and to give the right amount of macrotexture for bonding, special attention to surface preparation tasks is necessary. Pre-overlay repairs may also be necessary to treat severe cracking, spalling, patches, punchouts, pumping, and/or settlement/heaving in the existing pavement in order to reduce the likelihood of reflective cracking [5].

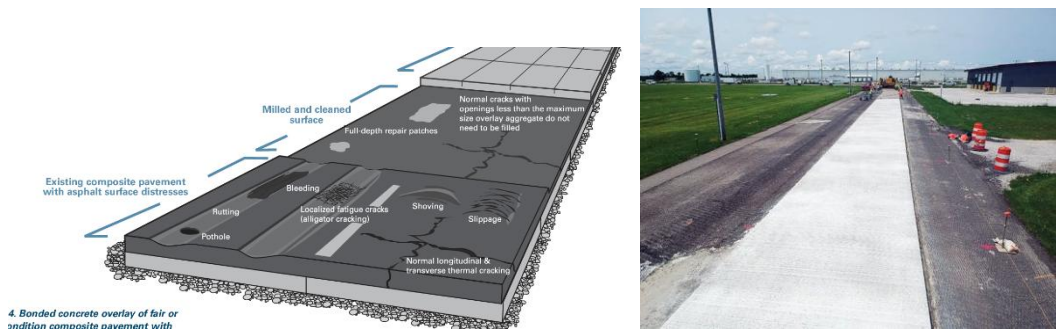


Figure 1. Bonded concrete overlay applications (adapted from guide to concrete overlays, 2012)

BCOA pavements can extend their service life by 10-20 years and are a cost-effective rehabilitation option for moderately damaged asphalt pavements. They are popular due to their low overlay thickness and ease of construction [6]. As project performance data becomes available, better design guidelines may be created to advance their use. These include factors like traffic, climate, existing asphalt pavement structure, and concrete mix design. The design takes economy and utility into account in addition to mechanical factors. The design of bonded concrete overlay thickness is influenced by a number of input factors as traffic, temperature gradient, and existing asphalt modulus, traffic (ESAL), fiber content and joint spacing. The predicted ESALs are the sensitive input and need to be carefully evaluated to fulfill the bonded overlay's performance requirements. The current state of the pavement affects the drainage coefficients, load transmission, and modulus of rupture. In order to avoid overdesigning the thickness of the concrete overlay, pre-overlay repairs are usually carried out to correct significant load transfer and/or drainage defects prior to a bonded overlay being applied. In addition, a number of crucial design factors are listed by Riley (2006) and Roesler et al. (2008). These include the thickness and stiffness of the existing asphalt, the flexural strength of the concrete overlay, the size of the slab, the effective

temperature gradient, and the use of structural fibers. In order to prevent excessive concrete drying shrinkage, caution must be used while choosing the concrete mixture design. The proportions of the concrete mixture chosen will still have a big impact on this attribute, even if adequate curing can lessen concrete's early-age shrinkage. Additionally, proper surface preparation is crucial. Debonding at the concrete-asphalt contact may result from excessive shrinkage and/or inadequate surface preparation [7-8].

2. Materials and Methods

This study selected three provinces in Türkiye's cold regions (Afyonkarahisar, Kayseri, Erzurum), each representing unique climatic conditions, to develop design charts and examine the factors influencing the design of BCOA pavements. The mechanistic-empirical (M-E) design approach was employed using the BCOA-ME software, a finite element-based tool developed by the University of Pittsburgh [9]. BCOA-ME allows for precise overlay thickness predictions for bonded concrete overlays on distressed Hot Mix Asphalt (HMA) pavements of various panel sizes. This tool is advantageous for designers, offering a comprehensive analysis platform for all bonded concrete overlays on HMA, and facilitates the evaluation of design variables such as traffic loads, soil conditions, climate, fiber reinforcement, and joint spacing on overlay performance [9-11].

A 20-year service life was selected to reflect typical performance expectations across the provinces. The study considered three subgrade quality levels (poor, moderate, and good), four levels of Average Annual Daily Truck Traffic (AADT) to represent traffic volume ranges (low, low-moderate, moderate-high, and high), and a C30 concrete strength class. The reliability coefficient was consistently set at 85%, and the maximum allowable cracked slab percentage was limited to 15% in accordance with GHD project demands. Additionally, given the increasing preference for fiber reinforcement in thin concrete overlay applications, synthetic fiber was incorporated at three dosages (0, 2.5, and 3.5 kg/m³) to evaluate its impact on overlay design. Joint spacings of 1x1 m (3x3 ft) and 2x2 m (6x6 ft) were also included in the analysis. Moreover, the condition of the existing asphalt pavement where the overlay will be applied was categorized into two levels: moderate (adequate) and severe (marginal). Accordingly, the percentage of transverse cracks on the existing pavement was taken into consideration in the analysis. The parameters used in the analysis are summarized in Table 1, resulting in a total of 432 idealized design scenarios.

Table 1. Design variable values entered into the BCOA-ME Design Program.

Percent Trucks %	Low Traffic=3,3	Low-Moderate Traffic=16	Moderate-High Traffic=25	High Traffic=50
ESAL	6231000	30211000	47204000	94408000
Composite Modulus of Subgrade Reaction, k-value (Mpa/m)	Good=95	Moderate=41	Poor=14	
Fiber Content (kg/m ³)	0%	2,5%	3,5%	
Existing HMA Performance	Adequate		Marginal	
Joint Spacing (m)	1x1 (Small Slab)		2x2 (Large Slab)	

The climate data required for the M-E design approach for the selected provinces (Afyonkarahisar, Kayseri, Erzurum) were determined by matching them with values observed at a U.S. station. This method was necessary due to the lack of comprehensive climate data in Türkiye compatible with the BCOA-ME program. The matching process adhered to specified tolerance limits to ensure the selected provinces accurately represented the average conditions for each climate category, as referenced in a previous study [12]. In this way, the equivalent climate stations required for input into the BCOA-ME design program were identified. Figure 2 shows the selected provinces along with their corresponding related maps. AMDAT Region of three provinces is Zone 3. Sunshine zone is Zone 3 for Afyonkarahisar and Kayseri beside Zone 4 for Erzurum.

Table 3. Recommended C30 Thin Concrete Overlay Thickness and Joint Spacing Under Different Conditions for Kayseri

KAYSERİ																											
HMA Fatigue	ADEQUATE																										
Joint Spacing (m)	1.00X1.00 (SMALL SLAB)																										
ESAL Traffic	LOW									LOW-MODERATE									MODERATE-HIGH								
Fiber Content (kg/m ³)	0			2,5			3,5			0			2,5			3,5			0			2,5			3,5		
K value (Alpha m)	G	M	P	G	M	P	G	M	P	G	M	P	G	M	P	G	M	P	G	M	P	G	M	P	G	M	P
Calculated PCC Overlay Thickness (mm)	138	138	137	121	120	119	117	116	115	>140	>140	>140	126	126	124	122	121	120	>140	>140	>140	128	127	126	123	123	121
Joint Spacing (m)	2.00X2.00 (LARGE SLAB)																										
ESAL Traffic	LOW									LOW-MODERATE									MODERATE-HIGH								
Fiber Content (kg/m ³)	0			2,5			3,5			0			2,5			3,5			0			2,5			3,5		
K value (Alpha m)	G	M	P	G	M	P	G	M	P	G	M	P	G	M	P	G	M	P	G	M	P	G	M	P	G	M	P
Calculated PCC Overlay Thickness (mm)	136	144	156	111	117	126	105	110	118	141	149	161	115	121	131	109	115	123	142	151	163	116	122	132	110	116	124
HMA Fatigue	MARGINAL																										
Joint Spacing (m)	1.00X1.00 (SMALL SLAB)																										
ESAL Traffic	LOW									LOW-MODERATE									MODERATE-HIGH								
Fiber Content (kg/m ³)	0			2,5			3,5			0			2,5			3,5			0			2,5			3,5		
K value (Alpha m)	G	M	P	G	M	P	G	M	P	G	M	P	G	M	P	G	M	P	G	M	P	G	M	P	G	M	P
Calculated PCC Overlay Thickness (mm)	139	139	138	122	122	120	118	117	116	>140	>140	>140	127	127	126	123	122	121	>140	>140	>140	129	128	127	124	124	123
Joint Spacing (m)	2.00X2.00 (LARGE SLAB)																										
ESAL Traffic	LOW									LOW-MODERATE									MODERATE-HIGH								
Fiber Content (kg/m ³)	0			2,5			3,5			0			2,5			3,5			0			2,5			3,5		
K value (Alpha m)	G	M	P	G	M	P	G	M	P	G	M	P	G	M	P	G	M	P	G	M	P	G	M	P	G	M	P
Calculated PCC Overlay Thickness (mm)	139	147	159	114	120	129	107	113	121	144	152	165	118	124	134	112	117	126	145	154	>165	119	125	135	113	118	127

Table 4. Recommended C30 Thin Concrete Overlay Thickness and Joint Spacing Under Different Conditions for Erzurum

ERZURUM																											
HMA Fatigue	ADEQUATE																										
Joint Spacing (m)	1.00X1.00 (SMALL SLAB)																										
ESAL Traffic	LOW									LOW-MODERATE									MODERATE-HIGH								
Fiber Content (kg/m ³)	0			2,5			3,5			0			2,5			3,5			0			2,5			3,5		
K value (Alpha m)	G	M	P	G	M	P	G	M	P	G	M	P	G	M	P	G	M	P	G	M	P	G	M	P	G	M	P
Calculated PCC Overlay Thickness (mm)	137	137	136	120	120	119	116	116	114	>140	>140	>140	125	125	124	121	121	120	>140	>140	>140	127	126	125	123	122	121
Joint Spacing (m)	2.00X2.00 (LARGE SLAB)																										
ESAL Traffic	LOW									LOW-MODERATE									MODERATE-HIGH								
Fiber Content (kg/m ³)	0			2,5			3,5			0			2,5			3,5			0			2,5			3,5		
K value (Alpha m)	G	M	P	G	M	P	G	M	P	G	M	P	G	M	P	G	M	P	G	M	P	G	M	P	G	M	P
Calculated PCC Overlay Thickness (mm)	136	144	155	110	120	119	104	109	118	140	148	161	115	121	130	108	114	122	141	150	162	116	122	131	109	115	123
HMA Fatigue	MARGINAL																										
Joint Spacing (m)	1.00X1.00 (SMALL SLAB)																										
ESAL Traffic	LOW									LOW-MODERATE									MODERATE-HIGH								
Fiber Content (kg/m ³)	0			2,5			3,5			0			2,5			3,5			0			2,5			3,5		
K value (Alpha m)	G	M	P	G	M	P	G	M	P	G	M	P	G	M	P	G	M	P	G	M	P	G	M	P	G	M	P
Calculated PCC Overlay Thickness (mm)	138	138	137	122	121	120	117	117	116	>140	>140	>140	127	126	125	122	122	121	>140	>140	>140	128	128	127	124	123	122
Joint Spacing (m)	2.00X2.00 (LARGE SLAB)																										
ESAL Traffic	LOW									LOW-MODERATE									MODERATE-HIGH								
Fiber Content (kg/m ³)	0			2,5			3,5			0			2,5			3,5			0			2,5			3,5		
K value (Alpha m)	G	M	P	G	M	P	G	M	P	G	M	P	G	M	P	G	M	P	G	M	P	G	M	P	G	M	P
Calculated PCC Overlay Thickness (mm)	138	146	158	113	119	128	107	112	120	143	151	164	117	123	133	111	117	125	144	153	165	118	125	134	112	118	126

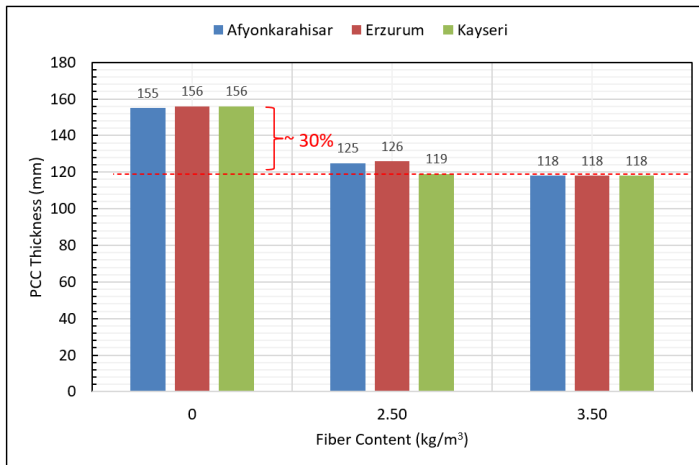


Figure 3. PCC Thickness vs Fiber Amount Graphics of three provinces (for the case of ESAL-low, k value-poor, 2x2 m).

4. Conclusion and Recommendations

With the increasing traffic volumes, growing freight and passenger transportation demands, and rising vehicle ownership per capita, the exploration of new-generation pavement technologies has become crucial for Türkiye. Currently dominated by asphalt pavements, the nation's highway infrastructure requires frequent maintenance and major rehabilitation due to the damage of heavy traffic. In this context, concrete overlays on asphalt pavements, in other words thin whitetopping solution, present a significant opportunity for Türkiye, offering extended service life, ride quality and increased durability. This study focused on applying the BCOA-ME design methodology developed by Pittsburgh University to three provinces representing Türkiye's cold climate regions (Afyonkarahisar, Kayseri, Erzurum). Various scenarios were analyzed, incorporating different traffic levels, subgrade conditions, existing pavement structures, fiber reinforcement dosages, and slab sizes. Using the finite element-based BCOA-ME design program, a total of 432 scenarios were evaluated to generate recommended thickness charts under these conditions. The findings highlighted the substantial impact of fiber reinforcement on the structural design of thin overlay, with thickness reductions of up to 30% observed in certain cases. This can bring to mind the potential of fiber-reinforced thin concrete overlays as a cost-effective and durable solution for Türkiye's high-traffic roads, paving the way for future advancements in sustainable pavement technology.

Acknowledgement

This study is based on the master's thesis research conducted by graduate student Duygu Kaplanca.

References

- [1] Strateji Geliştirme Dairesi Başkanlığı. (2023). 2023 Faaliyet Raporu, Retrieved from <https://www.kgm.gov.tr/SiteCollectionDocuments/KGMdocuments/MerkezBirimler/Kurumsal/FaaliyetRaporu/2023Faaliyet.pdf>
- [2] Karayolu Ulaşım İstatistikleri. (2023). Karayolu Ulaşım İstatistikleri (2023). Retrieved from <https://www.kgm.gov.tr/SiteCollectionDocuments/KGMdocuments/Yayinlar/YayinPdf/KarayoluUlasimIstatistikleri2023.pdf>
- [3] Performans Programı Strateji Geliştirme Dairesi Başkanlığı. (2024). Performans Programı 2024. Retrieved from <https://www.kgm.gov.tr/SiteCollectionDocuments/KGMdocuments/MerkezBirimler/Kurumsal/PerformansProgrami/2024Performans.pdf>
- [4] Sengun,E., Yaman, I. O., & Ceylan, H. “An overview on Rigid Pavement Specifications”, 1st European IRF Europe & Central Asia Regional Congress & Exhibition, presented, İstanbul, Türkiye, 15-18 September 2015.
- [5] Vandenbossche, J.M. and Barman, M. Bonded Whitetopping Overlay Design Considerations for Prevention of Reflection Cracking, Joint Sealing, and the Use of Dowel Bars. Transportation Research Record, No. 2155, 2010, pp. 3-11
- [6] Agar, E., Sütas, İ., & Öztas, G. Beton Asfalt Kaplama ile Beton Yol Karşılaştırması. Türkiye Hazır Beton Birliği, Beton Yollar Özel Sayısı, 48- 51. (2001).
- [7] Mateos A., Millan M.A., Harvey J.T., Paniagua F., Wu R. (2021) Mechanisms of asphalt cracking and concrete-asphalt debonding in concrete overlay on asphalt pavements. Construction and Building Materials, Volume 301
- [8] Barman M., Vandenbossche J.M., Li Z., Influence of Interface Bond on the Performance of Bonded Concrete Overlays on Asphalt Pavements. Journal of Transportation Engineering, Part B: Pavements, Volume 143, Issue 3
- [9] DeSantis, J.W. Modeling the Development of Joint Faulting for Bonded Concrete Overlays of Asphalt Pavements (BCOA). Ph.D. Dissertation, University of Pittsburgh, Pittsburgh, PA, 2020.
- [10] Vandenbossche, J.M. and Barman, M. Bonded Whitetopping Overlay Design Considerations for Prevention of Reflection Cracking, Joint Sealing, and the Use of Dowel Bars. Transportation Research Record, No. 2155, 2010, pp. 3-11
- [11] DeSantis, J.W., and J.M. Vandenbossche, “Redevelopment of Artificial Neural Networks for Predicting the Response of Bonded Concrete Overlays of Asphalt in a Faulting Prediction Model,”Transportation Research Record: Journal of the Transportation Research Board, TRB, NationalResearch Council, DOI:10.1177/03611981211001075, 2021.
- [12] Öztürk, Hİ., Şengün E., Yaman İÖ. (2019). Comparison of jointed plain concrete pavement systems designed by mechanistic empirical (M-E) method for different traffic, subgrade, material and climatic conditions. Journal of the Faculty of Engineering and Architecture of Gazi University.



Application and Essential Components of Serial and Parallel Chopper Converters

Samatar ALI^{1,*} , ***Murat ARI***² , ***Mahmud Esad YİĞİT***³ 

¹Department of Electrical and Electronics Engineering, Çankırı Karatekin University, Çankırı, Türkiye

²Department of Electrical and Electronics Engineering, Çankırı Karatekin University, Çankırı, Türkiye

³Department of Electrical and Electronics Engineering, Çankırı Karatekin University, Çankırı, Türkiye

Abstract

This article discusses the use of a chopper to convert a fixed DC input into a DC output voltage. Choppers are commonly employed in applications such as power supply and motor control. There are types of choppers, including series and parallel choppers. The primary goal of this research is to examine the practical aspects of choppers, in series and parallel configurations to enhance comprehension of their operation principles and control system design well as evaluate their performance in various uses cases. In a series chopper setup, the current (DC) voltage source is connected in series with the motor with the chopper controlling the voltage supplied to the motor. In contrast in a parallel configuration multiple choppers are linked together to increase output current while ensuring a voltage level, across each chopper. This special converter enables the use of devices that require an amount of current to function.

Keywords: *the current result, direct current voltage , the energy source ,control motor.*

1. Introduction

Chopper converters are a type of power electronics devices that are commonly employed to regulate and transform power supply operations by adjusting the voltage and current to suit the load through the manipulation of semiconductor switch timings effectively managing power distribution in applications, like industrial motor drives and electric vehicles. Chopper converters – also called DC to DC converters – work to adjust the current (DC) voltage from a source to a different level of DC voltage, at the output by utilizing high frequency switching through components like transistors and inductors along, with diodes. The main types of chopper converters are buck converters that decrease the input voltage and boost converters that increase the input voltage as buck boost converters that can perform either function based on the control method employed. Different types of chopper converters have their functions and circuit setups designed to meet specific performance standards and application demands [1-2]. The importance of chopper converters in today's technology landscape cannot be overlooked as they play a role in converting energy to reduce losses and enhance the overall effectiveness of electronic systems. For example : in energy setups like panels and wind turbines, chopper converters are crucial for streamlining the energy conversion process and ensuring it works seamlessly with the grid or the load. In industry these converters are crucial for electric cars as they regulate the battery power to ensure consistent performance for the driving system. Their efficiency and quick adjustment to varying power needs are also essential in devices such as laptops and smartphones aiding in maintaining stable voltage levels and effective power control.

2. Fundamentals Concepts

2.1 Basic Operation

Chopper converters are circuits that are built to manage the voltage level between the power source and the device by utilizing high speed switching elements specifically designed for this purpose. The main concept involves turning the power supply both on and off into a process known as duty cycle modulation which determines how long it is switched 'on' in relation, to the time elapsed. This manipulation of duty cycle enables regulation of the power reaching the device resulting in customized output voltage control as needed. Important elements that support this process consist of components, like transistors and diodes, as well as passive devices such as capacitors and inductors that aid in regulating the output and reducing fluctuations in voltage levels. The effectiveness of a chopper converter heavily relies on the frequency at which it switches and the quality of its

* Corresponding author. e-mail address: samataralimigul@gmail.com

parts; higher frequencies typically result in operation. Can also cause more heat stress, on the electronic components[3].

2.2 Types of Converters

Chopper converters come in varieties depending on their circuit setups. The connection, between input and output voltages are categorized broadly into various types such, as buck converters boost converters buck boost converters and Cuk converters A buck converter is used when there is a need to decrease the voltage from the input to the output bringing down the voltage while possibly boosting the current capacity On the side of things a boost converter works to raise the input voltage to an output voltage. This is usually applied in situations where the source voltage must be increased for use. The buck. Boost converter provides flexibility by being able to raise or lower the voltage based on the duty cycle, which proves handy in power supplies that must function under input voltage scenarios. The Cuk converter stands out for utilizing two inductors and capacitors to offer output flexibility along, with the advantage of maintaining pulsating input and output currents to reduce noise and enhance power supply quality—a key consideration when selecting the right converter, for a particular application based on specific electrical needs and operational conditions. Categorizing these systems do not help in the development and application but also highlights the wide-ranging potential and versatility of chopper converters, in today's electronics and power setups [4].

3. Serial Chopper Converters

3.1 Design and Components

The setup of chopper converters prominently features an arrangement of semiconductor switches, like transistors or Mosfets and a diode for freewheeling and an inductor to manage energy during switching cycles. The functioning relies on regulating the flow of current in the circuit through the series switch with precision to control the output voltage effectively. The duration for which the switch conducts electricity. Known as the duty cycle. Plays a role in determining the output voltage supplied to the load. It's important to use an inductor because it helps to out the changes in current caused by switching actions and keeps the output stable to avoid voltage spikes. Moreover, you can also use capacitors at the output to reduce any remaining voltage fluctuations and ensure a DC output that works well for electronic devices[5].

3.2 Applications and Advantages

Serial chopper converters are widely used in scenarios that require voltage regulation and optimal efficiency as a priority. Hence, it's common to find them in gadgets powered by batteries to prolong battery life, by converting energy. Their presence is also crucial in electronics for vehicles to effectively handle the power flow between batteries and motors. Serial choppers excel at delivering an regulated output which makes them perfect, for supplying power to delicate systems needing consistent voltage even when the load changes. One of the benefits of chopper converters is their high efficiency and simple design approach compared to parallel converters. In a setup energy flows through components decreasing energy losses, from component resistance and leakage currents. This efficiency is especially advantageous for battery operated devices where conservating energy's key to prolong device life. Moreover, the uncomplicated circuit design makes implementation easier. Lowers manufacturing expenses making chopper converters a cost-efficient option, for various applications.

4. Parallel Chopper Converters

4.1 Design and Components

In the setup of chopper converters design framework that you see around a lot these days involves using a transistor or some other fancy switching device hooked up parallel to the load. The main job of this switch in this setup is to take turns powering the load by diversifying the current flow away from it now and then to manage how much voltage is hitting the load when it's not being powered. A key part of this design is having a freewheel diode set up across the load to help keep the current flowing during those times when the switch takes a break from powering things up – this way there aren't any hiccups in how the load runs. This setup requires an inductor to be used connected in a row, with the power source to ensure a flow of current while switching occurs. Additionally, capacitors are utilized to stabilize the voltage and reduce any fluctuations. [6]

4.2 Applications and Advantages

In situations where quick and efficient voltage regulation's crucial and a rapid response is needed to handle changing load demands or potential faults in power systems, like applications for overload protection in power supplies. Parallel chopper converters are commonly used for their ability to swiftly redirect current flow. Their setup allows them to deliver performance in systems, with load changes which helps maintain stability and reliability of the voltage supply. The benefits of chopper converters are highlighted by their ability to handle abrupt shifts, in load demands effectively—a crucial aspect in scenarios with dynamic power needs. Encapsulated within the structure is a built-in safety net; should a switch falter, the load can be supplied power via the freewheel diode albeit at a diminished rate—thus guaranteeing equipment continuity. This aspect positions parallel converters as an option, for systems requiring constant power supply. Furthermore, these converters generally experience voltage strain on the switching parts, which can result in increased component longevity and decreased maintenance requirements. This adds to their attractiveness, in high reliability contexts[7].

5. Managing and Regulating Series and Parallel Power Converters

This research delves into the synchronization of phases in power converters that are vital for maintaining resilient power supply systems in various applications. By utilizing synchronization methods in these converters, they can efficiently handle loads and improve system reliability by enhancing current load distribution. The significance of this lies in energy scenarios where the dependable integration of power sources is crucial. The study merges ideas from dynamics and control theory to enhance converter efficiency and stability for performance, in demanding settings [8-9]. This research delves into the control techniques for transforming series configurations into systems. Discusses the crucial factors in distributing voltage and current among converter units to enhance the efficiency and dependability of intricate power networks. The study focuses on applications, in power arrangements commonly found in renewable energy systems where adaptability and expandability are key considerations. By examining theories and conducting experiments to confirm findings in practice; the research offers strategies, for regulating DC to Dc converters and DC, to Ac inverters in both series and parallel setups to maintain optimal performance when dealing with different loads.

6. Simulation Results

Understanding the behavior of choppers through simulations is essential for understanding their characteristics and evaluating their efficiency before putting them into use. Monitoring how voltage and current switches influence the optimization of design parameters and predicting problems such, as interference or current fluctuations is highly significant. Analyzing timing diagrams in simulations contributes to the enhancement and fine tuning of chopper converters. The diagram demonstrates the operation of the printer by depicting both its on) and inactive (off) states based on the switching mechanism. The setup includes: A DC power supply, $E > 0$. A functioning electrical switch (when the connection is made $u=0$), with one-way current flow H. A device that consumes electricity.

The circuit is defined by the following relationship [10]:

$$E = u_h + u \quad (1)$$

When the switch labeled H moves back and forth it switches between being open and closed.

$$T = t_f + t_u \quad (2)$$

where; t_f is the time when H closes and t_u is the initial period.

$$f = 1/T \quad (3)$$

The cyclic ratio α is given by:

$$\alpha = \frac{t_f}{T}; \quad 0 \leq \alpha \leq 1 \quad (5)$$

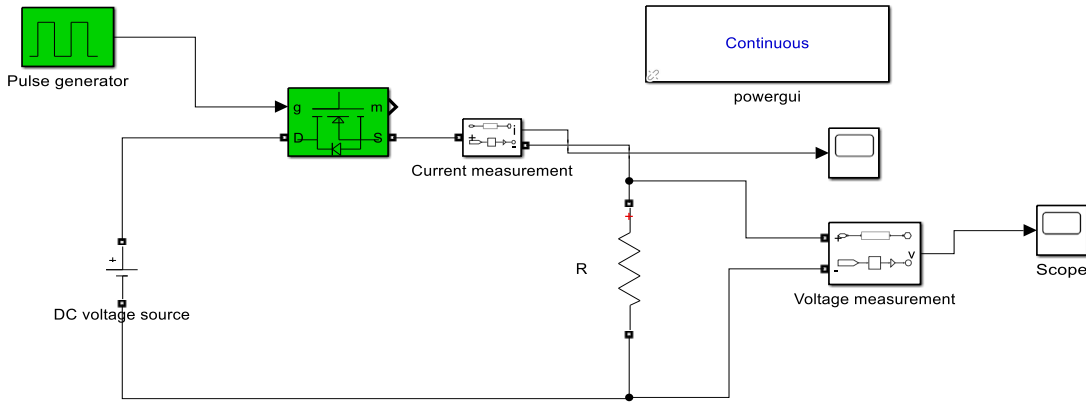


Figure 1. Circuit of step-down Serial chopper.

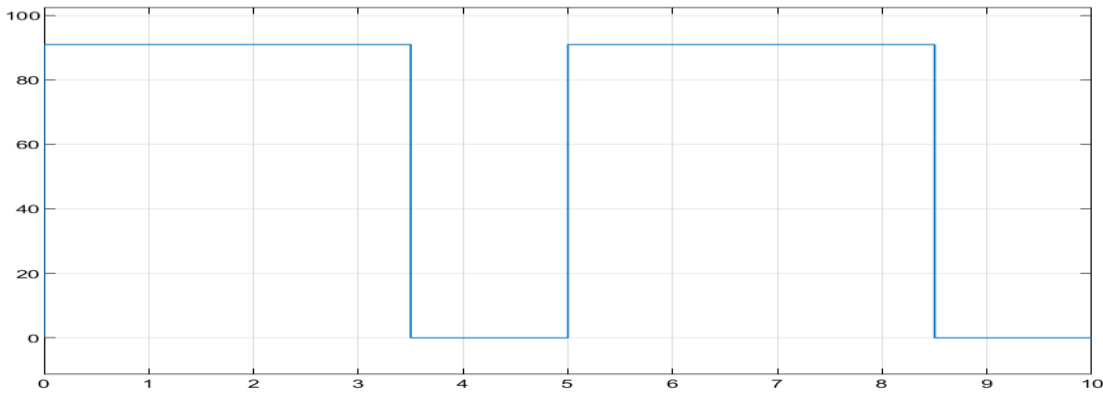


Figure 2. Serial chopper circuit diagram.

Analyzing and fine tuning the performance of a DC converter using a chopper parallel simulation allows for optimization without physically constructing the circuit. By utilizing software to model its behavior adjustments, to parameters can be made seamlessly. This predictive approach aids in assessing response, energy efficiency and overall stability paving the way for the creation of dependable solutions, across a range of industrial and technological settings.

The voltage output expression is given as:

$$V_{out} = \frac{D}{1-d} * V_{in} \quad (6)$$

Equation (6) can be used to relate the input voltage V_{in} to the output voltage V_{out} . Since D is a variable (usually indicating the duty cycle in electronics), perform these steps:

1. Determine Range of D : Typically, D ranges from 0 to 1 (0% to 100%).
2. Plot D on the x -axis; this is the cycle ratio. Determine V_{out} for D values: Calculate V_{out} using the equation with D values from 0 to 1.
3. Plot V_{out} on the y -axis: This shows the voltage at the output.

The objective of the two rotor simulation experiments is to investigate the effect of load fluctuations on voltage and current levels in a configuration consisting of a DC power supply in combination with elements such as keyhole transistors (such as MOSFET or IGBT). Free-rotating code for protected flux control. The BUCK converter acts as a reducing converter. It reduces the output amplitude compared to the input amplitude. The BOOST converter increases the output voltage above the input voltage level. As revealed by simulations and experimental tests. This is consistent with calculation errors resulting from readout errors and instrument inaccuracies. The decision to use a configuration depends on the application requirements, such as voltage and current requirements, and desired level of performance together with considerations of the complexity of designing and maintaining peak power and impedance in electrical systems.

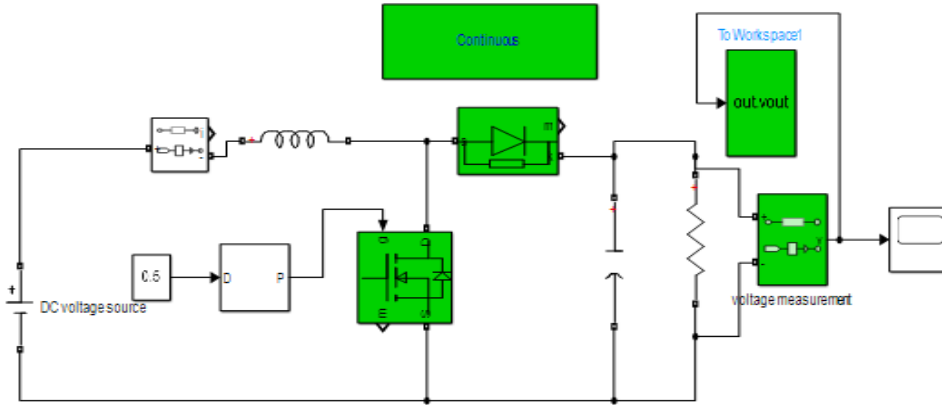


Figure 3. Parallel chopper circuit board.

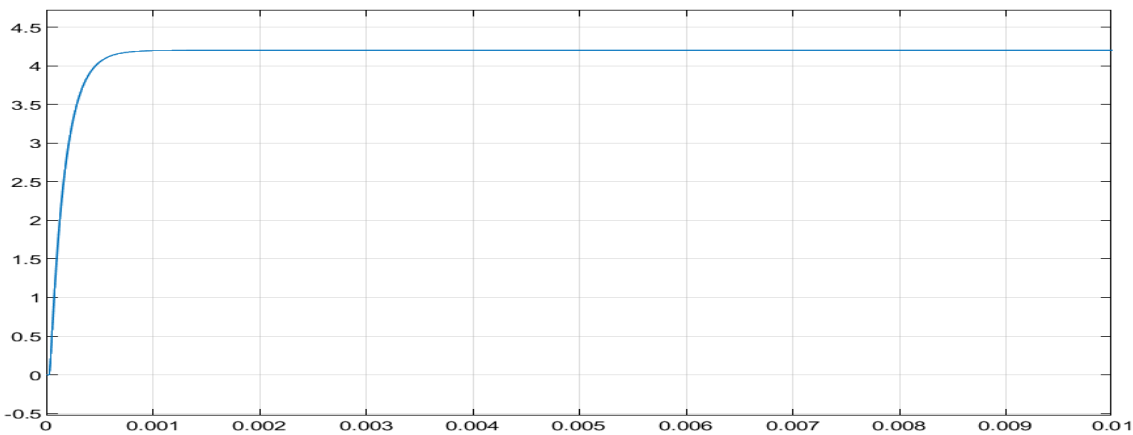


Figure 4. diagram parallel circuit.

In simulations studies have shown that the choice, between a chopper and a parallel chopper largely depends on the needs of the application at hand. Serial choppers are known for their ability to regulate voltage and respond swiftly to changes in contrast to parallel choppers which can adjust to loads and maintain power efficiency in diverse scenarios. When deciding in this regard it is crucial to consider the intricacy of the design as the associated costs involved. Both types of choppers effectively handle output voltage requirements. With serial choppers being particularly strong, in accuracy and responsiveness while parallel choppers excel in providing stability for fluctuating or long-term loads.

7. Conclusion

In this study paper we have delved into the design and operational concepts of parallel chopper converters to explain their crucial functions, in today's electronic and power systems world. After analyzing both setups thoroughly, each converter type comes with benefits tailored for uses which emphasize the flexibility and adjustability of chopper converters in efficiently handling and enhancing power distribution in diverse situations. Serial chopper converters are known for their effective design and high efficiency levels which make them valuable for situations where a consistent and reliable power supply is needed even with fluctuating conditions in operation settings. They can prolong the battery life of handheld devices. Are cost efficient to produce making them a popular choice in the consumer electronics and automotive sectors. On the chopper converters exhibit excellent performance, in scenarios that need quick dynamic responses, and strong operational safety measures These converters have a knack, for managing changes in workload and their fail safe mode makes them essential, for crucial power supply setups and protective electronic uses.

References

- [1] Ahmad, H., & Hagiwara, M. (2020). Interleaved bidirectional chopper with auxiliary converters for DC electric railways. *IEEE Transactions on Power Electronics*, 36(5), pp.5336-5347.
- [2] Du, S., & Liu, J. (2013). A study on DC voltage control for chopper-cell-based modular multilevel converters in D-STATCOM application. *IEEE Transactions on Power Delivery*, 28(4), 2030-2038.
- [3] Bououd R., & Sbita L. An overview of chopper topologies. International Conference on Green Energy Conversion Systems (GECS), Hammamet, Tunisia, 2017.
- [4] Luo, F. L., & Ye, H. (2016). *Advanced DC/DC Converters*. CRC Press.
- [5] Salinas, F., Ghanes, M., Barbot, J. P., Escalante, M. F., & Amghar, B. (2014). Modeling and control design based on petri nets for serial multicellular choppers. *IEEE Transactions on Control Systems Technology*, 23(1), pp.91-100.
- [6] Ajami, A., Shokri, H., & Mokhberdoran, A. (2014). Parallel switch-based chopper circuit for DC capacitor voltage balancing in diode-clamped multilevel inverter. *IET Power Electronics*, 7(3), pp.503-514.
- [7] Melkebeek, A., & Melkebeek, J. (2018). DC Chopper. *Electrical Machines and Drives: Fundamentals and Advanced Modelling*, pp.263-275.
- [8] Giral, R., Martinez-Salamero, L., & Singer, S. (1999). Interleaved converters operation based on CMC. *IEEE Transactions on Power Electronics*, 14(4), pp.643-652.
- [9] Mazumder, S., Nayfeh, A., & Borojevic, D. (2002). Robust control of parallel DC-DC buck converters by combining integral-variable-structure and multiple-sliding-surface control schemes. *IEEE Transactions on Power Electronics*, 17(3), pp.428-437.
- [10] Ruan, X., Chen, W., Fang, T., Zhuang, K., Zhang, T., & Yan, H. (2019). *Control of Series-Parallel Conversion Systems*. Springer, Singapore.



Comparison of the Performance of Different PV System Configurations Under Partial Shading

Ismail ALI ABDIRAHMAN^{1,*} , *Murat ARI*¹ , *Mahmud Esad YİĞİT*¹ 

¹Department of Electrical and Electronics Engineering, Çankırı Karatekin University, Çankırı, Turkey

Abstract

This paper aims to analyze the performance of various photovoltaic (PV) array configurations under different partial shading conditions. With the growth of solar energy adoption, PV systems are increasingly installed in environments where shading from buildings, trees, or obstacles is common. Partial shading disrupts light distribution on PV modules, leading to power losses, particularly in series configurations where shading of a single module can affect the entire string. To address this, configurations like Serie (S), Series-Parallel (SP), Honey-Comb (HC), Total Cross-Tied (TCT), and Bridged-Link (BL) have been developed to enhance shading resilience. Using MATLAB/Simulink simulations, these configurations were tested under four shading levels—0%, 20%, 40%, and 60%—to observe their power-voltage (P - V) and current-voltage (I - V) characteristics. The TCT configuration demonstrated the highest resilience to shading, maintaining a higher fill factor and power output compared to the other configurations. Results indicate that TCT configuration offers the highest resilience, producing 2672 W and 2524 W at 40% and 60% shading, respectively, significantly outperforming series configurations, which show substantial power reductions. The BL and HC configurations also demonstrate superior performance, with fill factor values that confirm the robustness of Total-Cross-Tied (TCT) against shading effects. Overall, The Total-Cross-Tied (TCT) configuration proved the most effective in reducing energy losses in shaded conditions. These findings suggest that the TCT configuration is best suited for environments with high shading risk, while the Series configuration performs well in unshaded conditions. This research underscores the importance of PV configuration choice for sustainable energy performance in real-world settings where shading is a concern.

Keywords: Photovoltaic Configurations, Partial Shading, MATLAB/Simulink, Power Output, Fill factor

1. Introduction

As the adoption of solar energy continues to grow, photovoltaic systems are increasingly deployed in diverse environments, including those susceptible to shading from buildings, trees, or other obstacles. Partial shading can significantly reduce the energy yield of PV arrays, as it disrupts the uniform distribution of light across the modules, leading to mismatched outputs within the system [1]. This shading effect is especially problematic for series configurations, where even a small portion of shading on a single module can lead to substantial power losses [2]. Consequently, improving the resilience of PV configurations to shading has become essential for enhancing their efficiency and reliability in practical applications. Various array configurations, such as Series (S), Series-Parallel (SP), Bridged-Link (BL), Total Cross-Tied (TCT) and Honey-Comb (HC), have been developed in the literature. These configurations are designed to handle shading differently, enabling some systems to sustain higher power outputs and maintain efficiency even when shaded. [3]. This study measures the performance of these configurations under varying shading scenarios using MATLAB/Simulink simulations. By examining characteristics of PV module under controlled shading scenarios, the study aims to determine which configurations best retain performance. The results demonstrate that the TCT configuration shows the greatest resilience to shading, the TCT may be the optimal choice for shading-prone environments [4].

2. PV array configuration

The photovoltaic system configurations mentioned in the literature to mitigate the shading effect are shown in Figure 1.

2.1. Series Configuration

In the series configuration, the photovoltaic panels are connected to each other in a single string. This arrangement increases the total voltage, as the voltage of each module adds to that of the others [5]. The maximum voltage (V_{max}), current (I_{max}), and power (P_{max}) of each panel are its output parameters while the

* Corresponding author. e-mail address: ismail.a.abdirahman@gmail.com

photovoltaic system is working correctly. The main advantage of this configuration is its simplicity and efficiency under optimal sunlight conditions, allowing for maximum power output. nevertheless, an important weakness is that the performance of the whole series will be limited, leading to significant power losses, if one panel in the string is shaded. The model used in this research is a 4x4 panels [6].

2.2. Serie-Parallel Configuration

Initially, the PV modules get connected in series to form strings. Several strings then connect in parallel. This configuration allows both voltage (via series connection) and current (via parallel connection) to be increased. The advantage of this configuration is that in the event of partial shading, only the affected string experiences reduced performance, while the other strings continue to operate normally. However, shading on an entire string can lead to significant power losses [7].

2.3. Total Cross-Tied Configuration

The TCT configuration is an improvement over the Serie-Parallel configuration, where cross ties are added between the modules in each row. This helps balance the voltage across rows of modules and distribute the current more evenly among columns. In the event of partial shading, this configuration allows losses to be limited by distributing the current through unaffected modules. As a result, the system's performance is less sensitive to shading compared to series or series-parallel configurations [7].

2.4. Bridged-Link Configuration

The bridged-link configuration is another variant that combines features of both series and parallel connections, while introducing "bridges" between some modules. These bridges are formed by connecting two modules in series, and then linking those series connections in parallel. The bridges are further connected by cross ties to create a more robust structure against partial shading. The main advantage of this configuration is that it reduces power losses under shading conditions, as currents can flow through multiple alternative paths [8].

2.5. Honey-Comb Configuration

The HC configuration is an adaptation of the bridged-link array, featuring adjustable bridge sizes. The panels are connected in series within small bridges, which are connected by cross ties, just like in the BL array. The honey-comb structure allows for more efficient current distribution across the modules, minimizing power losses [9].

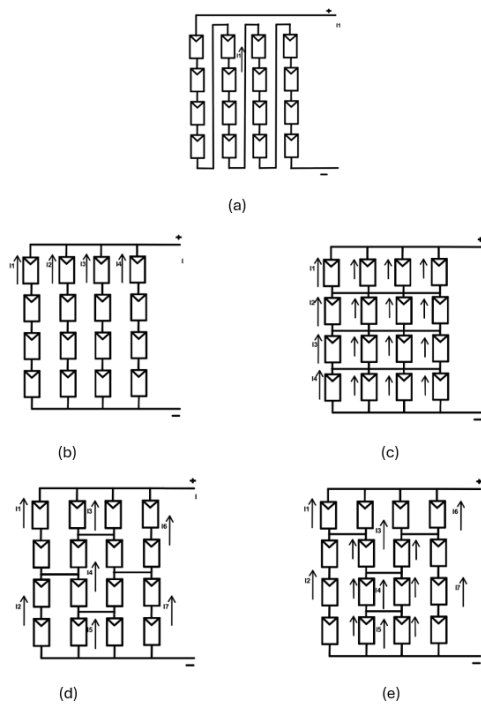


Figure 1: PV configurations: a) Serie, b) Serie-Parallel, c) Total-Cross-Tied, d) Bridged-Link, e) Honey-Comb

3. Analysis of partial shading conditions

3.1. MATLAB/Simulink Simulation of PV Configurations

In this section, the different configurations previously mentioned are simulated using MATLAB/Simulink. Table 1 presents the characteristics of the panel. The simulation models for the five topologies are shown, with the Total-Cross-Tied (TCT) topology illustrated in Figure 2. The main inputs for the simulations are temperature and irradiation. Since we are only focusing on the effects of partial shading, At 25°C, the temperature is maintained consistently.

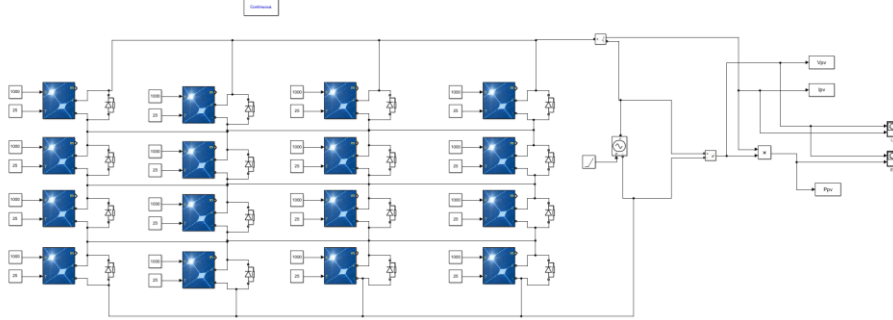


Figure 2. Simulink model for TCT configuration.

Table 1. characteristics of PV panel [10]

Parameters	Values
P_{max}	250 W
V_{mpp}	30.96 V
I_{mpp}	8.07 A
V_{oc}	37.92 V
I_{sc}	8.62 A
a	0.99132
R_{sh}	82.1161 Ω
$V_{oc}(\%/deg.C)$	-0.33969
$I_{sc}(\%/deg.C)$	0.063701

3.2. Shading patterns

We have simulated various partial shading scenarios to evaluate their impact on the performance of different photovoltaic configurations. Specifically, we applied targeted partial shading to four modules located on the left-hand side and the bottom of each configuration. These areas were chosen due to their susceptibility to common sources of shading, such as buildings, trees, or other obstacles in real-world environments [11]. As shown in Figure 3, shading was applied at four levels: 0% (no shading), 20%, 40%, and 60%, to replicate a range of realistic partial shading conditions that could impact energy production. This variation allowed us to assess how each PV system configuration responds to reduced irradiance, which can significantly impact the system's overall efficiency.

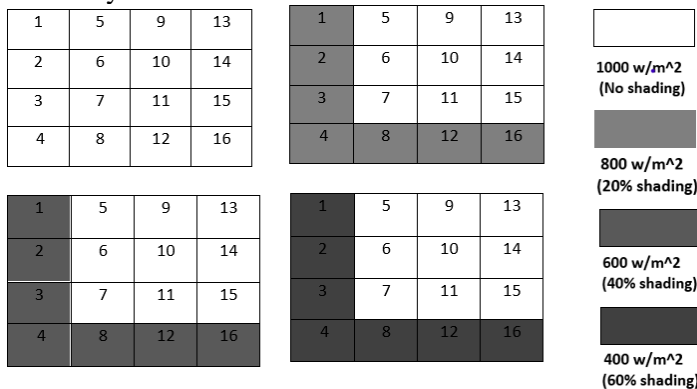


Figure 3. Pattern shading scenario.

4. Results and Discussion

We have generated the P - V (power-voltage) and I - V (current-voltage) curves for each configuration, simulating various levels of partial shading: 0%, 20%, 40%, and 60%. These curves allow us to visualize the impact of shading on system performance and observe changes in the maximum power point (MPP), as well as fluctuations in current and voltage. This analysis will serve as the basis for evaluating which configuration is the most resilient to the negative effects of partial shading. Table 2 presents the simulation results for maximum output current voltage, and power under different shading levels.

Table 2. Output power, current, and voltage under various shading levels.

Shading level	Configuration	P_{\max} (W)	V_{\max} (V)	I_{\max} (A)
No Shading	S	3997	497.5	8.033
	SP	3997	124.4	32.13
	TCT	3997	124.4	32.13
	BL	3997	124.4	32.13
	HC	3997	124.4	32.13
20% Shading	S	3398	509.6	6.68
	SP	3391	127.4	26.61
	TCT	3441	127.4	27
	BL	3419	127.4	26.84
	HC	3402	127.4	26.7
40% Shading	S	2617	521.8	5.015
	SP	2581	130.4	19.79
	TCT	2672	133.5	20.02
	BL	2634	130.4	20.19
	HC	2604	130.4	19.97
60% Shading	S	2193	279.1	7.857
	SP	2540	94.04	27.01
	TCT	2524	91.01	27.73
	BL	2529	91.01	27.79
	HC	2533	94.04	26.93

According to Table 2, the TCT configuration demonstrates the higher power output under shading scenarios, producing 2672 W at 40% shading and 2524 W at 60% shading. In contrast, the series(S) configuration drops to 2617 W and 2193 W, respectively. The Serie-Parallel (SP), Bridged-Link (BL), and Honey-comb (HC) configurations yield slightly lower outputs, with SP at 2540 W, BL at 2529 W, and HC at 2533 W at 60% shading. The superiority of the Total-Cross-Tied can be attributed to its ability to bypass shaded panels effectively, allowing for better energy harvesting. On the other hand, the series configuration suffers from its dependence on all panels, leading to significant performance losses. This analysis confirms that Total-Cross-Tied is the most resilient configuration, when there is shading, the series structure is extremely vulnerable. Moreover, the effect of shading on photovoltaic field performance is also determined by comparing the fill factor results of shading situations.

4.1 Fill factor

This factor is crucial for identifying the effect of shading, as a noticeable decrease in the fill factor indicates an efficiency loss due to shaded areas. The fill factor can be determined using Equation. Table 3 shows the short-circuit current (I_{sc}) and open-circuit voltage (V_{oc}). Table 4 shows the filling factor values. [12]:

$$FF = \frac{P_{max}}{V_{oc}I_{sc}} \quad (1)$$

Table 3. The short circuit current and open circuit voltage of various configurations.

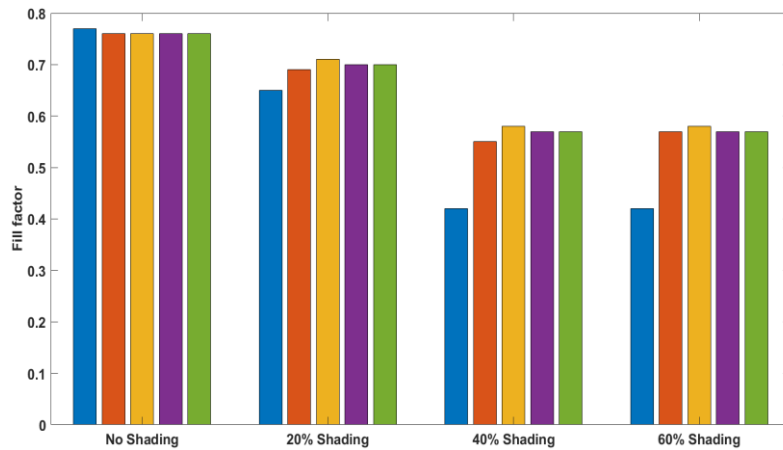
Shading level		S	SP	TCT	BL	HC
No Shading	V_{oc} (V)	606.72	151.7	151.6	151.7	151.7
	I_{sc} (I)	8.62	34.52	34.52	34.52	34.52
20%Shading	V_{oc} (V)	603	148.6	148.6	148.6	148.6
	I_{sc} (I)	8.62	32.79	32.79	32.79	32.79
40%Shading	V_{oc} (V)	600	150	150.1	148	147
	I_{sc} (I)	8.62	31.07	31.02	31.02	31.02
60%Shading	V_{oc} (V)	594.6	149.6	149.6	149.6	149.6
	I_{sc} (I)	8.62	29.29	29.29	29.34	29.4

Table 4: Fill factor values

Configurations	No Shading	20%Shading	40%Shading	60%Shading
S	0.77	0.65	0.42	0.42
SP	0.76	0.69	0.55	0.57
TCT	0.76	0.71	0.58	0.58
BL	0.76	0.70	0.57	0.57
HC	0.76	0.70	0.57	0.57

Figure 4 provides a graph illustrating the impact of different shading levels on the performance of various photovoltaic configurations. Without shading, all configurations show a high fill factor, around 0.76 to 0.77, indicating optimal performance. However, with 20% shading, there is a slight decrease for all configurations, although TCT (0.71) and BL (0.70) maintain the highest performance, showing better shade tolerance compared to others.

At 40% and 60% shading, the impact becomes more significant, especially for configuration S, which drops to 0.42, while Total-cross-Tied (TCT) remains higher at 0.58, followed by Bridged-Link (BL) and Honey-Comb (HC) at 0.57. This increased resilience of TCT under partial shading makes it the most performant configuration in shaded environments, while S is better suited for non-shaded conditions to achieve optimal performance.

**Figure 4.** Fill factor for different configurations

5. Conclusion

This article analyzed partial shading on different configurations of *PV* systems using MATLAB/Simulink simulations. Configurations like Series-Parallel (SP), Serie (S), Total Cross-Tied (TCT), Honey-Comb (HC), and

Bridged-Link (BL), were evaluated for their performance under shading scenarios. conditions. The results show that the Total-Cross-Tied (TCT) configuration offers the best resilience and superior energy production even in challenging conditions. In contrast, series systems experience significant performance losses. The efficiency of all other configurations was verified by the examination of I - V and P - V curves and fill factor values. These findings emphasize the importance of making a judicious choice of PV system configuration to optimize energy production in shading-prone environments.

References

- [1] Patel, H., & Agarwal, V. (2008). MATLAB-based modeling to study the effects of partial shading on PV array characteristics. *IEEE Transactions on Energy Conversion*, 23(1), 302-310. <https://doi.org/10.1109/PVSC.2016.7750368>
- [2] Jha, V., & Triar, U. S. (2019). A detailed comparative analysis of different photovoltaic array configurations under partial shading conditions. *International Transactions on Electrical Energy Systems*, 29(6), e12020. <https://doi.org/10.1002/2050-7038.12020>
- [3] Bingöl, O., & Özkaya, B. (2018). Analysis and comparison of different PV array configurations under partial shading conditions. *Solar Energy*, 160, 336–343. <https://doi.org/10.1016/j.solener.2017.12.004>
- [4] Tubniyom, C., Jaideaw, W., Chatthaworn, R., Suksri, A., & Wongwuttanasatian, T. (2018). Effect of partial shading patterns and degrees of shading on Total Cross-Tied (TCT) photovoltaic array configuration. *Energy Procedia*, 153, 35-41. <https://doi.org/10.1016/j.egypro.2018.10.028>
- [5] Sharma, S., Varshney, L., Elavarasan, R. M., Singh S. Vardhan, A., Singh S. Vardhan, A., Saket, R. K., Subramaniam, U., & Hossain, E. (2021). Performance enhancement of PV system configurations under partial shading conditions using MS method. *IEEE Access*. <https://doi.org/10.1109/ACCESS.2021.3071340>
- [6] Desai, A. A., & Mikkili, S. (2022). Modeling and analysis of PV configurations to extract maximum power under partial shading conditions. *CSEE Journal of Power and Energy Systems*, 8(6), 1670-1677. <https://doi.org/10.17775/CSEEJPES.2020.00900>
- [7] Darussalam, R., Pramana, R. I., & Rajani, A. (2017). Experimental investigation of serial parallel and total-cross-tied configuration photovoltaic under partial shading conditions. *Proceedings of the 2017 International Conference on Sustainable Energy Engineering and Application (ICSEEA)*. IEEE. <https://doi.org/10.1109/ICSEEA.2017>
- [8] Jazayeri, M., Uysal, S., & Jazayeri, K. (2014). A comparative study on different photovoltaic array topologies under partial shading conditions. In *2014 IEEE PES T&D Conference and Exposition* (pp. 1–5). IEEE. <https://doi.org/10.1109/TDC.2014.6863196>
- [9] Amin, M., Bailey, J., Tapia, C., & Thodimeladine, V. (2016, June). Comparison of PV array configuration efficiency under partial shading condition. In *2016 IEEE 43rd Photovoltaic Specialists Conference (PVSC)* (pp. 3704-3707). IEEE. <https://doi.org/10.1109/PVSC.2016.7750368>
- [10] Abdulmawjood, K., Alsadi, S., Refaat, S. S., & Morsi, W. G. (2022). Characteristic study of solar photovoltaic array under different partial shading conditions. *IEEE Access*, 10, 6856-6866. <https://doi.org/10.1109/ACCESS.2022.3142168>
- [11] Xu, C., Itako, K., Kudoh, T., Koh, K., & Ge, Q. (2021). Proposal for an active PV array to improve system efficiency during partial shading. *IEEE Access*, 9, 143423–143426. <https://doi.org/10.1109/ACCESS.2021.3121700>
- [12] Jalil, M. F., Khatoon, S., Nasiruddin, I., & Bansal, R. C. (2020). An improved feasibility analysis of photovoltaic array configurations and reconfiguration under partial shading conditions. *Electric Power Components and Systems*, 48(9–10), 1077–1089. <https://doi.org/10.1080/15325008.2020.1821842>



Investigation of Midwives' Satisfaction with Supportive Personnel Assigned to Vaginal Birth and Their Practice: Mixed Method Research

Engin DİNÇ¹ , Tuğba ARSLAN^{2*} , Serdar ARSLAN³

¹ Department of Public Health Services, Konya Provincial Health Directorate, Konya, Türkiye

² Faculty of Health Sciences, Department of Occupational Therapy, Çankırı Karatekin University, Çankırı, Türkiye

³ Nezahat Keleşoğlu Faculty of Health Sciences, Department of Physiotherapy and Rehabilitation, Necmettin Erbakan University, Konya, Türkiye

Abstract

The objective of this study is to evaluate the satisfaction of midwives with the level of support provided by the personnel assigned to vaginal births. The population of the research will be midwives working in the hospital to provide medical care. Given that the research is a focus group interview, it was decided that 12 participants would be appropriate. The following questions were posed: "Does the supportive staff communicate correctly with the hospital staff and the pregnant woman?", "Did the supportive staff pay attention to the guidance of the delivery room midwives in the selection of the pregnant woman?", and "Are you satisfied with this practice?" In terms of the communication skills of the supportive staff, 53.85% of the participants rated them as very good, while 46.15% rated them as good. In regard to the attention paid by the supportive staff to the guidance provided by midwives in the selection of pregnant women, 66.67% of the participants responded that it was very good, while 33.33% indicated that it was good. With regard to their satisfaction with the practice, eight participants answered "very good," three answered "good," and one answered "bad." The majority of participants expressed satisfaction with the practice and the conduct of the supportive staff. Qualitative analysis revealed that some support staff were perceived to disregard working hours and provide inadequate assistance to pregnant women. This reduces the midwife's workload, aligning with the anticipated outcomes. However, the research also illuminated the underlying issues.

Keywords: Personal Satisfaction, Midwifery, Qualitative Research

1. Introduction

The provision of continuous support throughout the process of labour has been demonstrated to have a positive impact on the outcomes for both the mother and the infant. These include an increased incidence of spontaneous vaginal birth, a shorter duration of labour and caesarean section, instrumental vaginal delivery, the use of any analgesia, the use of regional analgesia, a lower five-minute Apgar score and negative feelings about the birth experience. It is recommended that healthcare organisations integrate the provision of continuous support during labour into their policies and guidelines [1]. In-service training on supportive interventions was provided to volunteer midwives employed by the Konya Provincial Health Directorate. Those who completed this training were subsequently assigned to provide supportive care in addition to medical care. In order to achieve their goals and to retain invested employees, businesses must continuously invest in human resources [2]. It is therefore important to conduct research into employee satisfaction in the health sector [3]. Nevertheless, research has tended to concentrate on patient satisfaction, and the number of studies examining employee satisfaction is limited [4]. Furthermore, in contrast to this standard procedure, it would be advantageous to interpret the planned dissemination of the aforementioned supportive care directly by the relevant personnel.

The objective of this study was to assess the satisfaction of midwives with the personnel responsible for providing supportive care during vaginal births.

2. Materials and Methods

Volunteer midwives working in Konya Provincial Health Directorate were given in-service training on supportive interventions and the midwives who completed this training were assigned to Konya Training and Research Hospital, Dr. Ali Kemal Berivanlı Obstetrics and Gynaecology Hospital for supportive care in addition to medical care. Midwives working in the relevant hospital to provide medical care constituted the population of the study. Since the research was a focus group interview, it was decided to take 12 participants [5]. Participant Selection and Information: Participants were selected on the basis of volunteerism and demographic diversity. Each

* Corresponding author. e-mail address: tugbaarslan@karatekin.edu.tr

participant was given detailed information about the purpose, scope and process of the research and their written consent was obtained.

Data Collection Methods

An independent researcher from Konya Provincial Directorate of Health met face-to-face with the participants to inform them about the research. The research was conducted with semi-structured interview techniques using a qualitative approach. Individual interviews with each participant were conducted at their convenience and in an environment where they would feel comfortable. One-to-one interviews with the participants were planned and a combination of selected questions and open-ended questions were used to gain an in-depth understanding of the participants' experiences. Participants were asked to answer the questions 'Do the supportive staff communicate correctly with the hospital staff and the pregnant woman?', 'Did the supportive staff pay attention to the guidance of the midwives in the delivery room in the selection of the pregnant woman?', 'Are you satisfied with this practice?' in three options as very good, good and bad. In addition, an open-ended question was asked as 'What are your opinions and suggestions about this practice?' and 'What are your opinions and suggestions about the supportive staff?'. During these interviews, in-depth conversations about the participants' experiences were encouraged. The interview lasting approximately 15 minutes to a half hour. With the permission of the participants, all interviews were recorded through audio recorders. This ensured accurate transcription of the data for later analysis. Protecting the identity of the participants was a top priority and names and identifying information were anonymised. Audio recordings and transcripts were stored in encrypted files accessible only by the research team and securely destroyed after analysis.

Data Preparation and Organisation

The audio recordings were transcribed and converted into written texts. These texts will be organised and coded to be used in the analysis process. The data were analysed using thematic analysis method. This method is a qualitative form of analysis used to reveal the main themes, patterns and meanings in the data set. Initially, open coding was used, i.e. the data were carefully examined and the important parts were labelled and coded. These codes were then combined to form broader themes. As a result of analysing and comparing the codes, similar codes were grouped under themes and these themes represented the findings of the study.

Data Analysis

The themes were interpreted and evaluated in relation to the purpose of the research and the literature. In this process, main themes and patterns were extracted from participant responses and a comparative analysis was conducted [6]. This process aimed to answer the research questions and provide an in-depth understanding of participant experiences. To ensure the accuracy of the findings, feedback from participants was taken into account throughout the analysis process and the findings were adjusted to accurately reflect the participants' experiences.

Reporting and Presentation

The results of the analyses were reported and presented in accordance with the aims and hypotheses of the study. The findings were presented in accordance with scientific ethics and research standards and the confidentiality of the participants was protected.

Ethical Considerations

Ethical approval for the research was obtained from Çankırı Karatekin University Ethics Committee (unique decision code: 687d967ba1fa4fb0). Participants gave written informed consent. They were informed about the purpose of the study, their rights and the voluntary nature of their participation. Confidentiality and anonymity were maintained throughout the study by removing identifying information from transcripts and replacing it with unique participant codes.

3. Results

In this study, the satisfaction status of midwives working in the hospital to provide medical care from the practice of assignment to support women who give vaginal birth was examined. In this study, all of the participants were midwives with a bachelor's degree. All of the participants were women. The satisfaction of the participants was analysed quantitatively with a multiple-choice question in the form of 'Are you satisfied with this practice?' and very good, good, bad. To the related question, 8 (66.67%) participants answered very good, 3 (25%) participants answered good, and 1 (8.33%) participant answered bad. In the questions examining the opinions of the participants about the supportive staff, 53.85% of the participants answered very good and 46.15% answered

good for the communication skills of the supportive staff. Regarding the attention of the supportive staff to the guidance of midwives in pregnancy selection, 8 (66.67%) of the participants answered very good and 4 (33.33%) answered good.

1. What are your opinions and suggestions about this application?

Thematic Analysis of the Practice

Sample Answer: 'I often had to take care of the birth of more than one pregnant woman and this made me feel that I was not doing my job well enough. Thanks to this application, I feel comfortable taking care of other pregnant women'

Themes:

Satisfaction with the practice: In general, it was determined that midwives were satisfied with this practice.

2. What are your opinions and suggestions about the supportive staff?

Sample Answers: 'I like our friend's pregnancy support very much. She follows her work carefully and devotedly to the end. '

'Opening up to the pregnant woman and postnatal practices are good, but some support staff could spend more time with the pregnant woman. '

'Careful care is given to the pregnant woman, but the staff did not inform the midwives of the labour ward about the rest period, which created a negative observation. '

Themes:

Supportive staff behaviours: It was determined that the supportive staff did not always work in harmony with the medical midwife during rest breaks and working hours.

4. Discussion

In this study, the satisfaction of the midwives working in the hospital for medical intervention with the practices and behaviours of the midwives assigned to support the woman in vaginal birth was examined. Most of the practices and attitudes were mostly satisfied and a few negative feedbacks were received, such as determining the break times. Research has focused on the satisfaction of women who have given birth in larger numbers. And high satisfaction levels were reported in these studies [7,8]. The reason for satisfaction was determined as the presence of a doula and a family member in the room during labour and the practices performed before and during labour [7].

In a study examining the satisfaction level of midwives working in Greece, only 45.5% of midwives reported that they were satisfied with their jobs [9] prioritising the satisfaction of a professional group in which about half of them are not satisfied with their work will increase their work efficiency. In a study examining the satisfaction of midwives, the physical structure of the delivery room was examined [10]. Vaginal birth is an important process in which midwives play the most important role for both maternal and neonatal health. The findings of this study are important because all kinds of applications to be made in this process will affect not only the women in labour but also the work efficiency of midwives.

Acknowledgement

There is no financial support for the research.

References

- [1] Lunda, P., Minnie, C. S., & Benadé, P. (2018). Women's experiences of continuous support during childbirth: A meta-synthesis. *BMC Pregnancy and Childbirth*, 18(1), 167. <https://doi.org/10.1186/s12884-018-1755-8>
- [2] Bayraç, A. (2008). *İşletmelerde stratejik insan kaynakları yönetiminde eğitim ve geliştirme*. MSc Thesis, Selçuk University, Social Sciences Institute, 2008, 239, Konya.
- [3] . Vural, F., Dura, A. A., Fil, Ş., Çiftçi, S., Torun, S. D., & Patan, R. (2012). Sağlık çalışanlarında memnuniyet, kurumda kalma ve örgütsel bağlılığa etki eden faktörler. *Balıkesir Sağlık Bilimleri Dergisi*, 1(3), 137-144.
- [4] Meng, R., Li, J., Zhang, Y., Yu, Y., Luo, Y., Liu, X., ... & Yu, C. (2018). Evaluation of patient and medical staff satisfaction regarding healthcare services in Wuhan Public Hospitals. *International journal of environmental research and public health*, 15(4), 769.
- [5] Yağar, F. (2023). Nitel araştırmalarda örneklem büyüklüğünün belirlenmesi: veri doygunluğu. *Aksaray Üniversitesi Sosyal Bilimler Enstitüsü Dergisi*, 7(2), 138-152.
- [6] Braun V, Clarke V. Thematic analysis. *APA handbook of research methods in psychology*, Vol 2: Research designs: Quantitative, qualitative, neuropsychological, and biological. APA handbooks in psychology®. Washington, DC, US: American Psychological Association; 2012. p. 57-71.
- [7] Liu, Y., Li, T., Guo, N., Jiang, H., Li, Y., Xu, C., & Yao, X. (2021). Women's experience and satisfaction with midwife-led maternity care: A cross-sectional survey in China. *BMC Pregnancy and Childbirth*, 21, 151. <https://doi.org/10.1186/s12884-021-03638-3>
- [8] Shahbazi Sighaldehy, S., Azadpour, A., Vakilian, K., Rahimi Foroushani, A., Vasegh Rahimparvar, S. F., & Hantoushzadeh, S. (2023). Comparison of maternal outcomes in caring by Doula, trained lay companion and routine midwifery care. *BMC Pregnancy and Childbirth*, 23(1), 765. <https://doi.org/10.1186/s12884-023-05987-7>
- [9] Papoutsis, D., Labiris, G., & Niakas, D. (2014). Midwives' job satisfaction and its main determinants: A survey of midwifery practice in Greece. *British Journal of Midwifery*, 22(7), 480-486.
- [10] Wangler, S., Simon, A., Meyer, G., & Ayerle, G. M. (2023). Influence of the birthing room design on midwives' job satisfaction – A cross-sectional online survey embedded in the 'Be-Up' study. *Sexual & Reproductive Healthcare*, 37, 100867.



Flow and Heat Transfer in an Asymmetric Trapezoidal Duct with Turbulators

Nasser Abdoul Halim ISMAEL¹, , Selma AKÇAY², , Maher Abdulhameed Sadeq SADEQ³, 

¹ Department of Mechanical Engineering, Çankırı Karatekin University, Çankırı, Türkiye2

² Çankırı Karatekin University, Engineering Faculty, Department of Mechanical Engineering, Çankırı, Türkiye

³ Department of Mechanical Engineering, Çankırı Karatekin University, Çankırı, Türkiye

Abstract

Channels with wavy/corrugated surfaces, which are passive heat transfer improvement methods, have attracted great attention for a long time [1,2]. Corrugated channels provide significant improvement in heat transfer because they increase surface area [3]. Another passive method is the turbulators/obstacles added to channel [4]. The purpose of these turbulators is to direct the flow in a certain direction, improve flow mixing and increase heat transfer [5]. To date, heat transfer in wavy channels with different geometries with or without turbulators has been investigated by many numerical and experimental studies and as a result, it has been reported that significant improvements in heat transfer are obtained in these channels compared to straight channels [6-8]. In this study, a trapezoidal duct with asymmetric geometry was used and circular turbulators were placed inside the wavy channel. The heat transfer behavior of circular turbulators in three different diameters was investigated. The analyses were performed with the finite volume method and the standard k- ϵ turbulence model was used as the viscous model. The wavy surfaces of the channel were kept constant at $T_w=340$ K and the channel outlet temperature (T_{out}), convection heat transfer coefficient (h), Nusselt number (Nu) and heat transfer improvement rate (ER) were found at different Reynolds numbers ($3000 \leq Re \leq 6000$). The results were presented as graphs. The velocity and temperature images were obtained for different parameters in the channel and the results were discussed. In addition, the results were compared with the wavy channel without turbulators. As a result of the study, it was observed that heat transfer improved by increasing inlet velocity. It was seen that the circular turbulators added to the channel significantly affected the heat transfer and the heat transfer increased with the increase in the circular turbulator diameters.

Keywords: Asymmetric trapezoidal duct, Heat transfer, Turbulator

1. Introduction

Channels with wavy/corrugated surfaces, which are passive heat transfer improvement methods, have attracted great attention for a long time [1, 2]. Corrugated channels provide significant improvements in heat transfer because they increase surface area [3]. Another passive method is the obstacles/turbulators added to the channel [4]. The purpose of these turbulators is to direct the flow in a certain direction, improve flow mixing and increase heat transfer [5]. To date, heat transfer in wavy channels with different geometries with or without turbulators has been investigated by many numerical and experimental studies and as a result, it has been reported that significant improvements in heat transfer are obtained in these channels compared to straight channels [6-8]. Uysal and Akcay [6] investigated the flow and heat transfer in hybrid wavy channels and showed that the hybrid wave profile improved the heat transfer compared to the uniform wave profile. Zheng et al. [7] numerically investigated the effects of vortex generators with different shapes on heat transfer and nanofluid flow and reported that the flow and heat transfer behavior were significantly affected by the vortex shapes. Brodniansk'a, & Kot'smíd [8] investigated the heat transfer enhancement in a new type of corrugated channel heat exchanger with circular cylinders. They reported that the circular vortex generator provided improved heat transfer, and the heat transfer in corrugated channels was improved by 1.98 times compared to the flat channel.

The geometry of the wave profile, the geometry of the vortex generators added into the channel, their locations, their sizes, flow and fluid conditions affect the flow and heat transfer. Studies on this subject have increased due to the large number of parameters to be examined. Therefore, in this study, the effects of circular turbulators on the flow and heat transfer in an asymmetric wavy channel were investigated numerically under turbulent flow conditions.

* Corresponding author. e-mail address: selmaakcay@karatekin.edu.tr

2. Materials and Methods

2.1. Numerical geometry

Figure 1 indicates the geometry of the asymmetric trapezoidal duct with turbulators used in this work. There are adiabatic straight parts with a length of $L_1 = 100$ mm at the inlet and outlet of the channel. The asymmetric trapezoidal duct part (L_2) is heated. This part is kept at a constant temperature of 340 K. Circular cylinders are placed inside the wavy channel. Analyses were performed for three different diameters values of circular turbulators (d : 2 mm, 4 mm, 6 mm). The geometric parameters of the numerical model are given in Figure 1.

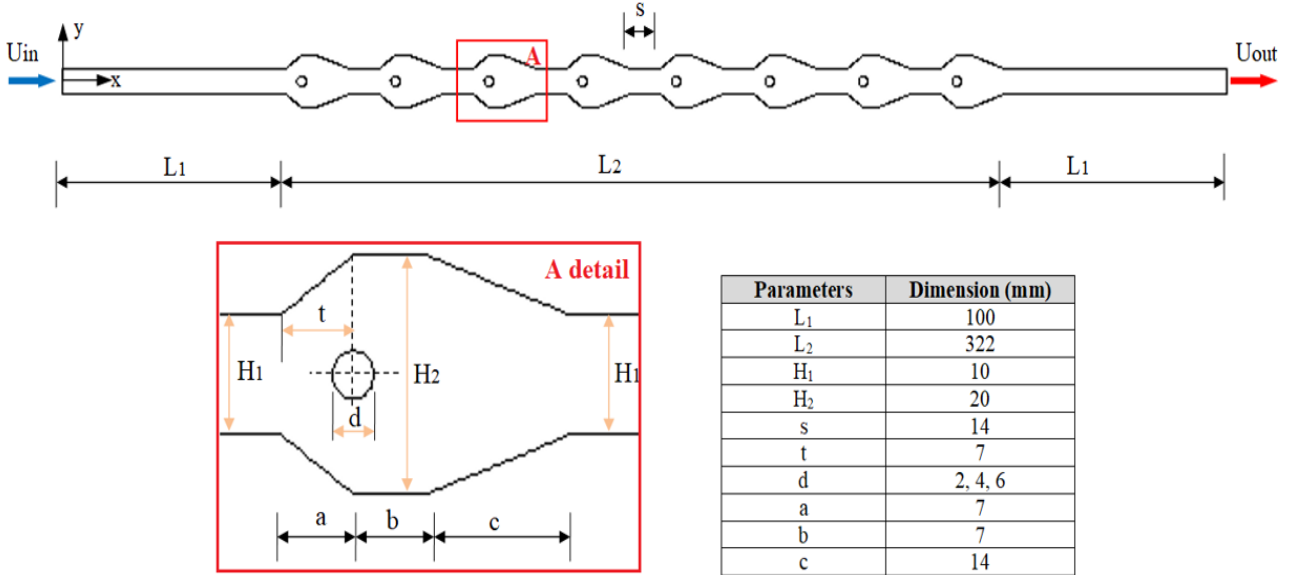


Figure 1. Geometry of the numerical model (with details)

2.2. Governing equations

In the numerical study, the solution field is 2d. The fluid is considered single-phase, incompressible and Newtonian. The flow is turbulent and steady case. Viscous terms are ignored. Fluid properties are constant. The effects of gravity and radiation are neglected. According to these assumptions, the governing equations are given below:

$$\frac{\partial}{\partial x_i}(\rho \bar{u}_i) = 0 \quad (1)$$

$$\frac{\partial}{\partial t}(\rho \bar{u}_i) + \frac{\partial}{\partial x_j}(\rho \bar{u}_i \bar{u}_j) = -\frac{\partial \bar{p}}{\partial x_i} + \frac{\partial}{\partial x_j} \left[(\mu + \mu_t) \left(\frac{\partial \bar{u}_i}{\partial x_j} + \frac{\partial \bar{u}_j}{\partial x_i} \right) \right] - \rho \overline{u'_i u'_j} \quad (2)$$

$$\frac{\partial}{\partial t}(\rho c \bar{T}) + \frac{\partial}{\partial x_j}(\rho \bar{u}_j \bar{T}) = \frac{\partial}{\partial x_j} \left[(\Gamma + \Gamma_t) \left(\frac{\partial \bar{T}}{\partial x_j} \right) \right] \quad (3)$$

$$-\rho \overline{u'_i u'_j} = (\mu_t) \left(\frac{\partial u_i}{\partial x_j} + \frac{\partial u_j}{\partial x_i} \right) \quad (4)$$

$$\frac{\partial}{\partial t}(\rho k) + \frac{\partial}{\partial x_i}(\rho k \bar{u}_i) = \frac{\partial}{\partial x_j} \left[\left(\mu + \frac{\mu_t}{\sigma_k} \right) \frac{\partial k}{\partial x_j} \right] + G_k - \rho \varepsilon \quad (5)$$

$$\frac{\partial}{\partial t}(\rho \varepsilon) + \frac{\partial}{\partial x_i}(\rho \varepsilon \bar{u}_i) = \frac{\partial}{\partial x_j} \left[\left(\mu + \frac{\mu_t}{\sigma_\varepsilon} \right) \frac{\partial \varepsilon}{\partial x_j} \right] + C_{1\varepsilon} \frac{\varepsilon}{k} G_k - C_{2\varepsilon} \rho \frac{\varepsilon^2}{k} \quad (6)$$

In this study, the heat transfer in the asymmetric trapezoidal duct with different diameters of circular turbulators were studied at different Reynolds numbers ($3000 \leq Re \leq 6000$).

2.3. Numerical method and boundary conditions

The numerical study was conducted by the ANSYS Fluent solver. The standard k- ϵ turbulence model was used as the flow model. Governing equations were discretized with the finite volume approach and the velocity-pressure relationship was used with the SIMPLE algorithm. The convergence criterion was set as 10^{-7} for the energy equations and 10^{-4} for the other equations. For the mesh independence testing, the Nusselt numbers were calculated for different element numbers. As a result of this calculations, it was decided that 164122 element numbers are sufficient for the numerical solutions.

The working fluid is air. The air enters the channel at a constant velocity (U_{in}) and temperature ($T_{in}=293$ K). In the study, Reynolds number varied in the range of $3000 \leq Re \leq 6000$. The surfaces of the wavy duct (L_2) were kept constant at $T_s=340$ K. The non-slip wall condition was defined for the all surfaces. Straight parts at the inlet and outlet of the channel are adiabatic. The circular turbulators were assumed to be adiabatic and non-slip conditions.

2.4. Mathematical Model

The Reynolds number (Re) is calculated by Equation (7):

$$Re = \frac{\rho U_{in} D_h}{\mu} \quad (7)$$

where, D_h is the hydraulic diameter, ρ is the density, μ is the dynamic viscosity, and U_{in} is the inlet velocity.

The average Nusselt number (Nu) is obtained by Equation (8):

$$Nu = \frac{h D_h}{k_f} \quad (8)$$

where, k_f and h are thermal conductivity and convective heat transfer coefficient, respectively.

$$h = \frac{q''}{\Delta T_{log}}$$

where, q'' and ΔT_{log} are heat flux and logarithmic temperature difference, respectively.

Logarithmic temperature difference is calculated by Equation (9):

$$\Delta T_{log} = \frac{[(T_w - T_{out}) - (T_w - T_{in})]}{\ln \left[\frac{(T_w - T_{out})}{(T_w - T_{in})} \right]} \quad (9)$$

where, T_{in} , T_{out} , and T_w represent the inlet and outlet temperatures of the fluid and the temperature of the wavy surface, respectively.

The improvement ratio (ER) is described with Equation (10).

$$ER = \frac{Nu_w}{Nu_o} \quad (10)$$

where, Nu_w shows the Nusselt number obtained in the asymmetric trapezoidal wavy duct with circular turbulators, and Nu_o shows the Nusselt number obtained in the asymmetric trapezoidal wavy duct without turbulators.

Results and Discussion

2.5. Validation of the numerical results

The numerical results obtained in this work were validated with the results of previous studies. Wang et al. [9] experimentally examined heat transfer for the turbulent flow of air in a flat channel. Fig. 2 indicates the comparison of the results of this study with Wang et al. [9].

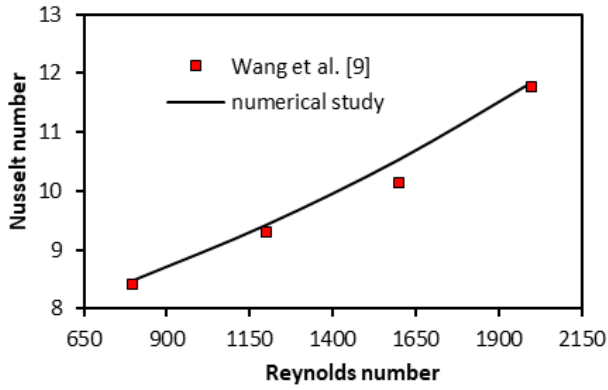


Figure 2. Validation of the numerical study

In this study, the velocity and temperature contours were presented to indicate the effects of the asymmetric trapezoidal wavy duct, circular turbulators and Reynolds number on heat transfer.

In Figure 3, the velocity contours are indicated in the asymmetric trapezoidal wavy duct with different diameters of circular turbulators for $Re=6000$. The circular turbulators in the wavy channel were considerably changed the flow fields. The presence of stagnant liquid regions in trapezoidal wavy gaps in the channel without circular turbulators is remarkable. It was observed that as the diameter of the circular turbulators increased, the fluid penetrated better into the wavy channel surfaces. However, the increase in the turbulator diameters caused the low pressure regions formed behind the turbulators to increase.

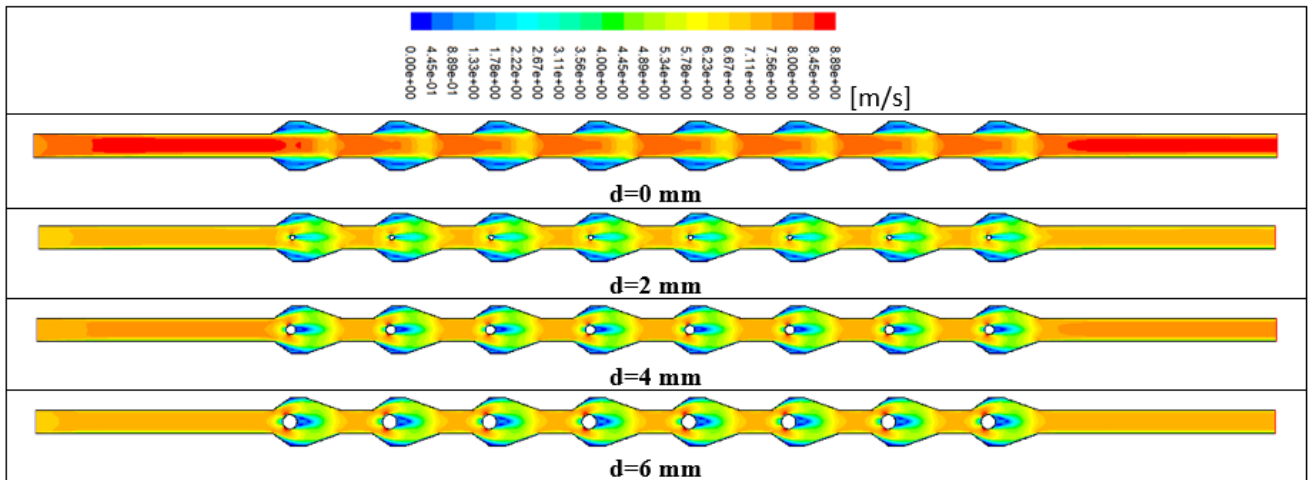


Figure 3. Velocity contours for different diameters of the circular turbulators at $Re=6000$

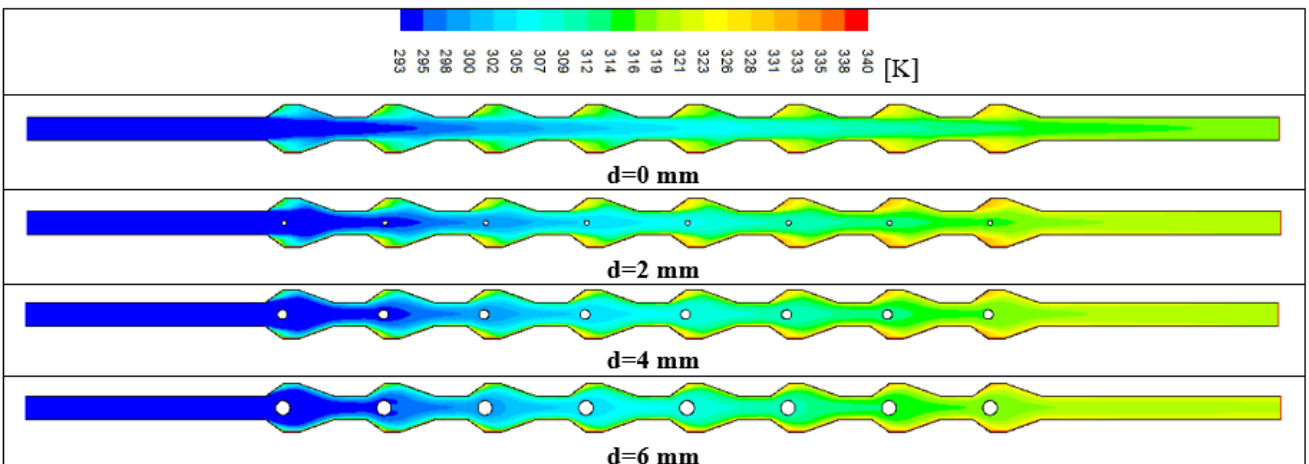


Figure 4. Temperature contours for different diameters of the circular turbulators at $Re=6000$

Figure 4 shows the temperature contours in the asymmetric trapezoidal wavy duct with different diameters of circular turbulators for $Re=6000$. The circular turbulators significantly affected the thermal fields. It was observed that the temperature gradient within the channel decreased by increasing the size of the circular turbulators. A decrease in the temperature of the wavy surfaces was observed with increasing turbulator diameters. In the channel with the turbulator diameter of $d=6$ mm, the temperature of the wavy surfaces decreased significantly compared to the turbulator diameter of $d=2$ mm. It was also observed that the channel temperature increased in the flow direction for all the channels with and without turbulators.

Figure 5 indicates the outlet temperature of the fluid (a), heat transfer coefficient (W/m^2K) (b), Nusselt number (c), and heat transfer enhancement ratio (d) with Reynolds number for the asymmetric trapezoidal wavy duct with/without turbulators. It was observed that the outlet temperature decreased with increasing Reynolds number for all channel flows. The highest outlet temperature was obtained in the channel with $d=6$ mm turbulator diameter (Fig. 5a). Increasing Reynolds number increased the heat transfer coefficient in all channel cases. The highest heat transfer coefficient was obtained in the turbulator diameter of $d=6$ mm (Fig. 5b). Increasing Reynolds number also increased the Nusselt number in all channels. It is seen that higher heat transfer is provided in the highest turbulator diameter studied ($d=6$ mm) (Fig. 5c). In Figure 5d, the channel without turbulators is considered as reference and the effects of different turbulator diameters on heat transfer improvement are calculated. The heat transfer improvement rate also increased with increasing turbulator diameters. At $Re=6000$, heat transfer in the turbulator diameter of $d=6$ mm increased by 1.27 times compared to the channel without turbulator (Fig. 5d).

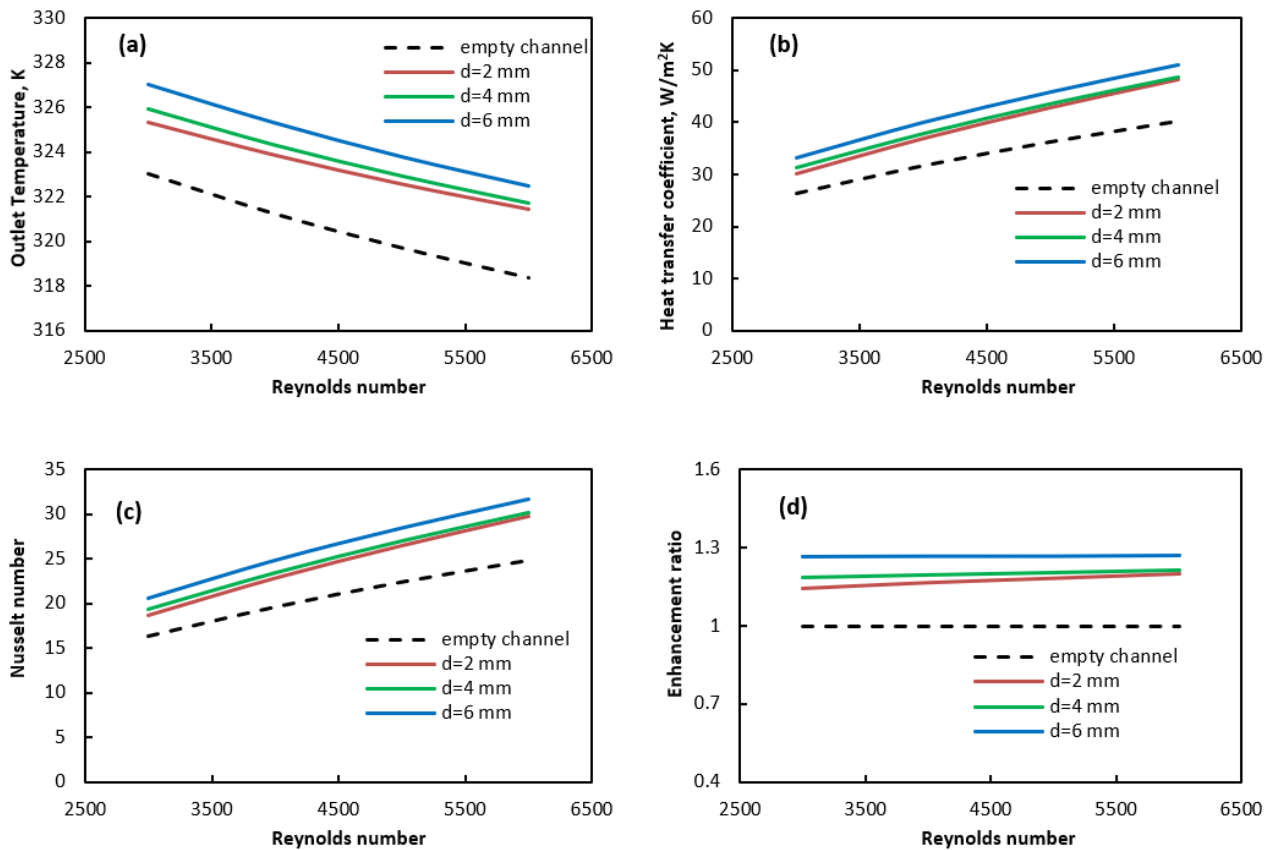


Figure 5. a- Outlet temperature, b- Heat transfer coefficient, c- Nusselt number, d- Enhancement ratio with Re

3. Conclusion

In this study, the effects of circular turbulators on the flow and heat transfer in an asymmetric trapezoidal wavy channel were numerically investigated under turbulent flow conditions. The analyses were carried out for

different diameters of turbulators and Reynolds numbers in the range of $3000 \leq Re \leq 6000$. In the study, the channel outlet temperature (T_{out}), convection heat transfer coefficient (h), Nusselt number (Nu) and heat transfer improvement ratio (ER) obtained for different parameters were presented as graphs. The velocity and temperature images were obtained in the channel. The main findings are listed below:

- It was seen that the circular turbulators added to the channel significantly affected the flow and heat transfer.
- The outlet temperature of the channel decreased with increasing Reynolds number for all channel flows. The highest outlet temperature was obtained in the channel with $d=6$ mm turbulator diameter.
- Increasing Reynolds number increased the heat transfer coefficient in all channel cases. The highest heat transfer coefficient was obtained in the turbulator diameter of $d=6$ mm.
- Increasing Reynolds number increased the Nusselt number in all channel flows. It is seen that higher heat transfer is provided in the highest turbulator diameter studied ($d=6$ mm).
- Heat transfer enhancement ratio increased with increasing turbulator diameters. At $Re=6000$, heat transfer in the turbulator diameter of $d=6$ mm increased by 1.27 times compared to the channel without turbulators.

Acknowledgement

In this study, the financial support was provided by The Scientific and Technological Research Council of Turkey (TUBITAK), Project No: 1919B012319076 (2209A, University Students Research Projects Support Program, 2023-2). All numerical work was conducted in Çankırı Karatekin University Computer Laboratory. The authors would like to thanks to all supporters due to their precious contributions.

References

- [1] Zhang, J., Zhu, X., Mondejar, M. E., & Haglind, F. (2019). A review of heat transfer enhancement techniques in plate heat exchangers. *Renewable and Sustainable Energy Reviews*, 101, 305-328.
- [2] Nitturi, L. K., Kapu, V. K. S., Gugulothu, R., Kaleru, A., Vuyyuri, V., & Farid, A. (2023). Augmentation of heat transfer through passive techniques. *Heat Transfer*, <https://doi.org/10.1002/htj.22877>
- [3] Alfellag, M.A., Ahmed, H.E., Jehad, M.G., & Farhan, A.A. (2022). The hydrothermal performance enhancement techniques of corrugated channels: A review. *Journal of Thermal Analysis and Calorimetry*, 147, 10177-10206.
- [4] Alam, T., & Kim, M. H. (2018). A comprehensive review on single phase heat transfer enhancement techniques in heat exchanger applications. *Renewable and Sustainable Energy Reviews*, 81, 813-839.
- [5] Akçay, S. (2023). Numerical study of turbulent heat transfer process in different wavy channels with solid and perforated baffles, *Heat Transfer Research*, 54(18), 53-82.
- [6] Uysal, D., & Akçay, S. (2024). Numerical study of thermal and hydrodynamic characteristics of turbulent flow in hybrid corrugated channels with different wave profiles. *Journal of Mechanical Engineering and Sciences*, 18(2), 10026–10045
- [7] Zheng, Y., Yang, H., Mazaheri, H., Aghaei, A., Mokhtari, N., & Afrand, M. (2021). An investigation on the influence of the shape of the vortex generator on fluid flow and turbulent heat transfer of hybrid nanofluid in a channel. *Journal Thermal Analysis and Calorimetry*, 143,1425–1438.
- [8] Brodniansk'a, Z., & Kot'smíd, S. (2023). Heat transfer enhancement in the novel wavy shaped heat exchanger channel with cylindrical vortex generators. *Applied Thermal Engineering*, 220, 119720
- [9] Wang, G., Qia, C., Liu, M., Li, C., Yan, Y., & Liang, L. (2019). Effect of corrugation pitch on thermo-hydraulic performance of nanofluids in corrugated tubes of heat exchanger system based on exergy efficiency. *Energy Conversion and Management*, 186, 51–65.



Investigation of Properties of Waste Concrete Powder Substituted Cement-based Mortars

Selahattin GUZELKUCUK^{1,}*

¹ Ayas Vocational School, Department of Architecture and Urban Planning, Ankara University, Ankara, Türkiye.

Abstract

As a result of the demolition of buildings, that have reached the end of their lifespan and do not meet current needs, whether due to urban transformation activities or the damage from natural disasters, a large amount of construction and demolition waste (CDW) is generated. However, urbanization, industrialization and rapid population growth and rising construction activities continue to increase the demand for cement day by day. This study aimed to assess the properties of CDW-incorporated cement-based mortars and evaluate CDW's potential as a substitute to cement. In this study, the properties of mortars produced by replacing cement with 10%, 20% and 30% waste concrete powder were compared with reference samples (without waste concrete powder) through workability, flexural strength, compressive strength and ultrasonic pulse velocity tests. The substitution of waste concrete powder in mortar mixtures reduced 7- and 28-day flexural and compressive strength values. However, the strength values of samples with a 10% substitution rate were close to those of the reference samples. It was observed that the ultrasonic pulse velocity measurements taken after 28 days correlated with the compressive strength values. As the strength of the samples increased, the ultrasonic pulse speeds increased. As a result, it was concluded that waste concrete powder can be used in cement-based systems and the properties of mortars prepared with varying ratios of concrete waste as a substitute for cement in concrete should be examined in greater detail.

Keywords: *Waste concrete powder, compressive strength, flexural strength, ultrasonic pulse velocity*

1. Introduction

It is estimated that construction and demolition waste represents at least 30% of the total solid waste produced in the world, and therefore, the construction industry is considered one of the largest producers of solid waste worldwide [1]. Engineering studies today aim to both improve the strength and durability of concrete and minimize the negative impacts on the environment. Recycling construction and demolition waste, which occurs as a result of demolition of buildings that have completed their lifespan through urban transformation and natural disasters such as earthquakes, is very important both economically and environmentally [2,3]. The huge demand for concrete worldwide causes high greenhouse gas emissions [4]. In addition to the need for tons of aggregate to meet the current market for concrete, a large amount of fossil fuel resources are required to be used in cement furnaces. Therefore, recycling of concrete waste which is the largest portion of the construction and demolition waste generated can contribute to the gradual reduction of the utilization of fossil fuels [5]. Adding this waste into cement as substitute materials can improve the properties of concrete, reduce the pressure on natural resources [6], and positively reduce greenhouse gas emissions [7]. The large amount of concrete waste generated in recent years, which has caused negative environmental problems, makes it necessary to turn this waste into a recyclable building material [8]. This study aimed to determine the properties of construction and demolition waste and evaluate its usability as an alternative to cement use.

2. Materials and Methods

2.1. Materials

According to the TS EN 196-1 standard, cement mortars were prepared by replacing cement with 10%, 20%, and 30% waste concrete powder. The chemical compositions of the cement and waste concrete powder used in the study are given in Table 1. CEM I 42.5 R type Portland cement by TS EN 197-1 was used in the study.

The concrete rubble fragments obtained from the demolition process of the buildings in urban transformation areas were ground until reached approximately the fineness of the cement to obtain the waste concrete powder. Sand used in this study was CEN reference sand mentioned in the TS EN 196-1 standard.

* Corresponding author. e-mail address: sguzelkucuk@ankara.edu.tr

Table 1. Chemical compositions of materials

Chemical Composition	Cement (%)	Waste Concrete Powder (%)
SiO ₂	24.30	31.6
Al ₂ O ₃	3.96	4.8
Fe ₂ O ₃	3.34	3.5
CaO	59.98	31.5
MgO	2.01	5.1
SO ₃	4.20	0.9
K ₂ O	0.42	0.7
Na ₂ O	0.35	0.45
TiO ₂	-	0.2
P ₂ O ₅	-	0.1
Loss on ignition	1.43	21.1

2.2. Preparation of Mixtures

The material quantities of mortar samples prepared according to the TS EN 196 – 1 standard are given in Table 2. In the table, “WCP” refers to waste concrete powder, while “0, 10, 20, and 30” refer to the substitution rate.

Table 2. Material quantities of mortar mixtures

Sample Code	Cement (Gram)	WCP (Gram)	Aggregate (Gram)	Water (Gram)
WCP0	450	0	1350	225
WCP10	405	45	1350	225
WCP20	360	90	1350	225
WCP30	315	135	1350	225

2.3. Testing of Samples

Flow table, compressive strength, flexural strength, and ultrasonic pulse velocity tests were performed on the samples.

2.3.1. Flow Table Test

The workability conditions of cement mortars were examined with the flow table test by ASTM C1437 standard.

2.3.2. Flexural Strength Test

At the end of 7 and 28 days, 40×40×160 mm prism-shaped samples were subjected to a flexural load at a constant speed of 50 ± 10 N/s according to TS EN 196-1 standard.

2.3.3. Compressive Strength Test

Compressive strength tests were performed at the end of 7 and 28 days of the curing process by TS EN 196-1 standard by applying a load at a constant speed of 2400 ± 200 N/s.

2.3.4. Ultrasonic Pulse Velocity Test

Ultrasonic pulse velocity test was performed on at least three oven-dried prism-shaped samples of 50 x 50 x 50 mm, and the average values were determined as the result. The values obtained from the device were used for direct comparison without any processing.

3. Results and Discussion

3.1. Flow Table Test

The results obtained from the flow table test conducted to determine the workability properties of waste concrete powder substituted cement mortars are given in Figure 1. according to the flow table test results in the graph, it was observed that the initial flow values were equal and 100 mm for all samples. The highest fluidity was in the WCP0-coded cement mortar without additives, with a final flow value of 148.5 mm, while the lowest fluidity was in the WCP30-coded cement mortar, with a final flow value of 141 mm. It is thought that this situation is because the water absorption capacity of waste concrete powder is higher than that of cement.

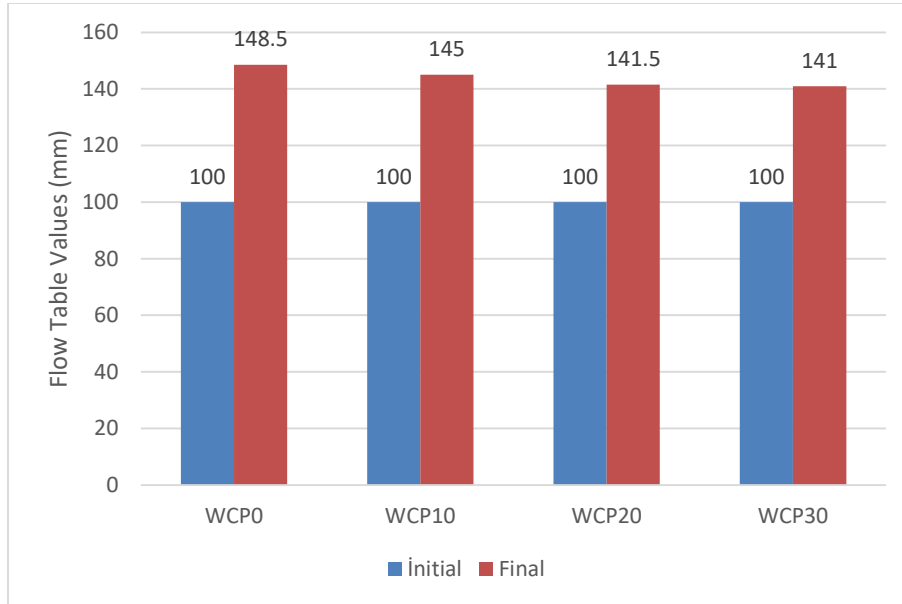


Figure 1. Flow table values of mortar mixtures.

3.2. Compressive and Flexural Strength Test

Compressive and flexural strength tests were performed on the prepared samples at the end of the 7th and 28th days, and the results are presented in Figure 2. In some studies in the literature, it has been stated that the mechanical properties of cement-based materials, where waste concrete powder has low reactivity, will decrease as the replacement rate increases [9-10]. When the results are examined, the highest compressive strength test results were obtained from the WCP0 sample as 44.55 MPa in 7-day samples and 53.13 MPa in 28-day samples. The highest flexural strength results of the samples were obtained as 5.74 MPa for the 7th day and 6.55 MPa for the 28th day in the WCP0 sample. It is seen that the strength values at the end of 28 days are close to the highest strength of the WCP10 sample. It is seen that the lowest strengths are in the WCP30 sample. This shows that there is a decrease in strength with the decrease in the amount of cement.

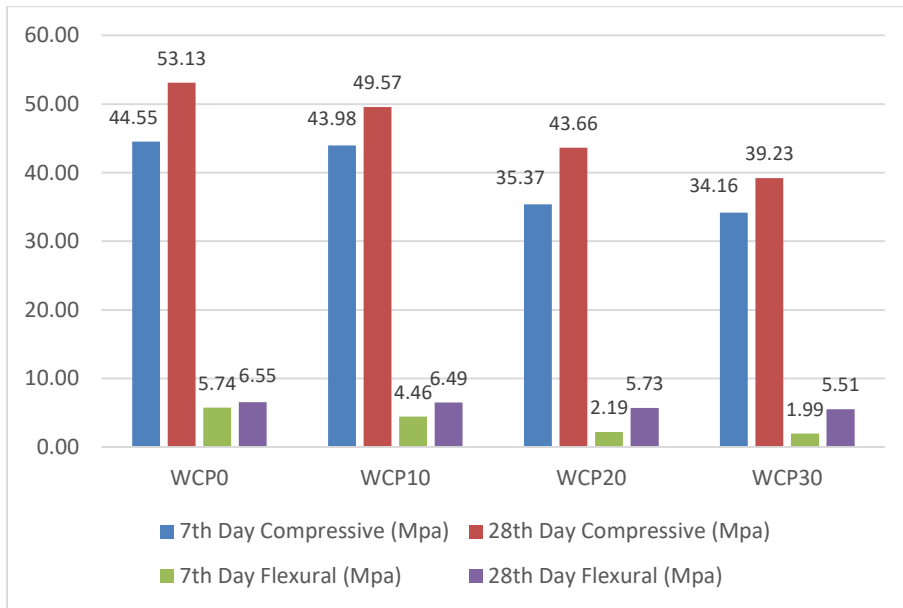


Figure 2. 7th and 28th day flexural and compressive strength values of mortar mixtures.

3.3. Ultrasonic Pulse Velocity Test

The results obtained from the ultrasonic pulse velocity test performed for 28-day-old mortar samples are given in Figure 3. The ultrasonic pulse velocity of concrete increases in systems with less porosity and a denser microstructure [11]. Based on this, when the ultrasonic pulse velocity values are examined, it can be said that the results obtained are parallel to the mechanical test results. In other words, the highest ultrasonic pulse velocity value was obtained in the WCP0 sample, which exhibited the highest mechanical performance.

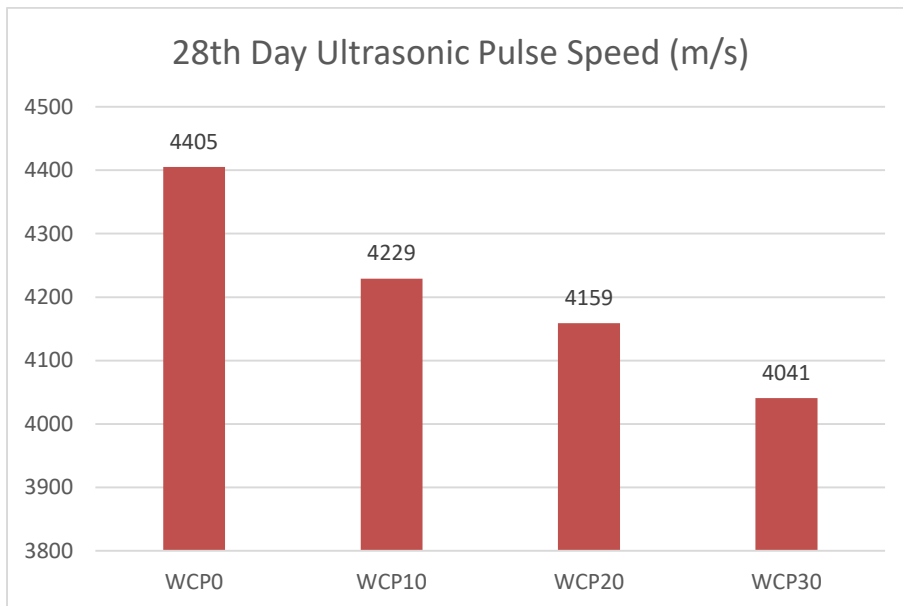


Figure 3. Ultrasonic pulse velocity values of mortar mixtures on the 28th day.

4. Conclusion

In this study, waste concrete powder was substituted instead of cement at 10%, 20% and 30% rates. Fresh property evaluation, mechanical property tests, and ultrasonic pulse velocity measurements were performed on the samples. The findings obtained as a result of the study are as follows:

- Waste concrete powder substitution in mortar mixtures decreased fluidity.

- Waste concrete powder substitution in mortar mixtures decreased 7- and 28-day flexural and compressive strength values. However, the strength values of the samples with a 10% substitution rate are close to the reference samples.
- As a result of the ultrasonic pulse velocity measurements performed at the end of 28 days, it was observed that the values were parallel to the compressive strength values. The ultrasonic pulse velocities increased as the strength of the samples increased.

As a result, recycling construction and demolition waste can provide great economic and environmental benefits. Therefore, it was concluded that waste concrete powder can be used in cement-based systems, and the properties of mortars prepared with varying ratios of concrete waste as a substitute for cement in concrete should be examined in greater detail.

References

- [1] Soto-Paz J., Arroyo O., Brayan A., Torres-Guevara L.H., Parra-Orobio B.A., Casallas-Ojeda M. 2023. The circular economy in the construction and demolition waste management: A comparative analysis in emerging and developed countries, *Journal of Building Engineering*, 78,107724.
- [2] Kul A., Ozel B.H., Ulugol H., Ozcelikci E., Yildirim G., Gunal M.F., Sahmaran M. 2023. Characterization and life cycle assessment of geopolymer mortars with masonry units and recycled concrete aggregates assorted from construction and demolition waste, *Journal of Building Engineering*, 78, 107546.
- [3] Shi Y., Xu J. 2021. BIM-based information system for econo-enviro-friendly end-of-life disposal of construction and demolition waste. *Automation in Construction*, 125,10361.
- [4] Miller S.A., Moore F.C. 2020. Climate and health damages from global concrete production, *Nature Climate Change*, 10,439–443.
- [5] Zhang C., Hu M., Meide M., Maio F.D., Yang X., Gao X., Li K., Zhao H., Li C. 2023. Life cycle assessment of material footprint in recycling: A case of concrete recycling. *Waste Management*, 155, 311–319.
- [6] Ashraf, M., Iqbal, M. F., Rauf, M., Ashraf, M. U., Ulhaq, A., Muhammad, H., & Liu, Q. F. (2022). Developing a sustainable concrete incorporating bentonite clay and silica fume: Mechanical and durability performance. *Journal of Cleaner Production*, 337, 130315.
- [7] Knight, K. A., Cunningham, P. R., & Miller, S. A. (2023). Optimizing supplementary cementitious material replacement to minimize the environmental impacts of concrete. *Cement and Concrete Composites*, 139, 105049.
- [8] Tuğla, R. K. (2020). Kendiliğinden Yerleşen Betonda Atık Beton Tozu Etkisinin İncelenmesi. *Bayburt Üniversitesi Fen Bilimleri Dergisi*, 3(1), 53-62.
- [9] Xiao, J., Ma, Z., Sui, T., Akbarnezhad, A., & Duan, Z. (2018). Mechanical properties of concrete mixed with recycled powder produced from construction and demolition waste. *Journal of Cleaner Production*, 188, 720-731.
- [10] Horsakulthai, V. (2021). Effect of recycled concrete powder on strength, electrical resistivity, and water absorption of self-compacting mortars. *Case Studies in Construction Materials*, 15, e00725.
- [11] Hong, G., Oh, S., Choi, S., Chin, W. J., Kim, Y. J., & Song, C. (2021). Correlation between the compressive strength and ultrasonic pulse velocity of cement mortars blended with silica fume: An analysis of microstructure and hydration kinetics. *Materials*, 14(10), 2476.



The Reactive Power Compensation to Improve Wind Turbine Stability

Zakaria IDRİSS^{1,*} , Murat ARI¹ , Mahmud Esad YİĞİT¹ 

¹ Department of Electrical and Electronics Engineering, Cankiri Karatekin University, Çankırı, Türkiye

Abstract

The efficiency of the power supply network is an important factor in ensuring network reliability. Due to the rapid development of power generation, the requirements for wind system stability have become more important. In this study, the effects of reactive power on wind turbines were examined to see if the wind turbine system is unstable. The studies revealed that there are several factors affecting the stability of the wind turbine system. Wind speed and blade angle are important parameters influencing the energy production of a wind turbine. Wind speed is influenced by air temperature, which modifies air density and thus leads to variations in wind speed. The wind turbine model has been simulated in Matlab/Simulink. Reactive power compensation is a technique that can improve power efficiency by reducing current and voltage distortion. Turbine power characteristics for different pitch angles and the reactive power of wind turbines for different wind speeds are given. Some reactive power compensation techniques for improving wind turbine stability have been examined and a comparison between bibliographic methods is discussed.

Keywords: Electric quality, Wind speed, Reactive power compensation, Statcom

1. Introduction

Power efficiency and energy savings are issues that are creating more and more concern among policymakers, economists, and academics who look at them from technological, economic, policy, and human behavior perspectives [1]. As a result, it is necessary to continue to discover and promote power efficiency, dependability, and sustainability technologies, such as the use of synchronous capacitors for reactive power correction in electrical systems [2].

Reactive power describes the power of inductive devices such as motors or capacitive loads. It is frequently calculated in volt-amperes reactive (VAR) [3]. To maintain the best possible circumstances for a power system from an engineering and financial standpoint, the electrical power system must always employ the best technology for compensating reactive power [4].

It is critical to comprehend wind qualities to effectively utilize wind energy from a wind turbine system. The wind's velocity varies greatly with space, time, season, and hourly variations [5]. There are certain fluctuations in wind speed on a shorter time scale in addition to seasonal variations [6]. These oscillations, which are known as synoptic variations, peak at approximately four days. Seasonal and synoptic wind speed components are not the only factors causing turbulence. Turbulence is the term used to describe variations in wind speed during short periods, usually less than ten minutes [7].

There are many technologies for compensating power, but some are more adapted than others to electrical networks [8]. This article examines how wind speed and blade orientation affect wind power and reactive power [9].

2. Win Turbine Modeling

A wind farm has been simulated using Matlab/Simulink software. Figure 1 shows the simulation model corresponding to the diagram described below.

The simulated system consists of a 2 MW wind turbine connected to a 400 kVA load and a 25 kV grid via a three-phase transformer. The driving and reactive power have been evaluated as a function of wind speed and blade angles. In general, wind power stability depends on the following parameters [10]:

- The relationship between wind speed and wind turbine speed

* Corresponding author. e-mail address: zakariaidriss223@gmail.com

- Blade angle as a function of wind speed
- Turbine output power
- Speed and blade angle

Electrical power is the amount of energy that flows through a given point in an electrical circuit during a unit of time. Energy storage components like capacitors and inductors in alternating-current (AC) circuits can periodically reverse the direction in which energy is moving [11]. The term active power refers to the portion of the power that is highest on average during an AC waveform is whole cycle. (The suggested of method approach is shown in Figure 1.

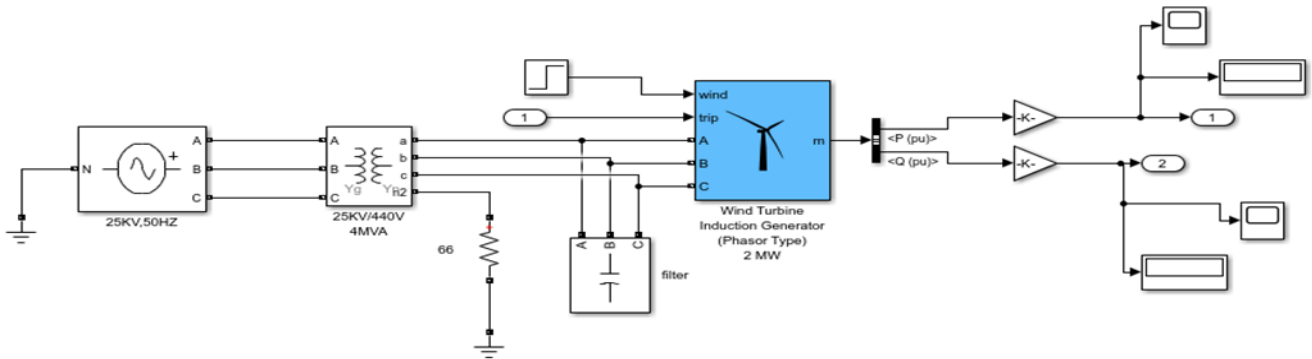


Figure 1. The framework of the suggested method.

In this study, the effect of varying wind speed on the output power of a wind turbine has been examined. The wind turbine under investigation has a maximum output power of 2 MW. This is reached at wind speeds of 12 m/s and above. Below 12 m/s, output power decreases. The output power of the wind turbine rises with increasing wind speed.

Controlling the position of the turbine's pitch angle can be used to raise the power output of the turbine. In changing the pitch angle of the blade, the wind turbine can be rotated at higher speeds as shown in Table 1 [12].

First, the wind turbine speed has been set to 12m/s and the pitch angle will be set to zero to observe the effect of the blade angle. The maximum power is obtained as shown in Figure 2. In Figure 3, the effect of the blade angle is observed more precisely, where the blade angle is changed to 10° while keeping the turbine speed unchanged. It has been noticed that the wind turbine is performance decreased.

Table 1. Function of turbine speed on pitch angle

Pitch angle	Wind speed
0 deg	12 m/s
10 deg	12 m/s
0 deg	10 m/s
0 deg	12 m/s
0 deg	14 m/s

In order to demonstrate the inherent instability of wind turbine systems further, an investigation was conducted to examine the influence of varying wind speeds on deliberate reactive power. This analysis stems from recognition that wind speed is not uniform across the entire length of the turbine blades, leading to power fluctuations. Initially, the wind speed has been set to a constant value of 10 m/s. Examination of the results revealed that during the first and second seconds of operation, the deliberate reactive power was more significant than in subsequent seconds.

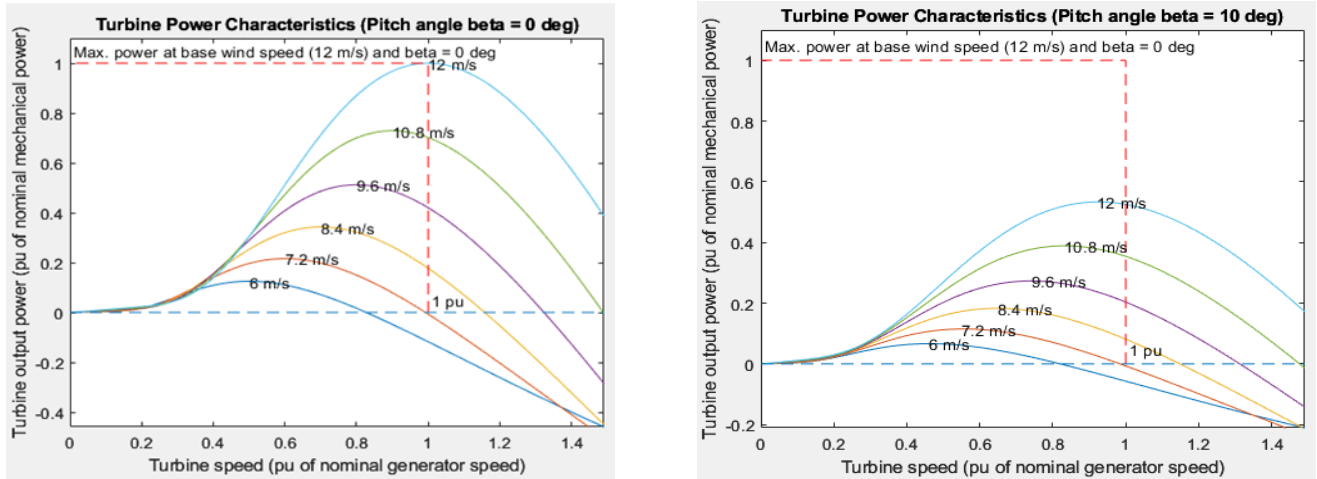


Figure 2. Turbine power characteristics for a stable pitch angle.

To delve deeper into the analysis, simulations were carried out considering wind speeds of 12m/s and 14m/s, as depicted in Figure 3. These simulations corroborated the crucial role of wind speed in the stability of the wind turbine system.

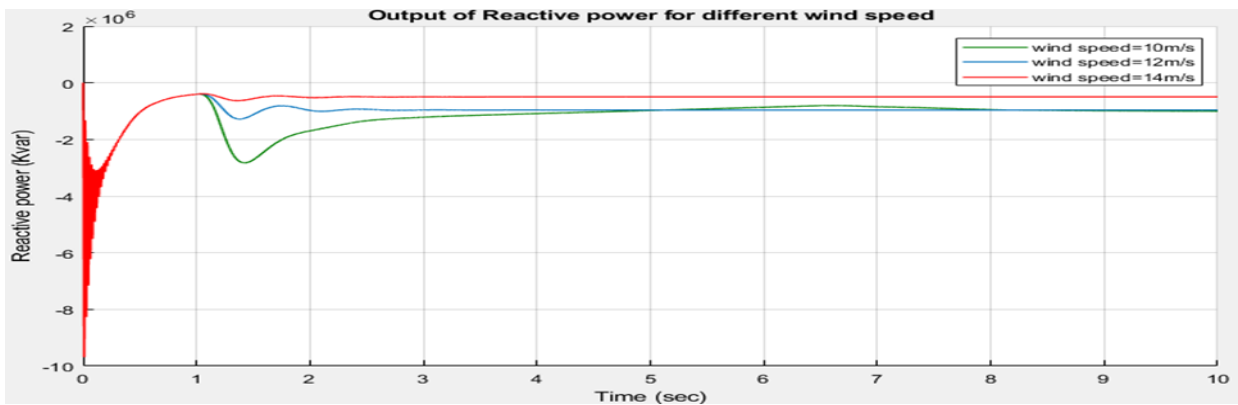


Figure 3. Reactive power for different wind speed.

3. Literature Review

Some techniques in the literature for reactive power compensation to improve wind turbine stability have been reviewed.

Farees et al. [13] highlight the significance of using devices in the flexible AC transmission system (FACTS) to increase the system's reactive power handling capability to prevent voltage instability. The study suggests the higher performance of STATCOM over traditional Static VAR Compensators (SVC). The authors present a fuzzy logic control technique for SVC and STATCOM, namely a double input, single output (DISO) FLC of the Mamdani type, to successfully reduce oscillations and enhance voltage stability. The fuzzy rule base, fuzzy inference engine, fuzzy fuzzification interface, and defuzzification interface are the four main parts of the FLC [13].

Bisen et. al [14] investigate how well SVC and STATCOM perform in comparison when it comes to improving the power system's multiple machines transient stability, which spans two areas. They highlight the increasing intricacy of power systems and the difficulties in maintaining power system stability, especially when it comes to transient and small-signal stability [14].

Elsady et al. [15] focus on improving the operation of electricity networks with integrated wind farms by a FACTS controller known as the static STATCOM. The authors highlight the capacity of the STATCOM to quickly absorb or inject reactive power into the electrical grid as a means of facilitating efficient voltage

management and stability restoration when wind farms are present. They create a dynamic power system model with a wind farm integrated, managed by the suggested STATCOM, and simulate a range of extreme disturbances to verify the model's efficacy. The outcomes show how well the STATCOM controller works to quickly reduce oscillations in the electrical grid and provide reliability [15].

Hosseini et. al [16] investigate the consequences on wind farm stability of using SVC, STACOM, or DBR and the steadiness of induction generator-based wind farms with fixed speeds. They credit the asynchronous functioning of FSIG-based wind farms, which causes FSIG to take in a considerable quantity of reactive power owing to large rotor slip during faults, as the cause of the system is instability. The authors model a wind farm with SVC, STATCOM, or DBR installed, based on fixed-speed induction generators, using MATLAB/SIMULINK. To find out more about the effects of these devices on wind power plant stability under various circumstances and with different variables, they compare the outcomes of system simulations in Figure 5 and Figure 6 [16].

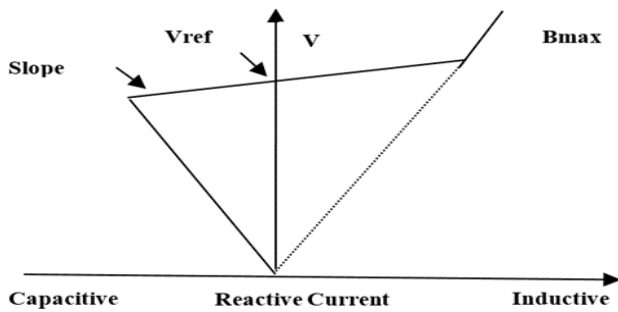


Figure 5. V-I characteristics of SVC.

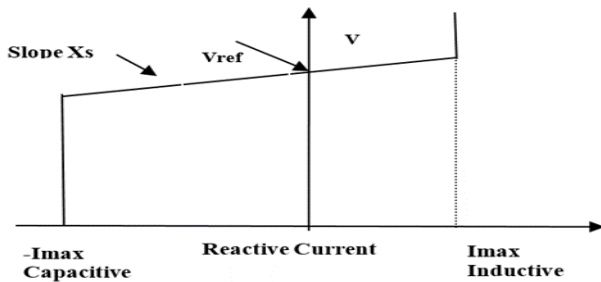


Figure 6. V-I characteristics of STATCOM.

Sedighizadeh et al. [17] studied the impact of STATCOM and SVC power wind farms stability when their fixed-speed induction generators are connected to the power grid. Owing to the asynchronous nature of FSIGs, the excessive consumption of reactive power by FISG following a malfunction is the main source of instability in FSIG-based wind farms. These phenomena result from the increase in reactive power consumption brought on by the FISG is enhanced rotor slide during the failure. A comparison has been made by the authors to show how well wind farms that use SVC and STATCOM can increase stability of wind farms during and following a fault.

Wang et al.[18] studied reactive power management in wind farms to regulate voltage and minimize power loss. They analyzed a real-world wind farm in Hubei, China, considering factors like bus voltage, power factor, transformer taps, and reactive power correction. By comparing different optimization methods, they identified strategies to reduce power loss under varying wind power conditions. Additionally, through simulations, they investigated the impact of various parameters on power loss and optimized transformer taps, capacitor switching, and reactive power output to minimize system losses. Their findings highlight the significant role of transmission line losses and the effectiveness of reactive power optimization, especially at higher wind power levels [18].

Zhou et al. [19] emphasize the importance of maintaining the level of electrical power in a network to guarantee a dependable electrical power infrastructure. They specifically investigate technologies for compensating reactive power as a way to achieve this objective. The paper compares three devices: synchronous condensers, SVCs, and STATCOMs. The authors provide an overview of their technological development, principles, and performance. Additionally, the paper discusses the potential of reactive power compensation technology in the future,

highlighting STATCOM is advantages, such as its superior dynamic behavior and ability to control multiple variables. The authors suggest that STATCOM is likely to become more widely used in the future [19].

4. The comparison Between the Methods of the Literature

Farees, Sedighzadeh, Bisen, Shrivastava, Elsady, and Hosseini all concluded that STATCOMs are more effective than SVCs in damping oscillations, enhancing voltage stability, and restoring stability after disturbances in wind farm systems. Wang's research highlighted the importance of reactive power management in wind farms, which STATCOMs can effectively address. Zhou predicted a rise in STATCOM usage due to their superior dynamic capabilities and multi-variable control. While SVCs remain viable in specific scenarios, STATCOMs generally offer better performance in power quality and stability enhancement for wind power integration. Table 2 shows the comparison of the different methods.

Table 2. Comparison between the methods of the Literature.

Authors	Methods	Findings
Farees et al. [11]	Fuzzy logic control technique for SVC and STATCOM	Successfully reduces oscillations and enhances voltage stability
Bisen et al. [12]	Evaluating SVC versus STATCOM	STATCOM improves transient stability more than SVC
Elsady et al. [13]	Dynamic power system model with a wind farm integrated, managed by the suggested STATCOM	STATCOM controller works well to quickly reduce oscillations in the power system and bring stability back
Hosseini et al [14]	Comparison of SVC, STATCOM, and DBR	STATCOM is the greatest option for enhancing the stability of network-connected wind farms
Sedighzadeh et al. [15]	A comparison between STATCOM and SVC	STATCOM performs better in boosting wind farm stability than SVC
Wang et al. [16]	Wind turbines capacity for reactive power management	Power losses in the wind farm system can be efficiently minimized by reactive power optimization
Zhou et al. [17]	Comparison of synchronous condensers, SVCs, and static synchronous compensators (STATCOMs)	STATCOM is likely to become more widely used in the future due to its superior dynamic behavior and ability to control multiple variables

5. Conclusion

Wind power for electricity generation has recently attracted much attention in the electricity industry. Used correctly, wind power can contribute to competitively priced electricity generation, improve the capacity factor of renewable energy sources, and extend regeneration capabilities. The power coefficient as a function of air density, wind speed, blade angle and other factors are all considered when producing or installing wind turbines. In this paper, a wind turbine generator was modeled and simulated using MATLAB/SIMULINK. Different levels of wind speed with different angles of inclination were taken into account to show the power characteristics of the wind turbine when integrated into a power system. These characteristics show that the wind energy system is unstable. Different wind levels were used to predict and monitor the system is active and reactive power. It is concluded that the wind energy system needs compensation techniques to reduce energy loss. Literary studies have revealed several reactive power compensation techniques such as STATCOM, SVC, static capacitor, and FLC. The scientific authors have examined the reactive power compensation system and a comparison of these approaches is also given that STATCOM is the best reactive power compensator.

References

- [1] Upadhyai R., & Garg L. An Integration of the SVC and STATCOM Technologies into Wind-Based Power Systems. International Conference on Futuristic Technologies (INCOFT), Belgaum, India, 2022, pp. 1–6.
- [2] Sumper, A. & Baggini, A. (2012). Electrical Energy Efficiency Technologies and Application. John Wiley

- and Sons, West Sussex, United Kingdom, ISBN: 9780470975510.
- [3] Kushwah R. & Gupta M. Modelling & simulation OF SVC and statcom for enhancement of power system transient stability using Matlab. International Conference on Electrical, Electronics, and Optimization Techniques (ICEEOT), Chennai, India, 2016, pp. 4041–4045.
 - [4] Continental Control Systems, Reactive Power, *Continental Control Systems*, Boulder CO, USA, 2012.
 - [5] Rafiqi I. & Bhat A. Role of STATCOM in improving the power quality issues in hybrid power plant connected to a power grid, 4th International Conference on Recent Developments in Control, Automation & Power Engineering (RDCAPE), Noida, India, 2021, pp. 384–387.
 - [6] 11-IJTPE-Issue57-Vol15-No4-Dec2023-pp72-82.pdf.
 - [7] Ahmad, R., & Abdul-Hussain, M. (2021). Modeling and Simulation of Wind Turbine Generator Using Matlab-Simulink. *J. Al-Rafidain Univ. Coll. Sci.* ISSN 1681-6870 Online ISSN 2790-2293, 2(1), pp. 282–300.
 - [8] 9-IJTPE-Issue56-Vol15-No3-Sep2023-pp.68-76.pdf.
 - [9] Demirovic N. Impact of STATCOM and SVC to voltage control in systems with wind farms using induction generators (IG). Mediterranean Conference on Power Generation, Transmission, Distribution and Energy Conversion (MedPower), Belgrade, Serbia, 2016, pp.16-29.
 - [10] Ayaz M., Colak I., & Bayindir R. Matlab/gui based wind turbine generator types on smart grid systems. International Conference on Renewable Energy Research and Applications (ICRERA), Birmingham, United Kingdom, 2016, pp. 1158–1162.
 - [11] Wei X., Qiu X., Xu J., & Li X. Reactive Power Optimization in Smart Grid With Wind Power Generator. Asia-Pacific Power and Energy Engineering Conference, Chengdu, China, 2010, pp. 1–4.
 - [12] Apata, O., & Oyedokun, D. (2018). Novel Reactive Power Compensation Technique for Fixed Speed Wind Turbine Generators. *IEEE PES/IAS PowerAfrica* (pp. 628–633). Cape Town.
 - [13] Farees, S., Gayatri, M., & Umanth, D. (2014). Performance Comparison between SVC and STATCOM for Reactive Power Compensation by Using Fuzzy Logic Controller. *ISS N*, 3(1).
 - [14] Bisen P., & Shrivastava A. Comparison between SVC and STATCOM FACTS Devices for Power System Stability Enhancement. International Journal on Emerging Technologies, 2010, pp. 101-109.
 - [15] Elsady G., Mobarak A., & Youssef A. (2010). STATCOM for Improved Dynamic Performance of Wind Farms in Power Grid. International Middle East Power Systems Conference (MEPCON), Cairo University, Egypt, pp.19-21.
 - [16] *International Journal of Engineering and Applied Sciences (IJEAS)* Int. J. Eng. Appl. Sci. IJEAS, 2018, 0(1).
 - [17] Sedighizadeh, M., Rezazadeh, A., & Parayandeh, M. (2010). Comparison of SVC and STATCOM impacts on wind farm stability connected to power system. *International Journal of Engineering and Applied Sciences (IJEAS)*, 2(2), Issue (2), pp.13-22.
 - [18] Wang, Y. (2019). Reactive Power Optimization of Wind Farm Considering Reactive Power Regulation Capacity of Wind Generators. *Innovative Smart Grid Technologies (ISGT Asia)*, Chengdu, China, pp. 4031–4035.
 - [19] Zhou X., Wei K., Ma Y., & Gao Z. A Review of Reactive Power Compensation Devices. *International Conference on Mechatronics and Automation (ICMA)*, Changchun, China, 2018, pp. 2020–2024.



Optimization Based Energy Management Approach for Prosumers Located in Small-scale Microgrids

Enes BEKTAŞ^{1,*} , **Mohammad Ruhul Amin BHUIYAN²** 

¹Engineering Faculty, Electrical and Electronics Engineering Department, Çankırı Karatekin University, Çankırı, Türkiye

²Faculty of Engineering and Technology, Electrical and Electronic Engineering Department, Islamic University, Dhaka, Bangladesh

Abstract

Benefits of integrating renewable energy resources (RESs) into the electrical grid include increased efficiency and less strain on transmission lines and the need for significant infrastructure investments. Therefore, presents new difficulties, though, like over-voltage and stability issues, which could endanger the dependability and safety of the power supply. Energy management system (EMS) can increase efficient use of produced renewable energies. Thus, EMS contributes positively to solving the mentioned problems in networks. This paper proposes and presents an optimization-based energy management system for prosumers with PV panel and battery equipment located in small scale microgrids. The objective function is determined as to prosumer bill minimization ensuring maximum power injection to the grid.

Keywords: Energy management system, Microgrid, Optimization, Prosumer

1. Introduction

The global demand for clean and sustainable energy has intensified research into advanced materials capable of driving efficient energy conversion technologies. Thin-film materials form the foundation of both photovoltaic (PV) and thermoelectric (TE) technologies [1-3], facilitating the development of efficient and sustainable energy conversion devices. Their integration offers significant potential for advancing next-generation energy systems.

Over the past ten years, a lot of residential clients have expressed a strong desire to install PV plants on their property, although on a small scale on the roofs of their homes. The LV distribution network is where these PV installations are situated. The distribution system's typical operating behaviour is impacted as a result of the quick increase in PV penetration.

The grid is supported by energy storage devices in terms of voltage. An association with battery energy storage systems (BESS) is also offered as an alternative for the issues driven on by the widespread installation of PV systems. The goal is to temporarily store extra active power for usage at night or during times of high demand [4, 5]. In this situation, creating an efficient solution requires careful design of numerous important elements. These factors include storage capacity, infrequent charging, protection against deep discharge or overcharging, and compatibility with the current infrastructure (load characteristics, load types, etc.).

[6] examines prosumer-based energy management systems (PEMS) in smart grid systems and their effects on energy sustainability and power system dependability in detail PEMS has tremendous promise for peak load balancing, energy conservation, and cost reduction. EMS for energy sharing between neighbours in residential micro grids is presented in [7]. Depending on whether solar photovoltaic (PV) and battery energy storage systems are installed, homes in residential micro grids are divided into three categories: traditional, proactive, and enthusiastic. [8] describes an energy management system to help prosumers coordinate their operations. It has been found that working cooperatively with other prosumers in a local setting result in greater performance. Both PV and ESS are part of the system. The objective function is to maximize the usage of available generation and reduce each household's load disconnection.

[9] investigations into grid-connected AC-coupled PV and BESS configurations. The goal of this study is to solve the over-voltage problems generated on by PV penetration by using customer-owned BESS devices. The BESS unit's active power set points are determined using an optimization-based scheduling technique. It has been shown that over-voltage problems can be resolved with residential BESS units without materially altering the main requirements of BES owners.

[10] seeks to maximize PV use, increase load supply, and reduce cost from the use of generating units. The system consists of PV, ESS, and wind. There are two stages in the best planning strategy. The first step involves fixing

the voltage fluctuations brought on by P. Investments in equipment and line losses are employed to optimize ESS operation.

By taking into account both physical limitations and prerequisites for a practical deployment in the real network, [11] maximizes income for selling energy produced by photovoltaic arrays while minimizing the cost of electricity received from the main grid.

In order to reduce the operational and maintenance costs of PV and ESS, [12] works on the basic microgrid topology, emphasizing that PV maintenance costs should be disregarded. The forecasting module is in charge of temperature, load demand, and solar irradiance. The best day-ahead scheduling is carried out by the optimization module. The only constraint applied is power balance [12]. Reliable intra-day forecasting methods are necessary to optimize the EMS's benefits. In order to generate the prediction, the applied tools mostly rely on modelling the PV or using previous data [13]. So as to maintain the day-ahead energy forecasts and give the system operator relevant data, it is necessary to have a self-adjusting forecasting tool.

This research offers an optimization-based energy management system for prosumers equipped with photovoltaic panels and battery systems inside small-scale microgrids. The objective function is established to minimize the prosumer's bill while maximizing power injection to the grid. The total of the bill is determined as a value, indicating that the prosumer can earn by selling generated solar electricity to the grid. The profit derived by augmenting battery capacity and photovoltaic output capacity could be further enhanced.

2. Defining of Basis Formulation for EMS

A simple structure of prosumer at low voltage grid and connection to medium voltage can be expressed as in Figure 1. As shown in Figure 1, DC or AC microgrid system term is not included. Because this paper focuses on not microgrid type but control of AC or DC microgrid with EMS.

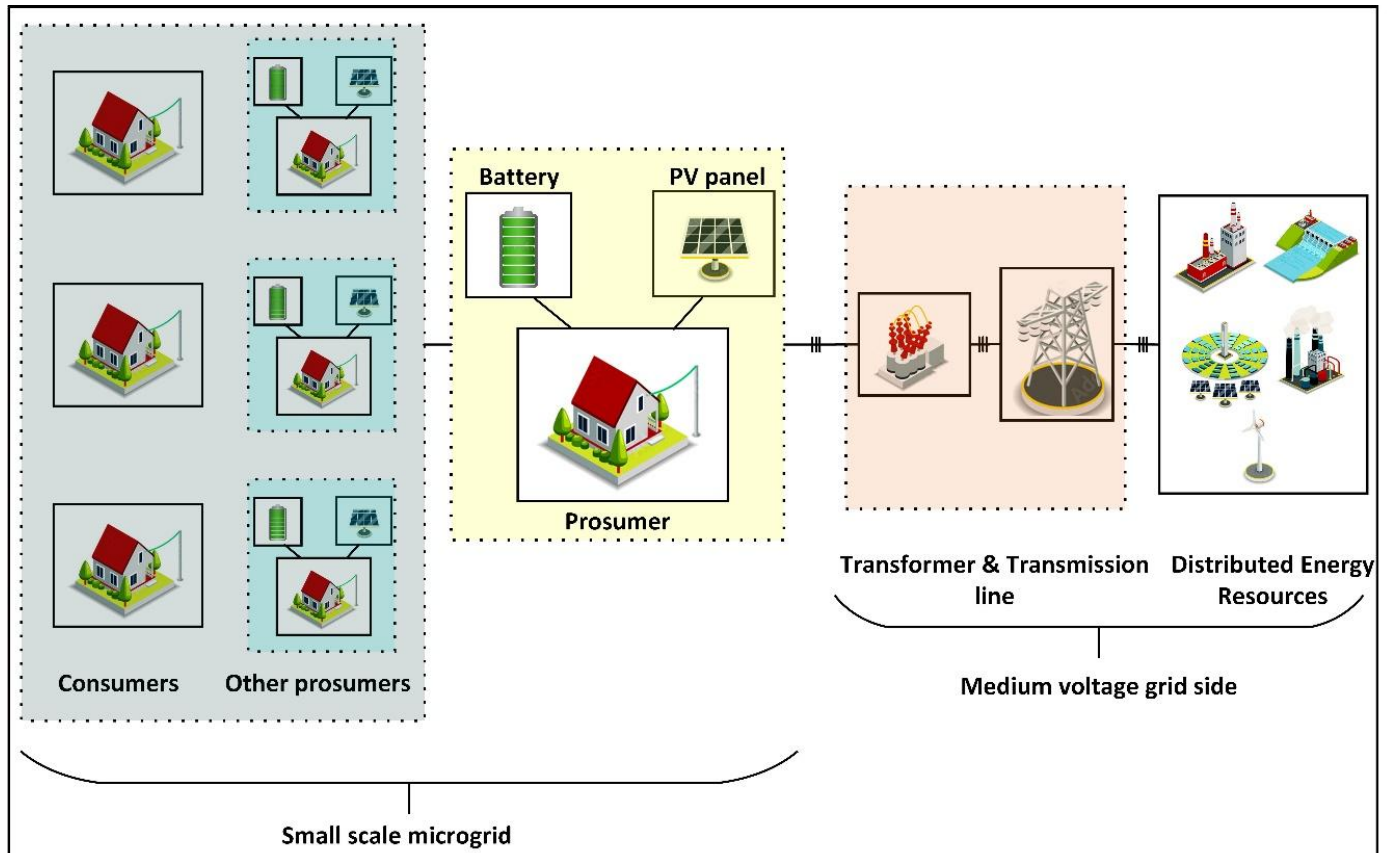


Figure 1. General diagram of low voltage microgrid and connections medium voltage

Proposed EMS concentrates on one prosumer energy management system and minimizing of bill of the prosumer. Energy management formulations can be derived by using parameters given in Table 1.

Table 1. Basic parameters of EMS formulations

Variable	Description	Unit
t	Time of 24 hour	[Hour]
P_t^{Panel}	Solar power generation of PV panel (average)	[kW]
$P_t^{Prosumer}$	Load demand of prosumer (average)	[kW]
P_t^{Charge}	Battery charge	[kW]
$P_t^{Discharge}$	Battery discharge	[kW]
SOC_{max}	Battery maximum capacity	[kWh]
SOC_{min}	Battery minimum capacity	[kWh]
SOC_t	Battery capacity	[kWh]

Objective function, to be minimized in optimization process, includes prosumer bill formulations. Bill formulation can be derived by using parameters given in Table 2. Prosumer's bill can be formulized as in Equation (1).

Table 2. Parameters of bill in EMS formulations

Variable	Description	Unit
P_t^{Inj}	Injected power from prosumer to grid (average)	[kW]
P_t^{Abs}	Absorbed power from grid to prosumer (average)	[kW]
p_t^{Inj}	Price of average injected power	[TL]/[kWh]
p_t^{Abs}	Price of average absorbed power	[TL]/[kWh]
B	Calculated bill of prosumer	[TL]

$$B = \sum_{t=1}^{24} (p_t^{Abs} \cdot P_t^{Abs} - p_t^{Inj} \cdot P_t^{Inj}) \quad (1)$$

It can be understood from Equation (1) that if bill is lower than zero, prosumer can make profit from the EMS. Therefore, the further the bill value is from 0, the more profit the producing prosumer makes.

The power balance, an equality constraint for the EMS optimization problem, must be formulated and presented in Equation (2). The total of the PV power, battery charge and discharge power, power absorbed from the grid, and electricity supplied to the grid must equal zero for every hourly interval. The values for battery charging and discharging, as well as absorbed and injected grid power—which are opposing values—can simultaneously be zero, or only one of them must equal zero. The optimization configuration must adhere to this guideline. The principle can be highlighted in solver-based optimization techniques. Nonetheless, particularly optimization strategies based on soft computing do not permit this. In soft computing-based optimization methods, the difference between the two values must be computed, and the charge/discharge or received/given value should be assessed based on whether the difference is positive or negative, necessitating a corresponding modification of the objective function. The identified issue can be regarded as the most challenging aspect in the implementation of soft computing-based energy management techniques.

$$P_t^{Panel} + P_t^{Discharge} + P_t^{Abs} - P_t^{Inj} - P_t^{Charge} - P_t^{Prosumer} = 0 \quad (2)$$

Other constraints are defined for Battery. Battery charge and discharge power cannot be lower than zero and greater than battery power. And, state of charge (SOC) at ant t time, time interval of (t-1) hour and t hour, affects next time period and is affected by previous time period. The SOC equation is given in equation (3). Thus, the battery inequalities can be defined as in Equations (4)-(6)

$$SOC_{t+1} = SOC_t + \left(\eta_{chg} * P_t^{Charge} - \frac{P_t^{Discharge}}{\eta_{dchg}} \right) \quad (3)$$

where SOC_{t+1} is the battery state of charge value for next time interval, η_{chg} is the battery charge efficiency and η_{dchg} is the battery discharge efficiency. And, P_{max} is defined as battery power. Generally, in the literature, the initial energy value of the battery, SOC_0 , is taken as between 90% and 70% of its energy capacity. For this reason, in this paper optimization is run with 70% SOC value. Battery power is determined as 50kW and energy capacity is 85kWh.

$$P_t^{Charge} \leq P_{max} \quad (4)$$

$$P_t^{Discharge} \leq P_{max} \quad (5)$$

$$SOC_{min} \leq P_t^{Discharge} \leq SOC_{max} \quad (6)$$

In this paper, GLPK solver/Python is used for optimization tool. The GLPK (GNU Linear Programming Kit) software is designed for addressing large-scale linear programming (LP), mixed integer programming (MIP), and associated difficulties. It comprises a collection of routines authored in ANSI C and structured as a callable library [14]. Finally, optimization-based EMS input and outputs is illustrated in Figure 2.

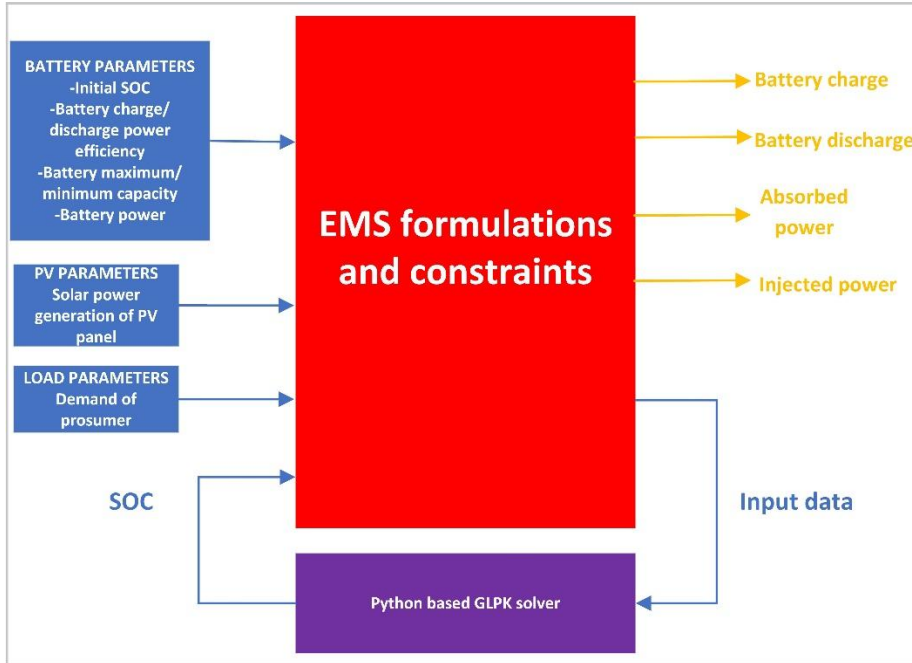


Figure 2. Interaction of Python based GLPK Solver and input/output data for EMS

3. Results

By running the optimization tool battery charge and discharge power are scheduled. In Figure 3, obtained results are given.

Time interval	Battery		Grid power		SoC	EMS inputs		Bill	
	P_chg	P_dis	P_abs	P_inj		Demand	SolarPro	End of one hour period	Total
1	0	6.98	0	0	60	6.98	0	0	0
2	0	6.44	0	0	52.87755	6.44	0	0	0
3	0	4.79296	1.44704	0	46.30612	6.24	0	1.1865728	1.1865728
4	0	6.22	0	0	41.41535	6.22	0	0	1.1865728
5	0	6.36	0	0	35.06841	6.36	0	0	1.1865728
6	0	6.66	0	0	28.57861	6.66	0	0	1.1865728
7	0	0	6.8	0	21.78269	6.8	0	5.576	6.7625728
8	0	0	7.64	0	21.78269	7.64	0	6.2648	13.0273728
9	0	4.68704	0	0	21.78269	5.04	0.35296	0	13.0273728
10	0	0	2.076316	0	17	4.6	2.523684	1.7025791	14.7299519
11	15.78762	0	0	0.390846	17	2.7	18.87846	-0.183698	14.5462541
12	20	0	0	7.260516	32.47187	3.46	30.72052	-3.412443	11.1338116
13	0	0	0	1.70436	52.07187	2.78	4.48436	-0.801049	10.3327624
14	20	0	0	1.59008	52.07187	3.38	24.97008	-0.747338	9.58542482
15	0	0	0	9.073868	71.67187	3.14	12.21387	-4.264718	5.32070686
16	0	0.212624	0	0	71.67187	2.42	2.207376	0	5.32070686
17	0	3.825804	0	0	71.4549	3.9	0.074196	0	5.32070686
18	0	8.32	0	0	67.55102	8.32	0	0	5.32070686
19	0	9.44	0	0	59.06122	9.44	0	0	5.32070686
20	0	8.04	0	0	49.42857	8.04	0	0	5.32070686
21	0	7.86	0	0	41.22449	7.86	0	0	5.32070686
22	0	8.44	0	0	33.20408	8.44	0	0	5.32070686
23	0	7.44	0	0	24.59184	7.44	0	0	5.32070686
24	0	20	0	12.84	17	7.16	0	-6.0348	-0.7140931

Figure 3. Results of Python based GLPK Solver based EMS

As seen in Figure 3, the battery is discharged between 0 and 01:00 hour (for $t=0$) and quantity of discharged is 6.98 kWh. And power balance equation is satisfied and can be verified using Equation (2) as; $0 + 6980 + 0 - 6980 - 0 - 0 = 0$. At the end of first-time interval, final SOC is calculated as 52.83 kWh with Equation (3). Calculated SOC is the initial SOC parameter for second time interval. For each time interval, calculated hourly bill is illustrated too. The total bill is calculated as – value, means that prosumer can make profit by selling generated solar power to the grid side. The profit obtained by increasing the battery capacity and PV production capacity can be further increased. For this purpose, it is recommended to conduct more detailed studies considering the system installation cost. In Figure 4, optimization outputs are given visually for the system operation, load profile and PV profile to be more easily interpreted together. Power balance is equal to zero as desired for optimization output. As stated in Section 2, Battery charging and discharging values, absorbed grid power and injected grid power which are opposite values. In EMS, power quality equality constraints are satisfied successfully by proposed method.

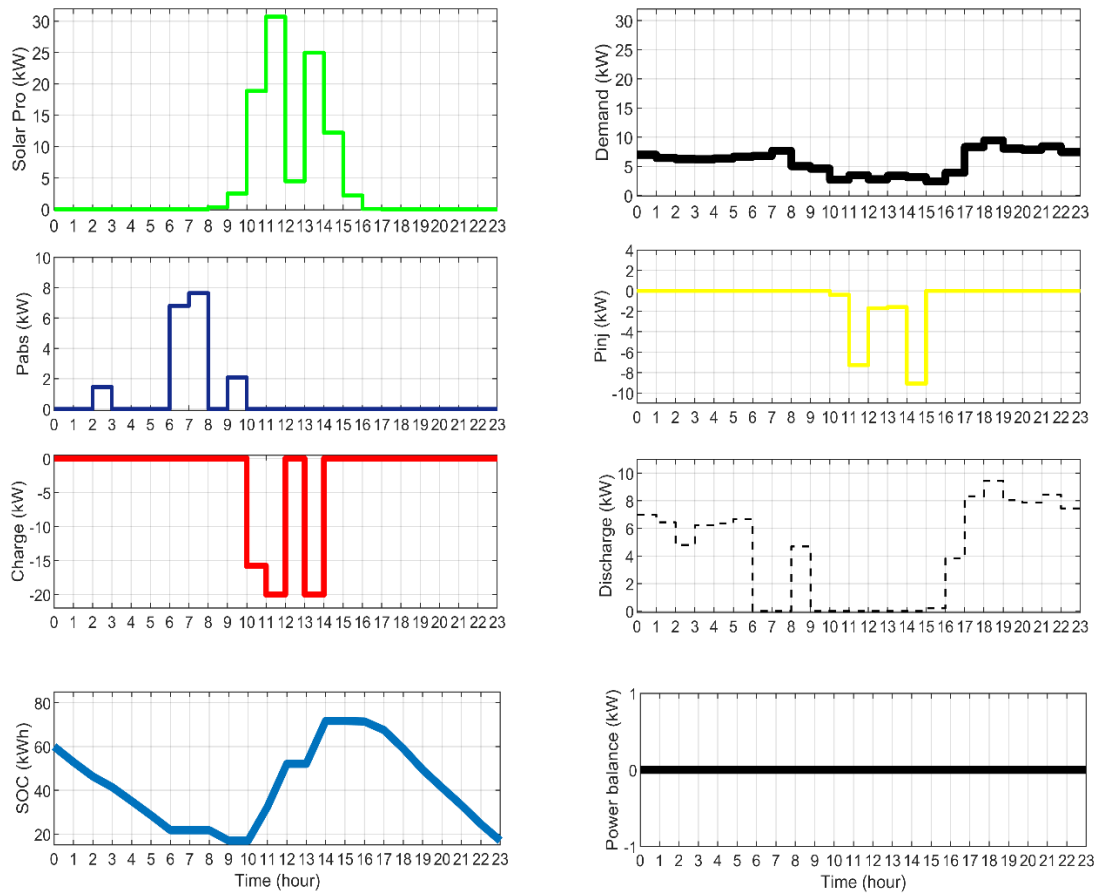


Figure 4. Demand, PV production, SOC, hourly charge and discharge, Pabs, Pinj for 24-hour

4. Conclusion

Within the scope of this investigation, an optimization-based method to energy management is provided and meticulously discussed. Both the load profile and the PV profile of the prosumer have been chosen at random in accordance with certain generic characteristics. For prosumer, the constraints are described in extensively. For the purpose of making it easier to grasp the results of optimization simultaneously, the system operation, load profile, and PV profile are all displayed graphically. It is necessary for there to be no power imbalance in order to achieve maximum production. It has been demonstrated that the proposed method is capable of successfully satisfying the power quality equality restrictions with minimized prosumer bill.

References

- [1] Bhuiyan, M. R. A., Alam, M. M., & Momin, M. A. (2010). Effect of substrate temperature on the optical properties of thermally evaporated ZnS thin films. *TURKISH JOURNAL OF PHYSICS*. <https://doi.org/10.3906/fiz-0902-9>
- [2] Bhuiyan, M. R. A. (2022). Overcome the future environmental challenges through sustainable and renewable energy resources. *Micro & Nano Letters*, 17(14), 402–416. <https://doi.org/10.1049/mna2.12148>
- [3] Bhuiyan, M. R. A., Mamur, H., & Dilmaç, Ö. F. (2020). Review on Performance Evaluation of Bi₂Te₃-based and some other Thermoelectric Nanostructured Materials. *Current Nanoscience*, 17(3), 423–446. <https://doi.org/10.2174/1573413716999200820144753>.
- [4] Alam, M. J. E., Muttaqi, K. M., & Sutanto, D. (2013). Mitigation of Rooftop Solar PV Impacts and Evening Peak Support by Managing Available Capacity of Distributed Energy Storage Systems. *IEEE Transactions on Power Systems*, 28(4), 3874–3884. <https://doi.org/10.1109/tpwrs.2013.2259269>
- [5] Liu, X., Aichhorn, A., Liu, L., & Li, H. (2012). Coordinated Control of Distributed Energy Storage System With Tap Changer Transformers for Voltage Rise Mitigation Under High Photovoltaic Penetration. *IEEE Transactions on Smart Grid*, 3(2), 897–906. <https://doi.org/10.1109/tsg.2011.2177501>
- [6] Rehman, Z., Mahmood, A., Razzaq, S., Ali, W., Naeem, U., EE, (2017, July). Prosumer based energy management and sharing in smart grid (journal-article). *Renewable and Sustainable Energy Reviews*. Retrieved from <http://dx.doi.org/10.1016/j.rser.2017.07.018>
- [7] Akter, M., Mahmud, M., & Oo, A. (2017). A Hierarchical Transactive Energy Management System for Energy Sharing in Residential Microgrids. *Energies*, 10(12), 2098. <https://doi.org/10.3390/en10122098>
- [8] Luna, A. C., Díaz, N. L., Graells, M., Vásquez, J. C., & Guerrero, J. M. (2016, September). Cooperative Energy Management for a Cluster of Households Prosumers. *Department of Energy Technology*.
- [9] Ranaweera, I., Midtgård, O., & Korpås, M. (2017). Distributed control scheme for residential battery energy storage units coupled with PV systems. *Renewable Energy*, 113, 1099–1110. <https://doi.org/10.1016/j.renene.2017.06.084>
- [10] Xu, T., Meng, H., Zhu, J., Wei, W., Zhao, H., Yang, H., Ren, Y. (2018). Considering the Life-Cycle Cost of Distributed Energy-Storage Planning in Distribution Grids. *Applied Sciences*, 8(12), 2615. <https://doi.org/10.3390/app812261>
- [11] Luna, A., Diaz, N., Savaghebi, M., Vasquez, J. C., Guerrero, J. M., Sun, L. (2016). Optimal Power Scheduling for a Grid-Connected Hybrid PV-Wind-Battery Microgrid System (journal-article). *IEEE* (p. 1227). <https://ieeexplore.ieee.org/document/7472016>
- [12] Tayab, U. B., B., Yang, F., El-Hendawi, M., & Lu, J. (2018). Energy Management System for a Grid-Connected Microgrid with Photovoltaic and Battery Energy Storage System. (Swinburne University of Technology), *2018 Australian & New Zealand Control Conference (ANZCC)* (p. 141). IEEE. <https://doi.org/10.1109/ANZCC.2018.8602017>
- [13] International Energy Agency. (2013). World Energy Outlook 2013. *World Energy Outlook*. <https://iea.blob.core.windows.net/assets/a22dedb8-c2c3-448c-b104-051236618b38/WEO2013.pdf>
- [14] <https://anaconda.org/conda-forge/glpk>



Lung Cancer Detection with Machine Learning Supported Image Processing Techniques

Furkan ÜSTÜNER¹ , **Mustafa SAZ²** , **İdris GENÇ³** , **Mahmut BÜYÜKBAŞ^{4,*}**

^{1,2,3,4} Faculty of Engineering, Electrical and Electronics Engineering, Abdullah Gül University, Kayseri, Turkey

Abstract

Fast processes play an important role in the diagnosis of lung cancer. This study aims to develop a computer-aided diagnostic (CAD) system using machine learning algorithms and advanced image processing techniques. The dataset used contains computed tomography (CT) scans obtained from two different private hospitals in Iraq and considers healthy individuals as well as lung cancer patients at different stages of the disease. The process has three important stages. The first is initial image preprocessing to get better output and improve image quality, followed by segmentation and feature extraction to identify relevant features, show the diseased area, and finally feature selection to optimize the inputs and make the best choices for the classification stage. In the project, various machine learning algorithms such as random forest, decision trees and neural networks are tested to distinguish benign and malignant cases, and the most ideal classification method for the data set is selected. The performance of these classification methods is evaluated using metrics such as accuracy, precision, and F1 score to ensure the reliability of the system. This study aims to significantly increase the effective treatment of patients by contributing positively to the lung cancer diagnosis process.

Keywords: Lung Cancer Detection, Image Processing, CT Scan Analysis, Classification, Feature Extraction

1. Introduction

Lung cancer is one of the most lethal types of cancer and millions of people die from this disease every year. Accurate diagnosis of lung cancer plays a critical role in the success of treatment. Computer-aided diagnosis (CAD) systems provide visualization of medical data using advanced technology and can significantly speed up the diagnosis process. In our project, computed tomography (CT) images of healthy and lung cancer patients at different stages in the IQ-OTH/NCCD dataset obtained from two private hospitals in Iraq were used[1]. Our aim is to accurately classify tumors as healthy, benign and malignant using image processing and machine learning algorithms. We aim to increase the classification accuracy, sensitivity and F1 score. In this direction, methods such as Contrast, Energy, Gabor filters and HomogeneityGLCM are used in the segmentation and feature extraction stages. Hasan Hejbari Zargar and his team demonstrated the effectiveness of these techniques by reaching 92.08% sensitivity, 91% accuracy and 93% AUC values with the VGG16 algorithm [2]. For classification and performance evaluation, algorithms such as artificial neural networks, decision trees and random forests are tested, and the correct classification success of each algorithm is examined. This model will provide significant contributions to correct diagnosis and appropriate treatment planning with high accuracy, sensitivity and F1 score.

2. Materials and Methods

2.1. Importing of the Datasets

Importing datasets is used in the first phase of a machine learning project and is especially used when it comes to diagnosis using computer-aided imaging. This study divided the dataset into three different cases: benign, malignant, and normal. After the necessary definitions were made using the Python coding language, the files were downloaded to the computer. This setting makes it easier to manipulate data programmatically. It helps the data to be used in subsequent stages such as pre-processing, feature extraction, feature selection and classification. Keeping the data set organized is an important way to ensure the success of the project and plays an important role in increasing efficiency in the analysis process. Additionally, a sample image from the dataset is included as shown in Figure 1.

* Corresponding author. e-mail address: mahmut.buyukbas@agu.edu.tr

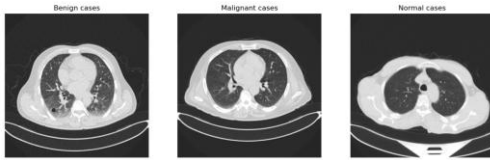


Figure 1. Importation of the dataset

2.2. Image Processing Procedures

In medical imaging, image processing methods are of great importance in the detection of diseases. Processes such as median filter, edge detection and Gaussian blur have been used to minimize noise, identify morphological changes and select important features. Color images are reduced to a single channel by converting to grayscale, thus reducing data size and increasing processing efficiency. Gaussian filter provides clearer and more processable images by reducing noise in sensitive medical data. Median filter provides clearer tumor segmentation in CT scans by eliminating random noise (e.g. salt and pepper). Edge detection provides detailed analysis by emphasizing density changes in the image and highlighting tumor boundaries. These methods contribute to a clearer view of anatomical structures in particular. You can also see the image processing operations performed on benign cases (Figure 2), malignant cases (Figure 3), and normal cases (Figure 4).

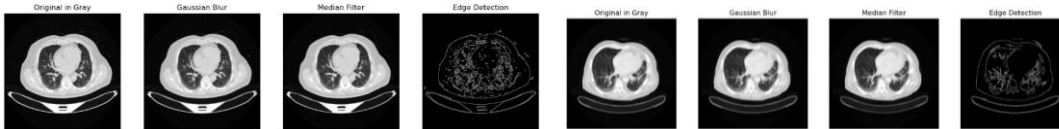


Figure 2. Benign Cases

Figure 3. Malignant Cases

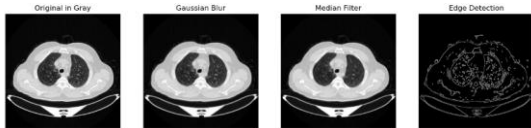


Figure 4. Normal Cases

2.3. Segmentation

The operations performed in the previous steps make the data obtained in the segmentation section clearer and more accurate. Particularly in medical imaging and in our project, segmentation separates diseased tissues from healthy tissues, making them more visible and increasing the accuracy of diagnoses at the stage of medical diagnosis. Segmentation on computed tomography (CT) scans used to diagnose lung cancer is crucial for determining the precise boundaries of tumors or other abnormal structures. This study used the segmentation method to mark and examine malignant (Figure 6) and benign (Figure 5) structures within the lung tissue. Segmentation on computed tomography (CT) scans used to diagnose lung cancer is crucial for determining the precise boundaries of tumors or other abnormal structures. This study used the segmentation method to mark and examine malignant (Figure 6) and benign (Figure 5) structures within the lung tissue. Clearer and more accurate data was obtained during feature extraction due to the separation of two different tissue parts. As a result, this separation process helps the machine learning procedures we use for classification work more effectively.



Figure 5. Benign Cases Segmentation



Figure 6. Malignant Cases Segmentation

2.4. Feature Extraction and Feature Selection

Feature extraction is an important step in machine learning and data analysis aimed at obtaining meaningful and more processable information from the raw data set. It is also the process of extracting the necessary information from the raw data set, aiming to facilitate the classification prediction of the model. The features extracted from the data aim to increase the accuracy of the model and its generalization capacity in different

situations. Feature extraction also reduces the size of the raw data set to make the data more manageable due to the large size of the raw data set. Thus, while the data set is represented in a more concise form, the processing time is reduced, and performance is increased due to the elimination of unnecessary information. In our project, we tried to perform feature extraction of Computerized Tomography (CT) images, which is a critical step in detecting and analyzing pathological conditions of lung CT images. In addition, the 50 different features extracted in this project allow us to analyze different aspects and textural qualities of the images in detail. ANOVA feature selection method was used to identify the extracted features associated with tumourous tissues. ANOVA analyses group means and variances. ANOVA feature selection helps to determine which features are relevant to tumourous tissue. ANOVA calculates the differences between the means of different groups, and if the calculated F value is within the desired range ($p < 0.05$) Figure 7 and Figure 8, it indicates that the feature makes a statistically significant difference between the groups.

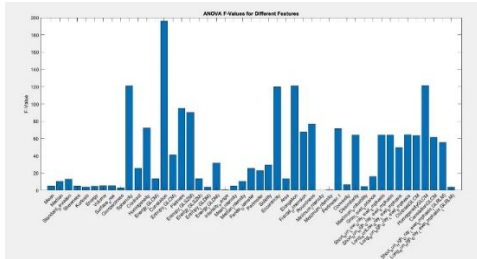


Figure 7. ANOVA F-Value for Different Features

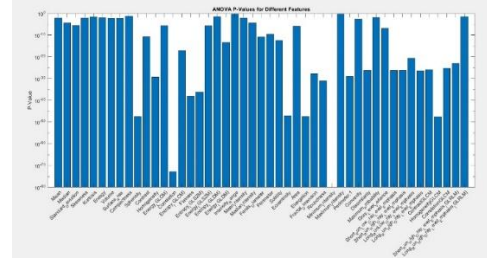


Figure 8. ANOVA p-Value for Different Features

The feature being important for the model and having a strong relationship with the target helps to create a model with a more understandable and general structure by increasing the model performance. Selection of meaningful features reduces the risk of overfitting and allows elimination of misleading data. The features that are important in our project are: Correlation expresses pixel relationship; HomogeneityGLCM is effective in showing textural consistency and separating tumor tissue; Elongation determines tumor shape differences; Sphericity separates tumor tissue from regular structures; Eccentricity helps to understand the morphological structure of the tumor; Flatness contributes to the analysis of tissue abnormalities; Entropy (GLSZM) and Roundness are used to detect irregular tumor shapes.

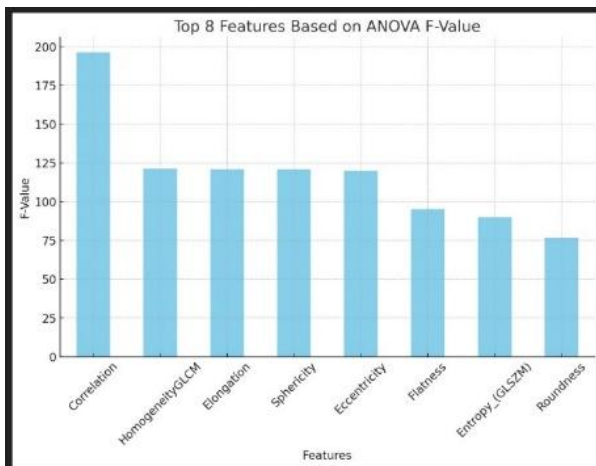


Figure 9. Top 8 Features Based on ANOVA F-Value

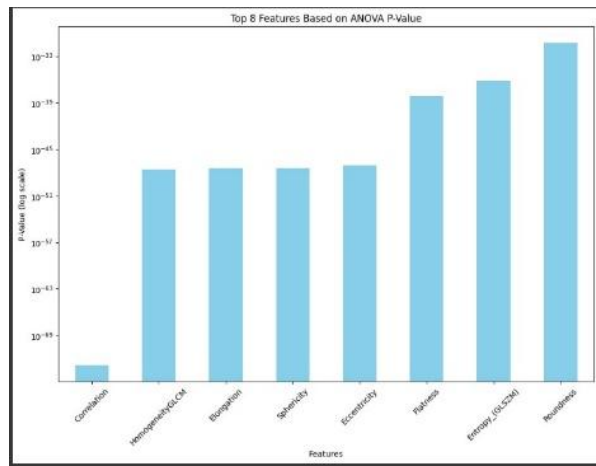


Figure 10. Top 8 Features Based on ANOVA p-Value

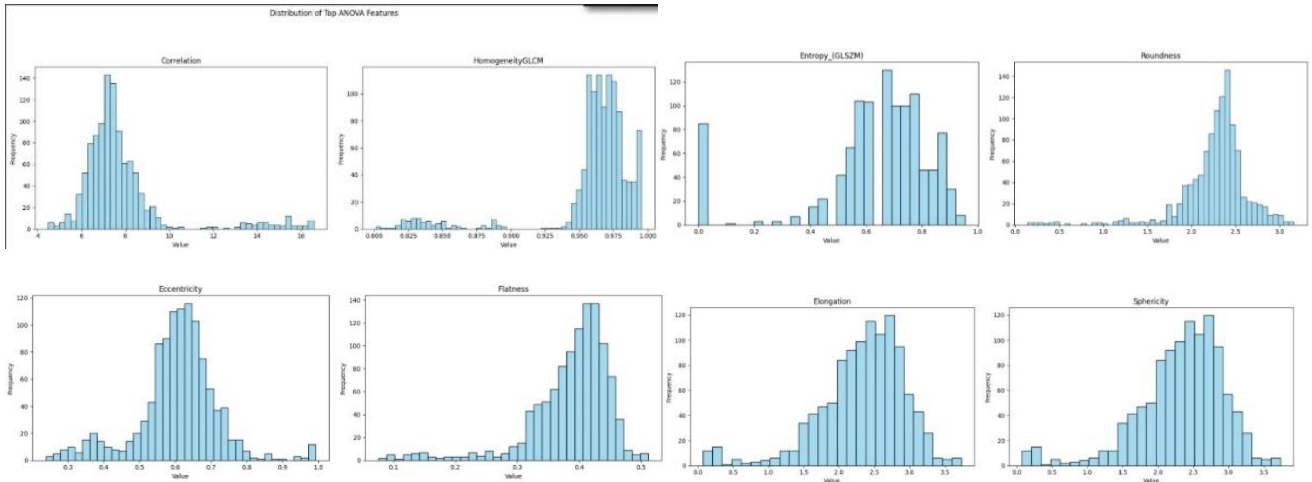


Figure 11. Histogram Graph of Selected Features

In summary, meaningful and important features in an image are the data processed for tumor detection. These features are essential for disease classification and detection in the later stages and incorrect feature extraction and selection of these features is directly related to the model's performance. Feature extraction and selection, which has a direct impact on the training and performance of the model, is essential for the other stages of the project.

3. Results and Discussion

3.1. Classification

In machine learning, classification is the process of dividing a dataset into subcategories. Especially thanks to the classification techniques used in the field of medical imaging, the images obtained are divided into groups in terms of identifying diseases. In this project, classification methods such as decision trees, Deep Neural Networks (DNN) and Random Forests were used (Figure 12). The Random Forest method is an interesting approach; it brings together many decision trees and evaluates the results produced by each tree and selects the most common result. Another advantage of this method is that it provides diversity and a wide perspective, because each decision tree looks at the data differently. The advantage of this method is that it provides high accuracy rates and reduces the risk of overfitting. Deep Neural Networks (DNN), which are high-layer artificial neural networks, are also a very successful classification method in recognizing and classifying complex patterns. (Figure 13). This allows the DNN to discover small details in the images. Decision trees are a simple but effective method that divides the data according to certain criteria and classifies the results by creating decision points on each branch (Figure 14). The feature selection research in the project highlighted that these three classification methods are suitable for lung cancer diagnosis. We ranked the features extracted from our dataset according to their importance and selected the most significant ones. This strategy greatly increased the success and accuracy of our model. In particular, selecting the right features can be life-saving for patients about to be diagnosed. This method aims to obtain more robust and reliable results by examining.

NUMBER OF CLASSES	3
ACCURACY	89.0909 %
RECALL	0.865030
PRECISION	0.867162
F1 SCORE	0.846024

Figure 12. Decision Trees Classification

NUMBER OF CLASSES	3
ACCURACY	98.8567 %
RECALL	0.953765
PRECISION	0.988735
F1 SCORE	0.97681

Figure 13. DNN Classification

NUMBER OF CLASSES	3
ACCURACY	91.8181 %
RECALL	0.816117
PRECISION	0.936752
F1 SCORE	0.844392

Figure 14. Random Forest Classification

Three different classification models (Random Forest, Decision Trees and Deep Neural Network, also known as DNN) were measured and their performances were compared. Each of the models was evaluated using important metrics such as accuracy, recall, precision and F1 score. Observations and graphical result (Figure 15) show that the DNN model is better than other classification models in every aspect. For this reason, we

decided to use the Deep Neural Network (DNN) method because it provides better results and is better suited to the data set. This decision was made after examining the models in more depth.

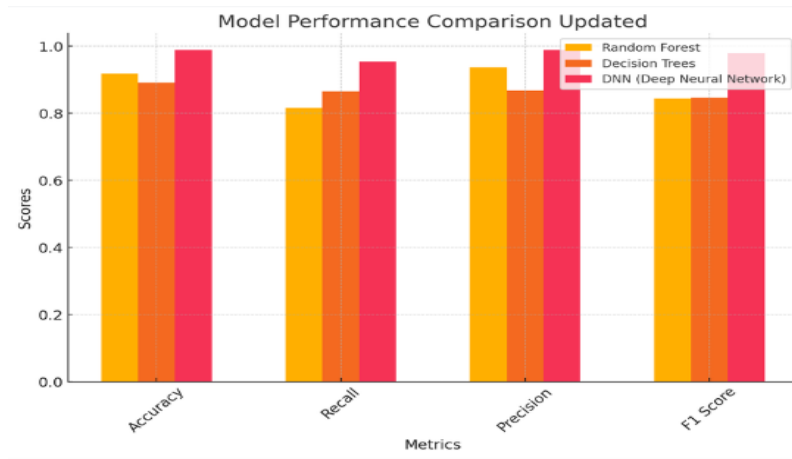


Figure 15. Model Comparison Table

3.2. Cross Validation

Cross-validation is used to evaluate the accuracy of classification models and avoid overfitting. Particular attention should be paid to complex structures such as Deep Neural Networks (DNN). Cross-validation is based on the principle of splitting a dataset into random subsets and using each subset as testing and training sets. This method is known as “k-fold cross validation”; where “k” indicates how many subsets the “k” dataset will be divided into. This increases the reliability of the model. The DNN model used in the project uses cross-validation to accurately evaluate how effective selected features are in diagnosing lung cancer. This prevents the model from fitting too many subsets of data. Once feature selection is completed in the project, evaluating the impact of the DNN model on various datasets allows determining the best feature combinations. This procedure is important to understand how the model will respond to various patient data. Cross-validation improves the final diagnostic success of the project by increasing the reliability of the model prior to medical application. In the project, various studies were carried out to increase the number of layers in the structure of the Deep Neural Networks (DNN) model in order to increase its effectiveness. Biden was tested by trying multilayer numbers. DNNs leverage multiple hidden layers to gain insight into complex data views. These layers affect the accuracy of predictions because each processes data differently. Therefore, the number of layers in the DNN model had to be adjusted to determine the most suitable structure for the project. As a result of our observations, increasing the number of layers allows the model to understand the data better, but increasing the number of layers too much negatively affects the generalization ability of the model. Therefore, experiments were conducted to determine the ideal number of layers that meet the highest accuracy and generalization performance in the diagnosis of lung cancer images in our dataset.

NUMBER OF LAYERS	4	6	8
ACCURACY	98.8567 %	94.8579 %	96.2542 %
RECALL	0.953765	0.912109	0.922398
PRECISION	0.988735	0.943092	0.965867
F1 SCORE	0.97681	0.939589	0.957638

Figure 16. Effect of change in the number of layers

The work done in the project to maximize the performance of the model using Deep Neural Networks (DNN) changed not only the number of layers but also the number of epochs and test set size. There is an epoch number, which indicates how many times the entire training data set will be processed in the learning process. Increasing the number of epochs allows the model to learn the training data better, but too many epochs may

cause the model's generalization ability to decrease and overfit. The project tried to find the ideal value that tried to maximize the model's performance on both training and validation datasets by trying different epoch numbers.

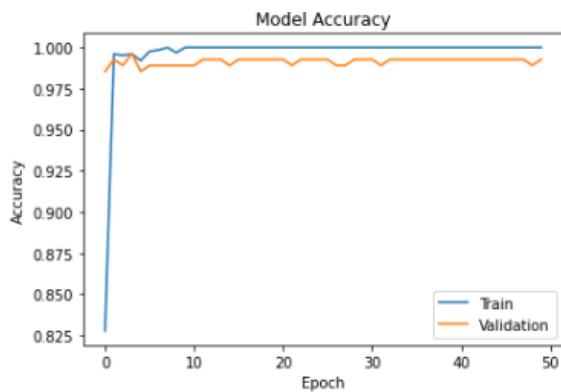


Figure 17. Effect of change in the number of Epoch Model Accuracy

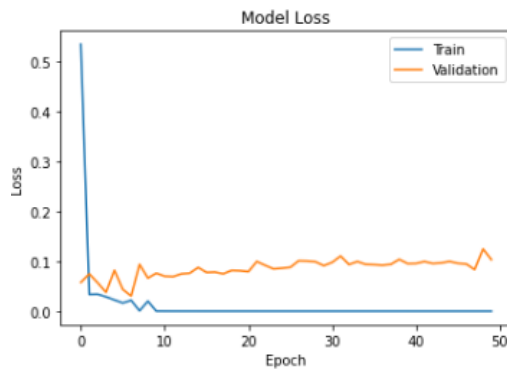


Figure 18. Effect of change in the number of Epoch Model Loss

However, adjustments to the test set size are important to the accuracy and reliability of the model. The test set allows the model to be compared with data it has not seen during the training process. This is usually set as a certain percentage of the data set. As the size of the test set increases, more accurate predictions can be made about how the model will perform with real data. However, a test set that is too large may be negatively affected as it will reduce the amount of data required for training the model. The project efforts achieved an ideal balance between the model's training dataset and validation dataset by manipulating the test set size, optimizing the success of the model both in the training process and in real-world conditions. These changes helped the DNN model provide high accuracy and reliability in diagnosing lung cancer.

TEST SIZE	0.2	0.5	0.8
ACCURACY	98.8567 %	92.6042 %	90.7810%
RECALL	0.953765	0.803345	0.913333
PRECISION	0.988735	0.943342	0.789458
F1 SCORE	0.97681	0.919903	0.901701

Figure 19. Effect of change in the ratio of Test Size

4. Conclusion

This study examines a new CAD system for lung cancer diagnosis. This project aims to significantly increase patient survival rates through rapid diagnosis, supported by data collected from private hospitals in Iraq. This study distinguishes benign and malignant cases by detailing processes such as image preprocessing, segmentation, feature extraction and feature selection. Various machine learning algorithms are used, such as SVMs, decision trees, and artificial neural networks. The findings support our system's correct detection capability, supported by high accuracy, sensitivity, and metrics such as F1 score. As a result, it seems that this project contributes to the development of treatment methods by creating an effective tool in the rapid diagnosis of lung cancer and has the potential to extend the lifespan of patients. These achievements show once again what impact technological innovations will have on health and how important rapid diagnosis is.

References

- [1] Mahimkar, A. (2021). IQ-OTH/NCCD lung cancer dataset [Data set]. Kaggle.
- [2] Zargar, H. H., Zargar, S. H., Mehri, R., & Tajidini, F. (2023). Using VGG16 Algorithms for classification of lung cancer in CT scans Image. arXiv preprint arXiv:2305.18367.
- [3] Alsaadi, E. M. T. A., & Rahman, Z. H. A. A. (2023, December). Automatic lung cancer recognition in chest CT-scan images using SVM classifier. In AIP Conference Proceedings (Vol. 2977, No. 1). AIP Publishing.

An Evaluation of Dynamic Compaction: Limits and Effects on Geotechnical Performance

Mehmet Salih YILDIZ^{1,*} , İnan KESKİN²

¹ Vocational School of Social Sciences, Cankiri Karatekin University, Cankiri, Türkiye

² Faculty of Engineering, Civil Engineering Department, Karabük Üniversitesi, Karabük, Türkiye

Abstract

Dynamic Compaction (DC) is a soil improvement method used to increase the bearing capacity and stability of soils. This method is based on the principle of repeatedly dropping a weight into the ground from a certain height and compacting the soil particles after the drops. This method offers higher efficiency in cohesionless soils such as sand and gravel, but is not effective for water-saturated and cohesive soils. DC has a wide range of applications from motorways and airports to coastal and harbour areas. In addition to its advantages, DC also has some disadvantages. The main disadvantages are noise and the danger posed by the vibration effect for the surrounding structures. However, these disadvantages can be overcome with proper planning, environmental precautions and working with expert teams. DC plays an important role in ground improvement projects by providing a fast and economical solution.

Keywords: Dynamic compaction, Soil improvement, Geotechnical performance

1. Introduction

The limited land resources are one of the main obstacles to the development of cities. Opening up more land for construction is inevitable for socio-economic development (Wei et al. 2023). Opening up land for construction is not only a matter of zoning planning, but also the structure to be built on it must be strong enough to meet the design criteria. Ground improvement methods are used to make limited zoning lands suitable for design criteria. Dynamic Compaction (DC) application is one of the ground improvement methods in civil engineering. This method; It provides the removal of air in the ground by repeatedly releasing a certain weight from a certain height, especially on weak and heterogeneous soils, and compaction of soil grains by positioning them closer to each other with this impact energy.

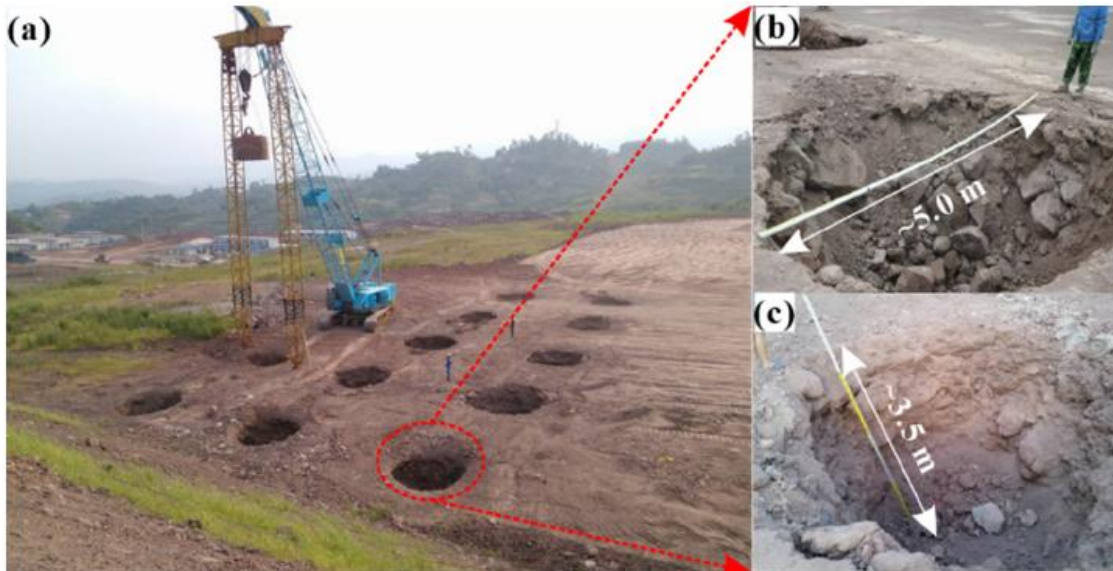


Figure 1. (a) A view of the DC application process and the application site (b) crater width and (c) crater depth (Wei et al. 2023)

* Corresponding author. e-mail address: msalihyldz@gmail.com

DC is an effective soil improvement method applied in the field of soil engineering to increase the bearing capacity of soils and reduce the liquefaction potential. This method is based on the principle of reducing air voids within the soil and compacting soil particles more tightly by applying high-energy impacts to the soil surface (Figure 1). The basic principle of DC is the rearrangement of soil particles by the impact effect of a heavy mass falling on the soil. This process leads to the reduction of voids within the soil and the densification of the soil structure. DC is particularly effective in stabilizing cohesionless soils, but under certain conditions it has limited effects on cohesive soils (Akan and Keskin 2018; Kundu and Viswanadham 2015; Pinarci, Taşçi, and Çetin 2017).

The DC method was introduced by Menard in the 1970s. Menard presented the healing depth as a metric energy data and formulated it as follows: (Eq. 1) (Ménard and Broise 1975).

$$D = (W \cdot H)^{0.5} \quad (1)$$

Here; (D) represents the healing depth, (W) represents the weight of the dropped object, and (H) represents the drop height.

After field tests carried out with this formula, it was stated in some studies that a coefficient defined by n in the improvement depth formula expressed by Eq. 1 (Eq. 2) and selected according to the soil type would be more representative in the calculations. It is stated that this coefficient can vary between 0.3 and 1.00 depending on the soil type. (Table 1) (Şengezer 2010).

$$D = n \cdot (W \cdot H)^{0.5} \quad (2)$$

Table 1. Evaluation of the relationship between soil type and n coefficient (Nashed 2005)

Reference	N value	Deposit
Menard and Broise (1975)	1.0	General
Leonards et al. (1980)	0.5	Dry fine to medium sand
Lukas (1980)	0.65 – 0.8	Miscellaneous fill
Bhandari (1981)	0.51	Saturated Sands
Charles et al. (1981)	0.35	Loose fills and alluvial soil
Bjølgerud and Haug (1983)	1.0	Sands
Smolczyk (1983)	0.5	Soils with unstable structure
	0.67	Silts and sands
	1.0	Purely frictional soils
Mayne (1984)	0.3 – 0.8	Sands and miscellaneous fill
Rollins and Kim (1994)	0.4	Collapsible soils
	$0.586(W H)^{0.5} - 0.009 W H$	

DC is based on two main processes: instantaneous compression due to the effect of impact loads and compression due to the dynamic effect of vibrations caused by the impact of the falling load on the ground (Jia et al. 2018).

When the literature on DC is analysed, 3 types of studies are encountered. These are field studies, model tests in the laboratory and numerical studies. These studies can be evaluated individually or they can be used together in some studies.

DC increases the bearing capacity of the soil and enables safer construction and utilisation of the structures. By reducing the total settlement, it accelerates the consolidation process and prevents non-uniform settlements during the use of the structure. It can be considered as a more economical option compared to other ground improvement methods. It increases the building safety against seismic movements by reducing the liquefaction potential of the soil.

DC is a soil improvement method that has a current literature from the 1970s to the present, and still has some limitations that are waiting to be explained. The aim of this study is to discuss the advantages and limitations of the DC method and its effects on geotechnical performance.

2. Application Areas and Technical Details of DC

Menard and Broise defined DC as the compaction of soils to a depth of 10-30 metres by repeatedly releasing loads weighing tens of tonnes from heights of 15-40 metres (Ménard and Broise 1975). In DC, an energy is transferred to the soil by releasing the weight from a certain height a certain number of times. This energy brings the soil grains closer to each other, reduces the voids and compresses the soil over a large area. Repeated impacts continue this compaction towards deeper layers of the ground. The water content in the soil is dispersed with these impacts, accelerating the total consolidation and preventing non-uniform settlements within the life of the structure. In addition, physical properties of the soil such as shear strength and free compressive strength are also improved during DC. With these improvements, the soil becomes more resistant to structural loads.

The processes of the DC application can be followed as follows: preparation phase, determination of weight amount and drop heights, realisation of impacts, control and measurements. In the first stage, which is the preparation stage, a suitable land is determined and the surface is prepared by drawing the grids of the points to be dropped. Then, depending on the soil type of the land and the desired degree of compaction, the weight to be dropped and the drop height are designed. On the determined grid, the soil is compacted by performing drops from the weight and drop height in accordance with the design criteria. Finally, the efficiency of the improvement is evaluated by comparing the measurements made in the initial state of the soil with the strength values of the land after the falls.

DC applications have a very common usage area such as strengthening the infrastructure in constructions such as highways and railways, strengthening the foundation soils of large structures such as industrial facilities, improving the runway and apron areas of airports, ensuring the ground stabilization of areas such as coasts and ports, and improving the pre-construction ground properties of residential areas.

There are some advantages and limitations in DC application. These limits, which will be discussed below, determine the effectiveness and applicability of the method. The main limits are; soil type, depth of effect of improvement, environmental factors, underground structures, control and measurements, weather conditions. DC can generally be applied in granular and non-saturated soil types. Compaction efficiency decreases in fine-grained soils and high water contents.

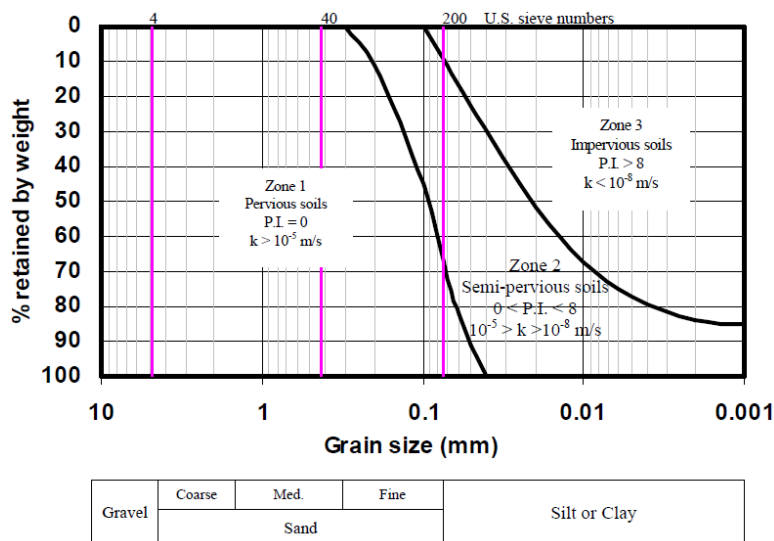


Figure 2. Grouping of soils for dynamic compaction (Lukas 1995)

Zone 1, shown in Figure 2 consists of highly permeable granular soils which are considered to be the most suitable for dynamic compaction. In this zone, as the load falls on the soil, the increasing pore water pressure dissipates almost immediately and densification occurs very quickly. (Lukas 1995).

Zone 3, contains soil types unfavourable for DC. Since the permeability in this zone is lower than 1×10^{-8} m/s, the damping of excessive pore water pressures during dynamic compaction takes a very long time, which is not practical for the application (Lukas 1995).

Zone 2, covers the area between the most favourable and unfavourable soils for DC. Silts, clayey silts and sandy silts are located in this zone. The permeability in this zone is between 10^{-5} and 10^{-8} m/s and time is needed to stabilise the excessive pore water pressure between the drops. In some projects, wick drains are installed for soils in this zone (Fig. 3) (Lukas 1995).

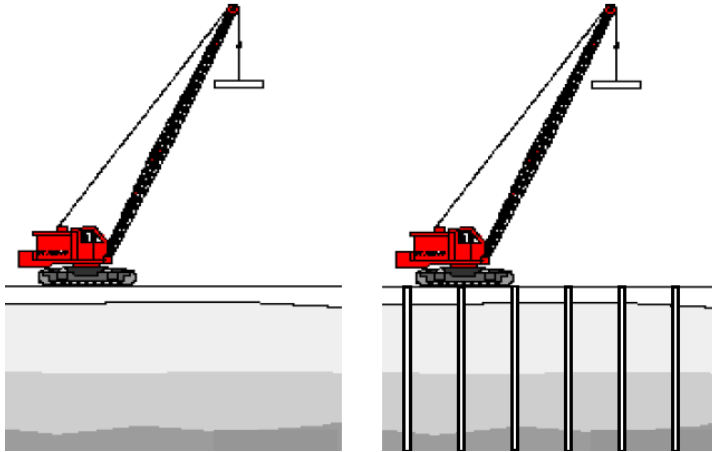


Figure 3. Example of DC with wick drain (Nashed 2005)

In previous studies, the depth of impact of DC was assessed as 10-12 meters. In places where deeper improvement is expected, sufficient compaction cannot be achieved. As an environmental effect, high noise and vibrations occurring during DC can be disturbing for neighboring structures and people. In addition, underground structures near the area where DC is performed can be negatively affected by the settlements and vibrations. Regular control and expert opinion are required for the degree of soil compaction and strength before and after DC. This may also require additional time and cost. In case of cold and rainy weather conditions, the DC process may become difficult. It can be said that the application will be more efficient in suitable weather conditions.

3. Results and Discussion

Studies on DC have revealed the following results. There are many factors affecting DC efficiency. The depth of the ground improved with DC does not depend only on the load, drop height and soil type. The most efficient improvement cannot always be achieved by dropping the heaviest load from the longest distance, and ground properties, number of drops, time between two drops, distance between drop points, shape and size of the dropped load, energy applied to the ground, ground water level and environmental conditions are also considered as parameters that need to be taken into consideration (Taghizadeh Valdi et al. 2018; Kim 2023; Kundu and Viswanadham 2018; Zhang, Wang, and Han 2021).

The parameters affecting DC can be summarized as soil properties; density (D_r), hydraulic conductivity (k), fines ratio (FC) and damping ratio. Studies have shown that the improvement depth of soils with high initial density decreases. Since it takes a long time to balance the excessive pore water pressure when the hydraulic conductivity decreases, more effective improvement is possible in soils with high hydraulic conductivity. The increase in the fines ratio will again create excessive pore water pressure, which negatively affects the improvement. Since the high damping ratio of the soil may cause the effects of the reduced load not to be seen at the desired level in the soil, it is one of the parameters that should be taken into consideration (Nashed 2005).

Since the number of falls increases the energy applied to the soil, it has a positive contribution to the improvement. However, since the improvement in the soil will remain constant after a certain number of falls, continuing to make falls is inefficient both in terms of time and economy. The effect of the time between two falls is a parameter that becomes important especially in soils with fine grains. The reason for this is waiting for the excessive pore water pressure to balance, that is, for the water to drain and for the settlement to be complete (Lukas 1995).

In the DC application, the distance between the drop points is determined by the field grid. This is an application made in order to ensure that the improvement is carried out homogeneously within the ground and to prevent non-uniform settlements. Each drop is carried out in a certain number of times to the specified points on this grid. Here, the drop distance, the weight of the falling object and the number of drops determine the energy applied to the ground. Again, control tests are carried out at certain points determined on the grid (Feng et al. 2013).

The shape and size of the dropped load also play a decisive role in the effectiveness of the DC process. These two parameters establish the pressure that the weight of the load exerts on the ground (Arslan, Baykal, and Ertas 2009).

In order to analyze the effects of groundwater level on DC, experiments were carried out on model tests at different water levels and as the groundwater level deepens, there were increases in the improvement. However, it is not suitable for compaction in completely dry soils. The optimum water content at maximum dry density for DC was determined as the value that provides the most suitable compaction (Hamid, Al-Amoudi, and Aiban 2019; Jia et al. 2021).

Another factor affecting the DC is the environmental conditions. The vibrations and sound that occur during the DC application can have negative consequences for the environment. Especially in areas where underground structures are located, vibrations can cause large lateral displacements and damage the structures. In order to eliminate this problem, there are studies on the creation of vibration isolation trenches between the areas where DC is applied and the surrounding structures (Wang, Yin, and Wang 2023; Zheng et al. 2023). At the same time, the resulting sound can exceed the limit conditions related to noise. For this reason, the relationship with the surrounding structures and people should also be taken into consideration in the area where DC will be applied (Abedini, Rafiee-Dehkharghani, and Laknejadi 2022; Gürkaynak 2012; Hwang and Tu 2006).

4. Conclusion

In this study, the advantages, limits and factors affecting the efficiency of the DC method are discussed in detail. It has been determined that DC has an important place in soil improvement projects and has a widespread use. It has been determined that the method has high efficiency especially in cohesionless and water-unsaturated soils, and that it contributes to the safer and more durable structures by increasing the soil bearing capacity and reducing the liquefaction potential. The improvement method, which also has some limits, has aspects that need to be clarified or resolved with the studies conducted. This study aims to shed light on future projects by addressing various aspects of DC application.

References

- Abedini, Farzaneh, Reza Rafiee-Dehkharghani, and Karim Laknejadi. 2022. "Mitigation of Vibrations Caused by Dynamic Compaction Considering Soil Nonlinearity." *International Journal of Civil Engineering* 20(7):809–26. doi: 10.1007/s40999-022-00700-9.
- Akan, Recep, and Sıddıka Nilay Keskin. 2018. "KOMPAKSİYÖYönteminin KohezyonlZeminlerin Serbest BasınçMukavemetinEtkisi." *Mühendislik Bilimleri ve Tasarım Dergisi* 6(2):250–57. doi: 10.21923/jesd.383872.
- Arslan, H., G. Baykal, and O. Ertas. 2009. "Discussion: Influence of Tamper Weight Shape on Dynamic Compaction." *Proceedings of the Institution of Civil Engineers: Ground Improvement* 162(3):153–54. doi: 10.1680/grim.2009.162.3.153.

- Feng, Shi Jin, Ke Tan, Wei Hou Shui, and Yan Zhang. 2013. "Densification of Desert Sands by High Energy Dynamic Compaction." *Engineering Geology* 157:48–54. doi: 10.1016/j.enggeo.2013.01.017.
- Gürkaynak, Ömer. 2012. "Dinamik Kompaksiyon Sonucu Oluşan Titreşim Verilerin Değerlendirilmesi." *İstanbul Teknik Üniversitesi*.
- Hamid, Abdulrahman M., Omar S. Baghabr. Al-Amoudi, and Saad A. Aiban. 2019. "Assessing the Effect of Density and Water Level on the Degree of Compaction of Sand Using Dynamic Cone Penetration Test." *Arabian Journal for Science and Engineering* 44(5):4921–30. doi: 10.1007/s13369-018-3641-0.
- Hwang, J. H., and T. Y. Tu. 2006. "Ground Vibration Due to Dynamic Compaction." *Soil Dynamics and Earthquake Engineering* 26(5):337–46. doi: 10.1016/j.soildyn.2005.12.004.
- Jia, Mincai, Ye Yang, Bo Liu, and Shaohai Wu. 2018. "PFC/FLAC Coupled Simulation of Dynamic Compaction in Granular Soils." *Granular Matter* 20(4):1–15. doi: 10.1007/s10035-018-0841-y.
- Jia, Mincai, Ye Yang, Bo Liu, and Shaohai Wu. 2021. "Densification Mechanism of Granular Soil under Dynamic Compaction of Proceeding Impacts." *Granular Matter* 23(3):1–15. doi: 10.1007/s10035-021-01136-z.
- Kim, Myeonghwan. 2023. "Enhancing Ground Improvement of Dredging Landfill in South Korea's Western Coastal Region: Insights into Dynamic Compaction Characteristics." *Buildings* 13(7). doi: 10.3390/buildings13071830.
- Kundu, Saptarshi, and B. V. S. Viswanadham. 2015. "Studies to Evaluate the Impact of Tamper on the Depth of Improvement in Dynamic Compaction." *15th Asian Regional Conference on Soil Mechanics and Geotechnical Engineering, ARC 2015: New Innovations and Sustainability (2011):2033–37*. doi: 10.3208/jgssp.IND-20.
- Kundu, Saptarshi, and B. V. S. Viswanadham. 2018. "Numerical Studies on the Effectiveness of Dynamic Compaction in Loose Granular Deposits Using Shear Wave Velocity Profiling." *Indian Geotechnical Journal* 48(2):305–15. doi: 10.1007/s40098-018-0298-2.
- Lukas, Robert G. 1995. "Geotechnical Engineering Circular No. 1, DYNAMIC COMPACTION." *Grouting, Soil Improvement, and Geosynthetics (Eds R. H. Borden, R. D. Holtz and I. Juran), ASCE Geotechnical Special Publication No. 30, Vol. 2, Pp. 940-953*. New York: ASCE.
- Ménard, L., and Y. Broise. 1975. "Theoretical and Practical Aspect of Dynamic Consolidation." *Geotechnique* 25(1):3–18. doi: 10.1680/geot.1975.25.1.3.
- Nashed, Rafeek. 2005. "Liquefaction Mitigation of Silty Soils." 6(4):5381.
- Pinarci, Emre, Meltem Taşçı, and Hasan ÇetİN. 2017. "Changes of Permeability and Effective Stress Compacted Clayey Soils Depending on the Compaction Energy." *Çukurova University Journal of the Faculty of Engineering and Achitecture* 32(3)(September):197–204.
- Şengezer, Levent. 2010. "GRANÜLER ZEMİNLERDE DİNAMİK KOMPAKSİYON UYGULAMASI." *İstanbul Teknik Üniversitesi*.
- Taghizadeh Valdi, Mohammad Hossein, Mohammad Reza Atrechian, Ata Jafary Shalkoohy, and Elham Chavoshi. 2018. "Numerical Investigation of Water Entry Problem of Pounders with Different Geometric Shapes and Drop Heights for Dynamic Compaction of the Seabed." *Geofluids* 2018. doi: 10.1155/2018/5980386.
- Wang, Guobo, Yao Yin, and Jianning Wang. 2023. "Vibration Safety Evaluation and Vibration Isolation Control Measures for Buried Oil Pipelines under Dynamic Compaction: A Case Study." *Soil Dynamics and Earthquake Engineering* 167(November 2022):107783. doi: 10.1016/j.soildyn.2023.107783.
- Wei, Yingjie, Yuyou Yang, Jintai Wang, Huancun Liu, Jianguang Li, and Yuxin Jie. 2023. "Performance Evaluation of High Energy Dynamic Compaction on Soil-Rock Mixture Geomaterials Based on Field Test." *Case Studies in Construction Materials* 18(November 2022):e01734. doi: 10.1016/j.cscm.2022.e01734.
- Zhang, Xiaoshuang, Min Wang, and Yunshan Han. 2021. "Model Test Study on the Effect of Dynamic Compaction under Low Water Content." *PLoS ONE* 16(6 June):1–14. doi: 10.1371/journal.pone.0253981.
- Zheng, Yonglai, Xin Lan, Tanbo Pan, Dingding Cui, Guangxin Li, Longyin Shen, and Xubing Xu. 2023. "Field Testing and Numerical Simulation of the Effectiveness of Trench Isolation for Reducing Vibration Due to Dynamic Compaction." *Applied Sciences (Switzerland)* 13(17). doi: 10.3390/app13179744.
- Applied Sciences (Switzerland)* 13(17). doi: 10.3390/app13179744.



Comparative Analysis of Floating and Ground-mounted Photovoltaic Systems: Performance, Environmental and Economic Perspectives in Istanbul

Ethar Sulaiman Yaseen YASEEN¹ , Abdülkerim FIRAT² , Mehmet Ali BİBERCİ^{2*} , İbrahim ÇİFTÇİ²

¹ Institute of Graduate Studies, Department of Electrical and Electronics Engineering, Çankırı Karatkin University, Çankırı, Türkiye

² Institute of Graduate Studies, Department of Mechanical Engineering, Çankırı Karatkin University, Çankırı, Türkiye

Abstract

This study conducts a comparative analysis of floating and ground-mounted photovoltaic (PV) systems in Istanbul, Turkey, focusing on their performance, environmental impact, and economic feasibility. Using PV-SOL Premium 2021 software, both systems each with an installed capacity of 154.8 kWp are simulated under identical climatic conditions. Performance metrics such as energy yield, specific yield, performance ratio (PR), CO₂ emission reduction, and financial outcomes are evaluated. Results show that the floating PV system outperformed the ground-mounted system, generating 200,467 kWh/year with a PR of 96.0%, compared to 190,260 kWh/year and a PR of 88.0% for the ground-mounted system. The superior performance of the floating system is attributed to reduced operational losses and enhanced cooling from the water surface. Additionally, the floating PV system demonstrated greater environmental benefits, offsetting 94,209 kg of CO₂ emissions annually, compared to 89,412 kg/year for the ground-mounted system. Despite these advantages, economic analysis revealed that neither system achieved financial profitability over a 20-year period. Both required an initial investment of 3,771,367 ₺, resulting in negative net cash flows of -2,419,049.15 ₺ for the floating system and -2,465,071.37 ₺ for the ground-mounted system. Furthermore, the floating PV system had a slightly lower electricity cost (1.03 ₺/kWh) compared to the ground-mounted system (1.09 ₺/kWh). These findings highlight the technical and environmental superiority of floating PV systems while emphasizing the critical need for subsidies, incentives, and supportive policies to enhance their financial feasibility and promote widespread adoption.

Keywords: Floating photovoltaic systems, Ground-mounted PV systems, Renewable energy.

1. Introduction

The increasing global demand for renewable energy necessitates innovative approaches that optimize energy output while minimizing environmental impacts. Photovoltaic (PV) systems are crucial for sustainable energy transition, but face challenges in environmental impact and efficiency. Recent research explores innovative approaches to optimize PV performance and sustainability. These include PV/T systems, sun-tracking mechanisms, bifacial configurations, and floating PV systems [1]. Environmental impacts of PV manufacturing and installation can be mitigated through optimized design, novel materials, recycling, and careful site selection [2]. Floating PV systems and solar trackers are gaining interest as methods to maximize power output and address land use concerns [3]. Agrivoltaic systems emerge as a promising solution, integrating food and energy production while considering landscape transformation and ecological impacts [4]. These advancements contribute to reducing greenhouse gas emissions, improving economic viability, and enhancing the overall sustainability of PV technology in meeting global energy demands.

Ground-mounted photovoltaic (PV) systems face significant land-use conflicts, particularly in densely populated areas where agricultural and urban needs compete with energy production. Agrivoltaic systems, which integrate crop production with solar energy generation, present a viable solution to this challenge by enhancing land use efficiency and promoting sustainable practices [5]. Research indicates that stilt-mounted PV panels can improve crop yields, even for shade-intolerant crops like corn, while simultaneously generating electricity [6]. These systems not only mitigate land competition but also contribute to lower greenhouse gas emissions and increased agricultural productivity. However, careful planning is essential to balance energy output and crop yields effectively. Overall, agrivoltaics represent a promising approach to addressing the dual demands of food and clean energy production.

Floating photovoltaic (FPV) systems have emerged as a promising solution to address land use challenges in solar energy production [7]. By utilizing water surfaces instead of land, FPVs offer several advantages, including increased land-use efficiency, reduced water evaporation, and improved cooling [8]. Studies have shown that covering just 1% of global reservoirs with FPVs could potentially generate 404 GWp of clean energy (Amer et

* Corresponding author. e-mail address:@.....

al., 2023). FPVs demonstrate significant land-sparing capabilities, with a mean land sparing ratio of 2.7:1 m² compared to ground-mounted PVs [9]. Additionally, FPVs exhibit higher water surface use efficiency, ranging from 35.2 to 94.5 W/m² depending on measurement criteria. However, further research is needed to fully understand the environmental impacts of FPVs on water quality and aquatic ecosystems [10].

The cooling effect of water is a particularly critical factor in the superior performance of FPV. Solar panels operate more efficiently at lower temperatures, and the proximity of FPV systems to water helps mitigate the heat buildup that typically reduces the efficiency of ground-mounted panels systems. This advantage is particularly beneficial in regions with high ambient temperatures, where cooling mechanisms are essential to maintaining optimal system performance [11]. FPVs can reduce water evaporation by up to 60% in reservoirs, contributing to water conservation in arid regions [12]. They also avoid land-use conflicts and can be deployed on degraded environments. A study estimated that FPV systems covering 27% of suitable man-made water bodies in the US could produce almost 10% of current national electricity generation (Spencer et al., 2018). However, challenges remain, including the need for supporting policies, development roadmaps, and ensuring long-term reliability of floating structures. Further research is needed to optimize FPV designs for maximum cooling benefits and economic competitiveness [13].

From an environmental perspective, FPV systems also present opportunities to minimize ecological impacts associated with land-based installations. The use of water surfaces reduces the need for land clearing, preserving natural habitats and maintaining biodiversity [14]. Moreover, FPV systems can be integrated with existing water infrastructure, such as hydropower reservoirs and irrigation canals, enhancing the overall efficiency of renewable energy systems. Despite these advantages, the adoption of FPV systems is not without challenges. Key barriers include higher initial investment costs, the need for specialized infrastructure to ensure system stability on water, and potential ecological impacts on aquatic ecosystems.

Economic considerations are a critical aspect of evaluating the feasibility of FPV systems. While the operational advantages of FPV systems may result in higher energy output and lower LCOE over the system's lifetime, the upfront costs associated with installation and maintenance are often higher than those of ground-mounted systems [15]. These costs are attributed to the specialized floating structures, anchoring systems, and corrosion-resistant materials required for water-based installations. Moreover, uncertainties related to system longevity and maintenance in aquatic environments add to the financial risks associated with FPV projects [16]. These challenges underscore the need for supportive policies, subsidies, and incentives to improve the financial viability of FPV systems and facilitate their widespread adoption.

Turkey, with its abundant solar energy potential and increasing focus on renewable energy development, provides an ideal setting for evaluating the performance of FPV systems [17]. The country has set ambitious targets for renewable energy capacity, aiming to diversify its energy mix and reduce dependence on fossil fuel imports. Istanbul, as a major urban and economic center, represents a critical region for implementing innovative energy solutions. The city's climatic conditions, characterized by high solar irradiance and moderate temperatures, make it an ideal location for testing the performance of both ground-mounted and floating PV systems.

This study aims to provide a comprehensive analysis of the performance, environmental impact, and economic feasibility of FPV systems compared to ground-mounted PV systems in Istanbul. Using PV-SOL Premium 2021 software, the study simulates the energy output, specific yield, and performance ratio (PR) of both systems under identical climatic conditions. It also evaluates the environmental benefits in terms of CO₂ emission reduction and assesses the financial outcomes, including investment costs, net cash flows, and electricity costs. By examining these factors, the study seeks to highlight the potential of FPV systems as a sustainable and innovative solution for renewable energy development in Turkey.

The findings of this research are contribute to the growing body of knowledge on FPV systems and provide valuable insights for policymakers, researchers, and industry stakeholders. By addressing the technical, environmental, and economic dimensions of FPV systems, this study aims to inform decision-making processes and promote the adoption of innovative renewable energy technologies. Ultimately, the research underscores the importance of integrating sustainability principles into energy planning and emphasizes the need for collaborative efforts to overcome the barriers to renewable energy deployment.

2. Materials and Methods

This study evaluates and compares the performance and environmental impact of two photovoltaic (PV) system models: The Ground-Mounted PV System and the Floating PV System. The analysis is conducted using consistent environmental and operational parameters to ensure a fair comparison. Both systems are assessed under identical climatic conditions, with key performance metrics calculated to understand their efficiency and sustainability.

2.1 Ground-Mounted PV System

The Ground-Mounted PV System is modeled with photovoltaic panels installed on fixed structures at ground level as shown in Fig. 1. The performance analysis focused on several parameters, including the system's annual energy output, which is determined using solar irradiance data and the system's design specifications. The Performance Ratio (PR) is evaluated to measure how effectively the system utilized its installed capacity, accounting for potential losses from heat and system components. To understand the energy efficiency of the installation, the Annual Specific Yield is calculated, representing the energy output per kilowatt-peak (kWp) of installed capacity. Additional factors such as shading losses are analyzed to ensure the system's placement and configuration would not hinder energy production. Lastly, the system's environmental impact is assessed by estimating the amount of CO₂ emissions avoided through its operation compared to conventional energy sources.

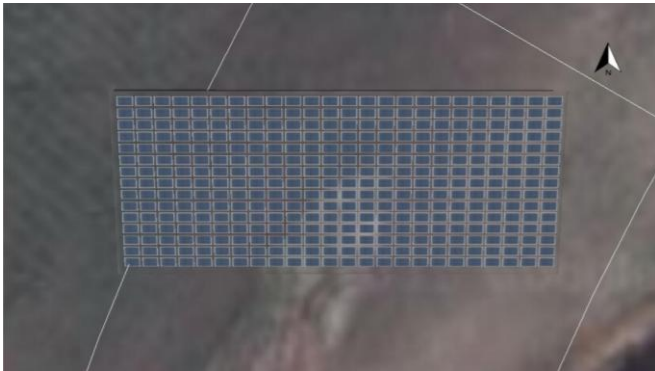


Figure 1. 3D model of the floating PV system

2.2 Floating PV System

The floating PV System is modeled with photovoltaic panels installed on water surfaces, taking advantage of environmental benefits like natural cooling and sunlight reflection. The system's annual energy output is calculated based on system-specific parameters and the same environmental data used for the ground-mounted model. The Performance Ratio (PR) is analyzed to assess the system's efficiency, with particular attention to the cooling effects of water, which reduce heat-induced energy losses. The Annual Specific Yield is calculated to quantify energy output per installed capacity, providing a basis for comparison with the ground-mounted system. Like the ground-mounted model, shading losses are considered to verify uninterrupted energy production potential. The system's contribution to environmental sustainability is also measured through an estimation of CO₂ emissions avoided, reflecting its role in reducing greenhouse gas emissions. Fig. 2 shows the 3D model of the floating PV system using Sol-PV simulation.

To ensure consistent and reliable comparisons, solar irradiance, temperature, and local climate data are input into simulation software for both systems. Standardized assumptions regarding panel efficiency, inverter performance, and operational losses are applied. The environmental assessment used standard conversion factors to correlate energy generation with CO₂ emission avoidance. This methodology offers a structured approach to evaluating the efficiency and environmental benefits of both PV systems, highlighting their potential applications in various contexts.

2.3 Data Collection and Simulation Parameters

The performance of both the Ground-Mounted PV System and the Floating PV System is simulated using PV-SOL Premium 2021 software. The simulations are conducted under climatic conditions specific to

Istanbul/Ataturk Airport, utilizing historical weather data from the period 1991–2010. This ensured accurate representation of the systems' behavior under realistic environmental conditions. Each system is modeled with identical hardware to provide a fair basis for comparison. The configurations included 360 SunPower SPR-MAX3-430 PV modules, covering a total area of 682.3 m², and 2 Huawei SUN2000-60KTL-M0 inverters. The Ground-Mounted PV System is designed with a tilt angle of 6°, optimizing solar capture under terrestrial conditions. In contrast, the Floating PV System employed a 0° tilt, reflecting its installation on a water surface where reflected sunlight enhances performance without the need for additional angling.

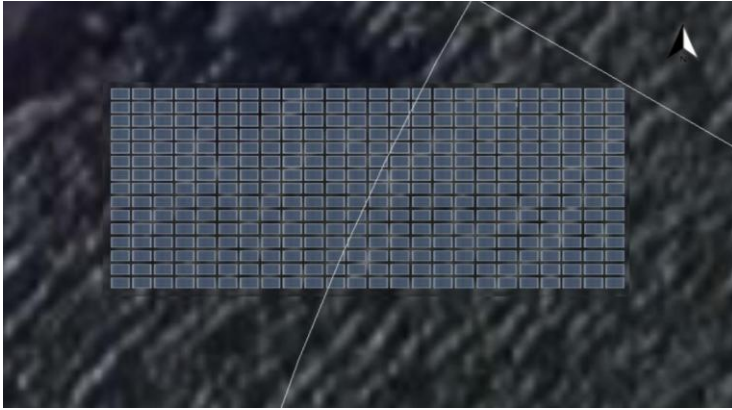


Figure 2. 3D model of the floating PV system

Key performance indicators are calculated for both systems to evaluate their operational efficiency and sustainability. These included annual specific yield, which measures the energy output per installed capacity; the performance ratio (PR), which indicates the systems' operational efficiency; and the total energy output in kilowatt-hours. Additionally, the CO₂ emissions offset by each system is assessed, reflecting their environmental benefits compared to conventional energy sources. Beyond technical metrics, financial indicators are also analyzed to understand the economic viability of each system. Parameters such as investment costs, payback periods, and net cash flow are calculated, providing insights into the long-term financial performance and feasibility of the systems. This comprehensive data collection and simulation process enabled a detailed comparison of the two PV systems, highlighting their strengths and potential applications in real-world scenarios.

3. Results and Discussion

3.1 Technical Performance

The floating PV system demonstrates clear technical superiority over the ground-mounted system, as evidenced by its enhanced energy generation and performance metrics. The floating system generated an impressive 200,467 kWh/year, surpassing the ground-mounted system's output of 190,260 kWh/year. This 10,207 kWh/year difference can be attributed to the floating system's ability to minimize operational losses and leverage the cooling effect of water surfaces. These factors significantly reduce the temperature of the photovoltaic modules, preventing efficiency losses typically caused by overheating in land-based systems. The Performance Ratio (PR) further highlights this difference in efficiency, with the floating PV system achieving a PR of 96.0%, compared to the ground-mounted system's 88.0%. This metric reflects the superior ability of the floating system to convert available sunlight into usable electricity, making it a more effective solution for maximizing energy output. The environmental benefits of the floating PV system are an additional advantage, as its higher energy generation directly correlates with greater reductions in carbon emissions.

3.2 Environmental Impact

The environmental benefits of photovoltaic systems are a key consideration in the evaluation of renewable energy technologies. In this comparison, the Floating PV System demonstrates superior performance in terms of reducing carbon emissions. By generating a higher annual energy output, the floating system offsets 94,209 kg of CO₂ emissions annually, significantly more than the 89,412 kg/year offset by the Ground-Mounted PV System. This difference highlights the enhanced environmental efficiency of the floating system, which is primarily driven by its reduced operational losses and improved cooling from the water surface. The ability to offset more carbon emissions makes the floating PV system a particularly attractive option for regions where environmental

sustainability is a priority. By contributing to a larger reduction in greenhouse gases, the floating PV system plays a critical role in combating climate change and supporting global efforts to transition to cleaner energy sources. Meanwhile, the ground-mounted system, though slightly less efficient in CO₂ reduction, still offers substantial environmental benefits compared to conventional fossil fuel-based energy generation. These findings underline the importance of selecting the appropriate PV system based on environmental goals. The floating PV system's superior CO₂ offset capability not only reflects its technical efficiency but also its potential to make a greater positive impact on the environment.

3.3 Economic Analysis

The financial analysis of the floating and ground-mounted PV systems reveals comparable installation costs and a marginal advantage for the floating system in terms of energy cost efficiency. Both systems required an initial investment of 3,771,367 ₺, reflecting identical hardware and installation expenses. Despite this similarity, the floating PV system demonstrated a slightly lower electricity cost at 1.03 ₺/kWh compared to 1.09 ₺/kWh for the ground-mounted system. This marginal difference stems from the floating system's higher energy generation efficiency and reduced operational losses. However, a critical observation is that neither system achieved positive financial returns within a 20-year operational period, underscoring the financial challenges associated with standalone renewable energy projects. Without the support of subsidies, tax incentives, or other forms of financial assistance, the economic feasibility of both systems remains limited. This highlights the need for supportive policies and frameworks to encourage investment in renewable technologies. As shown in Table 1, the floating PV system outperformed its ground-mounted counterpart in all technical and environmental metrics, including specific yield, performance ratio, and CO₂ emission reduction. Yet, the lack of profitability within 20 years emphasizes that while these systems contribute significantly to environmental sustainability, financial viability must be addressed through external funding or market adjustments to achieve widespread adoption.

Table 1. Performance comparison of floating vs. ground-mounted systems

Parameter	Floating PV System	Ground-Mounted PV System
Installed Capacity (kWp)	154.8	154.8
Annual Energy Yield (kWh/year)	200467.0	190260.0
Specific Yield (kWh/kWp/year)	1294.87	1228.93
Performance Ratio (PR, %)	96.0	88.0
CO ₂ Emission Reduction (kg/year)	94209.0	89412.0
Electricity Cost (€/kWh)	1.03	1.09
Total Investment Cost (₺)	3771367.0	3771367.0

The cash flow analysis for both the floating and ground-mounted PV systems underscores the financial challenges faced by renewable energy projects in the absence of robust incentives. Over a 21-year operational period, neither system achieved a positive net cash flow, with the floating PV system incurring a total loss of -2,419,049.15 €, slightly better than the -2,465,071.37 € loss for the ground-mounted system. This marginal advantage for the floating system reflects its higher energy efficiency and performance metrics, which translate to slightly improved financial outcomes. The analysis reveals that the floating PV system delivered a yearly specific yield of 1,294.87 kWh/kWp, surpassing the ground-mounted system's 1,228.93 kWh/kWp. This higher yield resulted in increased revenue from feed-in tariffs during the first year, with the floating system generating 22,392.48 €/year compared to 21,252.30 €/year for the ground-mounted system. While this additional revenue highlights the floating system's technical advantages, it remains insufficient to offset the high installation and operational costs over the system's lifetime.

4. Conclusion

This study evaluated and compared the performance, environmental impact, and financial feasibility of Ground-Mounted and Floating PV Systems under identical climatic and operational conditions. The Floating PV System demonstrated superior technical performance, generating higher annual energy output (200,467 kWh/year) compared to the Ground-Mounted PV System (190,260 kWh/year). The enhanced cooling effect of water surfaces reduced operational losses, resulting in a higher Performance Ratio (96.0%) and Specific Yield (1,294.87 kWh/kWp) for the floating system. Additionally, the Floating PV System achieved greater environmental benefits, offsetting 94,209 kg of CO₂ emissions annually, significantly more than the 89,412 kg/year offset by the Ground-Mounted system. Despite these technical and environmental advantages, neither system achieved financial profitability within a 20-year period. Both required a substantial initial investment (3,771,367 ₺) and

faced negative net cash flows over 21 years. The marginally lower electricity cost of the Floating PV System (1.03 £/kWh) compared to the Ground-Mounted system (1.09 £/kWh) highlights its economic efficiency. However, the lack of financial viability emphasizes the need for supportive mechanisms such as subsidies, tax incentives, and higher feed-in tariffs to make these renewable energy projects more attractive to investors. Future research should focus on optimizing system configurations and reducing installation costs, particularly for floating PV systems. Studies on the long-term durability and maintenance of floating systems in diverse water conditions would also enhance their applicability. Additionally, exploring hybrid renewable energy solutions and integrating energy storage systems could improve financial returns and operational flexibility. Policymakers must address the economic challenges through targeted incentives to drive the adoption of renewable technologies at scale.

References

- [1] Allouhi, A., Rehman, S., Buker, M. S., & Said, Z. (2023). Recent technical approaches for improving energy efficiency and sustainability of PV and PV-T systems: A comprehensive review. *Sustainable Energy Technologies and Assessments*, 56, 103026. <https://doi.org/10.1016/j.seta.2023.103026>
- [2] Tawalbeh, M., Al-Othman, A., Kafiah, F., Abdelsalam, E., Almomani, F., & Alkasrawi, M. (2020). Environmental impacts of solar photovoltaic systems: A critical review of recent progress and future outlook. *Science of the Total Environment*, 759(143528), 143528. <https://doi.org/10.1016/j.scitotenv.2020.143528>
- [3] El Hammoumi, A., Chtita, S., Motahhir, S., & El Ghzizal, A. (2022). Solar PV energy: From material to use, and the most commonly used techniques to maximize the power output of PV systems: A focus on solar trackers and floating solar panels. *Energy Reports*, 8, 11992–12010. <https://doi.org/10.1016/j.egy.2022.09.054>
- [4] Toledo, C., & Scognamiglio, A. (2021). Agrivoltaic Systems Design and Assessment: A Critical Review, and a Descriptive Model towards a Sustainable Landscape Vision (Three-Dimensional Agrivoltaic Patterns). *Sustainability*, 13(12), 6871. <https://doi.org/10.3390/su13126871>
- [5] Chopdar R.K., N. Sengar, Giri, N. C., & Halliday, D. (2024). Comprehensive review on agrivoltaics with technical, environmental and societal insights. *Renewable and Sustainable Energy Reviews*, 197, 114416–114416. <https://doi.org/10.1016/j.rser.2024.114416>
- [6] Sekiyama, T., & Nagashima, A. (2019). Solar Sharing for Both Food and Clean Energy Production: Performance of Agrivoltaic Systems for Corn, A Typical Shade-Intolerant Crop. *Environments*, 6(6), 65. <https://doi.org/10.3390/environments6060065>
- [7] Essak, L., & Ghosh, A. (2022). Floating Photovoltaics: A Review. *Clean Technologies*, 4(3), 752–769. <https://doi.org/10.3390/cleantechnol4030046>
- [8] Garrod, A., Neda Hussain, S., Ghosh, A., Nahata, S., Wynne, C., & Paver, S. (2024). An assessment of floating photovoltaic systems and energy storage methods: A comprehensive review. *Results in Engineering*, 21, 101940. <https://doi.org/10.1016/j.rineng.2024.101940>
- [9] Cagle, A. E., Armstrong, A., Exley, G., Grodsky, S. M., Macknick, J., Sherwin, J., & Hernandez, R. R. (2020). The Land Sparing, Water Surface Use Efficiency, and Water Surface Transformation of Floating Photovoltaic Solar Energy Installations. *Sustainability*, 12(19), 8154. <https://doi.org/10.3390/su12198154>
- [10] Amer, A., Attar, H., As'ad, S., Alsaqoor, S., Çolak, İ., Alahmer, A., Alali, M., Borowski, G., Moayyad Hmada, & Ahmed. (2023). Floating Photovoltaics: Assessing the Potential, Advantages, and Challenges of Harnessing Solar Energy on Water Bodies. *Journal of Ecological Engineering*, 24(10), 324–339. <https://doi.org/10.12911/22998993/170917>
- [11] Pouran, H. M., Padilha Campos Lopes, M., Nogueira, T., Alves Castelo Branco, D., & Sheng, Y. (2022). Environmental and technical impacts of floating photovoltaic plants as an emerging clean energy technology. *IScience*, 25(11), 105253. <https://doi.org/10.1016/j.isci.2022.105253>
- [12] Majumder, A., Kumar, A., Innamorati, R., Mastino, C. C., Cappellini, G., Baccoli, R., & Gatto, G. (2023). Cooling Methods for Standard and Floating PV Panels. *Energies*, 16(24), 7939. <https://doi.org/10.3390/en16247939>
- [13] Micheli, L. (2022). The temperature of floating photovoltaics: Case studies, models and recent findings. *Solar Energy*, 242, 234–245. <https://doi.org/10.1016/j.solener.2022.06.039>
- [14] Da Silva, G. D. P., & Branco, D. A. C. (2018). Is floating photovoltaic better than conventional photovoltaic? Assessing environmental impacts. *Impact Assessment and Project Appraisal*, 36(5), 390–400. <https://doi.org/10.1080/14615517.2018.1477498>
- [15] Ramasamy, V., & Margolis, R. (2021). *Floating Photovoltaic System Cost Benchmark: Q1 2021 Installations on Artificial Water Bodies*. <https://doi.org/10.2172/1828287>
- [16] Micheli, L., & Talavera, D. L. (2023). Economic feasibility of floating photovoltaic power plants: Profitability and competitiveness. *Renewable Energy*, 211, 607–616. <https://doi.org/10.1016/j.renene.2023.05.011>
- [17] Kayhan, V. A., Ulker, F., & Elma, O. (2015). *Photovoltaic system design, feasibility and financial outcomes for different regions in Turkey*. <https://doi.org/10.1109/epecs.2015.7368518>



Blockchain and the Nuclear Supply Chain: The Tracking Technology of the Future

İrem Nur ECEMİŞ^{1,*} , Mehmet Serdar GÜZEL² , Fatih EKİNCİ³ 

¹ Faculty of Engineering, Department of Computer Engineering, Cankiri Karatekin University, Cankiri, Türkiye

² Faculty of Engineering, Department of Computer Engineering, Ankara University, Ankara, Türkiye

³ Institute of Nuclear Sciences, Department of Medical Physics, Ankara University, Ankara, Türkiye

Abstract

The transportation and tracking of nuclear materials has become one of the leading areas of study in recent years. Nuclear material transportation includes many important parameters, such as sustainability, security, and transparency. Many factors (temperature, time, etc.) are critical in the transportation and tracking of these materials. This study focuses on the use of blockchain technology in nuclear material transportation. The security of the processes can be increased by using blockchain technology in nuclear material supply processes. An example architecture is presented based on the results of the studies conducted in the literature. In addition, the benefits that blockchain can provide and its usability in nuclear material transportation are evaluated. The main purpose of this study is to present how efficient blockchain technology can be in nuclear material transportation. The study has shown that nuclear material transportation using blockchain technology can significantly contribute to transportation methods.

Keywords: Blockchain, Nuclear Material, Tracking, Supply Chain, Transportation

1. Introduction

With the development of technology, using blockchain-based systems provides convenience in many areas. One of these areas is procurement processes. Blockchain technology's transparency, immutability, and decentralized structure allow for coping with problems encountered while transporting nuclear materials. Blockchain technology is a ledger structure where transactions recorded in a computer network can be shared and accessed by all participants. Certain codes and digital signatures make the created system reliable [1,2]. The decentralization of blockchain offers a structure that users can control in real-time. Thanks to its decentralization feature, the need for a central authority is significantly eliminated. In this way, costs and possible problems (unauthorized access and disruptions in transactions) are reduced.

The use of blockchain technology in the procurement process of critical nuclear materials worldwide provides trust in the procurement process. Research has shown that it is crucial to use secure intermediaries to prevent misuse and environmental hazards in transporting nuclear materials that can be used for medical needs and the energy sector from one location to another. The purpose of tracking nuclear materials in the procurement process is to maintain accountability and to demonstrate that nuclear materials are being used for appropriate approved uses and are not subject to theft, terrorism, and dangerous misuse. Financial or regulatory systems, such as those involved in the trade of these materials, can include tracking materials, eliminating the need for a separate activity. A robust, complete chain of custody for nuclear materials can create a direct line from the facility to the operator, designated inspector, NM accountant, agency, and nonproliferation officer [3-6].

To protect against nuclear theft or weapons use of nuclear materials, countries track nuclear materials. Ensuring that the investment in comprehensive material protection is worthwhile makes effective tracking programs essential. A more effective tracking system than traditional methods will benefit the international community. Increased capacity is possible due to the wider use of digital databases, increased computing power, advanced mathematics, smarter statistical methods, and various new types of data analytics. Identifying and verifying these digital transactions is a high priority in contemporary digital currency and blockchain technology [7-9].

Nuclear material tracking does not occur in isolation. Bilateral, multilateral, and international agreements provide a range of national and international regulatory frameworks that support nuclear material tracking. National and international guidelines also serve as guidelines. International organizations and forums often play

* Corresponding author. e-mail address: iremnurecemis@karatekin.edu.tr

a role in creating these regulations and guidelines. These regulations and guidelines emphasize integrating security into facilities and activities and the industry's responsibility to provide effective security [10,11]. When the studies in the literature are examined, it is seen that no study has been done for nuclear material transportation with blockchain [12].

This study discusses the potential use of blockchain technology in nuclear material transportation and the existing security, privacy, legislation, and regulations in this field. In this context, a blockchain architectural structure planned to be created is explained in general terms and the potential results are discussed.

2. Materials and Methods

Blockchain technology is a database technology with a decentralized structure. This technology contains blocks of data that are linked together with data structures called blocks and recorded reliably. Blocks are linked with cryptographic methods and made unchangeable, thus ensuring security. Nuclear material transportation is gaining increasing importance all over the world. Many countries depend on nuclear material transportation to meet their needs for nuclear material. Therefore, a secure and traceable transportation process is of great importance. Blockchain technology offers a logical solution to meet these needs. Blockchain makes sharing and updating documents in real-time during the material transportation process possible. This feature increases the traceability of nuclear material transportation and provides transparency. In addition, data in all logistics processes used in nuclear material transportation can be managed automatically with smart contracts on the blockchain. This increases the accuracy and security of transactions. With Blockchain, supply chain processes can be managed more efficiently, and dispute resolution among all stakeholders can be accelerated. In addition, thanks to Blockchain technology, storing and sharing data securely will be possible. This will prevent potential threats. Considering all these factors, it can be said that blockchain technology has an important place in nuclear material transportation processes. The transportation of nuclear materials is subject to strict regulations around the world. The International Atomic Energy Agency (IAEA) is a leading authority that sets nuclear safety and security standards.

Within the scope of this study, an architecture that can be developed using blockchain technology is presented. As a first step, nuclear materials are blocked with an RF coding system that will provide accuracy and reliability in international transportation. In this process, the authorization process and material certification will be carried out for users. In addition, continuous traceability of the nuclear material will be provided with an added time stamp. Afterward, material tracking codes will be assigned, and security tests such as radiation leakage tests will be performed. Then, the nuclear material will be safely entered into the supply process with the triple signature process. Unauthorized access will be restricted in this process. After the triple signature, international standard transportation protocols will be implemented. Transportation methods will be selected, and the licenses of the carrier companies will be checked. In order to ensure continuous monitoring with GPS during the transportation process, a GPS installation will be provided with a triple signature system, and it will be possible to see where the materials are at any time during the transportation process. In this process, GPS information during the transportation process will be continuously recorded on the blockchain and shipment will begin during this process.

Periodic security checks will be carried out during transportation, and everything in this process will be recorded on the blockchain. When the transported nuclear materials reach their final destination, they will be approved and accepted with a triple signature. Then, the delivery point information will be added to the blockchain. In this process, documents indicating that nuclear materials are received with triple signature and that leakage tests are performed afterward will be added to the blockchain. After using nuclear materials, nuclear materials with a half-life will be sent to the storage area, and this process will be recorded in the blockchain. Nuclear materials with expired life will be defined as waste and transported to storage. In this process, the carrier company will be selected, and their licenses will be checked. Waste materials will be brought to the storage area and blocked for storage here. Approval will be given with the triple signature system, and the waste monitoring counter will be started. The nuclear waste monitoring counter will be continuously monitored to prevent possible dangers. A general representation of this structure is shown in Figure 1.

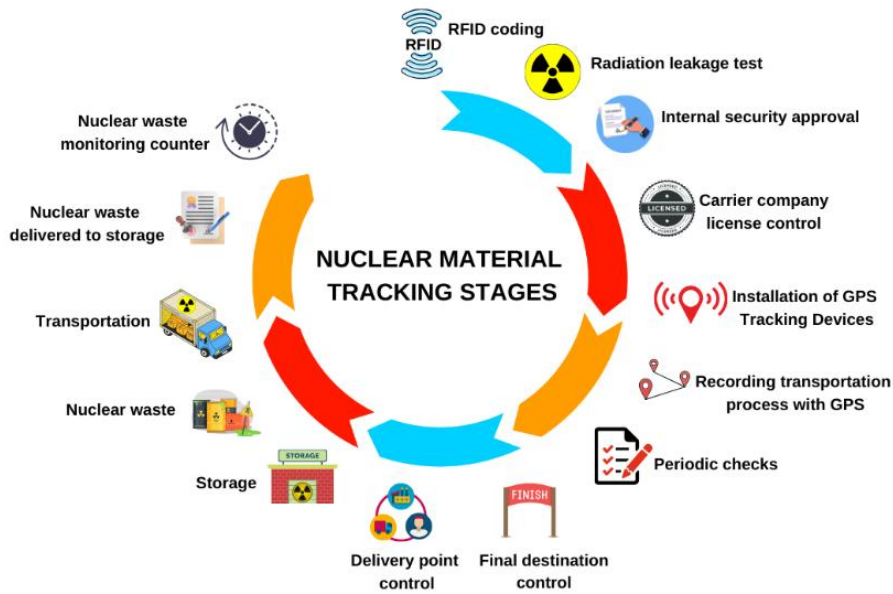


Figure 1. Nuclear material tracking stages.

Blockchain technology can prevent manipulation or incorrect information entry by recording the transactions made by carriers, controllers, suppliers, and other stakeholders while transporting nuclear materials in a decentralized database. In this way, transparent communication is provided between all stakeholders by recording the events and transactions at every stage of the transportation process. Blockchain technology also has the potential to provide automation of the transportation process through smart contracts. Blockchain technology can further increase the safety and inspection standards in the nuclear sector and provide operational excellence at every stage of the transportation process. Therefore, blockchain technology has great potential in nuclear material transportation.

3. Results and Discussion

Using traditional methods in nuclear material transportation, especially manual data recording and control processes can cause errors and delays in process processes. This situation can pose a risk regarding the security and transparency of transportation processes. With blockchain technology, data recording and monitoring processes become automatic, while a reliable infrastructure is created thanks to the immutability of data. Keeping data records in a distributed manner in blockchain-based systems increases data integrity and data security. A secure transportation process is provided thanks to the distributed structure. In this presented study, a blockchain architecture for the transportation of nuclear materials is presented. The architecture is explained in general terms. It is envisaged to create a highly secure supply chain internationally with the creation of this architecture.

Blockchain technology offers many advantages and reduces risks in nuclear material transportation. These advantages improve security, reliability, efficiency, and cost. Thanks to blockchain technology, every stage of nuclear material transportation becomes traceable. Thus, the risk of loss or damage to the material is greatly reduced. In addition, thanks to blockchain technology, unique digital codes are added to all nuclear materials transported, enabling the verification of the materials. The system automatically warns if any changes or problems are detected during transportation. Necessary precautions are taken with this warning. Another advantage of blockchain technology is the confidentiality of data. The information obtained during the material transportation process is encrypted in the blockchain network and stored in a distributed structure. In this way, the risk of data falling into the hands of unauthorized persons is greatly reduced. All participants can see the entire network and have the opportunity to verify changes in the records. With the blockchain network, the authorizations and access rights of the participants can be managed automatically. In this way, only authorized persons are included in the nuclear material transportation process, preventing unauthorized access.

In addition to the many advantages of blockchain technology in nuclear material transportation, there are also potential risks, such as hacking of blockchain platforms. In addition, technical difficulties (complexity of the blockchain network, scalability problems, and technical issues such as energy consumption, etc.) may also be encountered. For this reason, the advantages and risks of blockchain technology in nuclear material transportation should be meticulously evaluated. Appropriate precautions should be taken when necessary. Important elements such as security protocols, data encryption methods, and authorization processes should be considered while this process continues.

As a result, blockchain technology in nuclear material transportation offers significant advantages despite some disadvantages. Although many control points exist in the presented architecture, a blockchain network must always be created carefully and comprehensively. In addition, international cooperation is important in transporting nuclear materials between countries. All these factors should be considered, and the necessary steps should be taken. It can be concluded that blockchain technology has great potential to provide a safe, effective, and better future in nuclear material transportation.

4. Conclusion

There are many benefits provided by the use of blockchain technology in nuclear material transportation. Transparency and decentralization in blockchain structure significantly contribute to the efficiency of supply processes. Thanks to the blockchain structure, the risks of data manipulation or unauthorized access by employees in the supply process can be reduced. Real-time monitoring increases traceability throughout the supply chain. In this way, it creates trust at national and international levels. It is thought that a quality supply chain can be created by implementing the presented blockchain architecture. The potential of this technology offers a great advantage for making transportation processes more secure, transparent, and traceable. The scope of future studies aims to test these potential applications with real-world scenarios, review legislation and regulations, and increase blockchain-based collaborations among stakeholders in the nuclear industry. A continuation of this study aims to explain the architecture mentioned in detail and present the results by testing them in virtual environments. The results obtained can be used to strengthen the energy and health industries and increase nuclear safety. This study does not only prove the usability of blockchain on nuclear materials. It also sets a precedent for transporting many materials that are high in value and have difficult transportation processes. Blockchain is expected to be used more widely in the future as it is adopted in supply chains. In this way, increasing the use of blockchain will increase the industry's efficiency, security, and traceability. However, more research and development studies are needed in security, data integrity, and collaboration for future use. More research and development in this area can make a big difference in increasing the efficiency and safety of nuclear material transportation.

References

- [1] Poongodi, T., Sujatha, R., Sumathi, D., Suresh, P., & Balamurugan, B. (2020). Blockchain in social networking. *Cryptocurrencies and Blockchain Technology Applications*, 55-76.
- [2] Dong, S., Abbas, K., Li, M., & Kamruzzaman, J. (2023). Blockchain technology and application: An overview. *PeerJ Computer Science*.
- [3] Morgan, D., Pilania, G., Couet, A., Uberuaga, B. P., Sun, C., & Li, J. (2022). Machine learning in nuclear materials research. *Current Opinion in Solid State and Materials Science*, 26(2).
- [4] Marques, L., Vale, A., & Vaz, P. (2021). State-of-the-Art Mobile Radiation Detection Systems for Different Scenarios. *Sensors*, 21(4), 1051.
- [5] Hensley, C., Sisco, K., Beauchamp, S., Godfrey, A., Rezayat, H., McFalls, T., ... & Babu, S. S. (2021). Qualification pathways for additively manufactured components for nuclear applications. *Journal of Nuclear Materials*, 548.
- [6] Khan, A. U. R., & Ahmad, R. W. (2022). A blockchain-based IoT-enabled e-waste tracking and tracing system for smart cities. *IEEE Access*, 10, 86256–86269.
- [7] Ghimire, L. & Waller, E. (2022). The Role of Nuclear Forensics for Determining the Origin of Nuclear Materials Out of Regulatory Control and Nuclear Security. *International Journal of Nuclear Security*.
- [8] Zorkany, M., & Morsi, H. F. (2022). Safety of Radioactive Materials Transportation and Storing Assisted by Internet of Things. *Journal of Nuclear Engineering and Radiation Science*, 8(3), 031901.

- [9] Zubair, M., Radkiany, R., Akram, Y., & Ahmed, E. (2024). Nuclear safeguards: technology, challenges, and future perspectives. *Alexandria Engineering Journal*. 108, 188-205.
- [10] Sneve, M. K., Shandala, N., & Worthington, P. (2020, October). Regulatory framework of decommissioning, legacy sites and wastes from recognition to resolution: building optimization into the process. In Report of an international workshop, Tromsø.
- [11] Goodwin, M. A., Chester, D. L., Britton, R., Davies, A. V., & Border, J. (2022). Analysis of radionuclide detection events on the International Monitoring System. *Journal of Environmental Radioactivity*, 242, 106789.
- [12] Ecemis, I. N., Ekinici, F., Acici, K., Guzel, M. S., Medeni, I. T., & Asuroglu, T. (2024). Exploring Blockchain for Nuclear Material Tracking: A Scoping Review and Innovative Model Proposal. *Energies*, 17(12), 3028.



Biocomposites as Alternatives to Synthetic Fiber Composites: Types, Production Methods, and Mechanical Properties

Sakine KIRATLI ^{1,*} , Emin YUSIFOV ¹

¹ Engineering Faculty, Mechanical Engineering Department, Çankırı Karatekin University, Çankırı, Türkiye

Abstract

Global issues such as the depletion of resource reserves, environmental pollution, and economic concerns have shifted the focus of research across various disciplines. The concepts of recycling and sustainability have become ubiquitous across all sectors, leading to significant advancements in various economic aspects. In recent years, advances in nanotechnology and composite materials have led to major developments in the material sector. Composite materials have replaced metals to a certain extent in our daily lives. However, the desire for a cleaner world has spurred the idea of replacing the synthetic products used in these materials with natural ones. In recent years, researchers have examined natural fibers or polymers and investigated their usability. Researchers widely examine biocomposites based on their fiber matrix content, production methods, and application areas. This review presents an overview of existing natural fibers, categorization of biocomposites, mechanical properties, and production methods.

Keywords: Biofiber, Biopolymer, Recycling, Sustainability

1. Introduction

A composite material is a novel substance that possesses unique properties, combining two or more physically distinct phases that bear no resemblance to each other [1]. The matrix is one of the phases, while the reinforcement material, known as the fiber, serves to fortify it. The purpose of the matrix is to hold the fibers together and transfer the applied load to the fibers. It is also to protect the fibers from environmental and mechanical damage [2].

Due to concerns about recycling, the environment, and the economy, many sectors that previously favored composite materials over metals are now focusing on biocomposites. Biocomposites are materials consisting of biodegradable polymers (matrix) and biodegradable reinforcements. Biodegradable materials are substances that can be degraded by living organisms [3]. The fillers used in biocomposites are usually biofibers. Biocomposites made from natural biofibers are renewable, lightweight, biodegradable, and environmentally friendly. Biocomposites produced from renewable resources have gained universal importance due to their biodegradable nature. Although matrices provided from completely recyclable sources are preferred in obtaining biocomposites, biochemical technology is also in the works that enable the usability of synthetic thermoplastic and thermoset materials. For example, polyethylene and polypropylene are polymers used in commercial biocomposite production [4].

Biocomposites made from natural biofibers are composites with very wide application areas in biomedical, agricultural, packaging, and other related engineering fields [5]. For example, important industrial applications of PLA matrix biocomposites include the automobile industry, textile products, and foam materials [6]. As environmentally friendly materials, they have been extensively researched for use in various fields. Natural polymers and biofibers cannot be used as much as they should because they do not work well with the hydrophobic polymer matrix, get too hot, or can catch fire [6]. Solution proposals and studies to eliminate these negativities are ongoing.

2. Classification of Biocomposites

Biocomposites are generally classified according to matrix and reinforcement elements. Classification according to reinforcement is examined as short fiber, continuous fiber, and particulate composites. In the classification according to matrix, agropolymer and biopolyester matrix composites are examined. In addition, biocomposites are evaluated according to whether the matrix is petroleum-based plastic or bioplastic, with biofiber as the basis. When biofiber and bioplastic are used, they are called green composites.

* Corresponding author. e-mail address: skiratli@karatekin.edu.tr

2.1 Classification by matrix element

Agropolymer matrix biocomposites are an important class of biocomposites. They are obtained from biomass products. They mainly focus on starchy materials. The biggest disadvantage of starch is its sensitivity to water and its poor mechanical properties. This situation can be overcome by reinforcing the starch with natural fibers and coating both sides of the produced foam material with a biodegradable, low-hydrophilic polyester film such as polycaprolactone [7].

Biotechnological methods (e.g., PLA), microorganisms (e.g., PHB), and petroleum products (e.g., PCL) provide biomatrices for biopolyester matrix biocomposites. Polymerization of lactic acid monomers, produced by fermentation from natural sources, yields PLA, a biodegradable polymer. Microorganisms produce PHA as a carbon and energy reserve. Polyhydroxybutyrate (PHB), which is in this group, contains 3-hydroxybutyric acid amphoteric units. Caprolactone polymerization yields PCL, a petroleum-based biopolymer [8].

2.2 Classification by fiber element

Various methods (such as weaving, knitting, ribboning, felting, twisting, and netting) can draw fiber into yarn or transform it into fabric and other products. For thousands of years, the production of synthetic fibers limited the use of fiber to natural fibers like silk, wool, linen, and cotton.

Plant fibers contain millions of microfibrils arranged in lamellae within the cell walls. There are basically three types of cell wall polymers: cellulose, lignin, and polysaccharides (pectin and hemicellulose).

Biofibers are being investigated as cellulose (bast, leaf, and seed) and protein-based fibers (silk, wool).

2.2.1 Cellulose-based fibers

Bast fibers are formed in the bark or bark tube of some plants. The textile industry, which produces rope, string, paper, and sacking, heavily utilizes bast fibers. This group includes jute, flax, hemp, kenaf, and ramie fibers. Jute fiber is the cheapest and weakest natural fiber. Jute fibers are generally used in home textiles, some technical materials, sugar and coffee bags, carpet underlay, rope, twine, and rope production. Flax fiber is the oldest textile fiber. It is soluble in strong acids, resistant to alkalis, organic solvents, and high temperatures. Areas of use include various garments, technical products (such as luggage, bags, wallets, sewing thread), beds, tables, bathroom items, and linen fabrics with different textures. Hemp fiber bears a resemblance to linen, albeit with a coarser and tighter texture and greater strength. Kenaf fiber is shorter and coarser than jute fiber. It has many areas of use, such as textiles, paper products, composites, building materials, and absorbents. Ramie fiber is rigid and prone to breakage. Ramie's traditional uses are in heavy-duty products such as canvas or tent cloth, packaging materials, and upholstery fabrics [9].

Leaf fibers are hard and have a tighter, coarser structure than bast fibers, so their commercial value is limited. Typical examples are sisal, abaca, and henequen fibers. Sisal fiber is coarse and strong, has a high elongation under tension, but is less flexible than abaca fiber. Also, this fiber is resistant to salt water. Marine applications use abaca fibers as rope and cable materials due to their exceptional resistance to water, especially salt water. They are a preferred material in tea bags due to their water resistance, cleanliness, and easy extraction. Other uses include rope, mats, felt, tablecloths, and various garments. Henequen fiber is from the agave family of plants, very similar to sisal [10].

Seed fibers are called coir, cotton, and kapok fibers. Coir fibers are long, hard, and strong, but their softening and water absorption capacities are poor. Cotton fiber is a widely used natural fiber. Cotton is hydrophilic, its fibers swell significantly in water. Cotton is flexible, highly absorbent, and resistant to alkalis. Generally, people use kapok fiber as a fiber filling and insulation material. It is eight times lighter than cotton, non-allergenic and non-toxic, and resistant to odor and rot [11].

2.2.2 Protein-based fibers

Fibrous proteins are a class of proteins that are fibrous, strong, threadlike, and generally insoluble in water. Important protein fibers are silk, wool, fur, and some special hair fibers. Generally, alkalis, dry heat, and chlorine bleach degrade them, causing them to burn easily. Silk is the strongest natural fiber, it is light and has moderate abrasion resistance. Spider silk is elastic and the strongest known natural fiber. Sheep naturally produce wool, a hair-like protein fiber. Wool has moderate abrasion resistance, excellent flexibility, dimensional stability, and poor electrical conductivity [12].

3. Mechanical Properties of Biocomposites

Mechanical properties generally vary with the type of resin, its origin, the type, orientation, amount, and form of fiber, mixing, and the plasticizer used.

Tensile Strength-Tensile Modulus: Biopolymer matrix composites reinforced with biofibers exhibit significantly improved tensile properties. The tensile strength of fully biodegradable composites varies between 20 and 73 MPa. The hemp-reinforced PLA biopolymer composite (PLAHF: 73 MPa) exhibits the highest tensile strength, while the flax-reinforced polycaprolactone composite (PLCFF: 20-25 MPa) displays the lowest. The highest tensile modulus is 20 GPa for PLA/Sisal (PLASF) and the lowest for PCL/Flax (PLCFF) (0.8-0.9 GPa) [13].

Flexural Strength-Flexural Modulus: Flexural strength varies depending on the biofiber, biopolymer, and fabrication techniques in the biodegradable composite. The highest flexural strength belongs to hemp-reinforced PLA (PLAHF: 102 ± 2 MPa), while the lowest value belongs to flax-reinforced PCL (PLCFF: 30-35 MPa) biocomposites. The highest and lowest flexural modulus values are for sisal fiber-reinforced PLA (PLASF: 19 GPa) and flax fiber-reinforced PCL (PLCFF: 1.8-1.9 GPa), respectively [14].

Percentage Elongation-Impact Force: According to the tensile tests of sample biodegradable composites, the highest and lowest elongation values were determined as PLA/Jute (PLAJF: 1.5-4.71%) and PLA/Flax (PLAFF: 1.0%). In the impact tests showing the durability of the material, the biocomposites with the highest and lowest values were PLA/Jute (PLAJF: 15-80 kJ/m²) and PLA/Sisal (PLASF: 3-3.5 kJ/m²) [15].

4. Manufacturing of Biocomposites

Natural fibers have similar behaviors to fiberglass. Natural fibers require preparation for processing before use and necessary surface modifications to achieve these properties. This ensures good adhesion between the matrix and the fiber, achieves the appropriate degree of polymerization, and yields homogeneous physical properties [16].

The manufacturing techniques for biocomposites are mostly based on manufacturing processes for plastics or composites, such as press molding, hand lay-up, filament winding, pultrusion, extrusion, injection molding, compression molding, resin transfer molding, and sheet molding [17].

The compounding stage plays a crucial role in the production of biocomposites through various processes. The purpose of compounding is to prepare materials (such as pellets) with suitable properties for subsequent injection, molding, extrusion, or other processes. In compounding, polymers, fillers, fibers, and additives are generally mixed, a good dispersion is provided, and the aim is to obtain granules in suitable form and with processable properties [17].

5. Conclusion And Future Trends

Researchers are extensively studying composite materials, which have important application areas such as automotive, marine, and aviation. Numerous factors, including nanoscale developments, global innovations, economic challenges, and environmental factors, are driving these studies. Natural products are evaluated with the factors of being abundant in resources, clean, and recyclable. Researchers are exploring biofiber-reinforced composites in a variety of ways within this context. Researchers aim to tackle the challenges of obtaining and preparing biofibers for use, eliminating matrix and biofiber incompatibility, enhancing interface adhesion, and ultimately boosting strength. In the future, it is expected that these composites will reach the strength values of synthetic fiber-reinforced composites such as glass, carbon, and aramid and will find a very wide application area in all sectors.

References

- [1] Mortensen, A. (Ed.). (2006). Concise Encyclopedia of Composite Materials. Elsevier.
- [2] Rajak, D.K., Pagar, D.D., Menezes, P.L., & Linul, E. (2019). Fiber-reinforced polymer composites: Manufacturing, properties, and applications. *Polymers*, 11(10), 1667.
- [3] Karthika, M., Shaji, N., Johnson, A., Neelakandan, M.S., A. Gopakumar, D., & Thomas, S. (2019). Biodegradation of green polymeric composites materials. *Bio Monomers for Green Polymeric Composite Materials*, 141-159.

- [4] Manu, T., Nazmi, A.R., Shahri, B., Emerson, N., & Huber, T. (2022). Biocomposites: A review of materials and perception. *Materials Today Communications*, 31, 103308.
- [5] Akter, M., Uddin, M.H., & Tania, I.S. (2022). Biocomposites based on natural fibers and polymers: A review on properties and potential applications. *Journal of Reinforced Plastics and Composites*, 41(17-18), 705-742.
- [6] Akampumuza, O., Wambua, P.M., Ahmed, A., Li, W., & Qin, X.H. (2017). Review of the applications of biocomposites in the automotive industry. *Polymer Composites*, 38(11), 2553-2569.
- [7] Bhat, A.H., Dasan, Y.K., Khan, I., & Jawaaid, M. (2017). Cellulosic biocomposites: Potential materials for future. *Green Biocomposites: Design and Applications*, 69-100.
- [8] Shanks, R.A., Hodzic, A., & Wong, S. (2004). Thermoplastic biopolyester natural fiber composites. *Journal of Applied Polymer Science*, 91(4), 2114-2121.
- [9] Eyupoglu, S. (2020). Sustainable plant-based natural fibers. *Sustainability in the Textile and Apparel Industries: Sourcing Natural Raw Materials*, 27-48.
- [10] Thomas, S., Paul, S.A., Pothan, L.A., & Deepa, B. (2011). Natural fibres: Structure, properties and applications. *Cellulose Fibers: Bio-and Nano-Polymer Composites: Green Chemistry and Technology*, 3-42.
- [11] Lee, J.A. (2019). Plant fibers. In *CRC Handbook of Plant Science in Agriculture* (pp. 173-182). CRC press.
- [12] Boy, R., Narayanan, G., & Kotek, R. (2018). Formation of cellulose and protein blend biofibers. *Polysaccharide-Based Fibers and Composites: Chemical and Engineering Fundamentals and Industrial Applications*, 77-117.
- [13] Li, X., Chu, C.L., Liu, L., Liu, X.K., Bai, J., Guo, C., ... & Chu, P.K. (2015). Biodegradable poly-lactic acid based-composite reinforced unidirectionally with high-strength magnesium alloy wires. *Biomaterials*, 49, 135-144.
- [14] Chaitanya, S., Singh, I., & Song, J.I. (2019). Recyclability analysis of PLA/Sisal fiber biocomposites. *Composites Part B: Engineering*, 173, 106895.
- [15] Gunti, R., Ratna Prasad, A.V., & Gupta, A.V.S.S.K.S. (2018). Mechanical and degradation properties of natural fiber-reinforced PLA composites: Jute, sisal, and elephant grass. *Polymer Composites*, 39(4), 1125-1136.
- [16] Gholampour, A., & Ozbakkaloglu, T. (2020). A review of natural fiber composites: Properties, modification and processing techniques, characterization, applications. *Journal of Materials Science*, 55(3), 829-892.
- [17] Hasan, K.F., Horváth, P.G., Zsolt, K., & Alpár, T. (2021). Design and fabrication technology in biocomposite manufacturing. In *Value-Added Biocomposites* (pp. 157-188). CRC Press.



Hydrogen Production from Natural Gas

Riyadh Salah Hasan Hasan^{1*} , ***Zehra Gülten Yalçın¹*** , ***Mustafa Dağ¹*** 

¹ Institute of Graduate Studies, Department of Chemical Engineering, Çankırı, Turkey

Abstract

This research paper explores the history of gas production in Iraq, tracing its origins back to 1927. Gas production in the country is categorized into two types: associated gas and free gas. The study highlights the significance of the global transition from fossil fuels to renewable energy, emphasizing its critical role in environmental improvement. Hydrogen production is identified as a key component of this transition, with a focus on its generation from natural gas through steam-methane reforming at elevated temperatures. Furthermore, the paper examines the vital applications of hydrogen in the transportation sector and its broader environmental implications.

Keywords: Hydrogen, Natural gas, Carbon, Associated gas

1. Introduction

Iraq began natural gas production alongside oil extraction in 1927, starting with the flow of oil from the Baba Karkare field in Kirkuk and the associated natural gas in Iraq [1]. The country's natural gas sources are primarily classified into two categories: associated gas and free gas. Associated gas, which is extracted as a byproduct of oil production, accounts for 70% of Iraq's natural gas reserves. Its utilization is cost-effective as it requires no exploration, drilling, or extraction operations, given that it naturally accompanies the extracted oil. The main infrastructure needed for its exploitation involves extending pipelines and facilitating marketing efforts. In contrast, free gas constitutes 30% of Iraq's natural gas reserves and demands significantly higher investment due to the extensive processes required for exploration, drilling, and extraction operations [2]. The associated gas extracted from the Kirkuk oil fields is processed and purified by the North Gas Company. The company's primary objective is to process raw associated gas (ASSOCIATED GAS) to produce the following main products:

- 1- Sales gas
- 2- Liquefied Petroleum Gas (LPG)
- 3- Natural gasoline
- 4- Sulfur

Through a series of productivity operations, crude natural gas extracted from wells in Kirkuk is purified. Over the next 30-40 years, natural gas demand is expected to grow rapidly, driven by emerging economies such as China and India. This surge in demand, coupled with the anticipated rise in oil prices, current and projected oil dependency, and emissions of carbon dioxide (CO₂) from fossil fuels, underscores the importance of transitioning to alternative energy sources. The restrictions imposed by the Kyoto Protocol on emissions make hydrogen a viable and potentially limitless alternative energy source. However, the current challenge lies in its production costs and infrastructure development. Government support policies and private sector initiatives are expected to play a pivotal role in transforming the energy sector from an oil-dependent framework to one based on renewable energies, with hydrogen at the forefront. In the short to medium term, hydrogen demand will primarily be met by fossil fuels, particularly natural gas. This method is both environmentally and economically acceptable, as it allows hydrogen production at a reasonable cost without releasing CO₂ into the atmosphere.

To achieve this, two main options are available:

Steam Methane Reforming (SMR): A conventional method for producing hydrogen from natural gas, where CO₂ emissions are captured and stored in geological formations such as depleted oil and gas reservoirs or ocean floors.

* Corresponding author. e-mail address: riyadalshmary@gmail.com

Thermal Decomposition of Natural Gas: Producing hydrogen and pure carbon at high temperatures, this method allows carbon to be utilized in applications such as building materials, electricity generation, and soil improvement.

This study compares traditional steam methane reforming and catalytic thermal decomposition of natural gas from technological, environmental, and economic perspectives. Globally, approximately 50 million tons of hydrogen (H_2) are produced annually, with the majority used in industrial applications. Of this, 62.4% is consumed for ammonia (NH_3) production, 24.3% for refining, and 8.7% for methanol (CH_3OH) production [3]. Although hydrogen is increasingly considered for energy and heat production, natural gas steam reforming remains the dominant method, accounting for approximately 50% of global hydrogen production [4].

Despite its potential, the primary obstacle to hydrogen adoption is the carbon dioxide emissions associated with its production. Leading scientists highlight various global environmental, health, and societal issues such as climate change (greenhouse effect), air pollution, oxygen depletion, acid rain, ozone depletion, oil spills, and population growth. Among these, climate change remains a critical concern, with CO_2 emissions being a major contributor. Strategies to reduce CO_2 emissions include [5]:

- 1- Restricting population growth
- 2- Improving energy conversion and utilization efficiency
- 3- Transitioning to renewable energy sources such as solar, wind, hydro, and geothermal
- 4- Decarbonizing fossil fuels and producing hydrogen
- 5- Capturing and storing carbon from fossil fuels

Below is a histogram illustrating the distribution of hydrogen use by application, based on the data provided (Figure 1). The percentages for ammonia production, refining, methanol production, and other applications are shown.

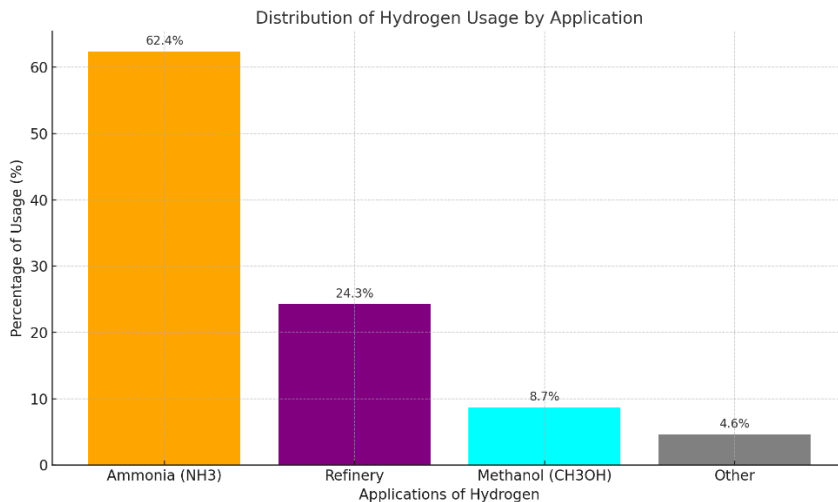


Figure 1. The distribution of hydrogen [4]

2. Materials and Methods

This section reviews the two fundamental principles for producing hydrogen from natural gas while capturing carbon dioxide:

- 1- Production of Hydrogen via Steam-Methane Reforming (SMR): Hydrogen is produced by reforming methane vapor, with the concurrent release of carbon dioxide.
- 2- Thermal Decomposition of Natural Gas: Natural gas is thermally decomposed into hydrogen and carbon, with the byproducts analyzed for potential applications.

The conservation of elemental carbon through separation processes is investigated from an environmental perspective. Additionally, the study outlines the potential applications of both hydrogen and carbon products generated during these processes. The proposed hydrogen and carbon infrastructure aims to provide

environmentally friendly solutions for hydrogen production, particularly those derived from natural gas, which currently dominate global production.

2.1. Hydrogen Production via Steam-Methane Reforming (SMR)

Steam-methane reforming consists of three main stages: reforming, the water-gas shift reaction, and gas purification [6]. Natural gas in the feedstock is first desulfurized, as illustrated in Figure 2, to prevent catalyst contamination. During this step, a small portion of recycled hydrogen is utilized to facilitate the process.

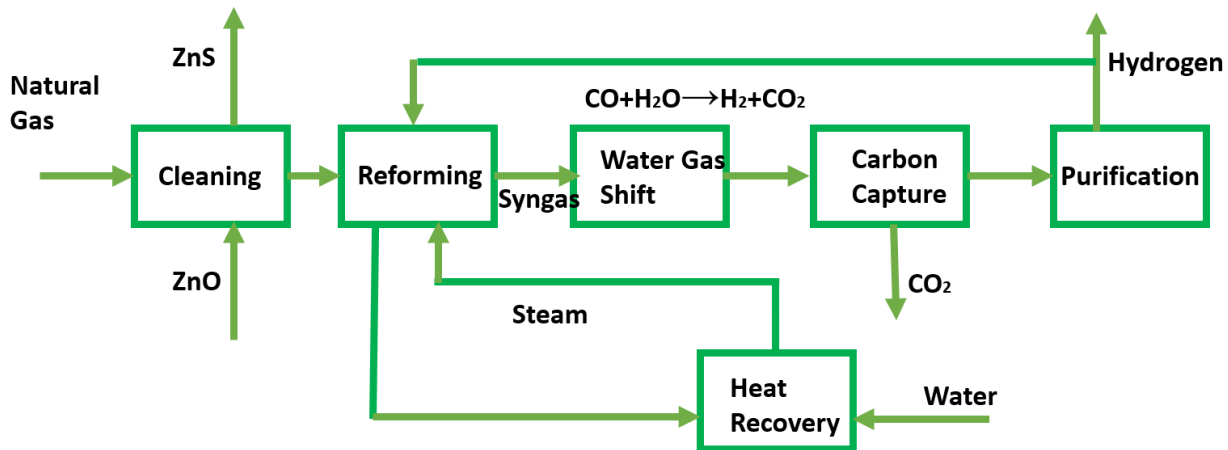


Figure 2. Block flow diagram of a hydrogen production plant with steam-methane reformation [7]

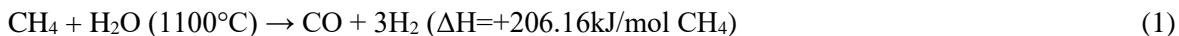
Hydrogen Production Process

After preliminary treatment, hydrogen sulfide (H_2S) is extracted using zinc oxide (ZnO) deposits. Following this step, natural gas is sent to the steam reformer under a pressure of 2.6 MPa. The processed gas is then transferred to high-temperature and low-temperature conversion reactors, where the water-gas shift reaction converts approximately 92% of the carbon monoxide (CO) into hydrogen. The resulting hydrogen is subsequently purified using a pressure swing adsorption (PSA) unit.

The PSA system primarily recovers hydrogen, but a portion of the natural gas is utilized to supply the steam reformer's fuel requirements. PSA exhaust gases typically comprise CO_2 (55 mol%), H_2 (27 mol%), CH_4 (14 mol%), CO (3 mol%), N_2 (0.4 mol%), and trace amounts of water vapor. The overall efficiency of the steam-methane reforming system typically ranges between 65% and 75%.

Steam-Methane Reforming Reaction

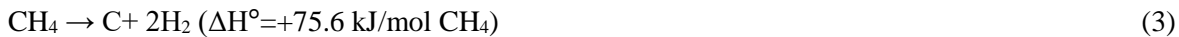
Steam-methane reforming is one of the most widely used industrial methods for hydrogen production. The inputs and efficiency of the process depend heavily on local factors such as raw material availability. The two primary steps involved are steam reforming and the water-gas shift reaction:



The water-gas shift reaction is an exothermic, heterogeneous catalytic process that serves as a crucial step in hydrogen and ammonia production. It is also employed for reducing atmospheric carbon monoxide. Depending on thermodynamic and kinetic conditions, the reaction can occur at high temperatures (320–450°C), typically using iron-based catalysts, or at low temperatures (200–250°C), where copper-based catalysts are preferred. The heat generated during the cooling of hot gases from the steam-methane reforming process is used to evaporate water. Additional hydrogen and carbon dioxide are produced when water vapor reacts with carbon monoxide. Only 50% of the hydrogen produced originates from hydrocarbons, while the remaining 50% is derived from water. The efficiency of the process is influenced by the careful management of thermodynamics and catalytic activity at various stages.

2.2. Thermocatalytic Separation of Metal

In this approach, methane is thermally decomposed into carbon and hydrogen at high temperatures (850–1200°C) in the presence of a catalyst. The reaction is represented as follows:



Since the reaction is endothermic, approximately 10% of the natural gas supply is utilized to meet the energy input requirements. The primary product of this process is hydrogen, while carbon is produced as a byproduct. Due to its granular structure, carbon is easily separable from hydrogen. Although this method holds great promise for large-scale hydrogen production, it is still under development, particularly in terms of improving conversion efficiency and optimizing process conditions.

2.3. Thermal Energy

Thermal energy is generated in a combustion chamber using a catalytic burner and a hydrogen/oxygen steam generator (in Figure 3). Similar to other end-use applications, hydrogen combustion produces minimal or no pollution, even during heat release. While the combustion of hydrogen at high temperatures may produce small amounts of nitrogen oxides (NO_x) due to thermal effects, recent tests have demonstrated that nitrogen oxide concentrations can be maintained at very low levels with proper combustion techniques. This makes hydrogen an environmentally friendly alternative for thermal energy production.

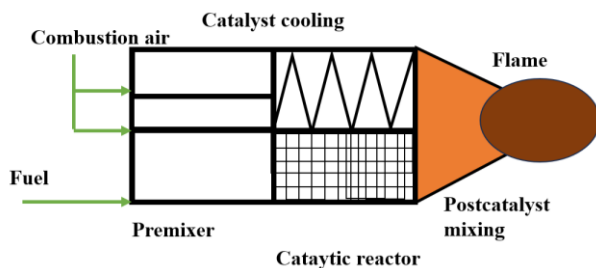


Figure 3. Catalytic combustion of hydrogen for heat production [8]

2.4. Hydrogen-Carbon Infrastructure System

This study proposes a hydrogen-carbon infrastructure system designed to optimize energy, environmental impact, and resource efficiency while emphasizing the economic interplay of its utilization. The system is based on natural gas (methane) for two key reasons:

1. Distribution network for natural gas
2. Current reserves of natural gas, which offer a longer supply lifespan compared to oil.

The proposed hydrogen-carbon infrastructure system leverages the thermal decomposition of natural gas, converting it into high-purity hydrogen (99.99% by volume) and carbon.

The applications of these products are diverse:

Hydrogen can be utilized in transportation, electricity generation, and heat production.

Carbon has four potential applications:

1. Building materials
2. Carbon-based fuel for electricity generation using batteries, with minimal CO_2 emissions
3. Soil reclamation
4. Carbon black production

This system represents a sustainable approach to harnessing natural gas as a transitional energy source while minimizing environmental impact and maximizing resource efficiency.

3. The Use of Hydrogen

Hydrogen fuel cell vehicles, which are three times more efficient than internal combustion engine vehicles, are becoming a viable alternative for transportation. Currently, five types of fuel cells are under development, with proton exchange membrane (PEM) fuel cells being the most suitable for transportation applications. Other fuel cell types include phosphoric acid, alkaline, molten carbonate, and solid oxide fuel cells.

Additionally, hydrogen gas can be utilized in vehicles equipped with internal combustion engines. Hydrogen-powered vehicles have several advantages, including a wide flammability range (4% to 75%), allowing for the use of broader air/fuel mixtures without ignition complications. Hydrogen engines operate at a 38% efficiency, which is approximately 20% higher than conventional internal combustion engines. Furthermore, since hydrogen fuel does not contain carbon, its combustion process produces no hydrocarbon or carbon dioxide emissions.

Considering these benefits, hydrogen emerges as a significant end-use product for transportation, supported by the following reasons:

1. National energy sustainability challenges are most critical in the transportation sector.
2. Pollution from the transportation sector significantly contributes to environmental issues.
3. Transportation is one of the most economically viable sectors for utilizing renewable resources.
4. Consumer loyalty and preference for hydrogen-powered transportation are high.

Hydrogen's efficiency, environmental advantages, and economic viability make it a crucial component of future transportation systems.

4. Conclusion

In the short and medium term, hydrogen production will continue to rely on fossil fuels, particularly natural gas, due to the existing pipeline infrastructure. Currently, hydrogen is primarily produced through steam methane reforming (SMR), a process that releases carbon dioxide (CO₂) as a byproduct. Instead of focusing solely on purifying and capturing this CO₂, an alternative approach involving the thermal separation of natural gas into hydrogen and carbon is proposed. This method offers both environmental and economic advantages by eliminating CO₂ emissions during production. In this context, researchers have proposed a hydrogen-carbon infrastructure system based on fossil fuels. The main advantage of this system lies in its reliance on the existing natural gas infrastructure, which significantly reduces the cost of transitioning to a hydrogen-carbon economy. The hydrogen-carbon system not only prevents CO₂ emissions from traditional industries such as power plants, cement production, and metallurgy but also promotes the substitution of carbon materials for cement and steel, further reducing emissions. Additionally, this system serves as a bridge between the current hydrocarbon-based economy and the future hydrogen economy, facilitating the transition to renewable energy sources.

References

- [1] Morton, Michael (2006). *In the Heart of the Desert, The Story of an Exploration Geologist and the Search for Oil in the Middle East*. Aylesford: Green Mountain Press. ISBN:9780955221200.
- [2] Reda, N. C. and a. p. Abdel-Aali (2015). *The oil and gas industry in Iraq: current and future trends for the period 2000-2020*, Emirates Center for Strategic Studies and Research.
- [3] Öztürk, M., *Investigation of Hydrogen Production Methods*, PhD Thesis, SDU Science Institute, 2009.
- [4] Middleton, P., Larson, R., Niclas, M., Collins, B., *Renewable Hydrogen Forum: A Summary of Expert Opinion and Policy Recommendations*. Forum presented by the American
- [5] Kaya, Y., et al., *A Grand Strategy for Global Warming*. Paper presented at Tokyo Conference on Global Environment, September 1989. Solar Energy Society. Washington, D.C. National Press Club, 473p, 2003.
- [6] Veziroglu, T. N., Barbir, F., *Hydrogen Energy Technologies*. Emerging Technology Series. Vienna, Austria: United Nations Industrial Development Organization, 122p, 1998.
- [7] Spath, P. L., Mann, M.K., *Life Cycle Assessment of Hydrogen Production via Natural Gas Steam Reforming*, NREL, 2001.
- [8] Baginski, O. (2009). "Crude oil prices: History, forecast, and impact on economy." *Russian Journal of General Chemistry* 79: 2486-2498.
- [9] Öztürk, M., *Investigation of Solar Energy Chemical Reactors*, Master Thesis, Science Sciences Institute, Süleyman Demirel University, 2005.



The Dual Role of Liver Enzymes in The Diagnosis and Monitoring of NAFL

Wasan Hussein Mezher AL-SULAIMAWI¹, , Melike BİLGİ^{2,*} 

¹ Çankırı Karatekin University, School of Natural and Applied Sciences, Chemistry Department, Çankırı, 18000, Türkiye

² Çankırı Karatekin University, Chemistry Department, Çankırı, 18000, Türkiye

Abstract

Non-alcoholic fatty liver disease (NAFLD) has emerged as a major global health concern, often leading to significant morbidity and mortality. Liver enzymes, including alanine aminotransferase (ALT), aspartate aminotransferase (AST), and alkaline phosphatase (ALP), are routinely measured in clinical practice. While these enzymes are traditionally used to assess liver function, their role in diagnosing, monitoring, and prognosis NAFLD is increasingly recognized. The results showed that there is a significant difference between the mean patient age of the two groups studied (control group and patient groups), the patient group was significantly excellent in the mean patient age which recorded 61.83 years as compared with 44.20 years for healthy persons in the control group. The results showed that the age groups above 70 years significantly outperformed the rest of the age groups in the prevalence of the disease, reaching 36%, followed by the age group 60-69 years, which recorded 30%, while the age group less than 30 years has not recorded any infection with the disease is 0%. The results presented that the average cumulative glucose concentration (HbA1C) achieved a significant increase in the patient group, amounting to 6.37% compared to 4.96% for the control group. The results indicated that the patient group was significantly superior to the control group in terms of a significant increase in the ALT level (67.11 vs. 34.60) U/L. The results revealed that the patient group was significantly superior to the control group in raising the average AST value to 39.22 U/L compared to 16.82 U/L for the control group. Data showed that there is a significant difference in the values of ALP levels between the two groups studied, but the patient group was significantly superior in raising the ALP values to 77.50 U/L compared to 49.60 U/L for the control group.

Keywords: NAFLD, ALT, AST, ALP

1. Introduction

Our lifestyle has become more sedentary due to industrialization, urbanization, and modernity. More people who use very little to no alcohol most commonly suffer from nonalcoholic fatty liver disease (NAFLD), a condition that affects the liver. In this disease, an excessive amount of fat accumulates in the liver. Because of the accumulation of fat in the liver, NAFLD disease is a severe type of fatty liver disease that causes the liver to enlarge and cause damage to the liver. There is a possibility that NAFLD could worsen, which might result in cirrhosis, significant scarring of the liver, and perhaps liver cancer. High alcohol consumption induces harm comparable to this damage. Overweight or obese individuals account for the majority of cases. About 25 percent of the world's population is affected by this kind of chronic liver disease, which is the most prevalent form [1-2]. To come up with a full treatment plan for people with NAFLD, it is important to diagnose NAFLD (at least basic steatosis) and severe hepatic fibrosis as soon as possible. Note that you can reverse non-alcoholic fatty liver disease, especially in its early stages. In certain high-risk individuals, the failure to recognize the illness at an early stage may have severe clinical consequences [3].

However, early detection of the disease could lead to adverse clinical effects. A liver biopsy, by its very nature, is an intrusive diagnostic, inherently linked to adverse clinical outcomes, and ineffective for some individuals. Furthermore, the process consumes a substantial amount of resources, operates under the guidance of ultrasonography, and frequently requires a day-case admission. Additionally, it is a very expensive operation [4]. These non-invasive liver tests (NILTs) are now used in clinical practice because imaging tests can diagnose and even stage non-alcoholic fatty liver disease and fibrosis without the problems that come with a biopsy and blood biomarkers that show how well the liver is working. The availability of the tests and their integration into clinical practice varies significantly among NHS providers [5]. Recently, there has been a growing acknowledgment on a worldwide scale of the existing and possible future burden of NAFLD. This has brought to light the significant need for effective pharmaceutical therapies for the illness, which is currently unfulfilled. Over the previous ten years, research in this field has advanced from pre-clinical investigations to randomized clinical trials. The use of

* Corresponding author. e-mail address: melikesahin@karatekin.edu.tr

appropriate histology and surrogate end-points in clinical trials of new therapies for NAFLD is growing on a global scale. This has helped improve the quality of trial design across the scientific community [6].

This study aimed to systematically review and meta-analyze the available literature on the diagnostic accuracy of liver enzymes (ALT, AST, ALP) in detecting NAFLD, to evaluate the prognostic significance of liver enzymes in predicting the progression of NAFLD to non-alcoholic steatohepatitis (NASH) and fibrosis, and to investigate the potential role of liver enzymes as biomarkers to monitor response to NAFLD treatment interventions.

2. Materials and Methods

In this study, a random sample of 150 people was selected for patients visiting health institutions in the city of Baghdad / Iraq, for the period from January 2 to June 30, 2024, to investigate the dual effect of liver enzymes in early diagnosis and detection of non-alcoholic fatty liver disease, thus facilitating control of the disease and reducing health harms and to prevent complications resulting from this disease. The random sample was divided into two groups as follows: The first group consisted of 50 healthy people who visited health institutions and did not suffer from non-alcoholic fatty liver disease. The second group consisted of 100 patients who visited health institutions and were diagnosed as suffering from non-alcoholic fatty liver disease through the diagnosis of a specialist doctor through a clinical examination and symptoms of the disease, which include: The patient suffers from type 2 diabetes, high blood pressure, high lipid levels, etc. Blood samples were drawn from patients, amounting to 5 ml for each patient, using a blood drawing device, and then the patient's information was taken, which included name, age, gender, weight, and medical history, and then the blood samples were transferred to the specialized laboratory to conduct the required tests. The cumulative HbA1C blood sugar level was measured for the patients under study using the Que-Test HbA1C analyzer device produced by EKF Diagnostics. ALT test is based on the ALT enzyme transferring the amino group from alanine to alpha-oxoglutarate to form pyruvate and glutamate. In the next step, pyruvate carries out a reductive reaction with NADH with the help of the lactate dehydrogenase enzyme to produce lactate and NAD^+ . The decrease in absorbance is due to the consumption of NADH, measured at 380 nm, equivalent to the activity of the ALT enzyme in the sample. AST test is for the AST enzyme to reduce the transfer of the amino group from aspartate to oxoglutarate, with the production of glutamate and oxacetate, and the latter reduces malate with the help of the MDH enzyme in the presence of reduced NADH. The reaction is measured kinetically at a temperature of 340 nm through the rate of decrease in absorbance resulting from the process of oxidizing NADH to NAD^+ which is equivalent to the activity of the AST enzyme present in the sample. First, all reagents, samples, and controls must be incubated at the incubation temperature. We added 50 microliters of the sample or control at 37 and 100 μL of the model or control at 30 °C, mixed well, then inserted the cuvette into the cell holder and incubated for 60 s. The initial absorbance reading is recorded, and the absorbance is re-read after 1, 2, and 3 minutes have passed, and the amount of difference between the absorbance and the rate of change in absorbance per minute is calculated ($\Delta A/\text{minute}$). The ALP enzyme catalyzes the hydrolysis of p-nitrophenylphosphate to a yellow product: nitrophenol and phosphate. This reaction occurs in a basic medium (pH 10.3), and the rate of change in absorbance is measured at 405 nm. This change in absorbance is equivalent to the amount of activity of the ALP enzyme in the sample. Incubate the working reagent at 37°C, then add 20 μL of the sample with 1 mL of the working reagent, then incubate at 37°C for 1 minute, read the amount of change in absorbance every minute for 3 minutes, and then calculate the rate of change in absorbance for every 1 minute. The statistical analysis of the variables in this study was conducted according to the statistical program SPSS, version 22.0, produced by the American company IBM. The average values between the tested groups were compared, and the standard deviation and standard error were extracted while the Pearson correlation between the different values was studied.

3. Results and Discussion

3.1 The Age of Patients of Groups Studied

The results of Table 1 showed that there is a significant difference between the mean patient ages of the two groups studied (control and patients' groups). The patient group was significantly excellent in the mean patient age, which recorded 61.83 years, as compared to 44.20 years for healthy persons in the control group. The standard deviation of the patient group recorded 12.13, while the control group recorded 8.29.

The results presented in Table 2 showed that the age groups above 70 years significantly outperformed the rest of the age groups in the prevalence of the disease, reaching 36%, followed by the age group 60-69 years, which recorded 30%, while the age group less than 30 years has not recorded any infection with the disease is 0%. [7]

found that the age group most affected by the disease was 56-60 years. Many studies indicated that the age group most affected by the disease was the age group over 65 years [8]. [9] also showed that older patients were more sensitive to contracting the disease in addition to other risk factors such as high blood pressure, diabetes, obesity, and high ALT values. Table 3 shows that there is a strong positive significant correlation between the patient's age and the tested groups, as it recorded a 0.605 at the 0.01 level.

Table 1. The age of patients in the groups studied

Group studied	Mean Year	N	Std. Deviation	Std. Error of Mean
Control	44.2000	50	8.29310	1.17282
Patients	61.8300	100	12.13315	1.21331
Total	55.9533	150	13.78275	1.12536

Table 2. Age period of patient group

Age period	Patients group N (%)
<30 Years	0 (0.0)
30-39 Years	4 (4.0)
40-49 Years	19 (19.0)
50-59 Years	11 (11.0)
60-69 Years	30 (30.0)
>70 Years	36 (36.0)
Total	100 (100.0)

Table 3. Correlation between the age of patients and groups studied

		Group studied	Age
Group studied	Pearson Correlation	1	0.605**
	Sig. (2-tailed)		0.000
	N	150	150
Age	Pearson Correlation	0.605**	1
	Sig. (2-tailed)	0.000	
	N	150	150

**Correlation is significant at the 0.01 level (2-tailed).

3.2. HbA1C level of groups studied

The results presented in Table 4 show that the average cumulative glucose concentration (HbA1C) achieved a significant increase in the patient group, amounting to 6.37% compared to 4.96% for the control group. Explained that insulin resistance is one of the influential factors that contribute to the development of non-alcoholic fatty liver disease. [10] found that patients with non-alcoholic fatty liver disease had elevated HbA1c concentrations ranging from 5.7 to 6.5%. [11] also showed that HbA1C levels are significantly associated with the presence of non-alcoholic fatty liver disease and concluded that HbA1C can be used as a biomarker to predict the disease. Table 5 revealed that there is a strong positive correlation between HbA1C level, and the groups studied which recorded 0.756 at a level of 0.01.

Table 4. The HbA1C level of groups studied

Group studied	Mean %	N	Std. Deviation	Std. Error of Mean
Control	4.9622	50	0.42863	0.06062
Patients	6.3740	100	0.64112	0.06411
Total	5.9034	150	0.88285	0.07208

Table 5. Correlation between HbA1C level and groups studied

		Group studied	HbA1C
Group studied	Pearson Correlation	1	0.756**
	Sig. (2-tailed)		0.000
	N	150	150
HbA1C	Pearson Correlation	0.756**	1
	Sig. (2-tailed)	0.000	
	N	150	150

**Correlation is significant at the 0.01 level (2-tailed)

3.3. ALT level of groups studied

Table 6 indicated that the patient group was significantly superior to the control group in terms of a significant increase in the ALT level (67.11 vs. 34.60) U/L. [12] found that there was an increase in ALT and AST levels in patients with non-alcoholic fatty liver disease. While [13] indicated that there is an increase in the level of ALT by 19 and 30 times for women and men with the disease, respectively. While [14] indicated that ALT is a poor predictor of non-alcoholic fatty liver disease. However [15], showed that the ALT level can be used as a high-risk indicator of the severity of non-alcoholic fatty liver disease, especially in patients with moderate conditions. Confirmed that the use of ALT levels in the medical diagnosis of non-alcoholic fatty liver disease still needs additional tests and studies. While [16] found that non-alcoholic fatty liver disease was significantly associated with elevated ALT [17] found that people who drink small amounts of alcohol have elevated ALT levels. The results of Table 7 showed that there is a positive strong significant correlation between ALT levels and the groups studied which recorded 0.869 at a level of 0.01.

Table 6. ALT level of groups studied

Group studied	Mean U/L	N	Std. Deviation	Std. Error of Mean
control	34.6000	50	9.68694	1.36994
patients	67.1112	100	8.28515	0.82851
Total	56.2741	150	17.68978	1.44436

Table 7. Correlation between ALT level and groups studied

Group studied	Pearson Correlation Sig. (2-tailed) N	Group studied	ALT
		1	0.869** 0.000
ALT	Pearson Correlation	150	150
	Sig. (2-tailed)	0.869**	1
	N	0.000	150

**Correlation is significant at the 0.01 level (2-tailed)

3.4. AST level of groups studied

The results of Table 8 revealed that the patient group was significantly superior to the control group in raising the average AST value to 39.22 U/L compared to 16.82 U/L for the control group. [18] point out that liver enzymes are commonly used to evaluate people for a wide range of diseases. It is known that AST is an enzyme found mainly in the liver, in addition to its presence in other organs of the body. When liver cells are destroyed, this leads to the release of this enzyme into the blood, and its concentrations in the blood rise, this helps us in diagnosing this disease [19]. It has been reported that patients with alcoholic fatty liver disease have a high AST/ALT ratio and that a high AST level is associated with an increased risk of non-alcoholic fatty liver disease [20-21]. The results of Table 9 pointed that there is a positive strong significant correlation between AST level and the groups studied which recorded 0.844 at a level of 0.01.

Table 8. AST level of groups studied

Group studied	Mean U/L	N	Std. Deviation	Std. Error of Mean
Control	16.8200	50	2.12555	0.30060
Patients	39.2260	100	8.11866	0.81187
Total	31.7573	150	12.55352	1.02499

Table 9. Correlation between AST level and groups studied

Group studied	Pearson Correlation Sig. (2-tailed) N	Group studied	AST
		1	0.844** 0.000
AST	Pearson Correlation	150	150
	Sig. (2-tailed)	0.844**	1
	N	0.000	150

**Correlation is significant at the 0.01 level (2-tailed)

3.5. ALP level of groups studied

Data from Table 10 showed that there is a significant difference in the values of ALP levels between the two groups studied, but the patient group was significantly superior in raising the ALP values to 77.50 U/L compared to 49.60 U/L for the control group. [22] revealed that the ALP level was 220 U/L for patients with type 2 diabetes. While [23] found that the ALP levels of about 99.94% of the population in his study were within the normal range. While [24] confirmed a slight increase in ALP levels in patients with non-alcoholic fatty liver disease. [25] indicated that ALP can be used as a good indicator for predicting non-alcoholic fatty liver disease, especially in obese patients. [26] found that there is a significant correlation between ALP levels and changes in dependent fatty liver disease and that this hormone can be used to predict this disease. The results of Table 11 revealed that there is a positive significant correlation between ALP level and the groups studied which recorded 0.852 at a level of 0.01.

Table 10. ALP-level of groups studied

Group studied	Mean U/L	N	Std. Deviation	Std. Error of Mean
Control	49.6000	50	4.52657	0.64015
Patients	77.5040	100	9.41900	0.94190
Total	68.2027	150	15.48792	1.26458

Table 11. Correlation between ALP level and groups studied

		Group studied	ALP
Group studied	Pearson Correlation	1	.852**
	Sig. (2-tailed)		.000
	N	150	150
ALP	Pearson Correlation	.852**	1
	Sig. (2-tailed)	.000	
	N	150	150

** Correlation is significant at the 0.01 level (2-tailed)

4. Conclusion

The results showed that there is a significant difference between the mean patient age of the two groups studied (control and patient groups), the patient group was significantly excellent in the mean patient age which recorded 61.83 years as compared with 44.20 years for healthy persons in the control group. The results showed that the age groups above 70 years significantly outperformed the rest of the age groups in the prevalence of the disease, reaching 36%, followed by the age group 60-69 years, which recorded 30%, while the age group less than 30 years has not recorded any infection with the disease is 0%. The results presented that the average cumulative glucose concentration (HbA1C) achieved a significant increase in the patient group, amounting to 6.37% compared to 4.96% for the control group. The results indicated that the patient group was significantly superior to the control group in terms of a significant increase in the ALT level (67.11 vs. 34.60) U/L. The results revealed that the patient group was significantly superior to the control group in raising the average AST value to 39.22 U/L compared to 16.82 U/L for the control group. Data showed that there is a significant difference in the values of ALP levels between the two groups studied, but the patient group was significantly superior in raising the ALP values to 77.50 U/L compared to 49.60 U/L for the control group.

References

- [1] Powell, E. E., Wong, V. W. S. and Rinella, M. 2021. Non-alcoholic fatty liver disease. *The Lancet*, 397(10290): 2212-2224.
- [2] Neuschwander-Tetri, B. A. 2017. Non-alcoholic fatty liver disease. *BMC medicine*: 15, 1-6.
- [3] Choudhari, S. and Jothipriya, M. A. 2016. Non-alcoholic fatty liver disease. *Research Journal of Pharmacy and Technology*, 9(10): 1782-1785.
- [4] Bellentani, S. 2017. The epidemiology of non-alcoholic fatty liver disease. *Liver international*, 37: 81-84.
- [5] Maurice, J. and Manousou, P. 2018. Non-alcoholic fatty liver disease. *Clinical medicine*, 18(3): 245.
- [6] Bedossa, P. 2017. Pathology of non-alcoholic fatty liver disease. *Liver International*, 37: 85-89.
- [7] Summart, U., Thinkhamrop, B., Chamadol, N., Khuntikeo, N., Songthamwat, M. and Kim, C. S. 2017. Gender differences in the prevalence of nonalcoholic fatty liver disease in the Northeast of Thailand: A population-based cross-sectional study. *F1000Research*, 6.

- [8] Lonardo, A., Nascimbeni, F., Ballestri, S., Fairweather, D., Win, S., Than, T. A. and Suzuki, A. 2019. Sex differences in nonalcoholic fatty liver disease: state of the art and identification of research gaps. *Hepatology*, 70(4): 1457-1469.
- [9] Frith, J., Day, C. P., Henderson, E., Burt, A. D. and Newton, J. L. 2009. Non-alcoholic fatty liver disease in older people. *Gerontology*, 55(6): 607-613.
- [10] Chen, C., Zhu, Z., Mao, Y., Xu, Y., Du, J., Tang, X. and Cao, H. 2020. HbA1c may contribute to the development of non-alcoholic fatty liver disease even at normal-range levels. *Biosci Rep.*, 40(1): BSR20193996.
- [11] Masroor, M. and Haque, Z. 2021. HbA1C as a biomarker of non-alcoholic fatty liver disease: comparison with anthropometric parameters. *Journal of Clinical and Translational Hepatology*, 9(1): 15.
- [12] Bayard, M., Holt, J. and Boroughs, E. 2006. Nonalcoholic fatty liver disease. *American Family Physician*, 73(11): 1961-1968.
- [13] Hadizadeh, F., Faghihimani, E. and Adibi, P. 2017. Nonalcoholic fatty liver disease: Diagnostic biomarkers. *World journal of Gastrointestinal Pathophysiology*, 8(2): 11.
- [14] Dyson, J. K., Anstee, Q. M. and McPherson, S. 2014. Non-alcoholic fatty liver disease: a practical approach to diagnosis and staging. *Frontline Gastroenterology*, 5(3): 211-218.
- [15] Thong, V. D. and Quynh, B. T. H. 2021. Correlation of serum transaminase levels with liver fibrosis assessed by transient elastography in vietnamese patients with nonalcoholic fatty liver disease. *International Journal of General Medicine*, 4(11): 1349-1355.
- [16] Sanyal, D., Mukherjee, P., Raychaudhuri, M., Ghosh, S., Mukherjee, S. and Chowdhury, S. 2015. Profile of liver enzymes in non-alcoholic fatty liver disease in patients with impaired glucose tolerance and newly detected untreated type 2 diabetes. *Indian Journal of Endocrinology and Metabolism*, 19(5): 597-601.
- [17] Sinn, D. H., Kang, D., Guallar, E., Hong, Y. S., Cho, J. and Gwak, G. Y. 2022. Modest alcohol intake and mortality in individuals with elevated alanine aminotransferase levels: a nationwide cohort study. *BMC Medicine*, 20(1): 18.
- [18] Hall, P. and Cash, J. 2012. What is the real function of the liver 'function' tests. *The Ulster Medical Journal*, 81(1): 30.
- [19] Huang, X. J., Choi, Y. K., Im, H. S., Yarimaga, O., Yoon, E. and Kim, H. S. 2006. Aspartate aminotransferase (AST/GOT) and alanine aminotransferase (ALT/GPT) detection techniques. *Sensors*, 6(7): 756-782.
- [20] Nath, P., Kumar, R., Mallick, B., Das, S., Anand, A., Panigrahi, S. C. and Acharya, S. 2022. Effect of nonalcoholic fatty liver disease (NAFLD) on COVID-19: a single-center study of 3983 patients with review of literature. *Cureus*, 14(7): e26683.
- [21] Nyblom, H. B. U. B. J., Berggren, U., Balldin, J. and Olsson, R. 2004. High AST/ALT ratio may indicate advanced alcoholic liver disease rather than heavy drinking. *Alcohol and Alcoholism*, 39(4): 336-339.
- [22] Chen, S. C. C., Tsai, S. P., Jhao, J. Y., Jiang, W. K., Tsao, C. K. and Chang, L. Y. 2017. Liver fat, hepatic enzymes, alkaline phosphatase and the risk of incident type 2 diabetes: a prospective study of 132,377 adults. *Scientific Reports*, 7(1): 4649.
- [23] Sheng, G., Peng, N., Hu, C., Zhong, L., Zhong, M. and Zou, Y. 2021. The albumin-to-alkaline phosphatase ratio as an independent predictor of future non-alcoholic fatty liver disease in a 5-year longitudinal cohort study of a non-obese Chinese population. *Lipids in Health and Disease*, 20: 1-10.
- [24] López-Amador, N., Nolasco-Hipolito, C., Rojas-Jimeno, M. D. and Carvajal-Zarrabal, O. 2017. Liver enzymes in patients diagnosed with non-alcoholic fatty liver disease (NAFLD) in Veracruz: a comparative analysis with the literature. *Clinical Investigation*, 7(1): 25-32.
- [25] Ali, A. H., Petroski, G. F., Diaz-Arias, A. A., Al Juboori, A., Wheeler, A. A., Ganga, R. R. and Ibdah, J. A. 2021. A model incorporating serum alkaline phosphatase for prediction of liver fibrosis in adults with obesity and nonalcoholic fatty liver disease. *Journal of Clinical Medicine*, 10(15): 3311.
- [26] Sohrabi, M., Aghapour, S., Khoonsari, M., Ajdarkosh, H., Nobakht, H., Zamani, F. and Nikkhah, M. 2023. Serum Alkaline Phosphate Level Associates with Metabolic Syndrome Components Regardless of Non-Alcoholic Fatty Liver; A Population-Based Study in Northern Iran. *Middle East Journal of Digestive Diseases*, 15(3): 175-179.



Transformation of Food Waste into Adsorbents and Methylene Blue Dye Removal

Tiba SALEH GHANI AL-OKAIDAT¹ , ***Muhammed Bora AKIN***^{2,*} 

¹ Ministry of Higher Education and Scientific Research, Ministry Headquarters, Baghdad, Iraq

² Faculty of Engineering, Department of Chemical Engineering, Çankırı Karatekin University, Çankırı, Türkiye

Abstract

Pollution caused by dyes from industrial processes poses serious environmental threats to aquatic ecosystems and increases the need for sustainable water treatment methods. This study focuses on examining the utilization of food waste as low-cost and environmentally friendly adsorbents. It is observed that common food wastes such as orange peels, coffee grounds, and eggshells can be used for the adsorption of methylene blue (MB) from water by optimizing their surface properties through chemical activation processes. Characterization procedures typically involve Fourier Transform Infrared Spectroscopy (FTIR), Scanning Electron Microscopy (SEM), and surface area analyses. Adsorption performance is assessed by exploring parameters such as solution pH, temperature, initial concentration, and contact time. The results demonstrate that adsorbents derived from food waste exhibit high adsorption capacity and provide an effective solution for methylene blue removal.

Keywords: Food waste, Methylene blue, Adsorption, Environmental sustainability, Biosorbent

1. Introduction

Industrial effluents containing synthetic dyes, particularly methylene blue (MB), represent a significant environmental challenge due to their toxicity and resistance to biodegradation. Methylene blue, a cationic dye prevalent in the textile, printing, and paper industries, poses severe risks to aquatic ecosystems and human health when released into water bodies [1]. The need for effective and sustainable water treatment methods has thus become paramount. Among various treatment techniques, adsorption has gained attention for its simplicity and cost-effectiveness in removing dyes from wastewater [2]. However, traditional adsorbents like activated carbon can be prohibitively expensive, prompting researchers to explore alternative materials that are both cost-effective and environmentally friendly.

Food waste, an abundant and often overlooked resource, has emerged as a promising precursor for the production of low-cost adsorbents. The transformation of food waste into adsorbents capable of efficiently removing MB from aqueous solutions is a focal point of recent studies. For instance, various food waste materials, such as banana peels and coffee grounds, have demonstrated significant adsorption capacities for volatile organic compounds and dyes [3, 4]. The chemical activation of these materials can enhance their adsorption properties, allowing for improved removal efficiencies of methylene blue [5]. Additionally, the optimization of adsorption conditions, including pH and adsorbent dosage, is crucial for maximizing dye removal rates. It has been shown that the surface charge of the adsorbent can significantly affect the adsorption process, particularly in the case of cationic dyes like MB, where an acidic environment can lead to decreased adsorption due to the positive charge on both the dye and the adsorbent surface [2].

Moreover, the use of agricultural and food waste not only provides a sustainable solution for dye removal but also addresses the pressing issue of waste management. By converting food waste into effective adsorbents, we can mitigate environmental pollution while simultaneously reducing the volume of waste sent to landfills [6, 7]. Studies have indicated that the adsorption capacities of these bio-based materials can rival those of conventional adsorbents, making them viable alternatives for wastewater treatment [8]. Furthermore, the incorporation of various treatment methods, such as chemical activation or blending with other materials, can further enhance the performance of these adsorbents [5].

2. Food Waste as Adsorbent Precursors

* Corresponding author. e-mail address: mbakin@karatekin.edu.tr

2.1. Chemical Composition and Suitability

Food wastes such as orange peels, coffee grounds, and eggshells are rich in carbonaceous and mineral components, making them suitable for adsorption applications. Orange peels contain significant amounts of pectin and lignin, which are inherently adsorptive due to their structural properties and functional groups that facilitate binding with pollutants [3]. Coffee grounds, primarily composed of cellulose and hemicellulose, also exhibit promising adsorption characteristics, attributed to their porous structure and high surface area [3]. Furthermore, eggshells, which are predominantly composed of calcium carbonate, provide a unique mineral-based adsorbent that can enhance the adsorption process through ion exchange mechanisms [9].

2.2. Pretreatment and Activation

To enhance the adsorption capacity of food waste materials, pretreatment and activation processes are necessary. Chemical activation, commonly using agents such as potassium hydroxide (KOH) or phosphoric acid (H_3PO_4), is employed to increase porosity and surface area, which are critical for effective adsorption [2]. This activation process not only enhances the surface characteristics of the adsorbent but also introduces functional groups that can interact with dye molecules, thereby improving adsorption efficiency [10]. Additionally, thermal treatment can be utilized to carbonize organic matter, creating high-surface-area adsorbents suitable for methylene blue removal [11]. The combination of these pretreatment methods can significantly improve the adsorption capacity of food waste-derived adsorbents, making them competitive alternatives to conventional materials [12].

3. Characterization of Food Waste Adsorbents

Characterization techniques provide essential insights into the surface properties and adsorption mechanisms of synthesized adsorbents derived from food waste. Understanding these characteristics is crucial for optimizing their performance in dye removal applications.

3.1. Fourier Transform Infrared Spectroscopy (FTIR)

Fourier Transform Infrared Spectroscopy (FTIR) is a powerful analytical tool used to identify functional groups responsible for adsorption in food waste-derived adsorbents. The presence of peaks corresponding to hydroxyl (-OH), carboxyl (-COOH), and amine ($-\text{NH}_2$) groups in the FTIR spectra confirms the existence of active sites that can interact with MB molecules [13]. These functional groups play a significant role in the adsorption process, as they can form hydrogen bonds and electrostatic interactions with the dye, enhancing the overall adsorption capacity of the material [14]. The ability to characterize these functional groups allows researchers to tailor the adsorbent properties for improved performance in wastewater treatment applications.

3.2. Scanning Electron Microscopy (SEM)

Scanning Electron Microscopy (SEM) analysis provides detailed information about the surface morphology of food waste adsorbents. Activated food waste typically exhibits a porous structure, which is advantageous for the adsorption of MB. SEM images reveal significant changes in texture following chemical activation, indicating an increase in surface area and the availability of active sites for adsorption [15]. The porous nature of the adsorbent not only facilitates the diffusion of dye molecules but also increases the contact area between the adsorbent and the dye, thereby enhancing the adsorption efficiency [16]. This morphological characterization is vital for understanding how structural changes influence the adsorbent's performance.

3.3. Surface Area and Porosity

Surface area analysis, commonly performed using the Brunauer-Emmett-Teller (BET) method, quantifies the adsorbent's capacity for dye adsorption. Higher surface areas correlate with improved MB removal efficiencies, as a larger surface area provides more active sites for interaction with the dye molecules [17]. The porosity of the adsorbent is equally important, as it affects the accessibility of the dye to the active sites. Studies have shown that food waste-derived adsorbents can achieve significant surface area enhancements through chemical activation and thermal treatment, making them competitive alternatives to traditional adsorbents like activated carbon [18]. The relationship between surface area, porosity, and adsorption capacity underscores the importance of these characterization techniques in the development of effective adsorbents for wastewater treatment.

4. Adsorption Mechanisms

4.1. Physical Adsorption

Physical adsorption, also known as physisorption, involves weak van der Waals interactions between MB molecules and the surface of the adsorbent. This mechanism is primarily influenced by the adsorbent's porosity and surface area, as a higher surface area provides more sites for dye molecules to adhere [19]. The effectiveness of physical adsorption is contingent upon the accessibility of these sites, which can be enhanced through the

activation of food waste materials, resulting in a more porous structure that facilitates greater interaction with the dye [20].

4.2. Chemical Adsorption

Chemical adsorption, or chemisorption, occurs through the formation of covalent or ionic bonds between MB and functional groups present on the adsorbent surface. Functional groups such as carboxyl (-COOH) and hydroxyl (-OH) are critical for this process, as they provide active sites that can interact strongly with the cationic dye [21]. The presence of these functional groups enhances the adsorption capacity of food waste-derived adsorbents, making them effective in removing MB from wastewater [22]. The strength of the interactions in chemical adsorption typically results in higher adsorption energies compared to physical adsorption, leading to more stable dye-adsorbent complexes.

4.3. Factors Affecting Adsorption

The solution pH significantly influences the adsorption process. Optimal MB removal is typically observed in slightly basic conditions (pH 7–9), where the surface charges of the adsorbent favor the uptake of cationic dyes [23]. At higher pH levels, the increased concentration of hydroxyl groups on the adsorbent surface can lead to reduced adsorption rates due to electrostatic repulsion between the negatively charged surface and the cationic dye [24]. Thus, pH is a critical parameter that must be optimized to enhance the adsorption efficiency of food waste-derived adsorbents.

Temperature also impacts the kinetics and equilibrium of the adsorption process. Generally, higher temperatures increase the adsorption capacity by enhancing molecular mobility and the rates of adsorption reactions [25]. This effect is particularly important in the context of food waste adsorbents, as elevated temperatures can facilitate the diffusion of dye molecules into the porous structure of the adsorbent, thereby improving overall removal efficiency [26].

The initial concentration of MB in solution serves as a driving force for mass transfer during the adsorption process. Adsorbents typically exhibit higher efficiencies at moderate dye concentrations, as excessive concentrations can lead to the saturation of active sites on the adsorbent [2]. Understanding the relationship between initial dye concentration and adsorption capacity is essential for optimizing the use of food waste-derived adsorbents in practical applications.

Contact time is another crucial factor affecting adsorption kinetics. Equilibrium is usually reached within 60–180 minutes for food waste adsorbents, depending on the specific material and dye concentration [27]. The rate of adsorption can vary significantly based on the characteristics of the adsorbent and the nature of the dye, highlighting the importance of conducting time-dependent studies to determine optimal contact times for effective dye removal.

4.4. Adsorption Isotherms and Kinetics

Adsorption isotherms are mathematical models that describe the interaction between adsorbates and adsorbents. The Langmuir model assumes monolayer adsorption on a homogeneous surface, indicating that there are a finite number of active sites available for adsorption. In contrast, the Freundlich model describes multilayer adsorption on heterogeneous surfaces. Food waste-derived adsorbents often fit the Langmuir model, suggesting high adsorption efficiency and a limited number of active sites available for MB [28]. This fitting emphasizes the potential of these adsorbents for effective dye removal in wastewater treatment applications.

Adsorption kinetics can be analyzed using pseudo-first-order and pseudo-second-order models. The pseudo-second-order model typically provides a better fit for food waste adsorbents, indicating that chemisorption is the dominant mechanism in the adsorption process [29]. This suggests that the rate of adsorption is primarily dependent on the number of available active sites and the concentration of the dye, further supporting the role of chemical interactions in enhancing adsorption capacity.

5. Comparative Studies and Performance Evaluation

5.1. Adsorption Capacities

Food waste-derived adsorbents demonstrate high MB adsorption capacities compared to conventional adsorbents. For instance, activated orange peels have been reported to achieve capacities of up to 200 mg/g, while coffee grounds and eggshells reach capacities of 150 mg/g and 120 mg/g, respectively [30]. This high adsorption capacity can be attributed to the porous structure and rich functional groups present in these materials, which facilitate effective interactions with the dye molecules [30]. The ability of food waste materials to serve as

efficient adsorbents not only highlights their potential in wastewater treatment but also underscores the value of utilizing agricultural by-products in environmental remediation efforts.

5.2. Economic and Environmental Benefits

Utilizing food waste for MB removal offers dual benefits: it mitigates food waste disposal issues and reduces costs associated with conventional adsorbents. The eco-friendly nature of food waste-derived adsorbents aligns with the principles of sustainable development, as they contribute to waste valorization and resource recovery [6]. By transforming food waste into valuable adsorbents, industries can lower their operational costs while simultaneously addressing environmental concerns related to waste management [6]. This approach not only promotes a circular economy but also encourages the adoption of sustainable practices in wastewater treatment.

5.3. Practical Applications and Future Directions

Food waste-based adsorbents can be integrated into industrial water treatment systems for large-scale dye removal. The scalability of production methods and the evaluation of long-term performance under real-world conditions are critical areas for future research [31]. Developing efficient methods for the synthesis and application of these adsorbents will enhance their practicality in various wastewater treatment scenarios.

Beyond orange peels, coffee grounds, and eggshells, other food wastes such as banana peels, potato skins, and nut shells hold potential as adsorbents. Exploring diverse food waste types can expand the applicability of this approach, allowing for the development of a wider range of low-cost and effective adsorbents [30]. This exploration can lead to the identification of new materials with superior adsorption properties, further enhancing the effectiveness of food waste-derived adsorbents in treating various pollutants.

The regeneration of food waste adsorbents is essential for economic feasibility. Chemical desorption and thermal regeneration methods show promise, though optimization is required to minimize efficiency losses during repeated cycles [32]. Ensuring that these adsorbents can be reused multiple times without significant degradation of their adsorption capacity will be vital for their long-term application in wastewater treatment [33]. Research into the regeneration processes will contribute to the overall sustainability and cost-effectiveness of using food waste-derived adsorbents in practical applications.

6. Conclusion

This study highlights the transformative potential of food waste as a resource for water treatment. By chemically activating food wastes such as orange peels, coffee grounds, and eggshells, high-efficiency adsorbents can be produced for MB dye removal. Characterization techniques confirm the presence of functional groups and porous structures essential for adsorption. The process is cost-effective, environmentally friendly, and scalable, providing a sustainable solution for industrial dye pollution. Future research should focus on optimizing adsorption parameters, exploring diverse food waste types, and integrating these adsorbents into practical water treatment systems.

References

- [1] M. Rafatullah, O. Sulaiman, R. Hashim, and A. Ahmad, "Adsorption of methylene blue on low-cost adsorbents: a review," *Journal of Hazardous Materials*, vol. 177, no. 1–3, pp. 70–80, 2010, doi: 10.1016/j.jhazmat.2009.12.047.
- [2] S. Bahari, F. Jahid, Y. Lian, R. Ramli, and L. Lee, "Adsorption of methylene blue using tea waste treated with alkaline-potassium hydroxide," *Key Engineering Materials*, vol. 932, pp. 59–69, 2022, doi: 10.4028/p-w80ye7.
- [3] M. Frezzini, L. Massimi, M. Astolfi, S. Canepari, and A. Giuliano, "Food waste materials as low-cost adsorbents for the removal of volatile organic compounds from wastewater," *Materials*, vol. 12, no. 24, p. 4242, 2019, doi: 10.3390/ma12244242.
- [4] E. Matei, M. Răpă, A. Predescu, A. Țurcanu, R. Vidu, C. Predescu, and C. Orbeci, "Valorization of agri-food wastes as sustainable eco-materials for wastewater treatment: current state and new perspectives," *Materials*, vol. 14, no. 16, p. 4581, 2021, doi: 10.3390/ma14164581.
- [5] M. Mohadesi, A. Gouran, and F. Shahbazi, "Combination process for dye removal based on photocatalyst and adsorption using low cost waste material adsorbent," *Environmental Progress & Sustainable Energy*, vol. 41, no. 6, 2022, doi: 10.1002/ep.13898.
- [6] F. Younas, A. Mustafa, Z. Farooqi, X. Wang, S. Younas, W. Mohy-Ud-Din, and M. Hussain, "Current and

- emerging adsorbent technologies for wastewater treatment: trends, limitations, and environmental implications," *Water*, vol. 13, no. 2, p. 215, 2021, doi: 10.3390/w13020215.
- [7] O. Bello, A. Olaniyan, and H. Abdulazeez, "Dye adsorption using biomass wastes and natural adsorbents: overview and future prospects," *Desalination and Water Treatment*, vol. 53, no. 5, pp. 1292–1315, 2015, doi: 10.1080/19443994.2013.862028.
 - [8] S. Gisi, G. Lofrano, M. Grassi, and M. Notarnicola, "Characteristics and adsorption capacities of low-cost sorbents for wastewater treatment: a review," *Sustainable Materials and Technologies*, vol. 9, pp. 10–40, 2016, doi: 10.1016/j.susmat.2016.06.002.
 - [9] A. Riduan, R. Rainiyati, S. Heraningsih, and B. Badariah, "Minimizing river pollution by batik dye wastewater using palm oil fuel ash (POFA) as an environmentally friendly, low-cost adsorbent alternative," *Journal of Degraded and Mining Lands Management*, vol. 10, no. 1, p. 3981, 2022, doi: 10.15243/jdmlm.2022.101.3981.
 - [10] H. Zhang, X. Yao, T. Qu, G. Owens, and L. Gao, "A sustainable natural clam shell derived photocatalyst for the effective adsorption and photodegradation of organic dyes," *ChemistrySelect*, vol. 4, no. 2, pp. 617–622, 2021, doi: 10.21203/rs.3.rs-1039754/v1.
 - [11] S. Idris, J. Yisa, A. Itodo, and K. Popoola, "Application of carbonized poultry waste in the removal of chemical oxygen demand (COD) from dye wastewater: kinetic study," *Resources and Environment*, vol. 2, no. 2, pp. 51–55, 2012, doi: 10.5923/j.re.20120202.08.
 - [12] D. Sikdar, S. Goswami, and P. Das, "Activated carbonaceous materials from tea waste and its removal capacity of indigo carmine present in solution: synthesis, batch and optimization study," *Sustainable Environment Research*, vol. 30, no. 1, 2020, doi: 10.1186/s42834-020-00070-8.
 - [13] H. Zhu and H. Zou, "Characterization of algae residue biochar and its application in methyl orange wastewater treatment," *Water Science & Technology*, vol. 84, no. 12, pp. 3716–3725, 2021, doi: 10.2166/wst.2021.473.
 - [14] A. Prajapati, P. Verma, S. Singh, and M. Mondal, "Adsorption-desorption surface bindings, kinetics, and mass transfer behavior of thermally and chemically treated great millet husk towards Cr(VI) removal from synthetic wastewater," *Adsorption Science & Technology*, 2022, doi: 10.1155/2022/3956977.
 - [15] M. El-Azazy, A. El-Shafie, and K. Al-Saad, "Application of infrared spectroscopy in the characterization of lignocellulosic biomasses utilized in wastewater treatment," *Environmental Progress & Sustainable Energy*, 2023, doi: 10.5772/intechopen.108878.
 - [16] I. Lobzenko, M. Burachevskaya, I. Zamulina, A. Barakhov, T. Bauer, S. Mandzhieva, and V. Rajput, "Development of a unique technology for the pyrolysis of rice husk biochar for promising heavy metal remediation," *Agriculture*, vol. 12, no. 10, p. 1689, 2022, doi: 10.3390/agriculture12101689.
 - [17] J. Bell, P. Nel, and B. Stuart, "Non-invasive identification of polymers in cultural heritage collections: evaluation, optimisation and application of portable FTIR (ATR and external reflectance) spectroscopy to three-dimensional polymer-based objects," *Heritage Science*, vol. 7, no. 1, 2019, doi: 10.1186/s40494-019-0336-0.
 - [18] U. Shoukat, E. Baumeister, and H. Knuutila, "ATR-FTIR model development and verification for qualitative and quantitative analysis in MDEA–H₂O–MEG/TEG–CO₂ blends," *Energies*, vol. 12, no. 17, p. 3285, 2019, doi: 10.3390/en12173285.
 - [19] Y. Hu, K. Li, Y. Li, H. Liu, M. Guo, X. Ye, and K. Lee, "Dyes adsorption onto Fe₃O₄-bis(trimethoxysilylpropyl)amine composite particles: effects of pH and ionic strength on electrostatic interactions," *ChemistrySelect*, vol. 4, no. 2, pp. 617–622, 2019, doi: 10.1002/slct.201803241.
 - [20] A. Soltani, M. Faramarzi, and S. Parsa, "A review on adsorbent parameters for removal of dye products from industrial wastewater," *Water Quality Research Journal*, vol. 56, no. 4, pp. 181–193, 2021, doi: 10.2166/wqrj.2021.023.
 - [21] A. Herrera-González, A. Peláez-Cid, and M. Caldera-Villalobos, "Adsorption of textile dyes present in aqueous solution and wastewater using polyelectrolytes derived from chitosan," *Journal of Chemical Technology & Biotechnology*, vol. 92, no. 7, pp. 1488–1495, 2017, doi: 10.1002/jctb.5214.
 - [22] A. Gneedy, A. R. Dryaz, M. Shaban, H. AlMohamadi, S. A. Ahmed, R. El-Sayed, and N. K. Soliman, "Application of marine algae separate and in combination with natural zeolite in dye adsorption from wastewater: A review," *Egyptian Journal of Chemistry*, vol. 65, no. 9, pp. 589–616, 2022, doi: 10.21608/ejchem.2022.86811.4356.
 - [23] N. Raval and P. Shah, "Adsorptive amputation of hazardous azo dye Congo red from wastewater: a critical review," *Environmental Science and Pollution Research*, vol. 23, no. 15, pp. 14810–14853, 2016, doi:

- 10.1007/s11356-016-6970-0.
- [24] O. Mouhtady, E. Obeid, M. Abu-Samha, K. Younes, and N. Murshid, "Evaluation of the adsorption efficiency of graphene oxide hydrogels in wastewater dye removal: application of principal component analysis," *Gels*, vol. 8, no. 7, p. 447, 2022, doi: 10.3390/gels8070447.
- [25] E. Alkhatib, P. Snetsinger, A. Alanazi, and S. Aanonsen, "Application of factorial design in the analysis of factors influencing textile dye adsorption on activated carbon," *Journal of Civil & Environmental Engineering*, vol. 7, no. 6, 2017, doi: 10.4172/2165-784x.1000287.
- [26] Z. Maděrová, E. Baldíková, K. Pospíšková, I. Šafařík, and M. Šafaříková, "Removal of dyes by adsorption on magnetically modified activated sludge," *International Journal of Environmental Science and Technology*, vol. 13, no. 7, pp. 1653–1664, 2016, doi: 10.1007/s13762-016-1001-8.
- [27] T. Yadav and P. Patil, "Pressmud as biosorbent for reactive dyes removal from wastewater," *International Journal for Research in Applied Science and Engineering Technology*, vol. 11, no. 1, pp. 262–271, 2023, doi: 10.22214/ijraset.2023.48546.
- [28] Y. Zhang, X. Ma, H. Xu, Z. Shi, J. Yin, and X. Jiang, "Selective adsorption and separation through molecular filtration by hyperbranched poly(ether amine)/carbon nanotube ultrathin membranes," *Langmuir*, vol. 32, no. 49, pp. 13073–13083, 2016, doi: 10.1021/acs.langmuir.6b03689.
- [29] L. Hevira, A. Rahmi, R. Zein, Z. Zilfa, and R. Rahmayeni, "The fast and low-cost adsorbent to the removal of cationic and anionic dye using chicken eggshell with its membrane," *Mediterranean Journal of Chemistry*, vol. 10, no. 3, pp. 294–301, 2020, doi: 10.13171/mjc02003261271lh.
- [30] W. Zhang, L. Hui-He, J. Tang, H. Lu, and Y. Liu, "Ginger straw waste-derived porous carbons as effective adsorbents toward methylene blue," *Molecules*, vol. 24, no. 3, p. 469, 2019, doi: 10.3390/molecules24030469.
- [31] C. Vaneckhaute, "Management of nutrient-rich wastes and wastewaters on board of ships," 2021, doi: 10.5772/intechopen.98683.
- [32] F. Fadzil, F. Fadzil, S. Sulaiman, A. Shaharoshaha, and R. Seswoya, "Mild thermal pre-treatment as a method for increasing the methane potential of food waste," *International Journal of Design & Nature and Ecodynamics*, vol. 15, no. 3, pp. 425–430, 2020, doi: 10.18280/ijdne.150316.
- [33] D. Zou, X. Wang, C. Wu, T. Li, M. Wang, L. Shu, and T. Shimaoka, "Dechlorination of municipal solid waste incineration fly ash by leaching with fermentation liquid of food waste," *Sustainability*, vol. 12, no. 11, p. 4389, 2020, doi: 10.3390/su12114389.



Can Artificial Intelligence Be Trained To Account For The Growth Laws And Biological Patterns Inherent in Tree Growth?

*İlker ERCANLI*¹ , *Muammer ŞENYURT*² 

¹ Forest Engineering Department, Forest Faculty Çankırı Karatekin University, Çankırı, Türkiye

Abstract

This study addresses a fundamental question in artificial intelligence applications within forestry science: Can AI models effectively learn and incorporate inherent biological growth patterns and laws governing tree development? Through systematic evaluation of Deep Learning Architecture (DLA) implementations in forestry modeling, we identify two distinct methodological paradigms: conventional adaptive learning-based models and optimized DLA frameworks incorporating hyperparameter and regularization techniques. While AI models demonstrate superior statistical performance compared to traditional regression approaches, their evaluation in forestry science necessitates consideration beyond mere performance metrics, particularly regarding biological plausibility. Our analysis reveals that standard adaptive learning-based AI models, despite achieving high training accuracy, often exhibit overfitting tendencies and fail to capture fundamental biological relationships. In contrast, hyperparameter-optimized and regularization-optimized DLA models, incorporating customized network parameters, demonstrate remarkable capacity in maintaining biological fidelity while mitigating overfitting challenges. These optimized frameworks successfully predict tree attributes while preserving consistency with established dendrometric principles, effectively addressing the traditional 'black-box' limitations of AI models. The study concludes that through proper optimization techniques, AI models can indeed be trained to account for biological growth patterns, though their full potential in forestry applications remains to be explored as our understanding of their capabilities continues to evolve.

Keywords: *Biological realistic predictions, Overfitting, Hyperparameter-optimized and regularization-optimized DLA models*

1. Introduction

In the mid-nineteenth century, Alan Turing's influential 1950 paper in the *Journal of Mind* introduced a pivotal question by juxtaposing two concepts: 'thinking' and 'machines' through his inquiry, 'Can machines think?' (Turing, 1950). This foundational concept of thinking machines has evolved into Artificial Intelligence (AI) systems capable of learning the dynamic mechanisms and interrelationships within living ecosystems (McCorduck, 2004; Nilsson, 2014). Turing's initial question has transformed into a more complex inquiry: 'Can artificial intelligence (AI) learn and comprehend living systems, such as forest ecosystems?'

From this perspective, a critical initial phase in developing AI systems involves enabling AI to gain comprehensive understanding of the living systems it encounters (Russell et al., 2015; Brynjolfsson and Mitchell, 2017). The predictive capabilities and effective learning processes of AI in relation to these living systems represent crucial developmental stages in AI model evolution (Armstrong et al., 2014; Taddeo and Floridi, 2018). Consequently, AI techniques increasingly focus on the quality of learning required to accurately model these complex biological systems.

Artificial Intelligence (AI) models have demonstrated remarkable success in learning processes across various engineering disciplines, including electronics, manufacturing, mechanical engineering, communications, and construction. Moreover, these models exhibit significant potential for understanding the complex interrelationships within natural ecosystem growth processes, particularly in forest systems.

Since the early 2000s, AI models—specifically Artificial Neural Network (ANN) models—have emerged as an innovative and increasingly prominent prediction methodology in forest modeling studies. The growing prominence of ANN models in forestry modeling literature can be attributed to two key advantages: first, their robust capability for nonlinear modeling without the need for predetermined statistical functions, and second, their ability to generate successful and robust predictions without adhering to traditional statistical assumptions

* Corresponding author. e-mail address: ilkerercanli@karatekin.edu.tr

(Özçelik et al., 2010; Ashraf et al., 2013; Diamantopoulou et al., 2015). Many studies focused on developing and evaluating ANN models by comparing their predictive capabilities for various individual tree and stand characteristics against conventional regression models—the latter having served as the classical statistical estimation methodology in forestry for approximately eight decades. Comparative analyses consistently demonstrated that ANN models exhibited superior predictive performance in estimating individual tree and stand attributes compared to traditional regression approaches. In this evolving landscape of predictive modeling, AI models—particularly ANN models and more recently, Deep Learning Architecture (DLA) models—have emerged as viable alternatives to classical regression approaches. This shift is particularly significant given the longstanding criticisms of AI models with ANN or DLA regarding their reliance on biological assumptions and limitations in modeling complex growth relationships within tree and forest systems, especially in certain data structures. In forestry biometrics, while statistical validity and model fit are essential criteria, the biological realism of predicted individual tree and stand attributes holds paramount importance. This emphasis on biological realism was first articulated by Levins (1966), who established it as a fundamental requirement for developing robust and predictive models in forest systems. Subsequently, Lei and Parresol (2001) further advanced this concept by delineating specific biologically realistic characteristics crucial for modeling individual tree growth.

Within this theoretical framework, prediction systems developed for forestry applications must demonstrate consistency with established biological growth patterns. These patterns typically manifest as sigmoid growth curves with distinct inflection points, multiple asymptotes, and monotonically non-decreasing trajectories over time—characteristics that reflect the underlying biological processes of tree and forest development. This study evaluates the potential of artificial intelligence models, particularly Deep Learning Architecture (DLA) models, to generate predictions that align with biological realism and fundamental growth laws governing both individual tree and stand development in forestry. The present research may explore the fundamental challenge of training artificial intelligence systems to effectively recognize and account for the inherent biological patterns and growth laws that characterize tree development processes within forest ecosystems.

2. Overfitting problem: A significant challenge and limitation in artificial intelligence

AI models, characterized by multiple non-linear hidden layers and thousands of neuronal weights, demonstrate remarkable flexibility and non-linear modeling capabilities in their complex architectural structures when modeling various individual tree and stand attributes. While this inherent flexibility in non-linear modeling potentially offers superior predictive performance compared to traditional linear and non-linear regression approaches, it simultaneously introduces the risk of overfitting during the training process. In overfitted challenges, AI models may generate predictions that almost perfectly align with observed training data, effectively memorizing the dataset—including its noise components—rather than learning the fundamental input-output relationships. This phenomenon, formally known as the 'overfitting or generalization problem,' represents a critical limitation that frequently impairs the model's ability to generalize effectively to unseen or validation datasets.

The manifestation of overfitting typically presents as a distinct pattern: while the model achieves exceptionally low residual errors for the training dataset, it exhibits substantially larger errors when applied to unseen validation data. Consequently, overfitted AI models often demonstrate poor statistical performance metrics when evaluated against validation datasets. The hallmark symptoms of overfitting and generalization problems can be characterized by low bias in training set predictions coupled with high variance and unsatisfactory predictive capability when applied to validation datasets.

The implications of the overfitting problem extend beyond mere validation error metrics, significantly impacting the ability to achieve biological realism in modeling individual tree and stand growth dynamics within forestry science. When AI models succumb to overfitting, failing to learn intrinsic data relationships and instead defaulting to memorization patterns, they may fundamentally violate principles of biological realism. The core challenge with overfitted AI models lies in their tendency to memorize rather than learn the underlying relationships in the training data, thereby compromising their ability to capture genuine biological patterns and growth dynamics.

3. The hyperparameter-optimized or regularization-optimized AI models

In addressing the overfitting phenomenon within artificial intelligence frameworks, the optimization of hyperparameters and regularization parameters emerges as a critical component in the development of AI models. Neural network architectures incorporating such optimized hyperparameters are formally classified as

'hyperparameter-optimized ANN' models, reflecting their enhanced configurational sophistication. Also, Within the artificial intelligence literature, AI models incorporating optimized regularization parameters are formally designated as 'regularization-optimized ANN' models, reflecting their enhanced capacity for generalization through systematic parameter adjustment. Artificial Neural Networks trained through adaptive learning processes typically incorporate hyperparameters such as learning and momentum rates, with these parameters traditionally optimized through error minimization between observed and predicted values. However, this approach differs substantially from hyperparameter-optimized ANN models in their fundamental methodology. While adaptive learning processes employ automatic parameter determination for residual minimization, hyperparameter-optimized ANNs implement a more sophisticated approach, requiring meticulous customization of network topology parameters. This optimization process demands systematic trial-and-error experimentation, with particular emphasis on two critical objectives: mitigating overfitting tendencies and preserving biological realism. The careful calibration of architectural parameters, including learning and momentum rates, represents a more rigorous and controlled approach to network optimization compared to adaptive learning methodologies. To address overfitting challenges and maintain biological realism in neural networks, various regularization optimization strategies have emerged as effective methodological approaches. These techniques include early stopping protocols based on Root Mean Square Error (RMSE) metrics, regularization implementations incorporating L1 and L2 penalty terms, and dropout mechanisms utilizing randomly excluded neural units. These methodologies collectively serve to reduce network model complexity while enhancing the robustness of neural network architectures (McCorduck, 2004; Goodfellow et al., 2016).

4. The growth laws and biological realism in tree growth

In forestry science about tree and stand growth and yield modeling studies, while the assessment of statistical prediction models such as regression analyses traditionally relies on various metrics including Akaike Information Criterion (AIC), Bayesian Information Criterion (BIC), coefficient of determination (R^2), Bias, and Root Mean Square Error (RMSE), the biological coherence of these models holds paramount importance. Specifically, the predictive behavior patterns generated by these prediction models must demonstrate fundamental consistency with the inherent biological development trends and natural characteristics of the modeled attributes. As stated in many studies such as Bailey and Clutter (1974) and Cieszewski (2002), desirable characteristics of height growth curves are: (1) a sigmoidal structure (known as an “S curve”); (2) a logical behavior with a zero value of height at age zero; (3) polymorphism; (4) an asymptotic behavior; and (5) base-age invariance.

The fundamental principles of biological realism in tree growth volumetrics were initially established by Heinrich Cotta in the early nineteenth century (Clark, 1902). A primary tenet of this biological framework establishes that tree stem volume is fundamentally determined by the interaction of three key parameters: diameter at breast height (DBH), total tree height (TTH), and tree form (Avery and Burkhart, 1983). While many contemporary volume prediction systems primarily utilize DBH and TTH as independent variables for total tree volume (TTV) estimation, often excluding tree form considerations (van Laar and Akca, 1997), the underlying biological relationships remain crucial. The relationship between these parameters exhibits specific biological patterns: TTV demonstrates a positive correlation with DBH when TTH remains constant, and similarly, TTV increases with increasing TTH for constant DBH values. Significantly, these relationships follow allometric curvilinear patterns rather than linear trajectories (Spurr, 1952; Avery and Burkhart, 1983). For hyperparametrized Deep Learning Architecture (DLA) models to gain acceptance within the forestry literature as effective prediction systems, they must demonstrate consistency with these established biological patterns. Any deviation from expected trends, such as decreases or unexpected fluctuations in TTV values at higher DBH and TTH values, would constitute a violation of biological realism, potentially compromising the model's validity and utility in forestry applications.

In addition to comparing and evaluating various models for estimating individual tree and stand characteristics according to different performance criteria (R^2 , Bias, RMSE, AIC, BIC, etc.), the assessment of prediction accuracies obtained through these prediction models is also conducted using graphical methods. In a related evaluation, Ercanli et al. (2023) presented graphs of dominant height growth predictions for five site index values (i.e., 5, 10, 15, 20, 25, and 30 m at base age 100) obtained through both ANN models and a nonlinear mixed effects model with one random parameter (Fig. 1). Upon examination of Figure 1, while biologically consistent estimates of dominant height development are observed in the left corner of the graph (Fig. 1a), the standard feed-forward ANN model - trained with an adaptive learning process without any hyperparameter or regularization parameter specifications - produced predictions that significantly violate and are highly inconsistent with growth

laws and biological realism about dominant tree heights. Ercanli (2024), in a study utilizing Deep Learning Algorithm - a multilayer artificial neural network - to predict individual tree taper using stem diameters outside bark (DOB) and total tree volume (TTV), obtained results highly inconsistent with biological realistic patterns for both characteristics when using a standard DLA model based on adaptive learning (Fig. 2b and 3b). The implementation of optimized DLA architectures—specifically, a hyperparameter-optimized model with 0.8 momentum and seven hidden layers for TTV predictions, and a regularization-optimized model with 1×10^{-6} dropout ratio and three hidden layers for DOB estimations—yielded statistically robust results across both training and validation datasets while preserving biological plausibility in their predictions (Fig 2a and 3a). The predictive outcomes generated by both hyperparameter-optimized and regularization-optimized DLA models for TTV (Fig. 2a) and DOB (Fig. 3a) demonstrate strong adherence to established biological principles governing tree volume and diameter growth patterns in dendrometric science (Avery and Burkhart, 1983; van Laar and Akca, 1997; Pretzsch, 2009).

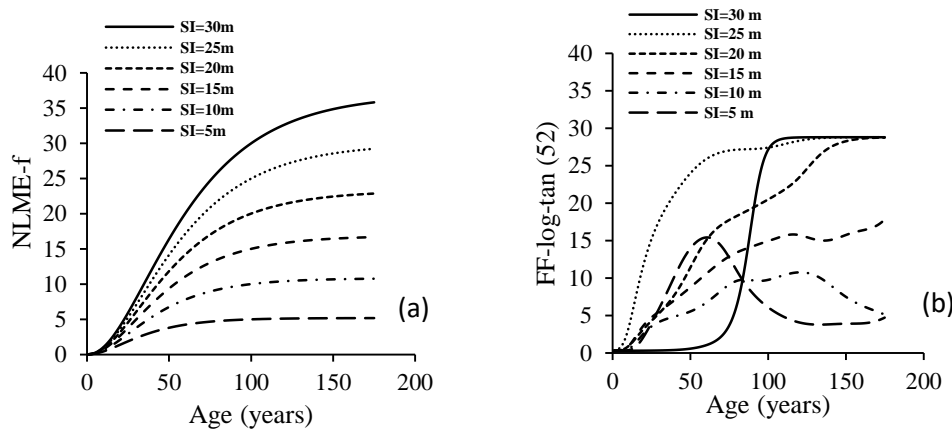


Figure 1. Predicted site index curves for five site index values by Nonlinear mixed effect regression, feed-forward network architectures and ANN with feed forward learning-log-tan of activation functions and 52 number of neurons (Ercanli et. al. 2023)

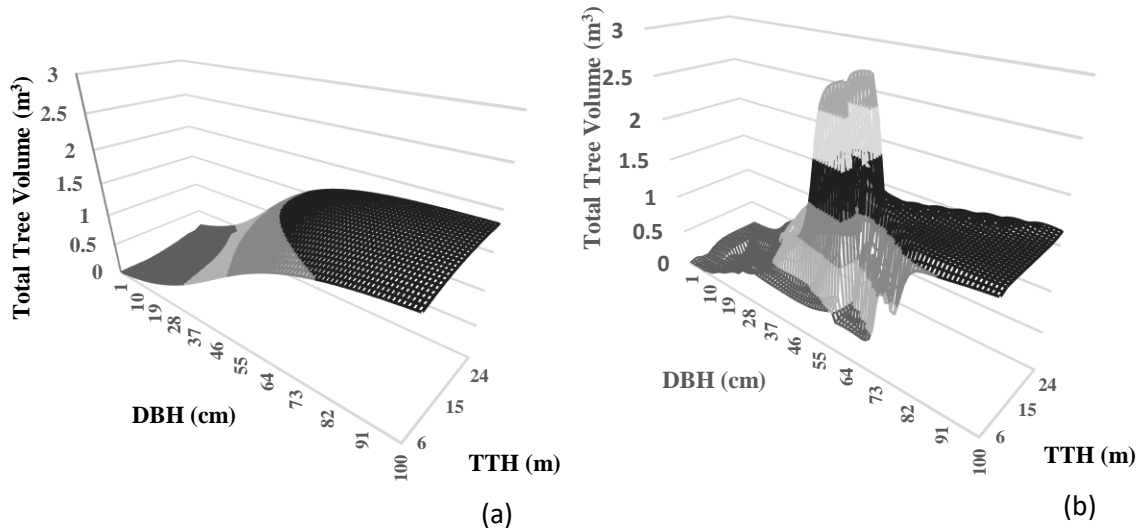


Figure 2. The change of total tree volumes predicted by the best predictive hyper-parametrized DLA (a) and the standard DLA including 10 (b) number of hidden layer and according to DBHs and Total tree height (TTH) (Ercanli, 2024)

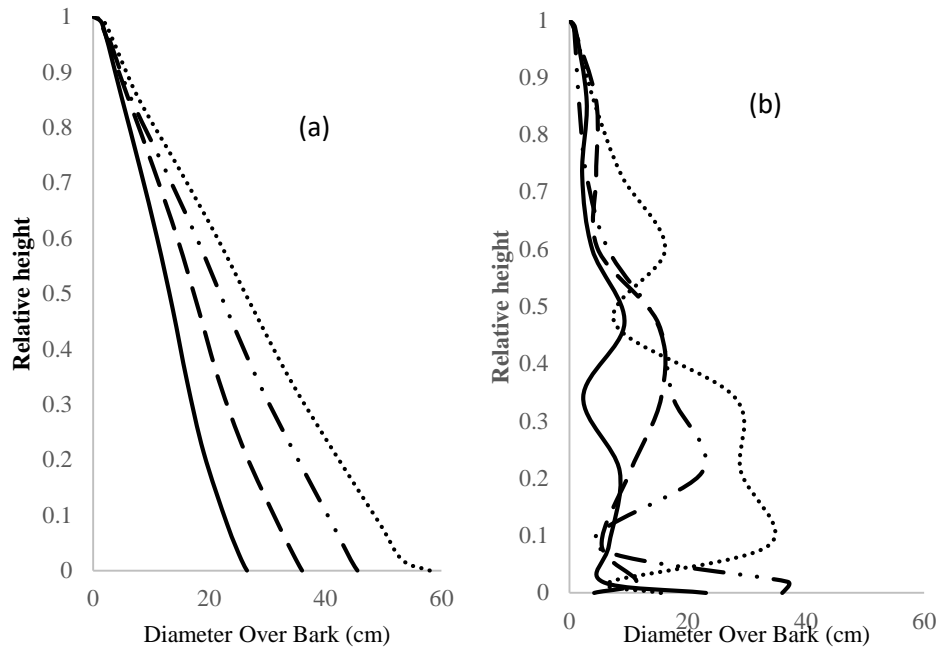


Figure 3. The predicted stem profiles by the Fang et. al (2000)'s taper equation based on NLS (a), CAR (1) (b), the best predictive regularization-optimized DLA and the standard DLA with a 3 # hidden layer (d) (Ercanlı, 2024)

Conclusion

This investigation explores the fundamental question of whether artificial intelligence can be effectively trained to incorporate inherent biological patterns and growth laws of tree development, while providing a systematic assessment of AI model implementations in forestry applications, a distinct branch of natural sciences. Despite artificial intelligence models demonstrating superior performance metrics compared to traditional regression models from statistical science, the evaluation of predictive models in natural sciences, particularly in forestry, extends beyond mere statistical performance criteria. While artificial intelligence models demonstrate remarkable predictive ability through their sophisticated nonlinear fitting capabilities, their training process necessitates consideration of factors beyond conventional adaptive learning approaches, which traditionally focus on minimizing the residuals between observed and predicted values. The employment of hyperparameter-optimized and regularization-optimized DLA models, trained via an innovative methodology incorporating customized network parameters, presents a significant advancement in simultaneously addressing two critical challenges in forest modeling: (i) the statistical issues of overfitting and generalization capacity, and (ii) the maintenance of biological realism in tree and stand attribute predictions. In addressing the fundamental question 'Can artificial intelligence be trained to account for the growth laws and biological patterns inherent in tree growth?', two distinct methodological approaches emerge in the implementation of AI models with DLA for forestry applications:

(i) Adaptive learning-based AI models prone to overfitting, which demonstrate high fidelity to training data but fail to capture underlying biological relationships, essentially resulting in data memorization rather than pattern recognition;

(ii) Advanced DLA implementations incorporating hyperparameter optimization and regularization techniques, characterized by systematic customization of network parameters to enhance model generalization and biological consistency. The optimization-based approach represents a significant advancement in elucidating the 'black-box' nature of these models, enabling the capture of intricate data relationships. Through the systematic implementation of hyperparameter optimization and regularization techniques, these advanced DLA frameworks demonstrate remarkable capacity in maintaining biological fidelity while mitigating overfitting and enhancing generalization capabilities. In this context, the Human-Centered Artificial Intelligence (HCAI) paradigm has been comprehensively conceptualized by Holzinger et al. (2022). The application of this paradigm to forest science represents a symbiotic integration of artificial and natural intelligence. This integration aims to augment, support, and optimize artificial intelligence systems, such as Artificial Neural Networks (ANN) or Deep Learning Algorithms (DLA), with human knowledge and perspective in forest growth and yield predictions. This approach facilitates a synergistic confluence of technological innovation and human experiential expertise. However, the

full potential of DLA applications in forestry science remains to be fully explored as our understanding of its inherent capabilities and limitations continues to advance.

References

- [1] Armstrong, S., Sotala, K., and O. S. Heigeartaigh. 2014. The errors, insights and lessons of famous AI predictions – and what they mean for the future. *J. Exp. Theor. Artif. Intell.* 26: 317-342.
- [2] Ashraf, M.I., Zhao, Z., Bourque, C.P.A, MacLean, D.A., and F.R. Meng. 2013. Integrating biophysical controls in forest growth and yield predictions with artificial intelligence technology. *Can. J. For. Res.* 43: 1162-1171.
- [3] Avery, T.E. and H.E. Burkhardt. 1983. *Forest Measurement*. Third Edition. McGraw-Hill, New York. 331 p.
- [4] Bailey, R. L. and Clutter J. L. 1974. Base-age invariant polymorphic site curves. *Forest Sci* 20: 155–159.
- [5] Brynjolfsson, E. and T. Mitchell. 2015. What can machine learning do? Workforce implications. *Science* 358: 1530–1534.
- [6] Cieszewski, C. J. 2002. Comparing fixed and variable-base-age site equations having single versus multiple asymptotes. *Forest Sci* 48 (1): 7-23.
- [7] Clark, J.F. 1902. Volume tables and the bases on which they may be built. *Forestry* 1: 6–11.
- [8] Diamantopoulou, M.J., Özçelik, R., Crecente-Campo, F. and Ü. Eler. 2015. Estimation of Weibull function parameters for modelling tree diameter distribution using least squares and artificial neural networks methods. *Biosyst. Eng.* 133: 33-45.
- [9] Ercanlı, İ., Bolat, F. and H. Yavuz. 2023. A comparison of artificial neural networks and regression modeling techniques for predicting dominant heights of Oriental spruce in a mixed stand. *Forest Systems*, 32 (1).
- [10] Ercanlı, İ. 2024. Deep learning algorithms for addressing overfitting and biological realism in tree taper and volume predictions, *Can. J. For. Res.* First: 1–19 (2024)
- [11] Goodfellow, I., Bengio, Y. and A. Courville. 2016. *Deep learning*. MIT press.
- [12] Holzinger, A., Saranti, A., Angerschmid, A., Retzlaff, C. O., Gronauer, A., Pejakovic, V., Medel-Jimenez, F., Krexner, T., Gollob, C., K. Stampfer, K. 2022. “Digital transformation in smart farm and forest operations needs human-centered AI: Challenges and future directions.” *Sensors*, 22(8), 3043.
- [13] Lei, Y. and B.R. Parresol. 2001. Remarks on heightdiameter modelling. *Res. Pap. SRS-10*. Asheville, NC: U.S. Department of Agriculture, Forest Service, Southern Research Station. 6p
- [14] Levins, R. 1966. The strategy of model building in population biology. *Am. Sci.* 54(4), 421-431.
- [15] McCorduck, P. 2004. *Machines who think: A personal inquiry into the history and prospects of artificial intelligence* (2nd ed.). CRC Press. 598 p.
- [16] Nilsson, N. J. 2014. *Understanding beliefs*. The MIT Press Essential Knowledge series. 168 p.
- [17] Özçelik, R., Diamantopoulou, M.J., Brooks, J.R. and H.V. Wiant Jr. 2010. Estimating tree bole volume using artificial neural network models for four species in Turkey. *J. Environ. Manage.* 91: 742-753.
- [18] Russell, S., Hauert, S., Altman, R. and M. Veloso. 2015. Ethics of artificial intelligence. *Nature* 521: 415–416.
- [19] Spurr, S.H. 1952. *Forest inventory*. New York: Ronald Press Co. 476 p.
- [20] Taddeo, M. and L. Floridi. 2018. How AI can be a force for good. *Science* 361: 751–752.
- [21] Turing, A., 1950. Computing Machinery and Intelligence. *Mind* 59 (236): 433–60.
- [22] Van Laar A. and A. Akça. 2007. *Forest mensuration*. Springer, Dordrecht, Netherlands, 383 p.



The Effect of Dominant Side on Lower Extremity Flexibility in Adolescent Shooting Athletes

Mahmut BEŞLİ^{1,*}, **Burak ULUSOY**², **Hatice Reyhan BEŞLİ**³, **Dilara ÇAĞLAR**⁴,
Bahar ANAFOROĞLU⁵

¹ Institute of Health Sciences, Ankara Yildirim Beyazıt University, Ankara, Türkiye

² Department of Physical Therapy, Faculty of Health Sciences, Çankiri Karatekin University, Çankiri, Türkiye

³ Sports Physiotherapy, Provincial Directorate of Youth and Sports, Çankiri, Türkiye

⁴ Shooting Coach, Çankiri, Türkiye

⁵ Department of Physical Therapy, Faculty of Health Sciences, Ankara Yildirim Beyazıt University, Ankara, Türkiye

Abstract

Shooting athletes are observed to maintain a static posture for long periods during training and competitions. There are no studies yet examining the effect of the dominant extremity on lower extremity flexibility (LEF) in air rifle shooters (ARS). The purpose of this study was to investigate the effect of the dominant extremity on LEF and the relationship between LEF and core muscle strength (CMS) in ARS. This study included adolescent ARS in Çankiri. The athletes were questioned about their age, height, weight, experience levels, and dominant shooting extremities. They were evaluated using sit-and-reach tests for right and left lower extremities, trunk flexion endurance tests, plank tests, and the Sorensen test. The average age of the athletes was 15 (± 0.51) years. The average BMI was 21.63 (± 1.04) kg/m², and the average duration of shooting experience was 27 (± 6.52) months. The right side was the dominant extremity for all athletes in the study. According to the sit-and-reach test results, the right LEF was greater than the left LEF ($p < 0.001$). No correlation was found between LEF and CMS ($p > 0.05$). The results of this study show that the LEF of the dominant side is greater in ARS, and that LEF is not correlated with CMS. Similar to this study other studies found no correlation between CMS and flexibility in shooting athletes. Research found that the effect of flexibility on shooting success is 34%. It is shown that flexibility plays a crucial role in shooting athletes and can directly affect shooting performance, considering the importance of posture during shooting. Although no relationship was found between LEF and CMS, we suggest that flexibility and strength exercises should be incorporated to improve body symmetry and enhance shooting performance, considering the athletes' young age and relatively short experience.

Keywords: Shooting athletes, Lower extremity flexibility, Core muscle strength, Dominant extremity

1. Introduction

Flexibility is known to be influenced by personal characteristics such as age, gender, and body type, as well as by the specific sport [1]. Some researchers have suggested a negative relationship between flexibility and muscle strength in athletes [2, 3]. However, research does not provide a consensus on the relationship between flexibility and trunk strength in shooting athletes [4, 5]. Yapıcı et al. reported a relationship between flexibility and trunk strength in shooting athletes [6].

Shooting athletes are observed to maintain a static posture for long periods during training and competitions [4, 6]. Air rifle shooters shoot in a position involving head and trunk rotation and lateral flexion and typically do not move much between rounds. The highest level of technical proficiency is required to perform at an elite level. Target stability, postural control, emotional condition, and mental skills are all crucial [7].

There are no studies yet examining the effect of the dominant extremity on lower extremity flexibility in air rifle shooters. The purpose of this study was to investigate the effect of the dominant extremity on lower extremity flexibility and the relationship between lower extremity flexibility and core muscle strength in air rifle shooters.

* Corresponding author. e-mail address: fzt.mahmutbesli@gmail.com

2. Materials and Methods

This study included adolescent air rifle shooters from Çankırı. The athletes' demographic information—age, height, weight, sports experience, and dominant extremity used for shooting—was collected. Body mass index (BMI) was calculated based on height and weight data. In addition to demographic information, lower extremity flexibility and core muscle strength were assessed. The sit-and-reach test was used to evaluate lower extremity flexibility, with measurements taken for both the right and left lower extremities and recorded in centimeters [8]. Core muscle strength was assessed using the trunk flexion endurance test, the right and left side plank tests, and the Sorensen test. Results were recorded in seconds [9]. Examples of the tests are shown in Figure 1.



Figure 1. Examples of the tests. a) Right sit-and-reach test; b) Sorensen test; c) right side plank test; d) trunk flexion endurance test.

Data analysis was performed using SPSS 24.0 (IBM SPSS Statistics for Windows, Version 24.0, IBM Corporation, Armonk, NY, USA). The normality of the data distribution was tested using the Shapiro-Wilk test. Mean and standard deviation values were reported for normally distributed data, while median and interquartile ranges were reported for data that were not normally distributed. Paired sample tests were used for comparisons. Pearson correlation analysis was employed for normally distributed data, while Spearman correlation analysis was used for non-normally distributed data. Statistical significance was accepted as $p \leq 0.05$.

3. Results

The average age of the athletes (8 female, 6 male) was 15 (± 0.51) years. The average BMI was 21.63 (± 1.04) kg/m², and the average sports experience was 27 (± 6.52) months. The right side was the dominant extremity for all athletes in the study. Demographic information of the athletes included in the study is shown in Table 1 and Table 2.

Table 1. Demographics of the athletes included in the study

Demographic Information		Number	Percent
Gender	Female	8	57.2
	Male	6	42.8
Dominant Shooting Extremities	Right	14	100
	Left	0	0

Table 2. Demographics of the athletes included in the study (n=14)

Demographic Information	Mean	Standard Deviation
Age (years)	15.00	0.51
Weight (kg)	59.57	3.05
Height (cm)	166.00	2.26
BMI (kg/m ²)	21.63	1.04
Sports Experience Level	27.00	6.52

cm: centimeter; kg: kilogram; kg/m²: kilogram per square meters; n: number.

The sit-and-reach test results showed that the flexibility of the right lower extremity was 32.79 (± 1.62) cm, while the flexibility of the left lower extremity was 30.18 (± 1.57) cm. The flexibility of both lower extremities was 27.86 (± 1.44) cm. The data for lower extremity flexibility are shown in Table 3.

Table 3. Lower extremity flexibility values (n=14)

Sit and Reach Test	Mean (cm)	Standard Deviation
Both Lower Extremities	27.86	1.44
Right Lower Extremities	32.79	1.62
Left Lower Extremities	30.18	1.57

cm: centimeter; n: number.

The core muscle strength test results showed that the median duration of the trunk flexion endurance test was 69.00 (IQR: 56.75) seconds. The mean duration of the right side plank test was 63.29 (± 12.32) seconds, the mean duration of the left side plank test was 59.79 (± 10.70) seconds, and the mean duration of the Sorensen test was 174.93 (± 28.49) seconds. The core muscle strength results are shown in Table 4.

Table 4. Core Muscle Strength tests values (n=14)

Core Muscle Strength	Mean (sec)	Standard Deviation
Trunk Flexion Endurance Test ¹	94.93	23.49
Right Side Plank Test	63.29	12.32
Left Side Plank Test	59.79	10.70
Sorensen Test	174.93	28.49

n: number; sec: second; ¹: this data were not normal distribution, median: 69.00, interquartile range: 56.75.

In the comparison of the right and left sides, the sit-and-reach test results showed significantly greater flexibility in the right lower extremity compared to the left ($p < 0.0001$). No significant differences were found between the right and left side plank tests ($p > 0.05$). The results of the comparison tests are presented in Table 5.

Table 5. Comparisons of right and left side values (n=14)

	Right Side	Left Side	p-value
Sit-and-Reach Test (cm)	32.79 (± 1.62)	30.18 (± 1.57)	0.000* (t:5.52)
Side Plank Test (sec)	63.29 (± 12.32)	59.79 (± 10.70)	0.730 (t: 0.,45)

cm: centimeter; n: number; p: statistical significance value; sec: second; *: $p < 0.05$, statistically significant.

When evaluating the relationship between flexibility and core muscle strength tests, no significant correlation was found between flexibility and core muscle strength ($p > 0.05$). The correlation table is shown in Table 6.

Table 6. Correlation of lower extremity flexibility and core muscle strength tests value (n=14)

	Trunk Flexion Endurance Test	Right Side Plank Test	Left Side Plank Test	Sorensen Test
Sit-and-Reach Test	p: 0.59 r: 0.15	p: 0.78 r: -0.08	p: 0.77 r: 0.09	p: 0.86 r: 0.05
Right Sit-and- Reach Test	p: 0.38 r: 0.26	p: 0.73 r: -0.10	p: 0.66 r: 0.13	p: 0.73 r: -0.10
Left Sit-and- Reach Test	p: 0.38 r: 0.25	p: 0.74 r: -0.10	p: 0.59 r: 0.16	p: 0.77 r: -0.09

n: number; p: statistical significance value; r: correlation coefficient.

4. Discussion

This study found that the flexibility of the dominant lower extremity was greater in adolescent air rifle shooters, and that lower extremity flexibility did not correlate with core muscle strength. Similar to the study by Akinoğlu et al., no correlation was found between core muscle strength and flexibility in shooting athletes [5]. Diler et al. suggest that flexibility influenced shooting performance [10]. Ertürk et al. found that the effect of flexibility on shooting success was 34% [11]. Although this study did not directly analyze shooting performance, it was clear that flexibility plays an important role in shooting athletes, especially given the static posture required during shooting.

Shooting athletes compete in different disciplines, making it challenging to draw consistent conclusions about trunk performance across these athletes. However, it is reasonable to assume that air rifle shooters and archery athletes share similar characteristics, and comparisons could be drawn between these sports. Research has shown that flexibility and muscle strength tend to be greater in the dominant sides of athletes in various sports [12, 13]. Mair et al. reported that athletes in asymmetric sports have greater range of motion in their dominant extremities [14]. Core muscle strength is important in order to be successful during shooting and to tolerate the reaction force that occurs [15].

Air rifle shooters have the ability to reduce body sway before shooting. This can be achieved by affecting postural control, respiratory control, and pulse decreasing [16]. The organization of trunk muscles, upper extremity muscles, pelvic muscles, and lower extremity muscles becomes important in postural control [17-19]. Trunk muscles, in particular, continue to work actively to maintain body balance against unexpected biomechanical changes [20]. In addition, when we consider the direct relationship between respiratory control and core muscles, it may be expected that core muscles are equally strong. This may explain why the side plank times of the athletes in our study were not affected by the dominant side.

Target stability is important in air rifle shooting [21]. Kocahan et al. reported that different muscle strengths are expected in the upper extremity and related muscles due to the asymmetrical stance in the shooting posture, but the isometric strengths of the shoulder's muscles are similar [22]. During shooting, the stiffness of the pelvic and leg muscles rather than active muscle contraction plays an important role in target stability [23]. We think that

the core muscles are not affected by the dominant extremity due to the importance of postural control, but the flexibility of the lower extremity is affected due to the asymmetrical posture.

This study has several limitations: Postural analysis was not performed on the athletes included in the study. The dominant side of all participants was the right side.

5. Conclusion

Based on the results, we conclude that lower extremity flexibility is influenced by shooting posture and the dominant extremity. Although no correlation was found between lower extremity flexibility and core muscle strength, we recommend incorporating flexibility and strength exercises to improve body symmetry and enhance shooting performance, particularly considering the athletes' young age and limited experience.



References

- [1] Çon M, Akyol P, Tural E, Taşmektepligil MY. Voleybolcuların Esneklik Ve Vücut Yağ Yüzdesi Değerlerinin Dikey Sıçrama Performansına Etkisi. Selçuk Üniversitesi Beden Eğitimi Ve Spor Bilim Dergisi. 2012;14(2):202–7.
- [2] Alonso J, Mchugh MP, Mullaney MJ, Tyler TF. Effect Of Hamstring Flexibility On Isometric Knee Flexion Angle–Torque Relationship. Scand J Med Sci Sports. 2009 Apr 17;19(2):252–6.
- [3] Brockett Cl, Morgan Dl, Proske U. Predicting Hamstring Strain Injury In Elite Athletes. Med Sci Sports Exerc. 2004 Mar;36(3):379–87.
- [4] Peljha Z, Michaelides M, Collins D, Carson H. J. Assessment Of Physical Fitness Parameters In Olympic Clay Target Shooters And Their Relationship With Shooting Performance. Journal Of Physical Education And Sport. 2021;21(6).
- [5] Akınoğlu B, Kocahan T, Ünüvar E, Eroğlu İ, Hasanoğlu A. Investigation Of The Relationship Between Trunk Muscle Strength And Sit And Reach Flexibility In Athletes. Türkiye Klinikleri Journal Of Sports Sciences. 2020;12(1):9–15.
- [6] Yapıcı A, Bacak Ç, Çelik E. Relationship Between Shooting Performance And Motoric Characteristics, Respiratory Function Test Parameters Of The Competing Shooters In The Youth Category. European Journal Of Physical Education And Sport Science [Internet]. 2018;4(10). Available From: [Www.Oapub.Org/Edu](http://www.oapub.org/edu)
- [7] Spancken S, Steingrebe H, Stein T. Factors That Influence Performance In Olympic Air-Rifle And Small-Bore Shooting: A Systematic Review. Plos One. 2021 Mar 31;16(3):E0247353.
- [8] Miyamoto N, Hirata K, Kimura N, Miyamoto-Mikami E. Contributions Of Hamstring Stiffness To Straight-Leg-Raise And Sit-And-Reach Test Scores. Int J Sports Med. 2018 Feb 30;39(02):110–4.
- [9] Elliott TLP, Marshall KS, Lake DA, Wofford NH, Davies GJ. The Effect Of Sitting On Stability Balls On Nonspecific Lower Back Pain, Disability, And Core Endurance. Spine (Phila Pa 1976). 2016 Sep 15;41(18):E1074–80.
- [10] Diler K, Kizilin Mm, Özal M. Havalı Tabanca Atıcılığı Ve Bu Disiplindeki Performans Faktörleri. Rol Spor Bilimleri Dergisi. 2022;1(1):11–26.
- [11] Ertürk C, Can İ, Bayrakdaroglu S. Havalı Tüfek Sporcularının Bazı Fizyolojik Ve Motorik Özelliklerinin Atış Performansları Üzerine Etkisi. Spor Bilimleri Araştırmaları Dergisi. 2022 Dec 31;7(2):281–93.
- [12] Ellenbecker Ts, Roetert Ep, Bailie Ds, Davies Gj, Brown Sw. Glenohumeral Joint Total Rotation Range Of Motion In Elite Tennis Players And Baseball Pitchers. Med Sci Sports Exerc. 2002 Dec;34(12):2052–6.
- [13] Ihalainen S, Kuitunen S, Mononen K, Linnamo V. Determinants Of Elite-Level Air Rifle Shooting Performance. Scand J Med Sci Sports. 2016 Mar 8;26(3):266–74.
- [14] Mair SD, Uhl TL, Robbe RG, Brindle KA. Physseal Changes And Range-Of-Motion Differences In The Dominant Shoulders Of Skeletally Immature Baseball Players. J Shoulder Elbow Surg. 2004 Sep;13(5):487–91.
- [15] Zemková E, Zapletalová L. The Role Of Neuromuscular Control Of Postural And Core Stability In Functional Movement And Athlete Performance. Front Physiol. 2022 Feb 24;13.
- [16] Era P, Konttinen N, Mehto P, Saarela P, Lyytinen H. Postural Stability And Skilled Performance—A Study On Top-Level And Naive Rifle Shooters. J Biomech. 1996 Mar;29(3):301–6.

- [17] Mononen K, Konttinen N, Viitasalo J, Era P. Relationships Between Postural Balance, Rifle Stability And Shooting Accuracy Among Novice Rifle Shooters. *Scand J Med Sci Sports*. 2007 Apr 3;17(2):180–5.
- [18] Tang WT, Zhang WY, Huang CC, Young MS, Hwang IS. Postural Tremor And Control Of The Upper Limb In Air Pistol Shooters. *J Sports Sci*. 2008 Dec 15;26(14):1579–87.
- [19] Wojtków M, Korcz K, Szotek S. Assessment Of Body Posture And Feet Load Distribution In Sport Shooters. *Curr Probl Biomech*. 2016;(10):91–8.
- [20] Horak FB, Nashner LM. Central Programming Of Postural Movements: Adaptation To Altered Support-Surface Configurations. *J Neurophysiol*. 1986 Jun 1;55(6):1369–81.
- [21] Ihalainen S, Linnamo V, Mononen K, Kuitunen S. Relation Of Elite Rifle Shooters' Technique-Test Measures To Competition Performance. *Int J Sports Physiol Perform*. 2016 Jul;11(5):671–7.
- [22] Kocahan T, Akınoğlu B, Ünüvar E, Hasanoğlu A. Comparison Of Shoulder Joint Isometric Muscle Strength And Joint Position Sense Of Trigger Arm And Opposite Arm In Air Pistol Shooting Athletes. *Turkiye Klinikleri Journal Of Sports Sciences*. 2018;10(3):116–22.
- [23] Day BL, Steiger MJ, Thompson PD, Marsden CD. Effect Of Vision And Stance Width On Human Body Motion When Standing: Implications For Afferent Control Of Lateral Sway. *J Physiol*. 1993 Sep;469(1):479–99.



Use of Probability Density Functions to Predict Diameter Distributions in Forestry

Muammer ŞENYURT^{1,*} , İlker ERCANLI¹ 

¹ Forest Faculty, Forest Engineering Department, Çankırı Karatekin University, Çankırı, Türkiye

Abstract

This study discusses the role of diameter distribution models in providing more detailed insights into forest stand structures, essential for sustainable forest management and product determination. Traditional yield tables used in forestry provide stand-level predictions for growth and yield but lack specificity at finer scales like diameter classes. The paper highlights that, especially in Turkey, inventory studies for forest planning do not produce data detailed enough to fully support sustainable forestry practices. Diameter distribution models, using probability density functions, allow for the estimation of stand components, such as tree count, basal area, and volume, by diameter classes.

By integrating stand models with diameter distribution models, it becomes possible to derive more granular predictions that can benefit forestry applications, including forest management and silviculture. These models enable enhanced accuracy in predicting stand structure variations, which in turn supports planning for a broader array of forest products. The study emphasizes that the implementation of diameter distribution models can help mitigate current limitations in sustainable forestry efforts by enabling data from inventory studies to be analyzed at the diameter step level. As a result, this modeling approach offers a valuable foundation for forest management activities, aligning forestry practices with sustainability goals.

Keywords: Probability density function, Diameter distribution, Model

1. Introduction

The forest is a life community formed by a combination of forest soil and an array of vegetation, including trees, shrubs, herbaceous plants, mosses, ferns, and fungi of specific heights, structures, and densities, which collectively establish a unique climate over a broad area. This ecosystem is further enriched by microorganisms living both above and below the soil, as well as various insects and animals (Aytuğ, 1976). Forests serve as habitats not only for humankind but for all terrestrial living beings. In this regard, making optimal use of the services and values forests provide, while ensuring the integrity of the ecosystem and the sustainability of these areas, is achievable through their planned management. The consistency of such plans and the selection of an effective and systematic management approach depend on the quantification of the products and services offered by forests, as well as the modeling of the data obtained (Başkent & Keleş, 2004; Bolat, 2014).

Information about the increment and growth potential of forests, as well as stand structures, and the relationships between stand structures and site productivity, age, density, and species composition, is crucial for forest planning (Yavuz et al., 2002). Stand structures are defined by the distribution of trees within diameter classes in a stand, and the current and future diameter distributions provide a critical knowledge base, especially for forest management practices (Maltoma, 1997). Determining the variety of products that can be derived from forests depends on estimating the diameter distributions of stands, and this information is essential for effective forest planning (Rennols et al., 1985; Borders & Patterson, 1990; Laar & Akça, 2007).

Vanclay (1994), as well as Gadow and Hui (1999), defined models in the context of forestry science as systems of equations that estimate the growth and yield values of stands under various conditions. Burkhart (1995) and Garcia (2001) further described the applications of these estimates in forestry, including the evaluation of silvicultural treatment options, updating inventory data, and determining the timber yield obtainable from stands.

In the development process of models, which have a history of over 200 years in forestry, there are two primary types: empirical growth models and process-based (ecologically-based) growth models (Porté & Bartelink, 2002). Empirical growth models predict growth and yield elements for individual trees or stands using statistical functions (allometric relationships) that incorporate various tree and stand variables (Burkhart, 1997). Based on

* Corresponding author. e-mail address: msenyurt@karatekin.edu.tr

the unit used in modeling, empirical models are categorized into three types: Whole-Stand Models, Size-Class Models, and Individual-Tree Models (Mısır, 2003).

Diameter distribution models, which are part of size-class models, are widely used in forestry at the stand level. Compared to the other two model classes (whole-stand and individual-tree models), diameter distribution models offer several advantages: they provide insights into stand structure, include information at the diameter class level, and offer data that can be readily obtained from general forestry inventories. These models also provide information on the variety of products that can be derived from a stand, making them valuable for detailed stand-level information in forestry.

The need for predictions at the diameter class or diameter step level, rather than just at the stand level, has driven extensive research on diameter distribution models. Early studies include Gram's work in 1883, which modeled the diameter distribution of beech stands using a Normal distribution, and De Liocourt's 1898 study, which applied an Exponential distribution to the diameter distributions of uneven-aged stands. However, interest in modeling diameter distributions intensified particularly in the 1960s, when probability density functions (pdfs), a key concept in statistics, began to be applied for modeling diameter distributions in forestry (Packard, 2000).

This study provides information on probability density functions used in diameter distribution modeling, a significant area in forestry. Additionally, it briefly outlines the evaluation processes used to assess the effectiveness of these functions in modeling diameter distributions.

2. Probability Density Functions

Probability density functions are statistical functions that estimate the frequency value corresponding to a specific observed diameter as a ratio of the total number of individuals in the population from which the data were measured, yielding estimates between 0 and 1 (Bailey & Dell, 1973). Various researchers have developed different methods for modeling diameter distributions. For instance, the Johnson SB function was introduced by Johnson (1949), the Weibull function by Weibull (1951), the Gamma function by Nelson (1964), the Log-normal function by Bliss and Reineker (1964), and the Beta function by Clutter and Bennet (1965). Numerous studies have since used these functions to model diameter distributions (Bailey & Dell, 1973; Smalley & Bailey, 1974; Haffley & Schreuder, 1977; Rennols et al., 1985; Knoebel et al., 1986; Pukkala et al., 1990; Saramaki, 1992; Maltamo et al., 1995; Maltamo, 1997; Packard, 2000; Liu et al., 2004; Palahi et al., 2006; Podlaski, 2006; Nord-Larsen & Cao, 2006; Palahi et al., 2007).

In forestry, various probability density functions are used to model the distribution of trees within diameter classes in a stand, including the Normal (Bailey, 1980), Lognormal (Bliss & Reinker, 1964), Gamma (Nelson, 1964), Beta (Clutter & Bennet, 1965; Zöhrer, 1969), Johnson's SB (Johnson, 1949), and Weibull distributions (Weibull, 1951; Bailey & Dell, 1973) (Ercanlı & Yavuz, 2010). However, recent studies have highlighted the prominence of the 3-parameter Weibull distribution and 4-parameters Johnson SP. These probability density functions, with its flexible 3 and 4 parameters structure, have proven particularly effective in modeling diverse diameter distributions.

In addition to the traditional and widely recognized probability density functions (PDFs) such as the Gamma, Beta, Weibull, and Johnson's SB functions, statistical science has introduced other distribution functions, including the Laplace, Rayleigh, Nakagami, Lévy, Rice, and Kumaraswamy distributions (Michalowicz et al., 2013). The Rice distribution, applicable to positive real numbers, is closely related to several well-known distributions such as Chi-Square, Normal, Log-Normal, and Rayleigh (Jiang et al., 2018). The Rayleigh distribution is a specific case of the 2-parameter Weibull distribution, named after the English physicist Lord Rayleigh (Aslam et al., 2015). Emerging in 1960, the Nakagami distribution is relatively recent and is widely applied to model right-skewed, positive data sets (Akgül & Şenoğlu, 2023). The Lévy distribution is notable for its continuous, stable properties for non-negative random variables (Knopova & Schilling, 2013; Yousof et al., 2022). The Laplace distribution, one of the oldest known distributions, is unimodal and symmetric with a sharper peak than the Normal distribution (Liu & Kozubowski, 2015). Lastly, Kumaraswamy's distribution shares many properties with the Beta distribution but offers advantages in tractability and applicability to a range of natural phenomena, as it is a versatile PDF for double-bounded random processes (El-Sagheer, 2019). The structural models of the probability density functions mentioned are presented in Table 1 (Şahin and Ercanlı, 2023).

Table 1. Various PDFs for modelling diameter distributions (Şahin and Ercanlı, 2023)

No.	Distribution	Density function	Parameters
1	Gamma (3P)	$f(x) = \frac{(x - \gamma)^{\alpha-1}}{\beta^\alpha \Gamma(\alpha)} \exp(-(x - \gamma)/\beta)$	α : continuous shape parameter ($\alpha > 0$) β : continuous scale parameter ($\beta > 0$) γ : continuous location parameter Γ : Gamma function $\gamma \leq x < +\infty$
2	Johnson's S _B (4P)	$f(x) = \frac{\delta}{\lambda\sqrt{2\pi} z(1-z)} \exp\left(-\frac{1}{2}\left(\gamma + \delta \ln\left(\frac{z}{1-z}\right)\right)^2\right)$	γ, δ : continuous shape parameters ($\delta > 0$) λ : continuous scale parameter ($\lambda > 0$) ξ : continuous location parameter $\xi \leq x \leq \xi + \lambda$
3	Kumaraswamy (4P)	$f(x) = \frac{\alpha_1 \alpha_2 z^{\alpha_1-1} (1-z)^{\alpha_2-1}}{(b-a)}$	α_1, α_2 : continuous shape parameters ($\alpha_1, \alpha_2 > 0$) a, b : continuous boundary parameters ($a < b$) $a \leq x \leq b$
4	Laplace (2P)	$f(x) = \frac{\lambda}{2} \exp(-\lambda x - \mu)$	λ : continuous inverse scale parameter ($\lambda > 0$) μ : continuous location parameter $-\infty < x < +\infty$
5	Lévy (1P)	$f(x) = \sqrt{\frac{\sigma}{2\pi}} \frac{\exp(-0.5\sigma/x)}{(x - \gamma)^{3/2}}$	σ : continuous scale parameter ($\sigma > 0$)
6	Lévy (2P)	$f(x) = \sqrt{\frac{\sigma}{2\pi}} \frac{\exp(-0.5\sigma/(x - \gamma))}{(x - \gamma)^{3/2}}$	γ : continuous location parameter ($\gamma \equiv 0$ yields the one-parameter Lévy distribution) $\gamma < x < +\infty$
7	Lognormal (2P)	$f(x) = \frac{\exp\left(-\frac{1}{2}\left(\frac{\ln x - \mu}{\sigma}\right)^2\right)}{x\sigma\sqrt{2\pi}}$	σ and μ : continuous parameters ($\sigma > 0$)
8	Lognormal (3P)	$f(x) = \frac{\exp\left[-\frac{1}{2}\left(\frac{\ln(x-\gamma)-\mu}{\sigma}\right)^2\right]}{(x - \gamma)\sigma\sqrt{2\pi}}$	γ : continuous location parameter ($\gamma \equiv 0$ yields the two-parameter Lognormal distribution) $\gamma < x < +\infty$
9	Nakagami (2P)	$f(x) = \frac{2m^m}{\Gamma(m)\Omega^m} x^{2m-1} \exp\left(-\frac{m}{\Omega} x^2\right)$	m : continuous parameter ($m \geq 0.5$) Ω : continuous parameter ($\Omega > 0$) $0 \leq x < +\infty$
10	Normal (2P)	$f(x) = \frac{\exp\left(-\frac{1}{2}\left(\frac{x-\mu}{\sigma}\right)^2\right)}{\sigma\sqrt{2\pi}}$	σ : continuous scale parameter ($\sigma > 0$) μ : continuous location parameter $-\infty < x < +\infty$
11	Rayleigh (1P)	$f(x) = \frac{x}{\sigma^2} \exp\left(-\frac{1}{2}\left(\frac{x}{\sigma}\right)^2\right)$	σ : continuous scale parameter ($\sigma > 0$)
12	Rice (2P)	$f(x) = \frac{x}{\sigma^2} \exp\left(\frac{-(x^2 + v^2)}{2\sigma^2}\right) I_0\left(\frac{xv}{\sigma^2}\right)$	v, σ : continuous parameters ($v \geq 0; \sigma > 0$) I_0 : modified Bessel function of the first kind of zero $0 \leq x < +\infty$
13	Weibull (2P)	$f(x) = \frac{\alpha}{\beta} \left(\frac{x}{\beta}\right)^{\alpha-1} \exp\left[-\left(\frac{x}{\beta}\right)^\alpha\right]$	α : continuous shape parameter ($\alpha > 0$) β : continuous scale parameter ($\beta > 0$)
14	Weibull (3P)	$f(x) = \frac{\alpha}{\beta} \left(\frac{x - \gamma}{\beta}\right)^{\alpha-1} \exp\left(-\left(\frac{x - \gamma}{\beta}\right)^\alpha\right)$	γ : continuous location parameter ($\gamma \equiv 0$ yields the two-parameter Weibull distribution) $\gamma \leq x < +\infty$

* x is the tree diameter here

In forestry, various methods are used to estimate the parameters of the probability density functions (given in Table 1), which is widely applied in modeling diameter distributions. These methods include: (i) Nonlinear Regression Analysis, (ii) Maximum Likelihood Estimation, (iii) Moment-Based Parameter Recovery, and (iv) Percentile-Based Parameter Recovery. In this study, percentile-based equations, which provide a simple, practical, and effective approach, and the maximum likelihood method were employed for modeling diameter distributions (Knowe 1992, Bailey et al. 1989, Knowe et al. 1997, Liu et al. 2004, Cao 2004, Poduel 2011, Poduel and Cao 2013). The most used method, Maximum Likelihood Estimation (MLE), is based on the similarity between diameter classes obtained from measured diameter values in the field and those estimated by the model (Bailey

and Dell 1973, Borders et al. 1987). Estimating the parameters of probability density functions through MLE requires numerical solution techniques involving various iterations (Harter and Moore 1965). To apply MLE and estimate parameters, the likelihood function must be maximized. Statistical software such as SPSS, SAS, and R are commonly used for this purpose.

3. Conclusion

Diameter distribution models are essential for obtaining more detailed predictions about stand structures and determining the variety of products that can be derived from forests. In our country, yield tables based on normal and density-dependent estimates are currently used for predicting growth and yield, although these tables provide estimations for the stand as a whole. However, the need for more detailed predictions regarding stand structures is becoming increasingly apparent, especially in forest management and various forestry activities. Probability density functions and density-dependent yield tables allow for the estimation of the distribution of stand components—such as tree count, basal area, and volume—across diameter classes. By integrating stand and diameter distribution models, more detailed predictions can thus be obtained. Once the distribution of tree counts by diameter classes is achieved, the distributions of basal area and volume can also be derived using the tree count distributions. Diameter distribution models enable more detailed estimations of stand components, initially obtained for the entire stand, to be achieved at the level of diameter classes. These predictions, obtained with greater detail at the diameter class scale, form a valuable basis for various forestry applications, especially for forest management and silviculture.

Diameter distribution models enable predictions (such as stand volume, basal area, and tree count) provided by stand models and yield tables, typically at the whole-stand level, to be obtained in greater detail at the diameter class and step levels. This approach facilitates more precise predictions about stand structures and allows for a more accurate determination of the types of products that can be obtained from forests. In our country, Normal Yield Tables and Density-Dependent Yield Tables are used to predict growth and yield, providing estimations for the stand as a whole. However, the need for more detailed stand structure predictions is increasingly felt, especially in forest management and other forestry activities. The lack of detailed data obtained from inventory studies conducted for planning purposes in our country presents constraints on sustainable forestry practices. By enabling data obtained from inventory studies to be estimated at the diameter step level, diameter distribution models help alleviate some of these limitations in sustainable forestry efforts.

References

- [1] Akgül, F. G., & Şenoğlu, B. (2023). Comparison of wind speed distributions: a case study for Aegean coast of Turkey. *Energy Sources, Part A: Recovery, Utilization, and Environmental Effects*, 45(1), 2453-2470.
- [2] Aslam, M., Tahir, M., Hussain, Z., & Al-Zahrani, B. (2015). A 3-component mixture of Rayleigh distributions: properties and estimation in Bayesian framework. *PloS one*, 10(5), e0126183.
- [3] Aytuğ, B. (1976). Orman tanımlaması ve bu tanımlamada yer alan ağaç, ağaççık ve çalı kavramları. *I. Orman Kadastro Semineri*, OGM Yayın No: 607/13, Ankara
- [4] Bailey, R. L., & Dell, T. R. (1973). Quantifying diameter distributions with the Weibull function. *Forest science*, 19(2), 97-104.
- [5] Bailey, R. L. (1980). Individual tree growth derived from diameter distribution models. *Forest Science*, 26(4), 626-632.
- [6] Bailey, R. L., Burgan, T. M., & Jokela, E. J. (1989). Fertilized midrotation-aged slash pine plantations—stand structure and yield prediction models. *Southern Journal of Applied Forestry*, 13(2), 76-80.
- [7] Başkent, E. Z., & Keleş, S., (2004). Ormancılıkta Model ve Modelleme Kavramlarının Kullanımı ve Genel Değerlendirmesi, *Orman Mühendisliği Dergisi* , vol.41, 19-24.
- [8] Bliss, C. I., & Reinker, K. A. (1964). A lognormal approach to diameter distributions in even-aged stands. *Forest Science*, 10(3), 350-360.
- [9] Borders, B.E., Souter, R.A., Bailey, R.L. & Ware, K.D. 1987. Percentile based distributions characterize forest tables. *Forest Science*, 33(2); 570-576.
- [10] Burkhart, H. 1995. Modeling forest growth. *Encyclopedia of Environmental Biology*, (2); 535-543.
- [11] Burkhart, H. E. (1997). Development of empirical growth and yield models. *Empirical and process-based models for forest tree and stand growth simulation*. Lisboa: Salamandra, 53-60.

- [12] Cao, Q. V. (2004). Predicting parameters of a Weibull function for modeling diameter distribution. *Forest science*, 50(5), 682-685.
- [13] Clutter, J. L., & Bennett, F. A. (1965). Diameter distributions in old-field slash pine plantations.
- [14] EL-Sagheer, R. M. (2019). Estimating the parameters of Kumaraswamy distribution using progressively censored data. *Journal of Testing and Evaluation*, 47(2), 905-926.
- [15] Ercanlı, İ., & Yavuz, H. (2010). Doğu ladini (*Picea Orientalis* (L.) Link)-Sarıçam (*Pinus Sylvestris* L.) karışık meşcerelerinde çap dağılımlarının olasılık yoğunluk fonksiyonları ile belirlenmesi. *Kastamonu University Journal of Forestry Faculty*, 10(1), 68-83.
- [16] Gadown, K.V. & Hui, G.Y. 1999. Modeling forest development. *Kluwer Academic Publishers*, 213 p., Netherlands.
- [17] Garcia, O. (2001). Growth & Yield in British Columbia Background and discussion.
- [18] Hafley, W. L., & Schreuder, H. T. (1977). Statistical distributions for fitting diameter and height data in even-aged stands. *Canadian Journal of Forest Research*, 7(3), 481-487.
- [19] Johnson, N. L. (1949). Systems of frequency curves generated by methods of translation. *Biometrika*, 36(1/2), 149-176.
- [20] Jiang, K., Chen, X., Zhu, Q., Chen, L., Xu, D., & Chen, B. (2018). A novel simulation model for nonstationary rice fading channels. *Wireless Communications and Mobile Computing*, 2018(1), 8086073.
- [21] Knoebel, B. R., Burkhart, H. E., & Beck, D. E. (1986). A growth and yield model for thinned stands of yellow-poplar. *Forest Science*, 32(suppl_2), a0001-z0002.
- [22] Knopova, V., & Schilling, R. L. (2013, January). A note on the existence of transition probability densities of Lévy processes. In *Forum Mathematicum* (Vol. 25, No. 1, pp. 125-149). Walter de Gruyter GmbH.
- [23] Knowe, S. A. (1992). Basal area and diameter distribution models for loblolly pine plantations with hardwood competition in the Piedmont and Upper Coastal Plain. *Southern Journal of Applied Forestry*, 16(2), 93-98.
- [24] Knowe, S. A., Ahrens, G. R., & DeBell, D. S. (1997). Comparison of diameter-distribution-prediction, stand-table-projection, and individual-tree-growth modeling approaches for young red alder plantations. *Forest Ecology and Management*, 98(1), 49-60.
- [25] Liu, C., Zhang, S. Y., Lei, Y., Newton, P. F., & Zhang, L. (2004). Evaluation of three methods for predicting diameter distributions of black spruce (*Picea mariana*) plantations in central Canada. *Canadian Journal of Forest Research*, 34(12), 2424-2432.
- [26] Liu, Y., & Kozubowski, T. J. (2015). A folded Laplace distribution. *Journal of Statistical Distributions and Applications*, 2, 1-17.
- [27] Maltamo, M., Puumalainen, J., & Päivinen, R. (1995). Comparison of beta and Weibull functions for modelling basal area diameter distribution in stands of *Pinus sylvestris* and *Picea abies*. *Scandinavian Journal of Forest Research*, 10(1-4), 284-295.
- [28] Maltamo, M. 1997. Comparing basal area diameter distributions estimated by tree species and for the entire growing stocks in mixed stand. *Silva Fennica*, 31(1); 53-65.
- [29] Michalowicz, J. V., Nichols, J. M., & Bucholtz, F. (2013). *Handbook of differential entropy*. Crc Press.
- [30] Misir, N. (2003). *Karaçam ağaçlandırmalarına ilişkin büyüme modelleri* (Doctoral dissertation, Doktora Tezi, Karadeniz Teknik Üniversitesi, Fen Bilimleri Enstitüsü, Trabzon).
- [31] Nelson, T. C. (1964). Diameter distribution and growth of loblolly pine. *Forest Science*, 10(1), 105-114.
- [32] Nord-Larsen, T., & Cao, Q. V. (2006). A diameter distribution model for even-aged beech in Denmark. *Forest ecology and management*, 231(1-3), 218-225.
- [33] Packard, K. C. (2000). *Modeling tree diameter distributions for mixed-species conifer forests in the Northeast United States*. State University of New York College of Environmental Science and Forestry.
- [34] Palahí, M., Pukkala, T., & Trasobares, A. (2007). Calibrating predicted tree diameter distributions in Catalonia, Spain. *Silva Fennica*, 40(3), 487.
- [35] Podlaski, R. (2006). Suitability of the selected statistical distributions for fitting diameter data in distinguished development stages and phases of near-natural mixed forests in the Świętokrzyski National Park (Poland). *Forest Ecology and Management*, 236(2-3), 393-402.
- [36] Poudel, K. P., & Cao, Q. V. (2013). Evaluation of methods to predict Weibull parameters for characterizing diameter distributions. *Forest Science*, 59(2), 243-252.
- [37] Porte, A., & Bartelink, H. H. (2002). Modelling mixed forest growth: a review of models for forest management. *Ecological modelling*, 150(1-2), 141-188.

- [38] Pukkala, T., Saramäki, J., & Mubita, O. (1990). Management planning system for tree plantations. A case study for *Pinus kesiya*. *Silva Fennica*, 24(2), 171-180.
- [39] Rennolls, K., Geary, D.N. & Rollinson, T.J.D. 1985. Characterizing diameter distributions by the use of the Weibull distributions. *Forestry*, 58(1); 57-66.
- [40] Samaraki, J. (1992). A growth and yield prediction model of *pinus kesiya* in zambia. *Acta Forestalia Fennica*, 230, 68.
- [41] Smalley, G. W. (1974). *Yield tables and stand structure for shortleaf pine plantations in Tennessee, Alabama, and Georgia highlands* (Vol. 97). Southern Forest Experiment Station, Forest Service, US Department of Agriculture.
- [42] Şahin, A., & Ercanli, I. (2023). An evaluation of various probability density functions for predicting diameter distributions in pure and mixed-species stands in Türkiye. *Forest systems*, 32(3), 2.
- [43] Van Laar, A. & Akça, A. (2007). *Forest mensuration* (Vol. 13). Springer Science & Business Media.
- [44] Vanclay, J.K. 1994. Modelling forest growth: Applications to mixed tropical forests. *CAB International, Department of Economics and Natural Resource*, Royal Veterinary and Agricultural University, 312 p., Copenhagen, Denmark.
- [45] Weibull, W. (1951). A statistical distribution function of wide applicability. *Journal of applied mechanics*.
- [46] Yavuz, H., Gül, A.U., Mısır, N., Özçelik, R. & Sakıcı, O.E. 2002. Meşcerelerde çap dağılımının düzenlenmesi ve bu dağılımlara ilişkin parametreler ile çeşitli meşcere öğeleri arasındaki ilişkilerin belirlenmesi. *Orman Amenajmanı'nda Yeni Kavramsal Açılımlar ve Yeni Hedefler Sempozyumu*, 2012, İstanbul.
- [47] Yousof, H. M., Korkmaz, M. C., Hamedani, G. G., & Ibrahim, M. (2022). A novel Chen extension: Theory, characterizations and different estimation methods. *European Journal of Statistics*, 2, 1-1.
- [48] Zöhrer, F. (1969). Ausgleich von Häufigkeitsverteilungen mit hilfe der beta-funktion. *Forstarchiv*, 40(3), 37-42.



Meeting Common Area Energy Needs in Multi-Dwelling Buildings with Photovoltaic (PV) Panels: Design and Calculations

Baran ARAS^{1,*}, **Çağatay ERSİN²**

¹Vocational School, Electrical and Energy, Çankırı Karatekin University, Çankırı, Türkiye

² Vocational School, Electronics and Automation Department, Çankırı Karatekin University, Çankırı, Türkiye

Abstract

In recent years, PV (photovoltaic) electricity generation has been installed especially on the roof areas of newly meeting the energy consumption of independent housing sections is not preferred very often due to insufficient roof space. However, the use of roof space for common areas of housing is frequently preferred. Increasing energy unit prices, together constructed buildings; in order to meet the energy consumption for common areas. In multi-storey residential buildings, with the necessity of electric vehicle charging station systems in parking areas, have increased the energy costs of common areas of housing. Although PV energy systems are suitable for increasing energy costs, the installation cost of PV systems is also high. For this reason, it is inevitable that calculations and designs for PV systems should be made with high precision accuracy. In this study, the design of photovoltaic (PV) electricity energy systems for multi-storey residential buildings is discussed. The installed power and demand power calculations, which are mandatory in the project preparation stages of the buildings, were made on the basis of the electric power table in the common areas and the necessary calculations were performed. In line with the demand power calculations, the energy power, number of panels, inverter capacity, cable sections of the PV system were calculated and a 2D design was created in the AutoCAD program. Then, the connection elements of the designed PV system to the main distribution panel inside the building were calculated and integrated into the design. As a result, the applicability of PV electrical energy systems in common areas of multi-storey residential buildings was demonstrated. The use of such systems has great potential in terms of environmentally friendly energy production and low energy costs. In addition, it will contribute to energy efficiency in future building projects by providing an important step towards sustainable energy solutions. In the future, equipping more buildings with such systems will be an important development in terms of energy independence and environmental sustainability.

Keywords: 2D Desing, AutoCAD, Demand Power, Photovoltaic(PV), Power Calculate, Sustainable Energy

1. Introduction

In line with sustainable energy solutions, the necessity of environmentally friendly and low-energy-cost structures has become inevitable, considering current energy production and consumption costs. Consequently, the integration of renewable energy resources into buildings with structural features has been made mandatory during construction phases in many countries by governmental regulations. Türkiye is one of these countries [1]. According to the [1], at least 5% of the energy consumed in all buildings with an area of 5,000 square meters or more must be sourced from renewable energy resources. Suitable land for the installation of renewable energy systems is essential. High-rise buildings are predominantly located in urban areas and have limited available space. These areas are often insufficient for setting up renewable energy systems. Roof spaces, however, are the most suitable area for buildings. For this reason, solar energy systems, which are easy to integrate and install on roofs, are commonly preferred [2]. In buildings with multiple independent units, it is not possible to install a solar energy system capable of meeting the entire building's energy needs due to insufficient roof space. For mandatory renewable energy system installation, it is more likely that the energy consumption of the building's common areas will be met. According to the [3], electric vehicle charging stations have been made mandatory in building parking lots. With this requirement, the energy demand and consumption costs of the building's common areas have increased [4]. This has made the use of renewable energy systems, supported by current laws, inevitable. Although the installation of photovoltaic (PV) systems, referred to as solar energy systems, is easy, they are costly. At the same time, it is important that these PV energy systems meet the required power output [5, 6]. Therefore, the integration requirements of PV energy systems should be determined through calculations and models with high precision and accuracy. This study presents the calculations and 2D model drawings for the required PV energy system to meet the common area energy consumption in buildings with multiple independent

* Corresponding author. e-mail address: baranaras@karatekin.edu.tr

units, using a sample structure as an example. The aim is to create a model project that can be applied to all buildings within the framework of relevant laws and regulations.

2. Materials and Methods

The characteristics of the example building model with multiple independent units are provided in Table 1.

Table 1. Characteristics of the example building model.

Feature	Number
Houses	20
Workplace	0
Common Area	1
Lift	1
EVCS	1

The electrical power characteristics of the example model building are provided in Table 2 and Table 3. The electrical characteristics of the independent units (houses) in the building have been equivalently planned. According to the [7], The power of the dedicated lines is fixed, and the characteristics of the socket, lighting, and other power lines are determined based on their specifications.

Table 2. The electrical power distributions of the houses in the example building model.

Consumption Type	Power(W)
Boiler	150
Oven	2000
Dishwasher	2500
Washing Machine	2500
Electrical Socket	3600
Lamp	250
Total	11000

Table 3. The electrical power distributions of the common area in the example building model.

Consumption Type	Power(W)
EVCS	7500
Lift	8600
Hydrophore	1000
Water Pump	1500
Electrical Socket	3600
Multiswitch	250
Intercom	300
Shelter room	2000
Lamp	750
Fire systems	500
Total	26000

The powers provided in Table 2 and Table 3 are the installed power values. It is necessary to calculate the demand power. Subsequently, a building's simultaneous demand power calculation should be create [7, 8]. Bir dairenin talep güç hesabı;

$$\text{Demand Power} = ((\text{Installed Power}-8000) \times 0,4) + (8000 \times 0,6) \quad (1)$$

$$\text{Demand Power} = ((11000-8000) \times 0,4) + (8000 \times 0,6) = 6000W \text{ is found.}$$

Lift Demand Power;

$$\text{Demand Power} = \text{Installed Power} \times 0,55 \quad (2)$$

$$\text{Demand Power} = 8600 \times 0,55 = 4730W \text{ is found.}$$

The installed powers of all other common area electrical loads are assumed to be equal to the demand power. In this case, the demand power of the common area with an installed power of 26000 W is determined as 22130 W. Using the calculated installed power and demand power values, the building's simultaneous power table is created in Table 4.

Table 4. Power distribution table of the example building model.

Power Type	Power(W)	Explanation
Installed Power	11000	1 House
Demand Power	6000	1 House
Installed Power	26000	Common Area
Demand Power	22130	Common Area
Installed Power	220000	20 House(11000×20)
Demand Power	120000	20 House(6000×20)
Installed Power	246000	All Building(220000+26000)

The installed power of 246000 W is determined according to the building's estimated simultaneous demand power. Using the simultaneous demand power calculation, the selection and implementation of the building's electrical materials are made [7, 8]. The building's simultaneous demand power, with the power values in Table 4, is determined by multiplying the demand power of the houses by the simultaneity factor constant, and then adding the common area demand power to this value [7]. In this case;

$$\text{Simultaneous Demand Power} = (\text{Demand Power}_{(20 \text{ House})} \times 0,39) + \text{Demand Power}_{(\text{Common Area})} \quad (3)$$

$\text{Simultaneous Demand Power} = (120000 \times 0,39) + 22130 = 68930$ is found.

The power value of the PV energy system, which needs to be determined for the building's simultaneous demand power, is calculated based on the desired minimum 5% threshold in the structures; The minimum required installed PV system power should be 3446.5 We. The calculated power values of PV systems are based on high-efficiency conditions. However, since it is not possible to consistently maintain the highest efficiency conditions, the systems need to have power exceeding the We value. In this study, the Wp value has been taken 15% higher than the We value. In this case, the power of the installed PV energy system is approximately 4000 We. Electrical calculations for solar panels and inverters in PV energy systems with 4 kWe power are necessary for the correct integration of the system. The series and parallel string connections of the solar panels are the most important factors determining the current and voltage values. Although the series or parallel connection of the panels does not affect the power value, it is crucial for system performance. Considering all these factors, the electrical characteristics of the proposed solar panels and inverter are shown in Table 5.

Table 5. Electrical characteristics of solar panels and inverters.

PV Module and Inverter Information	
Panel Module Type	Polycrystalline
Panel P _{mpp}	400 Wp
Panel Power Tolerance	0-5
Panel V _{oc}	49,56V
Panel I _{sc}	11,23 A
Panel V _{mpp}	42,75 V
Panel I _{mpp}	10,53A
Inverter Output Power	4 kWe
Inverter Max. DC Input Voltage	1000 V
Inver Min. DC Voltage	100 V
Inverter Max. Output Current	10 A
Inverter Output Voltage	230 V/400 V

According to the electrical data in Table 5, 10 solar panels can meet the required 4 kWp/3.5 kWe power. However, it is not enough for only the power to be compatible. The other electrical characteristics must also be analyzed to determine whether they are suitable for the system's efficient operation. The important parameters for the compatibility analysis are as follows: the current-voltage values at the panel output should not exceed the inverter input values according to the number of panels; the DC voltage from the panels should be above the inverter's

minimum operating voltage; the inverter output voltage should not exceed the targeted kWe value; and the inverter output current should not exceed the maximum output current. If these parameters are met, the applicability of the model will be ensured.

3. Results and Discussion

The series-parallel string numbers and configurations of 10 solar panels with 400 Wp power must fall between the inverter's minimum DC voltage level of 100 V and the maximum DC input voltage level of 1000 V. To minimize system energy losses, it is desired that the current value remains as low as possible. In this case, if it is suitable to connect all 10 panels in series, the use of parallel strings is not recommended.

$$FV \text{ System Output Voltage} = \text{Number of Panels} \times V_{oc} \quad (4)$$

$$FV \text{ System Output Voltage} = 10 \times 49,56 = 495,6 \text{ V} < 1000 \text{ V}, 495,6 \text{ V} > 100 \text{ V}, 495,6 \text{ V} \text{ is suitable.}$$

The 100 V – 1000 V range may vary for each inverter; however, this value applies to a single MPPT (Maximum Power Point Tracker) input of the inverter. Based on the example model, it is assumed that only one MPPT is used. If desired, multiple MPPT inputs can also be utilized. Regardless of the input power of an inverter, its output power will match its rated output. In other words, the AC power obtained from the PV system at the We level will be 3.5 kWe in this case. Additionally, since the panels are connected in series, the current value remains below the 40-50 A level, making it suitable to use 6 mm² solar cables for interconnections. Based on the data obtained in the study, the 2D roof model drawing of the PV energy system in the AutoCAD environment is shown as a top view in Figure 1.

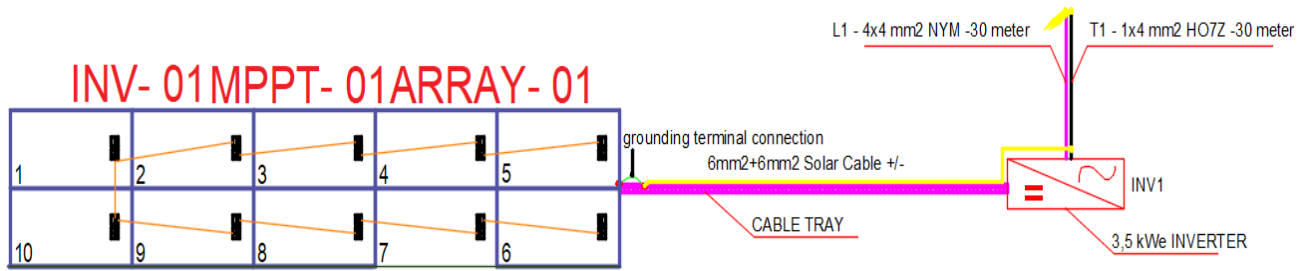


Figure 1. The 2D drawing of the designed PV energy system.

Conclusion

An example of a multi-story building with many independent units was considered. Electrical power calculations for the building were made in light of current regulations, laws, and research. Based on the power calculations, the requirements for a PV energy system that can be installed on the roof to meet the energy needs of the common areas were specified, and calculations were made to meet these requirements. Finally, the design of the 2D single-line diagram for the PV energy system was prepared. As a result, we believe that this model, which includes the necessary calculations for the design of PV energy systems in the rapidly developing construction sector, the parameters that need to be considered in the design, and the basic 2D project representation, can be easily adapted to all similar projects.

References

- [1] R. Gazete, "Binalarda Enerji Performansı Yönetmeliği'nde Değişiklik Yapılmasına Dair Yönetmelik," Erişim adresi: <https://www.resmigazete.gov.tr/eskiler/2022/02/20220219-2.htm> ve <https://www.mevzuat.gov.tr/File/GeneratePdf>, 2022.
- [2] B. Matpay, "Coğrafi bakımdan güneş enerji santrali (GES) için uygun yerlerin belirlenmesi: Van ili örneği," *Türk Coğrafya Dergisi*, no. 85, pp. 7-19, 2024.
- [3] R. Gazete, "Otopark Yönetmeliğinde Değişiklik Yapılmasına Dair Yönetmelik," ed: Madde, 2006.

- [4] M. U. Nawaz, M. S. Qureshi, and S. Umar, "Integration of Solar Energy Systems with Electric Vehicle Charging Infrastructure: Challenges and opportunity," *Revista Espanola de Documentacion Cientifica*, vol. 18, no. 02, pp. 1-18, 2024.
- [5] R. Foster, M. Ghassemi, and A. Cota, Solar energy: renewable energy and the environment. *CRC press*, 2009.
- [6] C. G. Granqvist, "Solar energy materials," *Advanced Materials*, vol. 15, no. 21, pp. 1789-1803, 2003.
- [7] R. Gazete, "ELEKTRİK İÇ TESİSLERİ YÖNETMELİĞİ, Resmî Gazete Tarihi: 04.11. 1984 Resmî Gazete Sayısı: 18565," ed, 1984.
- [8] M. F. Yapıcıoğlu, H. H. Sayan, and H. Terzioğlu, "Karabük ilindeki alçak gerilim dağıtım sistemlerinde elektrik tüketiminin analizi," *Avrupa Bilim ve Teknoloji Dergisi*, pp. 411-417, 2019.



Influence of Additives on Calcium Sulfate Crystal Size and Morphology

***Ghassan MUTTAR JASSEM JASSEM*¹** , ***Muhammed Bora AKIN*^{2,*}** 

¹ The Ministry of Industry and Minerals, General Company for Engineering Industries, Nassiriyh, Iraq

² Faculty of Engineering, Department of Chemical Engineering, Çankırı Karatekin University, Çankırı, Türkiye

Abstract

In this study, the effects of additives on the crystal size and morphology of calcium sulfate were examined through a literature review, and the findings were compiled and evaluated. It is well-known that the properties of calcium sulfate vary significantly due to the influence of various additives during its crystallization from solution, thereby altering its performance in various industrial and scientific applications. Studies in the literature investigate the effects of additives such as surfactants and polymers on the nucleation and growth mechanisms of calcium sulfate crystals. Notably, significant changes in crystal morphology are observed depending on the chemical structure of the additives. The knowledge gained from this review contributes to the production of calcium sulfate crystals with desired properties and the optimization of related processes.

Keywords: *Crystallization, Calcium Sulfate, Additive*

1. Introduction

Calcium sulfate is a compound with significant industrial and scientific relevance due to its diverse applications, ranging from construction materials to medical products. Its crystallization properties, including mechanical strength, thermal resistance, and solubility, are heavily influenced by crystal size and morphology, which are determined by the crystallization conditions and the presence of additives. The role of additives in modifying the crystallization pathways of calcium sulfate is well-documented, affecting both nucleation and growth mechanisms, thereby enhancing the performance of calcium sulfate in various applications [1-3].

Additives such as surfactants and polymers have been shown to exhibit distinct effects on the nucleation and growth mechanisms of calcium sulfate crystals. For instance, the addition of polyacrylic acid (PAA) has been found to significantly retard the transformation of amorphous calcium sulfate to calcium sulfate hemihydrate and ultimately to gypsum, providing insights into the mechanisms of these transformations [1]. Similarly, the use of reverse microemulsions has been demonstrated to control the morphology of α -calcium sulfate hemihydrate, highlighting the importance of the chemical nature and concentration of additives in determining crystal characteristics [2]. Furthermore, carboxylic acids have been observed to adsorb onto the crystal surfaces, potentially preventing crystal growth and leading to habit modification [4, 5].

The crystallization of calcium sulfate is also influenced by the presence of impurities and metal ions, which can alter the kinetics of the crystallization process. Studies have shown that the incorporation of certain ions can interfere with the crystal lattice arrangement, thereby affecting the growth rates and final morphology of the crystals [6]. For example, the presence of strontium ions has been reported to influence the crystallization kinetics of calcium sulfate dihydrate and hemihydrate, demonstrating the complex interplay between additives and crystallization dynamics [6]. Additionally, the crystallization conditions, such as supersaturation levels and temperature, play a crucial role in determining the phase stability and morphology of calcium sulfate crystals [7].

2. The Effect of Additives on Crystallization Processes

The crystallization of calcium sulfate, whether in its dihydrate (gypsum), hemihydrate, or anhydrite form, is a complex process influenced by supersaturation levels, solution pH, temperature, and the presence of additives. Among these factors, additives have drawn significant attention for their ability to control crystal nucleation, growth, and morphology. Table 1 illustrates the diverse effects of various additives on the crystallization of calcium sulfate.

* Corresponding author. e-mail address: mbakin@karatekin.edu.tr

Table 1. Effects of Additives on the Crystallization Behavior of Calcium Sulfate

Additive	Effect on Crystallization	References
Polyacrylic Acid	Retards the transformation from amorphous calcium sulfate to hemihydrate and gypsum; alters crystal aggregation.	[1]
Microemulsions	Control crystal morphology by adjusting droplet sizes, influencing reactant exchange.	[2]
Strontium Ions	Alters crystal lattice arrangement, affecting the morphology and growth rates of dihydrate and hemihydrate crystals.	[6]
Surfactants	Alter nucleation and growth mechanisms, providing tailored crystal sizes and shapes.	[7]
Sodium Ions	Reduces surface tension, promotes crystallization, and increases the average diameter of fine crystals.	[14]
Cefazolin	Changes crystal morphology from needle-like to block structures, affecting compressive strength.	[15]
Impurities	Modify nucleation kinetics and crystal morphology through selective adsorption on crystal surfaces.	[16, 17]
Aluminum Ions	Affects the transformation rate of α -calcium sulfate hemihydrate and alters crystal dimensions.	[18]
Trimesic Acid	Modifies crystallization kinetics and reduces mineral formation on production devices.	[19]
Carboxylic Acids	Inhibit nucleation and growth, causing changes in crystal morphology and filtration properties.	[5, 19]
Poly(sodium 4-styrenesulfonate)	Modifies BET specific surface area and pore size distribution of CaSO_4 after calcination.	[20, 21]
Conductive Copolymers (VPA-based)	Inhibit spontaneous precipitation of $\text{CaSO}_4 \cdot 2\text{H}_2\text{O}$, increasing induction time and reducing crystallization rate.	[22]
Tetraphosphonates	Act as effective retardants, increasing induction time and reducing the crystallization rate of $\text{CaSO}_4 \cdot 2\text{H}_2\text{O}$.	[23]

Additives influence the thermodynamics and kinetics of calcium sulfate crystallization by modifying the nucleation energy barriers and altering the growth dynamics. Lioliou et al. investigated the role of water-soluble polymers in calcium sulfate precipitation and observed that the polymers interact with specific crystallographic planes, inhibiting growth in certain directions and leading to morphological modifications [8]. Similarly, Feldmann and Demopoulos demonstrated that strong ionic interactions between additives and calcium ions significantly reduce the supersaturation required for nucleation, enhancing the control over crystal size and shape [9].

Studies by Liu and Nancollas explored the growth kinetics of calcium sulfate dihydrate in the presence of various additives. They found that organophosphorus compounds selectively adsorb on the crystal surfaces, leading to anisotropic growth and altered aspect ratios [10]. This behavior underscores the potential of additives in engineering crystals with desired geometric features.

Surfactants, with their amphiphilic nature, play a dual role in calcium sulfate crystallization. Anionic surfactants like sodium dodecyl sulfate (SDS) exhibit strong interactions with calcium ions, leading to the formation of stable complexes that hinder nucleation. Hamdona and Al Hadad reported that increasing the concentration of SDS results in smaller and more uniform crystals, beneficial for applications requiring precise control over particle size distribution [11]. Surfactants also influence the surface energy of specific crystal planes, thereby directing the growth patterns to achieve unique morphologies.

Polymers such as polyacrylic acid and polyethylene glycol have been widely studied for their ability to influence calcium sulfate crystallization. Rabizadeh et al. demonstrated that these polymers adsorb preferentially on high-energy sites of crystal surfaces, slowing down growth in specific directions and resulting in more equant morphologies [12]. The molecular weight and charge density of polymers are critical factors determining their

efficacy as crystal modifiers. For instance, higher molecular weight polymers create stronger steric barriers, further restricting growth and enhancing morphological control.

The implications of additive-induced modifications in calcium sulfate crystallization are profound in industries such as construction, pharmaceuticals, and water treatment. For example, Mao et al. conducted a study combining experimental techniques and molecular dynamics simulations to show that specific additives stabilize calcium sulfate hemihydrate in aqueous solutions, an essential property for producing construction materials like drywall [13]. Similarly, Wang and Meldrum reported that magnesium ions and certain organic molecules effectively inhibit calcium sulfate scaling in pipelines, a critical challenge in water treatment systems [1].

The use of additives in the crystallization of calcium sulfate significantly influences the morphology, size, and overall properties of the resulting crystals. The following table summarizes various additives, their effects on calcium sulfate crystallization, and relevant findings from the literature.

Carboxylic acids, for instance, have been shown to inhibit nucleation and growth, which can lead to significant changes in the morphology and filtration characteristics of the crystals produced [4, 5]. Polyacrylic acid (PAA) specifically retards the transformation from amorphous calcium sulfate to its more stable forms, thereby influencing the aggregation of crystals [1].

Moreover, the presence of metal ions such as strontium and sodium can significantly affect the crystallization process by altering the crystal lattice and promoting growth, respectively [6, 14]. The incorporation of surfactants and microemulsions has also been noted to control crystal morphology through modifications in the crystallization environment [2, 7].

The table also provides insights into the impact of various additives on the crystallization behavior of calcium sulfate (CaSO_4). Poly(sodium 4-styrenesulfonate) has been shown to modify the BET specific surface area and pore size distribution of CaSO_4 upon calcination, highlighting its potential in tailoring material properties for specific industrial applications [20], [21]. Conductive copolymers, particularly those based on vinylphosphonic acid (VPA), inhibit the spontaneous precipitation of $\text{CaSO}_4 \cdot 2\text{H}_2\text{O}$ by increasing the induction time and reducing the crystallization rate, thereby providing control over the scaling process in aqueous systems [22]. Similarly, tetraphosphonates, such as EDTMP and HDTMP, serve as highly effective retardants, further delaying the onset of crystallization and reducing the rate at which $\text{CaSO}_4 \cdot 2\text{H}_2\text{O}$ forms [23].

Understanding these interactions is crucial for optimizing the production processes of calcium sulfate in various industrial applications, as the choice of additive can lead to tailored properties that enhance performance in specific contexts.

3. Conclusion

This study provides a comprehensive review of the impact of additives on the crystallization of calcium sulfate, highlighting their role in influencing crystal size, morphology, and growth mechanisms. Additives such as surfactants and polymers interact with calcium sulfate crystals at a molecular level, altering their nucleation and growth pathways. These interactions are governed by the chemical structure, concentration, and specific adsorption characteristics of the additives.

The findings underscore the potential of using tailored additives to engineer calcium sulfate crystals with desired properties for specific applications. For instance, controlling crystal size and morphology can optimize the performance of calcium sulfate in construction materials, medical implants, and water treatment systems. Future research should focus on elucidating the molecular mechanisms underlying additive-crystal interactions and exploring environmentally friendly additives to enhance the sustainability of calcium sulfate production processes.

References

- [1] Y. Wang and F. Meldrum, "Additives stabilize calcium sulfate hemihydrate (bassanite) in solution," *Journal of Materials Chemistry*, vol. 22, no. 41, p. 22055, 2012. DOI: 10.1039/c2jm34087a.
- [2] B. Kong, B. Guan, M. Yates, and Z. Wu, "Control of α -calcium sulfate hemihydrate morphology using reverse microemulsions," *Langmuir*, vol. 28, no. 40, pp. 14137–14142, 2012. DOI: 10.1021/la302459z.

- [3] Y. Du, L. Chen, X. Zhao, and X. Wang, "Crystallization of calcium sulfate hemihydrate in the presence of sodium dodecyl sulfate," *Crystal Growth & Design*, vol. 14, no. 5, pp. 2205–2214, 2014.
- [4] S. Polat, "Characterization and kinetics of calcium sulfate dihydrate crystallization in the presence of trimesic acid," *Asia-Pacific Journal of Chemical Engineering*, vol. 12, no. 3, pp. 391–399, 2017. DOI: 10.1002/apj.2081.
- [5] T. Rabizadeh, C. Peacock, and L. Benning, "Carboxylic acids: Effective inhibitors for calcium sulfate precipitation?" *Mineralogical Magazine*, vol. 78, no. 6, pp. 1465–1472, 2014. DOI: 10.1180/minmag.2014.078.6.13.
- [6] T. Feldmann and G. Demopoulos, "Influence of impurities on crystallization kinetics of calcium sulfate dihydrate and hemihydrate in strong HCl-CaCl₂ solutions," *Industrial & Engineering Chemistry Research*, vol. 52, no. 19, pp. 6540–6549, 2013. DOI: 10.1021/ie302933v.
- [7] H. Fu, B. Guan, G. Jiang, M. Yates, and Z. Wu, "Effect of supersaturation on competitive nucleation of CaSO₄ phases in a concentrated CaCl₂ solution," *Crystal Growth & Design*, vol. 12, no. 3, pp. 1388–1394, 2012. DOI: 10.1021/cg201493w.
- [8] M.G. Lioliou, C.A. Paraskeva, P.G. Koutsoukos, "Calcium sulfate precipitation in the presence of water-soluble polymers," *Journal of Colloid and Interface Science*, vol. 294, pp. 419–426, 2006. DOI: 10.1016/j.jcis.2006.07.074
- [9] T. Feldmann, G.P. Demopoulos, "Effects of crystal habit modifiers on the morphology of calcium sulfate dihydrate grown in strong CaCl₂-HCl solutions," *Journal of Chemical Technology & Biotechnology*, vol. 89, no. 1, pp. 103–110, 2014. DOI: 10.1002/jctb.4231
- [10] S.T. Liu, G.H. Nancollas, "The crystal growth of calcium sulfate dihydrate in the presence of additives," *Journal of Colloid and Interface Science*, vol. 44, no. 2, pp. 422–429, 1973. DOI: 10.1016/0021-9797(73)90318-4
- [11] S.K. Hamdona, U.A. Al Hadad, "Crystallization of calcium sulfate dihydrate in the presence of some metal ions," *Journal of Crystal Growth*, vol. 308, no. 1, pp. 105–114, 2007. DOI: 10.1016/j.jcrysgro.2006.11.227
- [12] T. Rabizadeh, T.M. Stawski, D.J. Morgan, "The effects of inorganic additives on the nucleation and growth kinetics of calcium sulfate dihydrate crystals," *Crystal Growth & Design*, vol. 17, no. 5, pp. 2489–2499, 2017. DOI: 10.1021/acs.cgd.6b01441
- [13] X. Mao, X. Song, G. Lu, Y. Xu, Y. Sun, J. Yu, "Effect of additives on the morphology of calcium sulfate hemihydrate: Experimental and molecular dynamics simulation studies," *Chemical Engineering Journal*, vol. 264, pp. 349–357, 2015. DOI: 10.1016/j.cej.2014.11.073
- [14] X. Liu et al., "Recovery of tungsten in the process of preparation of calcium sulfate whiskers from scheelite decomposed residue," *ACS Sustainable Chemistry & Engineering*, vol. 10, no. 39, pp. 13194–13204, 2022. DOI: 10.1021/acssuschemeng.2c04787.
- [15] C. Chiang, W. Chang, Y. Shih, F. Lin, C. Wu, and K. Yang, "An assessment of physical properties and the viability of osteoblast-like cells of cefazolin-impregnated calcium sulfate bone-void filler," *Journal of Biomedical Materials Research Part B Applied Biomaterials*, vol. 111, no. 2, pp. 382–391, 2022. DOI: 10.1002/jbm.b.35157.
- [16] B. Guan, L. Yang, and Z. Wu, "Effect of Mg²⁺ ions on the nucleation kinetics of calcium sulfate in concentrated calcium chloride solutions," *Industrial & Engineering Chemistry Research*, vol. 49, no. 12, pp. 5569–5574, 2010. DOI: 10.1021/ie902022b.
- [17] X. Mao, X. Song, G. Lu, Y. Sun, Y. Xu, and J. Yu, "Effects of metal ions on crystal morphology and size of calcium sulfate whiskers in aqueous HCl solutions," *Industrial & Engineering Chemistry Research*, vol. 53, no. 45, pp. 17625–17635, 2014. DOI: 10.1021/ie5030134.
- [18] Y. Feng, R. Guo, and Z. Lin, "Effect of aluminum sulfate and succinic acid on the growth law of α -calcium sulfate hemihydrate under microwave irradiation," *Advances in Materials Science and Engineering*, vol. 2021, no. 1, 2021. DOI: 10.1155/2021/6630638.
- [19] S. Polat, "Determination of the effects of carboxylic acids on calcium sulfate dihydrate crystallization," *Chemical Engineering & Technology*, vol. 40, no. 7, pp. 1354–1361, 2017. DOI: 10.1002/ceat.201600525.
- [20] M. Uğur, M. B. Akın, and M. M. Kocakerim, "Investigation of specific surface area and pore size distribution changes of CaSO₄ in the presence of poly (sodium 4-styrenesulfonate)," in *Proceedings of the International Congress on Engineering and Life Science (ICELIS)*, Kastamonu, Turkey, Apr. 2018.

- [21] M. Uğur, Ö. D. Aydeniz, M. M. Kocakerim, and M. B. Akın, “Investigation of fractal dimension change in synthesized CaSO_4 using PSSS,” *Journal of Physical Chemistry and Functional Materials*, vol. 1, no. 1, pp. 66–72, 2018. Available: <http://dergipark.gov.tr/jphcfum>.
- [22] Ö. Dogan, C. S. Erdemir, E. Akyol, S. Kirboga, and M. Öner, “Effect of conductive copolymers on scale formation of gypsum,” *Pure and Applied Chemistry*, Dec. 2016. DOI: 10.1515/pac-2016-0810
- [23] E. Akyol, M. Öner, E. Barouda, and K. D. Demadis, “Systematic structural determinants of the effects of tetraphosphonates on gypsum crystallization,” *Crystal Growth & Design*, vol. 9, no. 11, pp. 5145–5154, Nov. 2009. DOI: 10.1021/cg9007205.



Integration of Gas Chromatography Mass Spectrometry Analysis of Phytochemicals in *Ziziphus jujuba* Targeting Multidrug Resistant *Shigella* species Complemented by Molecular Docking Study

Ahmed ALSHARKSI¹ , Adam MUSTAPHA² , Serhat SIREKBASAN³ and Tuğba GÜRKÖK TAN⁴

¹ Department of Biology, Faculty of Sciences, Cankiri Karatekin University, Çankırı, Turkey

² Department of Microbiology, Faculty of Life Sciences, University of Maiduguri, Borno State, Nigeria.

³ Department of Medical Laboratory Techniques, Eldivan Vocational School of Health Services, Cankiri Karatekin University, Çankırı, Turkey

⁴ Department of Field Crops, Food and Agriculture Vocational School, Cankiri Karatekin University, Çankırı, Turkey,

Abstract

Antibiotic resistance emerging at the rate that surpass the development of new class of antibiotic. This study was conducted to explore the antimicrobial activity of *Ziziphus jujuba* extract against multi-drug resistant *Shigella* species. In-vitro antibacterial activity was assayed using agar diffusion technique. Total biochemical profile of the extract was screen using Gas Chromatography Mass Spectroscopy (GC-MS) analysis. In silico molecular docking was employed to determine activities of the compounds against PDB ID: 1x7i and the binding energies identified the potency of the compounds. The results demonstrated significant inhibitory effects using methanol solvent their 7.00mm at 25ml/dl, 7.00mm at 50ml/dl, 71.00mm at 75ml/dl and 20.00mm at 100ml/dl respectively. The result obtain from on the docking results CID-537118 had the best binding of -7.89kcal/mol and was analyze to interact with 1 hydrogen bond each with Lys32, (distance = 2.84Å). Likewise, CID-12760132 possess the binding affinity of -7.31kcal/mol interacting 2 hydrogen bonds with Lys32 (distance = 3.02Å) and Ser10 with (distance = 2.56Å), CID-56634694 has a binding energy of -7.30kcal/mol which interact with RNA dependent RNA polymerase via 2 hydrogen bond with Lys32 (distance = 2.98Å) and Ser10 with (distance = 2.55Å), Compound with Pubchem I.D of CID-101771, has binding energy of -7.25 kcal/mol and was examined to interact with via 2 hydrogen bond with Tyr228(distance =2.47Å) and Lys32 (distance =2.89Å). Compound with Pubchem I.D of CID-537118, has binding energy of -7.29 kcal/mol and was examined to interact with via 1 hydrogen bond with Tyr228 (distance =2.88Å). Compound with Pubchem I.D of CID-985, has binding energy of -5.00 kcal/mol and was examined to interact with via 1 hydrogen bond with Lys32 (distance =2.84Å) and Lys32 (distance =2.89Å). The results underscore the potential of *Ziziphus jujuba* as a potential source of source of bioactive compound with antibacterial activity and could be considered as an alternative therapeutic strategies and candidate for drug development.

Keywords: Multidrug resistant, *Ziziphus jujube*, *Shigella*, Molecular docking, In-vitro evaluation.

1. Introduction

A major adversity for the mortality and morbidity amongst humans and animals are infectious diseases [1]. Antibiotics serve the main basis for the therapy of microbial infections, since the discovery of these antibiotics and their uses as chemotherapeutic agents there was a belief in the medical order that this would lead to the ultimate eradication of infectious diseases [2]. However, this headway is challenged by one of the 21st global challenge; antibiotic resistance and decline in development of novel antimicrobial agent [2].

Medicinal plants have been rich sources of bioactive compounds and been employed in the treatment of many infection in history [3]. Previous studies revealed the application of plants as source of bioactive compounds with antibacterial activities and have been recognized as promising in the process of drug discovery [4-7]. In fact, the use of medicinal plant have been recognized by World Health Organization (WHO) as widely used in many parts of the world in the treatment of many diseases [4]. Mustapha et al., [5] investigated the antibacterial activity of *Lawsonia inermis* Linn against multidrug resistant *Klebsiella pneumoniae*, and, Adeniyi et al., [6] confirmed the biological activities of plants found in certain regions of Ghana. In another review, plants such as *Matricaria*

* Corresponding author. e-mail address: t.gurkok@karatekin.edu.tr

recutita L. *Hypericum perforatum* L. *Equisetum arvense* L. have exhibited wide range of antibacterial activity against pathogens [7].

Ziziphus jujube Mill, is a plant in a member of Rhamnaceae, and it is described as a medium-sized with seeds and fruit and has been widely used as medicine and food globally [8]. The plant is indigenous to many parts of the world and has been used for medicinal and nutritional purposes [9-11]. *Z. jujuba* is a home to many phytochemicals including amino acids, alkaloids, calcium, cardiac glycoside, flavonoids, lipids, phosphate, potassium, protein, saponins, sugar, tannin, and terpenoids [12-14]. There is concern for the increase trends of antibiotic resistance by *Shigella* spp to important lines of treatments such as third-generation cephalosporins (TGC), azithromycin and fluoroquinolones, [15, 16]

The discovery and development of new drugs design is a time-consuming and costly process, there is need for two phased search of potential bioactive compounds [17]. The aim of this study is to identify the chemical composition of *Ziziphus mauritiana* and investigated the antibacterial activity of *Z. mauritiana* against multi-drug resistant *Shigella* spp using in-vitro and in-silico studies.

2. Materials and Methods

2.1. Bacterial Isolates

Shigella isolates were obtained from the Department of Microbiology, Faculty of Life Sciences, University of Maiduguri, Nigeria. Standard Microbiological and biochemical methods were used to phenotypically identify and characterize the *Shigella* isolates as described by Cheesbrough [18].

2.2. Phytochemical Plants Extraction

Fresh leaves of *Ziziphus jujube* M. were collected within Maiduguri Metropolis, Nigeria and taken to the Department of Botany, University of Maiduguri, Nigeria, and processed for preliminary phytochemical screening. Three solvents were used Methanol, Chloroform and Distilled water according to Gul et al., [19].

2.3. GC-MS Analysis

Gas Chromatography Mass Spectroscopy was used according to Idris et al. [20] Identification of chemical compounds relied on retention time from Gas Chromatography, and mass spectra were matched with the National Institute of Standards and Technology database.

2.4. Antibacterial activity of *Ziziphus jujube*

The agar well diffusion method was employed to determine the antibacterial activities of *Ziziphus jujube* M. extracts Mueller–Hinton agar (MHA) plates using 25, 50, 75 and 100 mg/mL concentrations. These plates were incubated at 37 °C for 24 h, followed by the measurement of the zones of inhibition in millimeters using a Vernier caliper. Each antibiotic underwent testing in triplicates over four days, and the averages were calculated (mean ± standard deviation).

2.5. Preparation of Crystal of Ix7i

In this study, the Ix7i crystal structure complex, involving GDP and 9PC ligands (PDB ID: Ix7i), was sourced from the Protein Data Bank (PDB) as per the work by Berman et al., 2000. Following acquisition, the associated ligands were excised, the structure underwent a comprehensive cleanup process. Finally, the protein structure was optimized, and its energy was computed utilizing a specific program integrated into SwissPDViewer [21].

2.6. Molecular docking

This study selected compounds with specific physicochemical properties for docking investigations. AutoDock 4.2, an extension of the Python Molecular Viewer, was employed for these docking studies. In this process, the torsion bonds and side chains of the ligands were allowed to rotate freely, while Ix7i remained rigid. The binding energy of the protein–ligand complex was calculated using the formula by Hariono et al. [23].

2.7. Pharmacokinetic Analysis

Following the docking studies, compounds exhibiting favorable binding energies were subjected to a secondary screening. This screening focused on evaluating their pharmacokinetic properties, encompassing absorption, distribution, metabolism, and excretion (ADME), to ensure their viability as potential drug candidates. Pharmacokinetic Screening: Tools Used include the AdmetSAR tool and ADME/TOX program. Toxicity

Assessment: Additionally, the toxicity of each identified compound was assessed to ascertain their safety profile. Tools Used include the DataWarrior tool, AdmetSAR tool and ADME/TOX program (<http://lmmd.ecust.edu.cn/admetSar3/>).

3. Results and Discussion

In the current study, the results of the phytochemical analysis were presented in table 1. Flavonoid, saponins and volatile oil were not detected and cardial glycoside only found in distilled water as solvent. The presence of some secondary metabolites could attribute to the antibacterial activity of the plant.

Table 1. Phytochemical Analysis of *using different Ziziphus jujuba* solvent

S/No.	Phytochemical Constituents	Methanol	Chloroform
1	Flavonoid	-	-
2	Saponins	-	-
3	Alkaloid	+	+
4	Volatile Oil test	-	-
5	Steroid	+	-
6	Tannin	+	+
7	Cardial glycoside	-	-

(-) indicate the absence, while
(+) indicate the presence

The results of the GC-MS analysis revealed the different constituents of the phytochemicals, including their compound names, chemical formula, peak value and retention time. The compounds identified from GC-MS analysis revealed different molecular weight (MW) ranging from 142 to 524 in the 39 compounds detected.

3.1. Antibacterial activity of *Ziziphus jujube*

The result of the antibacterial activity of the extracts of *Z. jujube* against *Shigella* ranging from 7.00-20.00mm for Methanol and 7.00-11.00 mm for Chloroform.

3.2. Pharmacokinetic analysis and Docking score

A molecular docking analysis was carried out on the twelve compounds to evaluate their binding energies with the *Shigella* protein (**Ix7i**). The molecular docking revealed free binding energies ranging from -0.00 kcal/mol to +8.07 kcal/mol.

Ziziphus jujuba a susceptibility testing was conducted in the research aiming to identify chemical compounds in, with potential drug activity against multidrug-resistant *Shigella*. Fresh leaves were collected, air-dried, and extracted using methanol and ethanol. The methanol extract exhibited a significant inhibition zone of 7.00mm at 25mg/dl, 7.00mm at 50mg/dl, 17.00mm at 75mg/dl and 20.00mm at 100 mg/dl concentrations. While in chloroform solvent the extract showed inhibition zone at 25 mg/dl, 50 mg/dl, 75mg/dl and 100mg/dl, and 7.00mm, 8.00mm, 10.00mm and 11.00mm respectively. This reveals the potential antibacterial effect of the plants against the bacterial isolates and could be attributed to the phytochemicals embedded.

The totals of 39 compounds were obtained from GC-MS analysis of *Ziziphus jujuba*, compounds were further filtered based on their physiochemical properties according to **Christopher A. Lipinski's rule of five or Pfizer's rule of five (Molecular weight (≤ 500), Number of HBA (≤ 10), Number of HBD (≤ 5), MolLogP (≤ 5))** to evaluate Drug likeness or determine the chemical and physical properties of pharmacological agent. This led to the selection of all the 39 compounds. These Molecules were assayed in docking studies using the **AutoDock 4.2 tool** to calculate the binding free of each protein-ligand complex. Based on the docking results CID_537118 had the best binding of -7.89kcal/mol and was analyze to interact with RNA dependent RNA polymerase via 1

hydrogen bond each with Lys32, (distance = 2.84Å). Compound with Pubchem I.D of CID_537118, has binding energy of -7.29 kcal/mol and was examined to interact with via 1 hydrogen bond with Tyr228 (distance = 2.88Å). Compound with Pubchem I.D of CID_985, has binding energy of -5.00 kcal/mol and was examined to interact with via 1 hydrogen bond with Lys32 (distance = 2.84Å) and Lys32 (distance = 2.89Å). Compound with Pubchem I.D of CID_550119, has binding energy of -5.45 kcal/mol and was examined to interact with via 1 hydrogen bond with Tyr228 (distance = 2.98Å). Moreover, other compounds interact with RNA dependent RNA polymerase via the weak hydrophobic bond, these include; CID_537083, CID_537671, CID_5364533, CID_13760785, CID_543346, CID_554143, CID_23618376, CID_319211683, CID_3449717, CID_5284421, CID_5319737, CID_11748436, CID_5364509, CID_5366244, CID_9601436, CID_554143, CID_24585, CID_5367644, CID_5367644, CID_13760785, CID_5283646, CID_554143, CID_535324, CID_249903130, CID_5364495, CID_550072, CID_249914677, CID_6420608, CID_550119, CID_523023, CID_445070, and CID_638072. which possessed the binding energy of -3.67 kcal/mol, -3.67 kcal/mol, -4.25 kcal/mol, -5.88 kcal/mol, -6.02 kcal/mol, -4.82 kcal/mol, -4.04 kcal/mol, -3.96 kcal/mol, -0.00 kcal/mol, -5.00 kcal/mol, -7.89 kcal/mol, -4.63 kcal/mol, -4.34 kcal/mol, -4.12 kcal/mol, -4.62 kcal/mol, -3.72 kcal/mol, -4.18 kcal/mol, -4.89 kcal/mol, -0.00 kcal/mol, -4.74 kcal/mol, -0.30 kcal/mol, -4.38 kcal/mol, -6.02 kcal/mol, -3.59 kcal/mol, -3.80 kcal/mol, -7.43 kcal/mol, +5.82 kcal/mol, -3.46 kcal/mol, +8.07 kcal/mol, +8.07 kcal/mol, +5.62 kcal/mol, -5.04 kcal/mol, -4.74 kcal/mol, -4.55 kcal/mol, -4.63 kcal/mol, respectively.

Based on the docking analysis, 7 out of 39 compounds had a good binding energies with the protein, these compounds were further subjected to pharmacokinetic analysis to scrutinize the pharmacokinetic properties of individual compound (via **absorption, distribution, metabolism, excretion, and toxicity**). The properties such as **Human Intestinal absorption (HIA), Cytochrome P450 (CYP450 2D6) inhibition, and Blood-Brain Barrier (BBB)** were determined using **ADMET SAR 2.0 tool**.

The toxicity parameters such as Mutagenicity, Tumorigenicity, Reproducibility, and Irritability was accessed using the DataWarrior tool, and two compounds (CID- 3449717 and CID-5364495) has **high mutagenicity**, one compound CID-609887 the others are none mutagenic. These compound CID-985 has high tumorigenic while two compounds with CID-5283646, CID-249903130 has low tumorigenic while the others are none tumorigenic. in the analysis, six compounds has high reproducibility (CID-101771, CID-537118, CID-319211683, CID-537118, CID-56634694, CID-5364495, CID-249914677, and CID-6420608) and the remaining compounds are non-reproducible. And finally, seven compounds has high irritability (CID- 537083, CID-543346, CID-537118, CID-985, CID-537118, CID-3449717, and CID-5364495) and CID-5364495 has low irritability, the rest of the compounds are none irritable.

4. Conclusion

The extracts of *Z. jujube* showed better inhibitory effect t of the *Shigelle* isolates due to the presence of the secondary metabolites in the plant. A total of 39 compounds with good affinities against RNA dependent RNA polymerase were selected and screened for pharmacokinetic properties. Seven compounds with desirable pharmacokinetic properties were selected. Therefore, these results could be considered as suitable prospective inhibitors of multidrug *Shigella* species.

References

- [1] The Lancet: Global burden of bacterial antimicrobial resistance 1990–2021: a systematic analysis with forecasts to 2050 2024; 404: 1199–226
- [2] de Kraker, M.E.A., Stewardson, A.J., & Harbarth S. (2016). Will 10 million people die a year due to antimicrobial resistance by 2050? *PLoS Med*, 13: e1002184
- [3] Isaac, A., Samuel, A.O., Woasiedem, T., Francis, A.A., & Lawrence, S.S. (2023). Applications of molecular docking in natural products-based drug discovery. <https://doi.org/10.1016/j.sciaf.2023.e01593>
- [4] Breijyeh, Z., & Karaman, R. (2024). Antibacterial activity of medicinal plants and their role in wound healing. *Futur J Pharm Sci* 10, 68. <https://doi.org/10.1186/s43094-024-00634-0>
- [5] Mustapha, A., AlSharksi, A.N., Eze, U.A., Samaila, R.K., Ukwah, B.N., Anyiam, A.F., Samarasinghe, S., & Ibrahim, M.A. (2024). Phytochemical Composition, In Silico Molecular Docking Analysis and Antibacterial Activity of *Lawsonia inermis* Linn Leaves Extracts against Extended Spectrum Beta-Lactamases-Producing Strains of *Klebsiella pneumoniae*. *BioMed*, 4, 277–292. <https://doi.org/10.3390/biomed4030022>
- [6] Adeniyi, A., Asase, A., Ekpe, P.K., Asitoakor, B.K., Adu-gyamfi, A., & Avekor, P.Y. (2018). Ethnobotanical study of medicinal plants from Ghana ; confirmation of ethnobotanical uses, and review of biological and toxicological studies on medicinal plants used in Apra Hills Sacred Grove, *J. Herb. Med.* 14 76–87, doi:10.1016/j.hermed.2018.02.001

- [7] Bittner, F.S., Rendecková, K., Mučaji, P., Nagy, M., & Slobodníková, L. (2012). Antibacterial Activity of Medicinal Plants and Their Constituents in the Context of Skin and Wound Infections, Considering European Legislation and Folk Medicine—A Review. *International Journal of Molecular Science*, 22(19):10746. doi: 10.3390/ijms221910746.
- [8] Priya, A., Talever, S., Devender, P., & Himansu, C. (2023). An updated review of Ziziphus jujube: Major focus on its phytochemicals and pharmacological properties. *Pharmacological Research - Modern Chinese Medicine*, 8, 100297, <https://doi.org/10.1016/j.prmcm.2023.100297>.
- [9] Pareek S. Nutritional composition of jujube fruit Emirates J. Food Agric., 25 (6) (2013), pp. 463-470, 10.9755/ejfa.v25i6.15552
- [10] Lu, Y., Bao, T., Mo, J., Ni, J., & Chen, W. (2021). Research advances in bioactive components and health benefits of jujube (*Ziziphus jujuba* Mill.) fruit. *J Zhejiang Univ Sci B*, 15;22(6):431-449. doi: 10.1631/jzus.B2000594.
- [11] Gao, Q.H., Wu, C.S., & Wang, M., (2013). The jujube (*Ziziphus jujuba* Mill.) fruit: a review of current knowledge of fruit composition and health benefits. *J Agric Food Chem*, 61(14): 3351-3363. 10.1021/jf4007032
- [12] Asma, H.S., Moza, T.H.G., Hossain, M.A. (2016). Comparative evaluation of total phenols, flavonoids content, and antioxidant potential of leaf and fruit extracts of Omani *Ziziphus jujuba* L Pac. *Sci. Rev. A Nat. Sci. Eng.*, 18 (1) 78-83
- [13] Shams, N., Najafabadi, M.A., Sahari, M.B., Hamidi, Z.E. (2017). Effects of concentration method and storage time on some bioactive compounds and color of jujube (*Ziziphus jujuba* var. *vulgaris*) concentrate. *J. Food Sci. Technol.*, 54 (9) (2017, August), pp. 2947-2955, 10.1007/s13197-017-2733-2
- [14] Miklavčič, A.V., Baruca, A.A., Hladnik, M., Ota, A., Skrt, M., & Butinar, B. (2019). An integrated characterization of jujube (*Ziziphus jujuba* Mill.) grown in the north adriatic region *Food Technol. Biotechnol.*, 57 (1) (2019), 17-28, 10.17113/ftb.57.01.19.5910
- [15] Taneja, N., Mewara, A. (2016). Shigellosis: epidemiology in India. *Indian J Med Res*. 2016;143(5):565. doi: 10.4103/0971-5916.187104
- [16] Li, Y.L., Tewari, D., Yealy, C.C., Fardig, D., & M'ikanatha, N.M. (2016). Surveillance for travel and domestically acquired multidrug-resistant human *Shigella* infections—Pennsylvania, 2006–2014. *Health Security* 14(3):143–151. doi: 10.1089/hs.2016.0026
- [17] El-Beltagi, H.S., Aziz, S.M.S., Aboshady, A.I., Ibrahim, M. A. R., Ibrahim, M. F. M., Alenezi, M. A., Darwish, D. B. E., Al-Qahtani, S. M., Al-Harbi, N. A., & Darwish, H. (2023). Isolation and Identification of Flavonoids from Black Cumin (*Nigella sativa*) by HPLC-MS and In Silico Molecular Interactions of Their Major Compounds with *Fusarium oxysporum* Trypsin-like Serine Protease. *Separations*. 10, 360.
- [18] Cheesbrough, M. (Ed.) Biochemical tests to identify bacteria. In *Laboratory Practice in Tropical Countries*; Cambridge Edition; Cambridge University Press: Cambridge, UK, 2002; pp. 36–70.
- [19] Gul, R., Jan, S.U., Faridullah, S., Sherani, S., & Jahan, N. (2017). Preliminary phytochemical screening, quantitative analysis of alkaloids, and antioxidant activity of crude plant extracts from *Ephedra intermedia* indigenous to Balochistan. *Science World Journal*, 5873648.
- [20] Idris, A.H., Haruna, Z., Iliyasu, M.Y., Sahal, M.R., Inusa, T., Salisu, A., Isma'il, S., Umar, R.D., Kabeer, Z.M.; Tahir, H. (2023). Antibacterial Activity of *Lawsonia inermis* Leaf Extracts against Multidrug-resistant *Pseudomonas aeruginosa* from Infected Wounds. *European Journal of Medicinal Plants*, 34, 1–8
- [21] Pettersen, E.F., Goddard, T.D., Huang, C.C., Couch, G.S., Greenblatt, D.M., Meng, E.C., & Ferrin, T.E. (2004). UCSF Chimera—A visualization system for exploratory research and analysis. *J. Comput. Chem*. 25, 1605–1612.
- [22] Morris, G.M., Huey, R., Lindstrom, W., Sanner, M.F., Belew, R.K., Goodsell, D.S., & Olson, A.J. AutoDock4 and AutoDockTools4: Automated Docking with Selective receptor flexibility. *J. Comput. Chem*. 1998, 30, 2785–2791.
- [23] Hariono, M., Abdullah, N., Damodaran, K.V., Kamarulzaman, E.E., Mohamed, N. Hassan, S.S. Shamsuddin, S., & Wahab, H.A. (2016). Potential new H1N1 neuraminidase inhibitors from ferulic acid and vanillin: Molecular modelling, synthesis and in vitro assay. *Scientific Report*, 6, 38692.



Determination of the Potential Inhibitory Potentials of Some Thiosemicarbazone Compounds on Glyceraldehyde-3-phosphate Dehydrogenase Enzyme

Zeyad ADIL HAMEED HAMEED^{1,*} , **Şevki ADEM**² 

¹ Faculty of Science, Chemistry Department, Çankırı Karatekin University, Çankırı, Türkiye

² Faculty of Science, Chemistry Department, Çankırı Karatekin University, Çankırı, Türkiye

Abstract

Glyceraldehyde-3-phosphate dehydrogenase (GAPDH) is a widely expressed enzyme essential for glycolysis and has gained significant attention for its diverse roles in cancer biology. Beyond its primary function in glycolysis, GAPDH exhibits non-enzymatic activities that are closely linked to cancer progression, invasiveness, and metastasis. Its enzymatic role involves catalyzing the conversion of glyceraldehyde-3-phosphate to 1,3-bisphosphoglycerate, a critical step in the glycolytic pathway. This process is particularly advantageous for cancer cells, supplying the energy necessary to sustain their rapid proliferation and adapt to the challenging conditions of the tumor microenvironment. In the presented study, the binding potential of some thiosemicarbazone compounds to the active site of this enzyme was investigated by molecular modeling method. In addition, detailed maps of the binding patterns of the molecules to the active site of GAPDH enzyme were obtained. As shown, the compound 5a has the best binding to the target, and this interpretation is based on its lowest moldock score (-129.858) and rerank score (-102.267). In addition, it has a relatively high number of Hbond (-4.26096), which could contribute to the strong binding. Also, compounds 3b and 3a have good binding, which indicates that they also have excellent efficacy.

Keywords: Glyceraldehyde-3-phosphate dehydrogenase, Thiosemicarbazone, Docking, Cancer

1. Introduction

Glyceraldehyde-3-phosphate dehydrogenase (GAPDH) is a glycolytic enzyme specifically catalyzing the reversible conversion of glyceraldehyde-3-phosphate (G-3-P) to 1,3-diphosphoglycerate. GAPDH participates in numerous cellular functions, in addition to glycolytic effects. For instance, GAPDH contributes to nuclear tRNA export, DNA replication and repair, endocytosis, exocytosis, cytoskeletal organization, iron metabolism, carcinogenesis, and cell death [1]. In normal cells, GAPDH is required for a variety of distinctive cell activities in diverse subcellular locales. Membrane GAPDH is required for membrane fusion and iron transport. In the cytosol, GAPDH is required for interorganelle trafficking as well as posttranscriptional mRNA expression. The latter may be of particular interest as, depending on the respective mRNA, GAPDH can increase or decrease mRNA stability as well as determine its rate of translation. In the nucleus, GAPDH is required for the maintenance of DNA integrity primarily through its telomeric association and its effect on DNA repair enzyme function; the control of gene transcription, histone biosynthesis and its role in apoptosis. In addition, GAPDH fulfills a fundamental role in the response of cells to environmental challenges, most notably oxidative stress, hypoxia and ischemia. On the other hand, with respect to the pathology of human disease, GAPDH is an a priori requirement for the onset of a series of age-related neurodegenerative disorders, the cellular and organ-specific pathologies associated with diabetes, and its diverse roles in tumor development and progression [2]. With respect to the latter, GAPDH is required for tumor survival and propagation, tumor-specific angiogenesis, tumorspecific gene expression, the stabilization of tumor-specific mRNA and, as tumors may be exposed to hypoxia, its role in ensuring tumor survival during oxygen deprivation or, conversely, oxidative stress. Regrettably, there appears to be an inverse relationship between GAPDH expression and patient survival. Programmed cell death can be considered an unusual biochemical pathway in as much as it does not facilitate cell viability. Instead, it is a means by which an organism preserves itself by removing damaged cells which may threaten its existence. Recent evidence indicates that GAPDH fulfills an important role in apoptosis [3]. As such, the ability of cancer cells to restrict or eliminate its apoptotic functions may provide a means to ensure tumor cell survival, growth, and metastases. The role of GAPDH in programmed cell death illustrates not only the breadth of its moonlighting activities but also several important basic mechanisms which underlie its functional diversity. These include the necessity of its normal posttranslational modification, the requirement for GAPDH protein/protein interactions, dynamic changes in its subcellular localization from a cytoplasmic to a nuclear protein, and, lastly, a series of

* Corresponding author. e-mail address: zeyad95adil@gmail.com

GAPDH mediated changes in nuclear structure and function. As the initiation of apoptosis is an existential threat to tumor survival, let alone its progression, invasiveness, and metastases, the ability of cancer cells to prevent programmed cell death would be a major selective advantage in tumorigenesis. Apoptosis is not the only program of gene expression which leads to cell destruction, i.e., caspase-independent cell death (CICD) represents a second mechanism through which an organism protects itself by ensuring the death of damaged cells. Recent evidence indicates that moonlighting GAPDH function is not only an important component of CICD but is also required for cell destruction by this pathway [4]. Thiosemicarbazones has occupied a prominent place in medicinal chemistry because of their broad profile of biological activities such as antitumor, antibacterial, antifungal, antiviral, antiprotozoal, among others. These classes of compounds present chelating properties, which favor the biochemical mechanisms, being the antineoplastic activity the most explored. The anti-tumor mechanism of thiosemicarbazones could be through the inhibition of DNA synthesis. Thiosemicarbazones could stabilize the cleavable complex between topoisomerase II and DNA through alkylation of thiol on the top II-DNA complex. In addition, thiosemicarbazones can inhibit iron-containing enzyme ribonucleotide reductase by metal ion chelation because iron has been shown to be an essential molecular target in the proliferation of cancer cells and generation of reactive oxygen species [5]. This study aims to understand the intricate mechanisms by which GAPDH performs its various functions in order to develop new cancer treatments using thiosemicarbazones associated with abnormal GAPDH activity.

2. Materials and Methods

Glyceraldehyde-3-phosphate dehydrogenase (GAPDH): Crystal Structure Of Human Placental Glyceraldehyde-3-Phosphate Dehydrogenase was retrieve from protein data base web site. Its PDB ID is 1U8F [6]. Molegro Virtual Docker software was used for the docking analyses [7]. Protein structure uploaded to software using File/Import molecules tool. Water molecules found in the protein crystal structure were removed. Molecules not necessary for activity were deleted. Compounds used docking studies were selected from a review article [8]. They were imported to docking software. Possible errors in the structure of molecules were checked and corrected. The position of docking area was determined as X:12.14, Y:-24.43 and Z:29.23. Its radius was 15 angstrom. Docking procedure started Docking/Docking Wizard tool. Ligands were chosen from workspace. MolDock Score was defined as a scoring function. Binding site origin, center and radius were checked. Search algorithm was determined as MolDock SE. The number of runs was 10. Energy minimization and optimize H-bond were selected for after docking. The docking operation was started after determining where the results file will record. After docking, the results were transferred to the program and the best results were selected for analysis. Protein structure and poses were exported as PDB file. These files were uploaded to Discovery Studio 2021 Client. The binding states of the molecules with the protein and the details of their interactions were determined using this program.

3. Results and Discussion

Through Table 1 we can see the results we obtained after performing the molecular docking study, and as shown in the table, the name of the compound, PubChem CID, MolDock Score, Rerank Score, and HBond.

Table 1. Molecular docking study results

Ligand	MolDock Score	Rerank Score	HBond
5a	-129.858	-102.267	-4.26096
3b	-129.454	-101.929	-6.11213
3a	-129.029	-101.808	-3.84993
5b	-125.479	-90.2582	-4.7077
1b	-123.292	-102.304	-4.66947
1a	-122.938	-98.8184	-6.36
4b	-120.525	-70.3087	-3.69325
6a	-118.599	-96.8953	-5.88936
6b	-118.133	-68.2495	-4.42705
4a	-117.04	-94.6059	-4.05389
7a	-116.983	-98.2596	0
2b	-113.208	-79.4179	-2.50267
7b	-112.944	-89.731	-5.91473
2a	-112.786	-73.346	-5.57123

A ligand's expected binding affinity to a receptor is indicated by its MolDock Score. In most cases, lower values indicate better binding. The Rerank Score is an improved version of the original that takes into account other variables, such as hydrogen bonding. HBond: The total amount of hydrogen bonds created by the receptor and ligand.

As shown in the table, 5a has the best binding to the target, and this interpretation is based on its lowest moldock score (-129.858) and rerank score (-102.267). In addition, it has a relatively high number of Hbond (-4.26096), which could contribute to the strong binding. Also, compounds 3b and 3a have good binding, which indicates that they also have excellent efficacy.

Figure 1 shows the complexes that were formed. Compound 5a binds to GAPDH through several bonds, including Carbon hydrogen bond (THR P:182, and GLU P:317), Conventional hydrogen bond (ASN P:316, and ILE P:14), Pi-anion (GLU P:317), Pi-alkyl (ARG P:13, ILE P:14, CYS P:152, ALA P:183, and TYR P:320), Pi-Pi stacked (TYR P:320), and van der Waals.

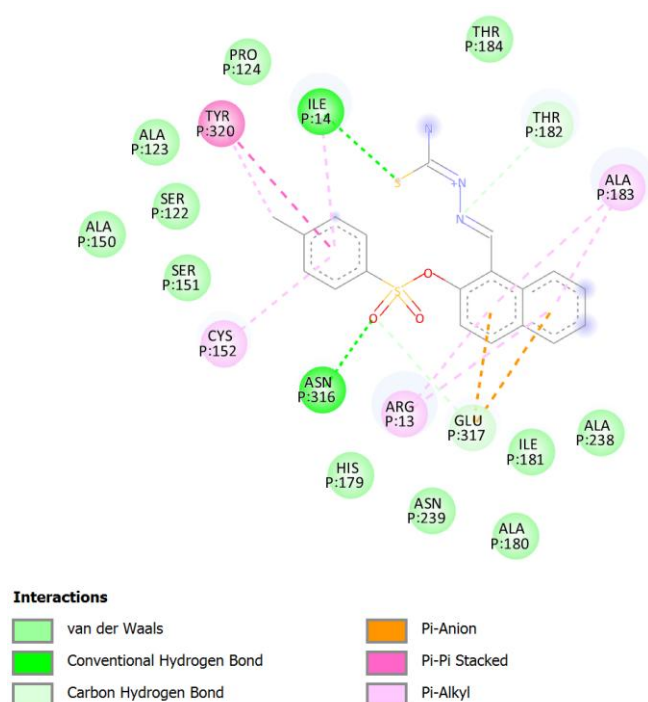


Figure 1. Interactions between 5a and GAPDH

Figure 2 shows the complexes that were formed. Compound 3b binds to GAPDH through several bonds, including Carbon hydrogen bond (THR P:99, and GLU P:10), Conventional hydrogen bond (ASN P:9, and ILE P:34), Alkyl (ILE P:38, and MET P:46), Pi-alkyl (PRO P:36, and ILE P:38), Pi-sulfur (PHE P:37), Pi-anion (ASP P:35) and van der Waals.

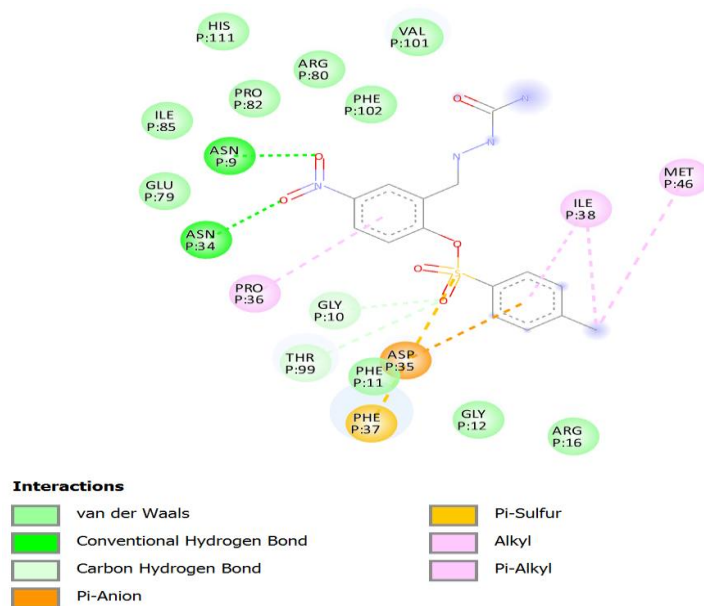


Figure 2. Interactions between 3b and GAPDH

Figure 3 shows the complexes that were formed. Compound 3a binds to GAPDH through several bonds, including Carbon hydrogen bond (CYS P:152), Conventional hydrogen bond (SER P:98, SER P:122, CYS P:152, and ASN P:316), Alkyl (ALA P:123, and PRO P:124), Pi-alkyl (ARG P:13, and ALA P:183), Pi-sulfur (HIS P:179), Pi-anion (GLU P:317), Pi-donor hydrogen bond (HIS P:179), Pi-Pi T-shaped (TYR P:320) and van der Waals.

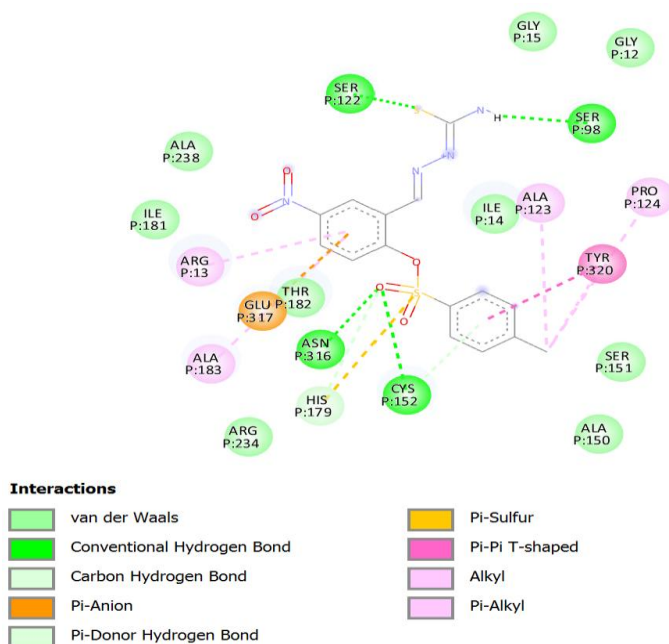


Figure 3. Interactions between 3a and GAPDH.

4. Conclusion

This computer study might give us new information about how GAPDH inhibitors bind and interact with each other, which could lead to the creation of better, safer treatments for human health. The results of the docking study show that 5a is the most promising candidate for binding to the target receptor.

References

- [1] Zhang, J. Y., Zhang, F., Hong, C. Q., Giuliano, A. E., Cui, X. J., Zhou, G. J., ... & Cui, Y. K. (2015). Critical protein GAPDH and its regulatory mechanisms in cancer cells. *Cancer biology & medicine*, 12(1), 10.
- [2] Sirover, M. (2017). *Glyceraldehyde-3-phosphate dehydrogenase (GAPDH): the quintessential moonlighting protein in normal cell function and in human disease*. London: Elsevier.
- [3] Sirover, M. A. (2018). Pleiotropic effects of moonlighting glyceraldehyde-3-phosphate dehydrogenase (GAPDH) in cancer progression, invasiveness, and metastases. *Cancer and Metastasis Reviews*, 37, 665-676.
- [4] Colell, A., Ricci, J.-E., Tait, S., et al. (2007). GAPDH and autophagy preserve survival after cytochrome c release in the absence of caspase activation. *Cell*, 129, 983–997.
- [5] de Siqueira, L. R. P., de Moraes Gomes, P. A. T., de Lima Ferreira, L. P., de Melo Rêgo, M. J. B., & Leite, A. C. L. (2019). Multi-target compounds acting in cancer progression: Focus on thiosemicarbazone, thiazole and thiazolidinone analogues. *European Journal of Medicinal Chemistry*, 170, 237-260.
- [6] Wong, K. S., Mabanglo, M. F., Seraphim, T. V., Mollica, A., Mao, Y. Q., Rizzolo, K. and Houry, W. A. 2018. Acyldepsipeptide analogs dysregulate human mitochondrial ClpP protease activity and cause apoptotic cell death. *Cell Chemical Biology*, 25(8): 1017-1030.
- [7] Thomsen, R. and Christensen, M. H. 2006. MolDock: a new technique for high-accuracy molecular docking. *Journal of Medicinal Chemistry*, 49(11): 3315-3321.
- [8] Kurşun-Aktar, B. S., Adem, Ş., Tatar-Yilmaz, G., Hameed, Z. A. H., & Oruç-Emre, E. E. (2023). Investigation of α -glucosidase and α -amylase inhibitory effects of phenoxy chalcones and molecular modeling studies. *Journal of Molecular Recognition*, 36(11), e3061.

Targeting Reprogrammed Glucose Metabolism in Cancer Therapy

Sevki ADEM^{1,*} 

¹ Faculty of Science, Chemistry Department, Çankırı Karatekin University, Çankırı, Türkiye

Abstract

Cancer cells alter their metabolic processes to fulfill the demands of rapid growth and to thrive in diverse microenvironments. The acceleration of glycolysis not only meets their energy needs but also supplies intermediates for biosynthetic pathways, enabling the production of essential molecules such as proteins, lipids, nucleotides, and fatty acids. This metabolic reprogramming is closely tied to key cancer traits, including uncontrolled cell growth, resistance to apoptosis, metastasis, and the formation of new blood vessels. Enzymes like hexokinase, phosphofructokinase-1, and pyruvate kinase, which are upregulated during these processes, have emerged as promising targets for cancer treatment. This study delves into the altered glucose metabolism in cancer cells and discusses its potential for therapeutic manipulation.

Keywords: Glucose, Cancer, Cancer Treatment, Metabolism

1. Introduction

Glucose plays a critical role in supporting the survival and rapid proliferation of cancer cells. Through a phenomenon known as the Warburg effect, cancer cells rely heavily on glycolysis for energy production, even in the presence of oxygen. This metabolic preference not only provides ATP but also generates essential intermediates for anabolic processes, such as nucleotide, protein, and lipid synthesis, which are vital for cell growth and division (Figure 1). Additionally, glucose metabolism contributes to maintaining redox balance by supplying NADPH through the pentose phosphate pathway, helping cancer cells counteract oxidative stress. This dependency on glucose underscores its importance as both an energy source and a building block provider, making it a central target for therapeutic intervention in cancer treatment [1,2].



Figure 1. Intracellular metabolic processes that use glucose

Cancer cells exhibit a distinct metabolic phenotype known as the Warburg effect, where they preferentially utilize glycolysis for energy production, even in the presence of adequate oxygen. This metabolic shift is driven by a reprogramming of glucose metabolism, orchestrated by key enzymes. Hexokinase (HK), particularly HK2, is often overexpressed in cancer cells, catalyzing the first step of glycolysis by phosphorylating glucose to glucose-6-phosphate. This modification traps glucose inside the cell and supports rapid glycolysis, which provides both energy and intermediates for biosynthetic pathways essential for tumor growth [3].

Another pivotal enzyme is pyruvate kinase M2 (PKM2), a variant predominantly expressed in cancer cells. PKM2 regulates the final step of glycolysis by converting phosphoenolpyruvate (PEP) to pyruvate. Unlike its normal

* Corresponding author. e-mail address: sevkiadem@gmail.com

counterpart PKM1, PKM2 exhibits lower enzymatic activity, allowing cancer cells to accumulate upstream glycolytic intermediates for anabolic processes such as nucleotide, lipid, and amino acid synthesis [4]. This enzymatic adaptation ensures that cancer cells can meet the demands of rapid proliferation. Additionally, lactate dehydrogenase A (LDHA) is upregulated to convert pyruvate to lactate, even in aerobic conditions, which acidifies the tumor microenvironment and facilitates cancer cell invasion and immune evasion [5].

The reprogramming of glucose metabolism in cancer cells also involves the activation of the pentose phosphate pathway (PPP) by glucose-6-phosphate dehydrogenase (G6PD). This pathway generates NADPH and ribose-5-phosphate, which are critical for antioxidant defense and nucleotide synthesis, respectively [6]. Furthermore, alterations in enzymes such as isocitrate dehydrogenase (IDH) and phosphofructokinase (PFK) contribute to the metabolic flexibility of cancer cells, enabling them to thrive under fluctuating nutrient and oxygen levels. Targeting these key enzymes offers promising therapeutic opportunities to disrupt the metabolic adaptations of cancer cells while sparing normal tissues.

2. Hexokinase 2

Hexokinase 2 (HK2) is a key enzyme in the glycolytic pathway, responsible for catalyzing the phosphorylation of glucose to glucose-6-phosphate (G6P), the first and irreversible step of glycolysis. In cancer cells, HK2 is often overexpressed and plays a pivotal role in facilitating the metabolic reprogramming known as the Warburg effect. This phenomenon describes the preference of cancer cells for glycolysis, even under aerobic conditions. The elevated expression of HK2 enhances the uptake and utilization of glucose, providing cancer cells with the energy and metabolic intermediates needed for biosynthesis and rapid proliferation. Unlike normal cells, which primarily express HK1, the specific upregulation of HK2 in tumors underscores its importance in supporting the unique metabolic demands of cancer (Figure 2) [7].

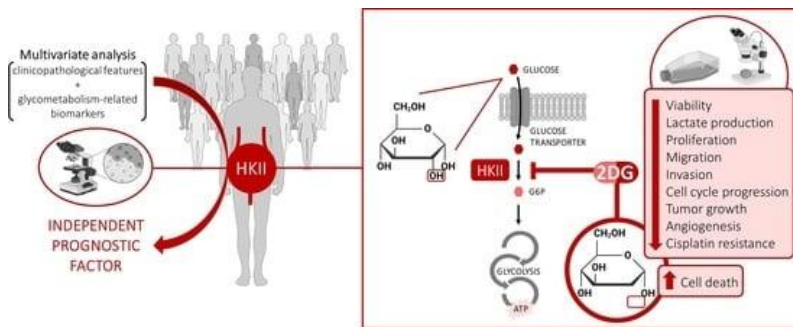


Figure 2. Hexokinase 2 as a therapeutic target [8]

A distinctive feature of HK2 in cancer cells is its association with the outer mitochondrial membrane. This localization is mediated by its interaction with the voltage-dependent anion channel (VDAC), which enables HK2 to access ATP generated by oxidative phosphorylation directly. This strategic positioning not only enhances the efficiency of glycolysis but also protects cancer cells from apoptosis. By binding to VDAC, HK2 prevents the release of pro-apoptotic factors such as cytochrome c, thereby promoting cell survival. This dual role in metabolism and apoptosis regulation highlights HK2's critical contribution to cancer cell resilience and progression.

HK2 also influences the tumor microenvironment by promoting lactate production through enhanced glycolysis. The secreted lactate acidifies the tumor surroundings, creating conditions that facilitate invasion, metastasis, and immune evasion. Furthermore, the increased glucose consumption mediated by HK2 deprives immune cells in the tumor microenvironment of the energy required for their functions, impairing anti-tumor immune responses. By driving metabolic alterations that support tumor growth and suppress the immune system, HK2 acts as a central player in shaping the tumor microenvironment to favor cancer progression [9].

HK2 has emerged as a promising therapeutic target due to its overexpression in tumors and minimal expression in most normal tissues. Inhibiting HK2 can disrupt glucose metabolism, depriving cancer cells of the energy and building blocks needed for growth. Additionally, targeting HK2 can disrupt its anti-apoptotic role, rendering cancer cells more susceptible to programmed cell death. Strategies to inhibit HK2 include small molecule inhibitors, RNA interference, and antisense oligonucleotides, many of which are under preclinical and clinical investigation. By specifically targeting HK2, these therapies aim to selectively impair cancer metabolism without significantly affecting normal cells [10].

Despite the therapeutic potential of targeting HK2, challenges remain. The redundancy of glycolytic enzymes and the metabolic plasticity of cancer cells may allow tumors to adapt to HK2 inhibition. Furthermore, given the role of HK2 in some normal tissues, off-target effects must be carefully managed. Advances in understanding the regulatory mechanisms of HK2, such as its transcriptional and post-translational modifications, are aiding the development of highly specific inhibitors. Combining HK2-targeted therapies with other metabolic, immune, or chemotherapeutic strategies may provide a more effective and comprehensive approach to cancer treatment. As research progresses, targeting HK2 holds significant promise for improving outcomes in cancer therapy.

3. Pyruvate kinase M2

Pyruvate kinase M2 (PKM2) is an isoform of the pyruvate kinase enzyme, essential in the final step of glycolysis, where it catalyzes the conversion of phosphoenolpyruvate (PEP) to pyruvate while generating ATP. In cancer cells, PKM2 is predominantly expressed, replacing the PKM1 isoform commonly found in normal tissues. Unlike PKM1, which is constitutively active, PKM2 exists in both active tetrameric and less active dimeric forms. This unique feature allows cancer cells to regulate glycolysis dynamically. By favoring the dimeric form, PKM2 slows down glycolysis, enabling the accumulation of glycolytic intermediates that are diverted into biosynthetic pathways necessary for nucleotide, lipid, and amino acid synthesis. This metabolic reprogramming, also known as the Warburg effect, provides cancer cells with the resources needed for rapid growth and proliferation [11].

Beyond its metabolic role, PKM2 also participates in non-metabolic functions that support tumorigenesis. PKM2 can translocate to the nucleus in response to growth signals or oxidative stress, where it acts as a transcriptional coactivator. In this capacity, PKM2 interacts with transcription factors like hypoxia-inducible factor-1 alpha (HIF-1 α) and β -catenin to regulate the expression of genes involved in glycolysis, angiogenesis, and cell cycle progression. For example, HIF-1 α activation promotes the expression of glucose transporters and glycolytic enzymes, enhancing glucose uptake and utilization in cancer cells. Additionally, PKM2-mediated activation of β -catenin supports stem-like properties in cancer cells, contributing to tumor initiation and resistance to therapy. These non-metabolic roles underscore PKM2's versatility as a driver of cancer progression [12].

PKM2 also helps cancer cells adapt to the challenging conditions of the tumor microenvironment. Under hypoxic conditions, common in solid tumors, PKM2 shifts cellular metabolism towards glycolysis, reducing reliance on oxygen-dependent oxidative phosphorylation. This metabolic adaptation not only supports ATP production but also leads to the secretion of lactate, acidifying the tumor microenvironment. The acidic environment promotes invasion, metastasis, and immune evasion, further enhancing cancer progression. Thus, PKM2 contributes to both intrinsic cellular functions and extrinsic interactions that promote tumor survival and dissemination [13].

Given its central role in cancer metabolism and signaling, PKM2 has emerged as an attractive target for cancer therapy. Strategies to inhibit PKM2 activity aim to disrupt the metabolic flexibility of cancer cells by forcing them to rely on oxidative phosphorylation, which is less efficient for biosynthesis. Alternatively, activating PKM2 to favor its tetrameric form can enhance glycolytic flux, depleting glycolytic intermediates needed for biosynthetic pathways and suppressing tumor growth. Small molecule inhibitors, activators, and RNA-based therapies are currently under investigation to modulate PKM2 activity and localization. Targeting PKM2 not only hampers cancer cell proliferation but also reduces their adaptability to the tumor microenvironment [14].

While targeting PKM2 offers significant promise, challenges remain. PKM2 is also expressed in some normal tissues, raising concerns about potential off-target effects. Additionally, the heterogeneity of cancer metabolism across tumor types may influence the effectiveness of PKM2-targeted therapies. Despite these challenges, advancements in understanding PKM2's molecular functions and regulatory mechanisms are enabling the development of highly specific inhibitors and combination therapies. By integrating PKM2-targeted treatments with other metabolic or immune-based therapies, there is significant potential to enhance cancer treatment outcomes and improve patient survival.

4. Phosphofructokinase 1

Phosphofructokinase 1 (PFK1) is a critical regulatory enzyme in glycolysis, catalyzing the irreversible conversion of fructose-6-phosphate to fructose-1,6-bisphosphate. As the rate-limiting step in glycolysis, PFK1 determines the flux of glucose through this pathway, making it a key point of control in cellular metabolism. In cancer cells, PFK1 activity is often upregulated to support the metabolic reprogramming characteristic of the *Warburg effect*. This enhanced glycolytic activity supplies the ATP and biosynthetic precursors necessary for rapid cell proliferation and tumor growth. The ability of PFK1 to integrate signals from cellular energy levels and metabolite availability positions it as a central regulator of cancer metabolism.

The regulation of PFK1 in cancer cells is influenced by oncogenic signaling pathways. For example, the activation of PI3K/AKT signaling promotes glycolysis by upregulating enzymes, including PFK1. Additionally, PFK1 is subject to allosteric regulation by metabolites such as fructose-2,6-bisphosphate (F2,6BP), which is elevated in many cancers. F2,6BP strongly activates PFK1, bypassing its usual inhibitory feedback mechanisms and driving glycolytic flux. Post-translational modifications, such as phosphorylation or acetylation, also modulate PFK1 activity in cancer cells, further enhancing its function and ensuring the metabolic flexibility required for tumor survival and growth [15].

PFK1 contributes to the adaptation of cancer cells to the hypoxic and nutrient-deprived conditions of the tumor microenvironment. Under low oxygen, the reliance on glycolysis increases, making PFK1 a crucial enzyme for energy production. This shift to glycolysis leads to lactate accumulation and acidification of the tumor microenvironment, promoting invasion, metastasis, and immune suppression. Furthermore, the intermediates generated by PFK1-driven glycolysis are diverted into anabolic pathways, supporting macromolecule biosynthesis and antioxidant defense, which are essential for cancer cell survival in harsh conditions.

Targeting PFK1 presents a promising strategy for cancer therapy due to its central role in tumor metabolism. Inhibiting PFK1 activity can disrupt the glycolytic flux, depriving cancer cells of energy and biosynthetic precursors. Small molecule inhibitors of PFK1 or its activator F2,6BP are being explored to block glycolysis selectively in tumor cells. Additionally, targeting the oncogenic signaling pathways that regulate PFK1 expression and activity, such as the PI3K/AKT pathway, offers an indirect approach to suppress PFK1-driven glycolysis. These strategies aim to exploit the metabolic vulnerabilities of cancer cells, making PFK1 a valuable therapeutic target [16].

While PFK1 is an attractive target for cancer therapy, challenges remain. The ubiquitous expression of PFK1 in normal tissues raises concerns about off-target effects, requiring the development of highly selective inhibitors. Additionally, the metabolic plasticity of cancer cells may allow them to bypass PFK1 inhibition by activating alternative pathways, such as oxidative phosphorylation or glutaminolysis. Combining PFK1-targeted therapies with other metabolic inhibitors, immune therapies, or traditional chemotherapies may enhance efficacy and overcome resistance. Further research into the regulatory mechanisms of PFK1 and its role in cancer biology will aid in the development of novel and effective therapeutic strategies.

5. Lactate Dehydrogenase A

Lactate dehydrogenase A (LDH-A) is a critical enzyme in cancer metabolism, catalyzing the conversion of pyruvate to lactate while regenerating NAD^+ for continued glycolysis. In cancer cells, LDH-A expression is often upregulated to support the metabolic shift known as the Warburg effect, where cells favor aerobic glycolysis over oxidative phosphorylation, even in the presence of oxygen. This metabolic reprogramming provides cancer cells with rapid ATP production and intermediates for biosynthesis. The overexpression of LDH-A enables cancer cells to sustain high glycolytic rates, making it a vital enzyme for energy production and survival under both hypoxic and normoxic conditions.

LDH-A plays a pivotal role in tumor progression by influencing both intracellular and extracellular environments. Intracellularly, the production of lactate helps cancer cells maintain redox balance by regenerating NAD^+ , essential for sustaining glycolysis. Extracellularly, the secretion of lactate acidifies the tumor microenvironment, creating conditions that promote invasion, metastasis, and immune evasion. Acidification also suppresses the activity of immune cells such as T cells and natural killer (NK) cells, enabling tumors to evade immune surveillance. By fostering an aggressive tumor phenotype and altering the microenvironment, LDH-A contributes significantly to cancer progression and resistance to therapy [17].

The expression and activity of LDH-A are tightly linked to the hypoxic conditions commonly found in tumors. Hypoxia-inducible factor-1 alpha (HIF-1 α), a transcription factor activated under low oxygen levels, directly upregulates LDH-A. This regulation ensures that cancer cells can adapt to hypoxic stress by relying on glycolysis and lactate production for energy. Additionally, HIF-1 α -induced LDH-A expression promotes angiogenesis, further supporting tumor growth. The reliance of hypoxic tumor cells on LDH-A underscores its importance as a survival mechanism and highlights its potential as a therapeutic target in the context of hypoxic tumors.

Targeting LDH-A presents a promising approach to cancer therapy due to its central role in glycolysis and tumor progression. Inhibiting LDH-A can disrupt lactate production, leading to reduced glycolytic flux, energy depletion, and impaired tumor growth. Moreover, blocking LDH-A activity can reverse the acidification of the tumor microenvironment, improving immune cell function and reducing invasion and metastasis. Small molecule

inhibitors of LDH-A, such as FX11 and galloflavin, have shown anti-tumor effects in preclinical studies. Combining LDH-A inhibitors with other therapies, such as immune checkpoint inhibitors or metabolic inhibitors, may enhance their efficacy and provide a multi-pronged approach to cancer treatment [18].

6. Glucose-6-Phosphate Dehydrogenase (G6PD)

Glucose-6-phosphate dehydrogenase (G6PD) is a key enzyme in the pentose phosphate pathway (PPP), responsible for the oxidation of glucose-6-phosphate (G6P) to 6-phosphoglucono- δ -lactone, producing NADPH in the process. NADPH is essential for maintaining cellular redox balance and for supporting biosynthesis, including fatty acid and nucleotide synthesis, which are critical for rapid cell division. In cancer cells, G6PD is often upregulated to meet the high metabolic demands of rapid proliferation. The increased activity of G6PD ensures an adequate supply of NADPH to neutralize the elevated levels of reactive oxygen species (ROS) that are generated by the accelerated metabolic processes in tumors [19].

G6PD plays a crucial role in supporting tumor growth by facilitating the generation of biosynthetic precursors and protecting cancer cells from oxidative damage. The increased production of NADPH via G6PD activation allows cancer cells to cope with the oxidative stress resulting from rapid metabolism, DNA replication, and mitochondrial activity. Additionally, G6PD helps maintain the cellular antioxidant defenses, such as glutathione, by providing the necessary reducing power. This protection against oxidative stress is essential for the survival of cancer cells in the harsh tumor microenvironment, where low oxygen levels and high nutrient consumption create challenging conditions.

In many cancers, metabolic reprogramming is a hallmark feature, and G6PD is an integral part of this process. Cancer cells often exhibit enhanced glycolysis, even in the presence of oxygen (the Warburg effect), which generates high amounts of lactate and ROS. To counterbalance these harmful byproducts, G6PD activity is upregulated to produce NADPH, which neutralizes ROS and allows cancer cells to continue proliferating. This metabolic shift also drives the biosynthesis of macromolecules, such as nucleotides, lipids, and proteins, which are essential for cell growth. G6PD, therefore, plays a critical role in sustaining the high-energy and biosynthetic demands of cancer cells, making it a crucial enzyme for tumor survival.

Given its central role in supporting the altered metabolic state of cancer cells, G6PD has become an attractive therapeutic target. Inhibiting G6PD could disrupt the pentose phosphate pathway, leading to reduced NADPH production, which would impair the antioxidant defense mechanisms of cancer cells. This would make tumor cells more vulnerable to oxidative damage and reduce their ability to proliferate. Moreover, blocking G6PD activity could also deprive cancer cells of essential biosynthetic precursors required for DNA and fatty acid synthesis, inhibiting tumor growth. Small molecule inhibitors targeting G6PD are being explored in preclinical studies, and their potential to enhance the effectiveness of chemotherapy and radiation therapy is under investigation.

While targeting G6PD offers a promising strategy for cancer treatment, there are challenges associated with its inhibition. G6PD is also expressed in normal cells, particularly in tissues with high oxidative stress, such as the liver and red blood cells. Therefore, selective inhibition of G6PD in tumor cells without affecting normal tissues is crucial to minimize off-target effects. Additionally, cancer cells may develop resistance mechanisms, such as compensatory activation of other antioxidant pathways. To address these challenges, ongoing research aims to identify biomarkers that predict patient response to G6PD inhibitors and explore combination therapies with other metabolic or immune-targeted treatments to enhance the effectiveness of G6PD inhibition in cancer therapy [20].

7. Conclusion

We Glycolysis represents an attractive target in cancer treatment due to its central role in supporting the unique metabolic demands of tumor cells. The reliance of cancer cells on glycolysis, even in the presence of oxygen (Warburg effect), provides a metabolic vulnerability that can be exploited therapeutically. Targeting key glycolytic enzymes such as hexokinase 2, glucose-6-phosphate dehydrogenase, phosphofructokinase 1, Pyruvate kinase M2, and lactate dehydrogenase A disrupts energy production, biosynthetic pathways, and redox balance, leading to impaired tumor growth and survival. Additionally, inhibiting glycolysis can reverse the acidification of the tumor microenvironment, enhancing immune responses and reducing metastatic potential. By integrating glycolysis-targeted therapies with existing treatments, such as chemotherapy and immunotherapy, it may be possible to achieve more effective and durable outcomes in cancer patients.

References

- [1] Ediriweera, M. K., & Jayasena, S. (2023). The role of reprogrammed glucose metabolism in cancer. *Metabolites*, 13(3), 345.
- [2] Abbaszadeh, Z., Çeşmeli, S., & Avcı, Ç. B. (2020). Crucial players in glycolysis: cancer progress. *Gene*, 726, 144158.
- [3] Gatenby, R. A., & Gillies, R. J. (2007). Glycolysis in cancer: a potential target for therapy. *The international journal of biochemistry & cell biology*, 39(7-8), 1358-1366.
- [4] Kim, J. W., Tchernyshyov, I., Semenza, G. L., & Dang, C. V. (2006). HIF-1-mediated expression of pyruvate dehydrogenase kinase: a metabolic switch required for cellular adaptation to hypoxia. *Cell metabolism*, 3(3), 177-185.
- [5] Yao, F., Zhao, T., Zhong, C., Zhu, J., & Zhao, H. (2013). LDHA is necessary for the tumorigenicity of esophageal squamous cell carcinoma. *tumor Biology*, 34, 25-31.
- [6] Zhang, Y., Xu, Y., Lu, W., Li, J., Yu, S., Brown, E. J., ... & Yang, X. (2022). G6PD-mediated increase in de novo NADP+ biosynthesis promotes antioxidant defense and tumor metastasis. *Science Advances*, 8(29), eabo0404.
- [7] Ciscato, F., Ferrone, L., Masgras, I., Laquatra, C., & Rasola, A. (2021). Hexokinase 2 in cancer: a prima donna playing multiple characters. *International journal of molecular sciences*, 22(9), 4716.
- [8] Afonso, J., Gonçalves, C., Costa, M., Ferreira, D., Santos, L., Longatto-Filho, A., & Baltazar, F. (2023). Glucose metabolism reprogramming in bladder cancer: hexokinase 2 (HK2) as prognostic biomarker and target for bladder cancer therapy. *Cancers*, 15(3), 982.
- [9] Li, R., Mei, S., Ding, Q., Wang, Q., Yu, L., & Zi, F. (2022). A pan-cancer analysis of the role of hexokinase II (HK2) in human tumors. *Scientific Reports*, 12(1), 18807.
- [10] Garcia, S. N., Guedes, R. C., & Marques, M. M. (2019). Unlocking the potential of HK2 in cancer metabolism and therapeutics. *Current medicinal chemistry*, 26(41), 7285-7322.
- [11] Upadhyay, S., Khan, S., & Hassan, M. I. (2024). Exploring the diverse role of pyruvate kinase M2 in cancer: Navigating beyond glycolysis and the Warburg effect. *Biochimica et Biophysica Acta (BBA)-Reviews on Cancer*, 189089.
- [12] İlhan, M. (2022). Non-metabolic functions of pyruvate kinase M2: PKM2 in tumorigenesis and therapy resistance. *Neoplasma*, 69(4).
- [13] Paredes, F., Williams, H. C., & San Martin, A. (2021). Metabolic adaptation in hypoxia and cancer. *Cancer letters*, 502, 133-142.
- [14] Adem, S., Rasul, A., Riaz, S., Sadiqa, A., Ahmad, M., Shahid Nazir, M., & Hassan, M. (2024). Pyruvate kinase modulators as a therapy target: an updated patent review 2018–2023. *Expert Opinion on Therapeutic Patents*, 34(10), 953-962.
- [15] Ni, X., Lu, C. P., Xu, G. Q., & Ma, J. J. (2024). Transcriptional regulation and post-translational modifications in the glycolytic pathway for targeted cancer therapy. *Acta Pharmacologica Sinica*, 1-23.
- [16] Simula, L., Alifano, M., & Icard, P. (2022). How phosphofructokinase-1 promotes PI3K and YAP/TAZ in cancer: therapeutic perspectives. *Cancers*, 14(10), 2478.
- [17] Certo, M., Tsai, C. H., Pucino, V., Ho, P. C., & Mauro, C. (2021). Lactate modulation of immune responses in inflammatory versus tumour microenvironments. *Nature Reviews Immunology*, 21(3), 151-161.
- [18] Tavartkiladze, A., Simonia, G., Lou, R., Revazishvili, P., Kasradze, D., & Maisuradze, M. (2024). Targeting Glycolysis in Tumor Cells: Therapeutic Inhibition of GLUT1 and LDH-A Using Phloretin and Melatonin for Metabolic Reprogramming and Tumor Regression in Triple Negative Breast Cancer. *Immunogenet Open Access*, 9, 235.
- [19] Song, J., Sun, H., Zhang, S., & Shan, C. (2022). The multiple roles of glucose-6-phosphate dehydrogenase in tumorigenesis and cancer chemoresistance. *Life*, 12(2), 271.
- [20] Yang, H. C., Wu, Y. H., Yen, W. C., Liu, H. Y., Hwang, T. L., Stern, A., & Chiu, D. T. Y. (2019). The redox role of G6PD in cell growth, cell death, and cancer. *Cells*, 8(9), 1055.



Determination of the Potential Inhibitory Potentials of Some Thiosemicarbazone Compounds on Glycogen Synthase Kinase 3 Enzymes: In Silico

Umar Ghali MUHAMMAD¹ , Şevki ADEM^{2,*}

¹Faculty of Science, Chemistry Department, Çankırı Karatekin University, Çankırı, Türkiye

² Faculty of Science, Chemistry Department, Çankırı Karatekin University, Çankırı, Türkiye

Abstract

Cancer is a major global public health that poses concern and lead to death. Enzymes usually serve as therapeutic targets in many diseases. Glycogen synthase kinase 3 (GSK-3) is a representative of the protein kinase family, and is extremely expressed in several tissues. GSK-3 is a serine/threonine kinase that phosphorylates serine or threonine residues of its substrate targets. Given its regulatory function in both tumor and immunological cells, GSK-3 has been suggested as a new cancer target.

In the present study, the binding potential of some thiosemicarbazone compounds to the active site of this enzyme was investigated by Molegro Virtual Docker software (2013) V6.0. Protein was repaired and water molecules were eliminated. In addition, detailed maps of the binding patterns of the molecules to the active site of GSK-3 enzyme were obtained using Discovery Studio 2024 Client. The result of the study revealed compound 2a has the highest binding score of -135.376 against GSK3 and hydrogen bond of -3.229. This is followed by compound 5b with moldock score of -134.954. The compound with least score is compound 7b with MolDock score of -117.832. This study shows high interaction between thiosemicarbazone compounds and GSK3. Therefore, it can be suggested to be used in designing therapeutic targets against GSK3 protein.

Keywords: Glycogen synthase kinase 3, Thiosemicarbazone, Docking, Cancer

1. Introduction

Cancer is a significant global public health concern, and it is one of the primary causes of mortality around the globe. Cancer as a multifactorial disease is usually targeted via different process, and inhibition of enzymes is one of those processes. GSK-3, a serine/threonine kinase, regulates several physiological processes through its vast variety of substrates, including glycogen synthase, β -catenin, Cyclin D1, and c-Myc. These substrates are necessary for important processes such as cell cycle progression, apoptosis, and glycogen metabolism. GSK-3 phosphorylates glycogen synthase, which reduces its activity and modulates glycogen storage and use [1-2].

GSK-3 contains two chains (chain A and chain B). GSK-3 α is usually inhibited by an external phosphorylation of the Ser21, while GSK-3 β is inhibited by Ser 9. GSK-3 β is considered the foremost and most promising therapeutic target [3]. Recent studies have identify novel competitive inhibitors of GSK-3 for therapeutic treatment of alzheimer's disease [4]. This is as a result of high rise in the level of the enzyme in AD patients. Recently, Ding et al [5] reported that gallic acid ameliorate cognitive impairment by inhibiting the activity of GSK-3 β . This is as a result of activation of Nrf to move to the nucleus.

GSK3 α/β is essential for the viability, survival, and proliferation of human tumors that are dependent on mutant KRas. Therefore suppression of GSK3 upregulates β -catenin and c-Myc to hinder the proliferation of Kras tumors [1]. One of the initial substrates of the oncogenic kinase AKT to be identified was GSK-3 β . PI3-Kinase/PDK1 is activated by growth factors and anti-apoptotic stimuli, which results in the phosphorylation of AKT kinase. This, in turn, phosphorylates GSK-3 β at Ser9, thereby inactivating it [6]. The evidence of involment of GSK-3 in proegression and survival of many cancer pathways cannot be ignored. Therefore the need for the design of both competitive and non-competitive inhibitors that will bind to the active site amino acids is needed.

* Corresponding author. e-mail address: sevkiadem@karatekin.edu.tr

Thiosemicarbazones are chelating ligands capable of forming a five-membered chelate ring involving the sulfur atom and the azomethine nitrogen atom with transition metal ions [7]. A number of characteristics of thiosemicarbazone render them promising candidates for anticancer drugs. Some of these include the cessation of ribonucleotide diphosphate reductase, which halts the production of deoxyribonucleic acid (DNA), the arrest of the cell cycle, and the production of an excessive amount of reactive oxygen species (ROS) [8].

This study investigated the binding potential of thiosemicarbazones compounds to the active site of GSK-3. The study elaborates the interaction of the compounds with the GSK-3 in order to develop anticancer agents that target the inhibition of the enzyme and slow the proliferation and survival of the cancer cells.

2. Materials and Methods

2.1. Protein preparation

The crystal structure of the target protein (PDB ID: 5F95) was downloaded from the Protein Data Bank with resolution 2.52 Å. The protein was then imported into Molegro Virtual Docker (MVD 2013, 6.0). Water molecules and ligands in the crystal structure were eliminated, and protein structural defects were identified. The structure defects of amino acid residues were examined, corrected, and optimized using neighboring residues. The surface was produced, and a cavity was identified for ligand binding.

2.2. Ligand preparation

All 14 ligands were downloaded from PubChem (<https://pubmed.ncbi.nlm.nih.gov>) in SDF format. They were all prepared in MVD to correct any found error.

2.3. Molecular docking

Molecular docking study was carried out at the identified cavity of glycogen synthase kinase 3 protein with binding site origin X: 67.14, Y: 5.94, and Z: 156.13; with radius of 15 and Grid resolution (Å) 0.30. Docking was carried out using dock wizard and best binding pose of ten trials were recorded. MolDock score, rerank score, HBond, and the predicted MW of all the ligands were tabulated.

3. Results and Discussion

Arginine residue was found to bind with both chain A and chain B of the GSK3 (ARG 144A and ARG 144B) through hydrogen and steric interactions for the 3 highest binding score recorded (Table 1). The 3 highest MolDock score are compound 2a (-135.376), compound 5b (-134.954) and compound 4a (-133.06). Compound 3a, 4b, and 5a gives almost similar score. Compound 7a has the lowest molDock score recorded from the 14 thiosemicarbazone compounds.

Table 1. Docking analysis of ligands against glycogen syntase kinase3

Ligand	MolDock Score	Rerank Score	HBond	MW
1a	-122.547	-91.225	-3.068	379.454
1b	-121.844	-97.172	-5.511	363.388
2a	-135.376	-99.831	-3.229	379.454
2b	-129.614	-80.600	-2.677	363.388
3a	-132.274	-97.654	-5.526	394.425
3b	-122.518	-83.856	-6.851	378.36
4a	-133.06	-94.925	-4.305	409.48
4b	-132.872	-107.005	-6.627	393.414
5a	-132.978	-97.082	-4.804	399.487
5b	-134.954	-80.227	-4.366	383.421
6a	-122.543	-99.761	-3.439	349.428
6b	-121.399	-103.853	-1.894	333.362
7a	-118.629	-60.515	-6.193	349.428
7b	-117.832	-92.881	-7.114	333.362

Table 2 shows the amino acids involved in the interactions between GSK-3 and thiosmecarbazone compounds. All the compounds shows hydrogen and steric interactions. Most of the compounds interact with both the chains of the enzyme.

Table 2. The binding interaction mechanisms of the top hits inhibitors with the target compound

Ligand	Hydrogen Bond	Steric Interactions
1a	Ser 147B, Tyr 222B, Arg 144B	Tyr 140B, Ser 147B, Arg 144B, Tyr 222B, Arg 220B
1b	Arg 144B, Tyr 221B	Pro 255, Ser 147B, Arg 144B, Tyr 140B, Tyr 221B, Tyr 222B, Arg 220B, Glu 249B
2a	Tyr 140A, Tyr 222A, Arg 144A, Tyr 221A, Arg 220A	Tyr 140A, Pro 255A, Tyr 222A, Arg 144A, Tyr 221A, Arg 220A, Ala 143A, Glu 249A, Pro 184A
2b	Ser 147B, Arg 144B	Tyr 222B, Ser 147B, Arg 144B, Arg 220B, Pro 184B, Tyr 140B
3a	Tyr 222B, Tyr 221B, Arg 144B	Pro 255B, Tyr 222B, Glu 249B, Arg 144B, Tyr 221B, Arg 220B
3b	Tyr 221B, Arg 144B, Tyr 140B, Ser 147B	Ser 219B, Tyr 221B, Pro 258B, Ser 147B, Arg 144B, Tyr 140B, Glu 249B
4a	Ser 147B, Tyr 222B, Asp 260A, Arg 144B	Glu 249B Ser 147B, Tyr 140B, Tyr 222B, Arg 144B, Asp 260A, Arg 220B
4b	Arg 144B, Ser 147B, Tyr 221B	Ser 147B, Arg 144B, Tyr 222B, Tyr 140B, Glu 249B, Arg 220B, Tyr 221B
5a	Tyr 221A, Arg 144A, Arg 220A, Tyr 140A	Arg 144A, Ala 143A, Glu 249A, Pro 184A, Lys 183A, Tyr 222A, Tyr 140A, Tyr 221A, Arg 220A
5b	Arg 144B, Tyr 221B, Tyr 140B, Arg 220A	Arg 144B, Gln 185B, Ser 219B, Tyr 221B, Arg 220A, Tyr 140B, Glu 249B, Ala 143B
6a	Ser 147B, Arg 144B	Arg 144B, Ser 147B, Glu 249B, Tyr 140B, Tyr 222B, Asp 260A
6b	Ser 147B, Leu 153B, Tyr 222B	Pro 255B, Tyr 222B, Gly 253B, Ala 143B, Ser 147B, Leu 153B
7a	Ser 147B, Arg 144B	Tyr 222B, Tyr 140B, Arg 144B, Ala 143B, Ser 147B
7b	Tyr 222B, Arg 220A, Tyr 140B, Arg 144B, Arg 220B	Glu 249B, Tyr 222B, Arg 144B, Arg 220A, Arg 220B

Five hydrogen binding with steric interactions are involved with compound 2a (Figure 1). A pi-sulfur bond and conventional hydrogen bond of chain A was created with Tyr A:140. Other conventional hydrogen bonds are with Tyr 222A, Arg 144A, Tyr 221A, Arg 220A, all of the A chain. Other types of interaction such as pi-pi, pi-alkyl, carbon hydrogen and alkyl bond can be depicted in Figure 1.

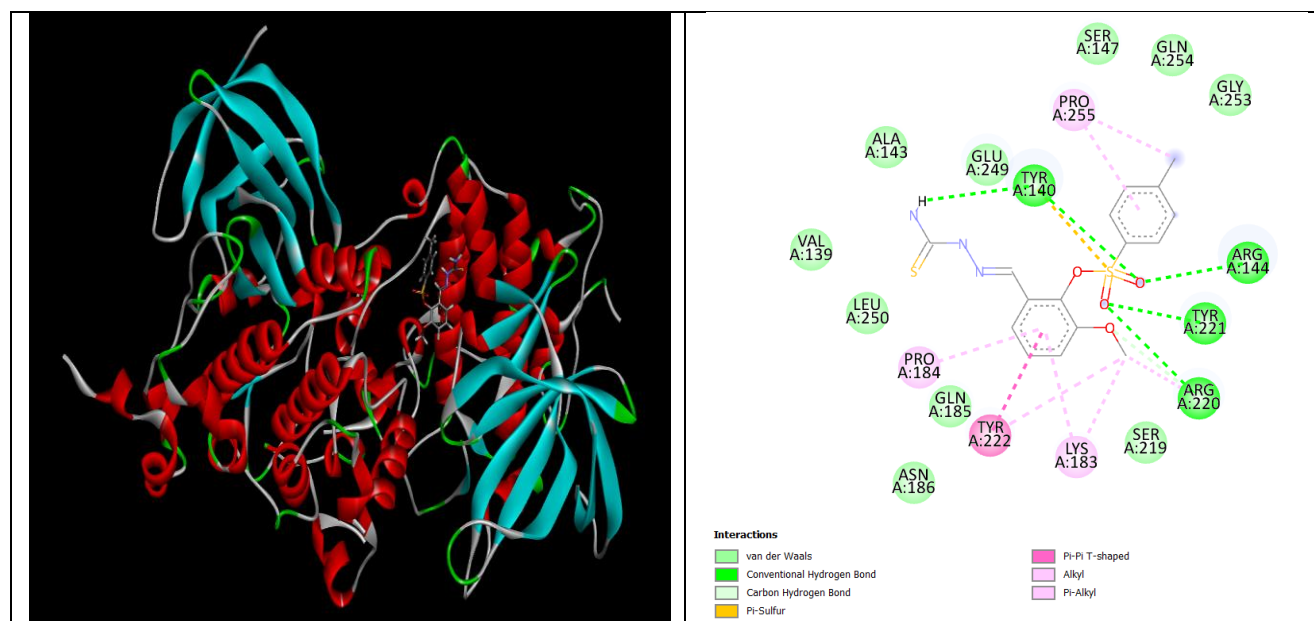


Figure 1. Interactions between compound 2a and GSK3.

Figure 5b shows hydrogen bonding with ARG A:220 and Van der Waals with ASP A:260. Asp residue has been reported to be part of the binding residues of the GSK-3 [9].

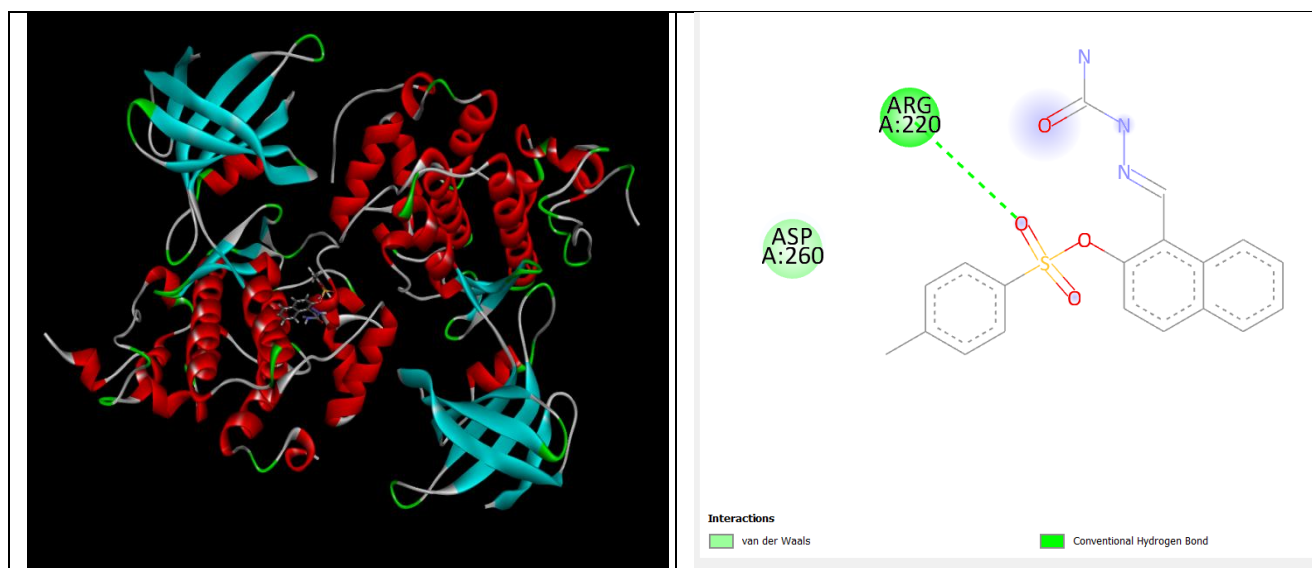


Figure 2. Interactions between compound 5b and GSK3

The hydrogen bond formed with Asp 260 of the A chain (Figure 3) with compound 4a, is similar to the one reported by Ding et al while using gallic acid for GSK-3 inhibition.

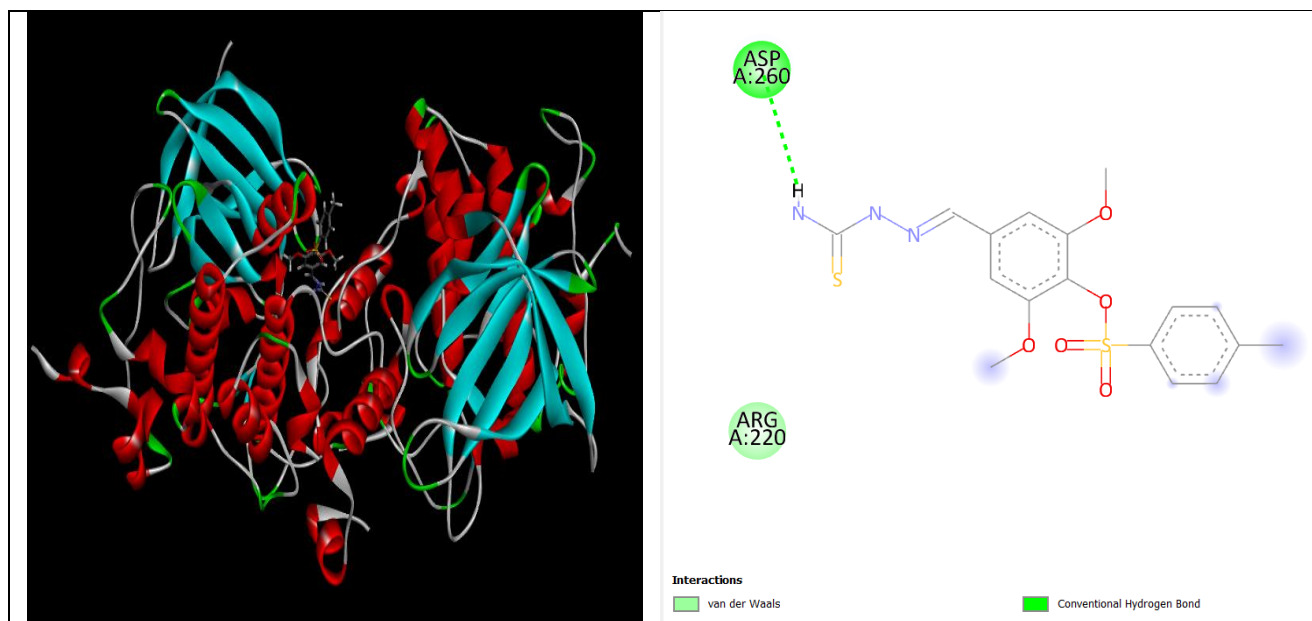


Figure 3. Interactions between compound 4a and GSK3. Van der Waals interaction with ARG A:220 and Conventional Hydrogen Bond with ASP A:260

4. Conclusion

The current study reveals a good interaction between thiosemicarbazone compounds and glycogen synthase kinase 3, thereby giving it an ideal opportunity for its drug likeness. This is as a result of its well fits in the active site of glycogen synthase kinase 3. Invitro and in vivo studies are recommended for further insights on the interactions and possible inhibition type

References

- [1] A. Kazi *et al.*, “GSK3 suppression upregulates β -catenin and c-Myc to abrogate KRas-dependent tumors,” *Nat. Commun.*, vol. 9, no. 1, pp. 1–9, 2018, doi: 10.1038/s41467-018-07644-6.
- [2] X. Fang, S. X. Yu, Y. Lu, R. C. Bast, J. R. Woodgett, and G. B. Mills, “Phosphorylation and inactivation of glycogen synthase kinase 3 by protein kinase A,” *Proc. Natl. Acad. Sci. U. S. A.*, vol. 97, no. 22, pp. 11960–11965, 2000, doi: 10.1073/pnas.220413597.
- [3] M. K. Pandey and T. R. DeGrado, “Glycogen synthase kinase-3 (GSK-3)-targeted therapy and imaging,” *Theranostics*, vol. 6, no. 4, pp. 571–593, 2016, doi: 10.7150/thno.14334.
- [4] S. R. Shri, Y. Nayak, and S. Ranganath Pai, “Molecular docking studies and molecular dynamic simulation analysis: To identify novel ATP-competitive inhibition of Glycogen synthase kinase-3 β for Alzheimer’s disease,” *F1000Research*, vol. 13, no. August, p. 773, 2024, doi: 10.12688/f1000research.145391.2.
- [5] Y. Ding *et al.*, “Gallic Acid Alleviates Cognitive Impairment by Promoting Neurogenesis via the GSK3 β -Nrf2 Signaling Pathway in an APP/PS1 Mouse Model,” *J. Alzheimer’s Dis. Reports*, vol. 8, no. 1, pp. 461–477, 2024, doi: 10.3233/ADR-230171.
- [6] G. Augello *et al.*, “The role of GSK-3 in cancer immunotherapy: GSK-3 inhibitors as a new frontier in cancer treatment,” *Cells*, vol. 9, no. 6, pp. 1–17, 2020, doi: 10.3390/cells9061427.
- [7] A. B. M. Ibrahim *et al.*, “Synthesis, structural studies and antimicrobial activities of manganese, nickel and copper complexes of two new tridentate 2-formylpyridine thiosemicarbazone ligands,” *Inorg. Chem. Commun.*, vol. 96, pp. 194–201, 2018, doi: 10.1016/j.inoche.2018.08.023.
- [8] A. Q. Ali, S. G. Teoh, N. E. Eltayeb, M. B. K. Ahamed, and A. A. Majid, “Synthesis of nickel(II) complexes of isatin thiosemicarbazone derivatives: In vitro anti-cancer, DNA binding, and cleavage activities,” *J. Coord. Chem.*, vol. 67, no. 20, pp. 3380–3400, 2014, doi: 10.1080/00958972.2014.959943.
- [9] J. Zhu, Y. Wu, L. Xu, and J. Jin, “Theoretical Studies on the Selectivity Mechanisms of Glycogen Synthase Kinase 3 β (GSK3 β) with Pyrazine ATP-competitive Inhibitors by 3DQSAR, Molecular Docking, Molecular Dynamics Simulation and Free Energy Calculations,” *Curr. Comput. Aided. Drug Des.*, vol. 16, no. 1, pp. 17–30, 2019, doi: 10.2174/1573409915666190708102459.



An Investigation of the Effect of Cupping (Al-Hijima) on Hematological, and Lipid Profile Parameters in Missan Province/South Iraq

Ali Mohsin Hasan AL-BEHADILI^{1,*} , Ali KARAIPEKLI² 

¹Institute of Graduate Studie, Department of Chemistry, Çankırı Karatekin University, Çankırı, Turkey

²Faculty of Science, Department of Chemistry, Çankırı Karatekin University, Çankırı, Turkey

Abstract

This research investigates the impact of cupping therapy on hematological and lipid profile parameters in patients in Missan Province, Southern Iraq. The study involves 50 patients, primarily suffering from chronic conditions such as obesity, high fat levels, joint pain, and headaches. Notably, cupping can significantly reduce total cholesterol, triglycerides, and LDL levels, while increasing HDL levels. The obtained results show that there are significant differences in the values of total cholesterol before and after cupping for 10, 20, and 30 days. A significant reduction in total cholesterol values was observed after cupping three times, as the values decreased to 209.08, 162.02, and 149.80 mg/dL, respectively. In the patient group, it was recorded as 234.24 mg/dL before cupping. The results confirm the presence of significant differences in the total triglyceride values before and after cupping. The total triglyceride values of 10, 20, and 30 days after cupping exhibit a significant decrease, as they are recorded at 147.08, 153.18, and 157.40 mg/dL, respectively, compared to 179.50 mg/dL before cupping. Notable differences in LDL values are also observed among the four groups studied before and after cupping. The groups recorded a substantial decrease in LDL levels 10, 20, and 30 days after cupping, with values of 117.34, 113.28, and 103.66 mg/dL, respectively, compared to 134.14 mg/dL prior to cupping. There are notable differences in HDL values before and after cupping. The results show a significant increase in HDL values following cupping. At 10, 20, and 30 days post-cupping, the HDL levels are 41.70, 43.50, and 45.98 mg/dL, respectively, compared to 32.21 mg/dL before cupping. These findings suggest that cupping therapy may have beneficial effects on hematological and lipid profiles, potentially contributing to improved overall health.

Keywords: *Cupping, Hematological, Lipid profile, Missan province*

1. Introduction

Al-Hijamah, a religious practice firmly ingrained in the Arab and Muslim world, is backed by several certified sayings (hadiths) of Prophet Mohammad (PBUH). Over 1400 years ago, Prophet Mohammad (PBUH) advised its usage in treating human maladies [1]. Cupping therapy has been shown to have positive effects in alleviating lower back pain, neck and shoulder discomfort, headache and migraine, knee pain, facial paralysis, brachialgia, carpal tunnel syndrome, hypertension, diabetes mellitus, rheumatoid arthritis, and asthma. The disorders may be classified into two categories: localized diseases, which include neck pain, lower back pain, and knee pain, and systemic diseases such as diabetes mellitus, hypertension, and rheumatoid arthritis [2].

There are three distinct forms of cupping therapy, which are dry cupping, wet cupping, and massage cupping. Dry cupping involves placing stationary cups on the skin without incisions, leaving them in one location for duration of five to 15 minutes. Wet cupping, on the other hand, utilizes a vacuum at various points on the body, accompanied by incisions, to extract 'harmful' blood located just beneath the skin's surface. In massage cupping, an application of oil is used on the skin to enhance the ease of movement and identify areas of tension and congestion before placing the cup [3]. Cupping treatment may be categorized into two main types: dry cupping and wet cupping. Dry cupping is the act of pulling the nearby tissue under the cup via suction, whereas wet cupping employs the same method but also includes the practices of scarification and bloodletting [4].

Several ideas elucidate the mechanism of action of cupping, including the immunomodulation hypothesis, which proposes that cupping and acupuncture have similar processes of action. The immunomodulation hypothesis proposes that the act of stimulating the skin might lead to the transformation of the microenvironment into biological signals, which in turn activate the neuroendocrine immuno system [5].

According to Wong [6], the mechanical stress on the skin caused by sub atmospheric pressure and the partial deprivation of oxygen during cupping suction might generate physiological and mechanical signals that have the potential to activate or inhibit gene expression. During wet cupping treatment, the process of making shallow

* Corresponding author. e-mail address: alimohsinalbahadili@gmail.com

cuts on the skin may stimulate the body's natural healing response and activate certain genes that control the wound-healing process.

Cupping treatment is generally considered safe, however adverse events (AEs) associated with cupping therapy are not often recorded but are not uncommon. The majority of adverse events are of mild to moderate intensity. The majority of adverse events associated with cupping treatment include the development of scars, followed by burns. The other adverse events that have been documented include cephalalgia, pruritus, vertigo, fatigue, myofascial tension, anemia, emesis, development of blisters, minor hematoma or discomfort at the site of cupping, formation of abscesses, cutaneous infection, sleeplessness, hyperpigmentation, and vasovagal syncope.

The study aims to evaluate the potential clinical benefits of cupping therapy on hematological and lipid profiles in patients with chronic conditions in Missan Province, South Iraq.

2. Materials and Methods

This research examined the effects of cupping on blood and lipid profile parameters in the people attending cupping centres in Amara, Maysan Governorate, Iraq, from January to June 2024. The patients had obesity, hypertension, elevated cholesterol, and triglycerides. Along with elevated haemoglobin, most individuals were smokers. To compare patients' haematological and lipid profiles before and after cupping. Approximately 200 patients are studied. Group A: 50 pre-cupping patients. In Group B, 50 patients cupped for 10 days. Group C: 50 cupping patients after 20 days. After 30 days of cupping, 50 patients were in Group D. Each patient should provide three 6-ml blood samples: before cupping, 10 days after cupping, and 20 days after cupping. The final sample was obtained 30 days after cupping. Using a lipid panel, blood lipid levels are measured. A typical panel comprises four cholesterol readings and a triglyceride measurement. Before commencing work, all reagents and samples are brought to room temperature and 1 ml of plank, sample, and standard Cal is added to Reagent R1. The Model Tube and standard Cal tubes each receive 10 microlitres of sample and standard Cal, respectively. The tubes are mixed and incubated at 25°C for 10 minutes, after which the absorbance at 500 nm for each sample and the standard is measured. The values are then applied to the Planck equation to calculate the total cholesterol in milligrams per deciliter. All the reagents and samples are transferred to room temperature; then, 1 ml each of the plank, model, and Cal Standard are added to the R1 reagent tube. Subsequently, 10 microlitres of the sample is added to the sample tube, and 10 microlitres of Cal Standard to the Cal Standard tube; then, they are mixed and incubated at room temperature. After 15 minutes, the samples' and standard's 500 nm absorbance are compared with the plank. LDL-cholesterol is dangerous. Too much cholesterol in the circulation causes atherosclerosis, which restricts blood flow. Good cholesterol, HDL, removes bad cholesterol, opening arteries and improving blood flow. The separation process uses phosphotannic acid and magnesium chloride to precipitate B-containing lipoproteins. Centrifugation and enzymatic analysis sediment the fine filtrates residual precipitated HDL cholesterol. All samples and reagents are kept at room temperature and mixed with 0.2 ml of the sample or standard with 0.4 ml of sedimentation reagent in designated centrifuge tubes. The tubes are thoroughly shaken and incubated at 25°C for 10 minutes. They are centrifuged at 4000 RPM for 10 minutes, and the clear filtrate is separated within two hours. 1 ml of the plank, sample, and standard are added into the R1 reagent tube. 50 microlitres of the sample filtrate is added into the filtrate and standard tubes. The tubes are mixed and incubated at room temperature for 10 minutes; then, the filtrate and standard absorbance at 500 nm are compared with the plank. Results are presented as mean \pm standard error (SE). SPSS 22 is performed by one-way ANOVA.

3. Results and Discussion

3.1. Total cholesterol level and cupping therapy

The results of Table 1 show that there are significant differences in the values of total cholesterol before and after cupping for 10, 20, and 30 days. The results confirm a significant reduction in the values of total cholesterol after cupping three times, as the values decrease to 209.08, 162.02, and 149.80 mg/dL, respectively. In the patient group, it was recorded as 234.24 mg/dL before cupping.

These results agree with the results of Mraisel et al. [7] who confirmed that the values of total cholesterol after cupping at 7 and 14 days decreased to 165.65 and 141.39 mg/dL compared to 208.89 mg/dL, respectively. Moreover, it was found that the values of total cholesterol decrease to 218.05 from 264.20 mg/dL, respectively. A decrease is also observed in total cholesterol values to 206.31 mg/dL from 313.94 mg/dL before cupping. It is found that Cupping therapy is given at meridian points to reduce high cholesterol in the blood. Giving

cupping therapy at the correct meridian points can increase the number of Lymphocytes, lymphocytes, and the endothelial system secrete adrenocorticotrophic hormone (ACTH), cortisol, and endorphins. Enkephalin and other humoral factors that also cause anti-inflammatory effects reduce serum triglycerides, phospholipids, and total cholesterol, especially LDL cholesterol [8]. Sutriyono et al. [9] indicated that cupping therapy may lead to lower values of total cholesterol and uric acid and lower blood pressure in patients suffering from high blood pressure.

Table 1. Total cholesterol level and cupping therapy

Group	Mean (mg/dL)	N	Std. Deviation	Std. Error of Mean
Pre cupping	234.2400	50	9.20417	1.30167
post 10 days of cupping	209.0800	50	5.88960	0.83291
post 20 days of cupping	162.0200	50	4.36821	0.61776
post 30 days of cupping	149.8000	50	5.80288	0.82065
Total	188.7850	200	35.02675	2.47677

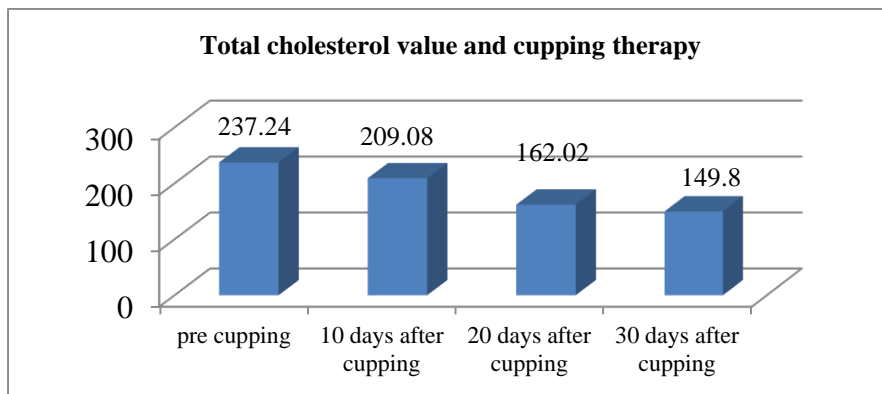


Figure 1. Total cholesterol value and cupping therapy

3.2. Total triglycerides value and cupping therapy

Table 2 shows the presence of significant differences in the values of total triglycerides before and after cupping. The results indicate a significant decrease in the values of total triglycerides 10, 20, and 20 days after cupping, as they were recorded at 147.08, 153.18, and 157.40 mg/dL, respectively, compared to 179.50 mg/dL before cupping. Suhaily et al. [10] concluded that after two sessions of wet cupping, total triglycerides, HDL, LDL and total cholesterol can be significantly improved by 20.8%, 13.7%, 16.4%, and 8.2%, respectively. Sultan et al. [11] indicated that cupping treatment can lead to a reduction in the level of triglycerides and total cholesterol to 102.5 and 147.5 mg/dL, compared to 125.62 and 160.75 mg/dL before cupping, respectively. Sungkawa [12] also showed that there is a significant decrease in the levels of triglycerides and total cholesterol after cupping to 159.0 and 220 mg/dL from 184 and 231 mg/dL, respectively, before cupping. Also, Niasari et al. [13], showed that treatment with cupping can lead to reducing the level of triglycerides from 126.27 mg/dL to 102.63 before cupping.

Table 2. Total triglycerides value and cupping therapy

Group	Mean (mg/dL)	N	Std. Deviation	Std. Error of Mean
Pre cupping	179.5000	50	6.65858	0.94167
post 10 days of cupping	147.0800	50	4.32289	0.61135
post 20 days of cupping	153.1800	50	4.90601	0.69382
post 30 days of cupping	157.4000	50	2.02031	0.28571
Total	159.2900	200	13.14572	0.92954

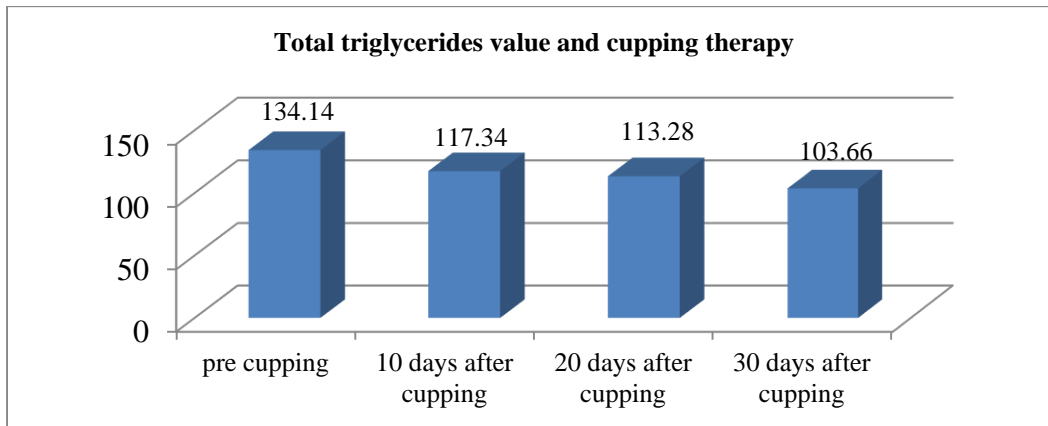


Figure 2. Total triglycerides value and cupping therapy

3.3. LDL value and cupping therapy

The results of Table 3 confirm that there are significant differences in the LDL values among the four groups studied before and after cupping, as the groups recorded 10, 20, and 30 days after cupping a significant decrease in the LDL rate, as they recorded 117.34, 113.28, and 103.66 mg/dL, respectively, compared to 134.14. mg/dL before cupping. These results agree with the results of the study conducted by Niasari et al. [13] in which it was found that the use of cupping can lead to a reduction in LDL values for men and prevent their levels from rising in the blood. It was also found that the use of cupping can result in a reduction in LDL values from 123.89 to 154.70 mg/dL. Moreover, cupping can significantly reduce the LDL values from 172.67 to 146.78 mg/dL. Sultan [11] also noted a decrease in LDL values after using cupping from 96.56 to 72.2 mg/dL.

Table 3. LDL value and cupping therapy

Group	Mean (mg/dL)	N	Std. Deviation	Std. Error of Mean
Pre cupping	134.1400	50	6.99565	0.98933
post 10 days of cupping	117.3400	50	5.25516	0.74319
post 20 days of cupping	113.2800	50	4.53575	0.64145
post 30 days of cupping	103.6600	50	3.55488	0.50274
Total	117.1050	200	12.20857	0.86328

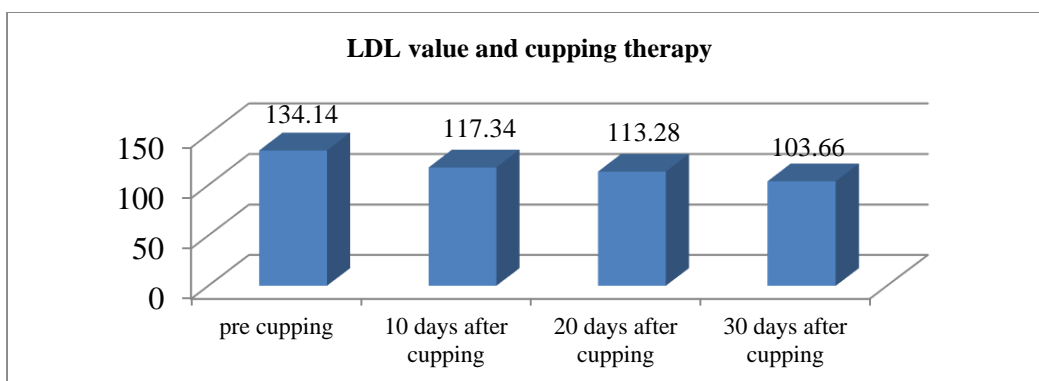


Figure 3. LDL value and cupping therapy

3.4. HDL value and cupping therapy

Table 4 showcases the significant differences in HDL values before and after cupping. The findings exhibit a significant increase in HDL values after cupping at 10, 20, and 30 days, amounting to 41.70, 43.50, and 45.98 mg/dL, respectively, compared to 32.21 mg/dL before cupping. These results agree with the results of, Mraisel

et al. [7], who confirmed that treatment with cupping for a period of 7 and 14 days significantly increased HDL values to 41.59 and 53.85 mg/dL, respectively, while the values before cupping were 33.98 mg/dL. Widada et al. [14] reported that HDL values increased from 33.03 mg/dL to 37.58 mg/dL after cupping. The present study agrees with the study by Widada et al. [14], which confirmed that HDL values increased significantly after cupping, and LDL values decreased after cupping treatment. It also agreed with the study by Ahmed et al. [15], which showed that HDL values increased from 1.12 in males and 1.30 in females to 1.43 and 1.81 mmol/L, respectively, after cupping.

Table 4. HDL value and cupping therapy

Group	Mean (mg/dL)	N	Std. Deviation	Std. Error of Mean
Pre cupping	32.2100	50	7.80443	1.10371
post 10 days of cupping	41.7000	50	1.68123	0.23776
post 20 days of cupping	43.5000	50	1.71726	0.24286
post 30 days of cupping	45.9800	50	1.51846	0.21474
Total	40.8475	200	6.65598	0.47065

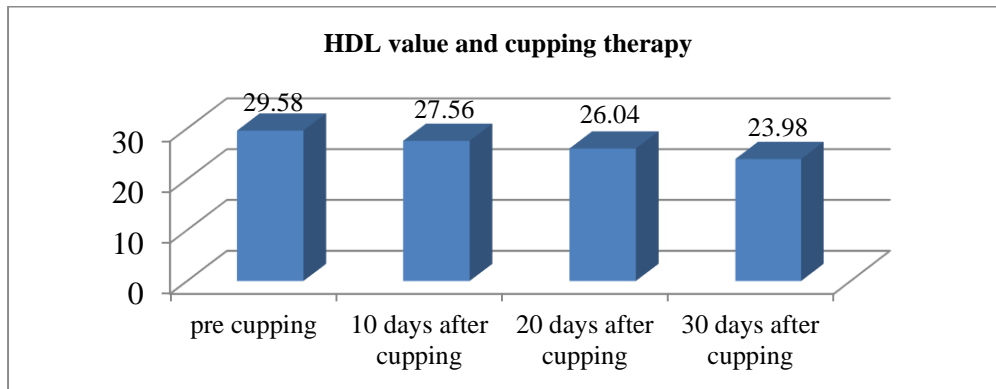


Figure 4. HDL value and cupping therapy

4. Conclusion

The average age of the patients under this study are 48.44, and their ages range from 30 to 58 years. Most of the people who underwent cupping suffered from chronic diseases such as obesity, high levels of fat, joint pain, and headaches, and they resorted to cupping as a popular treatment for these diseases. The results show that there are significant differences in the values of total cholesterol before and after cupping for 10, 20, and 30 days. The values of total cholesterol after cupping three times exhibit a significant decrease, as the values decrease to 209.08, 162.02, and 149.80 mg/dL, respectively. In the patient group, it was recorded as 234.24 mg/dL before cupping. Total triglycerides values before and after cupping exhibit considerable difference. A significant decrease in the values of total triglycerides 10, 20, and 20 days after cupping is observed, as they are recorded at 147.08, 153.18, and 157.40 mg/dL, respectively, compared to 179.50 mg/dL before cupping. There are differences in the LDL values for the four groups studied before and after cupping, as the groups recorded 10, 20, and 30 days after cupping. Moreover, a decrease in the LDL rate is noted, as they recorded 117.34, 113.28, and 103.66 mg/dL, respectively, compared to 134.14. mg/dL before cupping. The findings also show that there are considerable differences in HDL values before and after cupping. A significant increase in HDL values after cupping at 10, 20, and 30 days is noted, amounting to 41.70, 43.50, and 45.98 mg/dL, respectively, compared to 32.21 mg/dL before cupping.

References

- [1] Qureshi, N. A., Ali, G. I., Abushanab, T. S., El-Olemy, A. T., Alqaed, M. S., El-Subai, I. S., & Al-Bedah, A. M. (2017). History of cupping (Hijama): A narrative review of literature. *Journal of Integrative Medicine*, 15(3), 172-181.
- [2] Saha, F. J., Schumann, S., Cramer, H., Hohmann, C., Choi, K. E., Rolke, R., & Lauche, R. (2017). The effects of cupping massage in patients with chronic neck pain-A randomised controlled trial. *Complementary Medicine Research*, 24(1), 26-32.
- [3] Osman-Latib, F. (2013). *Islamic cupping & hijamah: A complete guide*. EDI Publishers.
- [4] Akhtar, H., Rashid, M., Siddiqi, M., & Ahmad, Q. Z. (2017). Role of Hijama'(Cupping Therapy) in the management of Niqras (Gouty Arthritis). *J Arthritis*, 6(256), 2.
- [5] Guo, Y., Chen, B., Wang, D. Q., Li, M. Y., Lim, C. H. M., Guo, Y., & Chen, Z. (2017). Cupping regulates local immunomodulation to activate neural-endocrine-immune worknet. *Complementary Therapies in Clinical Practice*, 28, 1-3.
- [6] Wong, C. (2019). Cupping therapy overview, benefits, and side effects. Medically reviewed by a board-certified physician.
- [7] Mraisel, A. C., Nama, M. A., & Ahmed, A. (2020). Effect of Cupping (Al-Hijima) on Hematological and Biochemical Parameters for some Volunteers in Missan Province. *Indian Journal of Forensic Medicine & Toxicology*, 14(3), 1520-1525.
- [8] Fikri, Z., Nursalam, N., & Has, E. M. M. A. (2010). The reduction of cholesterol with cupping therapy on cholesterol reduction in patients with hypercholesterolemia. *Jurnal Ners*, 5(2), 195.
- [9] Sutriyono, S., Robbina, M. R., & Ndii, M. Z. (2019). The effects of wet cupping therapy on blood pressure, glucose, uric acid, and total cholesterol levels. *Biology, Medicine, & Natural Product Chemistry*, 8(2), 33-36.
- [10] Suhaily, M. H., Ismail, A. A., & Najib, M. Y. (2017). Randomized control trial study on the effect of wet cupping on lipid profile. *IIUM Medical Journal Malaysia*, 16(2).
- [11] Sultan, M. Q. (2021). A correlation between wet cupping therapy treatment and serum lipids profile levels in Thi-Qar governorate-Iraq. *Annals of the Romanian Society for Cell Biology*, 2238-2242.
- [12] Sungkawa, H. B. (2019). Penurunan kadar kolesterol total dan trigliserida dengan teknik bekam pada penderita hiperkolesterolemia. *Meditory: The Journal of Medical Laboratory*, 7(1), 1-6.
- [13] Niasari, M., Kosari, F., & Ahmadi, A. (2007). The effect of wet cupping on serum lipid concentrations of clinically healthy young men: A randomized controlled trial. *J Altern Complement Med*, 13(1), 79-82.
- [14] Widada, W., Ontoseno, T., Purwanto, B., Subadi, I., & Notobroto, H. B. (2020). The effect of the blood cupping therapy on high density lipoprotein (HDL) and low density lipoprotein (LDL) in hypercholesterol patients. *Indian Journal of Forensic Medicine & Toxicology*, 14(4).
- [15] Ahmed, K. A. A., Ola, A. S., Haidar, A., Eskander, S., Al-qari, B. and Hamzah, A. 2022. Evaluating the Therapeutic Effects of Wet Cupping (Al-Hijamah) on Hematological Parameters, Kidney Function Tests and Lipid Profile in Adult Women. *Biomedical and Pharmacology Journal*, 15(1), 187-197.



Deep Learning Based Fault Detection For PCB Quality Control Using YOLO

Buğrahan BİLİR^{1,*}, **Adem ÇİÇEK²**

^{1,2} Department of Electrical Electronics Engineering, Çankırı Karatekin University, Çankırı, Türkiye

Abstract

Machine learning methods and image processing methods are increasingly used due to their high performance in different areas. This study aims to use the YOLO (You Only Look Once) algorithm to detect components and defects on printed circuit boards (PCBs). Since defects occurring in PCB manufacturing directly affect the performance of electronic devices, it is important to automatically detect these defects. In the study, a dataset consisting of PCB images is used and this dataset is labeled to include different types of defects. The model developed using the YOLO algorithm is subjected to hyperparameter optimization during the training process and the model performance is evaluated with metrics such as accuracy, precision and F1-score. The results show that the YOLO algorithm detects PCB defects with high accuracy and that the model provides an effective solution for quality control in manufacturing processes.

Keywords: YOLO, PCB, Fault detection, Deep Learning, Object detection, Quality control

1. Introduction

Printed circuit boards (PCBs) are of great importance as the basic building blocks of modern electronic devices, and it is necessary to detect errors occurring in production processes quickly and accurately. In this context, the inadequacies of traditional methods and the vulnerability of manual inspection processes to human-induced errors bring the use of computer vision and deep learning methods to the forefront [1]. In the field of object detection, the YOLO (You Only Look Once) algorithm has been frequently preferred in industrial applications due to its high accuracy and speed. The applicability of YOLO, especially in real-time production processes, has been proven in various studies. The study by Redmon and Farhadi, which introduced the YOLO algorithm, is considered groundbreaking in terms of speed and accuracy in object detection [2]. In addition, YOLOv4, developed by Bochkovskiy et al., has been adapted to PCB error detection and has shown that different types of errors can be successfully classified [3]. Research in the field of PCB error detection has generally focused on the detection of errors by manual labeling or traditional image processing methods. Lee and Kim developed a system that uses classical image processing methods to detect defects such as short circuits and missing holes on PCBs. However, the low generalization ability of these systems and the fact that they are affected by the diversity in the dataset have increased the importance of deep learning algorithms [4]. In studies on the use of machine learning methods in PCB production, it is stated that deep learning-based object detection algorithms exhibit superior performance compared to traditional machine learning methods [5]. In particular, Tan and Le's EfficientDet algorithm has offered an alternative approach for PCB defect detection and attracted attention with its high accuracy rates in smaller sizes [6]. The use of such algorithms ensures high success in real-time applications [7]. In studies on feature selection and model optimization, it has been seen that filter-based methods play a critical role in improving the performance of machine learning models. In particular, feature selection methods such as "Chi-square" and "ReliefF" have been found effective in classification problems. The work of Guyon and Elisseeff highlights that these techniques are effective tools to increase the accuracy rates of classification models [8]. In recent years, the use of hybrid models has emerged as an important solution for complex tasks such as PCB defect detection. For example, the hybrid model proposed by Wang et al. combined the YOLO algorithm with traditional CNN-based architectures to both increase accuracy and optimize processing speed [9]. Similarly, Zhao et al. developed a deep learning-based architecture for PCB defect detection and reported that the model achieved over 95% accuracy [10]. In summary, it clearly demonstrates the effectiveness of YOLO and similar algorithms in the field of PCB defect detection. However, issues such as the size of the datasets used, the variety of features, and the expansion of defect classes offer important research areas for future

* Corresponding author. e-mail address: bugra_bilir@hotmail.com

studies. In addition, applications of hybrid models and new generation deep learning architectures in this field are promising for further automation of industrial processes [9-11]. In this study, unlike similar studies in the literature, the dataset and hyperparameter optimization processes of previous projects are examined in order to increase the accuracy rate of the model, and special hyperparameter selections are made for the YOLO algorithm in line with the information obtained. In addition, the meticulous labeling of the dataset and enrichment with augmentation techniques significantly increased the generalization ability and performance of the model.

2. System Model

YOLO uses a set of deep learning-based architectures for object detection. The YOLO architecture used in this study consists of an EfficientNet-based structure that creates feature maps at different scales and combines them to provide detailed detection. A diagram explaining the YOLO architecture and the BiFPN (Bidirectional Feature Pyramid Network) layer is included (Figure 1).

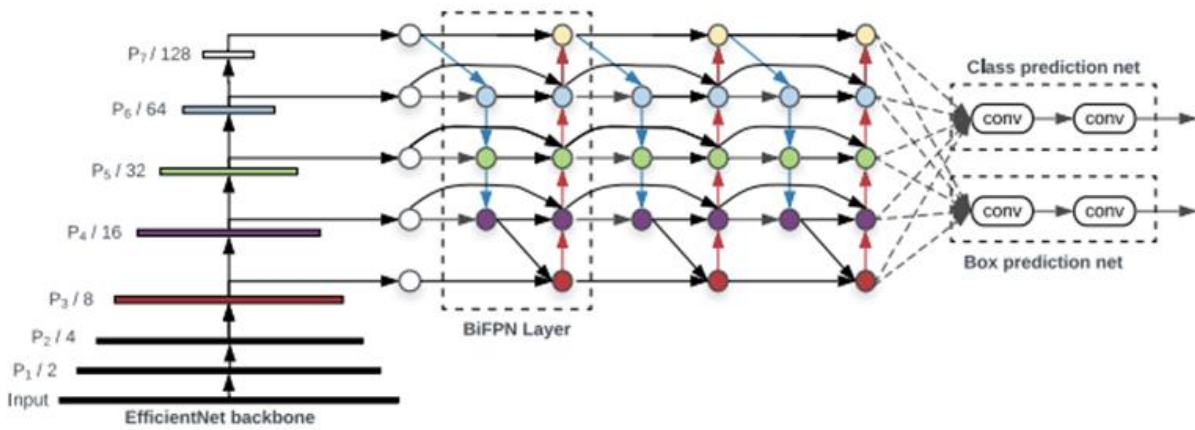


Figure 1. YOLO architecture and BiFPN layer[6]

BiFPN stands out as one of the most critical components of the YOLO architecture. BiFPN improves object detection accuracy by effectively combining feature maps of different resolutions. Unlike traditional feature pyramid networks, BiFPN has a bidirectional connection structure, which enables both upstream and downstream data flow. The merging process is performed to optimize the information contextually between these directions.

Node Structure and Weighted Sum: BiFPN provides data flow through nodes at each feature map level. These nodes combine information from different resolutions and optimize it with a weighted sum method. This approach provides more accurate detection of objects at different scales.

Dynamic Flow and Directional Structure: BiFPN has a bidirectional structure and enables the transfer of features from top to bottom and bottom to top. It combines low-level details for small objects and high-level contextual information for large objects.

Balance of Complexity and Performance: Another advantage of BiFPN is that it optimizes performance without increasing computational complexity. Especially for models that need to run fast, such as YOLO, such a feature fusion mechanism provides a balance between both accuracy and speed.

As a result, BiFPN and YOLO architecture provides an effective solution in cases where speed and accuracy are critical in object detection. This structure, which forms a strong foundation with EfficientNet, provides accurate and fast detection of objects with enriched feature maps and parallel prediction mechanism thanks to BiFPN.

3. Proposed YOLO Based PCB Defect Detection

In this study, a YOLO-based model is proposed for the detection and classification of defects on PCBs. The model aims to classify common defects in PCB images into categories such as "missing_hole", "short circuit", "spurious copper" and "mouse bite" and to classify these defects correctly. A comprehensive dataset is created, this dataset is labeled in detail for defects and the YOLO algorithm is trained. 70% of the dataset is separated for training and 30% for testing. The YOLO algorithm offers a fast and efficient object detection approach that can simultaneously predict both the locations and classes of objects by processing the input image at once.

The architecture of the model is built on an EfficientNet-based backbone network that extracts multi-scale feature maps from the input image. These feature maps are processed over the Bidirectional Feature Pyramid Network (BiFPN) layer and combine contextual information at different resolutions, allowing the detection of small and large defects. The bidirectional structure of BiFPN provides an efficient flow of information between low-resolution contextual information and high-resolution details. The final prediction process is performed by the model's prediction network, which determines both the error classes and their locations. Figure 1 shows the main components of the YOLO-based architecture in detail, such as the EfficientNet backbone network, the BiFPN layer, and the prediction network.

3.1 Dataset and Preprocessing

The dataset consists of high-resolution images containing different types of PCB defects. In the pre-processing phase of the dataset, irrelevant information such as background noise is filtered and the images are made suitable for the input dimensions of the YOLO algorithm. In addition, data augmentation techniques (such as rotation, scaling, translation) are applied to increase the generalization capacity of the model. The defect regions are carefully labeled and bounding boxes are created to ensure accurate inspection.

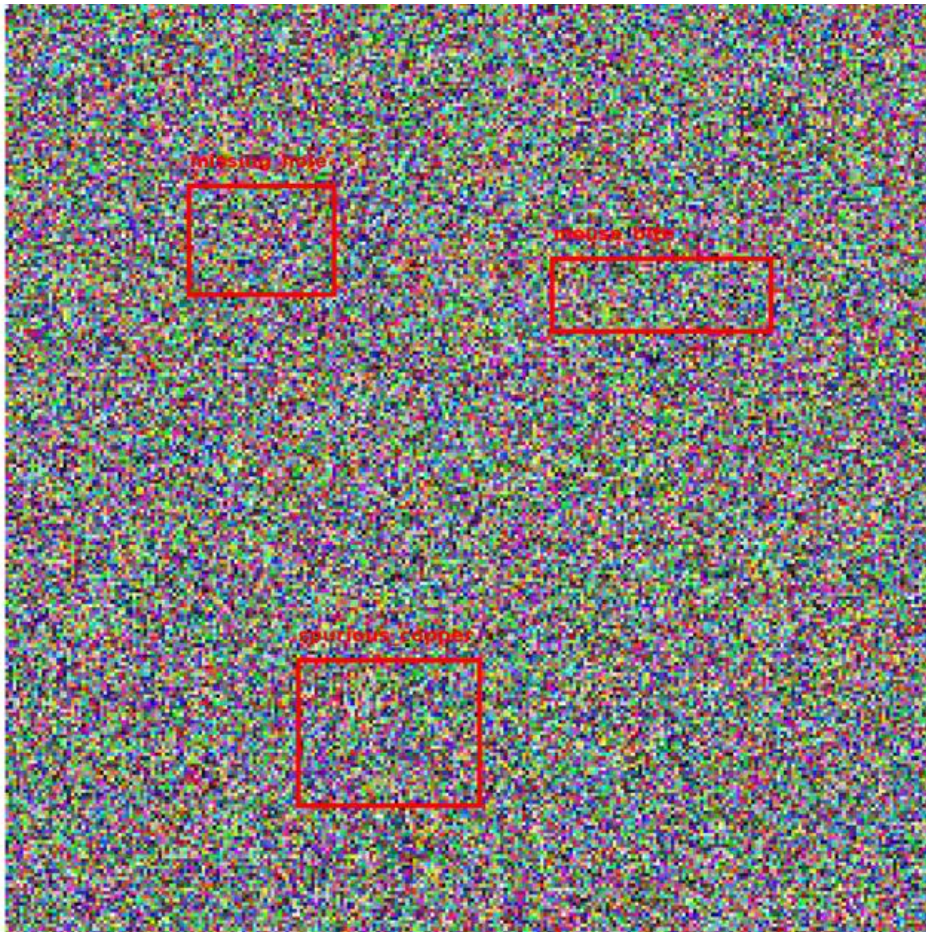


Figure 2. Annotated PCB Image with Defects

The data set is prepared by dividing it into different classes as "missing_hole", "short circuit", "spurious copper" and "mouse_bite".

3.2 Feature Extraction and BiFPN Layer

The EfficientNet backbone network of the model extracts feature maps (e.g., P1, P2, P3) from the input image at different resolutions. These feature maps are processed in the BiFPN layer and combine both low-level details and high-level contextual information with bidirectional information flow. For example, small-scale errors such as “spurious copper” benefit from high-resolution details, while large-scale errors such as “missing_hole” benefit from low-resolution contextual information. BiFPN optimizes the information at each level, enabling effective detection of errors of different sizes.

3.3 Model Training and Evaluation

The YOLO model is trained with a batch size of 16 and an adaptive learning rate. During the training process, categorical cross-entropy loss is used for classification and mean squared error loss for bounding box regression. The performance of the model is evaluated with standard metrics such as accuracy, precision, recall and F1-score. Analysis on the test set showed that the model provided over 99% accuracy, especially in the "missing_hole" and "short circuit" classes, and also operated at sufficient speed for real-time applications. In this study, labeling was performed on PCB images for YOLO-based model to detect various types of defects. Defect classes such as “missing_hole”, “short circuit”, “fake copper” and “mouse_bite” are included in the dataset. 70% of the dataset is used for training and 30% for testing. Statistical methods such as “Chi-square” and “ReliefF” is applied for feature selection on the data and the effects of these methods on the model performance is examined. The first 10 selected features are presented in Table 1.

Table 1. Features selected for each statistical methods

Chi-square	ReliefF	Gain Ratio	Information Gain
Feature1	Feature2	Feature1	Feature3
Feature2	Feature3	Feature4	Feature5
Feature3	Feature5	Feature6	Feature7
Feature4	Feature7	Feature8	Feature9
Feature5	Feature8	Feature9	Feature10
Feature6	Feature10	Feature11	Feature12
Feature7	Feature12	Feature13	Feature14
Feature8	Feature14	Feature15	Feature16
Feature9	Feature15	Feature16	Feature17
Feature10	Feature17	Feature18	Feature19

The expressions such as “Feature1”, “Feature2” in Table 3 represent specific features (variables) in the dataset used in the analysis of printed circuit boards (PCBs). These features are the basic inputs used for the model to learn to detect defects or components on each PCB. They are as follows:

Feature1: Number of holes or missing holes on the PCB.

Feature2: Measurement of line lengths or short circuit occurrences.

Feature3: Spurious copper on the copper layer or their surface area.

Feature4: Width and accuracy of traces on the PCB.

Feature5: Layout of connection points or open circuit.

Feature6: Presence of spurs on the PCB.

Feature7: Density of fine defects on the PCB (e.g. cracks or scratches).

Feature8: Measurement of surface irregularities or surface roughness.

Feature9: Electrical test results (such as voltage, current or resistance).

Feature10: Probability of defects occurring in different areas of the PCB (defect density distribution).

4. Simulation Results

Table 2 shows the model performances according to the feature selection methods used. The proposed YOLO-based model provided the highest accuracy rate, especially with the “Chi-square” and “ReliefF” techniques. While 99% accuracy is achieved with the “Chi-square” technique, 98% accuracy is achieved with “ReliefF”. In contrast, the accuracy of other singular-based algorithms such as DNN and RF varied between 85% and 92%. The findings show that feature selection methods have a significant effect on the model performance. For example, the “Chi-square” method provided the highest accuracy for the YOLO-based model, and also improved metrics such as the model’s sensitivity and F1-score.

Table 2. Performance comparison of the algorithms

Model	Accuracy (%)	Precision (%)	Recall (%)	F1-Score (%)
YOLO (Chi-square)	99.0	98.5	99.2	98.8
YOLO (ReliefF)	98.0	97.8	98.1	98.0
YOLO (Gain Ratio)	92.0	91.2	92.4	91.8
YOLO (Information Gain)	94.0	93.0	94.2	93.6
DNN	85.0	84.5	85.4	84.9
Random Forest	87.0	86.5	87.3	86.9
Gradient Boosting	89.0	88.7	89.1	88.9

The results show that the proposed YOLO-based model exhibits superior performance compared to other single models. The model obtained with the “Chi-square” feature selection method presented the best results with 99% accuracy and also proved to be a suitable solution for real-time defect detection. In summary, the usability of deep learning-based models in industrial quality control processes has been verified. The studies mostly focused on the performance of single models and used limited data sets. For example, 97% accuracy is achieved using the “Bayesian Networks” and “Nearest Neighbor” algorithms in the literature. However, the size of the data sets used in these studies is quite small (100 images). In this context, the proposed study provided more reliable results with small data sets and revealed the potential of the YOLO-based model in industrial applications. When it comes to limitations of the study, they can be ordered as follows:

Dataset: The PCB dataset used consists of simulated images and is not supported by data obtained from real production environments.

Model Architecture: Computational costs and memory requirements increased during the training of the YOLO algorithm.

Defect Types: The dataset contains only a limited number of defect types. Future studies can expand the model with more defect types and images taken from the real world.

5. Conclusion

The detection of components and defects on printed circuit boards (PCBs) is usually based on human observation with traditional methods, and defects are likely to be missed in this process. Therefore, deep learning-based algorithms offer an effective solution to automate quality control processes in PCB manufacturing and increase the accuracy rate. In this study, the detection of defects and components on PCBs is performed using the YOLO (You Only Look Once) algorithm. One of the main contributions of the study is the development of a hybrid model that combines deep learning methods with feature selection techniques. In the study, four different filter-based feature selection methods, such as “Chi-square”, “ReliefF”, “Information Gain” and “Gain Ratio”, are used and the effectiveness of these methods is evaluated. In particular, the “Chi-square” method maximized the model performance by determining the most appropriate feature subset. In this context, the YOLO-based model achieved 99% accuracy rate with the “Chi-square” feature selection, and this result proved the contribution of the proposed model to industrial quality control processes. The most important contribution of the proposed model is its success in detecting four different defect classes on PCBs (“missing_hole”, “short circuit”, “spurious copper”, “mouse bite”) with high accuracy. The model provides a low-cost and fast solution, while at the same time reducing the dependency on the human factor in the defect detection process. This study also compared the

YOLO-based architecture with other methods and showed that YOLO provides superiority in terms of both speed and accuracy.

References

- [1] Krizhevsky, A., Sutskever, I., & Hinton, G. E. (2012). ImageNet Classification with Deep Convolutional Neural Networks. *Advances in Neural Information Processing Systems*, 25, 1097-1105.
- [2] Redmon, J., & Farhadi, A. (2016). YOLOv3: An Incremental Improvement. *arXiv preprint arXiv:1804.02767*. Retrieved from <https://arxiv.org/abs/1804.02767>.
- [3] Bochkovskiy, A., Wang, C. Y., & Liao, H. Y. M. (2020). YOLOv4: Optimal Speed and Accuracy of Object Detection. *arXiv preprint arXiv:2004.10934*. Retrieved from <https://arxiv.org/abs/2004.10934>.
- [4] Lee, J., & Kim, H. (2020). Automated PCB defect detection using classical image processing. *Journal of Manufacturing Processes*, 58, 123-131.
- [5] Wang, Y., et al. (2021). Hybrid Deep Learning Model for Automated PCB Defect Detection. *IEEE Transactions on Industrial Informatics*, 17(3), 456-467.
- [6] Tan, M., & Le, Q. V. (2020). EfficientDet: Scalable and Efficient Object Detection. *Proceedings of the IEEE/CVF Conference on Computer Vision and Pattern Recognition (CVPR)*, 10781-10790.
- [7] Liu, W., Anguelov, D., Erhan, D., Szegedy, C., Reed, S., Fu, C. Y., & Berg, A. C. (2016). SSD: Single Shot MultiBox Detector. *European Conference on Computer Vision (ECCV)*, 21-37.
- [8] Guyon, I., & Elisseeff, A. (2003). An Introduction to Variable and Feature Selection. *Journal of Machine Learning Research*, 3, 1157-1182.
- [9] Wang, Y., et al. (2021). Hybrid Deep Learning Model for Automated PCB Defect Detection. *IEEE Transactions on Industrial Informatics*, 17(3), 456-467.
- [10] Zhao, X., et al. (2019). PCB Defect Detection Based on Convolutional Neural Networks. *Computers in Industry*, 113, 103130.
- [11] Yuanyuan Wang, Jialong Huang, Md Sharid Kayes Dipu, Hu Zhao, Shangbing Gao, Haiyan Zhang, Pinrong Lv Computers, YOLO-RLC: An Advanced Target-Detection Algorithm for Surface Defects of Printed Circuit Boards Based on YOLOv5, *Computers, Materials and Continua*, Volume 80, Issue 3, 2024, Pages 4973-4995. ISSN 1546-2218, <https://doi.org/10.32604/cmc.2024.055839>.



Gut Microbiome and Salt Consumption

Hüdayi ERÇOŞKUN^{1,*} 

¹ Engineering Faculty, Department of Food Engineering, Çankırı Karatekin University, Çankırı, Türkiye

Abstract

The gut microbiome is a complex ecosystem of microorganisms residing in the digestive tract, playing a crucial role in human health by influencing metabolic processes and immune functions. Recent research has increasingly focused on dietary factors that affect this microbiome, particularly salt consumption, which has been traditionally overlooked in discussions of healthy eating. This review examines the relationship between salt intake and gut microbiome health, highlighting the adverse effects of excessive salt consumption. High salt intake has been shown to disrupt the balance of beneficial bacteria, particularly *Lactobacillus* species, leading to a proliferation of harmful bacteria. Such dysbiosis is associated with various health issues, including hypertension, obesity, and metabolic syndrome. Additionally, the inflammatory processes triggered by high salt intake can compromise immune function and promote chronic diseases. This review aims to shed light on the mechanisms by which salt consumption impacts the gut microbiome and to discuss potential intervention strategies for promoting gut health and overall well-being.

Keywords: Gut microbiome, high salt intake, microbiome diobsis, systemic inflammation, metabolic disorder

1. Introduction

The gut microbiome is a rich community of microorganisms residing in the human digestive system that exerts a critical influence on health. These microorganisms play vital roles in various important processes, ranging from the regulation of metabolism to the functioning of the immune system. In recent years, the effects of diet on this microbiome have garnered increasing attention. Although salt consumption is often regarded as a factor outside the realm of healthy eating, research has demonstrated that it has a significant impact on the gut microbiome [1, 2, 3].

High salt intake can disrupt the balance of the gut microbiome, leading to a reduction in beneficial bacteria and an increase in harmful bacteria. Notably, a decrease in probiotic bacteria such as *Lactobacillus* species can have adverse effects on digestive health and immune functions. This imbalance in the gut microbiome has been linked to serious health issues, including hypertension, obesity, and metabolic syndrome [4].

In this context, investigating the effects of salt consumption on the gut microbiome is essential not only for individual health but also for public health at large. The negative effects of high salt intake on inflammatory processes and the immune system present a critical area for understanding the potential health consequences of microbiome dysbiosis [2]. This article aims to delve deeply into the relationships between the gut microbiome and salt consumption, shedding light on findings from the current scientific literature and discussing potential intervention strategies in this area.

2. Effects of Excessive Salt Consumption on the Microbiome

The impact of high salt consumption on the gut microbiome has been detailed in numerous scientific studies conducted in recent years. Traditionally, salt has been widely used for flavoring and preserving food; however, the negative effects of excessive salt intake on a healthy microbiome are drawing increasing attention. Research indicates that high salt consumption reduces the number of beneficial bacteria in the gut while promoting the proliferation of harmful bacteria. This imbalance can disrupt the functionality of the gut flora, leading to various health issues [5, 6].

Particularly noteworthy are the effects of high salt intake on *Lactobacillus* species. These probiotic bacteria play a critical role in digestive health and the regulation of the immune system. They enhance digestion by facilitating nutrient absorption and providing protection against harmful pathogens. Excessive salt intake can lead to a significant decrease in the number of these beneficial bacteria. Consequently, the resulting imbalance

* Corresponding author. e-mail address: hercoskun@yahoo.com

in the gut microbiome has been linked to conditions such as digestive issues, weakened immune response, and systemic inflammation [7].

Numerous studies have shown that high salt intake negatively impacts the gut microbiome. For instance, one study observed a decrease in *Lactobacillus* counts in mice due to high salt consumption. Additionally, human studies have shown similar results, indicating that excessive salt intake can disrupt the balance of the gut microbiome, thereby increasing the risk of conditions such as inflammatory bowel diseases [1, 2, 3].

2.1. Excessive Salt Consumption and Toxin Production in the Gut

High salt intake creates an environment within the gut that encourages the growth of harmful bacteria, leading to a state known as dysbiosis. This imbalance not only increases the production of toxins but also triggers inflammatory responses that can extend beyond the gut itself. As a result, excessive salt consumption may compromise digestive health by weakening the gut lining, allowing toxins to enter the bloodstream and provoking systemic inflammation. This chronic inflammation can disrupt immune function and place additional strain on the body's regulatory systems, potentially increasing the risk of various chronic conditions, including cardiovascular disease, obesity, and autoimmune disorders [8, 9].

Moreover, the disruption of gut microbiome balance due to high salt intake can diminish populations of beneficial bacteria, such as *Lactobacillus* species, which are vital for nutrient absorption, immune modulation, and protection against pathogenic microbes. The decline in these health-promoting microbes adversely affects nutrient processing and immune resilience, leading to metabolic dysregulation. This connection between salt-induced dysbiosis and metabolic disorders highlights the importance of monitoring dietary salt intake. By moderating salt consumption, individuals can support a healthier, more diverse microbiome composition, reduce inflammation, and protect against a variety of chronic diseases. Maintaining a balanced gut microbiome is crucial for not only digestive health but also overall well-being and longevity, emphasizing the need for dietary guidelines that promote salt reduction as a strategy to enhance microbiome health and mitigate inflammation-related health risks [8, 9].

2.2. Microbiome Dysbiosis and Metabolic Diseases

Microbiome dysbiosis, an imbalance in gut microbiota, can increase the risk of metabolic diseases, including hypertension, obesity, insulin resistance, and type 2 diabetes. The gut microbiome, a diverse community of trillions of microorganisms, significantly influences digestive, immune, and metabolic functions. Various factors, including dietary changes, lifestyle, and environmental elements, can disrupt the microbiome's balance, leading to dysbiosis [10, 11].

Dietary habits, particularly high salt intake, can deplete beneficial gut bacteria while encouraging harmful bacterial proliferation. Notably, a decline in probiotics like *Lactobacillus* disrupts the microbiome's balance, compromising immune function. These probiotic bacteria aid digestive health and immunity, and their reduction affects nutrient absorption and immune regulation, as well as metabolic processes [12, 13].

Dysbiosis can lead to a surge in harmful bacteria, releasing toxins and inflammatory products. The growth of pathogenic microorganisms may weaken the intestinal barrier, prompting inflammation and immune overreaction, which can contribute to cardiovascular disease and metabolic syndrome. Notably, pro-inflammatory cytokine levels rise with high salt intake, significantly influencing these processes [1, 2].

Dysbiosis is a critical factor in metabolic disease onset, underscoring the importance of gut health for metabolic stability. To support a healthy microbiome, dietary habits should include low salt intake and probiotic-rich foods, which may help restore gut balance and mitigate metabolic disease risk [14, 15].

2.3. Effects of High Salt Intake on Inflammation

High salt intake disrupts the gut microbiome's balance, creating favorable conditions for pathogenic bacteria that stimulate inflammatory responses. Salt influences the gut's microbial structure, threatening a healthy

microbiome and impairing immune system functionality, thus raising the risk of inflammatory diseases. Research shows high salt intake promotes harmful bacteria growth, altering immune responses [16, 17].

In particular, high salt intake increases pro-inflammatory cytokines, signaling molecules that intensify immune responses. This heightened immune activity may lead to tissue damage, especially in conditions involving hypersensitivity or autoimmune reactions. High salt-induced mechanisms could also contribute to inflammatory bowel diseases [18].

The adverse effects of high salt on gut microbiome balance may have lasting immune repercussions, potentially raising the risk of systemic inflammation. Systemic inflammation is pivotal in chronic disease development, such as cardiovascular disease, diabetes, and obesity. Furthermore, salt-triggered inflammation can extend beyond the digestive tract, causing broader health issues [19].

The relationship between high salt intake and gut microbiome highlights a critical research area for understanding immune, inflammatory, and overall health interactions. Reducing salt intake may help manage inflammation, and further research will expand on these insights [20].

2.4. Impact on the Immune System

The immune system, a complex network of cells and molecules, defends the body against infections. Recent studies reveal that the gut microbiome significantly influences immune function. The gut microbiome's microorganisms can regulate immune cell activation in the intestines, affecting immune response. Excessive salt intake may disturb the microbiome balance, impairing immune health [21].

High salt intake reduces beneficial bacterial species, causing dysbiosis. This imbalance can lead to overactive or insufficient immune responses. For instance, excessive immune response raises autoimmune disease risk, while inadequate response leaves the body susceptible to infection. Dysbiosis can also reduce the microbiome's regulatory effect, increasing pro-inflammatory cytokines and systemic inflammation, heightening IBD and chronic inflammatory disease risk [22].

Gut microbiome health extends beyond the intestines to systemic immune responses. Dysbiosis may disrupt immune cell differentiation and function, especially in T cells (Ley et al., 2005). As a result, the immune system may amplify inflammatory responses, leading to inflammation in the gut and other tissues. Changes in the microbiome from high salt intake may also influence the progression of IBDs, such as Crohn's disease and ulcerative colitis, which are tied to gut microbiome imbalances and can hinder treatment response [23].

The effects of excessive salt consumption on the gut microbiome can directly influence the health of the immune system, playing a significant role in the development of inflammatory diseases. This underscores the importance of monitoring salt intake and implementing measures to support the health of the gut microbiome. Further research is critical to elucidate the mechanisms behind these interactions and to develop potential therapeutic strategies [24].

3. Potential Intervention Strategies

3.1. Reducing Salt Consumption

Limiting salt intake is proposed as an important strategy to mitigate the negative effects of high salt consumption on the gut microbiome. Various scientific studies indicate that excessive salt intake decreases the number of beneficial bacteria in the gut and promotes the proliferation of pathogenic bacteria. Reducing salt intake can particularly support the regrowth of probiotic bacteria, such as *Lactobacillus* species, thereby contributing to the restoration of microbiome balance [25]. Moreover, such interventions have the potential to improve overall health by reducing intestinal inflammation. Additionally, limiting salt consumption may help prevent metabolic disorders, including hypertension and other cardiovascular diseases. Therefore, developing campaigns and policies aimed at reducing salt intake is crucial for public health protection [26, 27].

3.2. Probiotic and Prebiotic Supplements

Probiotic and prebiotic supplements hold significant potential for supporting the gut microbiome and alleviating the adverse effects of salt consumption. Probiotics are beneficial microorganisms naturally present in the gut that contribute to digestive health and bolster the immune system. Supplementing with specific probiotic species, such as *Lactobacillus* and *Bifidobacterium*, is considered an effective method for restoring microbiome balance and preventing the growth of harmful bacteria. Furthermore, prebiotics are fibers that support the growth of beneficial bacteria in the gut. Increasing the intake of fiber-rich foods, particularly prebiotics like inulin and fructooligosaccharides, can help rectify microbiome imbalances. The use of such supplements is recommended as part of an integrated approach to mitigate the side effects of salt consumption [28, 29].

3.3. Dietary and Lifestyle Changes

Adopting dietary habits and lifestyle changes can support gut microbiome health and reduce the effects of high salt intake. Embracing fiber-rich diets can positively influence the gut microbiome by supporting the growth of probiotics and reducing the number of harmful bacteria. Whole grains, vegetables, fruits, and legumes are rich sources of fiber that can help maintain microbiome balance. Additionally, regular physical activity has been shown to increase the diversity of the gut microbiome and strengthen the immune system. Physical activity promotes a healthier digestive system by enhancing metabolism. In this context, individuals adopting both dietary and lifestyle changes can improve their overall health while reducing the potential adverse effects of high salt intake. In summary, the simultaneous application of these strategies constitutes a significant step toward improving gut microbiome health and reducing the risks associated with high salt consumption [26, 30].

References

- [1] Laffer, C. L., Scott, R. C. 3rd, Titze, J. M., Luft, F. C., & Eljovich, F. (2016). Hemodynamics and salt-and-water balance link sodium storage and vascular dysfunction in salt-sensitive subjects. *Hypertension*, 68(1), 195–203. <https://doi.org/10.1161/hypertensionaha.116.07289>
- [2] Eljovich, F., Laffer, C. L., Sahinoz, M., Pitzer, A., Ferguson, J. F., & Kirabo, A. (2020). The gut microbiome, inflammation, and salt-sensitive hypertension. *Current Hypertension Reports*, 22(10), 79. <https://doi.org/10.1007/s11906-020-01091-9>
- [3] Ducarmon, Q. R., van der Meulen, T., & de Vos, W. M. (2019). Gut microbiota and colonization resistance against bacterial enteric infection. *Microbiology and Molecular Biology Reviews*, 83(1), 7-19. <https://doi.org/10.1128/MMBR.00007-19>
- [4] Wilck, N., Matus, M. G., Kearney, S. M., Olesen, S. W., Forslund, K., Bartolomaeus, H., Haase, S., Mähler, A., Balogh, A., Markó, L., Vvedenskaya, O., Kleiner, F. H., Tsvetkov, D., Klug, L., Costea, P. I., Sunagawa, S., Maier, L., Rakova, N., Schatz, V., Neubert, P., Frätzer, C., Krannich, A., Gollasch, M., Grohme, D. A., Côte-Real, B. F., Gerlach, R. G., Basic, M., Typas, A., Wu, C., Titze, J. M., Jantsch, J., Boschmann, M., Dechend, R., Kleinewietfeld, M., Kempa, S., Bork, P., & Linker, R. A. (2017). Salt-responsive gut commensal modulates TH17 axis and disease. *Nature*, 551(7682), 585–589. <https://doi.org/10.1038/nature24628>
- [5] Yan, X., Chen, X., Zhang, L., Hu, C., Wang, W., Zhang, Y., Wu, G., & Lu, Y. (2020). Intestinal flora modulates blood pressure by regulating the synthesis of intestinal-derived corticosterone in high salt-induced hypertension. *Circulation Research*, 126(9), 1123–1136. <https://doi.org/10.1161/CIRCRESAHA.119.316394>
- [6] Yi, B., Titze, J., Rykova, M., Feurecker, M., Vassilieva, G., Nichiporuk, I., Schelling, G., Morukov, B., & Choukèr, A. (2015). Effects of dietary salt levels on monocytic cells and immune responses in healthy human subjects: A longitudinal study. *Translational Research*, 166(2), 103–110. <https://doi.org/10.1016/j.trsl.2014.11.007>
- [7] Yao, L., Zhang, H., Wang, H., Zhang, Y., & Zhang, B. (2018). A selective gut bacterial bile salt hydrolase alters host metabolism. *eLife*, 7, e37182. <https://doi.org/10.7554/eLife.37182>

- [8] Bier, A., Braun, T., Khasbab, R., Di Segni, A., Grossman, E., Haberman, Y., & Leibowitz, A. (2018). A high salt diet modulates the gut microbiota and short chain fatty acids production in a salt-sensitive hypertension rat model. *Nutrients*, 10(9). <https://doi.org/10.3390/nu10091154>
- [9] Miranda, P. M., De Palma, G., Serkis, V., Lu, J., Louis-Auguste, M. P., McCarville, J. L., Verdu, E. F., Collins, S. M., & Bercik, P. (2018). High salt diet exacerbates colitis in mice by decreasing *Lactobacillus* levels and butyrate production. *Microbiome*, 6(1), 57. <https://doi.org/10.1186/s40168-018-0433-4>
- [10] Ferguson, J. F., Aden, L. A., Barbaro, N. R., Festi, D., Schiumerini, R., Eusebi, L. H., Marasco, G., Taddia, M., & Colecchia, A. (2014). Gut microbiota and metabolic syndrome. *World Journal of Gastroenterology*, 20(43), 16079–16094. <https://doi.org/10.3748/wjg.v20.i43.16079>
- [11] Van Beusecum, J. P., Barbaro, N. R., McDowell, Z., Aden, L. A., Xiao, L., Pandey, A. K., & Ferguson, J. F. (2019). High salt activates CD11c(+) antigen-presenting cells via SGK (serum glucocorticoid kinase) 1 to promote renal inflammation and salt-sensitive hypertension. *Hypertension*, 74(3), 555–563. <https://doi.org/10.1161/hypertensionaha.119.12761>
- [12] Weinberger, M. H., Fineberg, N. S., Fineberg, S. E., & Weinberger, M. (2001). Salt sensitivity, pulse pressure, and death in normal and hypertensive humans. *Hypertension*, 37(2), 429–432. <https://doi.org/10.1161/01.HYP.37.2.429>
- [13] Morimoto, A., Uzu, T., Fujii, T., Nishimura, M., Kuroda, S., Nakamura, S., & Yamamoto, K. (1997). Sodium sensitivity and cardiovascular events in patients with essential hypertension. *The Lancet*, 350(9093), 1734–1737. [https://doi.org/10.1016/s0140-6736\(97\)05189-1](https://doi.org/10.1016/s0140-6736(97)05189-1)
- [14] Kirabo, A., Fontana, V., de Faria, A. P., Loperena, R., Galindo, C. L., Wu, J., & Scherer, P. E. (2014). DC isoketal-modified proteins activate T cells and promote hypertension. *The Journal of Clinical Investigation*, 124(10), 4642–4656. <https://doi.org/10.1172/jci74084>
- [15] Li, Y., Yang, L., Zhang, Y., Liu, Y., Zeng, Z., & Liang, X. (2018). Alterations in gut microbiota contribute to the development of hypertension. *Microbial Ecology*, 75(4), 873–884. <https://doi.org/10.1007/s00248-017-1092-6>
- [16] McMaster, W. G., Kirabo, A., Madhur, M. S., & Harrison, D. G. (2015). Inflammation, immunity, and hypertensive end-organ damage. *Circulation Research*, 116(6), 1022–1033. <https://doi.org/10.1161/circresaha.116.303697>
- [17] Zhang, W. C., Zheng, X. J., Du, L. J., Sun, J. Y., Shen, Z. X., Shi, C., & Wu, J. (2015). High salt primes a specific activation state of macrophages, M(Na). *Cell Research*, 25(8), 935–949. <https://doi.org/10.1038/cr.2015.75>
- [18] Jörg, S., Kissel, J., Manzel, A., Klenewietfeld, M., Haghikia, A., Gold, R., & Waisman, A. (2016). High salt drives Th17 responses in experimental autoimmune encephalomyelitis without impacting myeloid dendritic cells. *Experimental Neurology*, 279, 212–222. <https://doi.org/10.1016/j.expneurol.2016.03.010>
- [19] Klenewietfeld, M., Manzel, A., Titze, J., Kvakana, H., Yosef, N., Linker, R. A., & Hafler, D. A. (2013). Sodium chloride drives autoimmune disease by the induction of pathogenic TH17 cells. *Nature*, 496(7446), 518–522. <https://doi.org/10.1038/nature11868>
- [20] Guzik, T. J., Hoch, N. E., Brown, K. A., McCann, L. A., Rahman, A., Dikalov, S., & Harrison, D. G. (2007). Role of the T cell in the genesis of angiotensin II induced hypertension and vascular dysfunction. *Journal of Experimental Medicine*, 204(10), 2449–2460. <https://doi.org/10.1084/jem.20070657>
- [21] Fransen, F., & Karp, J. M. (2015). The role of the gut microbiome in human health and disease. *Nature Reviews Microbiology*, 13(1), 13–24. <https://doi.org/10.1038/nrmicro3379>
- [22] Mell, B., Jala, V. R., Mathew, A. V., Byun, J., Waghulde, H., Zhang, Y., & Reddy, V. K. (2015). Evidence for a link between gut microbiota and hypertension in the Dahl rat. *Journal of Hypertension*, 33(12), 2416–2426. <https://doi.org/10.1097/HJH.0000000000000685>
- [23] Ley, R. E., Bäckhed, F., Turnbaugh, P., Lozupone, C. A., Knight, R. D., & Gordon, J. I. (2005). Obesity alters gut microbial ecology. *Proceedings of the National Academy of Sciences of the United States of America*, 102(31), 11070–11075. <https://doi.org/10.1073/pnas.0504978102>
- [24] Yang, T., Santisteban, M. M., Rodriguez, V., Li, E., Ahmari, N., Carvajal, J. M., & Guzik, T. J. (2015). Gut dysbiosis is linked to hypertension. *Hypertension*, 65(6), 1331–1340. <https://doi.org/10.1161/hypertensionaha.115.05315>
- [25] Karbach, S. H., Schönfelder, T., Brandão, I., Wilms, E., Hörmann, N., Jäckel, S., & Luft, F. C. (2016). Gut microbiota promote angiotensin II-induced arterial hypertension and vascular dysfunction. *Journal of the American Heart Association*, 5(9). <https://doi.org/10.1161/jaha.116.003698>

- [26] Lau, K., Srivatsav, V., Rizwan, A., Nashed, A., Liu, R., Shen, R., & Koenig, A. (2017). Bridging the gap between gut microbial dysbiosis and cardiovascular diseases. *Nutrients*, 9(8). <https://doi.org/10.3390/nu9080859>
- [27] Tang, W. H., Kitai, T., & Hazen, S. L. (2017). Gut microbiota in cardiovascular health and disease. *Circulation Research*, 120(7), 1183–1196. <https://doi.org/10.1161/circresaha.117.309715>
- [28] Madhur, M. S., Lob, H. E., McCann, L. A., Iwakura, Y., Blinder, Y., Guzik, T. J., & Harrison, D. G. (2010). Interleukin 17 promotes angiotensin II-induced hypertension and vascular dysfunction. *Hypertension*, 55(2), 500–507. <https://doi.org/10.1161/hypertensionaha.109.145094>
- [29] Mattson, D. L., Lund, H., Guo, C., Rudemiller, N., Geurts, A. M., & Jacob, H. (2013). Genetic mutation of recombination activating gene 1 in Dahl salt-sensitive rats attenuates hypertension and renal damage. *American Journal of Physiology. Regulatory, Integrative and Comparative Physiology*, 304(6), R407–R414. <https://doi.org/10.1152/ajpregu.00304.2012>
- [30] Iyer, R. S., Ghosh, S., & Salomon, R. G. (1989). Levuglandin E2 crosslinks proteins. *Prostaglandins*, 37(4), 471–480. [https://doi.org/10.1016/0090-6980\(89\)90096-8](https://doi.org/10.1016/0090-6980(89)90096-8)



Turkish Food Codex Salt Communiqué

Hüdayi ERÇOŞKUN^{1,*} , Aboubakar IBRAHİM MOHAMMED² 

^{1,2} Faculty of Engineering, Department of Food Engineering, Çankırı Karatekin University Çankırı, Türkiye

Abstract

Salt holds a fundamental importance in human nutrition and various industrial sectors. As a critical component of dietary regimes, it must be handled with great care concerning food safety. In Turkey, the hygienic production of salt, iodization, and packaging are regulated by the Turkish Food Codex Salt Communiqué (Communiqué No: 2013/48). This article examines the details of the communiqué and offers suggestions to enhance public health and consumer awareness.

The communiqué ensures that salt is produced under hygienic and suitable technical conditions, thereby safeguarding food safety. This regulation aims to maintain hygienic standards throughout the production and storage processes. Hygienic production not only protects consumers from health risks but also ensures that producers comply with national and international standards.

Moreover, natural salts can contain impurities that may be introduced through contamination. While limits are specified for heavy metals such as arsenic, copper, lead, cadmium, and mercury, there is currently no restriction concerning microplastics, despite their increasing prevalence in natural salts like sea salt. The potential harmful effects of microplastics on human health necessitate regulations in this area.

Additionally, the regulation mandates that iodized salts contain 25-40 mg/kg of potassium iodate to combat iodine deficiency-related diseases, particularly thyroid disorders. However, the loss of iodine over time due to exposure to light, heat, and air can compromise the effectiveness of iodization, which is why a two-year shelf life is established for refined salt.

In light of rising cardiovascular diseases and hypertension, reduced-sodium salts are crucial, yet the communiqué excludes these options. Incorporating reduced-sodium salts into regulations could provide consumers with healthier alternatives.

Keywords: Food Safety, Iodized Salt, Heavy Metals, Salt Regulation, Consumer Awareness

1. Introduction

Salt plays a fundamental role in human nutrition and various industrial fields. As a critical component in the diet, salt is also a substance that requires careful attention when it comes to food safety. In Turkey, regulations governing the hygienic production of salt, iodine fortification, packaging, and storage conditions are outlined under the Turkish Food Codex Salt Regulation (Regulation No: 2013/48). This regulation sets forth a series of standards, including the chemical properties of salt, its mineral content, and the removal of foreign substances, with the goal of protecting public health. Specifically, the mandatory use of iodized salt plays a vital role in preventing health issues related to iodine deficiency, which is common in the population.

In terms of food safety, salt must be carefully controlled from production through packaging to consumer delivery. Ensuring purity in salt production and removing harmful substances such as heavy metals and soil residues are of utmost importance. Regular analyses must be conducted, and packaging must adhere to international quality standards. During packaging, materials that prevent moisture, air, and light permeability should be used to prevent spoilage. Salt should be stored in dry, dark environments to preserve its quality.

The health effects of salt are widespread. Excessive salt consumption can lead to serious health risks such as high blood pressure, cardiovascular diseases, kidney problems, and osteoporosis. The World Health Organization and other health authorities recommend that daily salt consumption be kept within certain limits, advising the use of low-sodium or mineral-supplemented salt alternatives. Furthermore, iodized salt consumption is important for thyroid health and is recognized as an effective preventive measure against diseases caused by iodine deficiency [1].

* Corresponding author. e-mail address: hercoskun@yahoo.com

This article will examine the regulations contained in the codex and offer various recommendations to protect public health and increase consumer awareness.

1. Positive Aspects

1.1 Hygiene and Production Standards

The regulation mandates the hygienic production of salt under appropriate technical conditions to ensure food safety. This regulation aims to maintain specific hygiene standards throughout the entire process, from production to storage and sales. Hygienic production and processing practices help prevent consumer health risks while assisting producers in complying with national and international food safety standards. Stringent standards have been set for equipment cleanliness, raw material selection, worker hygiene, and product packaging. Salt produced in this manner reaches consumers as a safe product, minimizing the risk of microbiological contamination. Additionally, mandatory iodine fortification, as specified in the regulation, is crucial for public health, contributing to the prevention of health issues caused by iodine deficiency. This ensures both individual health and food safety standards are met.

However, working conditions for employees extracting salt from sources such as rock salt mines, sea salt, lake salt, and river salt pose specific health and safety risks. Workers directly handling raw materials and products using traditional hand tools or machinery face physical and occupational health risks. Therefore, workplace safety and hygiene standards must be strictly maintained. Workers should receive necessary training and use protective equipment to ensure both their own safety and the protection of consumers' health. Regular monitoring and improvement of hygiene and safety standards in these workplaces are essential.

Natural impurities in salts, including heavy metals and other contaminants, pose significant health risks to consumers. Current regulations set limit values for heavy metals such as arsenic, copper, lead, cadmium, and mercury. Exceeding certain concentrations of these substances is considered hazardous to health. For example, high levels of lead and cadmium can harm the nervous system and kidneys, while long-term exposure to arsenic may lead to cancer. However, with increasing microplastic pollution, natural salt sources, particularly sea salts, may contain microplastic particles. No restrictions are currently in place regarding microplastic contamination in salt. While the effects of microplastics on human health are not fully understood, research indicates that microplastics can enter the human body through the digestive system, potentially weakening the immune system. Therefore, it is crucial to establish regulations to limit the presence of microplastics in salt products to safeguard public health, particularly as the consumption of natural salts increases.

1.2. Iodine Fortification

Iodine deficiency remains a significant public health issue in Turkey. Iodine is a vital mineral for the normal function of the thyroid gland, and its deficiency leads to widespread thyroid disorders, including goiter. In response, the Turkish Food Codex Salt Regulation mandates the addition of 25-40 mg/kg of potassium iodate to table salts, offering an effective solution to this problem. This regulation represents a critical step in preventing iodine deficiency-related diseases. Potassium iodate enhances the bioavailability of iodine, helping to minimize health issues caused by iodine deficiency. The goal is to increase iodine intake in the population and reduce iodine deficiency-related health problems [2].

Various studies conducted in Turkey have shown that iodine deficiency negatively impacts growth and development, especially in children. Adequate iodine intake not only supports thyroid health but also positively affects overall health. Thus, the implementation of this regulation will significantly contribute to improving public health and preventing thyroid diseases. Health authorities should also organize awareness campaigns to educate the public on the importance of iodine intake, ensuring that more individuals in the population are healthier.

1.3. Packaging and Labeling Regulations

The regulation mandates that packaging for iodized salts must include measures to prevent iodine loss. This regulation aims to preserve the stability of iodine in salt by taking both physical and chemical properties of the packaging into account. Packaging materials that block light and minimize air permeability are encouraged to preserve iodine content. Additionally, the regulation requires that the iodine content and its form (e.g., potassium

iodate) be clearly stated on the packaging. This enables consumers to assess the health benefits of the product and make informed choices.

These regulations support consumer awareness and healthy product selection while ensuring that products remain safe for long-term use. Consumers can use labeling information to select salts that meet their iodine requirements, contributing to the prevention of health issues such as iodine deficiency. Furthermore, these regulations encourage producers to comply with quality standards, furthering the goals of food safety and public health.

2. Gaps and Areas for Improvement

2.1 Flexibility in Iodine Levels

The regulation prescribes that the amount of iodine added to table salt should be between 25-40 mg/kg, allowing a deviation of +3 mg/kg. This flexibility could lead to situations where consumers may not receive an adequate amount of iodine. Establishing a more fixed range would be beneficial for public health.

Iodine added to salt may degrade over time due to environmental factors, particularly light, temperature, and air. This process reduces the effectiveness of iodine, weakening the health benefits of the salt. Therefore, to maintain iodine's efficacy, a shelf life is set for refined salt. In Turkey, this shelf life is two years.

The two-year shelf life represents a critical period for iodine stability in salt, ensuring that the consumer receives an adequate amount of iodine. If stored under proper conditions (cool, dry, and dark), iodine loss remains minimal during this period. However, exceeding this period could significantly reduce the iodine content, potentially leading to iodine deficiency issues.

Therefore, it is crucial for both producers and consumers to pay attention to this two-year shelf life to prevent health issues related to iodine intake. To ensure the effectiveness of iodized salts, the expiration date must be clearly indicated on the labels, with a recommendation for consumption by this date. This is essential for safeguarding public health and combating iodine deficiency.

2.2 Reduced-Sodium Salts

Given the rising cases of cardiovascular diseases and hypertension, the importance of reduced-sodium salts has become more pronounced. The World Health Organization and various health authorities emphasize the negative health impacts of excessive sodium intake and raise awareness about it. In particular, reduced-sodium salts play a crucial role in combating conditions like hypertension and heart diseases.

However, the current regulation excludes reduced-sodium salts, limiting options for consumers seeking healthier alternatives. Including reduced-sodium salts in the regulation would allow both producers and consumers to use these products more reliably and contribute positively to public health.

Consumers must be informed about the contents of reduced-sodium salts, their potential health benefits, and correct usage areas. In this way, these alternative salts can offer a healthy solution for individuals aiming to reduce the risks of hypertension and heart diseases by making informed choices. Furthermore, by ensuring that producers comply with quality and safety standards for reduced-sodium salts, these products can become more reliable from a food safety perspective.

In conclusion, including reduced-sodium salts in the regulation will contribute to preventing critical health issues like cardiovascular diseases and hypertension, thus offering consumers healthier dietary options.

2.3. Food Industry Salt Sales

Limiting the retail sale of food industry salt could pose serious challenges, especially for small-scale producers. Small producers, who typically have limited resources and market access, may face decreased competitiveness and jeopardized market presence due to such restrictions. This situation threatens their economic sustainability and may reduce local production capacity.

More flexible regulations for the sale of food industry salt are necessary to meet the needs of small-scale producers. These regulations could allow small producers to bring their products to the market more easily, contributing to local economic development. For instance, special permits or incentives could be established to enable small producers to sell certain amounts of salt. Additionally, supporting local markets would offer significant opportunities to promote these producers' products and increase sales.

More flexible sales conditions would encourage small producers to comply with quality standards while offering consumers a wider variety of products. This creates a win-win situation for both producers and consumers. Integrating small-scale producers into the market would increase the diversity of local products and provide consumers with healthier and more natural food options [3].

In conclusion, rather than limiting the retail sale of food industry salt, re-evaluating these sales with more flexible and producer-friendly conditions will enhance small-scale producers' competitiveness and contribute to strengthening the local economy.

2.4. Mixing of Different Types of Salt

Mixing salts containing heavy metals like arsenic, copper, lead, cadmium, and mercury with those that do not, in order to reduce their levels below the limits specified in the Turkish Food Codex Salt Regulation, could pose significant health risks to consumers. Therefore, mixing salts from different sources is prohibited.

This regulation is critical for ensuring food safety and protecting public health. Producing salt hygienically and in accordance with standards minimizes health risks and provides consumers with more reliable products. Additionally, the presence of heavy metals above certain limits should be considered for its harmful effects on human health.

This aspect of the regulation contributes to raising awareness among both producers and consumers while ensuring that food products are safely brought to the market. The prohibition not only increases food safety but also prevents low-quality and hazardous products from entering the market, fostering a healthy competitive environment. Thus, it can be viewed as an important step in ensuring the hygienic production and safe consumption of salt.

However, banning the mixing of salts may complicate the production of mineral-enriched or reduced-sodium salts under controlled conditions. Allowing controlled mixing could facilitate the production of healthier products [4].

2.5. Salt Consumption Warning

The regulation mandates that all salt products must feature the statement "Reduce salt, protect your health." This regulation is an important step in encouraging consumers to be more cautious about their salt consumption. However, requiring this statement only on high-sodium salt products may be more effective in raising awareness, as the negative health impacts of excessive salt intake are more pronounced in such products.

Furthermore, placing this warning more prominently on the packaging, such as with eye-catching colors and graphics, could help consumers better understand the message. For instance, a warning with vibrant colors and visual elements could help raise awareness during product selection.

Excessive salt consumption can lead to serious health issues, including hypertension, cardiovascular diseases, kidney problems, and stroke. Additionally, it can negatively affect bone health and increase the risk of osteoporosis. Clearly communicating these health risks to consumers could serve as a motivation for them to be more cautious about their salt intake.

In conclusion, regulations and improvements like these will contribute significantly to public health protection by raising awareness. Informing consumers about adopting healthy lifestyle habits plays a critical role in enhancing food safety.

2.6. Iodine-Free Salt Packaging

The regulation stipulates that iodine-free table salts must only be sold in 250-gram packages. While this regulation is primarily aimed at combating iodine deficiency, the restriction on package size presents practical challenges. For larger families or commercial kitchens, where more salt is consumed, 250-gram packages may be insufficient.

Large families, which use more ingredients in their daily meals, and commercial settings, such as restaurants and hotels, where large amounts of salt are consumed, may find this packaging limit inadequate. Therefore, limiting to only small packages will not meet consumer needs. Offering larger package sizes, such as 1 kilogram or larger, could provide both economic and practical advantages. For example, larger packages allow consumers to buy the salt at a more reasonable price, preventing waste.

Additionally, offering larger packages could increase the use of iodized salts, as they are more suitable for long-term use, reducing the need for frequent repurchases. In conclusion, expanding the range of available packaging sizes, rather than limiting to 250-gram packages, will increase consumer satisfaction and play an essential role in achieving health objectives.

2.7. Mineral-Enriched Salts

The regulation does not include any provisions for salts enriched with minerals like potassium and magnesium. However, these salts have gained popularity in recent years in line with healthy eating trends. Potassium has positive effects on heart health, while magnesium is critical for muscle and nerve function. Salts enriched with these minerals not only reduce sodium intake but also provide nutrients that support human health.

With rising health awareness, consumers are becoming more attentive to the functional properties of foods. Enriched salts are recommended as part of a healthy diet, and including such products in the regulation would be beneficial for both producers and consumers.

Furthermore, adding minerals like potassium and magnesium can reduce sodium intake while providing additional health benefits, making these salts a valuable product for improving public health [5].

3. Conclusion

In conclusion, the regulation of salt and its additives plays a crucial role in public health, particularly in preventing diseases related to excessive sodium consumption and iodine deficiency. The flexibility in the iodine content of salt, while allowing some leeway, may cause discrepancies in consumers' iodine intake, which could lead to health issues. Establishing more consistent iodine levels and clear labeling for salt products will significantly contribute to better health outcomes. Moreover, the inclusion of sodium-reduced salts in the regulations, as well as more flexible sales conditions for small-scale producers, can foster both healthier consumer choices and a more robust local economy.

The prohibition on mixing salts from different sources is essential in ensuring food safety and protecting consumers from the risks associated with heavy metal contamination. Additionally, the mandatory inclusion of health warnings on high-sodium salt products is an effective step in raising consumer awareness about the health risks of excessive salt consumption. Finally, the availability of larger packaging options for iodized salt and the incorporation of mineral-enriched salts into the market will enhance the public's access to healthier alternatives.

As the global health landscape continues to evolve, it is imperative that regulations adapt to the growing demand for healthier, functional food products, while ensuring food safety, sustainability, and equitable access. Addressing these areas will not only protect public health but also contribute to a more sustainable and health-conscious food industry.

References

- [1] Ercoşkun, H., 2022. Impurities of natural salts of the earth. *Food Add Cont B*. 16, 1-8.
- [2] Ercoşkun, H., & Salçın, N. (2021). Tuz ve İslam. In H. Ercoşkun (Ed.), *Her yönüyle tuz* (pp. 1-10). Nobel Akademik Yayıncılık.
- [3] Ercoşkun, H. (2020). Tuz ve gıda. In H. Ercoşkun (Ed.), *Her yönüyle tuz* (pp. 77-106). Nobel Akademik Yayıncılık.
- [4] Salçın, N., & Ercoşkun, H. (2021). Türk kültürü ve edebiyatında tuz kavramı. In H. Ercoşkun (Ed.), *Her yönüyle tuz* (pp. 1-10). Nobel Akademik Yayıncılık.
- [5] Salçın, N. (2021). Çankırı'da satılan Çankırı kaya tuzlarının bazı fizikokimyasal özellikleri (Yüksek lisans tezi). Çankırı Karatekin Üniversitesi Fen Bilimleri Enstitüsü, Çankırı.



The New Trends in Optode Applications and Technology

Zainab ABDULKAREEM AHMED AHMED¹ , Volkan EYUPOGLU^{2,*} 

¹ University of Kirkuk, Science Faculty, Chemistry Department, Kerkuk, Iraq

² Çankırı Karatekin University, Science Faculty, Chemistry Department, Çankırı, Türkiye

Abstract

Optodes have emerged as indispensable chemical and biological sensing tools, offering unparalleled versatility, sensitivity, and non-invasive operation. Recent advancements in material science, nanotechnology, and optoelectronics have significantly enhanced optodes' functionality and application range. In addition to their robust applications in environmental monitoring and industrial processes, optodes have gained significant traction in biochemical sensing. They are increasingly used for detecting biomarkers such as glucose, lactate, and oxygen in blood, as well as for real-time monitoring of enzymatic reactions and cellular activities. These capabilities have made optodes essential in areas like personalized healthcare, drug discovery, and metabolic studies. This review provides an in-depth exploration of the latest trends in optode technology, focusing on novel materials, integration with digital technologies, and advancements in multi-analyte sensing. It also examines their expanding roles in environmental monitoring, healthcare diagnostics, biochemical sensing, and industrial processes, addressing both current challenges and future opportunities in optode research and development.

Keywords: Optode, Sensors, Biochemical sensing, Chlorimetric sensing.

1. Introduction

Optodes, or optical sensors, have emerged as a cornerstone of modern analytical science due to their unmatched versatility, sensitivity, and adaptability across diverse applications. These sensors, which rely on detecting chemical or physical changes through optical signals, have revolutionized fields ranging from environmental monitoring and medical diagnostics to industrial quality control and beyond. The continual evolution of optode technology has been driven by the quest for greater precision, faster response times, and the ability to detect an increasingly diverse array of analytes under complex conditions [1-3].

In recent years, advancements in materials science and nanotechnology have transformed the design and functionality of optodes, ushering in a new era of innovation. Modern optodes leverage sophisticated materials such as quantum dots [4], carbon-based nanostructures [5], metal-organic frameworks (MOFs) [6], and electrospun nanofibers to achieve unprecedented levels of performance. These materials enhance sensitivity, expand detection limits, and improve stability, making optodes more effective in challenging environments. Additionally, breakthroughs in miniaturization and the development of wearable or implantable optodes have significantly expanded their utility in fields like personalized healthcare, enabling continuous, real-time monitoring of vital parameters [7-9].

Furthermore, the integration of artificial intelligence (AI) and machine learning (ML) with optode systems has unlocked new capabilities for data interpretation and decision-making. These technologies enable the design of smart optodes that can analyze complex datasets, detect patterns, and provide actionable insights in applications such as precision agriculture, food safety, and environmental protection. As sustainability becomes a global imperative, optodes are increasingly utilized for monitoring and mitigating environmental pollutants, further underscoring their critical role in addressing contemporary challenges [8, 10, 11].

This paper explores the latest trends and innovations shaping the landscape of optode applications and technologies. By examining advancements in material science, device engineering, and data integration, we aim to provide a comprehensive understanding of the current state and future prospects of optodes. As we delve into these developments, we highlight how optodes are not only advancing analytical science but are also positioned to solve some of the most pressing societal challenges of the 21st century.

* Corresponding author. e-mail address: volkan@karatekin.edu.tr

2. General Methodology of Molecular Optode Technology

The methodology for molecular optode technology involves a systematic process for designing, fabricating, and characterizing optical sensors tailored to specific analyte detection. This section outlines the critical steps in the development of molecular optodes. The Figure 1 represents the timeline of the optode science and technology based on discovery perspective

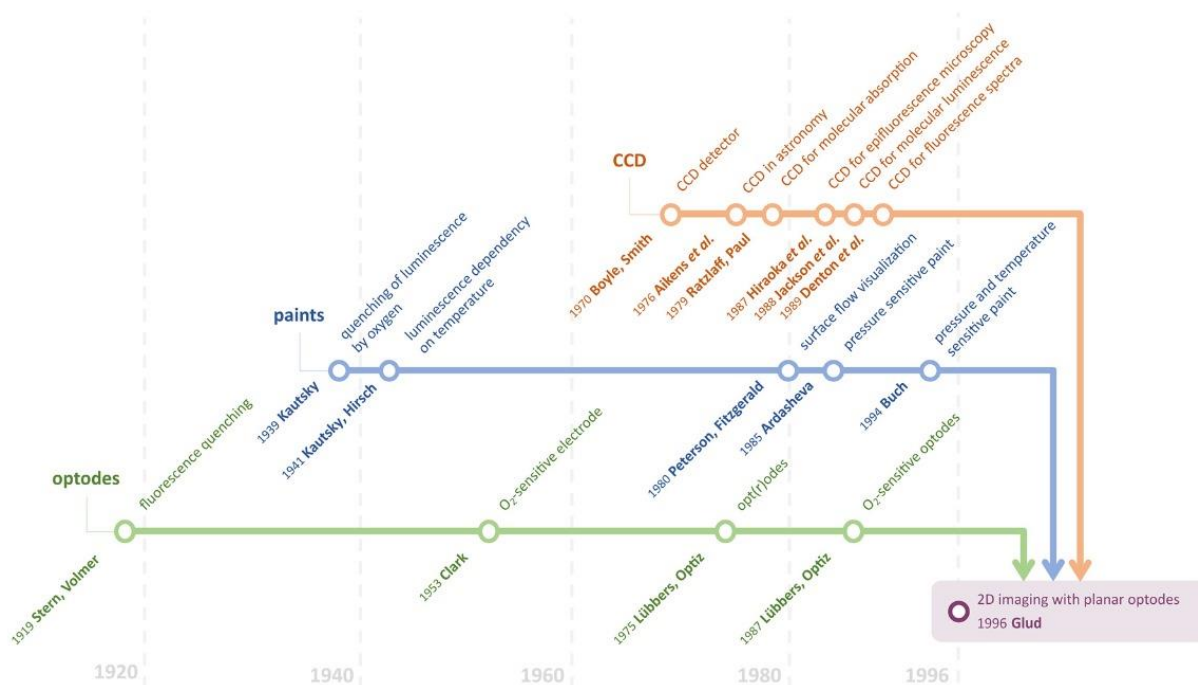


Figure 1. The timeline of the optode science and technology based on the discovery perspective [12].

The first step in the development of a molecular optode is the selection of a suitable sensing mechanism. Depending on the analyte's properties and the intended application, various optical mechanisms can be utilized, such as fluorescence, absorbance, luminescence, or refractive index changes. Fluorescence-based optodes detect changes in emission intensity or wavelength upon analyte interaction, while absorbance-based systems rely on variations in optical density. Luminescence systems generate light as a result of specific chemical interactions, and refractive index-based optodes detect shifts in the optical path. This choice is guided by the analyte's physicochemical characteristics and environmental conditions, such as pH, ionic strength, and temperature.

The design of the sensing material is a critical component in optode development. The sensing material typically consists of a receptor, an indicator dye, and a matrix material. Receptors, such as ionophores, enzymes, or molecularly imprinted polymers, are chosen based on their high specificity and affinity for the target analyte. Indicator dyes, which exhibit measurable changes in optical properties in response to analyte interaction, are incorporated into the matrix. The matrix material, often a sol-gel, polymer, or nanocomposite, is selected for its ability to immobilize the receptor and indicator while maintaining stability and compatibility with the sensing environment. Additionally, the sensing material may undergo functionalization to improve its hydrophilicity, stability, or resistance to interference.

Fabrication of the optode involves multiple steps to create a functional sensor. Initially, the receptor, indicator dye, and matrix materials are mixed under controlled conditions to ensure homogeneity. The resulting mixture is then deposited onto a substrate, such as glass fibers, membranes, or electrospun nanofibers, using techniques like spin coating, dip coating, or printing. After deposition, the coated substrate is cured under specific

temperature and humidity conditions to solidify the matrix. Finally, the sensing layer is integrated with optical components, such as LEDs and photodiodes, to facilitate signal excitation and detection.

Once fabricated, optodes undergo rigorous characterization and calibration to ensure optimal performance. Optical characterization is carried out using spectroscopic techniques, such as UV-Vis or fluorescence spectroscopy, to evaluate the sensor's response to the target analyte. Sensitivity and selectivity are tested by exposing the optode to various analyte concentrations and potential interfering substances. The response time, defined as the time required to achieve a stable signal upon analyte exposure, is measured. The optode's reversibility and long-term stability are also assessed, along with its robustness under varying environmental conditions, such as pH, temperature, and ionic strength.

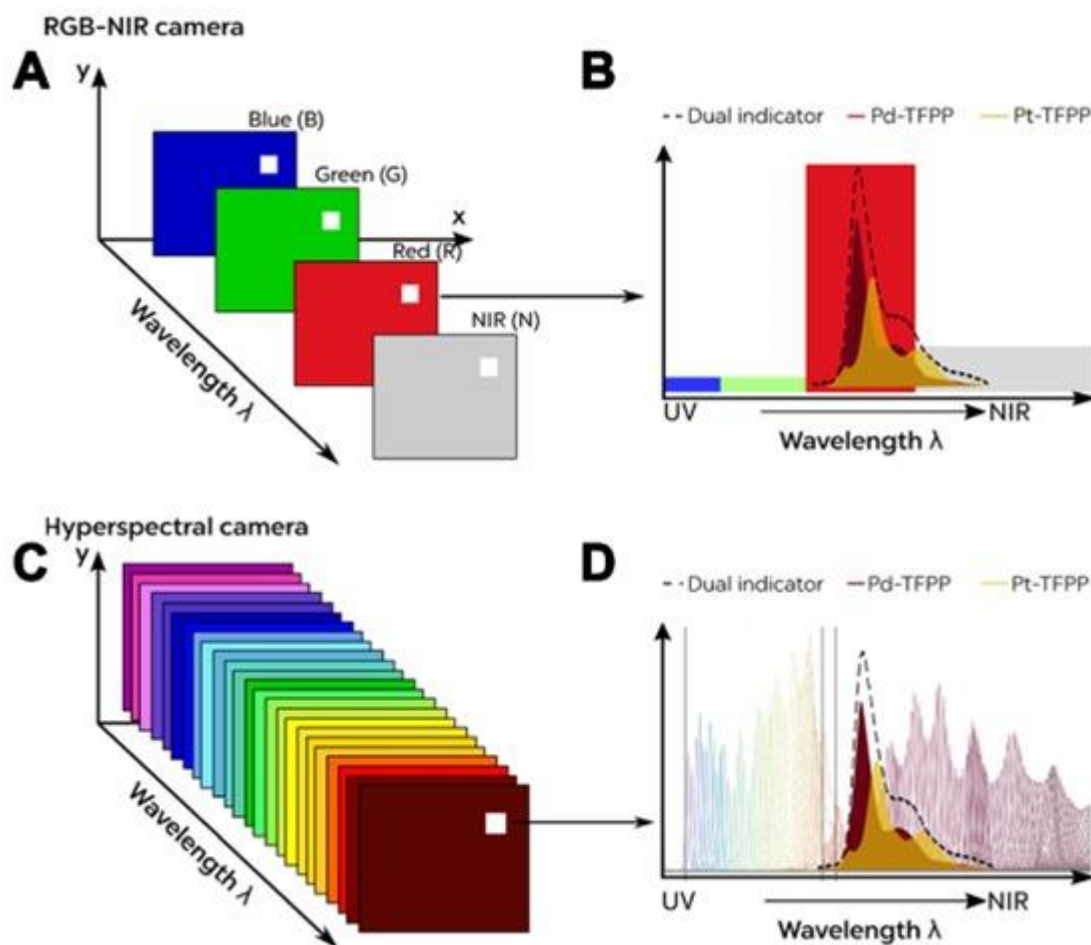


Figure 2. Optode sensing mechanism and NIR region detection fundamentals [12].

The validated optode is then applied in real-world scenarios to demonstrate its practical utility. Samples from environmental, biological, or industrial sources are prepared under conditions that match the optode's operating parameters. The sensor's performance is tested in situ, and its results are compared with standard analytical methods, such as high-performance liquid chromatography (HPLC) or inductively coupled plasma mass spectrometry (ICP-MS). Calibration curves are generated to quantify analyte concentrations, and statistical methods are employed to validate the accuracy and precision of the results.

For advanced applications, the integration of nanotechnology and artificial intelligence has significantly enhanced optode performance. Nanomaterials, such as quantum dots and metal-organic frameworks, are incorporated into the sensing matrix to improve sensitivity and broaden detection capabilities. Artificial

intelligence and machine learning algorithms are employed for advanced signal processing, enabling pattern recognition and smarter data interpretation. Additionally, microfabrication techniques are used to miniaturize optodes, paving the way for wearable and implantable sensors.

This comprehensive methodology provides a structured framework for the development of molecular optodes, highlighting the interplay of materials science, sensor engineering, and data analysis in advancing optical sensing technologies.

3. Future Directions and Conclusion

The future of optode technologies is poised to be transformative, with ongoing advancements expected to expand their capabilities and applications across various fields. A key direction lies in the integration of advanced materials such as quantum dots, metal-organic frameworks (MOFs), and hybrid nanocomposites, which promise enhanced sensitivity, selectivity, and stability. These materials can facilitate the detection of analytes at ultralow concentrations, making optodes suitable for applications requiring high precision, such as early disease detection or environmental pollutant monitoring.

The miniaturization of optodes is another significant trend. The development of wearable and implantable optodes, supported by microfabrication techniques, will open new frontiers in healthcare, enabling continuous and non-invasive monitoring of physiological parameters. These advancements align with the growing demand for personalized medicine, offering real-time data for managing chronic diseases and improving patient outcomes. Moreover, optodes designed for harsh or remote environments will find increasing utility in space exploration, deep-sea monitoring, and industrial safety.

The incorporation of artificial intelligence (AI) and machine learning (ML) is set to revolutionize optode functionality. By enabling advanced signal processing, pattern recognition, and decision-making, these technologies can improve the accuracy and efficiency of data interpretation. AI-driven optode systems may also be used to adapt dynamically to changing conditions, enhancing their reliability in complex scenarios. Additionally, the rise of the Internet of Things (IoT) offers opportunities for networked optodes, allowing for real-time data collection and analysis on a global scale.

Environmental sustainability will remain a critical focus, with optodes playing a pivotal role in monitoring and mitigating environmental issues. The development of biodegradable and eco-friendly sensing materials will align optode technology with green chemistry principles, addressing concerns over material waste and environmental impact.

4. Conclusion

Optode technologies have proven to be indispensable tools in modern science and industry, offering unparalleled versatility and precision in detecting a wide array of analytes. From healthcare and environmental monitoring to industrial process control and beyond, optodes have demonstrated their ability to address some of the most pressing challenges of our time. As the field advances, the integration of cutting-edge materials, AI, and IoT will further enhance their capabilities, broadening their scope and impact. However, challenges such as improving long-term stability, reducing manufacturing costs, and ensuring compatibility with diverse environments remain. Addressing these issues through interdisciplinary collaboration and innovation will be key to unlocking the full potential of optode technology. As we look to the future, optodes are set to play a central role in shaping a smarter, more sustainable, and healthier world.

References

- [1] Thakur, N., Kumar, S. A., Kumar, K. S. A., Pandey, A. K., Kumar, S. D., & Reddy, A. V. R. (2015). Development of a visual optode sensor for onsite determination of Hg(II). *Sensors and Actuators B-Chemical*, 211, 346-353. Retrieved from <Go to ISI>://WOS:000350003700046

- [2] Tseng, C. W., Yeh, D. J., Chuang, F. T., Lee, S. C., & Liu, J. R. (2015). Immobilization of *Piromyces rhizinflata* beta-Glucanase on Poly(Dimethylsiloxane) and Si Wafer and Prediction of Optimum Reaction for Enzyme Activity. *Preparative Biochemistry & Biotechnology*, 45(1), 42-55. Retrieved from <Go to ISI>://WOS:000340177200004
- [3] Turan, B., Bauer, A., Lambertz, A., Merdzhanova, T., & Haas, S. (2015). Novel interconnection scheme for thin-film silicon solar modules with conductive intermediate reflector. *Physica Status Solidi-Rapid Research Letters*, 9(2), 103-107. Retrieved from <Go to ISI>://WOS:000349974500001
- [4] Ahmadipour, F., Bahramifar, N., & Ghasempouri, S. M. (2014). Fractionation and mobility of cadmium and lead in soils of Amol area in Iran, using the modified BCR sequential extraction method. *Chemical Speciation and Bioavailability*, 26(1), 31-36. Retrieved from <Go to ISI>://WOS:000331866800004
- [5] Ahuja, P., Peshkova, M. A., Hemphill, B. D., & Gratzl, M. (2014). Minimizing color interference from biological samples in optode-based measurements. *Sensors and Actuators B-Chemical*, 204, 319-325. Retrieved from <Go to ISI>://WOS:000343116400038
- [6] Zhao, Y., Zhao, D., Kong, C., Zhou, F., Jiang, T., & Chen, L. (2019). Design of thin and tubular MOFs-polymer mixed matrix membranes for highly selective separation of H₂ and CO₂. *Separation and Purification Technology*, 220, 197-205. doi:10.1016/j.seppur.2019.03.037
- [7] Arvand, M., & Lashkari, Z. (2013). Sensitive and selective detection of trace copper in standard alloys, food and biological samples using a bulk optode based on N,N'-(4,4'-ethylene biphenyl) bis(3-methoxy salicylidine imine) as neutral carrier. *Spectrochimica Acta Part a-Molecular and Biomolecular Spectroscopy*, 107, 280-288. Retrieved from <Go to ISI>://WOS:000317029200034
- [8] Firooz, A. R., Ensafi, A. A., & Hajyani, Z. (2013). A highly sensitive and selective bulk optode based on dithiacyclooctadecane derivative incorporating chromoionophore V for determination of ultra trace amount of Hg(II). *Sensors and Actuators B-Chemical*, 177, 710-716. Retrieved from <Go to ISI>://WOS:000315751000094
- [9] Tavallali, H., Shaabanpur, E., & Vahdati, P. (2012). A highly selective optode for determination of Hg (II) by a modified immobilization of indigo carmine on a triacetylcellulose membrane. *Spectrochimica Acta Part a-Molecular and Biomolecular Spectroscopy*, 89, 216-221. Retrieved from <Go to ISI>://WOS:000301471600031
- [10] Ganjali, M. R., Gupta, V. K., Hosseini, M., Hariri, M., Faridbod, F., & Norouzi, P. (2012). Lanthanide recognition: A dysprosium(III) selective fluorimetric bulk optode. *Sensors and Actuators B-Chemical*, 171, 644-651. Retrieved from <Go to ISI>://WOS:000308572700083
- [11] Ge, Y. F., Zhu, J. W., Zhao, W. L., & Qin, Y. (2012). Ion-selective optodes based on near infrared fluorescent chromoionophores for pH and metal ion measurements. *Sensors and Actuators B-Chemical*, 166, 480-484. Retrieved from <Go to ISI>://WOS:000305356900065
- [12] Kalinichev, A. V., Zieger, S. E., & Koren, K. (2023). Optical sensors (optodes) for multiparameter chemical imaging: classification, challenges, and prospects. *Analyst*, 149(1), 29-45. doi:10.1039/d3an01661g



Molecular Docking Studies and Its Applications

Volkan EYUPOGLU^{1,*} 

¹ Çankırı Karatekin University, Chemistry Department, Çankırı, Türkiye.

Abstract

Molecular docking is a computational approach that predicts the interaction between a receptor (usually a macromolecule) and a ligand (often a small molecule). It is instrumental in understanding molecular interactions and in the identification and optimization of potential therapeutic agents. Docking studies leverage advanced software tools, including AutoDock, Glide, and Schrödinger Maestro, which incorporate algorithms for flexible docking, virtual screening, and scoring functions. This review explores molecular docking methodologies, widely used software, and their applications in drug discovery, structural biology, and other fields. Emphasis is placed on software capabilities, such as high-throughput screening and quantum mechanics/molecular mechanics (QM/MM) modeling. The review concludes by discussing limitations like scoring function inefficiencies and protein flexibility challenges while highlighting emerging technologies such as artificial intelligence (AI) integration to enhance predictive accuracy.

Keywords: Molecular Docking, Drug Discovery, Schrödinger, Virtual Screening, Computational Chemistry

1. Introduction

Molecular docking has become a pivotal computational approach for studying molecular interactions, particularly in the context of drug discovery, structural biology, and biomolecular engineering. This technique predicts the optimal binding orientation, conformation, and affinity of a ligand to its receptor, providing atomic-level insights into complex biological mechanisms [1, 2]. The rise of computational power, coupled with the evolution of advanced algorithms, has transformed molecular docking into a cornerstone of modern drug discovery. By accurately modeling ligand-receptor interactions, docking enables researchers to identify potential therapeutic agents, optimize lead compounds, understand enzymatic activity, and elucidate intricate signaling pathways fundamental to cellular processes [1, 3, 4].

Recent advancements have significantly enhanced the integration of molecular docking into multidisciplinary research. State-of-the-art software tools, such as Schrödinger Maestro, AutoDock, and MOE, offer robust functionalities that streamline workflows for virtual screening, protein-ligand interaction analysis, and binding affinity estimation [5-7]. These platforms incorporate sophisticated algorithms, including flexible docking, induced-fit modeling, and hybrid quantum mechanics/molecular mechanics (QM/MM) simulations, to address the inherent complexities of protein flexibility and solvent effects. Furthermore, docking studies now frequently leverage massive chemical libraries, enabling the rapid identification of promising drug candidates in areas ranging from oncology to infectious diseases [8].

The advent of artificial intelligence (AI) and machine learning (ML) has further revolutionized molecular docking. AI-driven scoring functions and pose prediction models have substantially improved docking accuracy, while ML algorithms facilitate the integration of docking data with high-throughput experimental results. These advancements have also enabled the development of cloud-based platforms that perform large-scale docking simulations, democratizing access to computational resources [9, 10].

In addition to its application in drug discovery, molecular docking plays a critical role in elucidating biomolecular interactions, such as protein-protein and protein-DNA complexes, and in enzyme inhibition studies. For example, docking has been instrumental in identifying potent inhibitors for enzymes such as G6PD, acetylcholinesterase, and kinases implicated in various diseases [1, 9-12]. This review explores the fundamental

* Corresponding author. e-mail address: volkan@karatekin.edu.tr

methodologies, cutting-edge tools, and diverse applications of molecular docking, with a focus on its transformative impact on scientific research and therapeutic development.

2. General Methodology of Molecular Docking

Molecular docking software provides powerful tools for simulating and analyzing molecular interactions, each with unique features tailored to specific research needs. AutoDock and its variant AutoDock Vina are widely used open-source tools that offer flexible ligand docking through grid-based energy evaluations and customizable scoring functions. Known for their computational efficiency, they are particularly popular in academic research for small-molecule docking studies and allow for batch processing of docking runs [9, 13].

The Schrödinger Suite [14] is a comprehensive platform for molecular modeling, integrating advanced tools such as Glide for high-precision docking and Induced-Fit Docking (IFD) for capturing receptor flexibility during ligand binding. Key features include the Virtual Screening Workflow for large-scale compound library screening, Protein Preparation Wizard for structure optimization, and Prime/MM-GBSA, which refines docking results by combining molecular mechanics with binding energy predictions. These capabilities make Schrödinger a preferred choice for structure-based drug design (SBDD) and detailed biomolecular studies.

MOE [15] (Molecular Operating Environment) excels in fragment-based drug discovery (FBDD) and computational pharmacology, offering tools for pharmacophore modeling, QSAR integration, and small-molecule design. Its versatility makes it well-suited for both academic and industrial research applications.

CHARMM-GUI and GROMACS [11, 16], although not docking software per se, are frequently employed alongside docking studies to perform molecular dynamics simulations. These tools help refine docking poses by exploring ligand stability within the receptor's binding pocket and provide insights into the dynamic nature of biomolecular interactions.

Collectively, these tools cater to a broad range of applications, from virtual screening to fragment assembly, enabling researchers to achieve precision in drug discovery and biomolecular interaction analysis.

3. Future Directions and Conclusion

The evolution of molecular docking is set to be driven by the integration of emerging technologies and innovative computational approaches, promising significant advancements in accuracy, efficiency, and scalability.

Artificial Intelligence (AI) and Machine Learning (ML): The incorporation of AI and ML into molecular docking workflows is revolutionizing how protein-ligand interactions are predicted and analyzed. AI-driven scoring functions and pose prediction models are enhancing the precision of docking outcomes by learning from vast datasets of experimental and computational binding data [2, 17]. Tools like DeepDock, which leverage neural networks, have demonstrated significant improvements in pose accuracy and binding affinity predictions. Furthermore, ML models are being utilized to optimize ligand libraries, prioritize high-potential candidates, and integrate multi-omics data for holistic drug discovery pipelines [18-20].

Quantum Mechanics/Molecular Mechanics (QM/MM): Hybrid computational techniques combining quantum mechanics and molecular mechanics are advancing the accuracy of binding energy predictions. QM/MM methods enable a detailed understanding of electronic interactions within active sites, particularly for systems involving covalent bonds or transition states. These techniques are becoming increasingly accessible, supported by the development of faster algorithms and hardware accelerations [21].

Cloud-Based High-Throughput Docking: The advent of cloud computing has transformed the scalability of molecular docking. Platforms such as RosettaDock and DockThor offer cloud-based high-throughput docking capabilities, enabling the screening of millions of compounds against biological targets in parallel. This not only accelerates drug discovery timelines but also democratizes access to computational resources, making cutting-edge docking studies feasible for researchers with limited local infrastructure [22].

Integration with Experimental Techniques: Future docking studies are expected to increasingly integrate with experimental methods such as cryo-electron microscopy (cryo-EM), X-ray crystallography, and NMR spectroscopy. These techniques provide high-resolution structural data, which, when combined with docking, can yield more reliable and biologically relevant predictions [18].

Multiscale Simulations: The coupling of docking with molecular dynamics (MD) simulations, coarse-grained modeling, and enhanced sampling techniques is gaining traction. This integration allows researchers to explore the dynamic behavior of ligand-receptor complexes, capturing transient interactions and improving docking accuracy in flexible or disordered protein regions [23].

4. Conclusion

Molecular docking remains a cornerstone of computational drug discovery and molecular biology, providing invaluable insights into biomolecular interactions and accelerating therapeutic development. With continual advancements in software capabilities and the integration of cutting-edge technologies such as AI, QM/MM, and cloud computing, molecular docking is poised to enter a new era of unprecedented accuracy and applicability. These innovations address longstanding challenges, such as scoring function limitations and protein flexibility, enabling researchers to confidently tackle complex biological questions. As docking evolves, its synergy with experimental validation and multiscale simulations will further solidify its role as an indispensable tool in modern science, driving progress in drug discovery, biomolecular engineering, and beyond.

Acknowledgement

The paper was presented in 3rd IKSTC in the workshop section.

References

- [1] Vijayakumar, S., & Rajalakshmi, S. (2021). Exploring novel natural compound inhibitors for Parkinsonian receptor (DJ1) by homology modeling, molecular docking and MD simulations. *Vegetos*, 34(4), 959-970. doi:10.1007/s42535-021-00263-5
- [2] Nadeem, M., Mumtaz, M. W., Danish, M., Rashid, U., Mukhtar, H., & Irfan, A. (2020). Antidiabetic functionality of *Vitex negundo* L. leaves based on UHPLC-QTOF-MS/MS based bioactives profiling and molecular docking insights. *Industrial Crops and Products*, 152. doi:10.1016/j.indcrop.2020.112445
- [3] Yang, B., Bai, L., Li, T., Deng, L., Liu, L., Zeng, S., . . . Zhang, X. (2021). Super selective ammonia separation through multiple-site interaction with ionic liquid-based hybrid membranes. *Journal of Membrane Science*, 628. doi:10.1016/j.memsci.2021.119264
- [4] Yang, B. B., Bai, L., Li, T. T., Deng, L. Y., Liu, L., Zeng, S. J., . . . Zhang, X. P. (2021). Super selective ammonia separation through multiple-site interaction with ionic liquid-based hybrid membranes. *Journal of Membrane Science*, 628. doi:ARTN 11926410.1016/j.memsci.2021.119264
- [5] Bitencourt-Ferreira, G., & de Azevedo, W. F. (2019) Molegro virtual docker for docking. In: Vol. 2053. *Methods in Molecular Biology* (pp. 149-167).
- [6] Misra, N., Patra, M. C., Panda, P. K., Sukla, L. B., & Mishra, B. K. (2013). Homology modeling and docking studies of FabH (beta-ketoacyl-ACP synthase III) enzyme involved in type II fatty acid biosynthesis of *Chlorella variabilis*: a potential algal feedstock for biofuel production. *Journal of Biomolecular Structure & Dynamics*, 31(3), 241-257. Retrieved from <Go to ISI>://WOS:000315774900001

- [7] Nabati, M., & Bodaghi-Namileh, V. (2020). In silico study of the active components (17 alpha-ethinyl estradiol and segesterone acetate) of annovera as a novel vaginal contraceptive system by docking of their binding to estrogen and progesterone receptors. *Eurasian Chemical Communication*, 2(2), 234-246. doi:10.33945/sami/ecc.2020.2.9
- [8] Moradi, H., & Vaezi, A. (2020). Lessons Learned From Korea: Covid-19 Pandemic. *Infect Control Hosp Epidemiol*, 1-5. doi:10.1017/ice.2020.104
- [9] Fadaka, A. O., Sibuyi, N. R. S., Madiehe, A. M., & Meyer, M. (2022). Computational insight of dexamethasone against potential targets of SARS-CoV-2. *Journal of Biomolecular Structure & Dynamics*, 40(2), 875-885. doi:10.1080/07391102.2020.1819880
- [10] Ibrahim, I. M., Abdelmalek, D. H., Elshahat, M. E., & Elfiky, A. A. (2020). COVID-19 spike-host cell receptor GRP78 binding site prediction. *J Infect*. doi:10.1016/j.jinf.2020.02.026
- [11] Kashfolgheta, S., Wang, S., Acree, W. E., & Hünenberger, P. H. (2021). Evaluation of nine condensed-phase force fields of the GROMOS, CHARMM, OPLS, AMBER, and OpenFF families against experimental cross-solvation free energies. *Physical Chemistry Chemical Physics*, 23(23), 13055-13074. doi:10.1039/d1cp00215e
- [12] V. Figueiredo, R., Srivastava, T., Skaar, T., Warning, N., Gravesteyn, P., van Os, P., . . . Goetheer, E. (2021). Impact of dissolved oxygen removal on solvent degradation for post-combustion CO₂ capture. *International Journal of Greenhouse Gas Control*, 112. doi:10.1016/j.ijggc.2021.103493
- [13] Elfiky, A. A. (2020). Anti-HCV, nucleotide inhibitors, repurposing against COVID-19. *Life Sciences*, 248, 117477. doi:10.1016/j.lfs.2020.117477
- [14] Ranjan, A., Chauhan, A., & Jindal, T. (2018). In-silico and in-vitro evaluation of human acetylcholinesterase inhibition by organophosphates. *Environ Toxicol Pharmacol*, 57, 131-140. doi:10.1016/j.etap.2017.12.014
- [15] Shah, R., Alharbi, A., Hameed, A. M., Saad, F., Zaky, R., Khedr, A. M., & El-Metwaly, N. (2020). Synthesis and Structural Elucidation for New Schiff Base Complexes; Conductance, Conformational, MOE-Docking and Biological Studies. *Journal of Inorganic and Organometallic Polymers and Materials*, 30(9), 3595-3607. doi:10.1007/s10904-020-01505-w
- [16] Urwin, D. J., & Alexandrova, A. N. (2021). Regularization of least squares problems in CHARMM parameter optimization by truncated singular value decompositions. *Journal of Chemical Physics*, 154(18). doi:10.1063/5.0045982
- [17] Vankadari, N., & Wilce, J. A. (2020). Emerging WuHan (COVID-19) coronavirus: glycan shield and structure prediction of spike glycoprotein and its interaction with human CD26. *Emerg Microbes Infect*, 9(1), 601-604. doi:10.1080/22221751.2020.1739565
- [18] Akue-Gedu, R., Nauton, L., Thery, V., Bain, J., Cohen, P., Anizon, F., & Moreau, P. (2010). Synthesis, Pim kinase inhibitory potencies and in vitro antiproliferative activities of diversely substituted pyrrolo[2,3-a]carbazoles. *Bioorganic & Medicinal Chemistry*, 18(18), 6865-6873. Retrieved from <Go to ISI>://WOS:000281524700028 http://ac.els-cdn.com/S0968089610006899/1-s2.0-S0968089610006899-main.pdf?_tid=32994b46-0e52-11e6-aa8b-00000aacb360&acdnat=1461965868_729089ccdd7aac399530f0d3b0119533
- [19] Sliman, F., Blairvacq, M., Durieu, E., Meijer, L., Rodrigo, J., & Desmaele, D. (2010). Identification and structure-activity relationship of 8-hydroxy-quinoline-7-carboxylic acid derivatives as inhibitors of Pim-1 kinase. *Bioorg Med Chem Lett*, 20(9), 2801-2805. Retrieved from <Go to ISI>://WOS:000276816600021 http://ac.els-cdn.com/S0960894X10003926/1-s2.0-S0960894X10003926-main.pdf?_tid=83d913e2-0e57-11e6-b1b4-00000aacb35f&acdnat=1461968151_8239e9811a4ad3f1396ec82ebac49dd0
- [20] Wu, Y., Wang, F. Y., Yu, H. X., Wang, Z. Y., & Wang, L. S. (2010). 3D-QSAR Study on the Inhibitory Activity of Flavonoids on PIM-1 Kinase. *Chinese Journal of Structural Chemistry*, 29(8), 1147-1154. Retrieved from <Go to ISI>://WOS:000281331200002
- [21] Zhen, G. L., Eggli, V., Voros, J., Zammaretti, P., Textor, M., Glockshuber, R., & Kuennemann, E. (2004). Immobilization of the enzyme beta-lactamase on biotin-derivatized poly(L-lysine)-g-poly(ethylene glycol)-coated sensor chips: A study on oriented attachment and surface activity by enzyme kinetics and in situ optical sensing. *Langmuir*, 20(24), 10464-10473. Retrieved from <Go to ISI>://WOS:000225207400017
- [22] Ren, J. X., Li, L. L., Zheng, R. L., Xie, H. Z., Cao, Z. X., Peng, S., . . . Yang, S. Y. (2011). Discovery of Novel Pim-1 Kinase Inhibitors by a Hierarchical Multistage Virtual Screening Approach Based on SVM Model, Pharmacophore, and Molecular Docking. *Journal of Chemical Information and Modeling*, 51(6),

1364-1375. Retrieved from <Go to ISI>://WOS:000292010100017
<http://pubs.acs.org/doi/pdfplus/10.1021/ci100464b>

- [23] Maiti, P., Nand, M., Joshi, T., Ramakrishnan, M. A., & Chandra, S. (2020). Identification of luteolin -7-glucoside and epicatechin gallate from *Vernonia cinerea*, as novel EGFR L858R kinase inhibitors against lung cancer: Docking and simulation-based study. *Journal of Biomolecular Structure & Dynamics*, 1-10. doi:10.1080/07391102.2020.1784791



Modeling and Simulation of Electric Vehicles: An Approach Using MATLAB

Tevfik ATAMAN^{1,*} 

¹ Vocational School, Machine and Metal Technologies, Çankırı Karatekin University, Çankırı, Türkiye

Abstract

Electric vehicles (EVs) are becoming progressively pivotal in the automotive sector owing to environmental issues and the necessity to diminish reliance on fossil fuels. This research centers on the modeling and simulation of an electric vehicle system with MATLAB/Simulink. The essential elements of electric vehicles, such as the battery, electric motor, power converter, and vehicle dynamics, are examined and modeled comprehensively. Lithium-ion batteries were selected for the battery module during the modeling process, focusing on charge-discharge characteristics and energy density. A permanent magnet synchronous motor (PMSM) was chosen as the electric motor, and its torque-speed relationship was dynamically modeled. Vector control algorithms were employed for motor control in the power converter. The vehicle dynamics model was developed to incorporate external elements such aerodynamic drag, rolling resistance, and gradient forces on the vehicle. The simulation findings offered a comprehensive examination of performance metrics including acceleration, energy consumption, and battery longevity of the electric car. The adaptable architecture of MATLAB/Simulink facilitated the seamless incorporation of various driving scenarios and battery capacity into the model. This project seeks to enhance the advancement of sustainable transportation systems by providing an efficient simulation environment for evaluating the performance of electric vehicles.

Keywords: Electric vehicle, Energy consumption, Vehicle modelling.

1. Introduction

The increase in the world population and the growth of the industrial branches continue to increase the need for production and increase the energy requirement. Today, most of the electricity needs are met by fossil fuels. After electricity generation, the oldest of fossil fuels is the transport and transportation sector, with the highest energy use growth rate [1]. Internal combustion engines operating with petroleum derivative fuels can operate around 40% efficiency today, despite the development of engine technologies. Most of the energy released by the burning of the fuel is expelled as heat. One of the alternatives recommended for cleaner and more efficient road vehicles is the use of hydrogen as fuel. Since only water vapor is released as a result of its combustion, hydrogen-powered vehicles will be zero-emission vehicles. However, the lack of hydrogen in nature and the use of fossil fuels in its production, the low energy efficiency until the hydrogen is obtained from the source and transformed into the road traveled in the vehicle, and the high emissions in this general cycle are the biggest obstacles to fuel cell studies [2]. In hybrid electric vehicles, the battery is used as a buffer in power requirement regions where internal combustion engines operate with low efficiency and high emissions, increasing the average efficiency of the internal combustion engine throughout the driving Cycle [3].

Innovations brought by hybridization such as recovery of brake energy, stopping of internal combustion engines and power management allow more efficient use of energy in road vehicles and travel with lower emissions. Energy efficiency in the conversion of vehicles operating with various energy systems calculated by Toyota from energy source to motion energy is shown in Figure 1 [4].

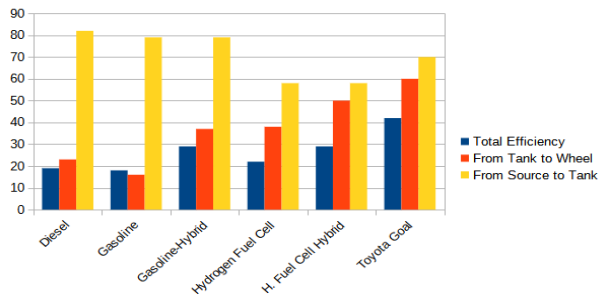


Figure 1. Efficiency of vehicles operating with various energy sources from source to wheel.

* Corresponding author. e-mail address: tevfikataman@karatekin.edu.tr

As can be seen from Figure 1, the fuels with the highest efficiency in the transformations from the source of energy to the energy storage on the vehicle are petroleum derivative fuels. In hybrid electric and fuel cell vehicles, the efficiency on the vehicle is higher and therefore the total efficiency of these vehicles is higher than the vehicles operating with petroleum-based fuels. The increased need for electrical energy in vehicles for higher HEV efficiency, low emission high fuel economy, driving comfort and cruise safety has made hybrid electric vehicles an important need today [5].

2. Materials and Methods

Hybrid electric vehicles provide a reduction in fuel consumption and exhaust gas emissions compared to conventional vehicles with the advantages they provide such as engine downsizing, engine stopping while driving, recovery of brake energy and energy management. The biggest problem encountered after determining the power components and their relationship with each other in hybrid electric vehicles is that this complex system can be controlled in the best way. To develop HEV control algorithms, first of all, the mathematical model of the designed system must be established in accordance with the calculations to be made. In order to make distribution calculations between power systems in HEV systems, longitudinal vehicle dynamics models should be established. This project aims to mimic a hybrid vehicle using the Matlab Simulink module. The study identified motor power, motor torque, and design parameters (projected area and drag coefficient) as input variables.

Vehicle Dynamics

In the first step, the parameters shown in Table 1 were used to model vehicle dynamics. This table also includes abbreviations for total vehicle load modeling. With the help of these parameters, it is possible to calculate the load forces applied to the vehicle. Also, the results to be obtained with changes in these parameters will be evaluated [6].

Table 1. Vehicle body parameters.

Abbreviation	Definition	Value	Unit
M	Mass	1250	Kg
g	Gravity	9.81	m/s ²
A	Slope of road	-	°
P	Air density	1.225	kg/m ³
A	Vehicle frontal area	1.7	m ²
C _d	Drag coefficient	0.3	-
C _f	Friction coefficient	0.02	-
V	Vehicle speed	-	m/s

2.1. Vehicle Model

HEVs can generally be classified into parallel HEVs and series HEVs based on their powertrain design. Parallel hybrid electric vehicles (HEVs) can be concurrently powered by an internal combustion engine (ICE) and an electric motor (EM). In a series hybrid electric vehicle (HEV), the propulsion system is exclusively driven by the electric motor (EM), which derives its energy from the onboard battery unit, charged by the vehicle's engine.

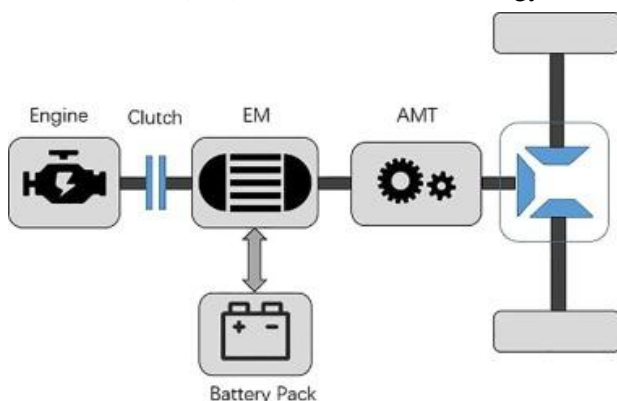


Figure 2. Configuration of the hybrid powertrain.

The powertrain design of the examined vehicle, featuring a single-shaft parallel hybrid layout, is seen in Fig. 2, which is often employed in numerous hybrid models. The automated machine transmission (AMT) is essential for optimizing the operational parameters of internal combustion engines (ICE) and electric motors (EM) to function within their respective high-efficiency ranges. The EM might function as a generator while recharging the battery. The clutch may be utilized to alter the operational modes of the powertrain, including EV mode, engine-drive mode, hybrid drive mode, and regenerative-brake model [6].

In this model, the speed profile that the driver must follow is given to the driver modeled with PI (proportional-integral), the driver model tries to reduce the error between the actual speed and the determined speed profiles by generating throttle, brake and clutch signals according to the actual vehicle speed. For any given cycle, the road forces corresponding to the vehicle speed are calculated, the loads on the wheels and the speed values are calculated backwards through the transmission organs, and the torque values that the motors must give with the rotation speeds are determined. All vehicle models created were prepared in MATLAB/Simulink environment (Figure 3).

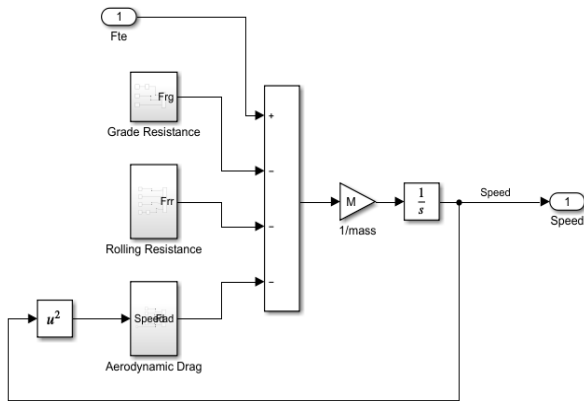


Figure 3. MATLAB/Simulink vehicle model.

Travel loads affecting the vehicle are calculated. These travel loads consist of wind resistance, rolling resistance in the wheels, braking and acceleration resistances and slope resistance. Travel resistances affecting the vehicle are given in Figure 4.

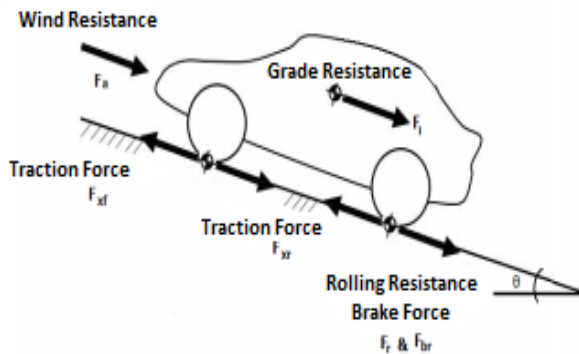


Figure 4. Forces acting on the vehicle.

2.2. Rolling Resistance

While the vehicle is in motion, rolling resistance acts on the wheels slightly in front of the wheel-road contact plane due to its elastic structure. A standard formulation was used to calculate the rolling resistance in the studies [6].

Rolling resistance arises from the tire's deflection during rotation on the road, resulting in a larger distribution of normal pressure in the leading half of the contact interface compared to the trailing half. Consequently, the horizontal corresponding force is generated at the interface between the tire and the road, referred to as rolling

resistance. Rolling resistance is influenced by various characteristics, notably tire shoulder temperature, ambient temperature, tire diameter, road conditions, tire inflation pressure, and tire type. Numerous empirical relationships are established for the rolling resistance coefficient as a function of velocity for different tire types and road conditions. The rolling resistance of each wheel can be computed using the following formulae:

$$F_{rr} = C_f * m * g * \cos \frac{\pi\alpha}{180^\circ} \quad (1)$$

2.3. Grade Resistance

Simple trigonometric calculations are used in the calculation of the grade resistance affecting the vehicle. This calculation is shown in equation 2.

$$F_{rg} = m * g * \sin \frac{\pi\alpha}{180^\circ} \quad (2)$$

3. Results and Discussion

The vehicle dynamics model was developed, and a Simulink model was created in the preceding section. The simulation results are derived by delineating several scenarios. The schematic diagram of the Simulink blocks, which includes the vehicle model, front wheels, rear wheels, and traction force, is depicted in the preceding drawings. The velocity of each wheel and the vehicle's overall velocity are computed at each time step during the simulation. The velocity determined by each block is input into the slip computation block to derive the slip corresponding to each wheel. These blocks compute the slip amount for each wheel using the equations, and these values are subsequently utilized by the traction force block to determine the longitudinal effective force, which is the force generated at the tire-road interface at the contact point that propels the vehicle forward. The orientation of this force alters during brake application, countering the vehicle's motion.

Owing to the dynamics of the brake model described, the velocity of the vehicle and each wheel reaches zero simultaneously. To assess the model's performance in scenarios where the vehicle comes to a halt and subsequently resumes movement, a test was conducted by simulating the conditions defined by the throttle opening position and brake pedal engagement.

Changes in vehicle speed were observed by entering different C_d and different C_f values. The relationship of these changes with other parameters and the changes of the change were evaluated.

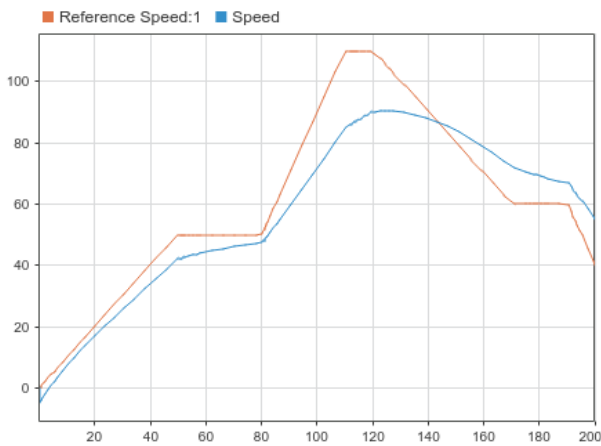


Figure 5. $C_d = 0.75$ situation.

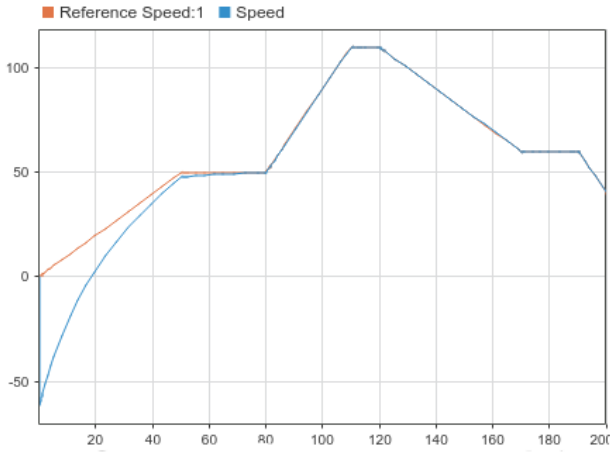


Figure 6. $C_f = 0.04$ situation.

4. Conclusion

This project aims to model a hybrid vehicle using the Matlab/Simulink module. In the analysis, rolling resistance, traction force, grade resistance, and design characteristics (frontal area and drag coefficient) were identified as input values. The study aims to determine the fuel consumption, specific fuel consumption, vehicle speed, and aerodynamic resistance parameters of a hybrid vehicle.

These inferences can be made by looking at real-time speed values compared to the reference speed. By looking at the changes in C_d and C_f values, optimization should be made to approach the reference speed values.

References

- [1] Guzzella L. and Sciarretta A., 2007, *Vehicle Propulsion Systems: Introduction to Modeling and Optimization*, Springer Science & Business Media, Berlin.
- [2] Boyalı A. and Güvenç L., 2010, *Hibrid Elektrikli Araçların Modellenmesi ve Kural Tabanlı Kontrolü*, İTÜ Engineering Magazine, Istanbul, 83-94.
- [3] Toyota Motor Corporation, *Toyota's Global Strategy Report*, 2003.
- [4] Pacejka, H. B., 2002, *Tyre and Vehicle Dynamics*, Butterworth – Heinemann, U.K.
- [5] Internet, 2005, *United States Environmental Protection Agency, National Air Toxics Assessment*, <http://www.epa.gov>.
- [6] Ehsani, M., 2004, *Modern Electric, Hybrid Electric, and Fuel Cell Vehicle Fundamentals Theory and Design*, CRC Press, 102-108.



ANSYS-Based Intake Manifold Flow Analysis: A Computational Fluid Dynamics Approach

Tevfik ATAMAN^{1,*} 

¹ Vocational School, Machine and Metal Technologies, Çankırı Karatekin University, Çankırı, Türkiye

Abstract

The varying performance requirements at all load and speed circumstances must permit an adequate supply of air to a sufficient number of cylinders. The primary function of the engine intake manifold is to uniformly distribute the fresh air-fuel combination to the combustion chamber. In an air intake system, reducing airflow resistance is crucial for enhancing performance. The intake manifold pressure fluctuates continuously due to variations in volume during the suction operation in each cylinder. The alteration of the valve opening area results in an erratic gas flow. This work numerically examined gas flow characteristics, including manifold pressure variations and velocity, utilizing Computational Fluid Dynamics. The findings from this investigation were thoroughly analyzed about variations in pressure and flow velocity of the fundamental parameters and illustrated graphically.

Keywords: Intake manifold, Computational fluid dynamics, Manifold flow analysis.

1. Introduction

The main function of the intake manifold is to carry the necessary and equal fresh air-fuel mixture to the combustion chamber. Intake manifolds are designed to provide a uniform air-fuel mixture to all cylinders. If they are incorrectly measured or designed, the engine cylinders will not be able to receive the necessary amount of air (cylinder charge) needed for good combustion. Changes can be made to the intake manifold depending on the variable performance needs of the engine. Only in this way can it be possible to provide the cylinders with sufficient air at all loads and speeds. This is possible with a multi-way intake manifold system. The intake manifold basically consists of two parts. The first is the plenum, which is the inlet part of the manifold under the butterfly body or carburetor. The second is the runner channels that connect the plenum to the cylinders. Manifold runners ensure that the fresh charge reaches each cylinder separately [1].

In an internal combustion engine, the air required for combustion is supplied to the cylinders by the intake manifold. Therefore, the Air Intake Manifold (AIM) has an important role. The desired amount of air delivered to the car engine increases combustion efficiency, thus reducing air pollution [1]. The intake air passes through the manifold vent, is distributed to the outlets connected to the vent, and passes into the combustion chamber. In order to optimize the air flow in the intake system, a good understanding of the air flows, inlet velocity, and pressure drop through the system is required [2].

Many studies have been done and are still being done for HEM flow optimization. Dal (2009) investigated the velocity and pressure distributions in the manifold by using the CFD method in his study to determine the flow characteristics in the intake manifold [3]. Khan and Salim (2013) determined the optimum flow conditions in the intake manifold of an SI engine under steady flow conditions by using different turbulence models in their study; They stated that CFD analysis is an effective method in determining the flow characteristics in the intake manifold [4]. Jemni et al. (2011) investigated the flow parameters in the manifold in terms of pressure and velocity by using the standard k- ϵ turbulence method in the intake manifold of an LPG spark ignition engine by using the CFD analysis [5]. Min-Ho Kim et al. (2000) investigated the internal flow characteristics of a six-cylinder diesel engine intake manifold computationally under steady state [6]. Safwan (2009) stated in his study that turbulent flow is the best method to estimate the flow conditions inside the manifold and that pressure and speed decrease occur with the decrease in turbulence value. The study by Angadi et al. (2010) also showed similar results and it was stated that the flow conditions change in direct proportion to the change in the amount of turbulence [7].

The main purpose of this study is to estimate the best flow conditions in the intake manifold by considering the flow parameters such as pressure and speed and using the standard k- ϵ turbulence model. A manifold model of a 4-cylinder vehicle was used for the HEM numerical model simulation. Air was used as the fluid in the analyses. In the numerical analysis, ANSYS Fluent15.0 software, which makes solutions based on the Finite Volume

* Corresponding author. e-mail address: tevfikataman@karatekin.edu.tr

Method, was used to analyze the internal flow of the air intake manifold. In line with the analysis results, this study aims to determine the best internal flow conditions for the intake manifold and to obtain the most appropriate design.

2. Materials and Methods

Numerical methods produce approximate solutions with the desired precision. As the precision increases, the processing steps increase, and depending on the type of problem being examined, more powerful and faster computers may be needed. Today, with the constantly developing computer technology, numerical analysis methods have also developed and have become an effective solution method for modeling and solving even complex problems.

The increasing development of computer technology and its capacities, the high cost of experimental and test equipment, and the long time required for the experimental process make CFD analyses attractive and all existing commercial CFD software includes three basic tools: Pre-processor, solver and post-processor [7].

The main operations performed in the pre-processor section are the creation of the geometry and mesh structure of the physical model, the definition of boundary conditions, the determination of solution techniques such as finite difference, finite volumes, finite elements and spectral methods, and the obtaining and evaluation of solution results in the solver section.

In the numerical study, the intake manifold geometry of a 4-cylinder, naturally aspirated and spark ignition engine was created in ANSYS Workbench as seen in Figure 1 and the meshing process was performed to determine the appropriate numerical mesh structure. The necessary flow analyses were performed on the initial geometry, new designs were made in line with the results obtained and a design with a better flow rate was attempted to be obtained. The boundary conditions in the study are given in Table 1.

Table 1. Boundary conditions.

Parameter	Value
Inlet velocity	50 m/s
Inlet Pressure	101300 Pa
Outlet Pressure	9500 Pa
Temperature	313 K

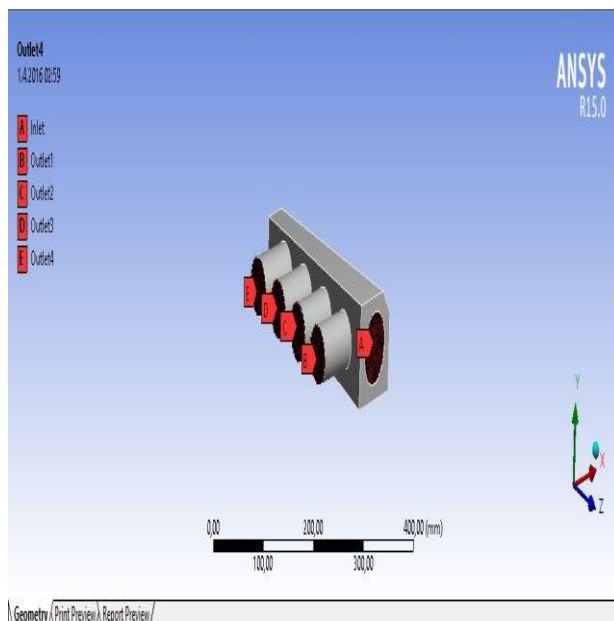


Figure 1. Initial geometry.

In the numerical simulation performed for the three-dimensional, steady flow condition, the Standard k-ε method was used as the turbulence model. The data obtained as a result of the analyses are presented in graphs in terms of pressure and velocity changes, which are the basic flow parameters, and are examined in detail below. The different values obtained from the flow analyses in different designs clearly provide information about the efficiency of the design. Theoretical calculations related to the Standard k-ε method are as follows.

It is a semi-empirical model that is widely used among two-equation turbulence models due to its economy and acceptable accuracy in many flow phenomena. It includes the solution of two transport equations written for turbulent kinetic energy (k) and dissipation rate (ε) and the calculation of turbulent viscosity. When the effect of buoyancy forces is neglected, these transport equations are given for k and ε, respectively;

$$\rho \frac{Dk}{Dt} = \frac{\partial}{\partial x_i} \left(\Gamma_k \frac{\partial k}{\partial x_i} \right) + G_k - \rho \varepsilon \quad (1)$$

$$\rho \frac{D\varepsilon}{Dt} = \frac{\partial}{\partial x_i} \left(\Gamma_\varepsilon \frac{\partial \varepsilon}{\partial x_i} \right) + C_{1\varepsilon} \frac{\varepsilon}{k} G_k - C_{2\varepsilon} \rho \frac{\varepsilon^2}{k} - R \quad (2)$$

$$\Gamma_k = \mu + \mu_t / \sigma_k \quad \Gamma_\varepsilon = \mu + \mu_t / \sigma_\varepsilon \quad (3)$$

$$G_k = \mu_t \left(\frac{\partial u_i}{\partial x_j} + \frac{\partial u_j}{\partial x_i} \right) \frac{\partial u_i}{\partial x_j} \quad (4)$$

$$\mu_t = \rho C_\mu \frac{k^2}{\varepsilon} \quad (5)$$

In this model, $R = 0$ and other empirical constants are: $C_{1\varepsilon} = 1.44$, $C_{2\varepsilon} = 1.92$, $C_\mu = 0.09$, turbulence Prandtl numbers defined for k and ε are $\sigma_k = 1.0$, $\sigma_\varepsilon = 1.3$.

3. Results and Discussion

In this study, numerical results were obtained using the CFD software for the intake manifold of a 4-cylinder, naturally aspirated and spark ignition engine, and the speed, pressure and turbulence kinetic energy changes of the flow for the HEM were investigated. Figure 2 shows the flow path of the first design manifold geometry.

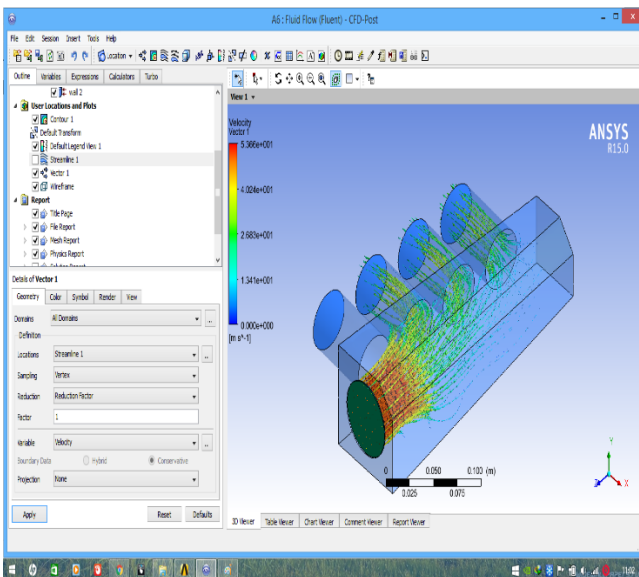


Figure 2. Initial geometry flow path.

As can be understood from Figure 2; it is seen that the 1st outlet section, which is very close to the inlet section and in a vertical position in the first design, cannot be used efficiently. The reason for this is that the air entering with a certain inlet speed rushes directly forward and goes to the other runners without stopping by the 1st outlet section. The outlet velocity values given in Table 2 clearly show this.

Table 2. Initial geometry outlet speeds.

Parameter	Speed (m/s)
Outlet 1	5.44
Outlet 2	21.45
Outlet 3	24.15
Outlet 4	30.85

In the design shown in Figure 3; while the inlet section remains the same, the outlet sections (runners) are made curved downwards. By changing the design to this state, the outlet velocities have improved a little more and the first outlet has been used more efficiently. The outlet velocities in this design are given in Table 3. The most important reason for the increase in the outlet velocities is that the flow is provided more efficiently from the softened edges without encountering sharp edges. This situation can be clearly seen with these improvements in the design. In addition, the outlets should be as close as possible to the vent center so that they can be fed with equal air. In the following designs, this situation will be taken into consideration and the necessary operations will be carried out and the most suitable design will be tried to be obtained.

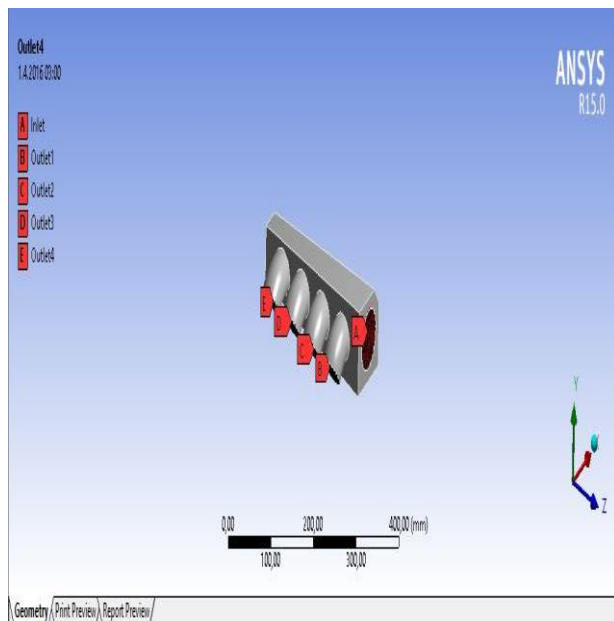


Figure 3. Second design.

Table 3. Second design outlet speeds.

Parameter	Speed (m/s)
Outlet 1	11.44
Outlet 2	25.64
Outlet 3	27.67
Outlet 4	31.95

It can be said that the runners are used more efficiently by considering the exit velocities in Table 3. The flow path of this design is as seen in Figure 4. As can be understood from here, more suitable designs can be made by taking these improvements into account in the next designs.

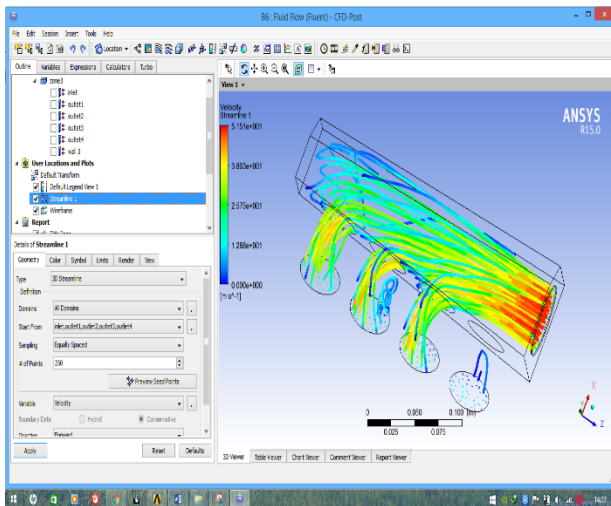


Figure 4. Second geometry flow path.

4. Conclusion

In this study, numerical results were obtained using Computational Fluid Dynamics software for the intake manifold of a 4-cylinder, naturally aspirated and spark ignition engine, and the speed and pressure changes of the flow for the considered intake manifolds were investigated. As a result of the analysis, the following conclusions were reached;

- The location of the manifold inlet is very important for the flow. By positioning the inlet perpendicular to the outlets, there may be outlets that the flow cannot reach. As in the first design, it was observed that the air entering from the inlet section was directed directly to the other outlets without directing to the first outlet section.
- Sharp edges inside the manifold negatively affect the flow path and flow rate. By softening these sharp edges, the flow becomes smoother and clearer, and the flow rate increases accordingly. In the first design, the outlet velocities are at the lowest levels due to the sharp edges inside the manifold.
- The vortices formed by the standard k- ϵ method best show the distribution of the flow in all connection points and the vent (pressure chamber). Therefore, this method is a good choice for analyzing the flow in the intake manifold.

References

- [1] Rajput, R., (2007). Internal Combustion Engine, Laxmi Publications.
- [2] Safwan, M., (2009). Pressure drop analysis of 1.6l car air intake system, Faculty of Mechanical Engineering, University Malaysia Pahang.
- [3] Dal, M. (2009). Emme manifoldu dizaynının motor performansına etkisi, Yüksek Lisans Tezi, Yıldız Teknik Üniversitesi Fen Bilimleri Enstitüsü, İstanbul. Pacejka, H. B., 2002, *Tyre and Vehicle Dynamics*, Butterworth – Heinemann, U.K.
- [4] Khan, M. M., and Salim, S.M., (2013). Evaluation of CFD Sub-Models for the intake manifold port flow analysis, School of Engineering, Taylor's University, Selangor, Malaysia.
- [5] Jemni, M. A., Kantchev, G., and Abid, M. S., (2011). Intake manifold design effect on air fuel mixing and flow for an LPG heavy duty engine, IJEE: Vol. 3, Issue 1, 61-72.
- [6] Min, H. K., Woo, I. C., and In-Bum, C., (2000). Three-dimensional flow characteristics and engine performance for the geometry modification of intake manifold in multi-cylinder diesel engine, FISITA World Automotive Congress, Seoul.
- [7] Angadi, B.M., Malipati, A. S., Nagathan. V. V., and Kattimani, R.S., (2010). Modelling and Analysis of Intake manifold of a Multi-cylinder SI engine, 4th International Conference on Fluid Mechanics and Fluid Power, Madras, Chennai.



SWOT Analysis of the Therapy Use of Çankırı Rock Salt Mine in Health Tourism

Hüdayi ERCOŞKUN^{1,*} , Mehmet SÖYLER² , Yakup ÖZTÜRK³ 

¹ Engineering Faculty, Department of Food Engineering, Çankırı Karatekin University, Çankırı, Türkiye

² Vocational School of Social Sciences, Çankırı Karatekin University, Çankırı, Türkiye

³ Ilgaz Tourism Faculty, Çankırı Karatekin University, Çankırı, Türkiye

Abstract

This study presents a SWOT analysis of the Çankırı Rock Salt Mine's potential for health tourism through salt therapy. With its unique natural resources and rich cultural heritage, Çankırı offers a promising environment for alternative therapies. The analysis identifies the region's strengths, such as its therapeutic mineral-rich salt, accessibility, and growing interest in natural remedies. It also highlights weaknesses, including infrastructure challenges and lack of awareness. Opportunities for growth include increasing health consciousness and government support, while threats encompass competition and economic fluctuations. This study aims to provide strategic insights for developing Çankırı as a prominent destination for health tourism.

Keywords: Health tourism, Salt therapy, SWOT analysis, Çankırı rock salt mine, Alternative therapies

1. Introduction

Health tourism has grown into a critical sector within the global tourism landscape, reflecting an escalating demand for alternative therapies and holistic wellness experiences. This trend is fueled by a rising awareness of personal health, a shift towards natural and non-invasive treatment methods, and a growing interest in preventive healthcare. As individuals increasingly seek therapies beyond conventional medicine, wellness practices like salt therapy, thermal baths, and herbal treatments have gained considerable attention. Salt therapy, in particular, stands out for its natural therapeutic effects, reputed to support respiratory health, alleviate skin conditions, and contribute to general well-being. Originating from ancient practices, salt therapy has gained modern relevance, attracting those who prefer natural healing methods [1-3].

In this context, Turkey's Çankırı Rock Salt Mine offers a compelling option for health tourism. Situated in Çankırı Province, the mine is renowned for its vast salt reserves and unique natural formations, which present both aesthetic and therapeutic appeal. The salt within the mine is rich in minerals like sodium chloride, potassium, magnesium, and calcium, which can contribute to respiratory and skin health when used in controlled environments. These characteristics, combined with Çankırı's cultural heritage and strategic location, position the region as a promising destination for visitors seeking alternative therapeutic options [4-6].

This study examines the potential of the Çankırı Rock Salt Mine to become a hub for health tourism, with a focus on salt therapy. Through a comprehensive SWOT analysis, the study identifies key strengths such as the mine's mineral composition, cultural and historical significance, and growing accessibility. It also considers weaknesses, including infrastructural limitations and a need for broader public awareness about the health benefits of salt therapy. Opportunities for growth lie in the increasing interest in wellness tourism and potential government support, while challenges include competition from other health tourism destinations and economic fluctuations [7-9].

By analyzing these factors, the research provides a strategic foundation for promoting Çankırı as a competitive player in the health tourism sector. Ultimately, this study aims to enhance awareness of

* Corresponding author. e-mail address: hercoskun@yahoo.com

Çankırı's natural therapeutic resources and highlight its potential for contributing to both local and international health tourism markets.

Strengths (S)

Natural Resource: Çankırı Rock Salt Mine is a unique natural resource known for its therapeutic properties. The mine contains mineral-rich salt that can provide significant health benefits. This natural resource can attract both domestic and international tourists seeking alternative therapies. The presence of natural salt formations offers a unique experience for visitors, enhancing their overall therapeutic journey.

Cultural Heritage: Çankırı has a rich historical and cultural background, contributing to its attractiveness as a health tourism destination. The region's traditional practices and local culture can enhance the appeal of salt therapy, providing a more holistic experience for visitors. By integrating local cultural elements into therapy programs, Çankırı can offer a distinctive and memorable experience for tourists.

Accessibility: Çankırı is located at a strategic point, with easy access to major transportation routes. This accessibility allows visitors to reach the salt mine more conveniently. Furthermore, the development of infrastructure, such as hotels and wellness centers, can enhance the overall experience of tourists and make the region more appealing for health tourism.

Expertise in Health: Çankırı has a range of healthcare professionals and researchers focused on salt therapy and its health benefits. Collaborations between health institutions and research centers can provide scientific backing for therapy practices, increasing credibility and attracting more visitors. The presence of qualified personnel can enhance the quality of services offered at the therapy centers.

Growing Interest in Alternative Therapies: There is a rising global interest in alternative and natural therapies. Many individuals are seeking non-pharmaceutical options for health management, making salt therapy an attractive choice. This trend presents an opportunity for Çankırı to promote its salt therapy services and attract health-conscious tourists.

Weaknesses (W)

Infrastructure Challenges: The existing infrastructure in Çankırı may not be sufficient to accommodate the influx of health tourism visitors. Limited transportation options, such as insufficient public transport and inadequate road conditions, can hinder access to the salt mine. Furthermore, the lack of comprehensive facilities for tourists, including accommodations and wellness centers, may limit the region's appeal.

Lack of Awareness: There is insufficient public awareness regarding salt therapy and its benefits. Many people may not be familiar with the concept, leading to a lack of interest in this treatment option. Furthermore, limited scientific research on the efficacy of salt therapy may contribute to skepticism among potential visitors. Increasing awareness through educational campaigns can help address this issue.

Competition: The health tourism sector is highly competitive, with numerous regions offering alternative therapies. To stand out, Çankırı needs to emphasize its unique characteristics and advantages over other destinations. Competition not only comes from local areas but also from international locations that may offer similar therapeutic experiences. Ensuring high-quality services and effective marketing strategies will be crucial for attracting visitors.

Limited Access: The transportation options to Çankırı Rock Salt Mine can be restricted, making it difficult for potential visitors to reach the region. Particularly for international tourists, limited flight connections and insufficient public transport can pose significant barriers. Enhancing transportation infrastructure will be vital for increasing accessibility and attracting a wider audience.

Regulatory Challenges: The absence of clear regulations governing health tourism and salt therapy practices can limit the operations of businesses in this sector. The lack of established standards may

create uncertainties for both investors and potential visitors. Developing a regulatory framework that ensures safety and quality in salt therapy services will be essential for building trust in the industry.

Opportunities (O)

Increasing Health Awareness: There is a growing awareness of health and wellness among the public, leading to increased interest in alternative treatment methods. Individuals are actively seeking natural therapies to enhance their well-being. Salt therapy, as a natural remedy, can benefit from this trend and attract more individuals seeking holistic health solutions.

Government Support: The Turkish government offers various incentives and support for health tourism initiatives. Tax reductions, grant programs, and financial assistance for health tourism businesses can facilitate the development of Çankırı Rock Salt Mine as a therapy destination. Information campaigns to raise awareness of these opportunities among potential investors can enhance the region's attractiveness.

Research and Development Opportunities: Scientific research focused on salt therapy can provide valuable insights into its health benefits and effectiveness. Collaborations with universities, research institutions, and healthcare organizations can strengthen the scientific foundation of therapy practices. This collaboration can lead to better marketing strategies and increased awareness of the region's therapeutic offerings.

New Markets: Exploring new markets for health tourism can open up opportunities for promoting Çankırı on an international scale. European and Middle Eastern markets, in particular, hold significant potential for attracting health tourists seeking alternative therapies. By positioning itself effectively, Çankırı can attract visitors from neighboring countries looking for natural treatment options.

Sustainable Tourism: The growing emphasis on sustainable tourism practices aligns well with the potential of Çankırı Rock Salt Mine. Implementing environmentally friendly practices in therapy centers can attract eco-conscious travelers. Promoting sustainable tourism initiatives can enhance the region's reputation and contribute to long-term economic growth.

Threats (T)

Competitive Market: The presence of numerous alternative therapy destinations poses a threat to Çankırı's market share. Competing regions may offer similar services, making it challenging for Çankırı to differentiate itself. Continuous innovation and improvement in service quality will be necessary to maintain a competitive edge.

Economic Conditions: Economic downturns can adversely affect health tourism demand. Reduced disposable income among potential visitors may limit their willingness to invest in health tourism experiences. Strategic planning to mitigate the impact of economic fluctuations will be crucial for sustaining the industry's growth.

Weather and Climate Change: The effectiveness of salt therapy may be influenced by climatic conditions. Extreme weather events or unfavorable conditions can affect visitor turnout at therapy centers. Preparing for climate variability and ensuring consistent accessibility will be essential for maintaining operations.

Public Perception of Health: Changes in public perception regarding alternative therapies can impact the acceptance of salt therapy. Skepticism towards non-traditional treatment methods may hinder the growth of salt therapy services. Efforts to educate the public about the benefits and effectiveness of salt therapy will be vital in overcoming these challenges.

Regulatory Uncertainties: Inadequate legal frameworks governing health tourism can pose risks for businesses operating in the sector. Changes in regulations may disrupt the operations of salt therapy centers. Establishing clear standards and regulations will be critical for fostering a secure and trustworthy environment for both businesses and visitors.

2. Results and Discussion

The SWOT analysis reveals several strengths of the Çankırı Rock Salt Mine as a health tourism destination. Its mineral-rich salt, coupled with the region's cultural heritage, enhances its appeal to tourists seeking holistic health solutions. Accessibility to the mine and the presence of healthcare professionals contribute positively to its therapeutic offerings. However, challenges such as inadequate infrastructure and limited public awareness hinder its growth potential. Opportunities for advancement include a rising interest in health and wellness, governmental support for health tourism initiatives, and potential collaborations for research and development. Conversely, the competitive market landscape and economic uncertainties pose significant threats to the region's aspirations in health tourism.

The Çankırı Rock Salt Mine holds considerable potential for establishing a health tourism hub centered around salt therapy. While the region benefits from its unique natural resources and cultural significance, addressing weaknesses such as infrastructure limitations and awareness gaps is crucial for attracting visitors. Capitalizing on opportunities like growing health consciousness and government incentives can significantly enhance the development of salt therapy in Çankırı. By strategically navigating the threats posed by competition and economic fluctuations, Çankırı can position itself as a leading destination for health tourism, offering visitors a unique and beneficial therapeutic experience.

3. Conclusion

This study's SWOT analysis of the Çankırı Rock Salt Mine's potential in health tourism reveals notable strengths, challenges, and opportunities, alongside external threats that may impact its growth.

The primary strength of the Çankırı Rock Salt Mine lies in its unique mineral-rich salt, which is scientifically recognized for various therapeutic benefits, especially in respiratory and skin conditions. This characteristic positions the mine as an attractive destination for tourists seeking alternative therapies. Additionally, Çankırı's cultural heritage adds significant value, as it enables a holistic tourism experience that combines wellness with a rich historical context. However, addressing the region's infrastructural limitations, particularly related to transportation and accommodation, is crucial to making Çankırı accessible to a broader audience. Improvements in these areas would support higher visitor capacity, enhancing the appeal for international tourists.

A major opportunity identified is the rising global interest in natural therapies and wellness tourism. Çankırı has the potential to capitalize on this trend, leveraging the growing health consciousness worldwide and aligning itself with eco-friendly, sustainable tourism practices. Moreover, Turkish government incentives for health tourism development present a unique opportunity for local stakeholders to enhance infrastructure and marketing efforts. Collaboration with health institutions and academic researchers could also provide a scientific foundation for salt therapy, increasing credibility among health-conscious visitors.

Nevertheless, competition within the alternative therapy and health tourism sectors is intensifying. Various destinations offer similar therapies, which can pose challenges in differentiating Çankırı's unique offerings. To sustain a competitive advantage, Çankırı must emphasize the distinctive properties of its salt resources and ensure high-quality services. Furthermore, regulatory uncertainties and economic volatility present significant risks. Clear regulations are essential for establishing trust and operational consistency in health tourism, while economic stability is critical for maintaining visitor demand.

In conclusion, this SWOT analysis highlights that while Çankırı Rock Salt Mine possesses considerable potential as a health tourism destination, strategic development of infrastructure, awareness campaigns, and effective marketing will be key to success. By addressing its weaknesses and capitalizing on emerging opportunities, Çankırı could position itself as a prominent location for health tourism, offering a distinct and therapeutic experience to a diverse audience.

References

- [1] Wu, T.-C., Xie, P. F., & Tsai, M.-C. (2015). Perceptions of attractiveness for salt heritage tourism: A tourist perspective. *Tourism Management*, 51, 201-209. <https://doi.org/10.1016/j.tourman.2015.05.026>
- [2] Kimic, K., Smaniotto Costa, C., & Negulescu, M. (2021). Creating tourism destinations of underground built heritage—The cases of salt mines in Poland, Portugal, and Romania. *Sustainability*, 13(17), 9676. <https://doi.org/10.3390/su13179676>
- [3] Akhmedenov, K. M., & Khalelova, R. A. (2021). Salt lakes of the West Kazakhstan region as objects of medical tourism. *GeoJournal of Tourism and Geosites*, 36(2), 637-645.
- [4] Ramos, J., & Campos, A. C. (2020). Tourism in a Salt Pan: Does Creativity Matter?. In M. Popescu & A. Iancu (Eds.), *Multilevel approach to competitiveness in the global tourism industry* (pp. 142-158). IGI Global.
- [5] Çılğınöğlu, H., & Yazgan, I. (2022). Speleotherapy in the scope of health tourism: case of Çankırı salt cave in Turkey. *International Journal of Tourism Policy*, 12(3), 333-350.
- [6] Hakan, T. (2022). Türkiye’deki Mağaraların Sağlık Turizmi Kapsamında İncelenmesi (Investigation of Caves in Turkey Within The Scope of Health Tourism). *Journal of Tourism & Gastronomy Studies*, 10(3), 1829-1843.
- [7] Dağdeviren, A. (2019). Çankırı Gastronomi Turizmine İlişkin Yerel Paydaşların Görüşleri (Local Stakeholders’ Views on Çankırı Gastronomy Tourism). *Journal of Tourism & Gastronomy Studies*, 7(4), 3124-3139.
- [8] Tülek, B. (2021). Somut ve somut olmayan kültürel miras değerleriyle Çankırı kenti ve turizme katkısı. *Avrupa Bilim ve Teknoloji Dergisi*, (23), 827-836.
- [9] Deniz, K., & Kadioglu, Y. K. (2023). Geochemistry of salts and the effect of trace elements on human health: Turkey salt resources. *International Journal of Environmental Analytical Chemistry*, 103(17), 5082-5100.



Dynamic Resynchronization Units in Microgrids Transitions

Nour Aboubakr Hasan FADHEEL^{1,*} , Fatih KORKMAZ² 

¹ Institute of Graduate Studies, Department of Electrical and Electronic Engineering, Çankırı Karatekin University, Çankırı, Türkiye

² Faculty of Engineering, Department of Electrical and Electronic Engineering, Çankırı Karatekin University, Çankırı, Türkiye

Abstract

Microgrids, as decentralized energy systems, play a pivotal role in the modern energy landscape, offering flexibility, resilience, and sustainability. At the heart of this system lies the resynchronization unit, a critical component ensuring the seamless transition of microgrids between grid-connected and islanded operational modes. This paper offers a comprehensive examination of the intricacies and nuances of the resynchronization unit within microgrids. The transition between grid-connected and islanded modes is not just a switch but a complex process that requires precision and reliability. The seamless nature of this transition is vital to prevent disruptions, power quality issues, and potential equipment damage. It is here that the resynchronization unit proves its mettle, ensuring that the transition occurs without hitches. Factors such as synchronization speed, voltage and frequency matching, and phase alignment are of paramount importance. However, designing such a unit is not without its challenges. Issues related to transient stability, harmonics introduction, and potential feedback loops can complicate the resynchronization process. To address these challenges, this paper presents several proposed solutions aimed at enhancing the reliability and efficiency of island microgrids during resynchronization. These include advanced control algorithms, integration of fast-response energy storage systems, and utilization of state-of-the-art power electronics.

Keywords: Microgrids, Resynchronization Unit, Grid-connected, Islanded Modes

1. Introduction

Microgrids are a new approach to localized energy generation, distribution, and consumption, particularly in remote or isolated regions [1]. These standalone electricity systems operate independently from the main grid, reducing dependency on fossil fuels and ensuring resilience against grid disturbances. They integrate diverse energy sources, such as solar, wind, and hydro, reducing dependency on fossil fuels and promoting a sustainable, eco-friendly energy mix. Advanced control mechanisms and state-of-the-art technologies optimize energy production, storage, and consumption, catering to varying demand profiles and resource availability [2]. The decentralized nature of island microgrids minimizes energy losses, enhances resilience against external shocks, and can be more cost-effective in regions where extending the main grid is impractical. Given the growing global focus on sustainability, energy security, and electrifying remote areas, island microgrids are a crucial solution in the modern energy landscape. Island microgrids require a seamless transition between operational modes, from grid-connected to islanded mode, to maintain system stability, prevent equipment damage, and ensure uninterrupted power supply to consumers [3]. Resynchronization is a crucial process that facilitates these transitions smoothly and efficiently. System stability and reliability are essential for resynchronization, as it ensures that the generated electricity matches the voltage, phase, and amplitude of the connected system or grid. Without proper resynchronization, significant mismatches can lead to system instability, such as voltage sags, frequency deviations, and complete system blackouts [4]. Unsynchronized transitions can also pose safety risks to electrical equipment, reducing their lifespan and potentially leading to catastrophic failures. Consumer experience and trust are crucial for a reliable electricity provider, and sudden power outages or fluctuations can disrupt daily activities, lead to financial losses, and erode trust in the utility provider [5]. Efficient resynchronization can prevent unforeseen expenses, contributing to the economic viability of the microgrid. Island microgrids often incorporate renewable energy sources like solar and wind, which can introduce fluctuations in the grid's voltage and frequency. Effective resynchronization is even more crucial in such scenarios to ensure the stability of the microgrid [6]. This paper analyzes the resynchronization unit in microgrids, highlighting its importance in maintaining system stability during operational mode transitions. It examines

* Corresponding author. e-mail address: nour.fadheel@gmail.com

current challenges and evaluates emerging solutions, contributing to the ongoing discourse on improving the reliability and efficiency of microgrids.

2. Design of Microgrid

In this study, Simulink model for analyzing the performance of a photovoltaic (PV) system and a battery energy storage system (BESS) in a hybrid microgrid. The system comprises a 1-megawatt solar energy generation system that links to the grid. Additionally, there is a 1-megawatt battery energy storage system (BESS). The Point of Common Coupling (PCC) serves as the juncture where the microgrid integrates with the primary utility grid, facilitating the amalgamation of distributed energy resources. This utility grid stands as the central electrical network to which the microgrid connects, supplying power as required and assimilating surplus power generated by the microgrid. Within the microgrid, the loads represent the electricity consumers. They source power from the solar system, the BESS, or the utility grid, contingent on power availability and consumption demand. Figure 1 shows the simple design of microgrid.

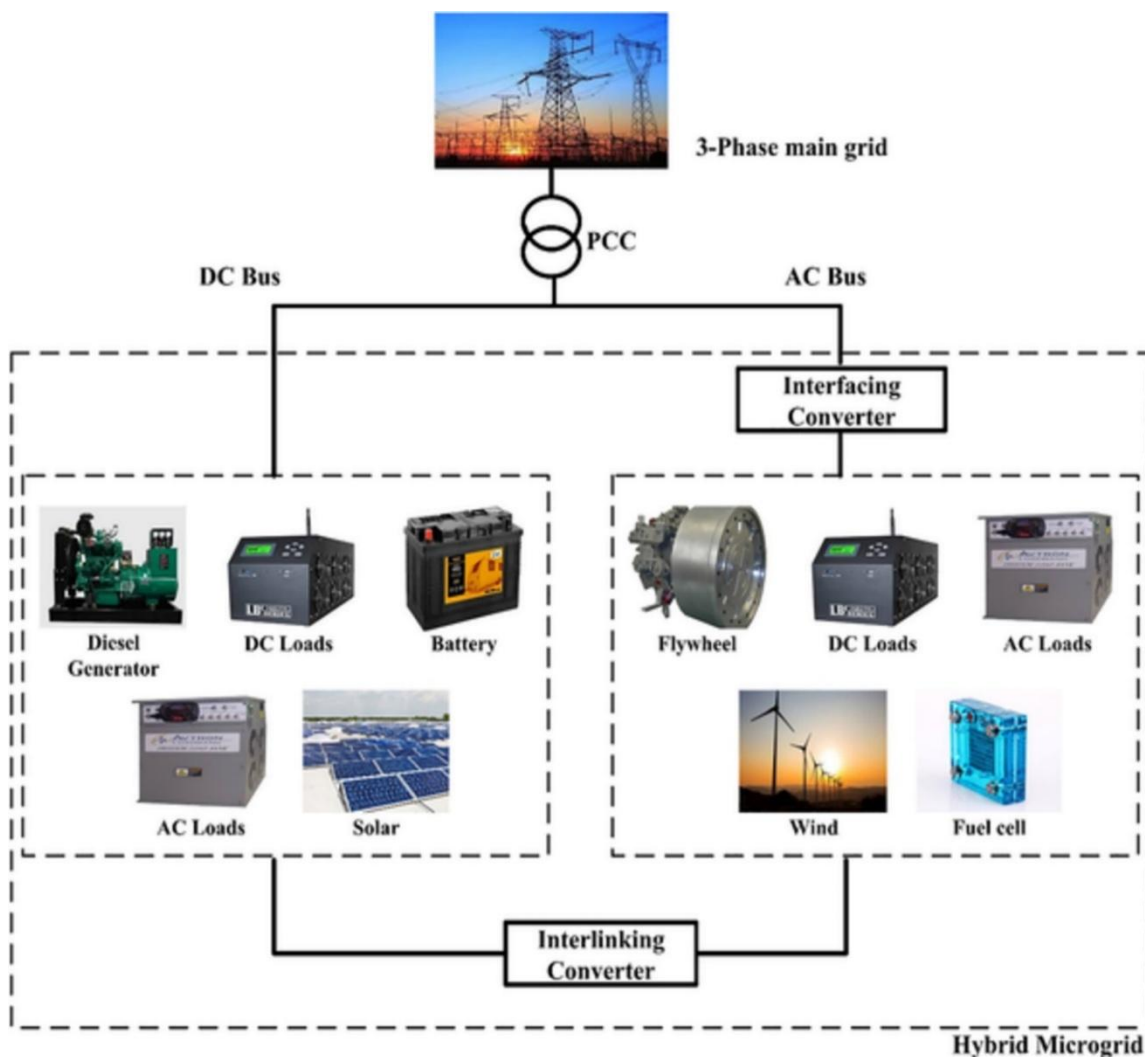


Figure 1. Design of Microgrid [7]

3. Principle of a Resynchronization Unit

A resynchronization unit is a specialized system designed to ensure that the electrical parameters of a localized energy system match those of a larger interconnected grid or another microgrid [8]. This matching involves aligning parameters such as frequency, voltage magnitude, and phase angle to ensure a seamless and safe connection or transition between different operational modes. The fundamental operation of a resynchronization

unit revolves around monitoring, comparing, and adjusting electrical parameters [9]. The unit continuously monitors the electrical parameters of both the microgrid and the main grid, tracking their frequency, voltage magnitude, and phase angle. If discrepancies are identified, the unit initiates corrective actions, such as frequency adjustment, voltage magnitude correction, and phase angle alignment. Once the electrical parameters are closely aligned, the microgrid can safely connect to the main grid or transition to another operational mode. Modern resynchronization units often incorporate feedback mechanisms to continuously adjust and optimize the synchronization process, ensuring real-time response to maintain synchronization even in dynamic grid conditions [10]. Safety protocols are equipped with resynchronization units to prevent potential damages or instabilities. If the unit detects that synchronization is not achievable within a specified timeframe or if discrepancies exceed safe limits, it will inhibit the connection to protect both the microgrid and the main grid. In essence, the resynchronization unit acts as a guardian, ensuring that the microgrid's electrical parameters are in harmony with those of the connecting system before any connection or transition occurs [11].

This unit brings the microgrid voltage in phase with the distribution system voltage before reclosing the grid breaker, ensuring a seamless reconnection without the risk of an out-of-phase reclosing. The resynchronization unit is crucial for ensuring a safe and reliable reconnection to the distribution system, ensuring all connected systems are in phase and operating correctly. It controls the frequency and voltages of the BESS, synchronizing it with the grid and providing the necessary power and voltage. It also regulates the current and voltage to prevent overloading. The synchronization process is an important step when connecting a microgrid to the main grid. During this process, PI regulators are used to slowly make the microgrid voltage and frequency equal to the main grid. This process is typically done over a period of 3 seconds, during which the PI regulators will adjust the microgrid voltage and frequency to match the main grid. The synchronization process helps ensure that the microgrid stays connected to the main grid and that power is being transferred properly. Once the synchronization process is complete, the microgrid is connected to the main grid and power can be exchanged. This process ensures that the microgrid is operating safely and efficiently, and that the main grid is not affected by the microgrid. In the BESS's Grid-forming mode, the voltage and frequency of a microgrid can be managed. Due to the mode's droop P/F setting of 0.5%, the microgrid frequency can vary between 60.3 and 59.7 hertz. With the droop Q/V setting at 3%, the microgrid voltage at the PCC bus can fluctuate between 609 Vrms and 582 Vrms. Given these parameters, the BESS can act as a reliable energy storage and power management system for the microgrid.

4. Results and Discussion

The synchronization unit closely monitors the microgrid's vital signs, continuously tracking its frequency and voltage. This real-time data is then compared with its counterparts on the master data grid. Regular monitoring is crucial when the microgrid is intentionally disconnected or when it operates in grid-forming mode. In such cases, the synchronization unit proactively adjusts the microgrid's frequency and voltage to align them with the main grid's parameters. Once the microgrid is reconnected to the grid, precise calibration is essential. The MEMS facilitates a smooth transition back to grid-following mode by ensuring a tight alignment between the microgrid's characteristics and those of the main grid. This not only ensures a consistent electricity supply but also safeguards the system against voltage and frequency variations. Figure 2 shows the performance of synchronization control unit.

The scenario described is a critical moment in the operation of a microgrid, showcasing its dynamic response to a sudden change in its operational status and subsequent recovery.

- *Initial Islanding (0-1 second):*

At the outset, the microgrid is suddenly islanded. This means it's disconnected from the main grid, which could be due to various reasons such as a fault in the main grid, maintenance activities, or a deliberate transition to off-grid mode. Upon islanding, the immediate effect observed is a change in frequency. The microgrid's frequency rises to 60.15 Hz, slightly above the standard nominal value of 60 Hz. This frequency deviation could be attributed to an imbalance between load and generation within the

microgrid. When disconnected, the excess power generated, which was initially accommodated by the main grid, causes the frequency to rise.

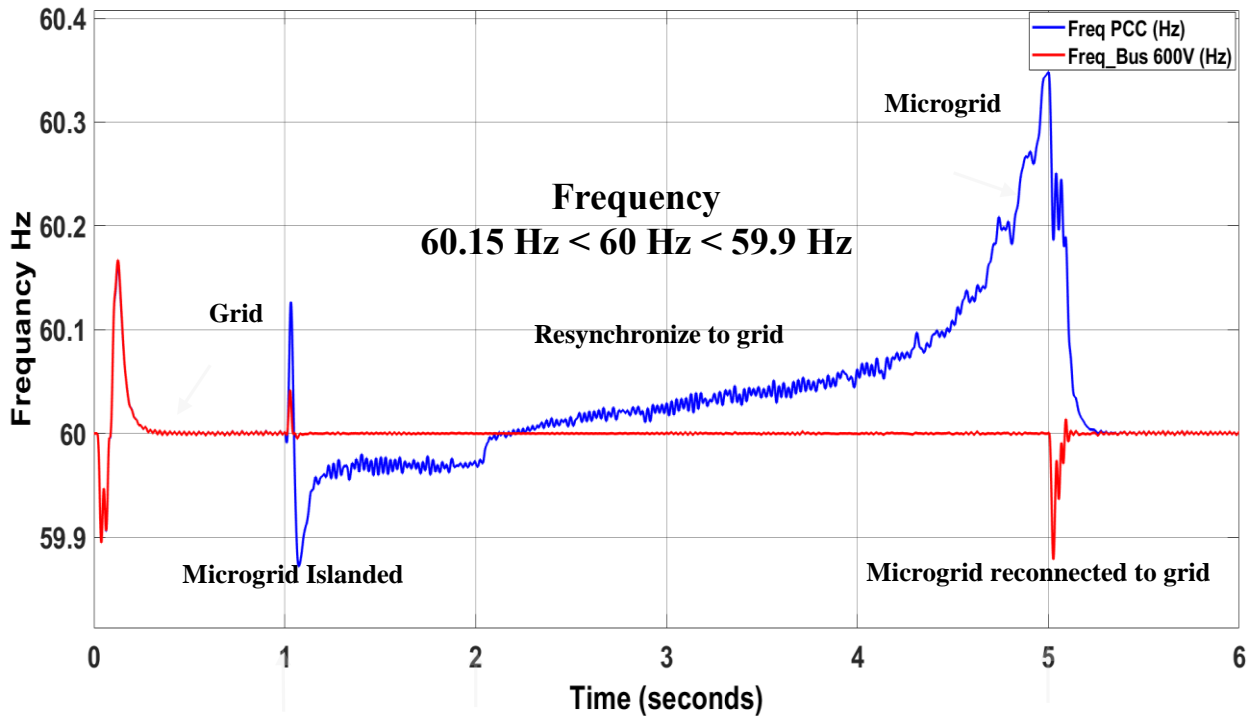


Figure 2. Frequency variations of PCC and 600V Bus

• *Response and Resynchronization Preparation (1-2 seconds):*

In this brief but crucial window, control systems within the microgrid respond to the frequency deviation. Advanced control strategies, possibly based on fast-acting power electronics and sophisticated software, are employed. These systems might adjust the output of generators, manage demand through load shedding or shifting, or leverage energy storage systems to absorb excess power. Concurrently, preparations to resynchronize with the main grid are initiated. This involves communicating with the main grid's operators, ensuring safety protocols are in place, and adjusting the microgrid's parameters to match those of the main grid (like frequency, voltage, and phase angle).

• *Stabilization and Resynchronization (2-5 seconds):*

Over these critical seconds, the control measures take effect, and the microgrid's frequency begins to stabilize. Sophisticated algorithms and high-speed communication systems play a crucial role in this rapid stabilization. By the 5-second mark, the frequency has been corrected back to the reference value of 60 Hz. This swift return to normal operating conditions highlights the resilience and advanced design of the microgrid, ensuring reliability and continuous power supply to the connected loads.

• *Post-Stabilization (5 seconds onwards):*

After frequency stabilization, the microgrid continues to operate in a stable state, with its operational parameters aligned with those of the main grid. The seamless transition back to the reference frequency, without any observable issues between the main grid and the microgrid, underscores the effectiveness

of the microgrid's control systems and its capability to operate in both grid-connected and islanded modes. This flexibility is vital for modern power systems, contributing to enhanced energy security, better integration of renewable resources, and improved resilience against disturbances. In Figure 3 appears to represent the behavior of the phase angle during a microgrid transitioning through three distinct stages: islanding from the main grid, resynchronization preparations, and finally, reconnection to the main grid. The phase angle is a crucial parameter when considering the synchronization of two power systems, as it reflects the difference in the position of the voltage waveforms in the power system.

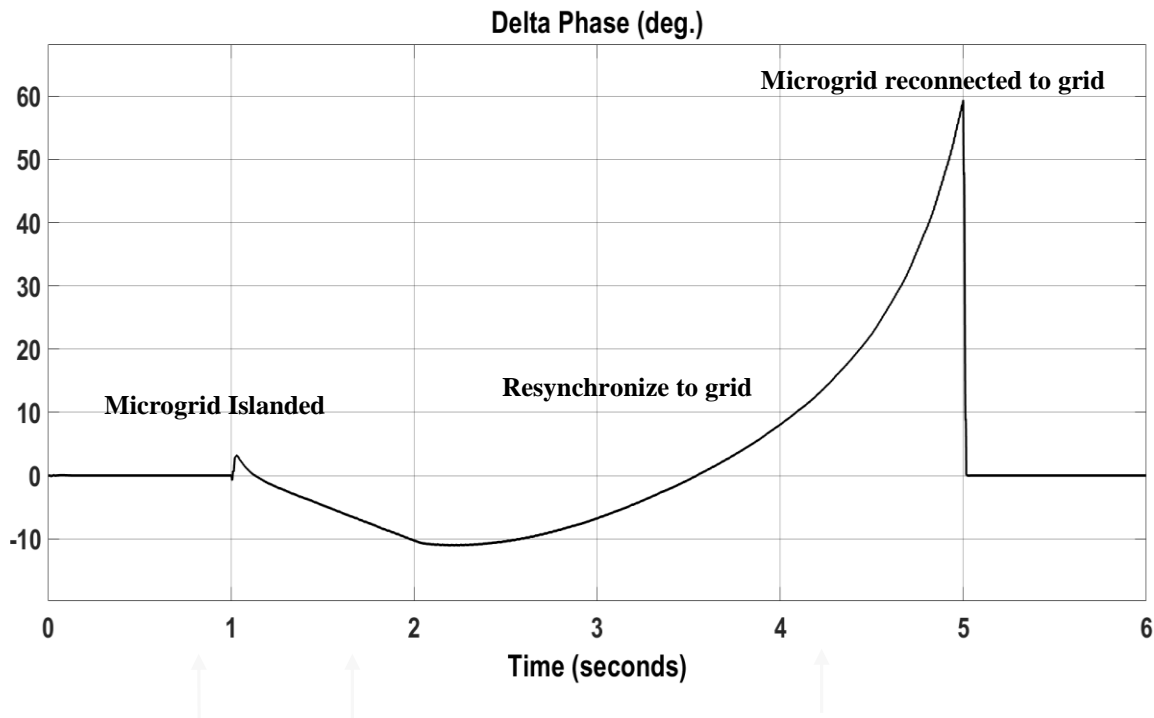


Figure 3. Phase difference between Microgrid and grid

5. Conclusion

This study underscores the significant advancements in microgrid technology facilitated by the integration of Resynchronization Unit Control. The observed enhancements in dependability during the pivotal transitions between grid-connected and islanded operations herald a new era in energy system operations. The seamless execution of resynchronization processes, evidenced by minimal disturbances and the assurance of uninterrupted energy provision, speaks volumes about the strides taken in this domain. The journey from an unexpected islanding event to a well-coordinated reconnection to the main grid illustrates the intricate ballet of real-time controls and automation that underpin modern microgrids. The ability to not only monitor and adjust but masterfully control the phase angle during these transitions is emblematic of the technological sophistication inherent in today's energy systems. This capability ensures fluidity between operational modes, safeguarding both the stability of the microgrid and the continuity of the power supply.

References

- [1] López-García, D., Arango-Manrique, A., & Carvajal-Quintero, S. X. (2018). Integration of distributed energy resources in isolated microgrids: The colombian paradigm. *TecnoLógicas*, 21(42), 13–30. <https://doi.org/10.22430/22565337.774>
- [2] Mahmood, D., Javaid, N., Ahmed, G., Khan, S., & Monteiro, V. (2021). A review on optimization strategies integrating renewable energy sources focusing uncertainty factor – Paving path to eco-friendly smart cities. *Sustainable Computing: Informatics and Systems*, 30, 100559. <https://doi.org/10.1016/j.suscom.2021.100559>

- [3] D'silva, S., Shadmand, M., Bayhan, S., & Abu-Rub, H. (2020). Towards grid of microgrids: Seamless transition between grid-connected and islanded modes of operation. *IEEE Open Journal of the Industrial Electronics Society*, 1, 66–81. <https://doi.org/10.1109/ojies.2020.2988618>
- [4] Shi, D., Luo, Y., & Sharma, R. K. (2014, October 1). Active synchronization control for microgrid reconnection after islanding. *IEEE Xplore*. <https://doi.org/10.1109/ISGTEurope.2014.7028802>
- [5] Aleem, S. K. A., Aftab, M. A., Hussain, S. M. S., Ali, I., Ganesh, V., & Ustun, T. S. (2019). Real-Time Microgrid Synchronization using Phasor Measurement Units. 2019 IEEE International Conference on Intelligent Systems and Green Technology (ICISGT). <https://doi.org/10.1109/icisgt44072.2019.00019>
- [6] Zacharia, L., Avgoustina Kyriakou, Lenos Hadjidemetriou, Kyriakides, E., Panayiotou, C., Martensen, N., & van. (2018). Islanding and Resynchronization Procedure of a University Campus Microgrid. 2018 International Conference on Smart Energy Systems and Technologies (SEST). <https://doi.org/10.1109/sest.2018.8495828>
- [7] Sarangi, S., Sahu, B. K., & Rout, P. K. (2020). Distributed generation hybrid AC/DC microgrid protection: A critical review on issues, strategies, and future directions. *International Journal of Energy Research*, 44(5), 3347–3364. <https://doi.org/10.1002/er.5128>
- [8] Kroposki, B., Basso, T., & DeBlasio, R. (2008, July 1). Microgrid standards and technologies. *IEEE Xplore*. <https://doi.org/10.1109/PES.2008.4596703>
- [9] Nishikawa, T., & Motter, A. E. (2015). Comparative analysis of existing models for power-grid synchronization. 17(1), 015012–015012. <https://doi.org/10.1088/1367-2630/17/1/015012>
- [10] Cho, C.-H., Jeon, J.-H., Kim, J.-Y., Kwon, S., Park, K.-Y., & Kim, S. (2011). Active Synchronizing Control of a Microgrid. *IEEE Transactions on Power Electronics*, 26(12), 3707–3719. <https://doi.org/10.1109/tpel.2011.2162532>
- [11] Taul, M. G., Wang, X., Davari, P., & Blaabjerg, F. (2019). An overview of assessment methods for synchronization stability of grid-connected converters under severe symmetrical grid faults. *IEEE Transactions on Power Electronics*, 34(10), 9655–9670. <https://doi.org/10.1109/tpel.2019.2892142>